Università degli Studi di Pisa - Dipartimento di Scienze della Terra

Scuola di Dottorato di Ricerca in Scienze di Base Galileo Galilei
Programma di Scienze della Terra
XXIV Ciclo 2009 – 2011

Dissertazione Finale

Ilaria Consoloni

Reconstruction of paleoenvironments and paleoclimate during the last and present interglacials over the Patagonian coast (Argentina), with particular reference to the shell geochemistry

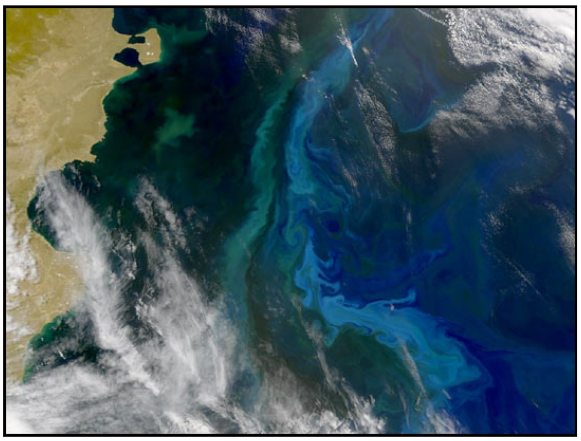

Tutore: *Dott. Giovanni Zanchetta*
Co-tutori: *Dott. Luigi Dallai*
Dott. Massimo Guidi

Referees: *Prof. Anthony E. Fallick*
Dott.ssa Barbara Stenni

Direttore della Scuola
prof. Fabrizio Broglia

Presidente del Programma
prof. Roberto Santacroce

A Camilla e Andrea

"La Patagonia!
È un'amante difficile.
Lancia il suo incantesimo.
Un'ammaliatrice!
Ti stringe nelle sue braccia
e non ti lascia più."
(Bruce Chatwin)

TABLE OF CONTENTS

ABSTRACT

The present study aims a better understating of the paleoceanographic, paleoclimatic and paleoenvironmental conditions of the Patagonia Atlantic coast in the in the vicinity of San Jorge Gulf (Chubut and Santa Cruz Provinces, Argentina) through the study of the geochemistry (stable isotopes and trace elements) of molluscs collected in the late Quaternary marine deposits.

On the basis of XRD powder analysis, petrographic and trace element screening tests (comparison between marine shells and paleosols), a large dataset of unaltered bivalves with aragonite (*Ameghinomya antiqua* species) or mixed aragonite-calcite (*Mytilus edulis* and *Aualcomya atra* species) composition of the shells was identified.

Analytical data definitively demonstrate the suitability of *Ameghinomya antiqua* and Mytilidae family specimens as potential proxies for paleoclimatic studies. Oxygen isotopic composition of modern *Mytilus edulis* in the study area is progressively more positive moving southward. The isotopic composition on modern mussels along the Atlantc coast of Patagonia seems to reflect the changes in seawater temperature. Stable isotope ($^{13}C/^{12}C$ and $^{18}O/^{16}O$ ratios) and trace elements (Ba/Ca, Sr/Ca, Mg/Ca, Mn/Ca, Fe/Ca) data indicate large variability of modern condition in the gulf, but in the past too systematic differences between old beach ridges sets existed and can be interpreted as substantial different paleoceanographic conditions, partly related also to local mixing with freshwater. Paleontological and geochemical data indicate that the Holocene and the previous interglacial appear consistently different from the present. In particular they seem to contain molluscs indicating a stronger influence of the warm and saltier Brazil current in the area and, then, fluctuations in the relative position between the two surface currents (Brazilian and Malvinas) over the time.

RIASSUNTO

Il progetto di ricerca svolto, è inserito in un più ampio progetto di ricerca finanziato dall'Università di Pisa e dal Ministero dell'Istruzione, dell'Università e della Ricerca in collaborazione con varie Università argentine che prevede lo studio della costa atlantica della Patagonia argentina durante il tardo Quaternario per ottenere delle ricostruzioni paleoambientali e paleoclimatiche di elevata risoluzione. Questo progetto è focalizzato sullo studio degli effetti delle variazioni del livello marino e del clima sull'ambiente costiero attraverso ricostruzioni paleogeografiche, paleoecologiche, paleobiogeografiche e paleoambientali su un'area selezionata della costa della Patagonia (Argentina) usando metodi geomorfologici, stratigrafici, paleontologici e geochimici.

L'area costiera della Patagonia è una regione remota che offre una straordinaria opportunità di studio dell'evoluzione climatica essendo l'unico tratto costiero dell'emisfero sud che si estende, quasi senza soluzione di continuità, dai tropici all'Antartide.

La maggior parte della costa atlantica della Patagonia è dominata dalla corrente fresca e a bassa salinità delle Malvinas (Falkland), mentre più a nord è caratterizzata dall'interazione con la Corrente Brasiliana più salata e calda.

Queste condizioni rendono la regione costiera un sito di importante scambio di acqua e calore tra l'Oceano Meridionale e i bacini subtropicali.

La posizione della confluenza tra le Correnti Brasiliana e delle Malvinas (BMC) migra latitudinalmente alla scala stagionale e pluriannuale, anche se poco è stato compreso circa le dinamiche che guidano queste variazioni su scala temporale più lunga.

Fin dai lavori pionieristici di Darwin e dalle ricostruzioni di Feruglio, i depositi costieri patagonici hanno attratto molti ricercatori per il loro notevole contenuto in molluschi, che in tempi recenti hanno offerto dati fondamentali riguardo l'evoluzione paleobiogeografica e paleoceanografica della costa atlantica.

Tuttavia, non esistono sistematiche ricerche che utilizzino proxies geochimici (es. isotopi stabili ed elementi in traccia) su questi archivi naturali.

In questo studio sono state proposte per la prima volta ricostruzioni paleoambientali e paleoclimatiche basate su analisi geochimiche (isotopi stabili ed elementi in traccia) di gusci di molluschi marini provenienti da depositi di spiaggia tardo quaternari affioranti

lungo la costa Atlantica della Patagonia Argentina al fine di comprendere gli effetti delle variazioni climatiche sull'ambiente costiero.

Nello specifico, il presente lavoro si concentra sulla costa atlantica patagonica in prossimità del Golfo di San Jorge (Province del Chubut e di Santa Cruz), dove affiorano successioni spettacolari di beach ridges, depositi di spiaggia sopraelevati, al cui interno sono molto frequenti accumuli di organismi marini trasportati sulla costa da tempeste. Sebbene questi accumuli siano molto diversificati, i molluschi costituiscono l'elemento dominante.

Questi depositi e il loro contenuto fossilifero costituiscono dei potenziali archivi per studiare le condizioni paleoclimatiche e paleoceanografiche dell'area e per ricostruire la circolazione costiera e le possibili variazioni locali nel contributo di acque continentali, poiché le correnti Brasiliana e delle Malvinas (Falkland) sono caratterizzate da una marcata differenza in salinità e temperatura che può essere tracciata attraverso l'utilizzo di analisi geochimiche sui gusci dei molluschi marini.

Durante il dottorato sono state compiute due campagne di circa un mese ciascuna in Patagonia che hanno riguardato il rilevamento geologico e geomorfologico ed il campionamento di circa 500 campioni di sedimento, paleosuoli e fossili prelevati dai depositi costieri di quest'area. Durante il lavoro di rilevamento e campionamento sono stati acquisiti tramite GPS oltre 1000 punti, grazie ai quali, è stato creato e implementato un database geografico costruito con ArcGIS® in cui sono state inserite la posizione dei punti, le descrizioni dei campioni raccolti ed è stato effettuato un collegamento ipertestuale attraverso cui visualizzare le fotografie scattate per ogni punto di campionamento. È stata eseguita, inoltre, prima dello svolgimento delle campagne, un'analisi di remote sensing, in cui, attraverso Google Earth, sono state individuate le principali forme del terreno (beach ridges, piattaforme in roccia, terrazzi marini e fluviali, ….) in modo da avere poi in campagna una migliore idea della geomorfologia dell'area.

Durante le campagne particolare attenzione è stata rivolta alla raccolta di campioni di molluschi ben conservati (preferibilmente a valve chiuse) e sono stati campionati i taxa più comuni tra le varie successioni per avere il massimo grado di confrontabilità dei dati. Per ogni unità sono state campionate più singole unità di beach ridges per verificare la variazione entro una fase trasgressiva-regressiva.

Durante il dottorato sono stati preparati (puliti e macinati) per le varie analisi circa 600 esemplari di Bivalvi. Per ogni stazione di campionamento, infatti, sono stati preparati da due a dieci esemplari. Per confermare l'assenza di alterazione degli stessi sono state

eseguite analisi diffrattometriche che hanno permesso di valutare che la conchiglia dei Bivalvi (attuali, olocenici e pleistocenici) avesse mantenuto l'originale composizione aragonitica o mista calcitico-aragonitica e non ci fosse stata una parziale ricristallizzazione in calcite. Il grado di alterazione dei Bivalvi è stato osservato anche tramite il contenuto in Mn, poiché questo elemento in traccia dà indicazioni sull'alterazione dei carbonati marini da parte di acque meteoriche (che contengono ≈ 40 volte più Mn dell'acqua di mare). Poiché sia i campioni attuali sia gli esemplari fossili mostrano un bassissimo contenuto in Mn, è possibile escludere la contaminazione da acque meteoriche per i bivalvi analizzati.
Attraverso l'analisi delle sezioni sottili è stato possibile osservare i due strati (interno ed esterno) di cui è composta la conchiglia della *Venus antiqua* ed è stato possibile stabilire che le alterazioni del guscio, quando osservabili, sono presenti solo all'interno dello strato esterno.
Per migliorare il quadro cronologico e stratigrafico dell'area di studio sono state effettuate, inoltre, 48 datazioni con il metodo del ^{14}C per fossili e sedimento di presunta età olocenica e 8 datazioni con il metodo U/Th su Bivalvi provenienti da cordoni pleistocenici. Datazioni su Molluschi ottenute con il metodo U/Th sono molto discusse in letteratura, in quanto il metodo sopra citato non è considerato attendibile se effettuato su Molluschi (a differenza, per esempio, dei Coralli), a causa dell'acquisizione da parte degli stessi dell'Uranio in fase diagenetica.
Durante il Dottorato, tuttavia, l'attività di ricerca principale ha riguardato lo studio degli elementi in traccia (circa 150 analisi) e l'analisi degli isotopi stabili ($\delta^{18}O$ e $\delta^{13}C$) sulle conchiglie di Bivalvi di età variabile tra l'attuale ed il Pleistocene medio (circa 500 analisi) .
Questi dati, considerati complessivamente, indicano chiaramente che i dati geochimici possono essere uno strumento potente per la ricostruzione regionale delle correnti marine.
Sulla base di analisi diffrattometriche ai raggi X, petrografiche e degli elementi in traccia, confrontando le conchiglie marine con i paleosuoli, è stato identificato un ampio set di bivalvi inalterati a guscio aragonitico (*Ameghinomya antiqua)* o misto calcitico-aragonitico (*Mytilus edulis* e *Aulacomya atra*).
I dati analitici dimostrano definitivamente l'attitudine di *A. antiqua* (mai utilizzata per studi di carattere geochimico) e dei Mitilidi come possibili proxies per studi paleoclimatici.
La composizione isotopica dell'ossigeno dei gusci attuali di *Mytilus edulis* nell'area di studio è progressivamente più positiva andando verso sud. La composizione isotopica dei mitilidi lungo la costa atlantica della Patagonia sembra riflettere le variazioni nella temperatura dell'acqua di mare, mentre la sua salinità rimane pressoché costante in tutta

l'area analizzata. Gli isotopi stabili (rapporti $^{13}C/^{12}C$ and $^{18}O/^{16}O$) e gli elementi in traccia (Ba/Ca, Sr/Ca, Mg/Ca, Mn/Ca, Fe/Ca) indicano una grande variabilità nelle condizioni attuali all'interno del golfo, ma anche nel passato hanno avuto luogo differenze sistematiche tra set di antichi beach ridges, che possono essere interpretate come condizioni paleoceanografiche sostanzialmente differenti, in parte connesse anche a mescolamenti con acque dolci.

Dati paleontologici e geochimici indicano che l'Olocene e il precedente interglaciale appaiono differenti dall'attuale. In particolare, sembrano contenere molluschi indicativi di un'influenza maggiore della corrente Brasiliana calda e salata nell'area e, quindi, di fluttuazioni nella posizione relativa tra le due correnti oceaniche superficiali (Brasiliana e delle Malvinas) nel tempo.

1. INTRODUCTION

The problem of global warming and the impact it is making and can make in the future climate and the environment are very important topics (CO_2 release, melting glaciers, sea level rise) and engage in a decisive way the Earth Sciences also in order to propose possible future climate scenarios and then evaluate strategies for mitigating plan.

In this context the study of past changes of climate and paleoenvironmental evolution is strategic.

The reconstruction of the climates and environments features of the past is crucial to understanding the influence that climate changes have on the evolution of the biosphere, hydrosphere and atmosphere. Many natural systems, in fact, are climate depending and various methods of investigation can be used in order to obtain important information on the paleoclimate. These include the stable isotope and trace element geochemistry (e.g. Dodd, 1965; Mook, 1971; Wefer & Berger, 1991; Klein *et al.,* 1996; Takesue & Van Geen; 2004; Gillikin et al., 2005; Lorrain et al., 2005; Freitas et al., 2008 Schone *et al.*, 2011).

The Patagonia is the only continental landmass emerging along the mid to low-latitudes in the Southern Hemisphere representing a unique region of the world. Patagonia represents a key area for understanding the role of the Southern Hemisphere in regulating climate during the last hundredth of thousand years. Overall, the collection of climatic data from Patagonian on land and on coastal deposits is of paramount importance for a complete understanding of climatic system. This is further highlighted by the fact that Patagonia not only offers a uniquely southern location, but the area is blown by the southern Westerlies, the dynamic component of the atmospheric circulation of the Southern Hemisphere. Furthermore its Atlantic coast is extremely interesting from a biogeographic point of view, as it is located between the marine zoographic provinces Argentinean and Magellanean and close to a surface currents convergence zone (Brasil-Malvinas confluence zone). It has been suggested that these provinces have been influenced by progressive weak latitudinal shifts during climate changes of the relative position of the surface currents (Aguirre, 2003).

The Atlantic coast of Patagonia preserves an impressive geological record of the glacial events and sea-level oscillations. The Quaternary coastal deposits, often organised in spectacular successions of raised beaches, contain an almost unexplored archive of past climate. These natural archives can offer precious information on local relative sea-level changes, tectonic and glacial isostasy component, and fundamental information on past surface ocean conditions and, through the study of the continental deposits related to beach ridge systems, information also on terrestrial climate. These deposits have been partially studies mainly with the purpose to reconstruct relative sea-level changes (Schellmann & Radtke, 2000) and/or disentangle the isostatic/tectonic component (Codignotto *et al*., 1992; Rostami *et al*., 2000); on the contrary they are practically unexplored as climatic archives (Isla & Bujalesky, 2008). Most of these deposits preserve rich and diversified fossil assemblages usually in the form of storm accumulations potentially very useful for paleoclimatological and paleoecological studies and to perform dating. In particular, the molluscs associations are good indicators for environmental parameters (substrate, depth, energy conditions) and changes in paleoclimate.

This study is is part of a larger research project, funded by the University of Pisa (Progetto Ateneo 2007) and the Ministry of Education, University and Research (PRIN 2009).

The aim of the PhD project focuses on the study of the effects of climate changes on the coastal environment through paleoenvironmental and paleoclimatic reconstructions based on the study of the geochemistry (stable isotopes and trace elements) of molluscs collected in the late project. The principles and techniques of stable isotopes and trace element geochemistry are applied to marine molluscs. The applicability of stable isotopes and other geochemical investigations are related on samples characterized by a low degree of alteration. So XRD and petrographic analyses have been used for inferring the shells preservation state. In addition detailed study of possible diagenitic overprint was undertaken also analysing carbonate-enriched soil horizons (Bk) present in the area used as proxy of potential fluid generating diagenetic alteration along with the analyses of modern, unaltered, molluscs shells collected in the area.

This project wants, then, provide new data for understand climate system in this strategically located region of the world. The results are important since the Patagonian coast is an environment of high natural values (however, it is threatened

by oil exploitation, mining and increasing tourism) and represents a natural heritage that need to be preserved for future generations as reserve of marine and terrestrial biodiversity.

This thesis is divided into three basic parts. The first describes the study area, the state of the art and the principles and techniques of stable isotopes and trace element geochemistry applied to marine molluscs for paleoclimatic reconstructions. The second part is devoted to the description of materials and analytical techniques used for the acquisition and processing of data. Finally, the third part describes and discusses the obtained results.

2. STUDY AREA

2.1 GEOGRAPHICAL SETTING

Patagonia represents the southernmost region of the South American continent and it extends from 37° S to Cape Horn, at 56° S, including the areas of southern Argentina and Chile (Fig. 1). With a surface area of approximately 790000 km^2, politically the region is divided in Argentinean Patagonia, to the east (it covers the provinces of Río Negro, Neuquén, Santa Cruz, Chubut and Tierra del Fuego) and the Chilean Patagonia, to the west (the Republic of Chile considers its Patagonian sector as that territory extending along the western slope of the Andes, from 43° S, in the province of Palena, and the southernmost archipelagos in the Cape Horn area, including the XIth (Aysén) and XIIth (Magallanes) administrative regions).

The natural boundaries of Patagonia are the Barrancas and Colorado rivers, the Provinces of Mendoza and La Pampa and the south portion of Buenos Aires Province to the north, the Andean Cordillera and the Republic of Chile to the west, the Atlantic Ocean to the east and the Beagle Channel and the Chilean Navarino Island archipelago to the south (Fig. 1).

Its main geographic feature is the Andean Cordillera, which is both the continental watershed and, in many areas, the international boundary between Argentina and Chile. It includes the Pacific and Atlantic lowlands and coasts, the southern archipelagos, and the valleys, tablelands and high plains extending between the Andes and the Atlantic Ocean.

The population density in Patagonia is approximately 1-2 persons per km^2, making it one of the most sparsely populated regions in the world.

Patagonia is also home to the Northern and Southern Icefields. The Northern Icefield runs for nearly 200 km and covers a surface of 4200 km^2. The Southern Icefield is over 350 km long and has a surface of approximately 13000 km^2. These icefields are located along the Andes at an average altitude of 1500 meters. Located mainly in Chile, some branches of the Southern Icefield extend into Argentina.

This region consists of an Andean zone (also called Western Patagonia) and the main Patagonian plateau south of the Pampa, which extends to the tip of South

America. The surface of Patagonia descends east of the Andes in a series of broad, flat steps extending to the Atlantic coast. The landscape is cut by eastward-flowing rivers, some of them of glacial origin in the Andes that have created broad valleys and steep-walled canyons.

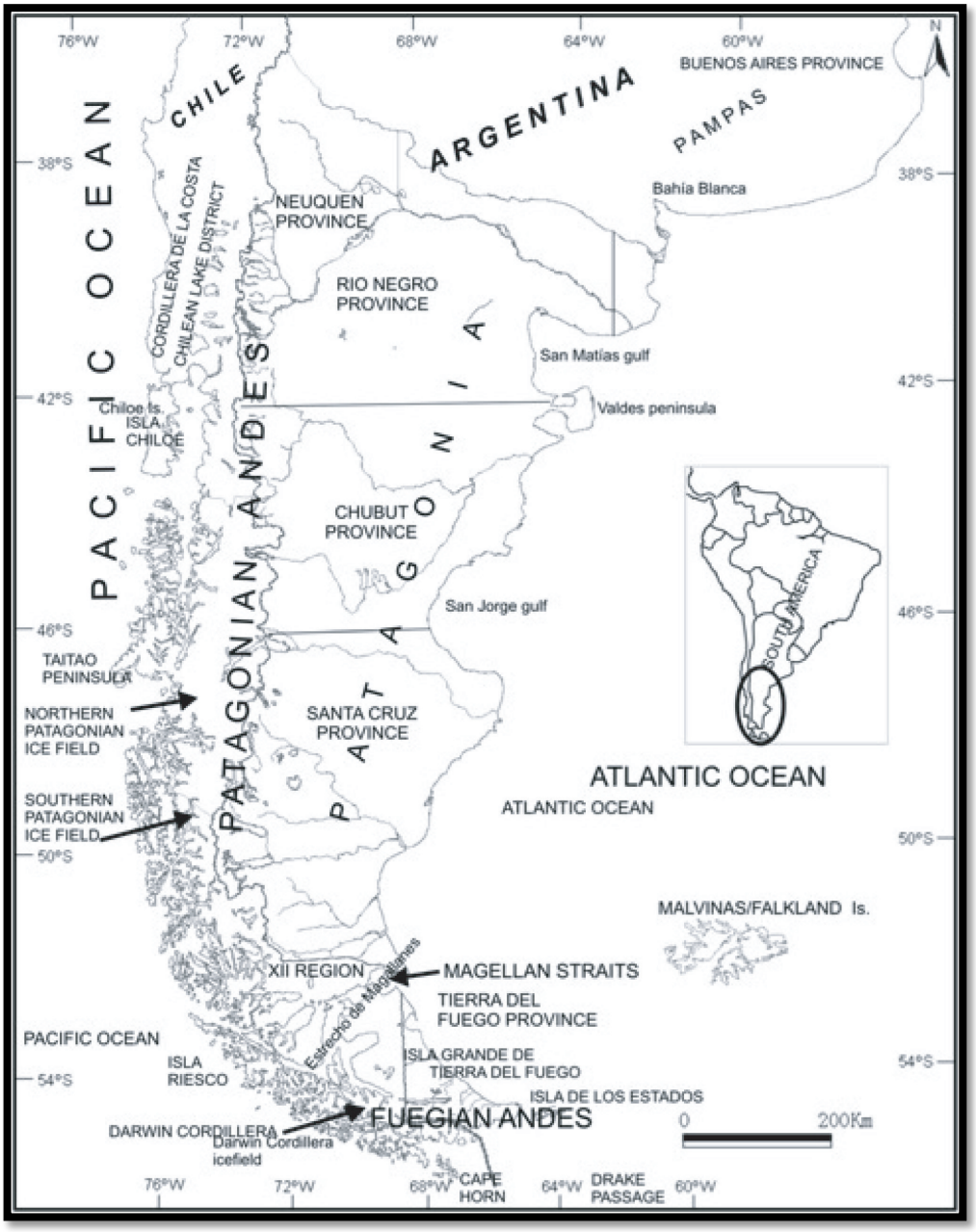

Figure 1 – Location map. Patagonia, main geographical regions (Rabassa & Coronato, 2009).

Other features of Patagonia include a series of basins, some of which contain lakes, nestled between the Patagonian Andes and the plateau, and volcanic hills in the

central plateau west of the city of Río Gallegos.

Specifically, the study area is located in the Golfo San Jorge and its immediate surrounding areas along the Atlantic coast of Patagonia (Figs. 1-2). The San Jorge basin is located in central Patagonia, between latitude 44º and 47º S and, politically, it lies on both the Santa Cruz and Chubut provinces and toward the east, on the continental shelf. The basin shows a clear elongated shape in the E-W direction.

Figure 2 – Study area with main localities.

2.2. GEOLOGICAL SETTING

The study area is located on the southern end of the South America Plate, which moving westward collides against the Nazca and the Antartic Plates (Coronato *et al.,* 2008). During the different tectonic regimes throughout time, four major tectono-sedimentary domains developed on the South American continent (Fig. 3).

The western continental margin of the South American Plate developed at least since Neoproterozoic to Early Paleozoic times and constitutes a convergent margin, along which eastward subduction of Pacific oceanic plates beneath the South American Plate takes place (Ramos, 1999). Through this process the Andean Chain developed. The eastern margin of the South American Plate forms a more than 10000 km long divergent margin, which developed as a result of the separation of the South American plate and the African plate since the Mesozoic through the opening of the South Atlantic and the break up of Gondwana. The northern and southern margins of the South American Plate developed along transform faults in transcurrent tectonic regimes due to the collision of the South American Plate with the Caribbean and the Scotia plates (Fig. 3).

Most authors agree about the participation of Patagonia in the Gondwana Supercontinent (i.e., Fitzgerald *et al.*, 1990; Peroni *et al.*, 1995). On the contrary, Ramos (1984, 1996) proposes that Patagonia may, with the Antartic Peninsula and other smaller fragments, have been accreted to Gondwana along a northward-dipping subduction zone during Middle to Late Permian.

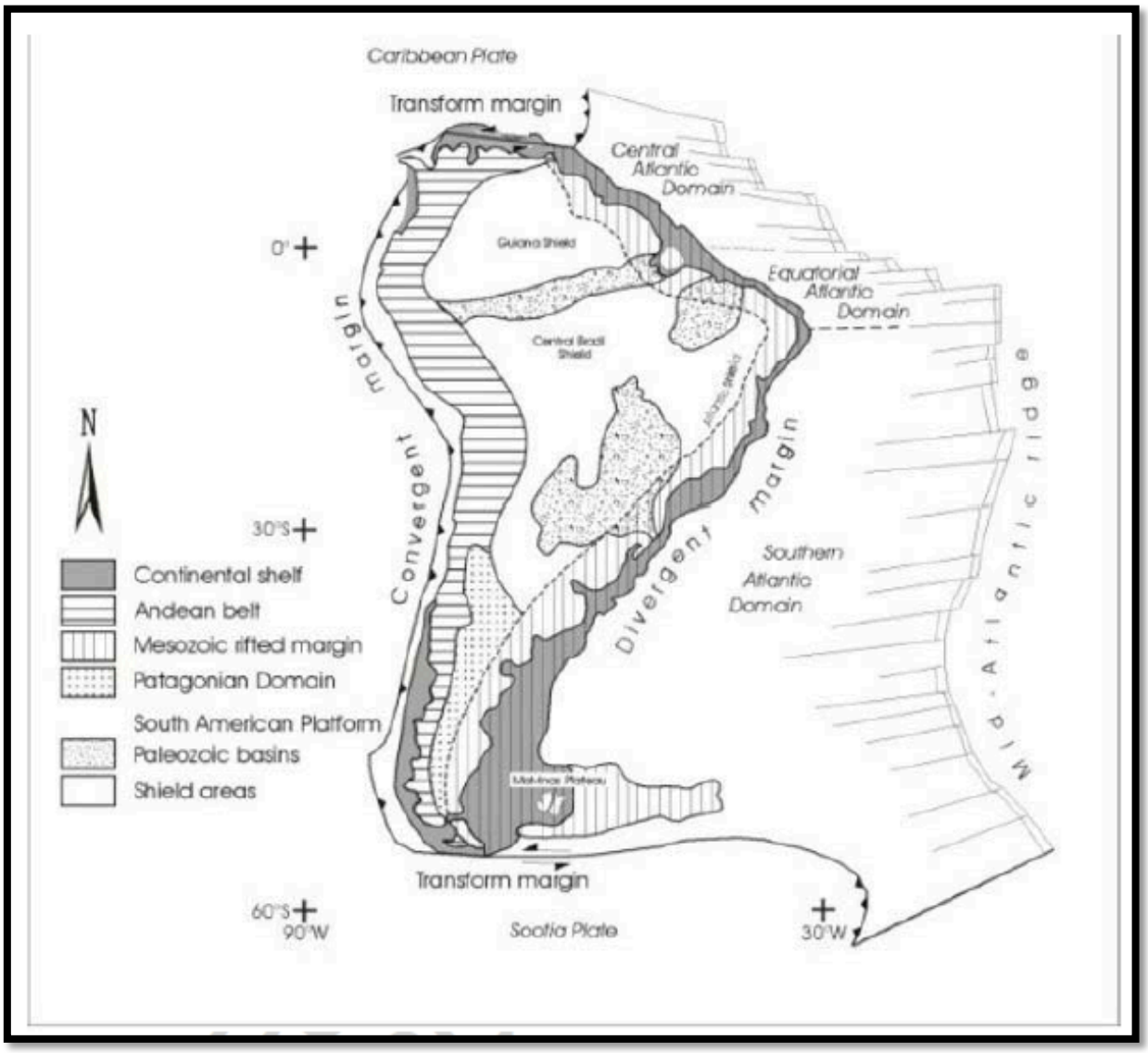

Figure 3 – Major tectono-sedimentary provinces of the South American Plate (modified after Milani and Thomaz Filho, 2000).

The Patagonian Platform (Fig. 4) mainly evolved during the Early Paleozoic and has been tectono-thermally active up to the Cenozoic. The Andes developed on the western continental margin of the plate, at least from the early Paleozoic on, and its evolution continues until today with active volcanism and seismicity due to continuous subduction of Pacific plates (Nazca and Antartic) beneath the South American Plate (Ramos, 1999; 2008).

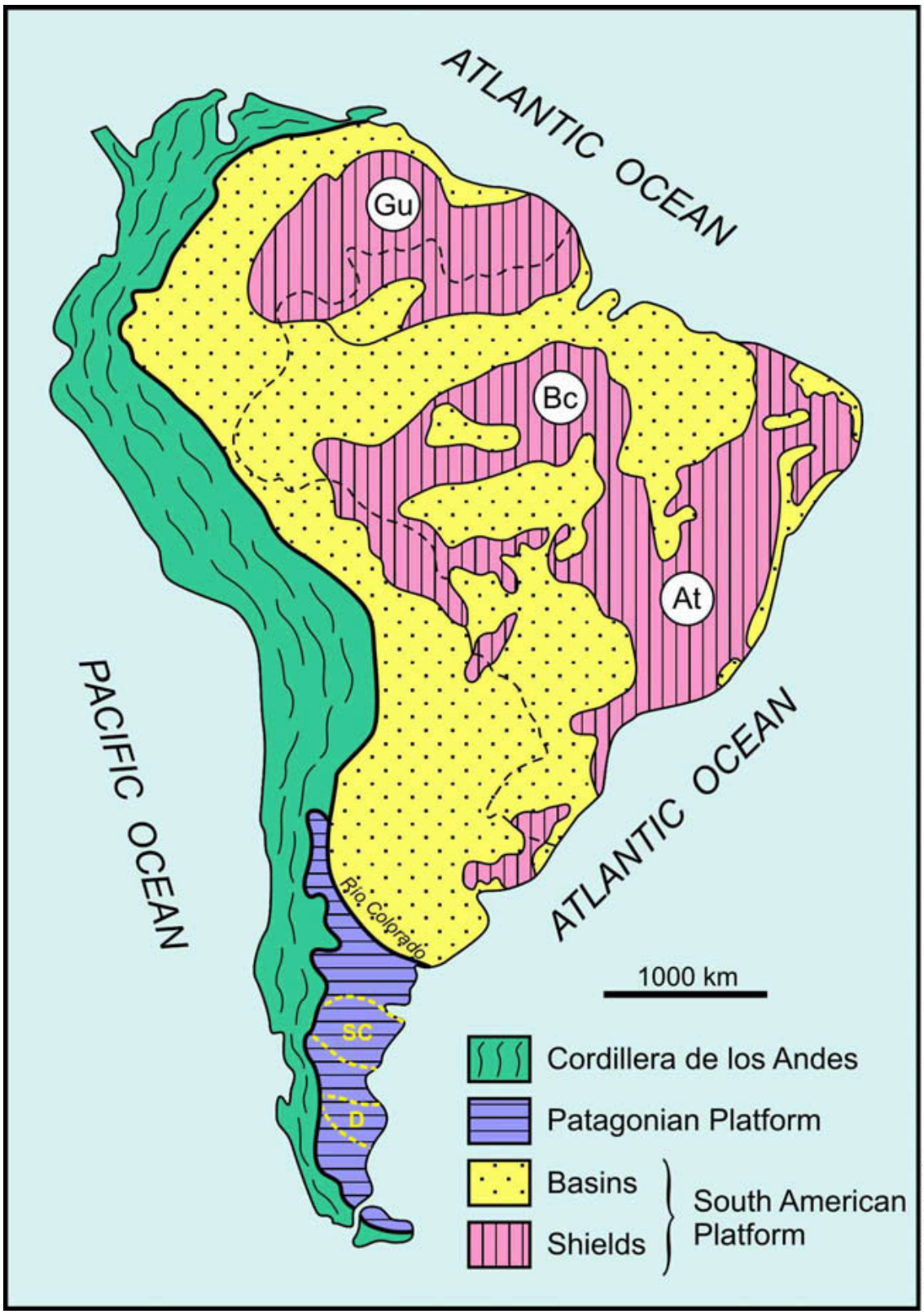

Figure 4 – Regional location of Patagonia Platform with most important basement massifs: the Somún Cura (SC) and Deseado (D). Gu: Guyana, Bc: Brasil Central, At: Atlantico (Ramos, 2008, based on Almeida *et al*., 1976).

Patagonia extends over a basement, remainder of Gondwana. The Patagonia geological province contains a series of basement outcrops, mainly exposed along the eastern side of the Andes, which can be grouped in two distinct massifs (Leanza ,1958; Harrington, 1962): the Somún Cura and Deseado massifs (Fig. 4). The northern block known as the Somún Cura (or northern Patagonian) massif is bounded in the north by the Neuquén and Colorado basins (Fig. 5). The Somún Cura Massif is bounded to the south by the Cañadón Asfalto Basin (Fígari, 2005). This basin was formed by NE–SW extension prior to 160 Ma during the opening of the Weddell Sea (Ghidella *et al*., 2002; Ramos, 2004a). The Cañadón Asfalto Basin extends to the north beneath the basalts of the central part of Somún Cura as noted by Cortiñas (1996), who proposed that the Somún Cura is formed by two highs, one in the north with an east–west trend, and another with a N30° W trend, defined as the Chubut high, consistent with two igneous–metamorphic belts. The present southern border is enhanced by the subsidence of the San Jorge Basin, which is interpreted as an aulacogen (De Wit, 1977; Fitzgerald *et al*., 1990; Ramos, 1996) formed as a consequence of the Weddell Sea opening, and reactivated during the opening of the South Atlantic. The Somún Cura Massif consists of gneisses, mica schists and granitoid rocks associated with low-grade metamorphics of Middle Proterozoic age (Ramos, 1999). In the eastern zone of the Massif, clastic, marine sedimentary rocks of Early to Middle Paleozoic age are located and penetrated by Paleozoic plutonic rocks. This basement is covered by pyroclastic rocks and acid lavas of Early to Middle Mesozoic age. Eastward and toward southeast, marine sedimentary rocks linked to Tertiary transgressions are located. Necks, domes and alkaline-type basalts are the result of the intense Middle Tertiary volcanism. The Massif structure is characterized by large basement blocks with inclined semi-grabens affected by the Andean orogeny (Ramos, 1999).

The Deseado Massif is exposed south of the San Jorge Basin and is bounded by the Austral (or Magallanes) Basin to the south (Fig. 5). It presents a sub-positive relief, stable since the Paleozoic, with a basement formed by phyllites and schists of Late Proterozoic to Early Paleozoic age, intruded by Middle Paleozoic granitoids and sub-volcanic rocks. The series, in the east-central portion of the area, continues with continental sedimentary rocks deposited during Late Paleozoic and Early Mesozoic. In the same area outcrops the Patagonian Central Batholith, acid plutonic

rocks of Triassic to Jurassic age. Tertiary marine and continental sedimentary rocks are interbedded with rhyolitic volcanics and pyroclastic flows (Leanza, 1958). Northward, Jurassic-Cretaceous continental sedimentary rocks are located, while the younger sedimentary rocks outcrop along the margins of the massif. During the Cenozoic , volcanic activity continued, erupting basaltic flows forming the center of the massif. Over these rocks, alluvial Early to Middle Pleistocene sediments have been deposited.

The structure of the Deseado Massif is characterized by subhorizontal Late Cretaceous to Cenozoic sequences; the Jurassic-Cretaceous rocks shows intense fracturing whereas the basement shows a strong deformation.

Consequently, the Patagonia is composed by two large basement massifs, bounded by Mesozoic basins, which were mildly deformed by the Andean orogeny (Ramos, 2004b).

Along the Patagonian littoral zone the coasts developed over Tertiary sediments and, in the southernmost sector, over Pleistocene glacial deposits. The coast of Atlantic Patagonia consists of active cliffs reaching over 50-60 m high in Rio Negro more than 100 m high in Santa Cruz and ca. 70 m high in Tierra del Fuego with wave-cut platforms. Less often sandy and gravel beaches occur.

Figure 5 – Main topographic features of Patagonia (Ramos, 2008).

The San Jorge basin is located in central Patagonia, between latitude 44º and 47ºS and it consists of an intracratonic basin predominantly extensional, trending roughly in an east-west direction, from the Andean belt to the Atlantic Ocean (Fig. 6). The basement of the basin consists of a sedimentary-volcanic complex associated to a rift process of Middle to Upper Jurassic age (Fig. 7). These deposits cover almost

the entire Patagonia. This is the most extent but not the only unit that underlies the sedimentary column. Depending upon the relative position into the basin there also are Precambrian to early Mesozoic igneous rocks as well as late Paleozoic to Mesozoic sedimentary units (Ramos, 1999; Sylwan, 2001).

Subsequently, the Neocomian sedimentary cycle took place under late rift conditions, synsedimentary filling grabens and half grabens, mostly continental but with some marine Pacific transgressions. After a regional tilt of the main axis of the basin, the Chubutian sedimentary cycle starts. During the Tertiary the basin shows an alternation of marine and continental deposits (Lema *et al*., 2001; Sylwan, 2001). The main phase of compression uplifts the N-S trending San Bernardo foldbelt by reactivating previous normal faults (Sylwan, 2001). The Quaternary deposits, very widespread in the whole Patagonia, represent drastic climatic changes, such as glaciations, and the consequent sea level fall (see Paragraph 2.2.1).

Volcanic activity throughout the history of the basin is expressed in the high tuffaceous content of the entire column.

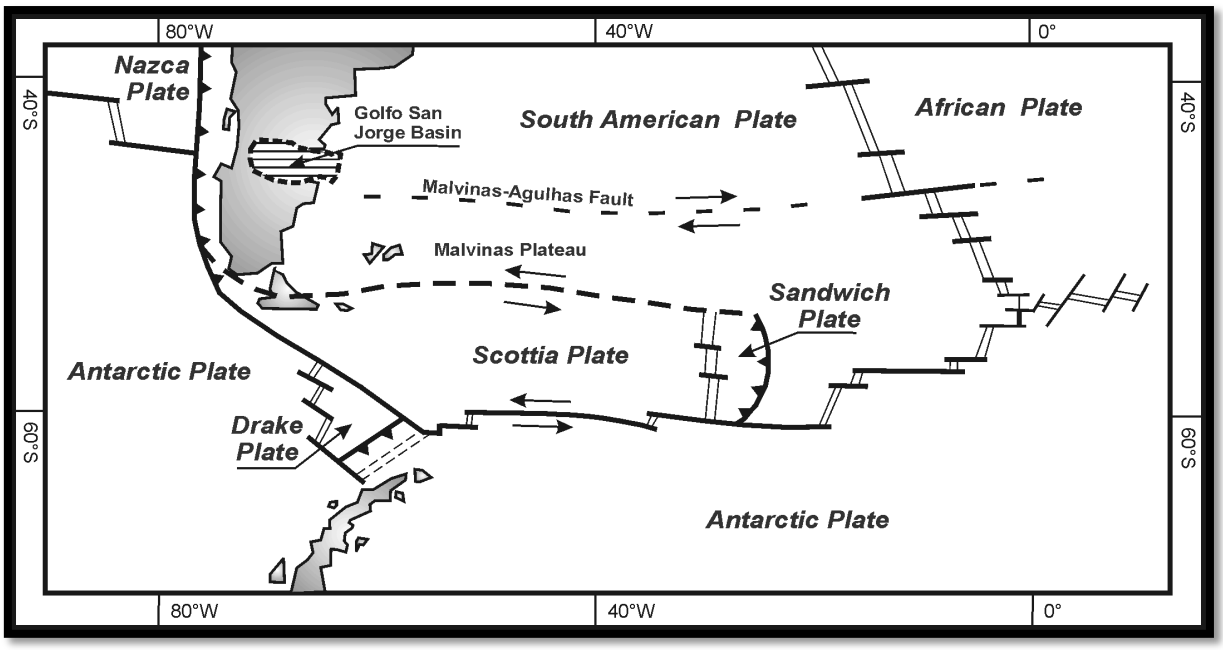

Figure 6 – San Jorge Basin and present macrogeotectonic map of the region. Redrawn after Biddle *et al*., 1996.

The sedimentary column is, at the basin center, thicker than 8,000 m, and is, in general, dominated by continental Mesozoic and Tertiary sediments (Lema *et al*., 2001; Sylwan, 2001).

Figure 7 – The “Marifil Complex”, the oldest geological unit in the San Jorge Basin.

The basin boundaries are the Somún Cura Massif to the north, the Deseado Massif to the south, the Cordillera de Los Andes to the west and the continental margin of the Atlantic Ocean to the east. Although the main features show a general E-W alignment as a result of a dominantly extensional tectonics, the San Bernardo foldbelt runs in the north-south direction, dividing the basin into two sectors, the east and the west ones. At its turn, the east sector is divided into the northern flank, the southern flank and the basin center. The offshore portion is considered to be a prolongation of the east sector (Baldi and Nevistic, 1996).

2.2.1. The Quaternary marine successions

Since the shallow marine molluscs analyzed within this PhD project come from the coastal Quaternary successions, particular attention is paid to the description of these deposits.

The fossilferous unconsolidated marine deposits along the Atlantic coast of Patagonia are the result of several factors related to changes in sea level, isostatic compensation, glacio-eustasy and neotectonic episodes (Feruglio, 1950; Codignotto, 1983; Cionchi, 1985; Codignotto *et al.*, 1992; Clapperton, 1993; Peltier and Rostami, 2000; Rostami *et al.*, 2000; Isla and Bujalesky, 2008; Schellmann & Radtke, 2010) and are known since the second half of the XIX century, when D'Orbigny (1834-1847; 1842-1844) studied fossil invertebrates contained within the deposits. Darwin (1846) also made reference to the marine deposits of southern Patagonia.

The most complete descriptions of the chronology, stratigraphy, lithology and paleontology of Quaternary marine successions of Patagonia derived from the pioneering work of Feruglio (1933; 1949; 1950). He recognized a succession of six marine fossil terraces. He was the first to propose a classification in marine terraces (also known as MT in the literature) ranging from a height approximately of 8 to 186 m above mean sea level (asl) (Fig. 8) and being (at least according Feruglio) more or less at the same height along the coast. In particular, Feruglio, although did not have modern dating techniques, interpreted the terraces as follows: the MTVI (+ 8-12 m) of Holocene age, the MTV (+15-30 m), MTIV (+30-40 m), MTIII (+40-95 m) and MTII (+105-140 m) Pleistocenic in age and the MTI (+170-186) of Pliocene age. In the light of modern geochronological studies (Rutter *et al*., 1990), only four of these (MTIII-VI) are Quaternary, 3 of which have deposited during the Middle - Late Pleistocene (MTIII, IV and V) and one during the Holocene (MTVI).

The marine terraces were subsequently studied from a geological, geomorphological, paleontological and geochronological point of view (Cionchi, 1987; 1988; Codignotto, 1983; 1987; Rutter *et al*., 1990; Rostami *et al.* 2000; Schellmann, 2000; Schellmann & Radtke, 2000; 2003; 2007; 2010; Aguirre, 2003; Aguirre *et al*., 2005; 2006; 2009; Ribolini *et al.*, 2010; Isola *et al.*, 2011; Zanchetta *et al*., 2012). The ages obtained through U/Th and ESR dating (Schellmann & Radtke, 2000; 2003) suggest that Pleistocene terraces have been deposited during at least

three marine highstands, which they interpret as being attributable to the Marine Isotope Stages 9/11, 7 and 5.

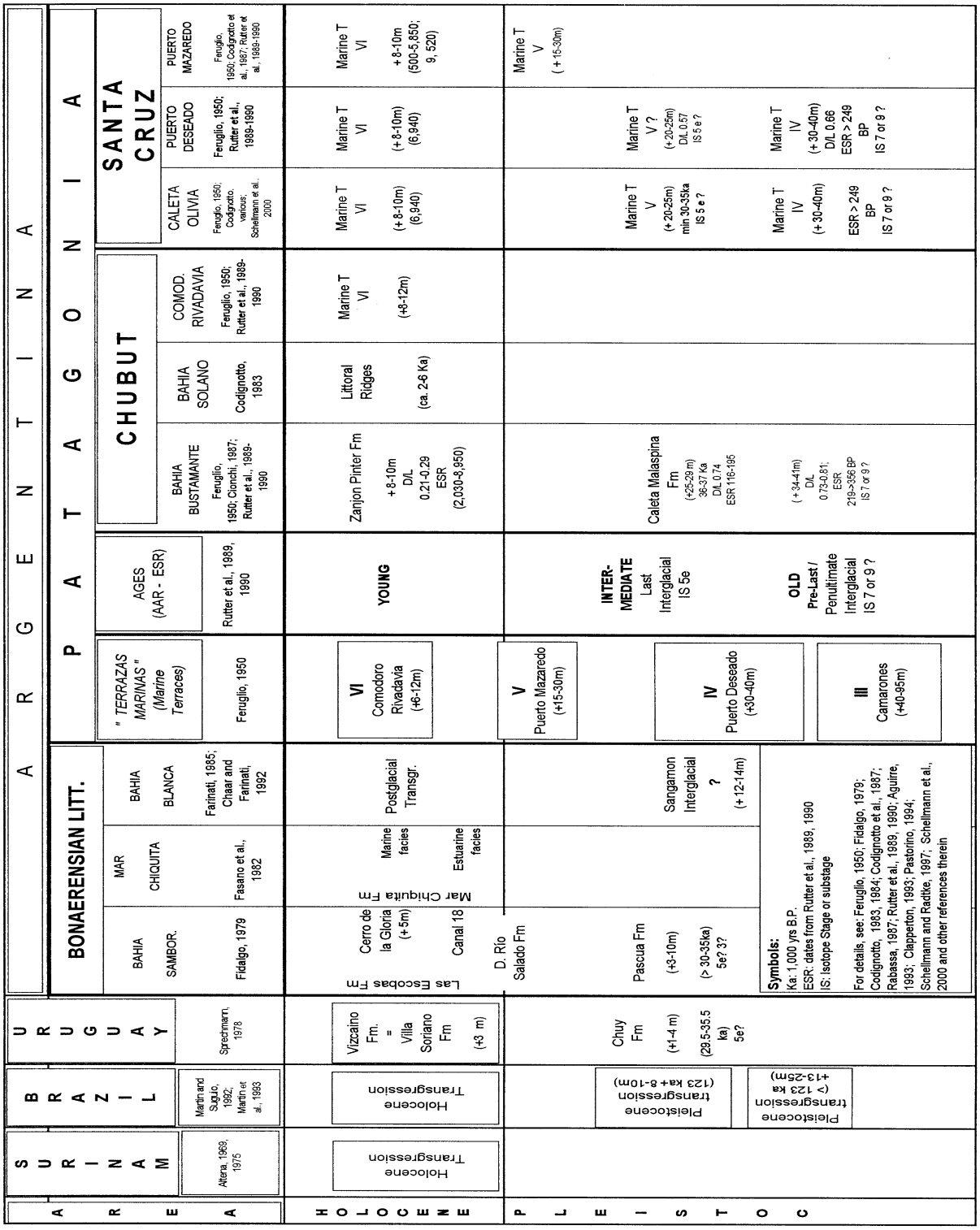

Figure 8 - Stratigraphical synthesis of present knowledge of the Late Quaternary coastal deposits from Golfo San Jorge and correlation with other coastal areas of the SW Atlantic margin (Aguirre, 2003).

Most of the "marine terraces", indeed, in this area are composed by successions of regressive coarse beach-ridges (“swash built ridges” *sensu* Tanner, 1995) mainly

related to intermittent storm activity. In wave-protected environments, instead, flat littoral terraces, consisting of sands or sandy gravels, outcrop. Beach ridges and marine terraces are usually interpreted as formed during phases of global marine highstand (Schellmann & Radtke, 2010). Another type of deposit outcropping in this area consists of valley-mouth terraces, terraces located at the mouth of “Cañadones” (dry valleys with periodical runoff), interfingerings of littoral sediments and fluvial deposits (Fig. 9).

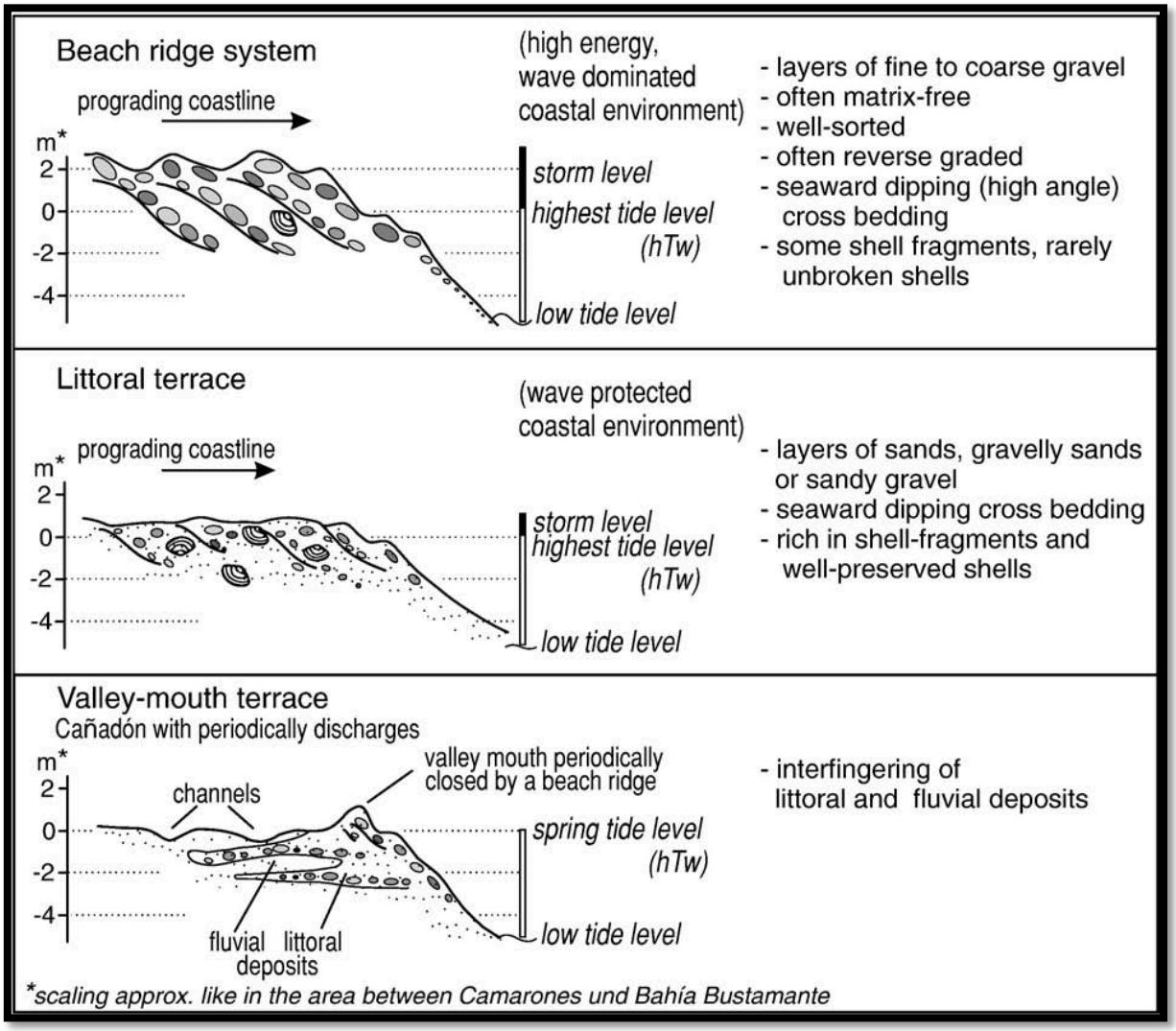

Figure 9 – Coastal deposits outcropping along the Atlantic coast of Patagonia (Schellmann & Radtke, 2010).

Schellmann & Radtke (2010) describe beach ridges outcropping along the Atlantic coast as “well sorted, coarse (granule-sized to boulder-sized) sediment layers with numerous matrix-free, frequently reverse graded gravel beds”. These deposits show large scale cross stratification. Every beach ridge, usually, is separated by swales

often running parallel to the coastline. Most contain highly fossiliferous marine strata, with abundant shell concentrations recently studied by Aguirre (2003) and Aguirre *et al.* (2005; 2006; 2009).

Mollusc shells represent the dominant biogenic elements within the fossil assemblages (80-95% according to Aguirre *et al*., 2008). The most abundant taxa are, among the bivalves, Mytilidae (mainly *Mytilus edulis, Brachidontes purpuratus, Aulacomya atra*), Pectinidae, Veneridae (i.e. *Ameghinomya antiqua*) and oysters and Patellacea, Muricidae and Volutidae among the gastropods (Tab. 1). Other macroinvertebrate taxa are represented by brachiopods, bryozoans, echinoderms, balanids, crabs, polyplacophors, scaphopods, polychaets and cnidarians (Aguirre & Farinati, 2000; Aguirre, 2003; Aguirre et al., 2005; 2006; 2008; 2009).

GROUPS I-IV	BIVALVIA	Marine quaternary								Modern malacol. provinces				Temperature	
		MIOCENE	PLEIST	HOLOC	SURINAM	BRAZIL	URUGUA	ARGENTINA		ANT	BRA	ARG	MAG		
								Buenos aires	Pata gonia						
II	*Glycymeris (G.) longior* (Sowerby)	X	X	X	X	X	X	X	X					W	
I	*Mytilus (M.) edulis* Linné	X		X		X	X	X	X						
IV	*Mytilus (M.) chilensis* Hupé								X					C	
III	*Brachidontes (B.) rodriguezi* (d'Orbigny)	X	X	X		X	X	X	X					W	
IV	*Brachidontes (B.) purpuratus* (Lamarck)	X	X	X			X		X					C	
I	*Brachidontes (B.) cf. purpuratus* (Lamk.)		X	X					X						
IV	*Aulacomya atra* (Molina)		X	X			X		X					C	
III	*Aequipecten tehuelchus* (d'Orbigny)	X	X	X	X	X	X	X	X						
IV	*Zygochlamys patagonicus* (King and Brod.)		X	X					X					C	
IV	*Chlamys lishkei* (Dunker)								X					C	
II	*Pododesmus rudis* Broderip		X	X					X					W	
II	*Plicatula gibbosa* Lamarck	X	X	X	X		X		X					W	
III	*Ostrea (O.) puelchana* Say	X	X	X	X	X	X	X	X						
	Ostrea tehuelcha Feruglio		X						X					W	
III	*Ostrea* sp.		X	X		X			X						
III	*Diplodonta patagonica* d´Orbigny		X	X		X	X	X	X					W	
III	*Diplodonta vilardeboana* (d´Orbigny)		X	X		X	X	X	X					W	
II	*Chama* sp.	X	X			X			X					W	
II	*Mactra (M.) isabelleana* d'Orbigny		X	X	X	X	X	X	X					W	
III	*Mactra (M.)* aff. *isabelleana* d'Orbigny	X	X	X			X		X						
IV	*Mulinia edulis* (King & Broderip)	X	X	X	X			X	X					C	
IV	*Darina solenoides* (King)		X	X	X		X	X	X					?	
III	*Solen tehuelchus* d'Orbigny		X	X	X	X	X	X	X					?	
III	*Solen* sp.				X		X		X						
IV	*Ensis macha* (Molina)			X	X				X					C	
II	*Macoma (P.) uruguayensis* (Smith)	X	X	X	X		X	X	X						
III	*Abra* sp.	X		X	X	X		X	X					W	
III	*Tivella isabelleana* (d´Orbigny)	X		X	X	X		X	X					W	
III	*Pitar (P.) rostratus* (Koch)	X	X	X	X	X	X	X	X						
IV	*Eurhomalea exalbida* (Dillwyn)		X	X				X	X					C	
IV	*Protothaca antiqua* (King)	X	X	X	X	X		X	X					C	
III	*Clausinella gayi* (Hupé)		X	X		X	X		X					C	
II	*Venericardia procera* Gould		X						X					W	
IV	*Petricola patagonica* d´Orbigny			X					X					C	
II	*Corbula (C.) patagonica* d'Orbigny	X	X	X	X	X	X	X	X					W	
I	*Hiatella arctica* (Linné)		X	X			X		X					C	
III	*Panopea abbreviata* Valenciennes	X	X	X		X	X	X	X					C	

GROUPS I-IV	GASTROPODA	MIOCENE	Marine quaternary							Modern malacol. provinces				Temperature	Absent
			PLEIST	HOLOC	SURINA	BRAZI	URUGUA	ARGENTINA		ANT	BRA	ARG	MAG		
								Buenos aires	Patagonia						
IV	*Fissurella picta* (Gmelin)		X	X	X				X					C	
IV	*Fissurella oriens* Sowerb y		X	X					X					C	
IV	*Fissurella radiosa* Lesson		X	X					X					C	
III	*Lucapinella henseli* (Martens)		X	X			X		X						
IV	*Nacella delicatissim a* (Strebel)		X	X					X					C	
IV	*Nacella (P.) magellanica* (Gmelin)		X	X					X					C	
IV	*Nacella (P.) deaurata* (Gmelin)		X	X				X	X					C	
IV	*Scurria ceciliana* (´Orb.)			X					X					C	
III	*Tegula (A.) patagonica* (d'Orbigny)	X	X	X		X	X	X	X					W	
IV	*Tegula (A.) blakei (*Clench & Aguayo)		X	X					X					W	
IV	*Tegula (C.) atra* (Lesson)		X						X					C	
III	*Photinula caerulescens* (King & Broderip)		X	X					X					C	
IV	*Ataxocerithium pullum* (Philippi)		X	X				X	X					C	
IV	*Callioslomа tehuelchum* Ihering		X						X						
III	*Callioslomа nordenskjoldi* Strebel		X	X		X		X	X						
III	*Littoridina australis* (d´Orbigny)	?	X	X		X	X		X						
I	*Crepidula aculeata* (Gmelin)		X	X		X	X	X	X					W	
III	*Crepidula protea* d'Orbigny	X	X	X		X	X	X	X					W	
III	*Crepidula onyx* Sowerby	X		X				X	X					W	
I	*Crepidula dilatata* Lamarc k	X		X				X	X					W	
I	*Crepidula* cf. *unguiformis Lamarc k*	X	X	X	X	X			X						
III	*Trochita pileus* (Lamarck)			X					X					C	
III	*Natica isabelleana* d'Orbigny	X	X	X		X	X	X	X					W	
IV	*Natica magellanica* Ihering		X						X						
IV	*Falsilunatia patagonica* (Philippi)			X					X					C	
III	*Epitonium georgettinum* (Kiener)	X		X	X	X	X	X	X					W	
I	*Epitonium (B.) magellanicum* (Philippi)			X	X				X					W	
III	*Trophon varians* (d'Orbigny)	X		X			X		X						
IV	*Trophon geversianus* (Pallas)	X		X				X	X						
IV	*Trophon necocheanum* Ihering			X					X						
IV	*Trophon elongatus* Strebel		X	X					X						
IV	*Fuegotrophon pallidus* (Broderip)		X	X					X					C	
IV	*Ximenopsis muriciformis* (King & Broder.)			X					X					C	
III	*Urosalpinx* sp.		X	X			X	X	X						
IV	*Acanthina monodon* (Pallas)		X	X					X					C	
III	*Zidona dufresnei* (Donovan)		X	X			X	X	X					W	
III	*Adelomelon ancilla* (Lightfoot)		X	X			X	X	X						
III	*Adelomelon beckii* (Broderip)	X		X			X	X	X						
III	*Adelomelon (P.) brasiliana* (Lamarck)		X	X		X	X	X	X					W	
IV	*Adelomelon ferussaci* (Donovan)		X	X					X						?
IV	*Odontocymbiola magellanica* (Gmelin)			X					X					C	
III	*Olivella (O.) tehuelcha* (Duclos)	X	X	X	X	X	X	X	X					W	
III	*Olivancillaria urceus* Roding)	X	X			X	X		X					W	
III	*Olivancillaria auricularia* (Lamarck)		X	X		X	X		X						?
III	*Olivancillaria carcellesi* Klappenbach		X	X		X	X	X	X					W	
IV	*Pareuthria plumbea* (Philippi)		X	X					X					C	
IV	*Pareuthria cerealis* Roch. & Mabille			X					X					C	
III	*Buccinanops cochlidium* (Dillwyn)	X		X			X	X	X					W	?
III	*Buccinanops globulosus* (Kiener)		X	X		X	X	X	X						
IV	*Buccinanops paytensis* (Kiener)		X	X					X					C	
I	*Siphonaria lessoni* (Blainville)		X	X		X	X	X	X						

Table 1 – Molluscan fauna typical of Quaternary deposits of Atlantic coast of Patagonia. Groups I-IV refer to groups of species according to their modern distribution. Modern zoogeographical provinces: ANT = Antillean Province, ARG = Argentine Province, MAG = Magellanean Province. Group I: pandemic; II: tropical or subtropical; III: warm-temperate to temperate waters: IV: cold waters. W: water or warm-temperate affinity. C: cold water affinity (Aguirre *et al*., 2008).

In her studies Aguirre observes that the original habitat of the molluscs collected within the Quaternary marine successions was characterized by varied hard substrates, high-energy, shallow euhaline waters, similar to the modern littoral conditions of the Patagonian Atlantic coast. Comparing fossil assemblages with the modern associations also Aguirre notes minor taxonomic differences, different percentages of the taxa in common, size variation of some taxa (*Ameghinomya, Tegula* and *Trophon*, generally bigger in the Quaternary), shape variability of individual taxa linked to local environmental conditions (*Tegula, Crepidula, Buccinanops, Pitar, Glycimeris, Brachidontes*) and latitudinal changes (i.e. *Littoridina australis, Tegula atra, Adelomenon, Ostrea tehuelcha*) due to SST of the shallow water masses.

Nevertheless, according to Aguirre *et al*. (2008), these differences are minor and seem to indicate that the Malvinas current (Paragraph 2.4) has been active in this area since at least the Mid-Late Pleistocene. Molluscs from Pleistocene deposits assigned to MIS 7 (MTIV), where *Tegula atra* and *Ameghinomya antiqua* are dominant, suggest colder SST than the Middle Holocene and the present. Throughout the study area the molluscan assemblage from MIS 5 (MTV) also indicate not warmer waters than at present (Aguirre *et al.,* 2003, 2005, 2006, 2008).

Aguirre (2001; 2002), however, highlights that during the Middle Holocene species of the groups II and III (tropical or subtropical and warm-temperate to temperate waters) were more abundant than in Late Pleistocene and at present, while typical cold water elements common at present were scarcer or absent. Aguirre (2002) ascribes this biogeographical change to the “Climatical Optimum” (Hypsithermal) that would be connected to a southward displacement of the warm Brazilian current (Paragraph 2.4) and a southward shift of the South Atlantic Anticyclonic Center.

Below the most significant locations in the study area that have been treated within this thesis will be described (Fig. 2).

Cabo Raso – Bahia Vera area (ca. 44°16’ S): this area is located on the Somún Cura Massif (Fig. 5), on the wave-exposed Chubut Province coast. The coast is dominated by gravely beach ridges and up to three distinctive Pleistocene beach ridge systems are preserved.

Feruglio (1950) first described in this area an inner ridge at +40 m above m.s.l. as

MTIII, intermediate ridges at +28–40 m as MTIV, and at +20–26 m above m.s.l. as MTV, and the most exterior ridge at +10–12 m above m.s.l. as MTVI.

Radtke (1989) assigned them a Middle Pleistocene, Last Interglacial and Holocene age, respectively. The ages (ESR, Th/U) obtained by Schellmann and Radtke (2000) for the Pleistocene terraces suggest at least three marine highstands which they interpreted as MIS 9 ?/11 (342–400 ka), MIS 7 (225 ka), and MIS 5 (125 ka) .

The exterior terrace (MTVI) consists of gravel and loose sand with abundant, very well preserved molluscan shells, in most cases retaining their original color. The ages of the oldest Holocene beach ridges (at ca. 8 m above hTw according to Schellmann & Radtke, 2007) range between 3600 and 2600 ^{14}C years ago (Schellmann & Radtke, 2007; 2010), while lower beach ridges (5 m and 4 m a hTw) formed around 2200 and 1200 years BP (Fig. 10).

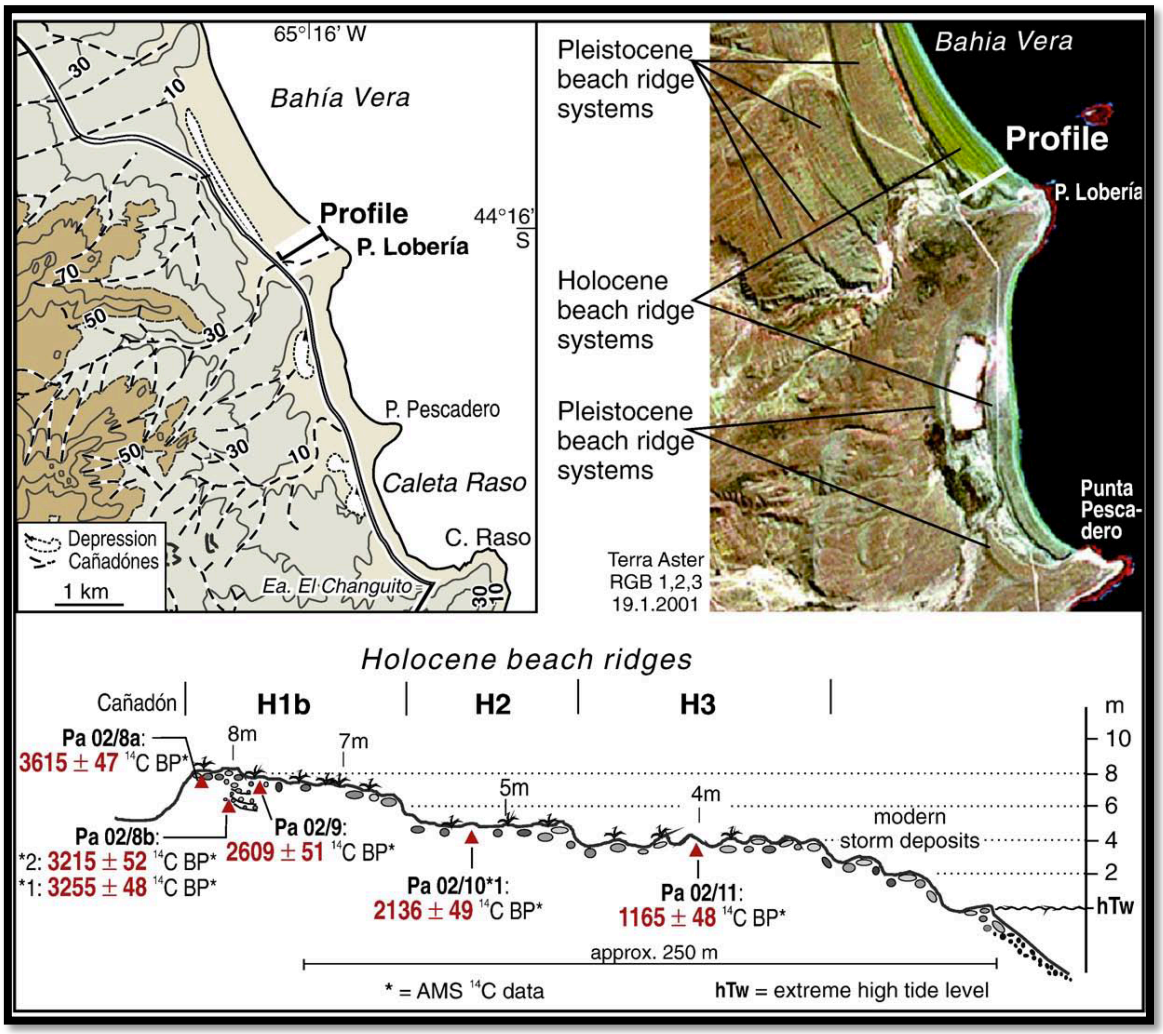

Figure 10 – Holocene beach ridges in Cabo Raso area (Schellmann & Radtke, 2010).

On the contrary, Ribolini *et al.* (2011) dated the Holocene maximum transgression in the Cabo Raso Bay at 6055 ± 20 years BP.

Bahia Camarones (44°40'-44°59' S): this locality, belonging to the Chubut Province, is characterised by different bays, cliffs and wave-cut platforms in the Mesozoic volcanic bedrock ("Marifil Complex, Fig. 7) and it is located on the southern border of the Somún Cura Massif (Fig. 5). In this area Feruglio (1950), as in Cabo Raso area, recognized four main littoral units: the inner ridge system, representing the oldest Pleistocene deposits (MTIII), is outcropping, with an elevation of 40 m above m.s.l., in the vicinity of Camarones and is composed of pebbles cemented by calcium carbonate and scarce molluscs like *Ostrea tehuelcha, Mactra* cf.*patagonica*, Pectinidae (Aguirre *et al*., 2006; 2008). This fossil assemblage suggests warmer conditions than at present (Aguirre *et al*., 2006; 2008). The ages for this unit correlate with MIS 9 or MIS 11 (Rostami *et al*., 2000; Schellmann & Radtke, 2000; Aguirre *et al*., 2006). The younger Pleistocene terraces (IV and V) are exposed both north and south of the village (Schellmann, 1998; Rostami *et al*., 2000; Schellmann & Radtke, 2000; 2003; Aguirre *et al*., 2006) and are composed of sand, gravel and shells. The ages for the MTV range between 92 and 135 ka (Schellmann, 1998; Rostami *et al*., 2000; Schellmann & Radtke, 2000; 2003), while for the MTIV between 178 and 250 ka (Schellmann, 1998; Rostami *et al*., 2000; Schellmann & Radtke, 2000), correlating the MTV to MIS 5 and the MTIV to MIS 7. These deposits are characterized by *Tegula atra, Tegula patagonica, Crepidula dilatata, Mytilus edulis, Ameghinomya antiqua* (biggest in MTIV), *Brachidontes purpuratus* (Aguirre *et al*., 2006; 2008). In a terrace located in the north of Camarones, Schellmann (1998) even assigns two sedimentary units of one fossil beach ridge system to isotopic substages 5c and 5e (Fig. 11). In the northern part of this area only the Last Interglacial has been identified.

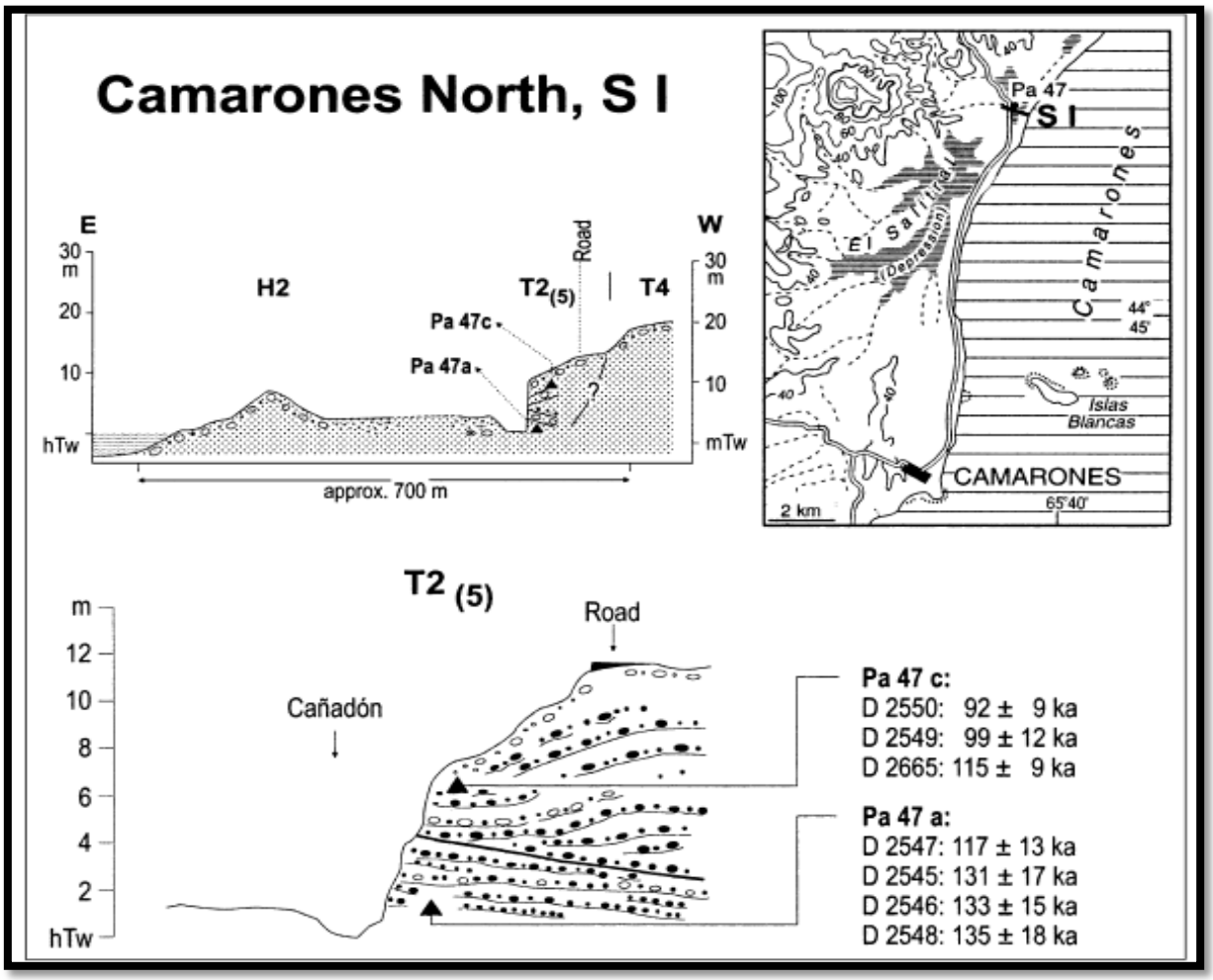

Figure 11 – Last Interglacial terrace in the north of Camarones (Schellmann & Radtke, 2000).

In the south of Camarones, on the contrary, a large number of datings (using both radiocarbon and Electron Spin Resonance dating methods) has been performed (Schellmann, 1998; Schellmann & Radtke, 2000; 2003; 2010), including Middle Pleistocene deposits (Fig. 12).

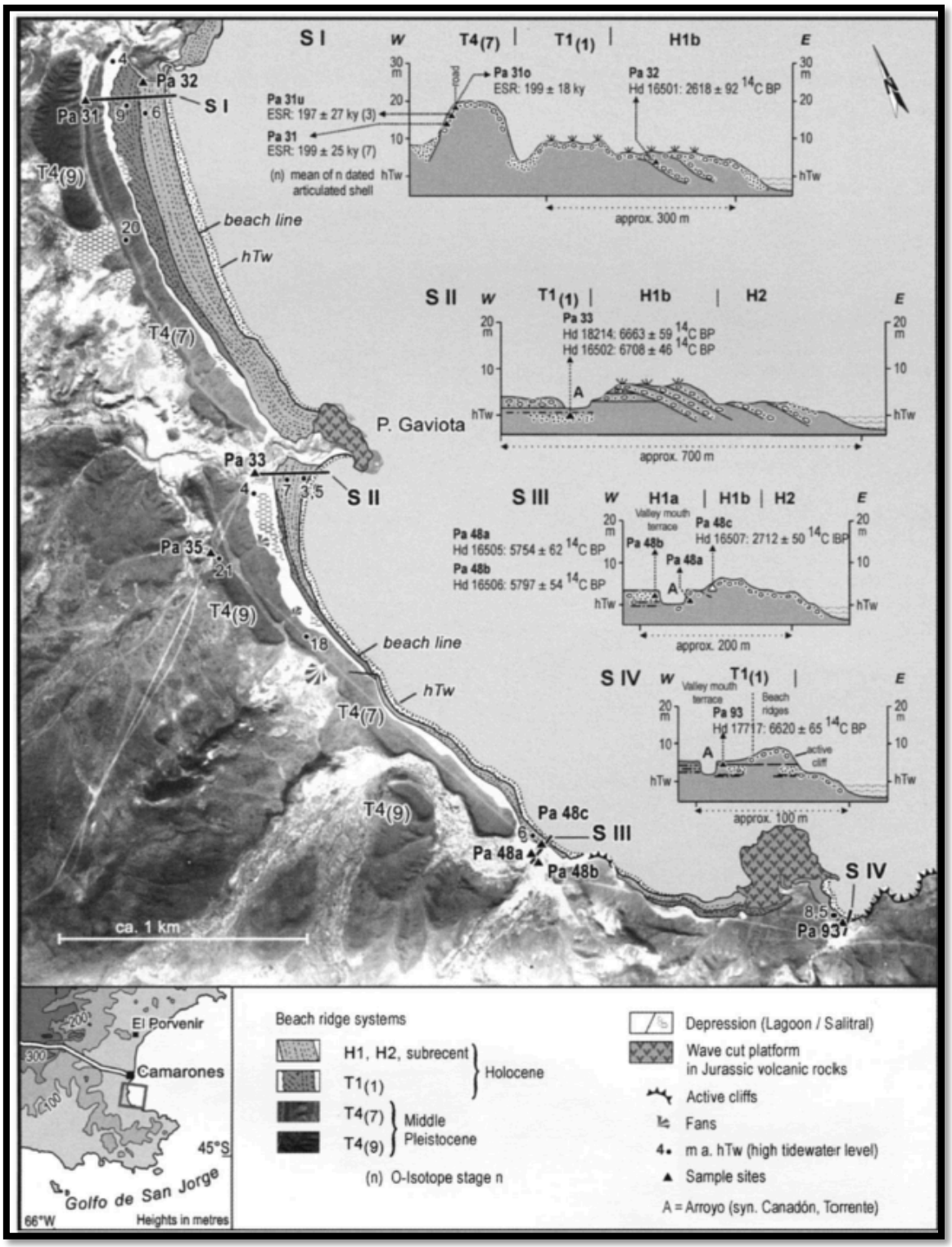

Figure 12 – Pleistocene and Holocene beach ridge systems south of Camarones (Schellmann & Radtke, 2003).

Codignotto (1983) reported the first radiocarbon data on mollusc shells from the littoral deposits, which allowed to relate the lowest beach ridge system (MTVI) to the Holocene.

The oldest mid-Holocene beach ridges, which developed more than 6200 ^{14}C years, can reach elevations of 8.5-9.5 m a hTw (Schellmann & Radtke, 2010). Furthermore, in this area younger beach ridges were deposited after the Mid-Holocene transgression maximum (between 5300 and 6000 ^{14}C years) and between 2600 and 3400 ^{14}C years. Finally, a second and a third group of beach ridges were deposited respectively about 2200 ^{14}C years ago and between 450 and 1400 ^{14}C BP (Schellmann & Radtke, 2010).

Holocene littoral deposits are characterized by *Brachidontes purpuratus, Nacella (Patinigera) magellanica, Nacella (Patinigera) deaurata, Aulacomya atra* (Aguirre et al., 2006). According to these authors this variation in fossil assemblage is a consequence of changes in sea-surface temperature (about 1-2° C warmer during the Middle Holocene than today).

As regards the Holocene deposits to the north of Camarones, no dating has been performed until the work of Zanchetta *et al.* (2012). The authors recognize a beach ridge system deposited at ca. 6600-5400 yr BP connected to a first phase of progradation of the coast. Two further phases of aggradation occurred, according to Zanchetta *et al.* (2012), between ca. 3300 and 2000 yr BP, and 1300-500 yr BP.

Bahia Bustamante area (45°08' S): this area is placed on the southern edge of the Somún Cura Massif (Fig. 5) and is probably one of the most interesting and studied areas of the Patagonia Atlantic coast (Feruglio, 1947; 1950; Cionchi, 1984; 1987; Radtke, 1989; Rutter *et al.,* 1989; 1990; Schellmann, 1998; Rostami *et al.,* 2000*;* Schellmann & Radtke, 2000; 2007; 2010; Aguirre *et al.,* 2005; Isola *et al.,* 2011).

Nowadays gravely beaches, bays and abrasion platforms characterise the coast. In the south of Bustamante village, Peninsula Gravina and Peninsula Aristizabal, separated by Caleta Malaspina bay, are present (Fig. 13). While along the open coast gravely beach ridge sequences outcrop, in the area of Caleta Malaspina tidal flats, marshes and littoral terraces are present.

The older Quaternary deposits dated by Schellmann (1998) yielded ages between 196 ± 33 and 225 ± 25 ka at his northernmost profile from Bahia Bustamante (Figs. 13, 16).

Beach deposits correlated to MIS 5 outcrop north to the village of Bahia Bustamante (Fig. 14) and at Caleta Malaspina (Schellmann, 1998; Schellmann & Radtke, 2000).

The oldest Bahia Bustamante Holocene beach ridges can reach, in this area, 10 m

a hTw of elevation (Fig. 15) and formed between 6200 and 6900 ^{14}C BP (Schellmann & Radtke, 2010), indicating the Holocene transgression maximum. Younger beach deposits formed about 5200 and 5400 ^{14}C BP, between 4500 and 4000 ^{14}C BP, and approximately at 2200 ^{14}C BP (Schellmann, 1998; 2007; Schellmann & Radtke, 2000; 2010). Fossil assemblages of Bahia Bustamante Pleistocene and Holocene coastal deposits coincide with those of Camarones and are representative of hard substrates, truly marine conditions and shallow waters (Aguirre *et al*., 2005).

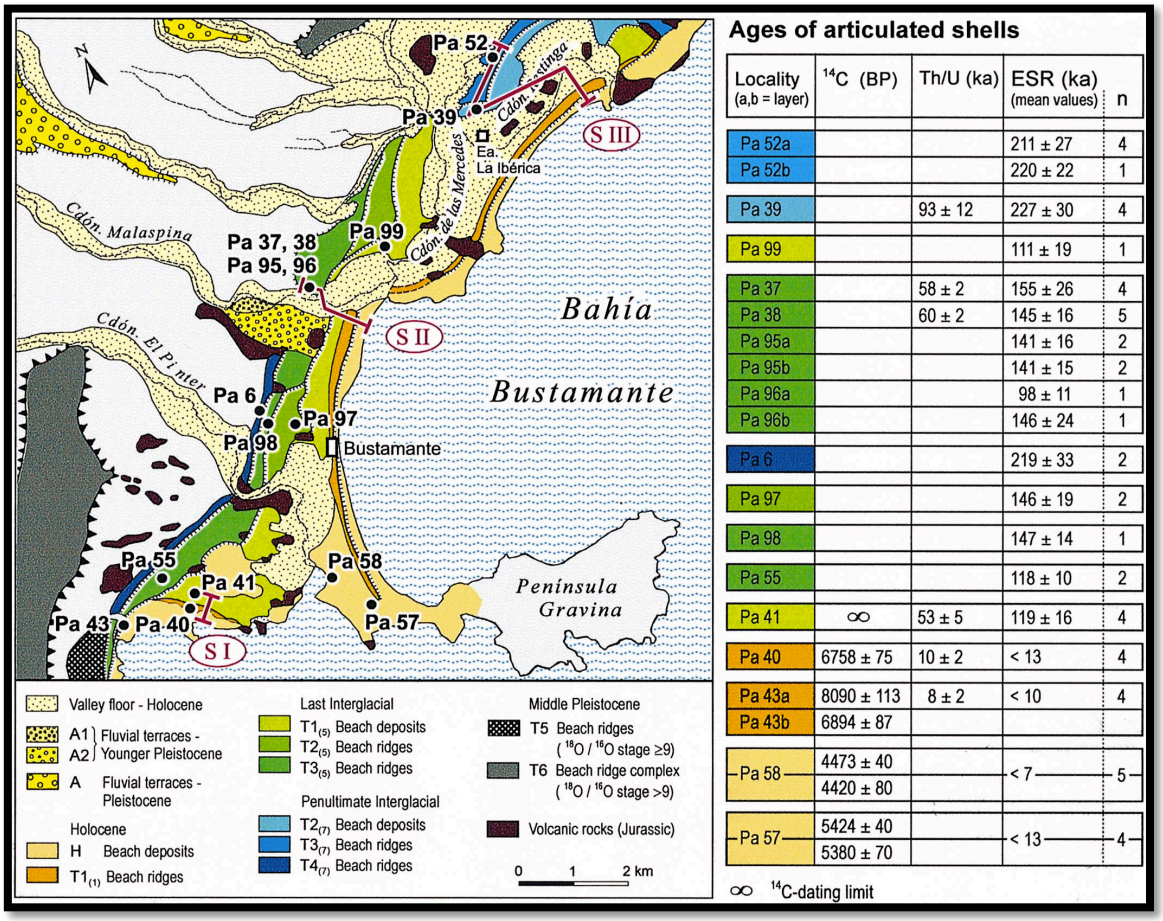

Figure 13 – Quaternary coastal deposits in the area of Bahia Bustamante with sampling location of the Pleistocene terraces (Schellmann & Radtke, 2000).

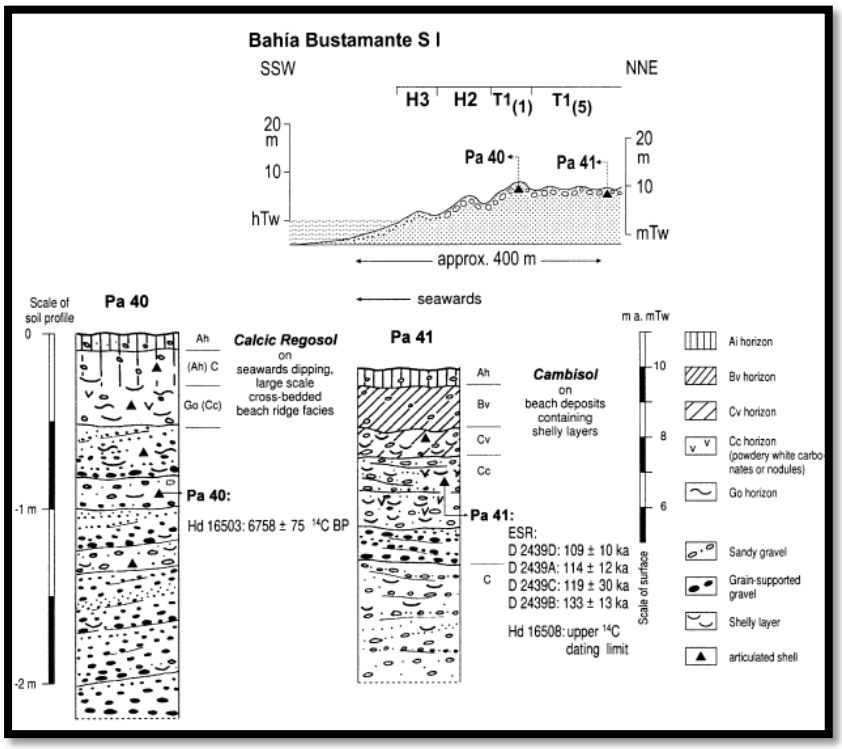

Figure 14 – Holocene and Last Interglacial coastal deposits in the southern part of Bahia Bustamante area (Schellmann & Radtke, 2000).

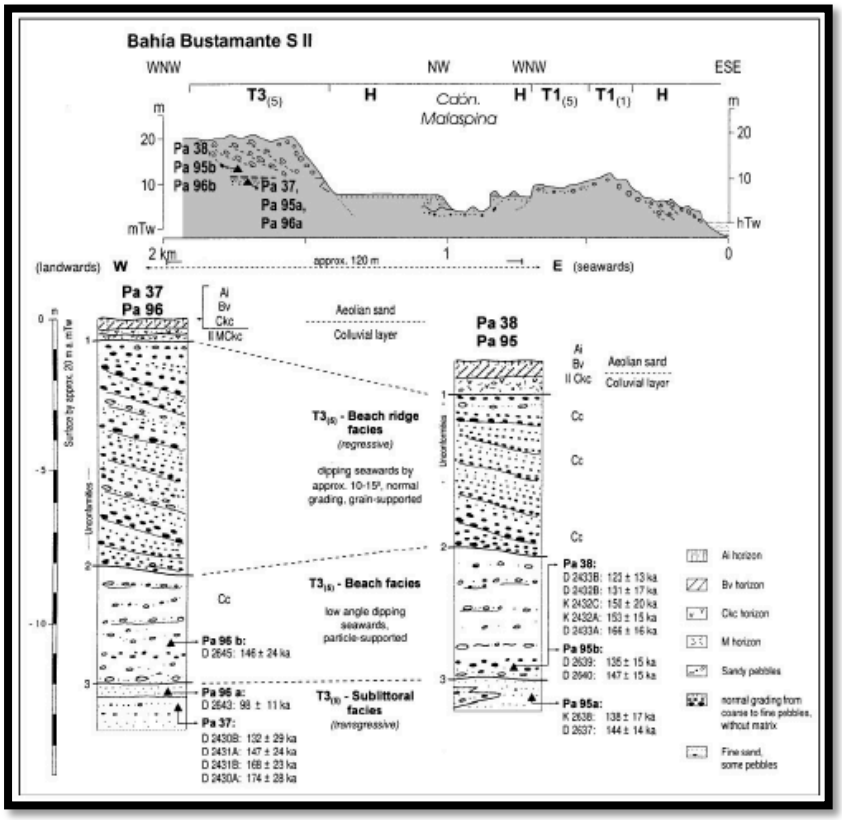

Figure 15 –Last Interglacial beach ridge system in the central part of Bahia Bustamante area (Schellmann & Radtke, 2000).

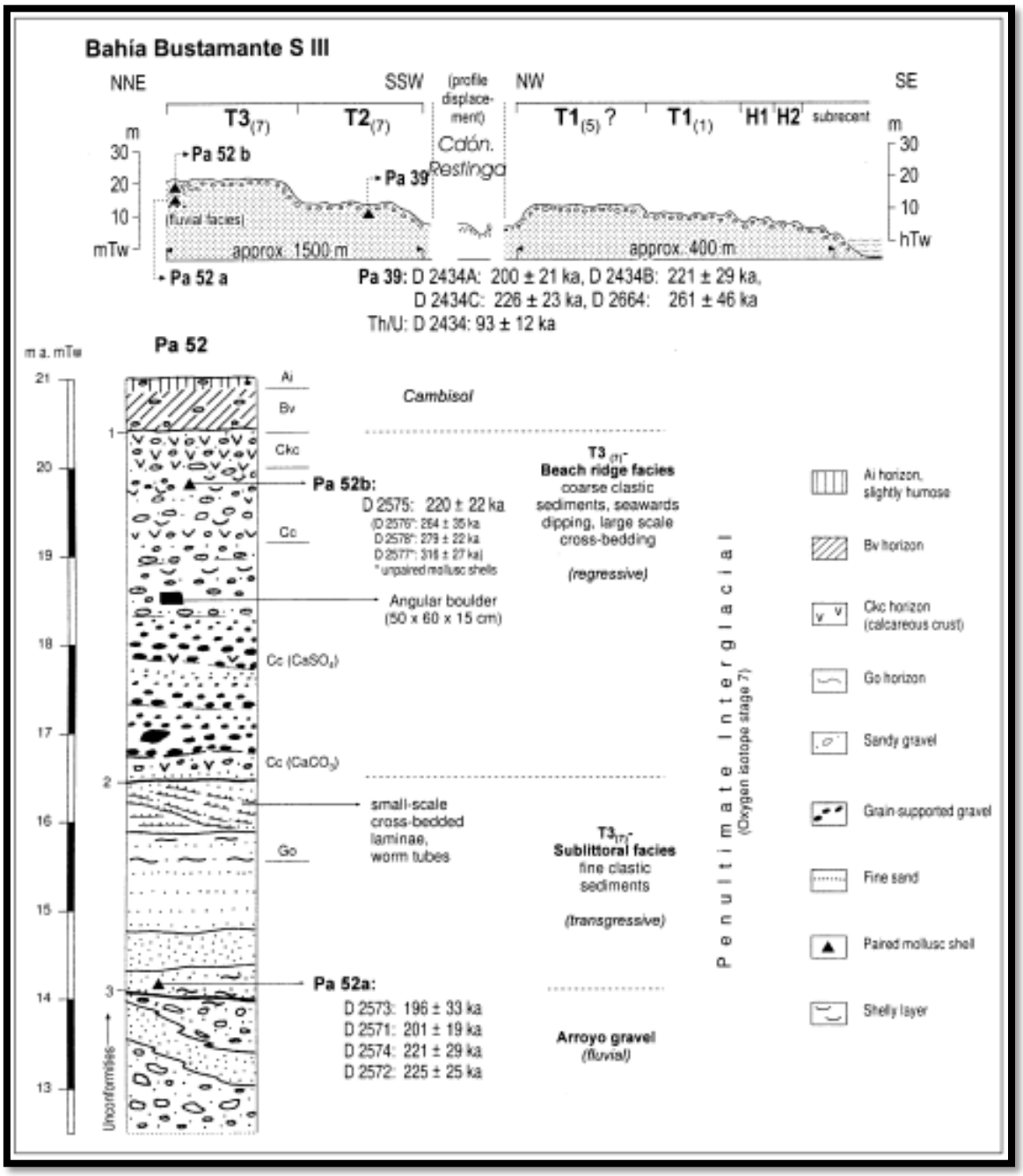

Figure 16 –Penultimate Interglacial beach ridge system in the nortern part of Bahia Bustamante area (Schellmann & Radtke, 2000).

The work of geomorphological mapping the most recent and most comprehensive for the Bahia Bustamante area was performed by Isola *et al*. (2011). This work presents a very accurate 1:100,000 scale geomorphologic map based on landform recognition via remote sensing analysis, supplemented by field surveys and ground control points.

Golfo San Jorge area (46° to 47°03' S): this area is located in the San Jorge Basin (Fig. 5), the Santa Cruz Province on the border with Chubut Province. The Late

Quaternary deposits lie on Tertiary successions (Zambrano & Urien, 1970; Sylwan, 2001), exposed in different abrasion platforms and cliffs and frequently constituted by marine deposits with enormous *Ostrea patagonica* shells. In this area Late Quaternary coastal deposits are described by Feruglio (1950), Codignotto (1983); Codignotto *et al.* (1988; 1990); Schellmann (1998); Aguirre *et al*. (2003); Schellmann & Radtke (2007; 2010).

In Bahia Solano (Fig. 2), Codignotto *et al.* (1990) dated mollusc shells from three Holocene systems of littoral successions respectively at 1700-2700, 3800-5000 and 5200-6500 yr BP (Fig. 17), while near Caleta Olivia (but without clear indications for the locations) Codignotto (1983) and Codignotto *et al.* (1988; 1992) dated single shells at 1550-6630 ^{14}C BP.

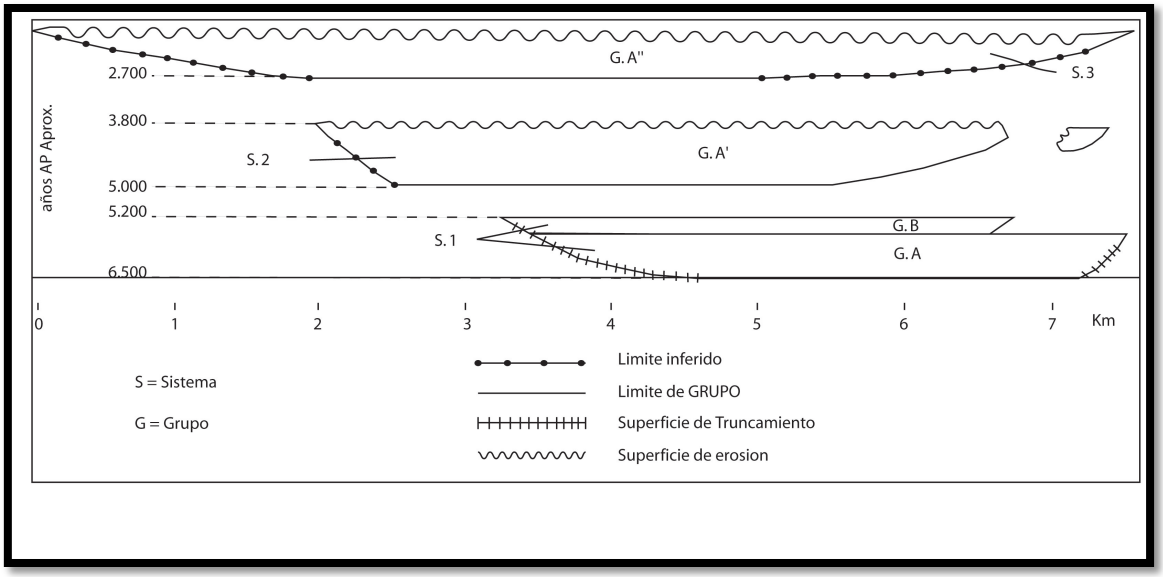

Figure 17 – Chronostratigraphic scheme of Bahia Solano beach ridges (redrawn from Codignotto, 1990).

North of Caleta Olivia, close to National Route 3 (Fig. 18), shells collected within a road section have been dated at 266 ± 36 and 496 ± 68 ka by Schellmann (1998) (Fig. 19). South of Caleta Olivia, always close to the National Route 3 (Fig. 18), mollusc shells from raised beach deposits yielded ages between 111 ± 30 and 157 ± 19 ka in the localities Pa 70 and 71 (Fig. 21) and ages between 172 ± 15 and 212 ± 26 in the localities Pa 124, 125, 126 (Fig. 20) (Schellmann, 1998). In the locality of Cantera Delgado, also studied by Aguirre *et al.* (2003) from a paleontological point of view, Schellmann (2007) get 2 ESR dating, that allow to assign these deposits to MIS 5. The elevation of raised beach deposits belonging to MIS 5 and MIS 7 is the same in this area (Schellmann, 1998; Schellmann & Radtke, 2003).

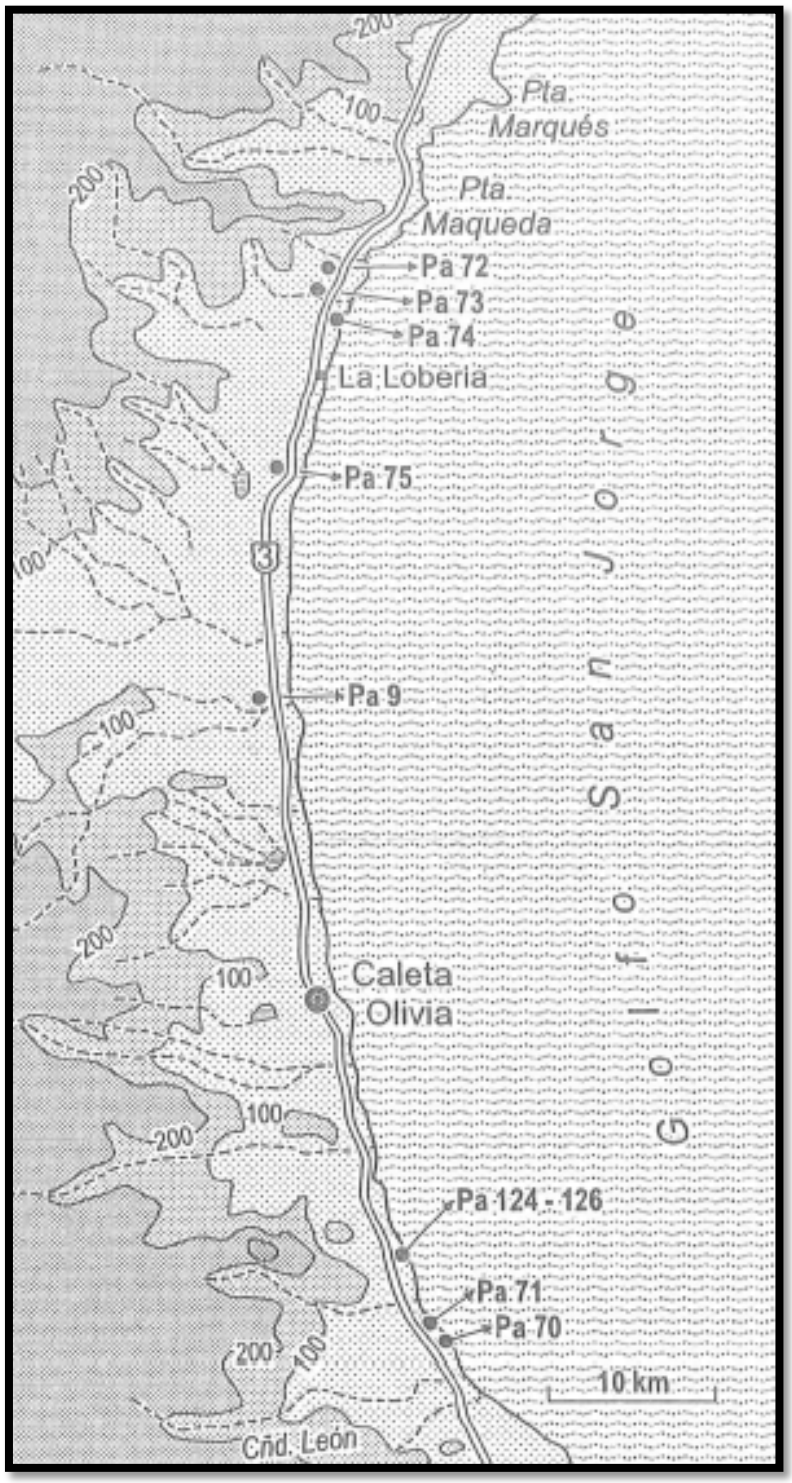

Figure 18 – Main sampling site in Caleta Olivia area (Schellmann, 1998).

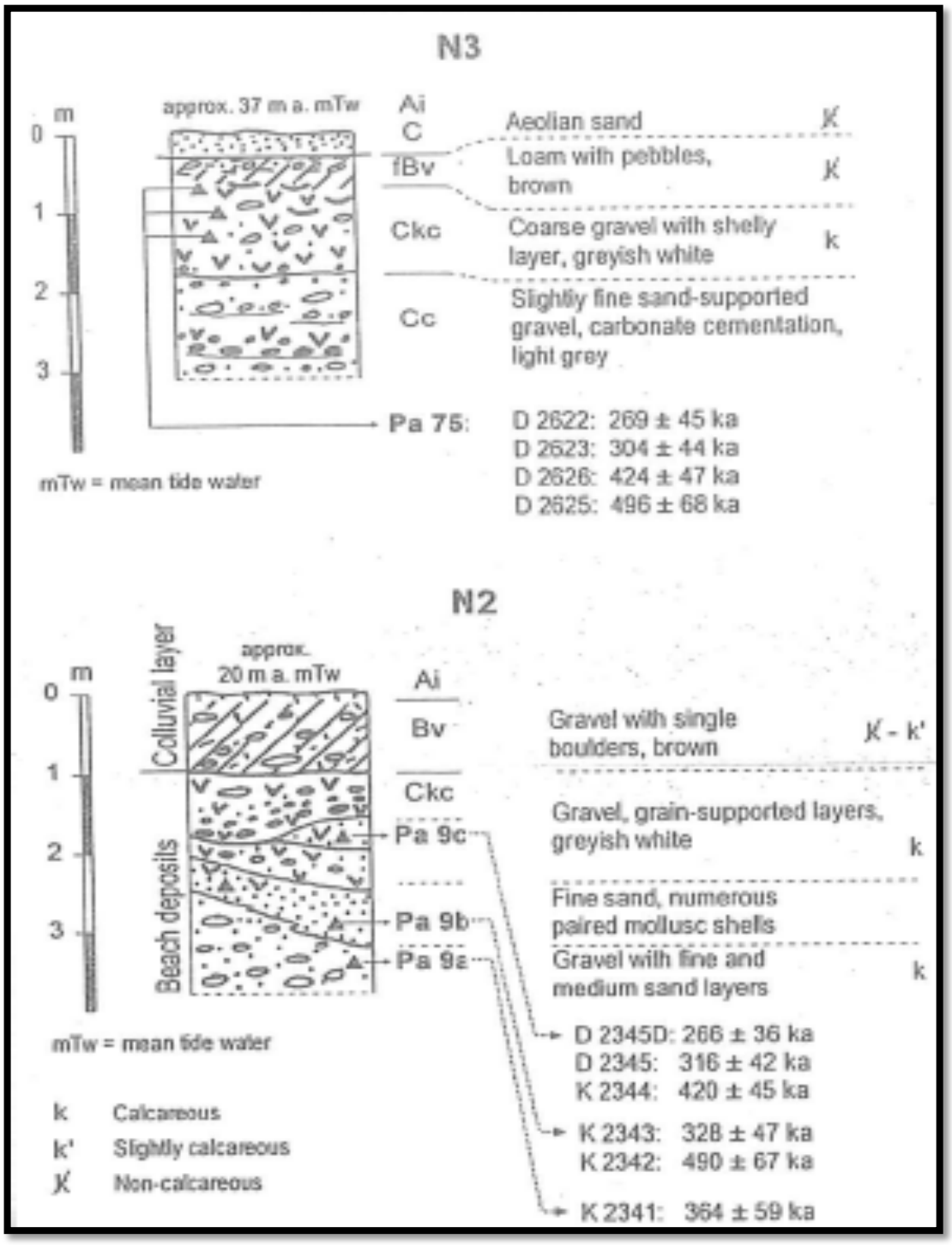

Figure 19 – Pleistocene beach deposits north of Caleta Olivia (Schellmann, 1998).

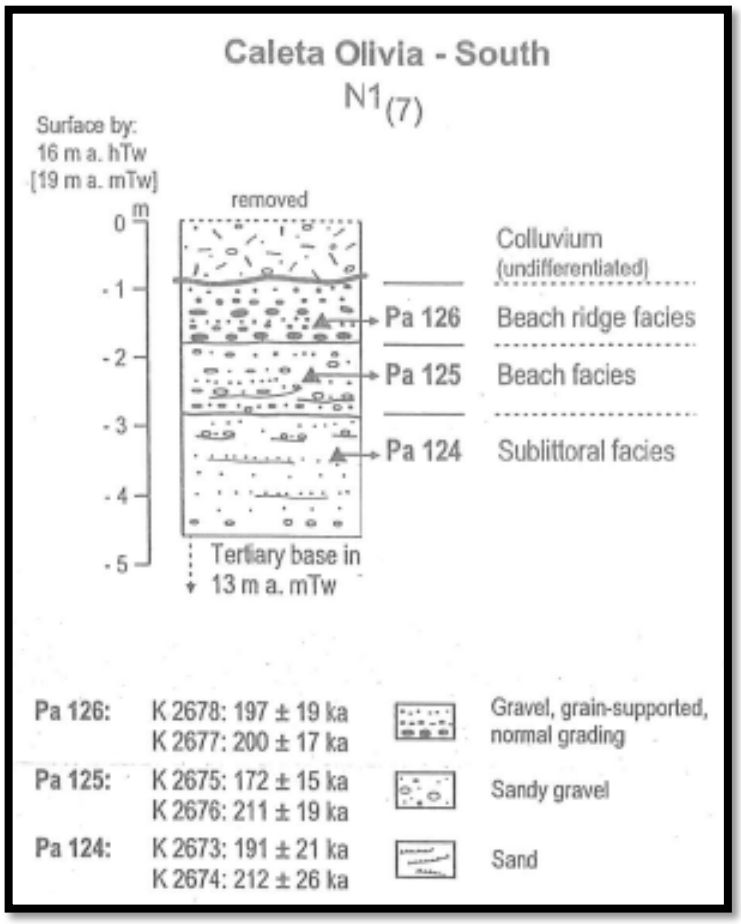

Figure 20 – Pleistocene coastal deposits south of Caleta Olivia (localities 124-126, Schellmann, 1998).

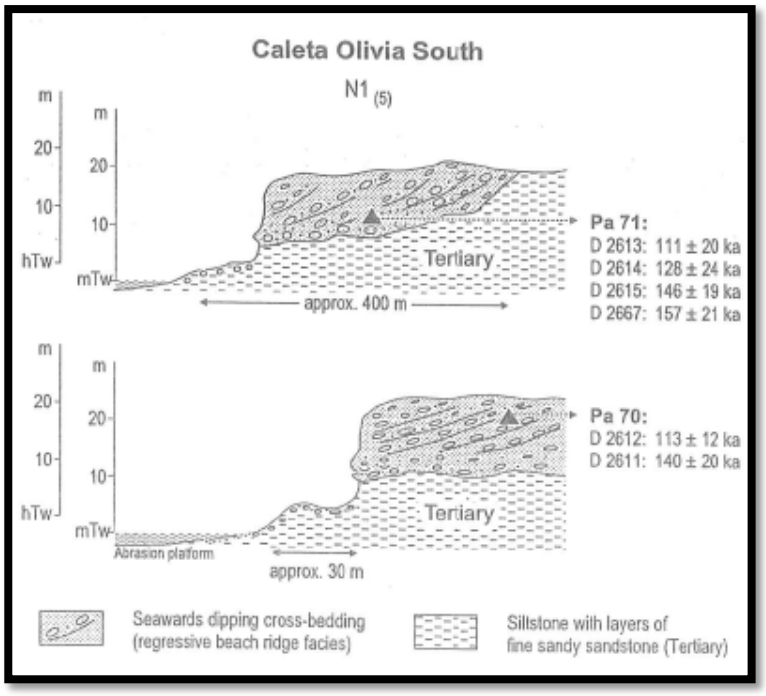

Figure 21 – Pleistocene coastal deposits south of Caleta Olivia (localities 70-71, from Schellmann, 1998).

Holocene coastal deposits have been studied by Schellmann (1998) north of Caleta Olivia, in the Punta Delgada locality (Fig. 22). In this area gravely beach ridges and littoral terraces are preserved and formed about 5200-5500 ^{14}C BP (Schellmann, 1998; Schellmann & Radtke, 2003; 2010).

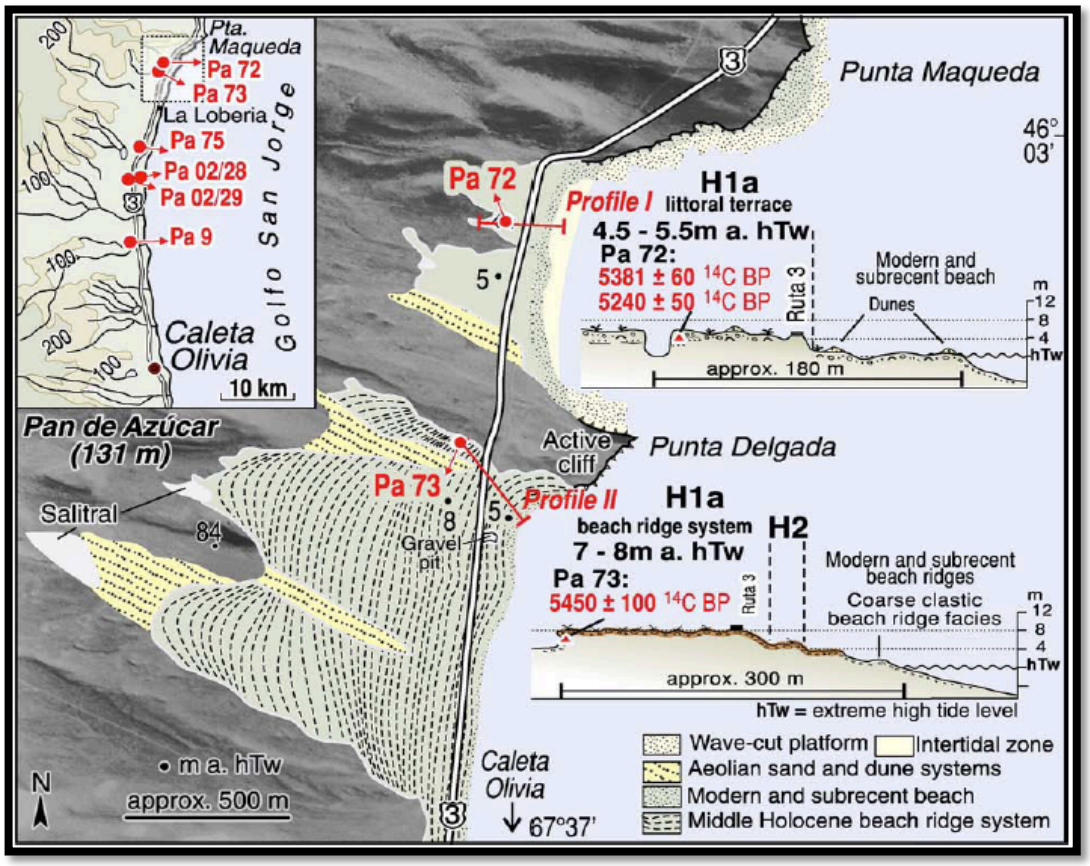

Figure 22 – Holocene coastal deposits north of Caleta Olivia (Schellmann & Radtke, 2010).

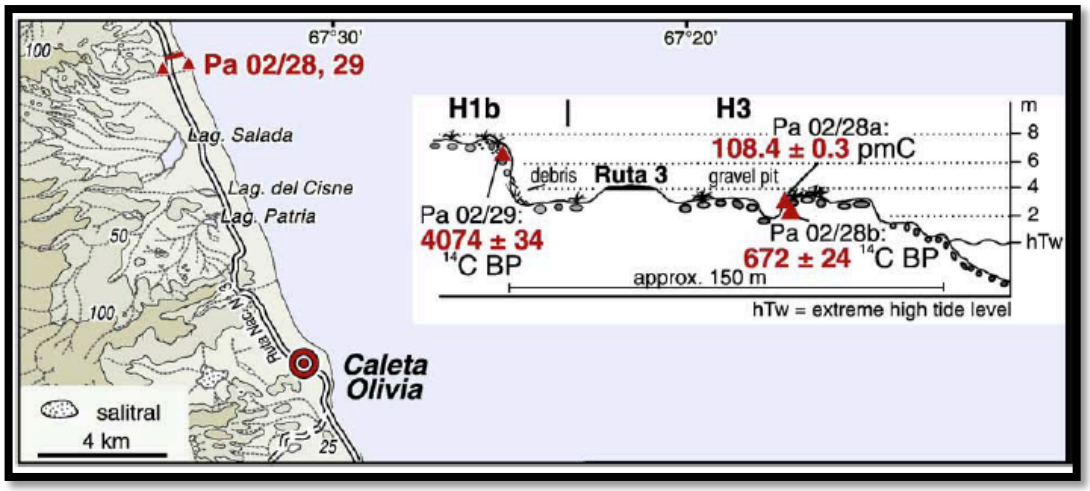

Figure 23 – Holocene beach ridges near Caleta Olivia (Schellmann & Radtke, 2010).

Always north of Caleta Olivia, late mid-Holocene beach ridges are preserved and have an age of 4074 ± 34 ^{14}C BP (Fig. 23).

The molluscan biodiversity of the Late Quaternary beach deposits in this area is lower than for the areas located northernmost and warm water taxa are not present (Aguirre *et al.*, 2009).

Puerto Deseado area (ca. 47°45 S): the city of Puerto Deseado (Fig. 2) is located on the Deaseado Massif (Fig. 5), in the Santa Cruz Province at the mouth of the Río Deseado. In this area abrasion platforms, steep cliffs, peninsulas and islands dominate the coast, while beach ridge systems are preserved only locally and mostly north of Puerto Deaseado.

Pleistocene coastal terraces have been described, in this area, by Feruglio (1947; 1950), Radtke (1989), Radtke *et al.* (1989) and Rutter *et al*. (1989; 1990).

Feruglio (1950) recognized 5 systems of marine platforms and beach deposits, but only the last three are considered late Quaternary. Rutter *et al*. (1990), using ESR and Amino Acid dating methods, assign the oldest of the three systems (system IV) to the penultimate interglacial (or older), the intermediate (system V) to the last interglacial and the youngest to the Holocene.

Radiocarbon date in Puerto Deseado have been performed for the first time by Schellmann (1998), which date the youngest Holocene beach ridge systems north of Puerto Deseado to about 1500 and 1300 ^{14}C BP (Pa 18 and 19, Fig. 24).

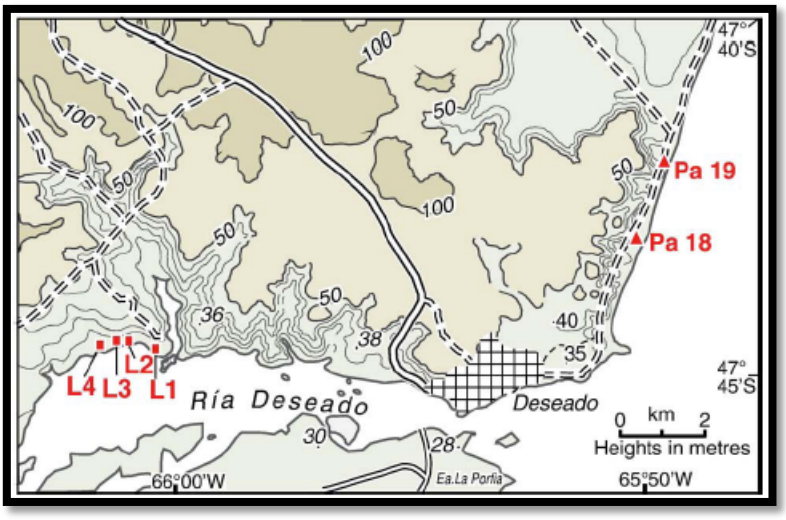

Figure 24 – Holocene sampling sites in Puerto Deseado area.

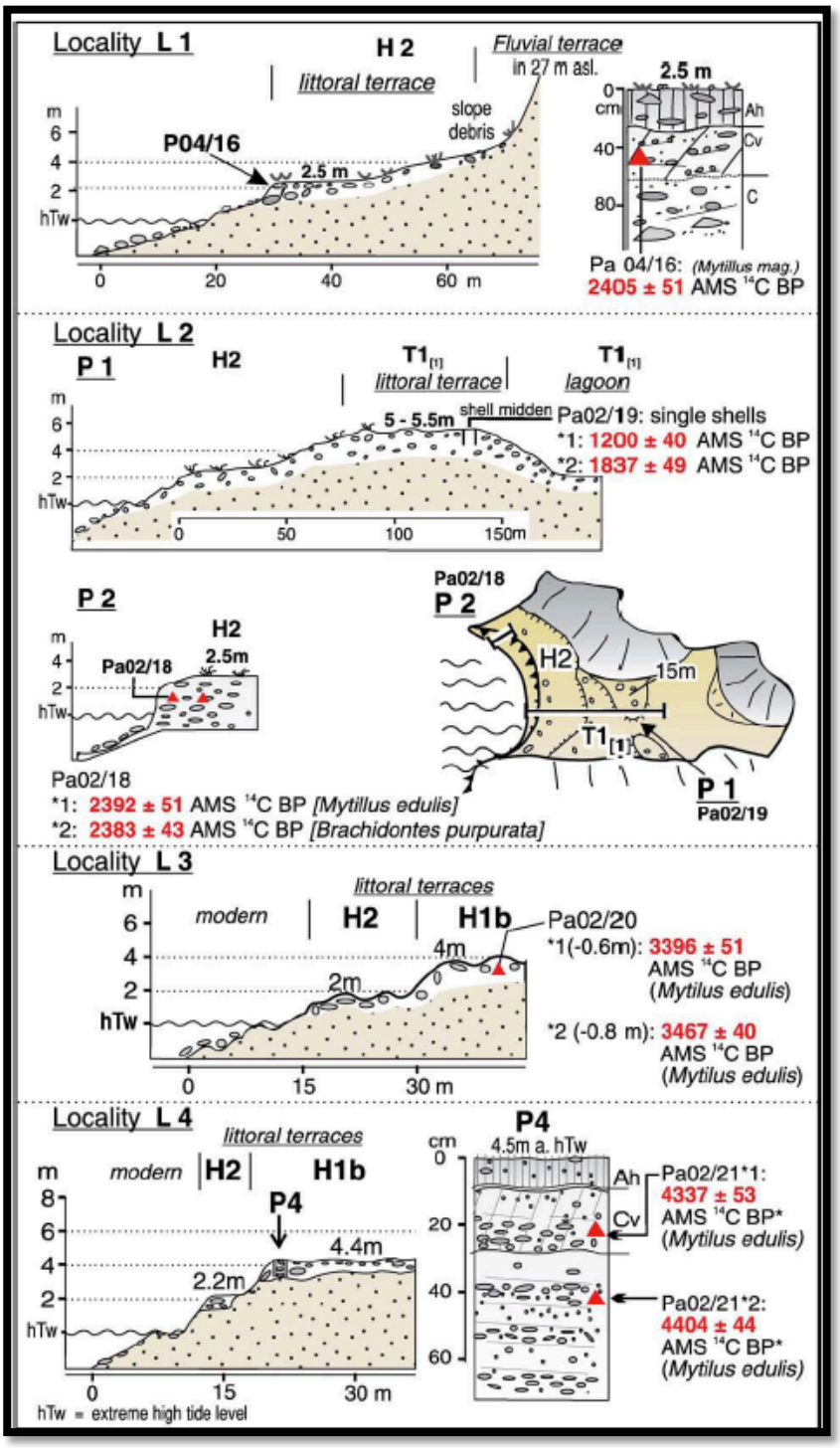

Figure 25 – Holocene littoral terraces in the Ría Deseado (Schellmann &Rdatke, 2010).

Along the Ría Deseado, the estuary of the Río Deseado, Holocene terraces are preserved. Schellmann (1998) and Schellmann & Radtke (2007) sampled and dated the oldest terraces to the mid-Holocene transgression maximum, while the next lower terraces formed about 3400-4400 ^{14}C BP and about 2400 ^{14}C BP (Figs. 24-25).

2.3. CLIMATE

Patagonia lies between the subtropical high-pressure belt and subpolar low-pressure areas (Prohaska, 1976) and is completely included in the circulation zone of the southern westerlies (Fig. 26). The Andes act as a topographic barrier, intercepting humid winds from the Pacific Ocean and defining a narrow western band (windward), with hyper-humid to humid climates, and a wider eastern area (leeward), where subhumid, semiarid and arid climates prevail.

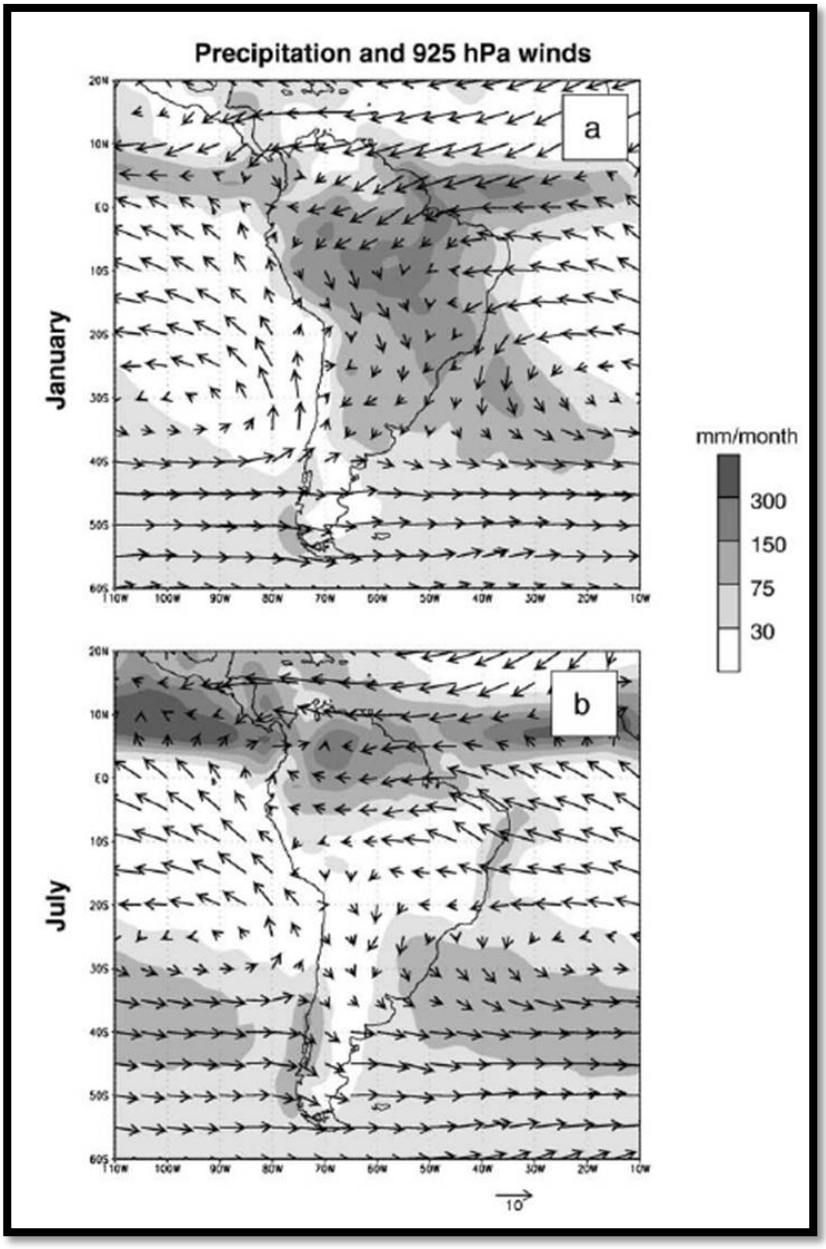

Figure 26 – Long-term mean CMAP precipitation and 925 hPa wind vectors for a) January and b) July (Garreaud *et al.,* 2009).

It is difficult to define the Patagonian climate in a global climatic classification. Eastern Patagonia shows a dry climate with moderate thermal amplitude, whereas western Patagonia has a markedly oceanic climate (Fig. 27).

The classification used by Coronato *et al.* (2008) is based on the superposition of three climatic elements: mean temperature, thermal amplitude and aridity index. The intersection or the superposition of the respective isolines defines climatically homogeneous areas. The code is:

First term: Mean Annual Temperature (MAT)

MAT > 10° C = Temperate (T)

MAT < 10° C =Cold (C)

Second term: Aridity Index (AI; UNESCO, 1977): mean annual rainfall/potential evapotranspiration

AI < 0.2 = Arid (A)

0.2 <AI < 0.5 = Semiarid (sA)

0.5 <AI < 0.75 = Subhumid (sH)

AI > 0.75 = Humid (H)

Third term: Mean Annual Temperature Range (MATR)

MATR > 16°C = Continental (c)

16°C > MATR > 10°C = Transitional (t)

10°C > MATR > 5°C = Oceanic (o)

MATR < 5°C = Hyper-oceanic (o+)

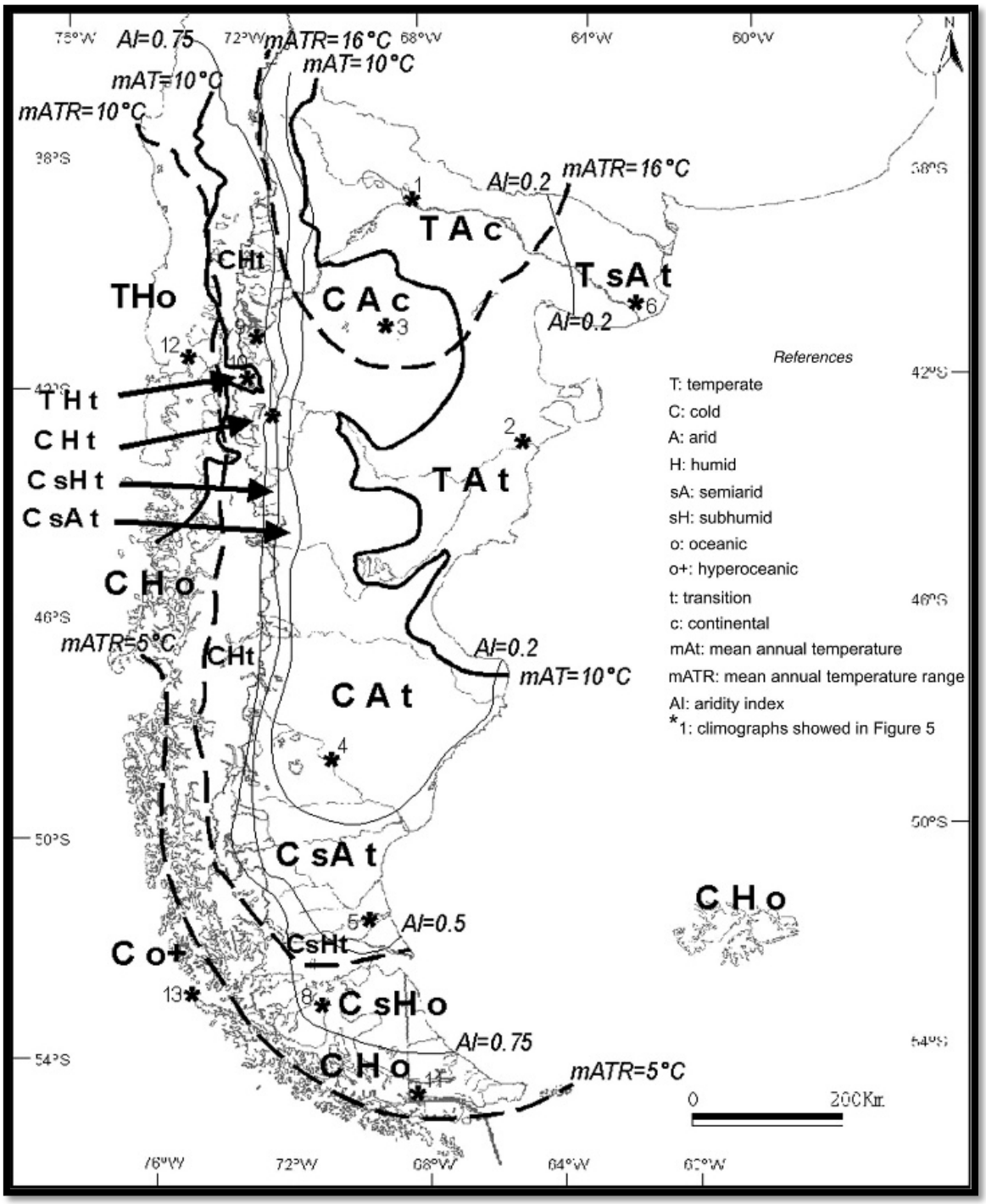

Figure 27 – Climates of Patagonia region (Coronato *et al.*, 2008).

2.3.1. Precipitation

Precipitation is mostly caused by mid-latitude storms that closely track the axis of the westerly wind maximum in the middle and upper troposphere. West of the Andes, uplift of low troposphere moist air produces significant orographic rainfall, which acts in concert with frontal precipitation (Garreaud et al., 2009). Therefore,

the Andes produces a major rainshadow effect leeward, and mean annual precipitation decreases abruptly from west to east from ca. 1400 mm at the Argentina–Chile border to less than 250 mm on the Patagonian plateau, with absolute values below 100 mm in the central region (Fig. 28). Rainfall is evenly distributed throughout the year close to the Andes, whereas towards the east, precipitation is restricted to autumn and winter, especially in the northern and central areas up to 46°S, where vegetation is scarce (Mazzoni & Vazquez, 2010).

Most of the extra-Andean Patagonia is situated within the winter maritime rainfall pattern, ruled by the northward displacement of the Southwestern Pacific anticyclone, which extends up to 46° S.

In eastern Chubut, due to a modest influence of the Atlantic Ocean, there is not a defined rainfall season and to the north, east of Río Negro, the increase of summer rainfall anticipates the subtropical continental pattern of central and northern Argentina (Coronato *et al.*, 2008). In the southern part of Patagonia and on the pacific coast until 47° S, a summer rainfall pattern is also recorded.

The area is dominated by westerlies winds, permanent strong winds coming from the west and southwest and blowing across the entire region, with a mean annual velocity of more than 6 m/s and which are more intense in spring and summer, (Fig. 26). The southern westerlies, extending through the entire troposphere and reaching a maximum speed (the jet stream) in the upper troposphere (Garreaud *et al.,* 2009) shift seasonally, towards the pole in summer and towards the equator in winter (about lat. 30°S). The windiest area is located between 47° and 49 °S, where mean annual velocities reach more than 10 m/s (Barros *et al*., 1997). After crossing the Andean Cordillera, the westerlies create rain shadow conditions in the eastern side of the Patagonia and they limit the Atlantic influence, expanding the Pacific impact across the region. The middle and high cloudiness recorded in the Atlantic coast of Patagonia is residual cloudiness generated by the orographic precipitations along the Pacific coast.

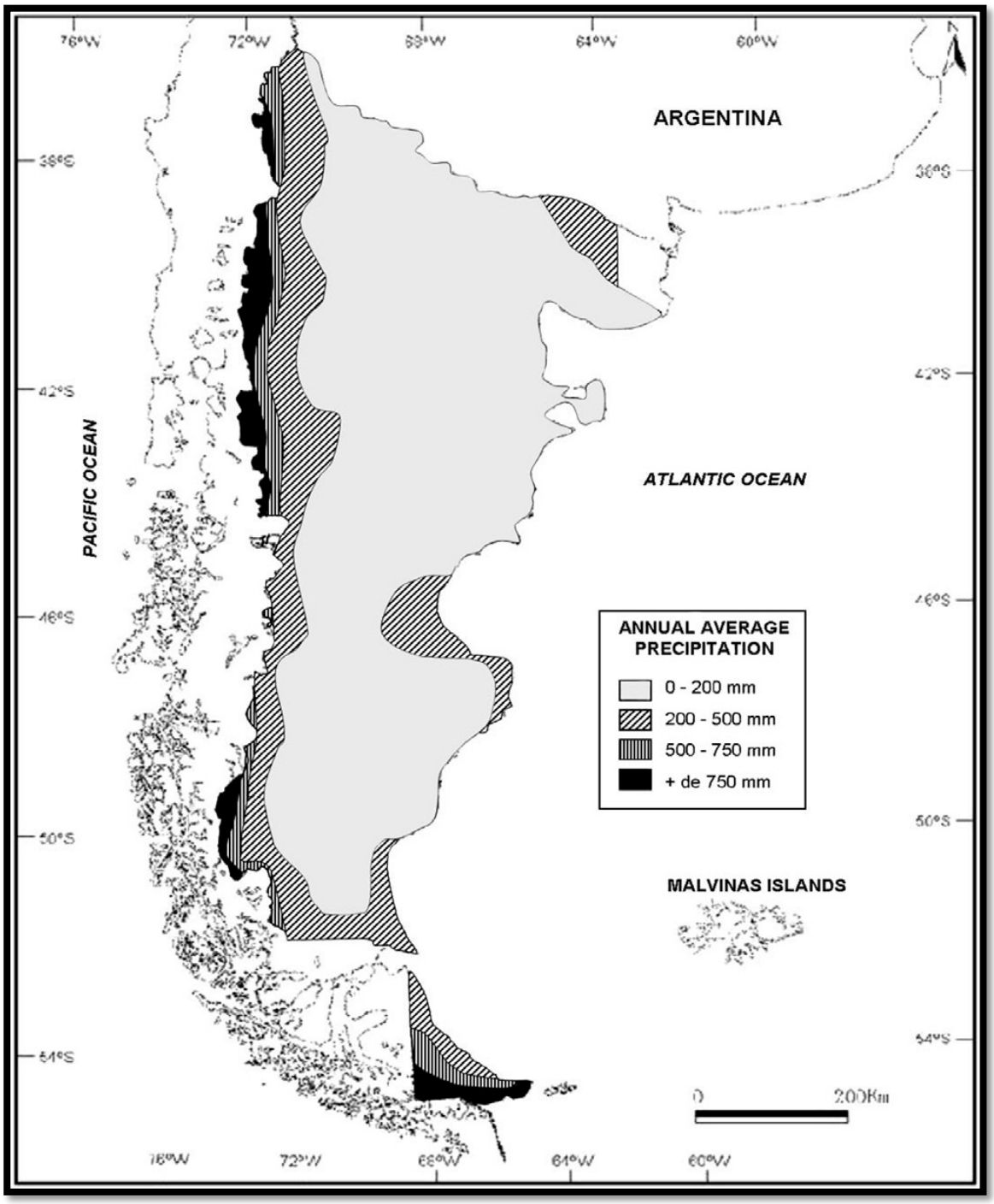

Figure 28 – Mean annual precipitation in Patagonia (Mazzoni & Vazquez, 2010).

2.3.2. Temperature

Temperature variations are very considerable in Patagonia, from temperate to cold climate conditions from the north to the south, with annual means ranging between 14 and 4 °C, respectively (Fig. 29).

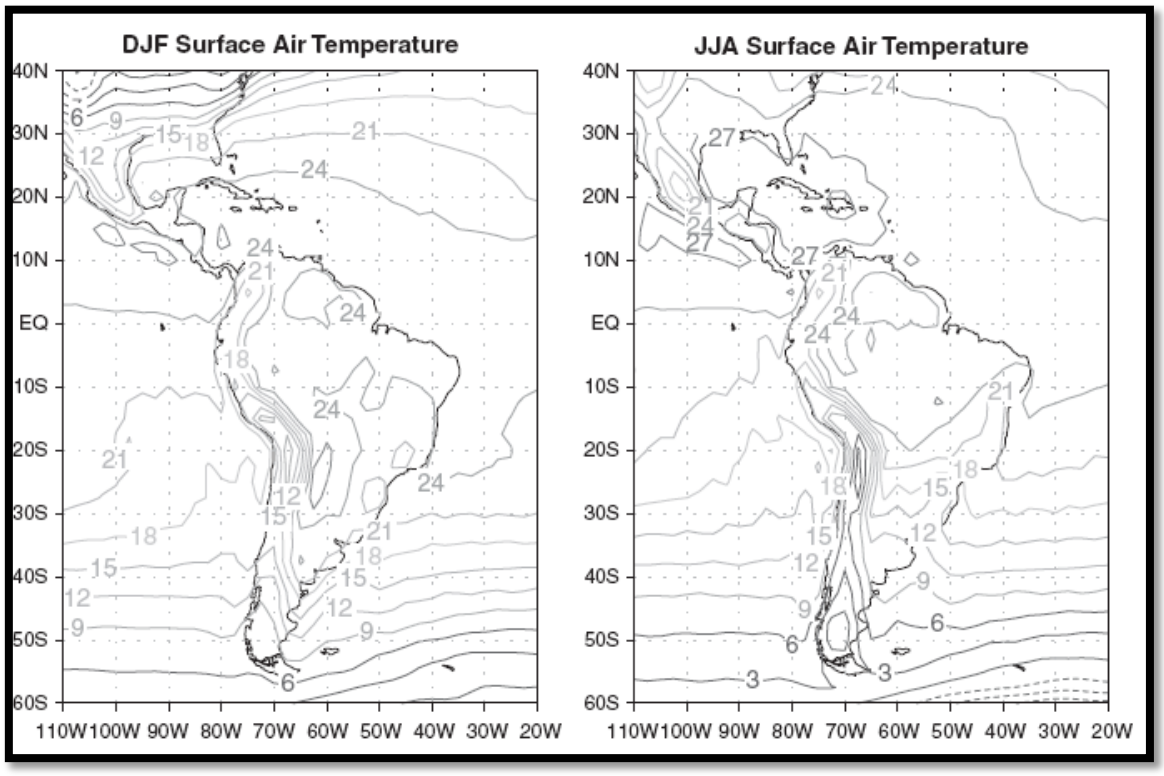

Figure 29 – Average (1979-2006) surface air temperature (°C) during December-January-February (DJF) and June-July-August (JJA) (Garcia *et al.,* 2010).

Differences in the solar radiation, changing from little above 180 W/m^2 (annual average) in the northernmost stations (e.g. Neuquen) to 100 W/m^2 in Tierra del Fuego (Paruelo *et al.,* 1998), are significant. According to the increase in latitude, the relationship between the incoming summer solar radiation and that of winter increases progressively from 4:1 at Neuquen (39° S) to 13:1 at Ushuaia (55° S). Conversely, the temperature pattern follows an opposite pattern. The mean annual thermal amplitude varies from 16°C in the north to 8°C in the south (Coronato *et al.*, 2008).

During the last two decades, a warming trend has been observed south of 46°S, both on the Pacific and Atlantic coasts (Rosenblüth *et al*., 1995). Since 1930 and 1940 a warming trend has been registered in the Orcadas del Sur and in Rio Gallegos.

Temperature and precipitation characteristics determine a dominant steppe vegetation in this area. The most representative vegetation types are the grassy-shrubby steppe of medium height (20-80 cm) and density, and dwarf cushion shrubs (5 to 20 cm) with scarce grasses and very low total cover (Leon *et al*., 1998). Vegetation in these ecosystems is distributed in a heterogeneous horizontal pattern of plant patches alternating with bare soil areas (Noy Meir, 1973).

Climatic characteristics largely influence the ecosystem structure and functioning in Patagonia, mainly through their effect on water dynamics (Leon and Facelli, 1981; Bertiller *et al.*, 1995). Relative abundance of grasses and shrubs varies with the amount and annual distribution of precipitation: shrubs increase as precipitation decreases and the proportion of rain in winter increases, whereas grasses increase with increasing precipitation (Paruelo and Lauenroth, 1996). Herbs distribution, on the contrary, is influenced by local-scale factors (i.e. landscape structure, edaphic characteristics and land-use history; Jobbagy *et al.,* 1996).

Desertification processes started at the end of the nineteenth century with the settlement of wool growers in different areas. Overgrazing has been the main factor causing desertification (Mazzoni, 2010).

2.3.3. Tides

The Patagonian coast is dominated by macrotides (Isla *et al.*, 2004; Isla & Bujalesky, 2008), increasing inside gulfs or in relation to the width of the continental shelf (Fig. 30). In this region tides are semidiurnal (Esteves *et al.,* 2000). Within northern Patagonian gulfs beach dynamics is conditioned by short fetchs (Isla *et al.*, 2001) and in the Golfo San Jorge tidal regime increases from mesotidal at entrance of the gulf to macrotidal at the westernmost coast (Isla *et al.*, 2002).

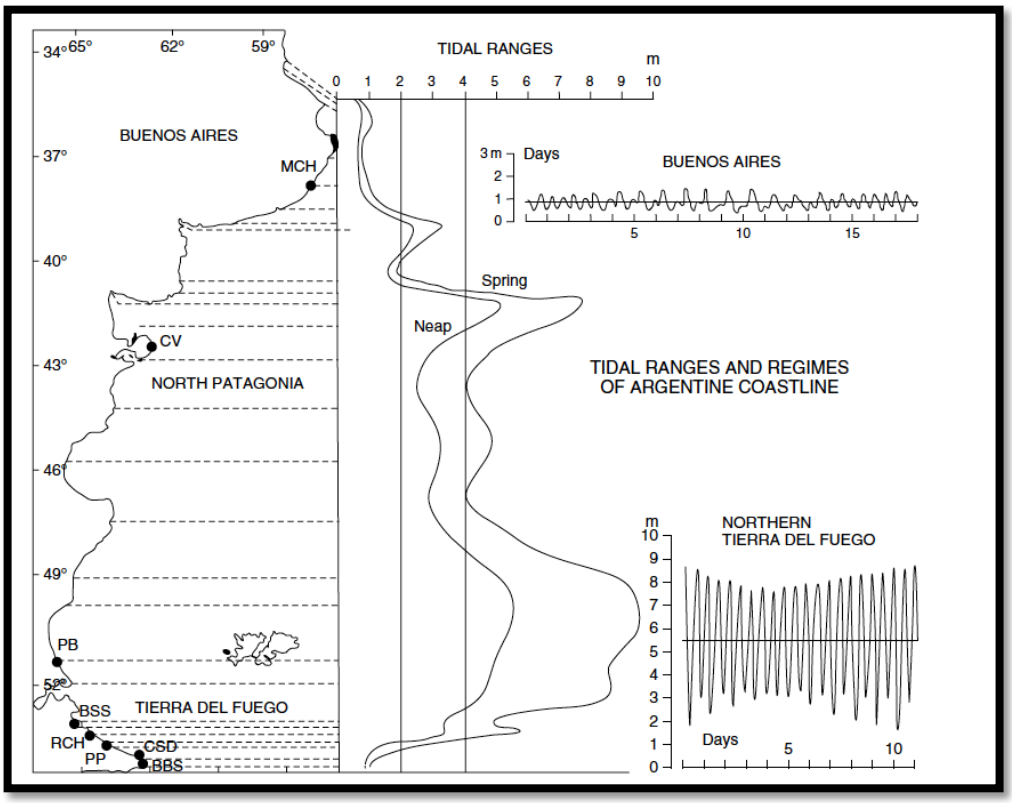

Figure 30 – Tidal ranges and regimes along the Patagonia coastline (modified from Isla and Bujalesky, 1995).

2.4. OCEANIC CURRENTS

Ocean currents play an important role in modulating local and global climate patterns. South America climate is strongly influenced by oceanic currents in both Atlantic and Pacific oceans, but the eastern coast of South America shows a seasonal behavior not observed along the Pacific coast (Garcia *et al.*, 2010)

The upper ocean circulation in the southwestern Atlantic is dominated by the presence of the warm and salty southward flowing Brazil Current and the cold and relatively fresh northward flowing Malvinas (Falkland) Current (Fig. 31).

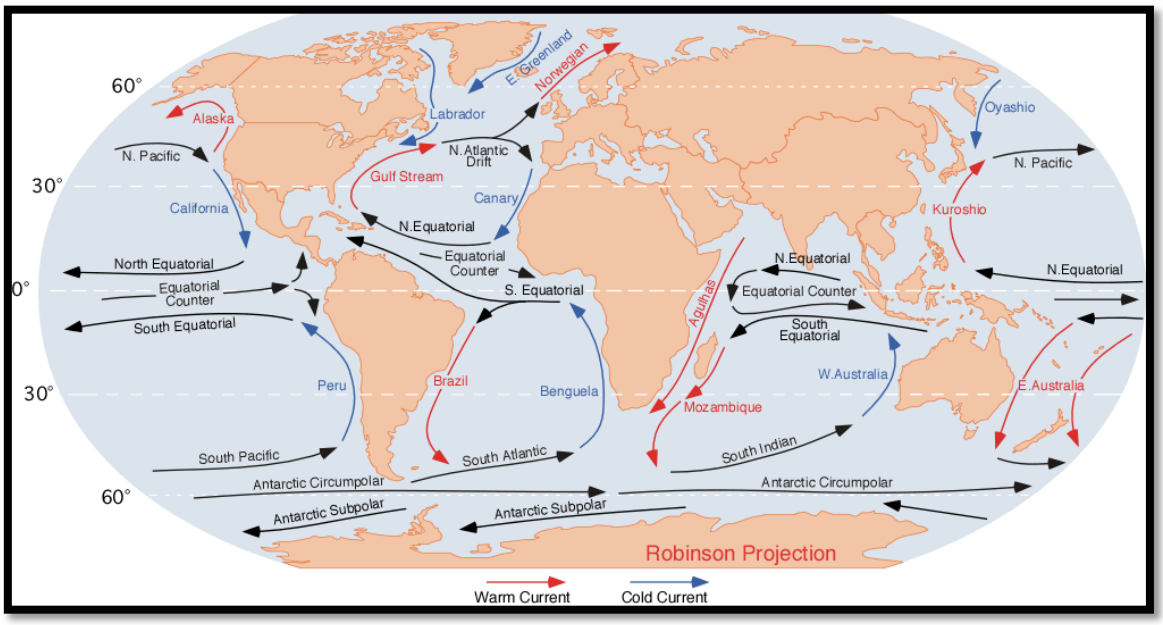

Figure 31 – Major ocean surface currents of the world (Pidwirny, 2006). Red arrows represent the warm currents; blue arrows represent the cold currents.

The Brazil Current originates from the Atlantic South Equatorial Current (Fig. 31), which bifurcates into two warm currents traveling along the South America coast, the northward-flowing Northern Brazil and Caribbean Currents, and the southward-flowing Brazil Current, and runs south along the coast of Brazil from about 9°S to about 38°S (Stramma *et al.*, 1990; Podesta *et al.*, 1991). It is generally confined to the upper 600 m of the water column. When the Brazil Current reaches about 33-38° S, it collides with the Malvinas Current (Fig. 32). The Brazil Current is then, in part, deflected to the east offshore of Rio de la Plata, a region known as the Brazil-Malvinas Confluence Zone (Gordon and Greengrove, 1986), one of the most energetic regions in all the oceans (Sarceno *et al.,* 2004).

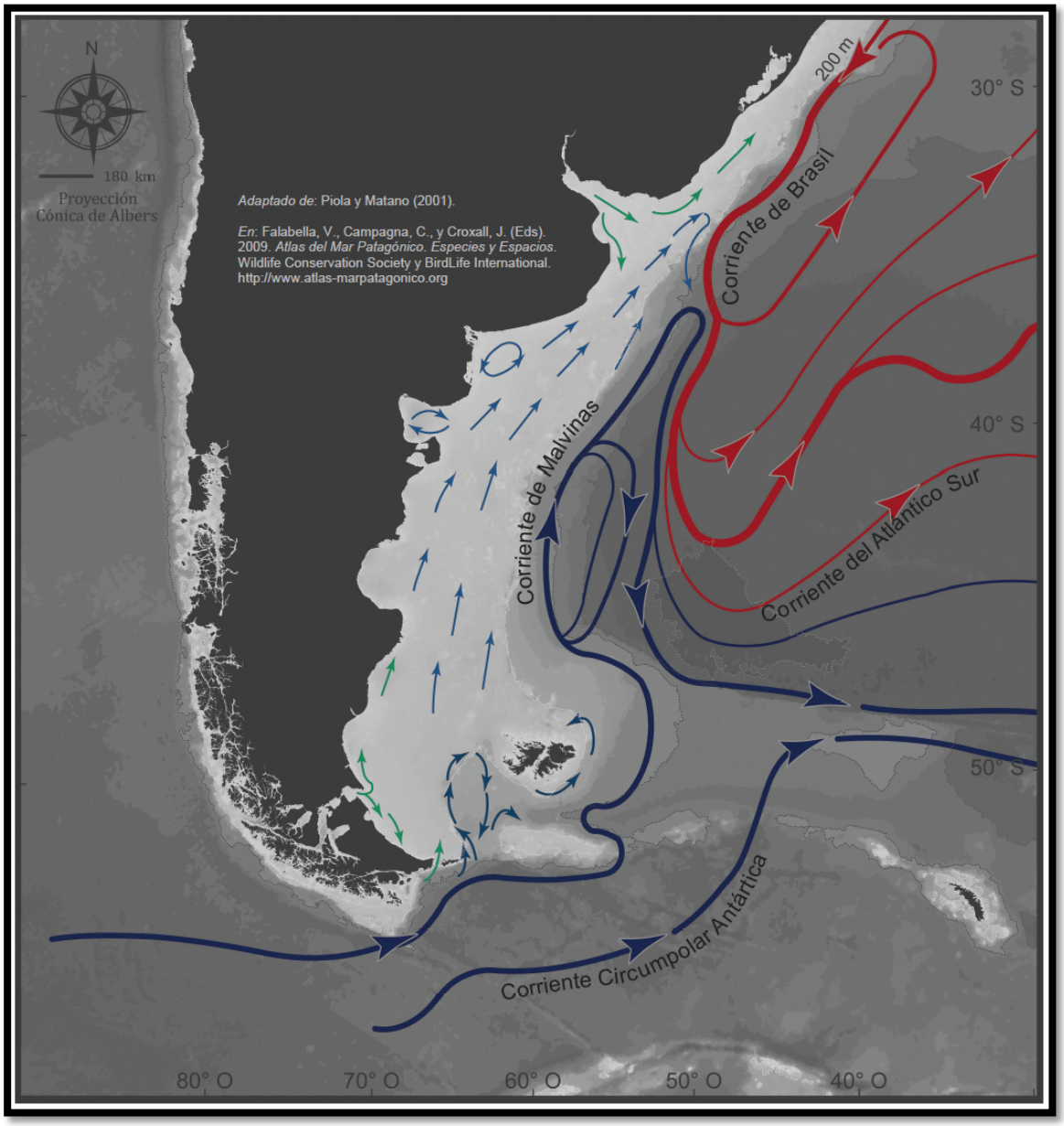

Figure 32 – Map of marine currents along the Patagonian Atlantic coast adapted from Piola and Matano (2001). Red arrows represent the warm currents; blue arrows represent the cold currents; green arrows represent freshwater inputs.

The transport of the Brazil Current is between 5 Sv and 6.5 Sv near surface waters (upper 500 m) around 20°S (Peterson and Stramma, 1990; Stramma *et al.,* 1990). As the Brazil Current flows south of 24°S, its flow intensifies by about 5% per 100 km, which is similar to the growth rate in the Gulf Stream, although transport values in the Brazil Current are considerably less (Peterson and Stramma, 1991). Thus, at about 33°S the total transport (which includes a recirculation cell in the upper 1400m) is about 18 Sv, and reaches values from 19-22 Sv at about 38°S, where it encounters the Malvinas Current (Olson et al., 1988; Peterson and Stramma, 1991).

On average, the temperature in the Brazil Current is about 18°C - 28°C, with essentially three meridional zones that experience several degrees of distinctly different annual temperature fluctuations, which corresponds to their proximity to shore. The first zone is located over the shelf and experiences temperature variability of 7-10 degrees, which is controlled by both winter invasions of subantarctic water from the Malvinas Current and discharges from Rio de la Plata and Patos-Mirim. The second or central portion, closer to the eastern margin of the continental shelf, experiences a 5-7 degree variance. The third, on the seaward-most zone, shows little fluctuation until the Confluence (Memery, *et al*., 2000; Zavialov *et al*., 1999). Temperatures in the southern section of the current (Figs. 33-34), near the Confluence, can change by 5-13 degrees, with the cooler temperatures occurring around August-September and the warmer values observed in February (Boebel *et al*., 1999; Podesta, *et al*., 1991). Almost yearly temperature anomalies of warm and cold fronts occur that seem to be related to the El Nino-Southern Oscillation (ENSO) events. Anomalous cold water extensions to the north occur on the shelf generally one year after every warm ENSO event, and anomalous warm water extensions occur generally one year after every cold ENSO (Lentini *et al.,* 2001). Surface salinities indicative of Brazil Current waters range from 35.1 to 36.2‰ (Fig. 35), with the maximum commonly found at around 20°S, where it can reach a salinity of 37.3‰ (Memery *et al*., 2000; Wilson & Rees, 2000).

The region of convergence of these two currents exhibits very complex frontal motions and patterns with the simultaneous presence of warm and cold eddies (Fig. 32). However, these two currents do not always collide, as there is evidence that leakage of water of the Malvinas Current mixes with water from the continental shelf and the Rio de La Plata discharge, flowing northward on the continental shelf break and east of the Brazil Current waters (Lentini *et al*., 2001; Piola *et al*., 2000; Sunye and Servain, 1998). The strong surface thermal front in the confluence region is characterized by the contrasting properties of the Thermocline and Subantarctic Surface Water masses. In situ estimates indicate that this frontal region can have horizontal gradients of up to 1°C $(250\ m)^{-1}$ (Garzoli and Garraffo, 1989). Hydrographic measurements also reveal that these frontal regions are associated with strong subsurface horizontal thermal gradients, which, in turn, can be related to the depth of a given isotherm (Roden, 1986; Garzoli and Garraffo, 1989).

The latitude of confluence, which determines where the Brazil Current will separate from the continent, is farther north during austral winter and spring (Fig. 33). This seasonality is presumed to be related to the general seasonal shift of wind systems and seasonal southern shift of the subtropical gyre (Peterson & Stramma, 1991). Maximum velocities at the confluence (at about 38°S) reach 55 cm s^{-1} with the average value of 35 cm s^{-1} with transports of 18 and 11 Sv respectively. Flow can increase up to 23 Sv at the Brazil-Malvinas Confluence (Garzoli, 1993) Mean conditions of circulation vary significantly, and more recent evidence shows that it is likely related to meteorological anomalies (Assireu *et al.*, 2003). Some short term variability in the southward extent of the Brazil Current has also been observed. Occasionally, when a Brazil Current meander that has extended unusually far south retreats, it can shed a series of warm core eddies that migrate into the Antarctic Circumpolar Current (Partos and Piccolo, 1988).

The range of the Confluence oscillate between about 54°W and 45°W, a total distance of about 770 km (at 38°S). The meanders appear to occur on a twelve month cycle and are likely correlate to changes in the separation latitude of the Brazil Current (Boebel *et al.*, 1999; Garzoli and Bianchi, 1987; Goni & Wainer, 2001; Maamaatuaiahutapu *et al.*, 1999; Zavialov *et al.,* 1999). The mean speed of the front is estimated to be about 14 cm s^{-1}. The front oscillates around its mean seasonal position (farther north and east during austral winter and farther south and west during austral summer) within a period of about one month and an amplitude that varies from 10-50 km per day. The mean velocity of the displacement of the front reaches values up to 10 km/day (Garzoli and Bianchi, 1987). This area is also rich in eddies, more often called Brazil Current Rings, averaging to about 7-9 rings per year. These elliptical rings can vary in size from about 56 to 225 km along the semi-major axis, and 23 to 108 km for the semi-minor axis. These anticyclones have a mean lifetime of about 35 days and translational speeds of anywhere between 4-27 km per day (Lentini *et al.*, 2002).

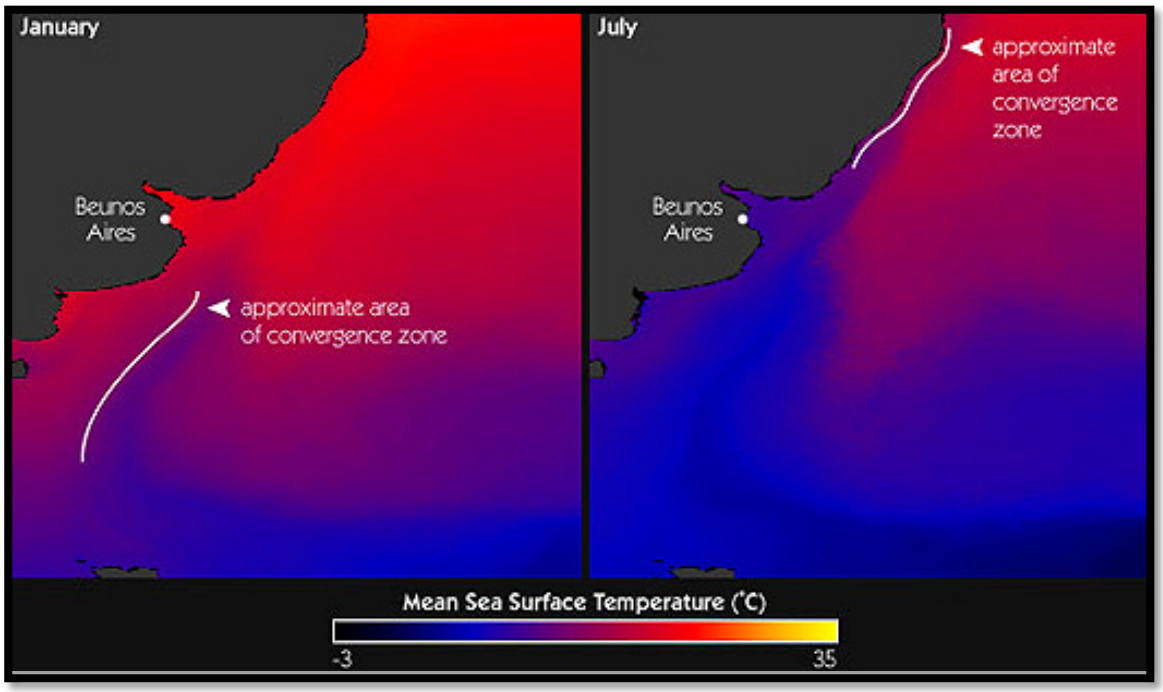

Figure 33 – Seasonal change of location of Brazil-Malvinas Confluence Zone http (www.disc.sci.gsfc.nasa.gov).

The Atlantic coast of Patagonia is dominated by the cold Malvinas (Falkland) Current (Fig. 32), a northward-running branch of the Circumpolar Current (Fig. 31). The Malvinas Current is modified by local prevailing winds, temperate thermal cycle and weakened through dilution by coastal input (Aguirre *et al.*, 2011). The Malvinas Current, formed when the West Wind Drift or Circumpolar Antarctic Current became active after the opening of the Drake Passage by the Oligocene-Miocene boundary (Beu *et al.*, 1997), moves northwards along the Argentine continental shelf until it reaches the Brazil Current offshore the Rio de la Plata estuary (Legeckis and Gordon 1982, Garzoli 1993, Vivier and Provost 1999). Its mean temperature ranges yearly from 4 to 11°C (Fig. 34) and salinity ranges yearly from 33.8 to 34.4‰ (Fig. 35). The Malvinas Current is strong, relatively fresh, and cold, with mean SST of 6°C (Brandini *et al.,* 2000). Thus, when it meets the weak, warm, southward-flowing Brazil Current at the Brazil-Malvinas Confluence, a sharp gradient in temperature and salinity can be observed (Goni 1996).

Estimates of the volume transport of the Malvinas Current vary widely in the literature, depending on the reference level that is chosen (Garzoli 1993). For example, using a reference level of 1000 m at 38°S, Garzoli (1993) obtained a transport of about 24 Sv. With a reference level of 3000 m at 42°S, Peterson (1992) found 60 Sv in the first 2000 m and 75 Sv in total, while at 46°S he found 70 Sv in

the first 2000 m and 88 Sv in total. Choosing the bottom as their reference level at 45°S, Saunders and King (1995) calculated 50 Sv in the thermocline and 60 Sv in total (Maamaatuaiahutapu *et al.,* 1998). Vigan *et al.* (2000) noticed that the transport values decreased from south to north. In particular, observations between 40°S and 38°S plummeted from about 20 ±5 Sv to zero. They attribute this to the fact that the Malvinas Current returns to the south at these latitudes. Thus, the location of the observations, relative to the location and orientation of both the high-velocity core of the Malvinas Current and its return flow, may also account for some of the variability in transport estimates. Direct measurements of the velocity of the Malvinas Current are scarce. According to Peterson (1992), surface drifters in the Malvinas Current travel at about 40 cm s^{-1}. Garzoli (1993) found geostrophic velocity values of 102 cm s^{-1} at 36.5°S and -61 to -62 cm s^{-1} at 36.6°S that were associated with the northward-flowing Malvinas Current and the southward return flow, respectively. The along-shelf flow of the Malvinas Current is highly variable from year to year, and it does not appear to have an annual or even a semi-annual cycle. However, there is a suggestion of significant energy at periods of about 135 days (Vivier and Provost 1999a, 1999b). On the other hand, the cross-shelf flow (perpendicular to the coast) clearly shows an annual cycle that is associated with the position of the subantarcitc front (Vivier and Provost 1999a).

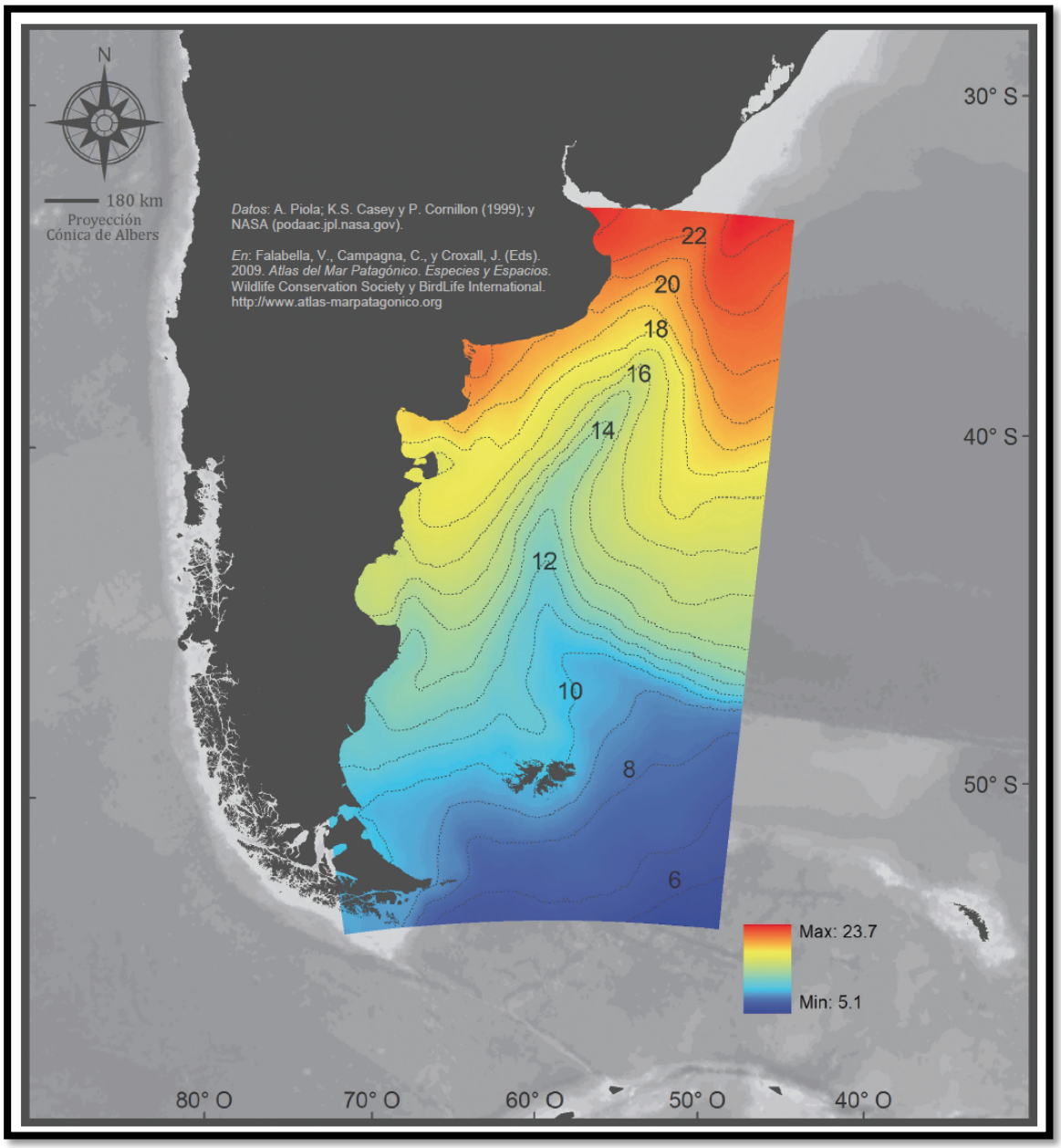

Figure 34 – Sea surface temperature in summer in °C (Flabella *et al*., 2009).

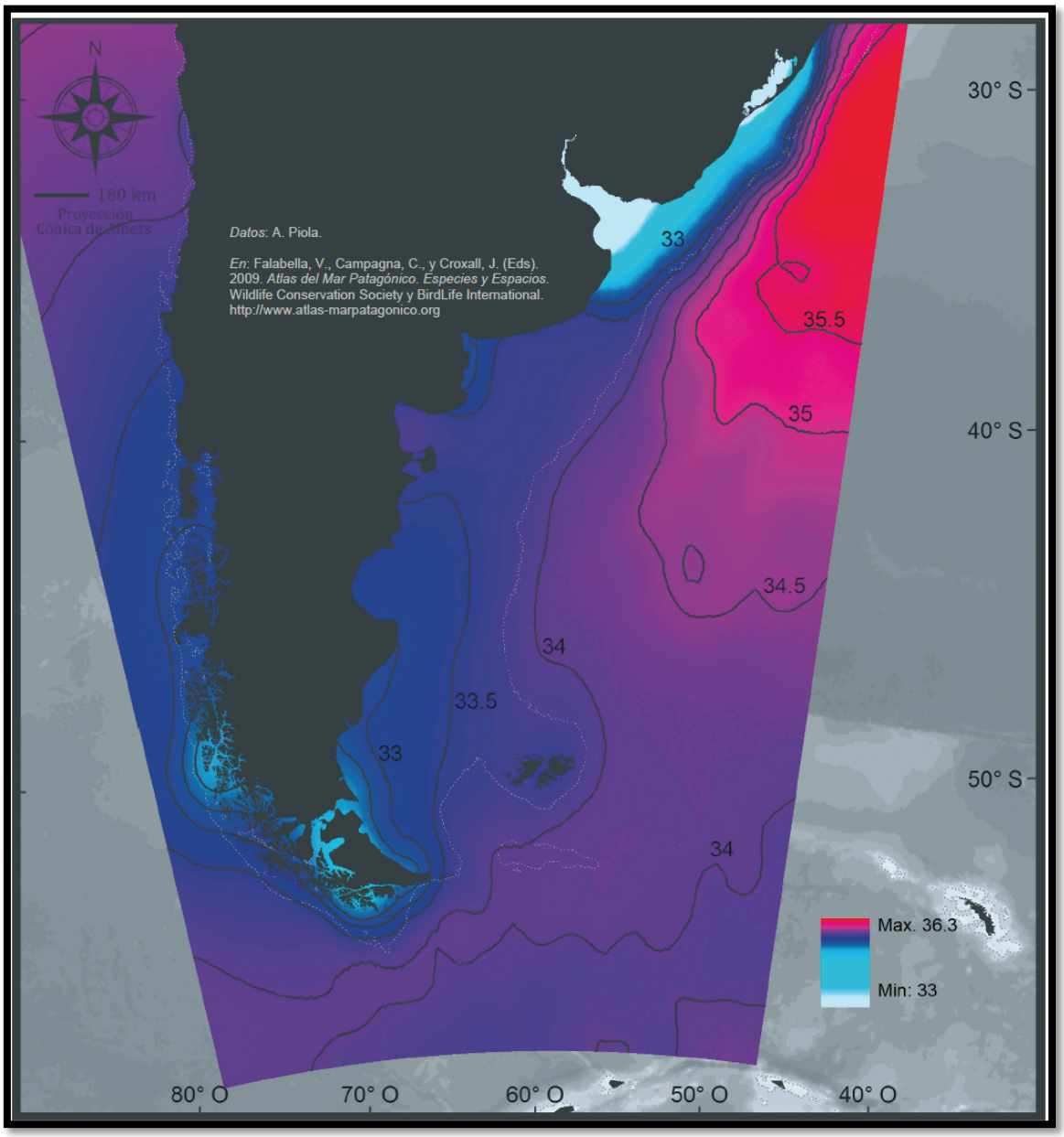

Figure 35 – Mean annual distribution of surface salinity (Flabella *et al*., 2009).

Along the coast between the Rio de La Plata-Paraná Delta and Tierra del Fuego, four salinity fronts and three thermal fronts are relevant for the study area. Three water masses are found in the upper thousand meters in this region (Maamaatuaiahutapu *et al*., 1992): the Thermocline Water, of subtropical origin and carried by the Brazil Current, is mostly confined to the continental break (Garfield, 1990). This water is characterized by a strong and deep thermocline with marked spatial and temporal variability. The Subantarctic Surface Water, which is carried by the Malvinas Current, meets the Thermocline Water in the upper 800 m, flows beneath the thermocline (Gordon, 1981), and forms the Antarctic Intermediate

Water, 500–1000 m deep, which recirculates with the subtropical gyre (Maamaatuaiahutapu *et al.*, 1998).

Surface salinity corresponds to the equilibrium between evaporation, precipitation, the contribution of currents and rivers with different physical and chemical characteristics and to the oceanic mixing processes. Most of the Patagonian Atlantic Ocean falls under the influence of sub-Antarctic waters, diluted by continental discharge, which originate in the southeastern Pacific and enter through the Magellan Strait and with the Malvinas Current (Fig. 35). In the northern zone, the discharge of continental waters from the Río de la Plata and the saline waters introduced with the Brazil Current, generate biologically important saline fronts.

The Atlantic coast of Patagonia belongs to the southwestern Atlantic sector of the Magellanean Zoogeographic Province (Fig. 36), extending from Golfo Nuevo (Chubut, ca 43°S) southwards to Cabo Hornos (55°S). From Golfo Nuevo to 28° S extends the Argentine Zoographic Province, a transitional area influenced by the cold Falkland Current and the warm Brazilian Current (Fig. 36).

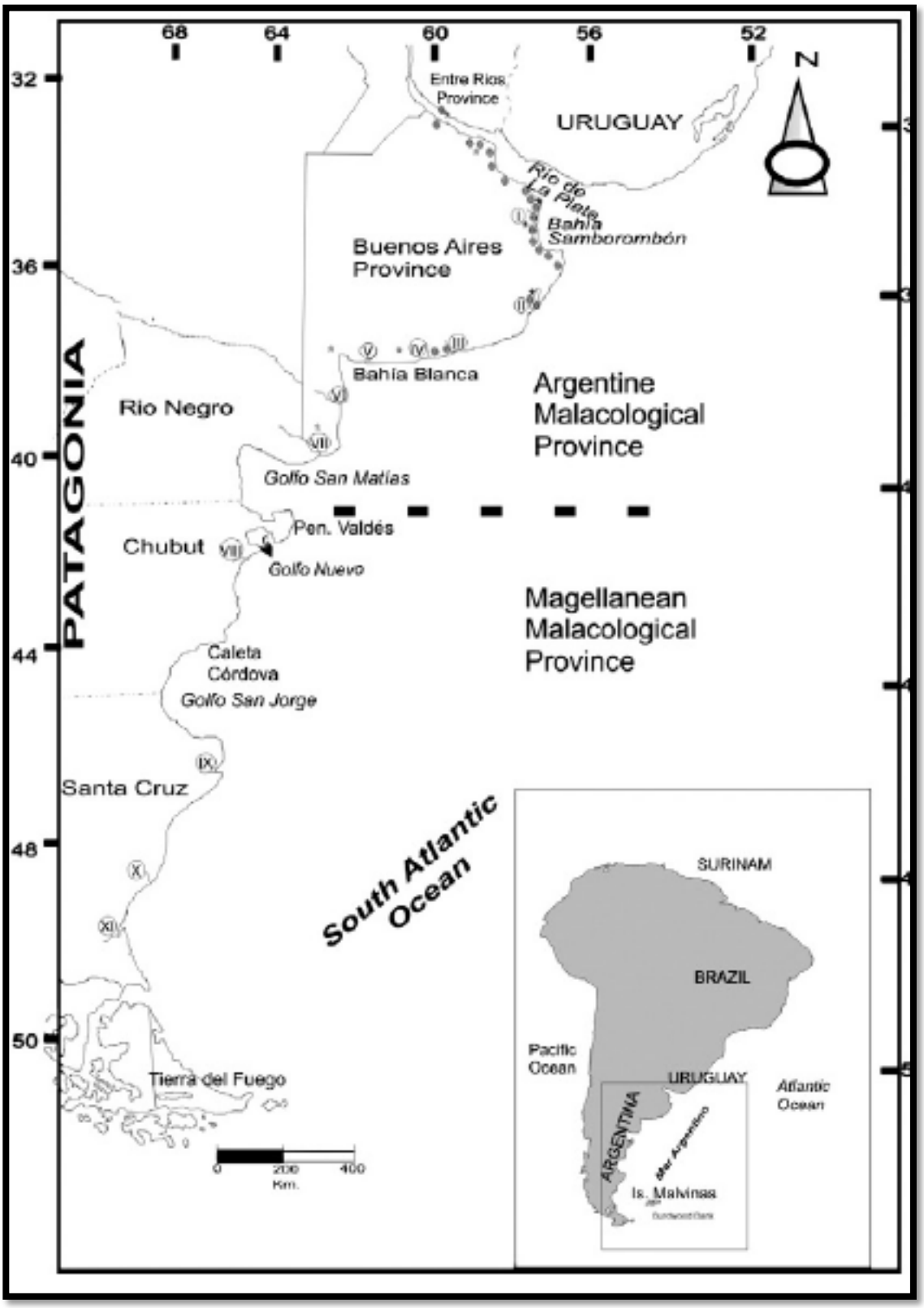

Figure 36 – Modern biogeographic regions (Argentine and Magellanean Malacological Provinces) (Aguirre *et al.* 2011).

In addition, the Malvinas current is a powerful source of nutrients (Fig. 37), stirring nutrients from the ocean depths and bringing them to the surface, where plants

thrive on them, producing plankton bloom. By contrast, the warm Brazilian current is shallow, and so the waters tend to be nutrient poor.

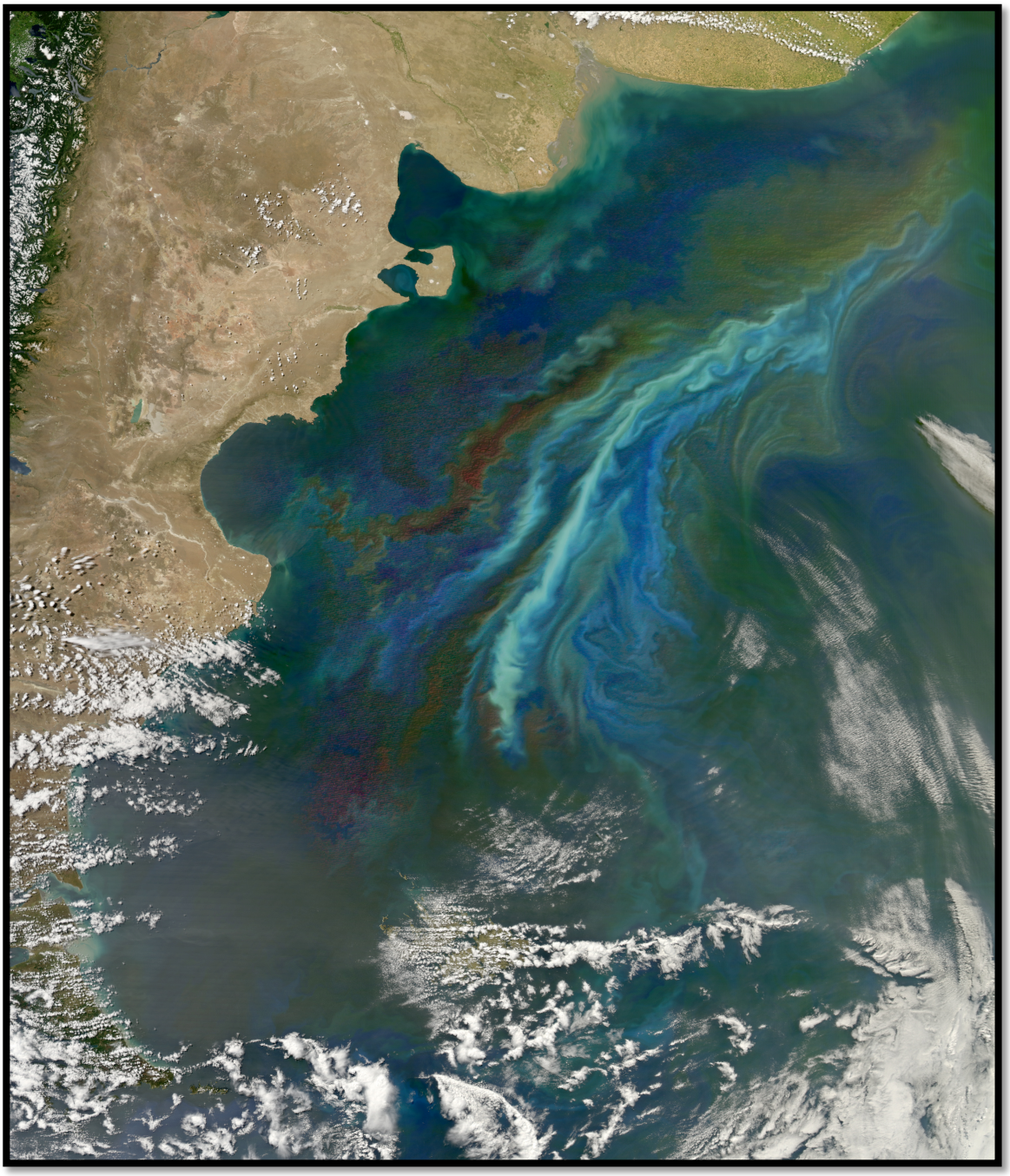

Figure 37 – Massive phytoplankton bloom off of the Atlantic coast of Patagonia on December 21, 2010 (http://earthobservatory.nasa.gov/IOTD/view.php?id=48244).

The oxygen isotopic composition of seawater in the study area shows very low values (Fig. 38) related to the relatively fresh Malvinas current, in contrast to higher isotopic composition of the saltier and warmer Brasilian current. In Figure 38 is possible to note the clear “indentation” of fresher water of Malvinas current to affect the Patagonian coast.

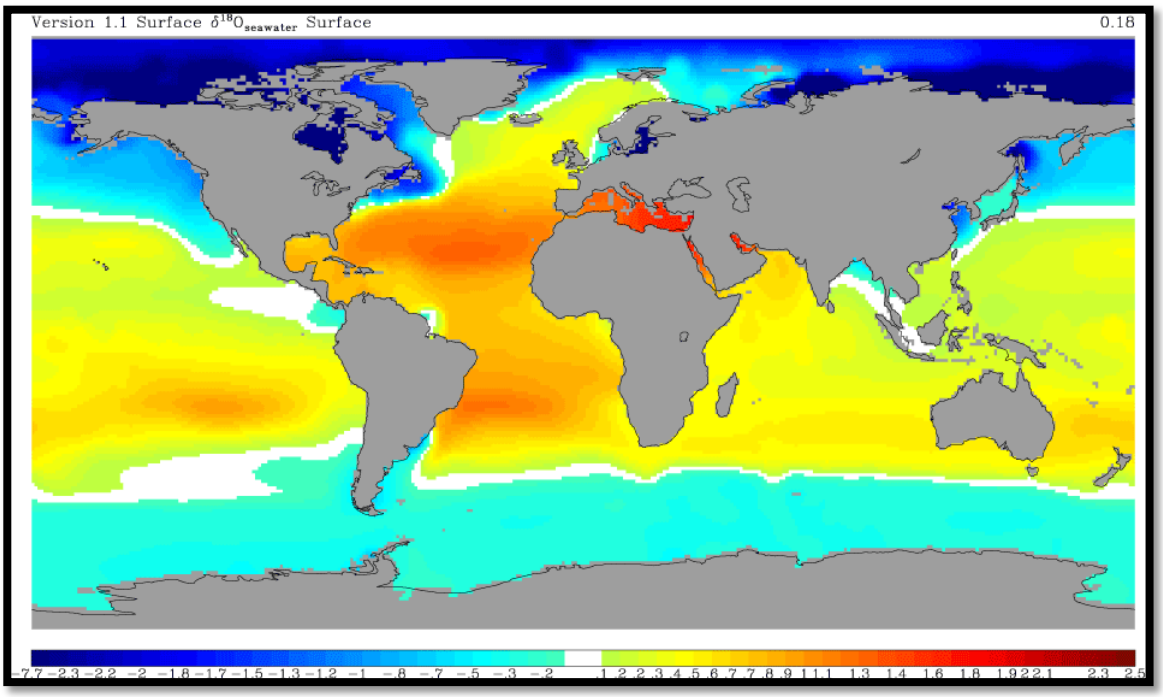

Figure 38 – Global oxygen isotopic composition of seawater (Schmidt *et al.*, 1999).

Despite sparse measurements, it is possible to observe that the carbon isotopic composition of total dissolved inorganic carbon (DIC) in the upper water column also increases from south to north showing an abrupt increase at the Brazil-Malvinas Confluence Zone (Kroopnick, 1980) .

3. PREVIOUS KNOWLEDGE ON STABLE ISOTOPES AND TRACE ELEMENTS OF MARINE MOLLUSCS OF THE ARGENTINE ATLANTIC COAST

The Atlantic coast of Patagonia has been partially studied from a geomorphological, stratigraphic and paleontological point of view, with the intent to reconstruct relative sea-level changes (Schellmann & Radtke 2000), paleobiogeographic variations of the fauna (Aguirre, 2003; Aguirre *et al*., 2005; 2006; 2009; 2011) and isostasy and tectonic component (Codignotto *et al.,* 1992; Rostami *et al.,* 2000) of the Atlantic coast, but the Quaternary marine deposits of this area are practically unexplored as climate archives (Isla & Bujalesky, 2008). Neither stable isotope ($\delta^{13}C$ and $\delta^{18}O$) nor trace elements data of modern and fossil shells are available for this area which should allow comparisons with the results obtained for the coastal deposits further north in Argentina (Aguirre *et al*., 1998; 2002) and south in Tierra del Fuego (Panarello, 1987; Obelic *et al*, 1998 Gordillo *et al*., 2010; Colonese *et al*., 2011; 2012; Saporiti *et al*., 2013).

3.1. STABLE ISOTOPES STUDIES ON MARINE MOLLUSCS OF ATLANTIC COAST OF ARGENTINA

In the Buenos Aires Province, to the north of the study area, stable isotope composition of Holocene *Mactra isabelleana* (Aguirre *et al*., 1998) and *Littoridina australis* (Aguirre *et al*., 2002) have been reported.

Aguirre *et al*. (1998) analyzed the variations in the $^{13}C/^{12}C$, $^{18}O/^{16}O$ and $^{87}Sr/^{86}Sr$ ratios of *Mactra isabelleana* collected from Holocene littoral deposits and from modern marine and estuarine environments along the coastal area of Buenos Aires Province between La Plata, on the Río de La Plata estuary, and Mar del Plata (Fig. 39).

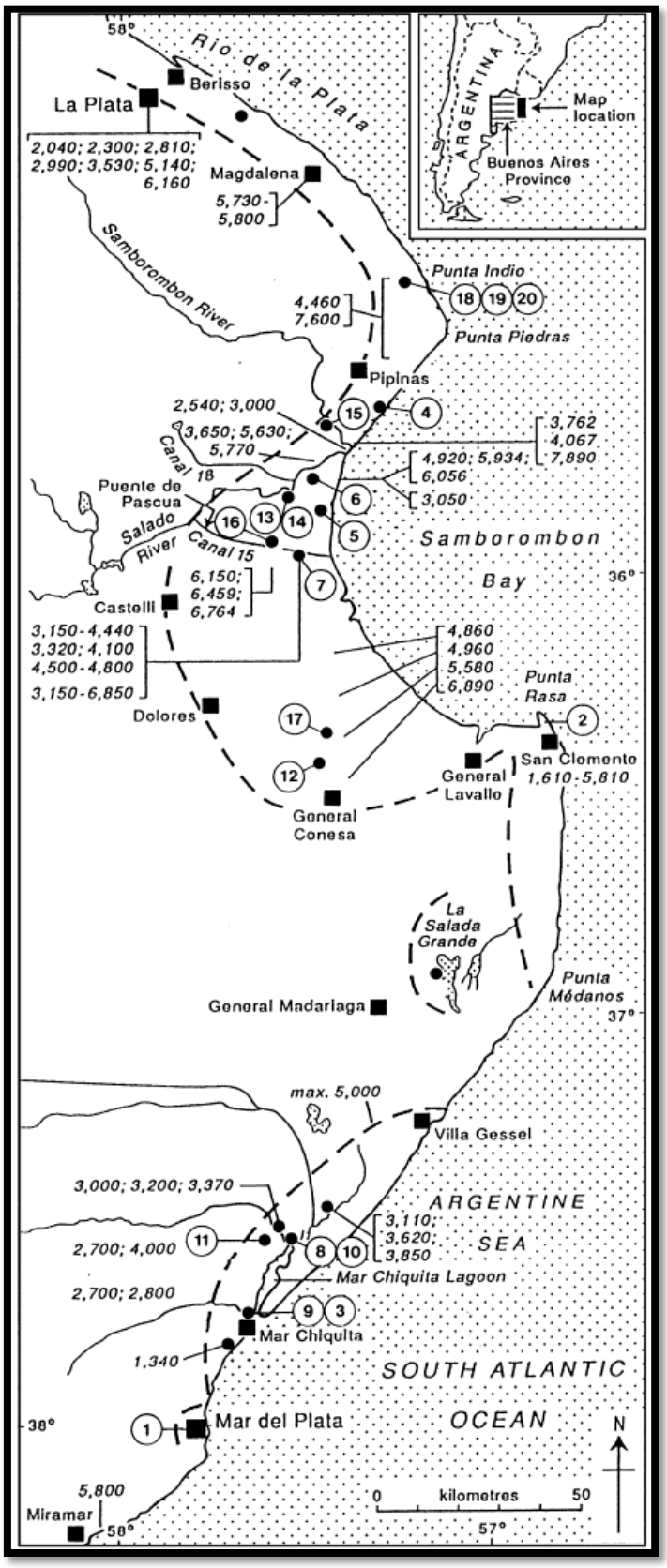

Figure 39 – Location map with position and range of age data for Holocene littoral ridges (Aguirre *et al*., 1998).

Isotopic analyses allowed to Aguirre *et al.* (1998) to identify three groups of data (Fig. 40), independent of age and partially supported by Sr data set: Group 1 shells, from Mar Chiquita, have isotopic values consistent with coastal marine waters. Group 2 shells, from the north and Samborombón Bay close to Río de La Plata, show lower $\delta^{18}O$ and generally $\delta^{13}C$ values than group 1 shells due to the fresh water influx from the Río de La Plata, that controls the isotopic composition of the coastal waters. Group 3 shells, coastal lagoonal samples from Samborombón Bay and Mar Chiquita, have low $\delta^{13}C$ values connected to abundant aquatic vegetation inside the lagoons.

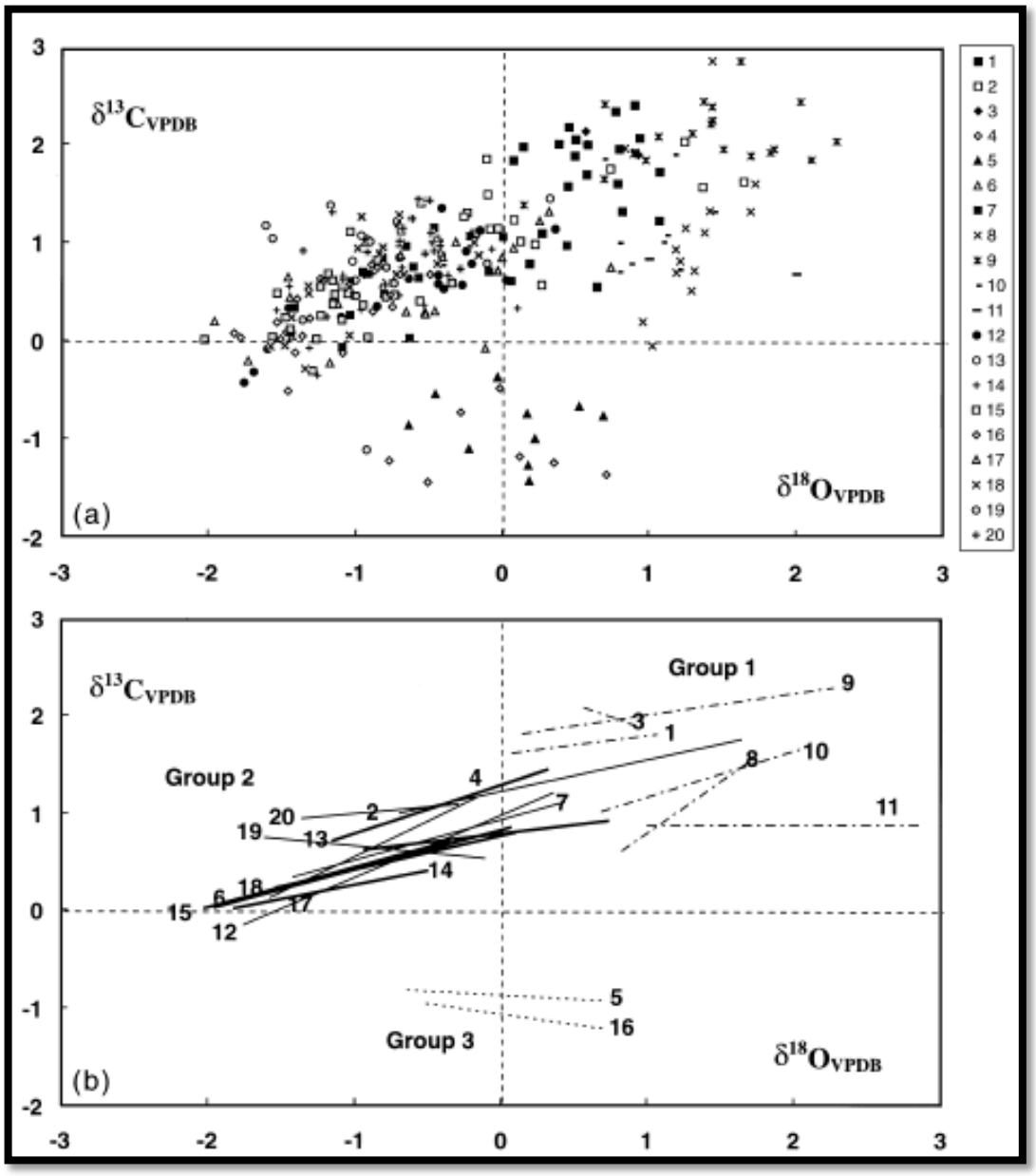

Figure 40 – Isotopic composition (a) and linear regressions (b) of the shells from 20 localities in the Buenos Aires Province (Aguirre *et al*., 1998).

Moreover, the changes in $\delta^{18}O$ and Sr values for shells from the south (Mar del Plata and Mar Chiquita) suggest that warmer temperature and a greater mixing with freshwater dominate the isotopic composition of molluscs during the Middle Holocene.

Aguirre et al. (2002) studied the isotopic composition (oxygen and carbon) of *Littoridina australis* shells collected from Holocene littoral deposits along the Buenos Aires province coastal area of Argentina (Fig. 41). *Littoridina australis* isotopic values were compared, in this work, with the isotope analyses from living freshwater *Littoridina parchappii*, collected in some Bonaerensean rivers (Bonadonna *et al*., 1999) and molluscs samples from Patagonia (Fig. 42).

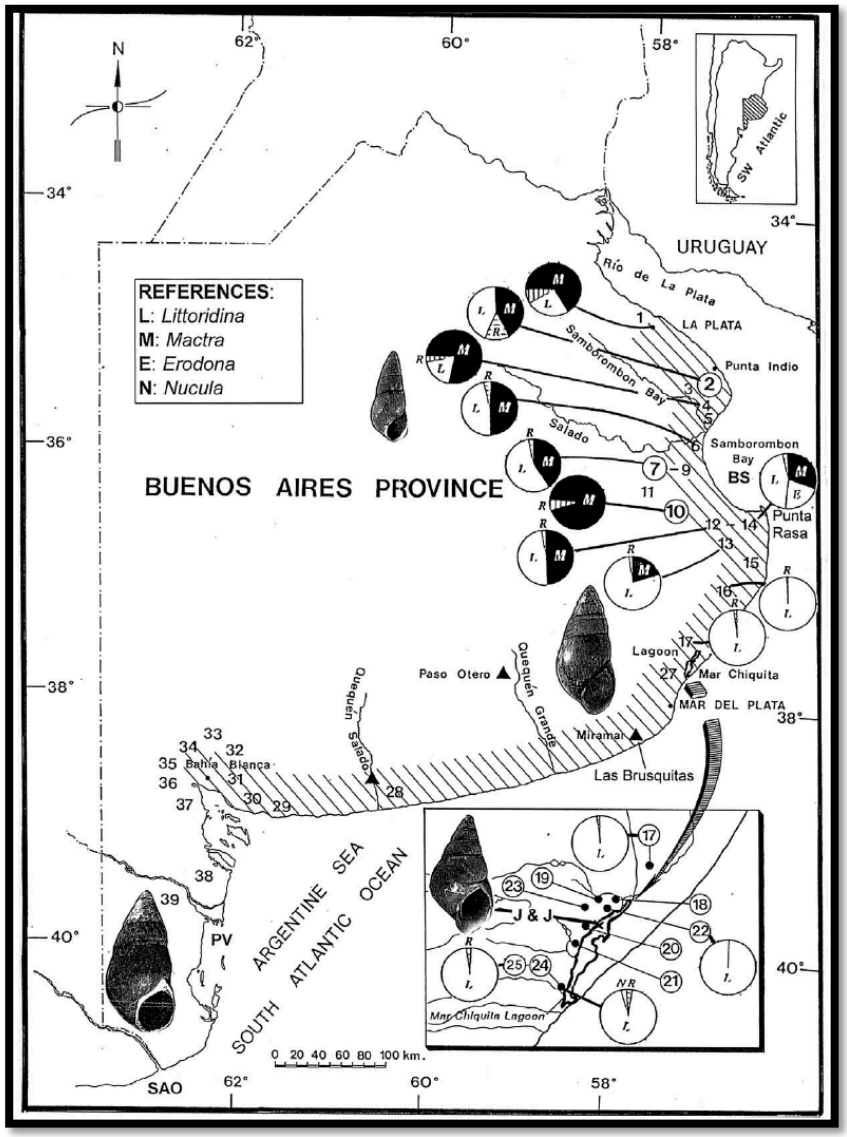

Figure 41 – Location of sampling site (Aguirre *et al*., 2002)

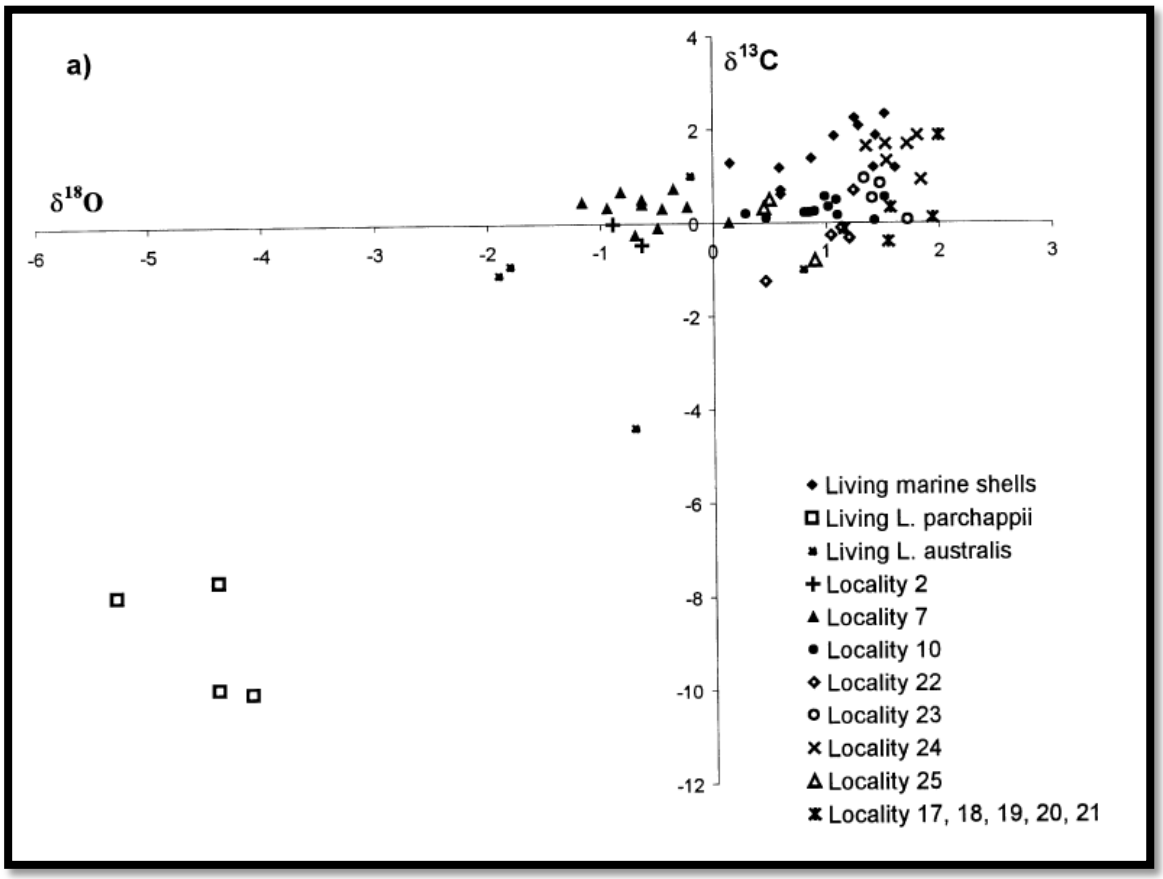

Figure 42 – Isotopic values of the Holocene *Littoridina australis,* modern *Littoridina australis, Littoridina parchapii* and marine mollusc samples (Aguirre *et al*., 2002).

Isotope data allowed the authors to define two distinct areas: the Samborombón Bay, where mixing between marine and freshwater dominates the isotopic composition of molluscs, and the Mar Chiquita lagoon, where the high isotope shell values was originated by evaporation of water that dominates the brackish environment (Fig. 43).

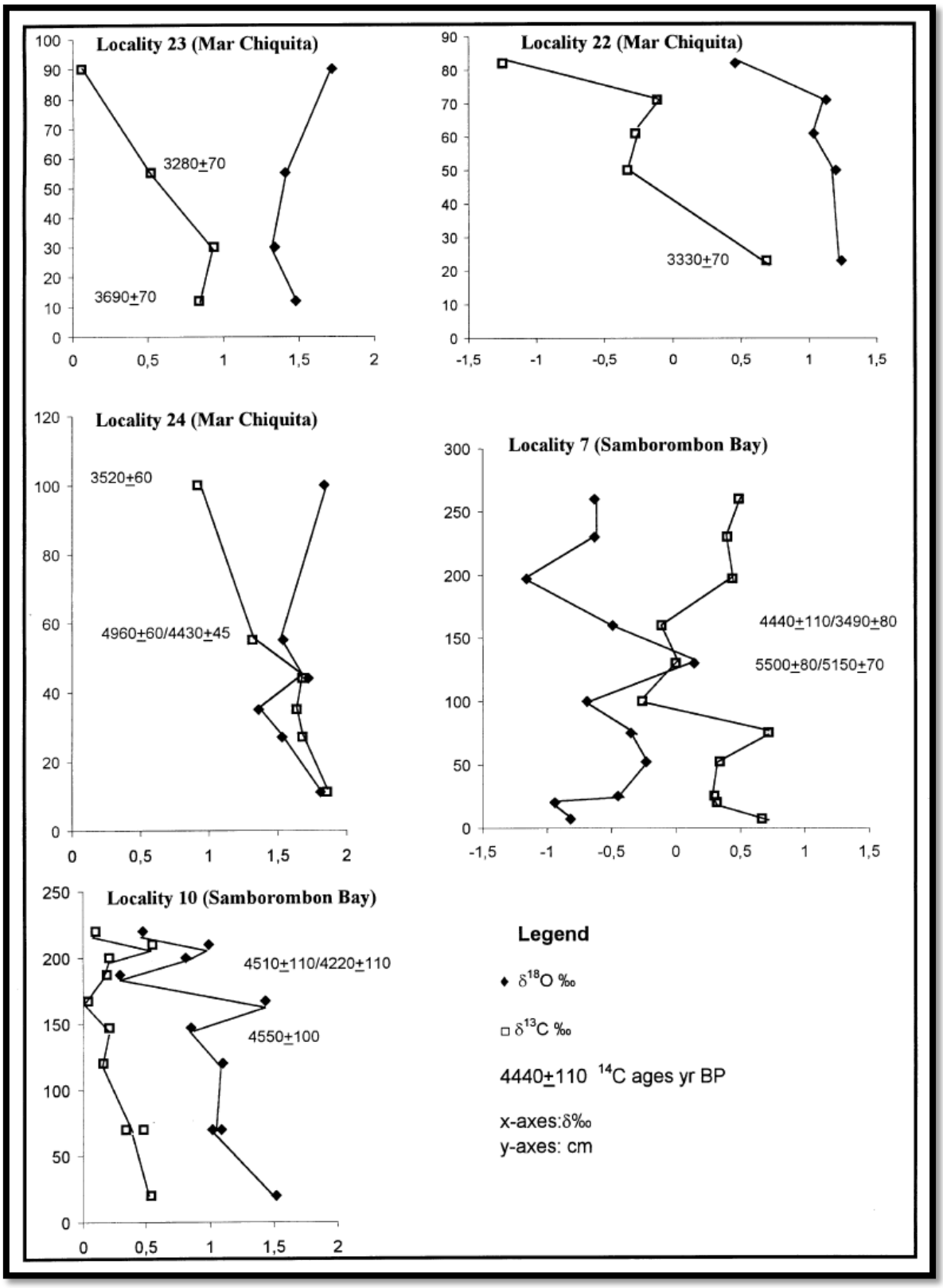

Figure 43 – Oxygen composition vs depth of some localities from Samborombón Bay and Mar Chiquita lagoon (Aguirre *et al*., 2002).

The first work on stable isotope composition of marine molluscs in the southernmost region of Argentina goes back to Panarello (1987), which studied carbon and

oxygen isotopic composition of fossil and modern molluscs from Tunel Site, in the Beagle Channel. He studied seven species (six species of molluscs and one of *Balanus*) from modern marine environment and from two Holocene shell middens (dated at 3030 ± 100 yr BP and 5630 ± 120 yr BP, respectively) and interpreted the isotopic record in terms of paleotemperature changes. According to this interpretation, results showed that the seawater temperature ca 5600 yr BP was lower than the present, while 3030 yr BP was higher.

Panarello (1987) interpreted that Holocene paleotemperatures are more related to local changes (e.g. marine stream pathway changes) and not to a worldwide trend. However, Panarello, correlates the variations in the oxygen isotopic composition only to variations in temperature, neglecting the large variability in water salinity which can be expected in the investigated area.

Still in the Beagle Channel, Obelic *et al.* (1998) analyzed the isotopic composition of *Mytilus edulis* shells from Holocene shell middens in order to reconstruct the surface water paleotemperature of the Beagle Channel in the last 6000 yr.

Obelic *et al.* (1998) observed that salinity may have influenced isotopic variations ($\delta^{18}O$ and $\delta^{13}C$) of *Mytilus edulis* shells from archaeological shell middens. These authors recognize a cooler period at 6000-5000 ^{14}C BP for the Beagle Channel, as well as a warming period at 4500-4000 ^{14}C BP (Fig. 44).

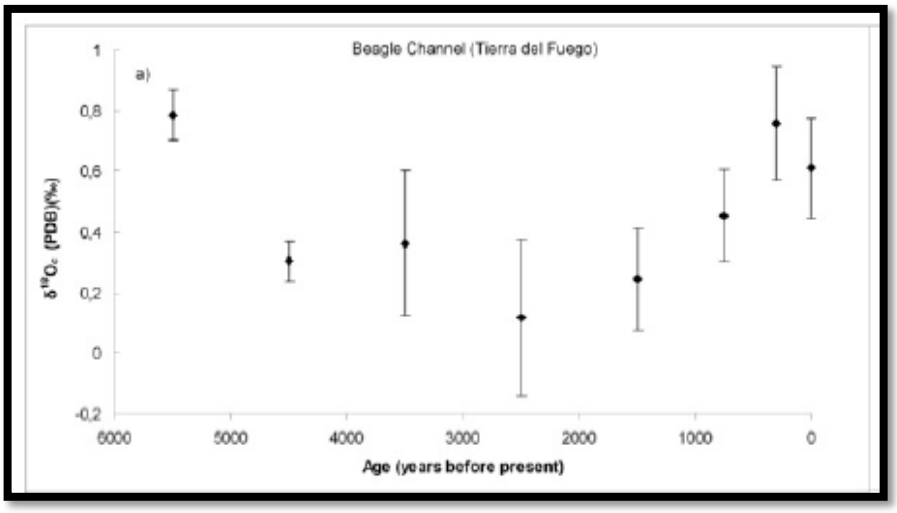

Figure 44 - $\delta^{18}O$ values of *Mytilus edulis* shells from Beagle Channel according to Obelic *et al.* (1998) (Saporiti *et al.,* 2013).

Gordillo *et al.* (2010) studied the isotopic composition ($\delta^{18}O$ and $\delta^{13}C$) of the bivalve *Hiatella* from the Beagle Channel (Fig. 45).

The isotopic values of the Holocene shells agreed with previous analyses of Panarello (1987) and Obelic *et al*. (1998). $\delta^{18}O$ of Pleistocene shells was slightly more positive and $\delta^{13}C$ more negative than the modern ones, while isotopic composition of Pleistocene *Hiatella* shells was similar to isotopic values obtained for Holocene *Hiatella* shells (Tab. 2 and Fig. 46). Gordillo *et al*. (2010) attributed this change in the isotopic composition to a deposition of the shells during the Pleistocene in a high energy marine environment during a cooler period relative to the present mean annual temperature.

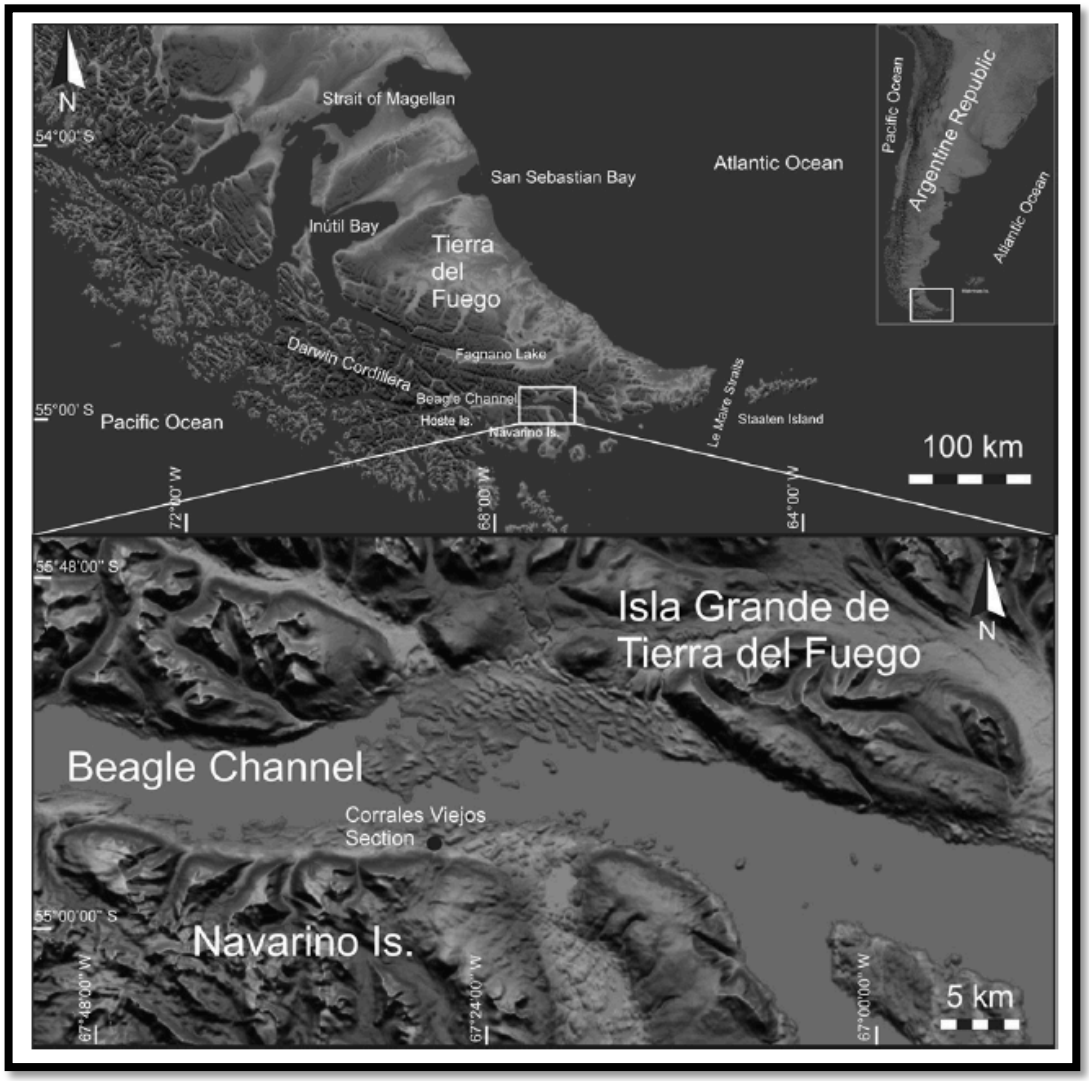

Figure 45 – Map of the study area of Gordillo *et al.* (2010).

Oxygen and carbon isotope obtained on fossil and modern *Hiatella* and *Mytilus* shells from the Beagle Channel.

Sample	Species	Age	$\delta^{13}C$ ‰	$\delta^{18}O$ ‰	Source
BG2	*Hiatella*	Modern/recent shell	0.4 ± 0.10	0.4 ± 0.10	This work
LR3	*Hiatella*	Holocene shell (ca. 7500)	1.6 ± 0.10	0.8 ± 0.10	This work
ER	*Hiatella*	Holocene shell (ca. 4000 yr BP)	1.5 ± 0.10	1.5 ± 0.10	This work
CV1	*Hiatella*	Pleistocene shell	1.1 ± 0.10	1.3 ± 0.10	This work
CV2	*Hiatella*	Pleistocene shell	1.1 ± 0.10	1.3 ± 0.10	This work
BG1	*Hiatella*	Modern/recent shell	1.97 ± 0.24	1.05 ± 0.10	Gordillo (1995)
AK	*Hiatella*	Holocene shell (ca. 4400 yr BP)	1.48 ± 0.18	1.29 ± 0.06	Gordillo (1995)
LR2	*Hiatella*	Holocene shell (ca. 5900 yr BP)	1.36 ± 0.10	0.23 ± 0.10	Gordillo (1995)
CB1	*Mytilus*	Modern shell / sea water	0.8 ± 0.1	0.3 ± 0.1	Panarello (1987)
CB2	Several species	Modern shells / sea water	1.6 ± 0.1[a]	0.87 ± 0.1[a]	Panarello (1987)
CB3	*Mytilus*	Modern shells/ pure sea water	−0.08 ± 0.31	0.17 ± 0.27	Obelic et al. (1998)
CB4	*Mytilus*	Modern shells/ influenced by freshwater	−0.35 ± 0.45	−0.16 ± 0.38	Obelic et al. (1998)

[a] Average values

Table 2 – Isotopic composition of *Hiatella* and *Mytilus edulis* shells from the Beagle Channel (Gordillo *et al.*, 2010).

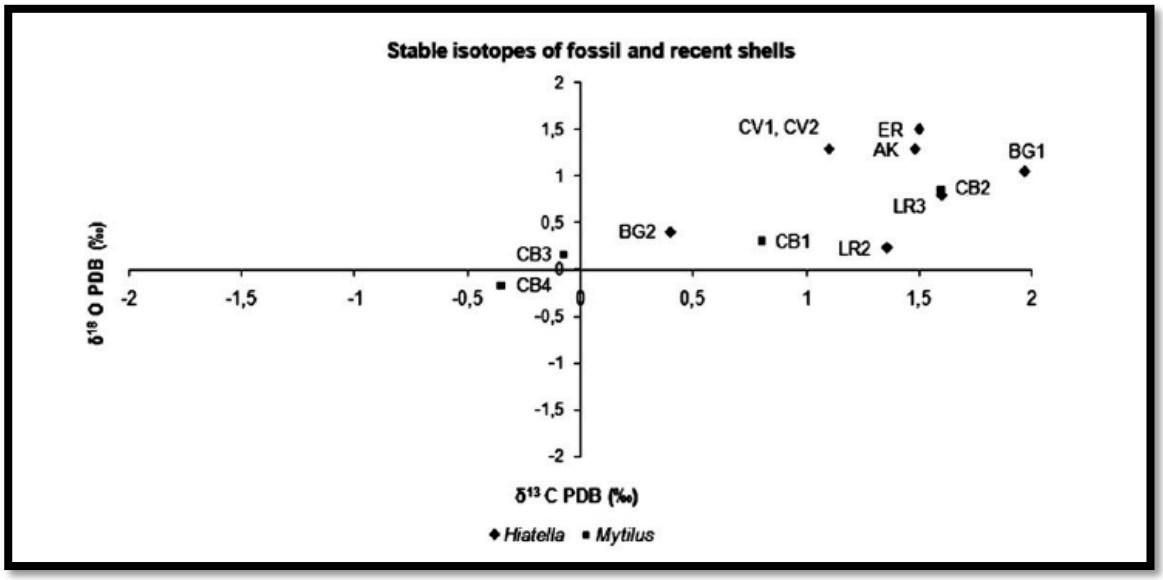

Figure 46 – Oxygen and carbon isotopic composition of *Hiatella* and *Mytilus* shells from the Beagle Channel. See Table 2 for abbreviations (Gordillo *et al*., 2010).

Colonese *et al.* (2011), instead, used the oxygen isotopic composition of *Nacella magellanica* shells collected from modern environment and shell middens along the Beagle Channel coast (Fig. 47) for sclerochronological studies, in order to reconstruct seasonal exploitation patterns of this species and to provide new insight into Yamana (a hunter-gatherer- fisher group which lived in Tierra del Fuego) coastal mobility and subsistence strategies.

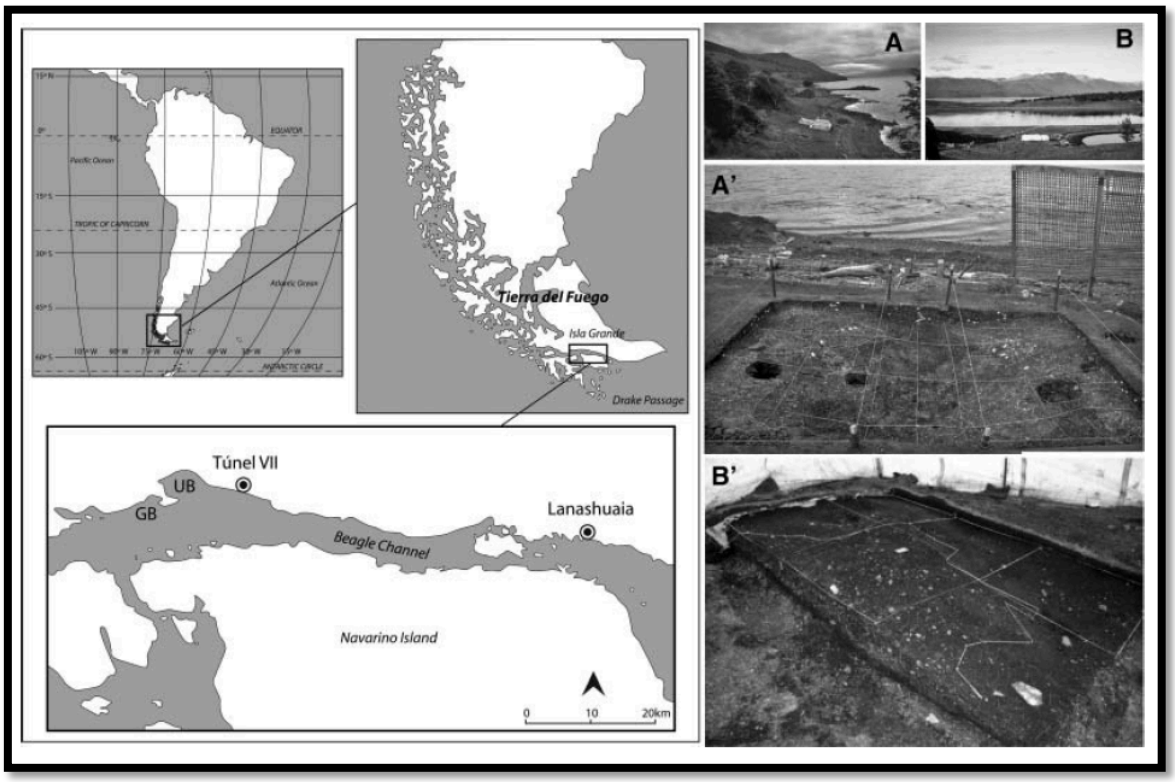

Figure 47 – Sample location of the shell middens (Tunel VII = A and A'; Lanashuaia = B and B') and of living specimens (GB = Golondrina Bay and UB = Ushuaia Bay) (Colonese *et al.*, 2011).

According to the authors the oxygen isotopic data indicate that *Nacella magellanica* was gatered in different seasons (Fig. 48) and that in the nineteenth century, Yamana people continuously occupied the Beagle Channel coast by means of short-lived campsites.

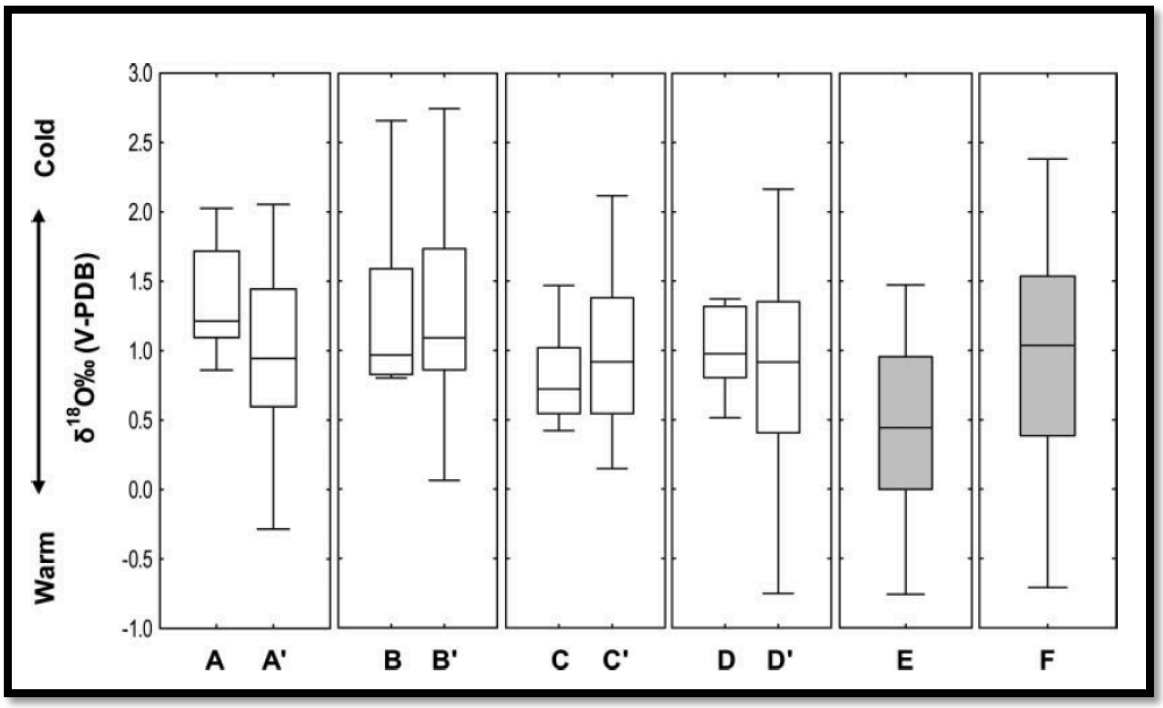

Figure 48 – Quartile distribution of archaeological shell-edge $\delta^{18}O$ from Tunel VII occupation phase in autumn-winter (A), spring (B), autumn (C) and Lanashuaia (D). Quartile distributions of ontogenic $\delta^{18}O$ values from Tunel VII occupation phase in autumn-winter (A'), spring (B'), autumn (C') and Lanashuaia (D') are used as seasonal reference. Quartile distribution of ontogenic $\delta^{18}O$ values of one modern shell collected in front of Lanashuaia (E) and of modern shells collected montly (F) are used to compare main $\delta^{18}O$ differences (Colonese *et al*., 2011).

With the same purposes Colonese et al. (2012) studied the oxygen isotopic composition of *Nacella deaurata* from Beagle Channel (Fig. 49).

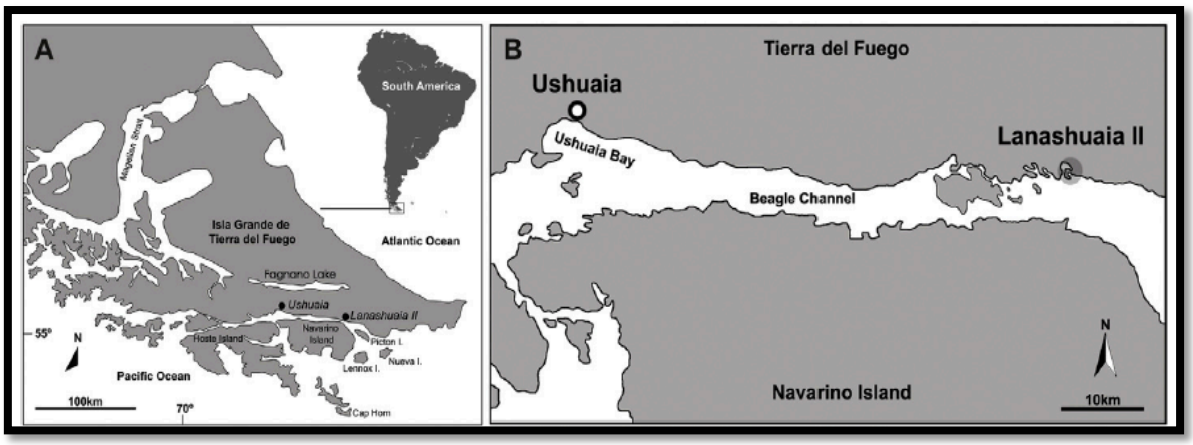

Figure 49 – Geographic position of the Beagle Channel (A) and location of the archaeological shell midden Lanashuaia II (B) (Colonese *et al.*, 2012).

Colonese *et al.* (2012) observe that sequential shell $\delta^{18}O$ of modern species tracks seasonal changes of sea surface temperature and ambient water $\delta^{18}O$. Moreover, the comparison of shell $\delta^{18}O$ profiles of *Nacella deaurata* and *Nacella magellanica*

suggests the occurrence of distinct growth rate and physiological adaptations between the species, while shell $\delta^{18}O$ of specimens collected from shell middens suggests that molluscs were exploited predominantly in winter. Results also indicate that specimens of *Nacella deaurata* experienced similar environmental conditions of present day at ca. 1320 yr BP (Fig. 50).

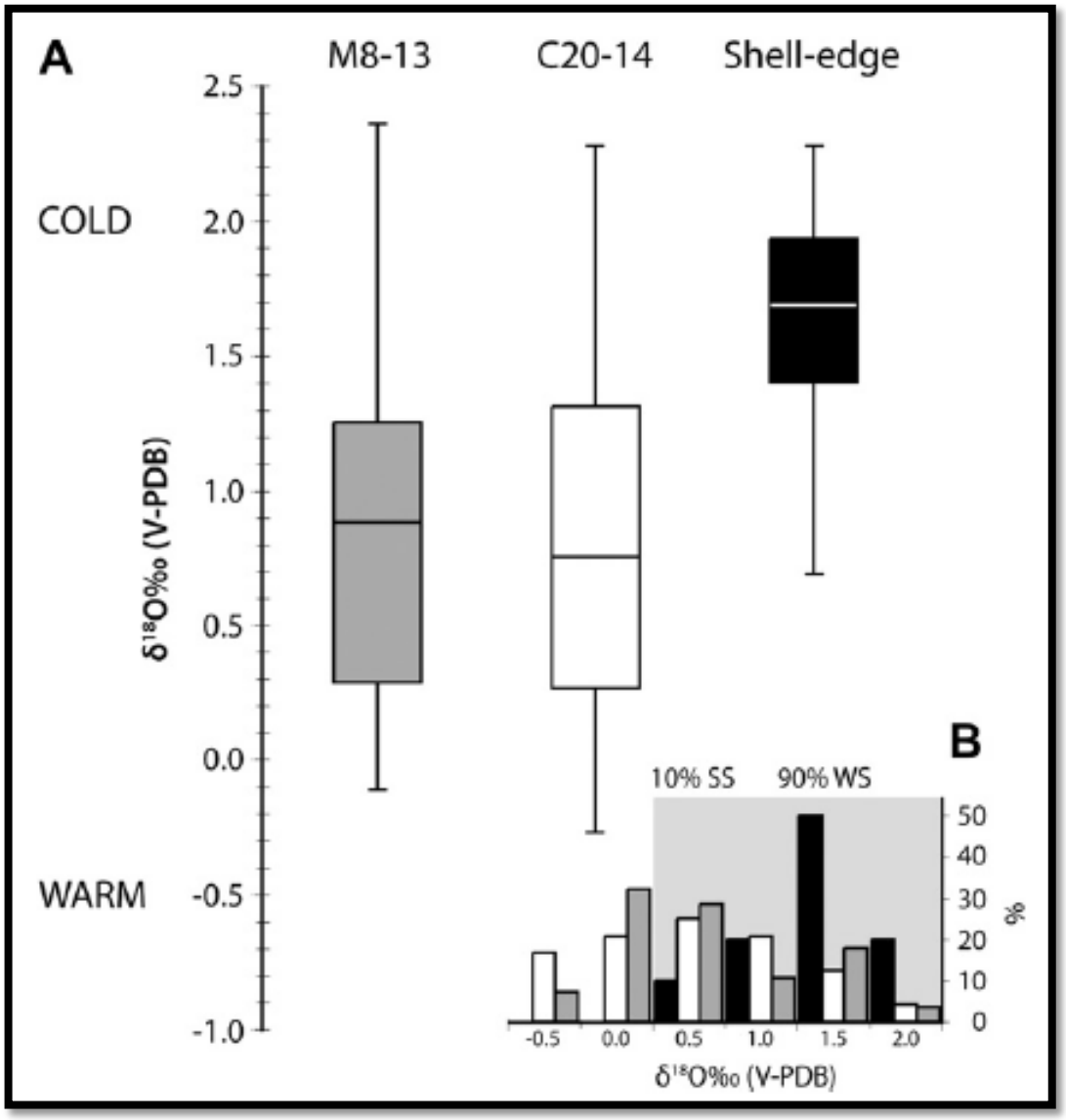

Figure 50 – A) Quartile distribution of shell-edge $\delta^{18}O$ values of *N. deaurata* from Lanashuaia II (M8-13 = modern *N. deaurata* specimen; C20-14 = archaeological *N. deaurata* specimens as comparisons). B) frequency distribution of shell-edge $\delta^{18}O$ values and sequential values of modern and archaeological specimens Colonese *et al.*, 2012).

Saporiti *et al.* (2013) used $\delta^{18}O$ composition of *Aulacomya atra atra* and *Mytilus edulis* shells collected from Beagle Channel and central-northern Patagonia archaeological sites as proxy for SST and to compare the $\delta^{18}O$ patterns with the patterns of resource exploitation by hunter-gatherers.

$\delta^{18}O$ values suggest that sea surface temperature increased both north and south at the beginning of the late Holocene and that was slightly higher than at present during most of that period, except during the Little Ice Age, showing similar values to those recorded at the end of middle Holocene (Figs. 51-52). Moreover Saporiti *et al.* (2013) conclude that changes in sea surface temperature are unlikely to be the major driver of the resource-exploitation patterns.

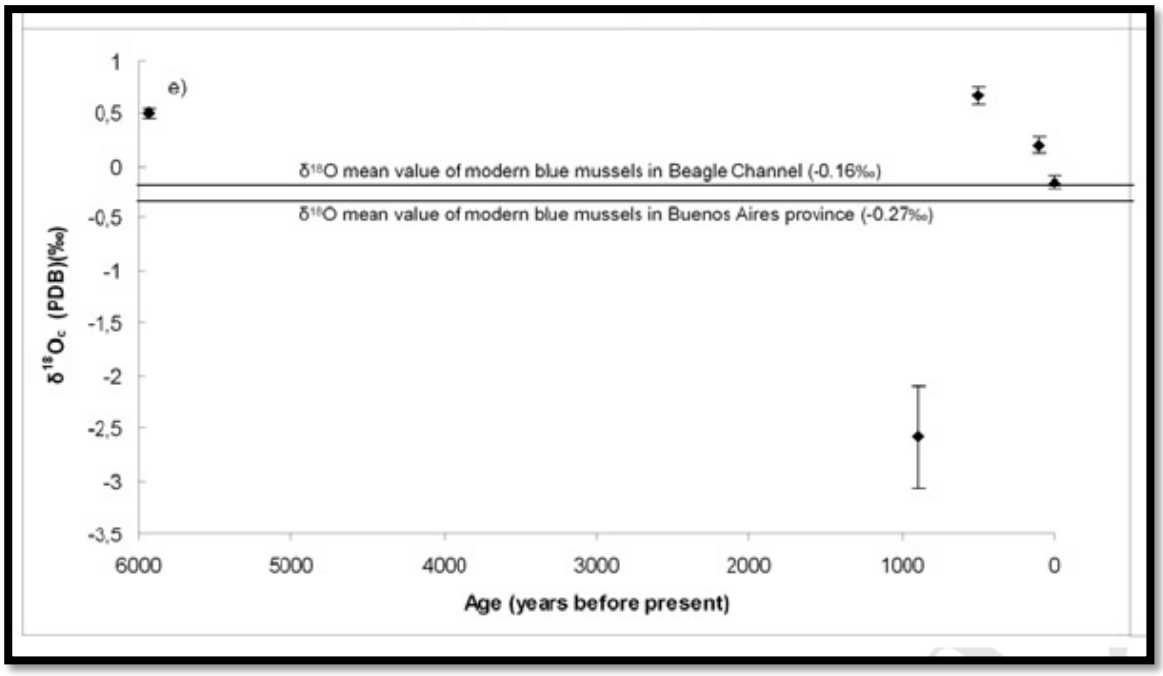

Figure 51 – Temporal profile of oxygen isotopic composition in bivalve shells from Beagle Channel according to Saporiti *et al.* (2013).

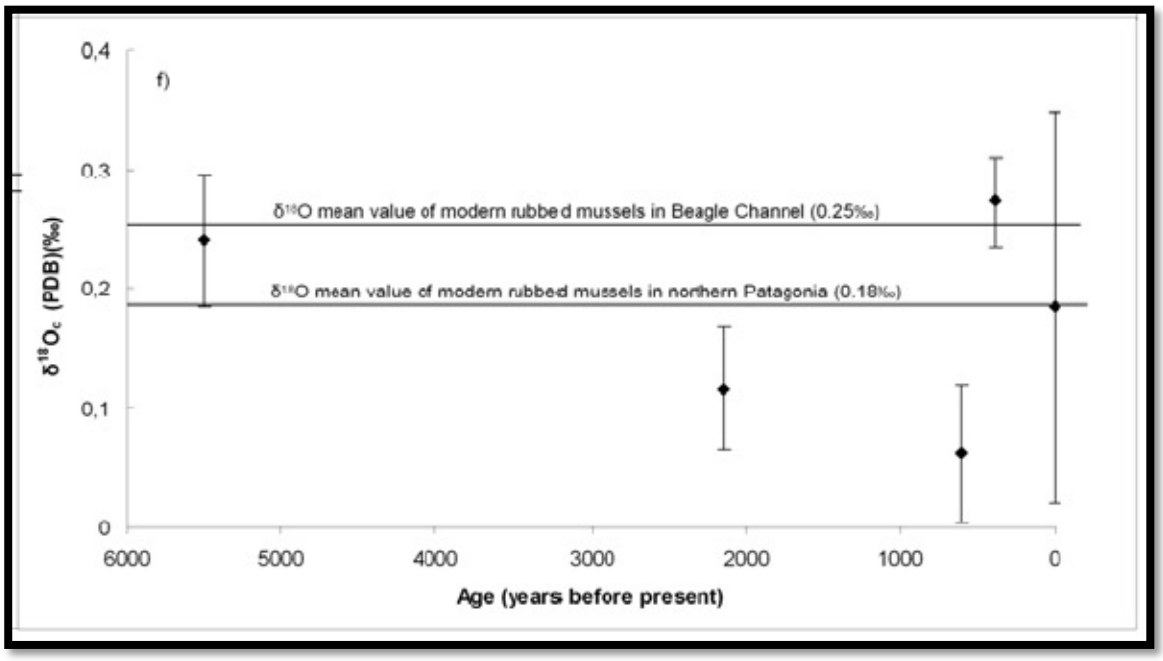

Figure 52 – Temporal profile of oxygen isotopic composition in bivalve shells from central-northern Patagonia according to Saporiti *et al.* (2013).

3.2. STABLE ISOTOPES FOR PALEOCLIMATIC STUDIES FROM OTHER ARCHIVES FROM ARGENTINA

3.2.1. Continental mollusc shells

In the Buenos Aires Province and Patagonia region Bonadonna *et al.* (1995; 1999) analyzed the stable isotope composition of fossil and living shells of terrestrial and freshwater molluscs for paleoclimatic and paleoenvironmental reconstructions.

Bonadonna *et al.* (1995) studied the carbon and oxygen composition of continental and littoral carbonatic shells from the Buenos Aires province to reconstruct the paleoclimate and the stratigraphy of the area during the last 30 ka.

Isotopic values seem to indicate a warm and dry environment around 30 ka, followed by a cold and dry environment before 10 ka, while temperate and humid conditions prevailed after 10 ka, with a humid event at 8-6 ka.

Bonadonna *et al.* (1999) used the isotopic composition ($\delta^{18}O$ and $\delta^{13}C$) of fresh water and terrestrial molluscs of the last 30 ka from Bonaerense and Patagonia regions in order to obtain paleoenvironmental and paleoclimatic information

According to Bonadonna *et al.* (1999), the isotopic values suggest that arid conditions occurred between 35 and 15 ka BP and warmer conditions around 35-25

ka BP. A new phase comparable with the present meteorological and climatic conditions began around 9 ka BP and a trend toward slightly arid seems to start after 5 ka.

3.2.2. Marine microfossils

Chiessi *et al.* (2007) studied the stable isotopic compositions of planktonic foraminifera as a proxy for the position of the Brazil- Malvinas Confluence in the Argentine Basin.

According to the authors the oxygen isotopic values of *Globorotalia inflata* and *G. truncatulinoides*, which result the most reliable indicators of the latitudinal position of the confluence zone, show a sharp gradient of 2‰ at the Brazil-Malvinas Confluence with stable values north and south of the confluence (Fig. 53).

The $\delta^{13}C$ of *Globigerinoides ruber, Globigerinoides trilobus, Globorotalia inflata* and *Globorotalia truncatulinoides* shows no significant trend across the front (Fig. 54).

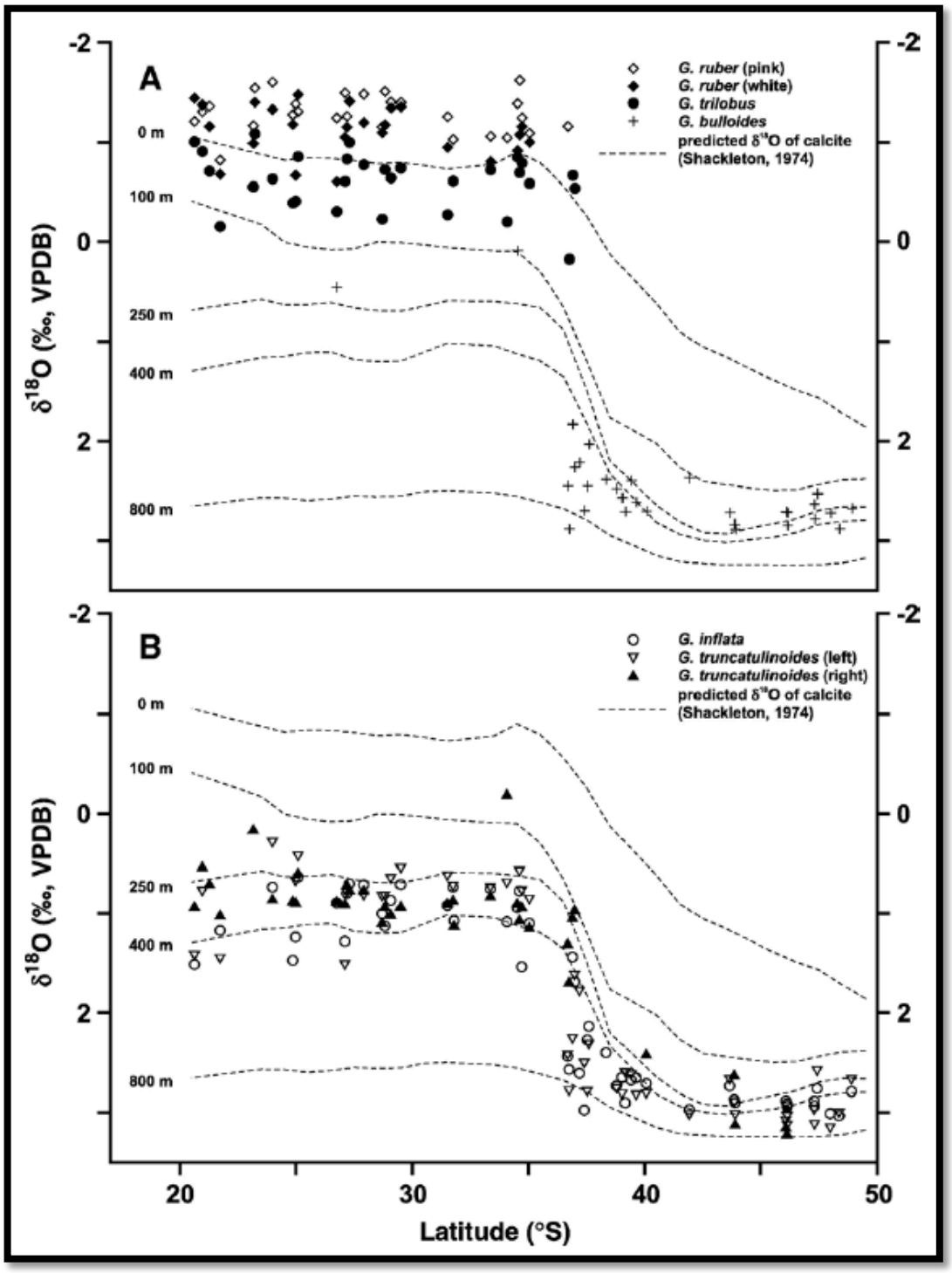

Figure 53 – Latitudinal variations in $\delta^{18}O$ of foraminifera according to Chiessi *et al*. (2007). Dashed lines represent the predicted $\delta^{18}O$ of calcite at selected depth levels.

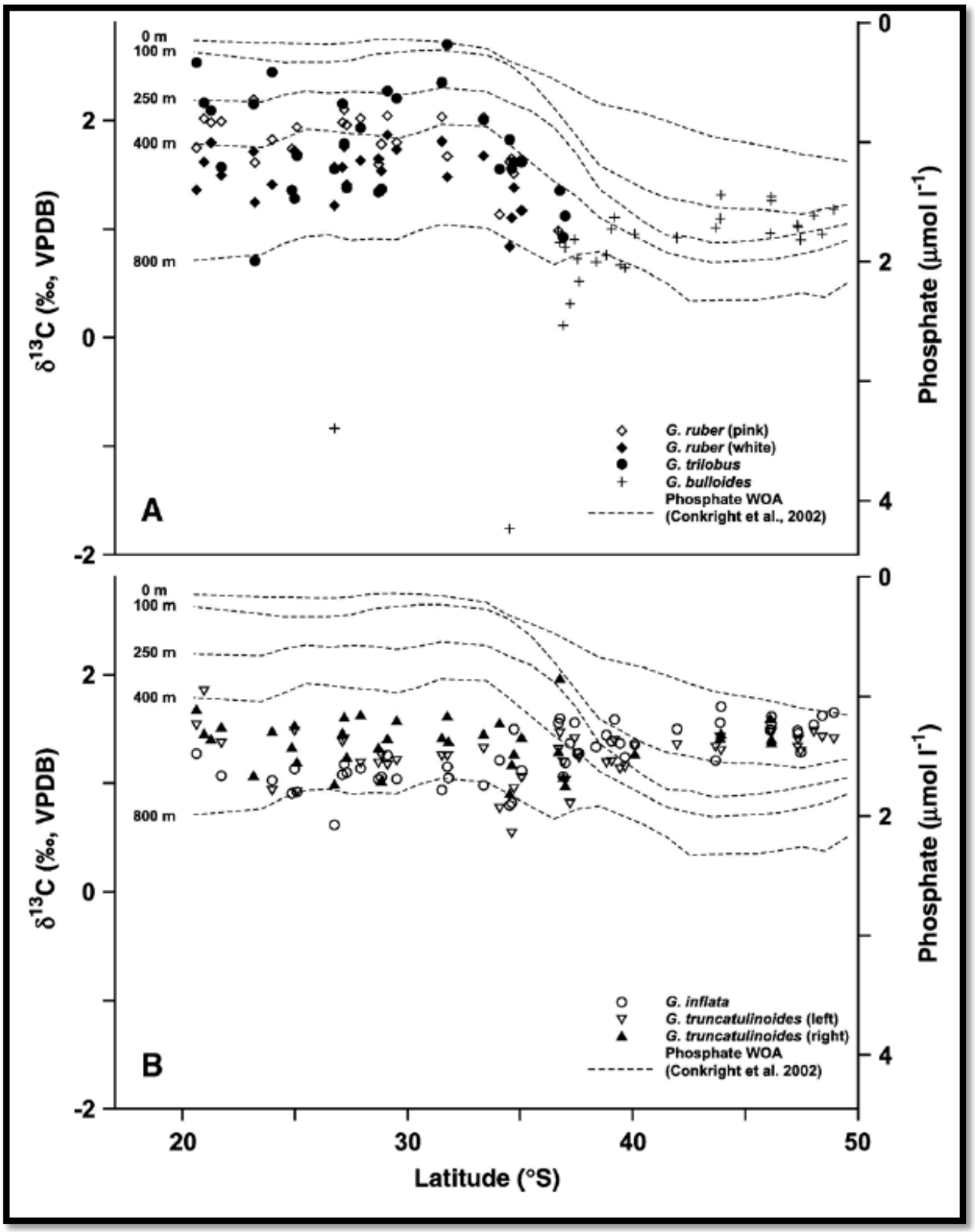

Figure 54 – Observed $\delta^{13}C$ values of foraminifera according to Chiessi *et al*. (2007). The isotopic values are compared with the latitudinal variations in phosphate concentration at selected depth levels.

3.2.3. Sediment cores from lakes

In the last twenty years there has been a major increase of limnogeological studies across different areas of Patagonia holding multiproxy results (e.g. Ariztegui *et al.*, 2008).

Markgraf *et al.* (2003), among the others, used a multyproxy approach, which includes stable isotopes on ostracodes, on two sediment cores dated to the Holocene from the Lago Cardiel (Fig. 55), located in the Extra-Andean Patagonian plateau of Argentina, for reconstructing the paleoenvironment and the paleoclimate of southern Patagonia during the Holocene.

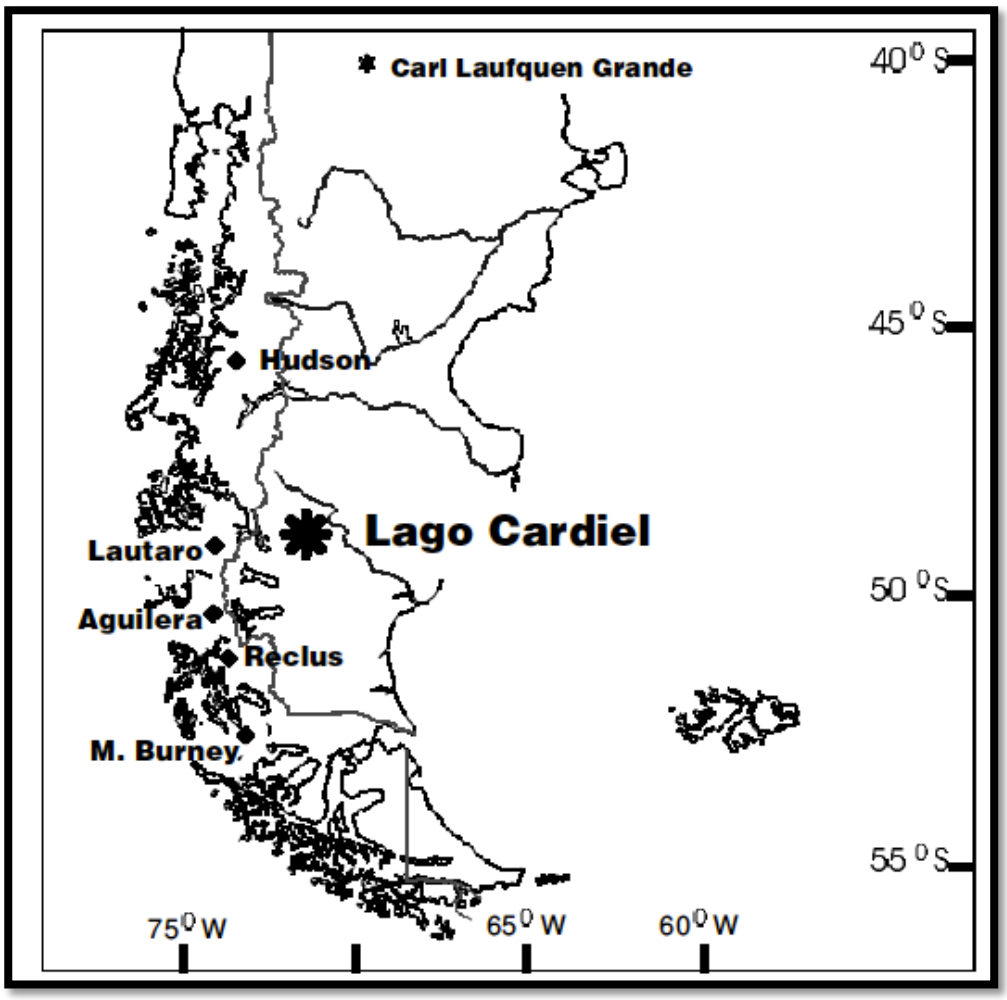

Figure 55 – Lago Cardiel location map from Markgraf *et al.* (2003).

The multyproxy analyses of sedimentary cores combined with seismic stratigraphy data indicate substantial lake-level changes during the late Pleistocene and Holocene (Fig. 56). Sedimentological and environmental indicators show lake levels higher than the present conditions during the early Holocene, following a lake-level

rise after a desiccation phase prior to 11 ka BP. After ca 6000 yr BP lake levels were generally lower but with repeated fluctuations. These changes support the view that the southern westerlies were focused north of latitude 50° S during the early Holocene, enabling the Antarctic cold fronts to bring easterly moisture to southern Patagonia, whereas during the late Holocene the westerly stormtracks shifted seasonally, with less and more variable moisture in the region.

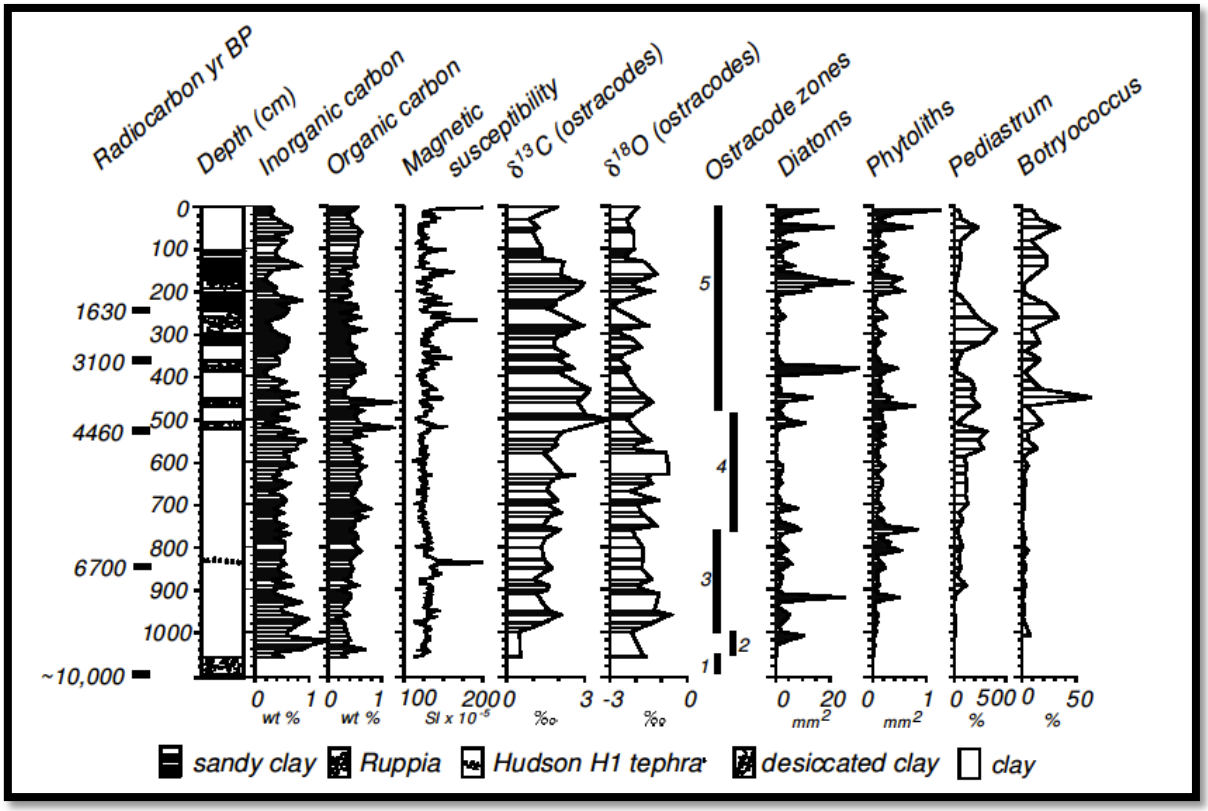

Figure 56 – Sedimentologic and paleoenvironmental record from a core from Lago Cardiel (Markgraf *et al.,* 2003).

3.2.4. Carbonatic crusts

Bonadonna *et al.* (1995) analyzed stable isotope composition of carbonatic crusts ("toscas" in the local literature) collected from the marine cliffs in the southeastern area of the Buenos Aires Province.

The isotopic values, very homogeneous for the oxygen and more variable for the carbon, indicate an evaporation influenced environment in a subhumid climate.

3.3. TRACE ELEMENT STUDIES ON MARINE MOLLUSCS OF ATLANTIC COAST OF ARGENTINA

Along the Atlantic coast of Patagonia, no trace element study on molluscs or other types of animals was performed in order to understand the climate and environmental variations of the area during the time.

The studies carried out on trace element concentrations within molluscs were performed mostly to understand the degree of pollution in seawater (e.g. Ribeiro Guevara *et al.,* 2004; Astorga España *et al.*, 2005; 2007; Gil *et al*., 2006; Conti *et al*., 2011; 2012; Duarte *et al.*, 2012).

Soldati *et al.* (2009) evaluated the seasonal periodicity of minor and trace elements of the freshwater mussel *Diplodon chilensis patagonicus* from Lago Steffen, situated on the west side of the Andean Cordillera.

They conclude that Mn, Sr and Ba are preferentially accumulated during the summer, while higher concentrations of Mg are present in the winter bands.

4. STABLE ISOTOPE AND TRACE ELEMENT GEOCHEMISTRY

4.1. STABLE ISOTOPES

4.1.1. General concepts

The term of *isotopes* comes from the Greek (meaning equal places) and implies that the various isotopes of the same element occupy the same position in the Periodic Table.

Isotopes are atoms of a given element whose nuclei contain the same number of protons, but a different number of neutrons and thus are ultimately characterized by the same atomic number (Z), but by a different mass number (A). Isotopes are usually denoted by writing the mass number as a superscript before the chemical symbol of the element (e.g. ^{2}H for deuterium).

Stable isotopes, whose processes show radioactive decay rates so low as to be insignificant in the time of observation, are about 300 (Hoefs, 2009).

For the light elements one isotope is prevailing, the others are present only in trace amounts.

Stable isotopes of oxygen and carbon, analyzed in this thesis, are three (^{16}O, ^{17}O and ^{18}O) and two (^{12}C and ^{13}C) respectively.

The isotopes of an element exhibit a broadly similar chemical behavior, having the same number of electrons in the same orbital position, but with a different physical behavior due to the difference in mass between the different species. However, not all chemical processes in the different isotopes of the same element behave exactly in the same way (for example, the rate of reaction between two isotopic forms is slightly different). The mass differences are particularly important in light elements (low numbers in the Periodic Table). Molecules vibrate with a fundamental frequency, which depends on the mass of the isotopes from which it is composed. The resultant differences in dissociation energy of the light and heavy isotopes imply that bonds formed by light isotopes are weaker than those formed by heavy

isotopes. Hence, molecules comprised of the light isotopes react more easily than those comprised of the heavy isotopes.

The disproportionate distribution of isotopes of the same element during a chemical reaction between two substances or between two phases of the same substance is defined isotope fractionation. The degree of isotopic fractionation is closely related to the difference in mass between the isotopes. Consequently, other conditions being equal, the isotopic fractionations will be more relevant to the isotopes of the light elements rather than heavy ones. This phenomenon is, in fact, related to the different bond energy characterizing the isotopes of the elements, whereby those with mass number greater require a higher amount of energy to dissociate than the light isotopes.

The partitioning of stable isotopes (e. g. ^{18}O and ^{16}O) within a two-phase system is described by an isotope fractionation factor because the isotope ratio of a given shared element can be different in the two phases. For example, for the precipitation of calcite from an aqueous solution corresponds to:

$$\alpha_{CaCO_3-H_2O} = (\frac{^{18}O}{^{16}O})_{CaCO_3} / (\frac{^{18}O}{^{16}O})_{H_2O}$$

The fractionation can be equilibrium or kinetic. Equilibrium fractionation describes isotopic exchange reactions occurring between two different phases of a compound at a rate maintaining equilibrium, as with the transformation of water vapor to liquid precipitation.

This type of reaction can be described as:

$$^1A + {}^2B \Leftrightarrow {}^2A + {}^1B$$

where A and B are the phases, and the superscripts 1 and 2 are isotopes.

The equilibrium constant may be expressed by:

$$K = \frac{\left[{}^1B\right]\left[{}^2A\right]}{\left[{}^2B\right]\left[{}^1A\right]}$$

This can also be expressed as a ratio of the isotopes in each phase:

$$R_A = \frac{\left[{}^2A\right]}{\left[{}^1A\right]} \text{ and } R_B = \frac{\left[{}^2B\right]}{\left[{}^1B\right]}$$

$$K = \frac{R_A}{R_B} = \alpha_{A-B}$$

where α_{A-B} is the fractionation factor, the ratio of the numbers of any two isotopes in one chemical compound A divided by the corresponding ratio for compound B (Urey, 1947).

Other factors come into play to influence equilibrium fractionation and isotope effects, chiefly vibrational energy, related to the zero-point energy difference and dependent on temperature. Different isotopes have different zero point energies for the vibrational mode of a bond. Temperature is a measure of energy in a system, translated to the energy of the bond. The zero point of energy changes with temperature increases. The difference in zero point energy between two isotopes decreases. Typically, the heavier isotope has a lower zero point energy, thus it takes more energy to break the bond of a heavy isotope compared to the light isotope. Processes of equilibrium fractionation are essentially temperature dependent. One may expect greater isotopic fractionation at low temperatures, and no isotopic fractionation at very high temperatures.

Kinetic fractionation is fractionation that is unidirectional, where equilibrium is not attained. Kinetic effects cause deviations from the simple equilibrium processes due to different rates of reactions for the various isotopic species. This type of fractionation applies to evaporation of surface waters and to most biogeochemical reactions, where the lighter isotope is faster reacting and becomes concentrated in the products.

While the absolute abundances of minor isotopes cannot be determined accurately, it is possible to get quantitative results by comparing the result given for a known external standard with that for the unknown sample. These differences in isotopic ratios, known as δ value, are defined as:

$$\delta = \frac{R_{sam} - R_{std}}{R_{std}} * 1000$$

Where *sam* is the sample values and *std* is the standard value. These variations in composition are given in delta (δ) notation, and are reported in parts per thousand (per mille, ‰). R stands for the heavy/light ratio between the abundances of any two isotopes (e.g. $^{18}O/^{16}O$). A positive δ value indicates enrichment in the heavy

isotope, relative to the standard, and conversely, depletion is shown by a negative δ value.

For two compounds A and B the δ-values and fractionation factor α are related by:

$$\delta_A - \delta_B = \Delta_{A-B} \approx 10^3 \ln \alpha_{A-B}$$

In order to compare isotopic data from different laboratories, an internationally accepted set of data was selected (Tab. 3).

Standard	Ratio	Accepted value ($\times 10^6$) (with 95% confidence interval)	Source
SMOW	D/H	155.76 ± 0.10	Hagemann et al. (1970)
	$^{18}O/^{16}O$	$2{,}005.20 \pm 0.43$	Bærtschi (1976)
	$^{17}O/^{16}O$	373 ± 15	Nier (1950), corrected by Hayes (1983)
PDB	$^{13}C/^{12}C$	$11{,}237.2 \pm 2.9$	Craig (1957)
	$^{18}O/^{16}O$	2067.1 ± 2.1	
	$^{17}O/^{16}O$	379 ± 15	
Air nitrogen	$^{15}N/^{14}N$	$3{,}676.5 \pm 8.1$	Junk and Svec (1958)
Canyon Diablo Troilite (CDT)	$^{34}S/^{32}S$	$45{,}004.5 \pm 9.3$	Jensen and Nakai (1962)

Table 3 – Absolute isotopic ratios of international standards (After Hayes, 1983).

In addition, to meet the shortage of Primary Reference Standards, new worldwide standards have been created and distributed by the IAEA. They are natural or synthetic compounds following the isotopic composition of the primary standards in respect of which have been calibrated (Tab. 4).

Element	Standard	Standard
H	Standard Mean Ocean Water	V-SMOW
B	Boric acid (NBS)	SRM 951
C	Belemnitella americana from the Cretaceous Peedee formation, South Carolina	V-PDB
N	Air nitrogen	N2 (atm.)
O	Standard Mean Ocean Water	V-SMOW
Si	Quartz sand	NBS-28
S	Troilite (FeS) from the Canyon Diablo iron meteorite	V-CDT
Cl	Seawater chloride	SMOC

Table 4 – Worldwide standards in use for the isotopic composition of hydrogren, boron, carbon, nitrogen, oxygen, silicium, sulfur and chlorine.

4.1.2. Oxygen isotopes

Oxygen is the most abundant element on the Earth and is “one of the most interesting elements in isotope geochemistry” (Hoefs, 2009). It has three stable isotopes, which are present with the following abundances (Rosman & Taylor, 1998):

^{16}O: 99.757%

^{17}O: 0.038%

^{18}O: 0.205%

Oxygen is highly abundant in gaseous, liquid and solid compounds and, because of the higher abundance and the largest mass difference, the $^{18}O/^{16}O$ ratio is normally determined.

Stable oxygen isotopic ratios of waters, silicates, phosphates, sulfates and high-temperature carbonates are normally reported relative to the SMOW standard ("Standard Mean Ocean Water" (Craig, 1961)) or the virtually equivalent VSMOW (Vienna-SMOW) standard. The oxygen stable isotope ratios of carbonates are commonly reported relative to PDB (for Pee Dee Belemnite according to Epstein *et al.*, 1953) or the equivalent VPDB (Vienna PDB), standard.

VSMOW and VPDB, estabilished in 1968 by the International Atomic Energy Agency, are virtually identical to the now-unavailable SMOW and PDB standards.

The conversion equations of $\delta^{18}O$ (VPDB) versus $\delta^{18}O$ (VSMOW) and vice versa (Coplen *et al.,* 1983) are:

$$\delta^{18}O \text{ (VSMOW)} = 1.03092\ \delta^{18}O \text{ (VPDB)} + 30.92$$

and

$$\delta^{18}O \text{ (VPDB)} = 0.97002\ \delta^{18}O \text{ (VSMOW)} - 29.98$$

The oxygen isotopic ratio of seawater is linked with fractionation processes within the hydrological cycle, which comprises of evaporation, atmospheric vapor transport, precipitation and subsequent return of freshwater to the ocean (directly via precipitation and via runoff or iceberg melting) and ocean circulation, such as upwelling and surface currents (Goman *et al*., 2008). Also long-term storage of freshwater in aquifers and ice sheets is important for seawater isotopic ratios (Fig. 57).

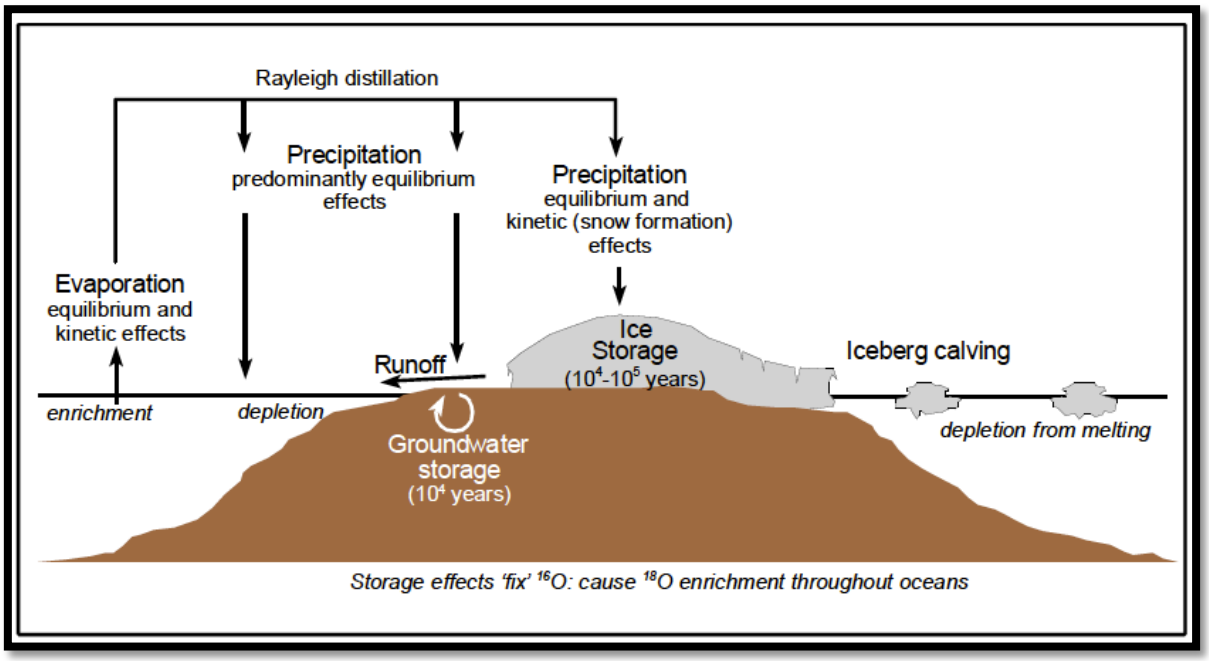

Figure 57 – Schematic presentation of the hydrological cycle influences on oxygen isotopic ratio. Effects on seawater are described in italics (after Rohling and Cooke, 1999).

Formation and melting of seasonal sea ice imposes strong local variability.

The spatial distribution of oxygen isotopes in the world oceans depends on processes od advection and mixing of water masses from different source regions with different isotopic signatures (Rohling, 2007).

Since the salinity of seawater is also affected by the processes just described, Craig & Gordon (1965) and later Fairbanks *et al*. (1992) defined a set of regression relationships between salinity and $\delta^{18}O$ with different slopes, ranging from 0.1 for

the masses of humid tropical surface water and 1.0 for the polar arid, with an overall average of 0.49. The greater gradients represent areas where evaporation exceeds the phenomenon of precipitation and vice versa (Fig. 58).

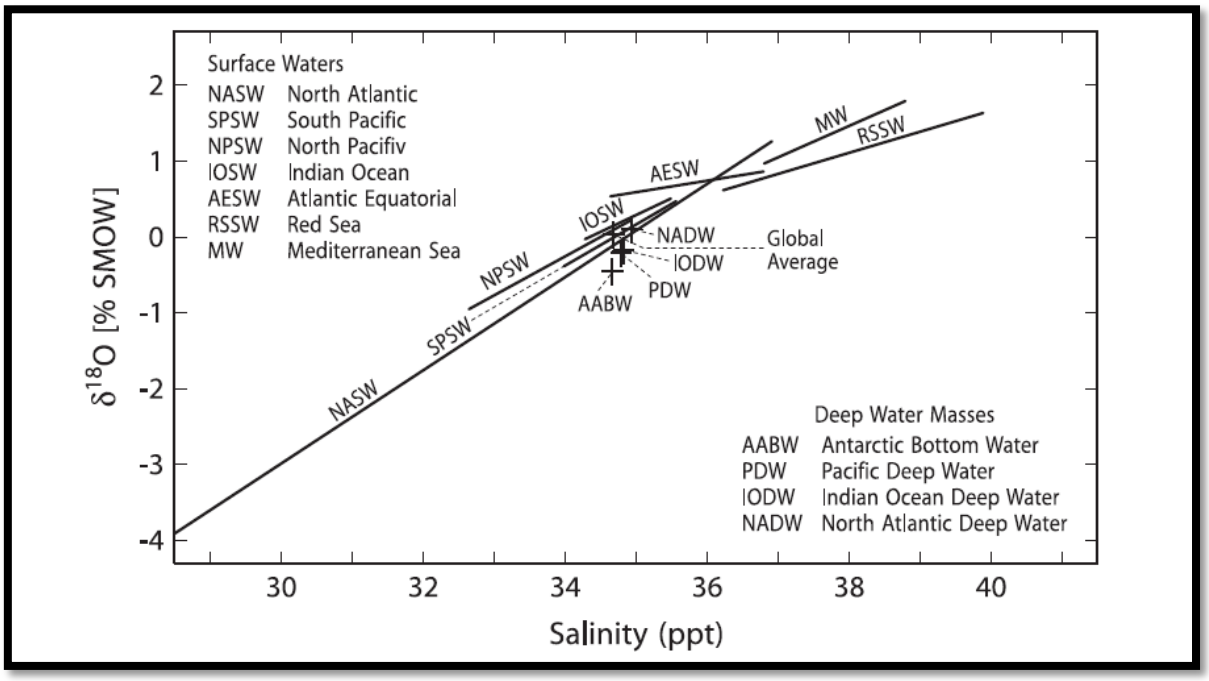

Figure 58 – Salinity versus $\delta^{18}O$ relationship in modern ocean surface and deep waters (after Railsback et al. 1989, modified by Hoefs, 2009).

The oceanic water currently shows a mean $\delta^{18}O$ equal to -0.1‰ (slight different from the one indicated by VSMOW) but this value varies, in different regions and at different ocean depths, between -2‰ and +4‰ (Ruddiman, 2008).

During the water evaporation from oceanic surfaces molecules containing ^{16}O are concentrated in the gaseous phase. The water vapor of the clouds will therefore be depleted in ^{18}O; on the contrary, the seawater surface will be enriched in this isotope. A further concentration of ^{16}O in the atmospheric water vapor will take place when it rains: in this case the water molecules containing ^{18}O enter preferentially in the condensed phase and spill at sea or on land.

The evaporation processes from the ocean surfaces are highest at low latitudes; the global atmospheric circulation shall carry the masses of water vapor to higher latitudes: during the transport the masses are repeatedly depleted in ^{18}O after fractionation processes that accompany the events of condensation and precipitation. Consequently the masses of atmospheric water vapor that reach the higher latitudes, feeding glacial oceanic and continental accumulations, are

extremely rich in ^{16}O ($\delta^{18}O$ = -20-40 ‰).

Another fundamental phenomenon of the oxygen isotope fractionation regards the crystallization of sedimentary minerals. The overall reaction involved in the precipitation of carbonate is:

$$Ca^{2+} + 2HCO_3^- \Leftrightarrow CaCO_3 + CO_2 + H_2O$$

Where oxygen is concerned, the various carbonate species in seawater are isotopically equilibrated with the water molecules. The equilibrium fractionation between calcite and water is a function of temperature. O'Neil *et al.* (1969) determined that for the range of = to 500°C the equilibrium fractionation factor $\alpha_{c\text{-}w}$ between water and calcite changes with temperature according to:

$$\alpha_{c\text{-}w} = \exp\left\{(2.78T^{-2}) * 10^3 - 3.39 * 10^{-3}\right\}$$

where T is in Kelvin. The summary effect of equilibrium fractionation is a ca. 0.2 ‰ depletion in the carbonate $\delta^{18}O$ for every 1°C temperature increase. However, the isotopic fractionation factor varies with temperature as predicted by Urey (1947) and measured in experimental work by for instance Kim and O'Neil (1997). They indicated a more pronounced $\delta^{18}O$ change with the temperature at low temperatures (up to 0.25‰ $°C^{-1}$) than at higher temperatures (about 0.2‰ $°C^{-1)}$.
Experimental observations on crystals of calcite growth by precipitation from an aqueous solution supersaturated in calcium carbonate show how the oxygen isotopic composition of the mineral is a function of the system temperature and of the oxygen isotope composition in the bicarbonate ions present in the solution; this parameter is controlled in turn by the isotopic composition of oxygen in water molecules.
Mineralogy of carbonate is also of important. For instance the experimental observations on synthetic aragonite show that the aragonite is enriched by about 0.8‰ at 25 °C than calcite (Kim *et al.,* 2007).

4.1.3. Carbon isotopes

Carbon has in nature two stable isotopes (^{12}C and ^{13}C), present on average according to the following abundances (Rosman & Taylor, 1998):

^{12}C = 98.93% and

^{13}C = 1.07%

In the Earth system there are two main carbon reservoirs: organic matters and sedimentary carbonates (Fig. 59).

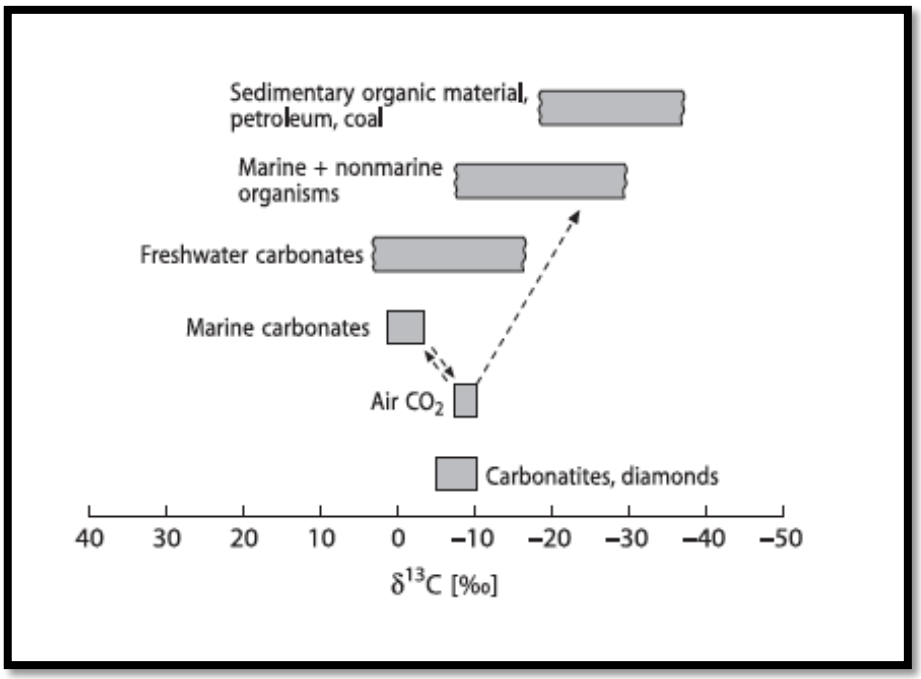

Figure 59 – Carbon isotopic composition of some important carbon reservoirs (Hoefs, 2009).

The carbon oxides, in particular CO_2, released into the atmosphere and dissolved in the hydrosphere, play an essential role of interaction between these geochemical reservoirs.

Modern isotope geochemistry make extensive use of the isotopic ratio $^{13}C/^{12}C$, for which the value of R_{st} suggested by IUPAC (Coplen, 1994) is relative to the VPDB, corresponding to: $R_{C(VPDB)} = 11237.2 \cdot 10^{-6}$.

The carbon isotopic composition of natural compounds is extremely variable ranging between $\delta^{13}C$ values greater than +20‰ (heavy carbonates) and less than -100‰ (e.g. light methane).

The isotopic effects observed in nature in relation to carbon are referring to two fundamental types: isotope equilibrium fractionation processes occurring within the inorganic carbon system (atmospheric CO_2 – dissolved bicarbonate – solid

carbonate) which tend to enrich ^{13}C in carbonates, and kinetic isotope effects occurring during photosynthesis which lead to an enrichment of ^{12}C (Hoefs, 2009).

The inorganic carbon system (Fig. 60) is composed by many chemical species, present in the form of gas (e.g. CO_2 and CO), minerals (various carbonates, mainly $CaCO_3$) or dissolved into the hydrosphere (e.g. H_2CO_3, HCO^{3-}, CO_3^{2-}). These species are related through equilibrium reactions, whose magnitude of isotopic fractionation is essentially due to the temperature. The inorganic carbon system in the ocean is controlled by the carbonate reactions. Most of the CO_2 in water is contained in the bicarbonate ion (HCO^{3-}), due to the reaction:

$$H_2O + CO_2 \Leftrightarrow H^+ + HCO^{3-}$$

The total dissolved inorganic carbon (DIC) in seawater is made from HCO^{3-}, CO_3^{2-} and dissolved CO_2. At normal seawater pH of 7.8-8.3, seawater contains mainly HCO^{3-} and small amounts of CO_3^{2-}. The biogenic and abiogenic calcium carbonate interacts with the inorganic carbon systems via the precipitation/dissolution equation:

$$2\ HCO^{3-} + Ca^{2+} \Leftrightarrow CaCO_3 + H_2O + CO_2$$

In the typical range of ocean water temperature, carbonates that precipitate show a strong enrichment in ^{13}C to the detriment of carbon dioxide dissolved.

The organic carbon cycle (Fig. 60) is intimately connected to photosynthesis processes, occurring in both the marine and the continental environments. The reaction simplified which describes photosynthesis is:

$$CO_2 + H_2O + \text{energy (sunlight)} \Rightarrow CH_2O + O_2$$

Inversely to the photosynthesis reaction, respiration under the presence of oxygen breaks down the organic biomass and releases energy and CO_2.

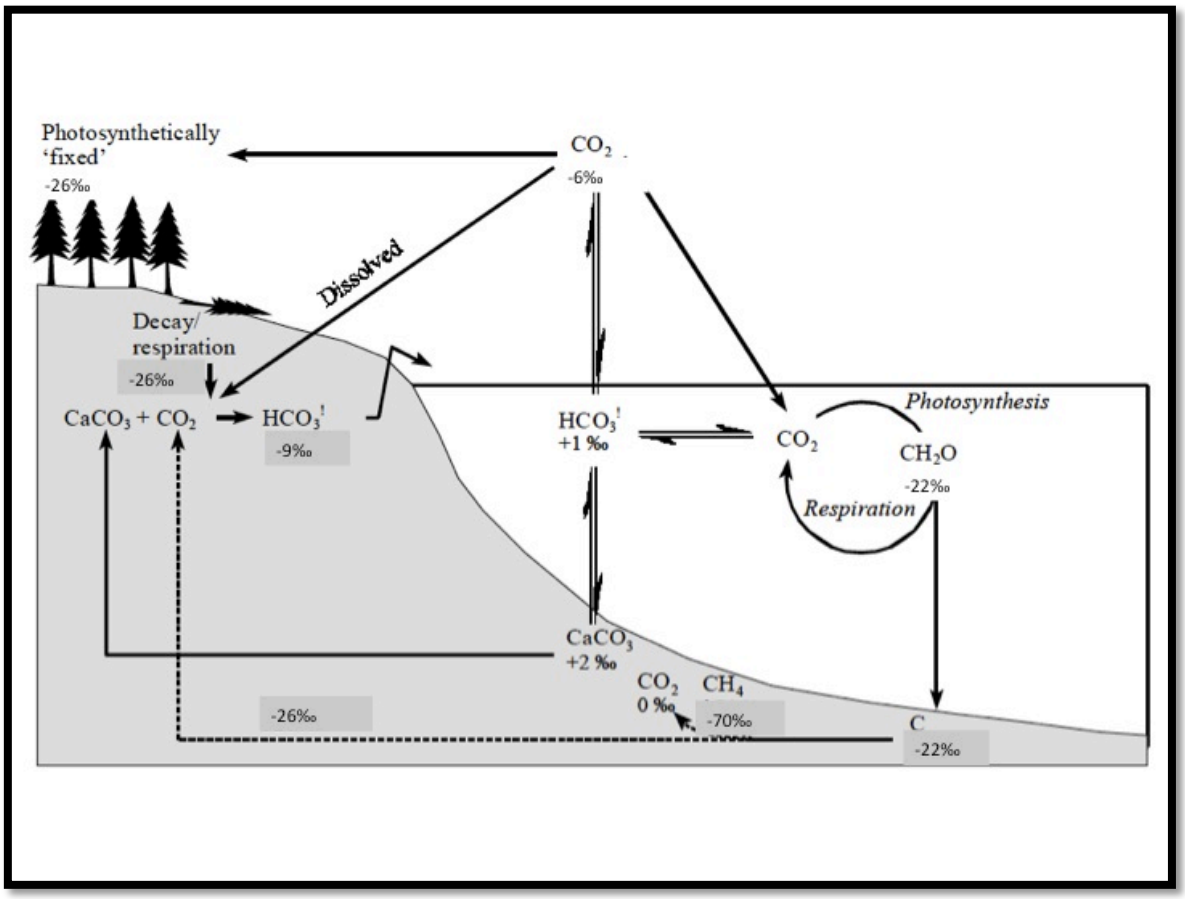

Figure 60 – Summary of the main isotopic interactions within the inorganic and organic carbon cycles (modified after Garlick, 1974 and Hoefs, 1997).

According to Park & Epstein (1960) the kinetic effect occurring during the photosynthesis processes is a temporally bipartite phenomenon in which before the incorporation and diffusion of CO_2 molecules take place and then the fixation of new organic matter takes place. Both phases involve a preferential selection of ^{12}C that is concentrated in the organic matter.

The isotope carbon distribution in the ocean system is the result of exchanges between three main reservoirs (Ruddiman, 2008): the atmosphere, whose carbon oxides are characterized by $\delta^{13}C$ values slightly negative (currently about -7‰); the organic matter, characterized by $\delta^{13}C$ values very negative (on average around -22‰) and very variable; carbonates, where the carbon isotope composition is closely related to that of the Dissolved Inorganic Carbon (DIC) from which the carbonate precipitated, but slightly more positive ($\delta^{13}C$ on average around 2‰).

The biogenic organic matter, isotopically very light, is mostly produced in the euphotic zone, which results depleted in dissolved ^{12}C. Following the death, a good part of this biomass in decomposition is transported in depth by means of the

"carbon biological pump", the sum of a suite of biogeochemical processes that transport the biomass to the lower layers of the water column. Here the organic matter, ^{12}C-rich, is re-oxidized and for this reason the deep ocean waters usually show slightly negative $\delta^{13}C$ values. For this geochemical studies carried out on the isotopic composition of carbonatic foraminifera shell indicate $\delta^{13}C$ values usually higher for planktonic forms than for benthic forms (Shackleton & Kennet, 1975).

4.1.4. Stable isotopes in biogenic carbonates: oxygen and carbon isotopes as paleoclimatic and paleoenvironmental proxies

Skeletal carbonate oxygen ($\delta^{18}O$) and carbon ($\delta^{13}C$) isotopic compositions are often used as geochemical archives of paleoenvironmental conditions.

Summing up in an equation (Maslin & Swann, 2006), the oxygen isotopic composition of a biogenic carbonate ($\Delta\delta^{18}O_M$) precipitated in ocean water equals to:

$$\Delta\delta^{18}O_M = \Delta\delta^{18}O_W + \Delta\delta_T = \Delta\delta_{GIV} + \Delta\delta_{local} + \Delta\delta_T + \text{vital effects}$$

where:

$\Delta\delta^{18}O_M$ = oxygen isotopic composition of the biogenic carbonate.

$\Delta\delta^{18}O_W$ = oxygen isotope composition of the water (combined effect of variations in global ice volume ($\Delta\delta_{GIV}$) and local influences ($\Delta\delta_{local}$)).

$\Delta\delta_T$ = water temperature.

Vital effects (Urey *et al.*, 1951) are "metabolic processes that modify the way in which environmental data are recorded in the geochemical composition of biogenic hard parts" (Schöne *et al.,* 2011) and could be connected to the ontogenic effect, to symbiont photosynthesis effect, to respiration effect, to the gametogenic calcite effect and to the effect of changes in $\left[CO_3^{2-}\right]$ (Rohling and Cooke, 1999). In order to minimize the influence of kinetic effects, analytical strategies for studying marine cores, for instance, have been designed focusing on time-series of single species and using very narrow size-windows from which specimens are picked for analysis.

Biogenic carbonates showing species-specific vital effects (Holmes and Chivas, 2002), are not precluded from palaeoclimatic studies as long as the offset is demonstrably independent of temperature or the factors that influence the offset from equilibrium are known. This is usually achieved by calibration studies to

investigate the precise systematics of isotopic fractionation.

Since the 50's, starting with the works of the Chicago School (Urey, 1947; McCrea, 1950; Epstein *et al.*, 1953; Craig, 1965; O'Neil *et al.,*1969; Shackleton, 1974; Erez and Luz, 1983), several transfer functions have been proposed to relate the value of the $\delta^{18}O$ measured in calcite ($\delta^{18}O_C$) with temperature (T_W) and $\delta^{18}O$ value of the water in which the mineral precipitated ($\delta^{18}O_W$) in equilibrium conditions. One of the most widely used is that proposed, for the calcite, by Erez & Luz in 1983:

$$T_w(°C) = 17.00 - 4.52 \bullet (\delta^{18}O_c - \delta^{18}O_w) + 0.03 \bullet (\delta^{18}O_c - \delta^{18}O_w)^2$$

For the aragonite, instead, can be used the equation:

$$T_w(°C) = 19.00 - 3.52 \bullet (\delta^{18}O_c - \delta^{18}O_w) + 0.03 \bullet (\delta^{18}O_c - \delta^{18}O_w)^2$$

Basically, keeping constant the value of $\delta^{18}O_W$, as the temperature decreases by 1°C the carbonate, which precipitates in equilibrium conditions from the aqueous solution, will be enriched by about 0.26‰ in the stable isotope (^{18}O).

Among the fossil forms usually used for paleoclimate reconstructions calcareous foraminifera are set. Emiliani (1955) first studied the isotopic composition of foraminifera and he reconstructed an isotopic curve where higher $\delta^{18}O$ values indicate cold periods and lower $\delta^{18}O$ represent warm intervals (Fig. 61).

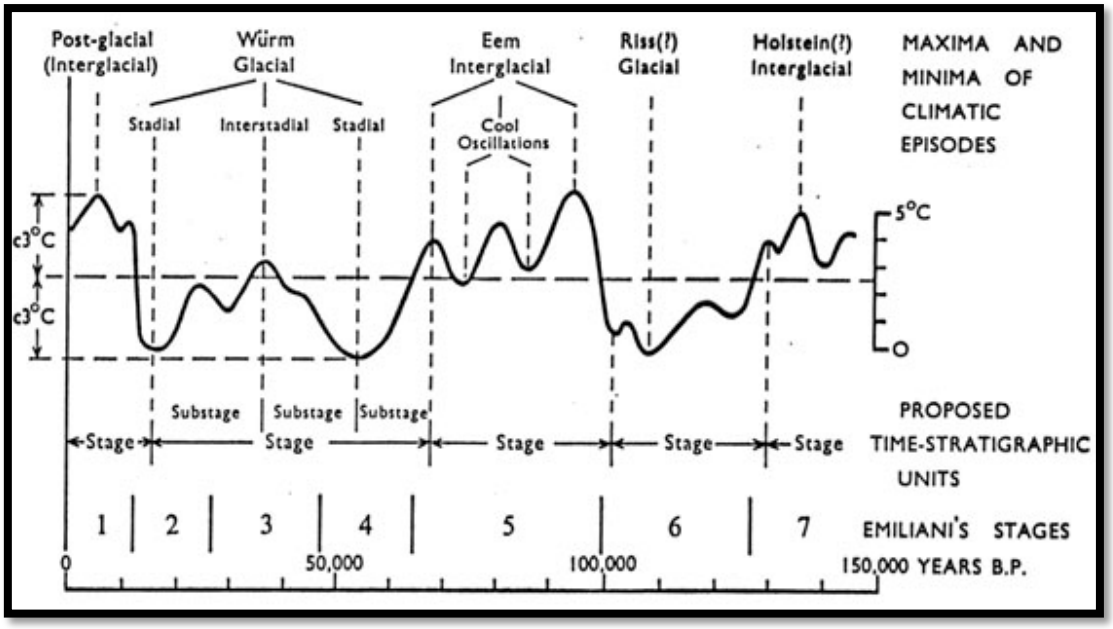

Figure 61 – Emiliani's isotopic curve for the last 150.000 years.

Emiliani believed that changes in ocean temperatures were the main factor acting on the oxygen isotope composition of biogenic marine carbonates, while a low percentage of the oxygen isotopic record was related to changes in the global ice volume.

Conversely, Craig (1965), Dansgaard & Tauber (1969), and Shacktleton & Opdyke (1973) demonstrated that the storage of isotopically light water in ice ("*ice volume effect*") is a factor by no means secondary, but it is the main factor in determining the oxygen isotopic composition of biogenic carbonates.

Time-series of foraminiferal $\delta^{18}O$ indicate that glacial ice volume has heavily varied during the Quaternary. During the last 400,000 years foraminiferal $\delta^{18}O$ shows a rough saw-tooth pattern with a 100,000-year cadence of glacial-interglacial cycles, mainly linked to the global ice-volume fluctuations (Fig. 62). Ice sheets grew over periods of approximately 90,000 years, reaching a maximum extent followed by a very abrupt ice-volume decrease that indicate the onset of an interglacial maximum with a typical mean duration of some 10,000 years. Between 0.4 and 1 million years ago, there was a less defined state, with a complex interaction for the glacial cycles between periods of 100,000 and 41,000 years. Particularly in the interval between 2.4 and 1 million years ago, the glacial cycles developed over a period of 41,000 years without having a noticeable saw-toothed temporal structure.

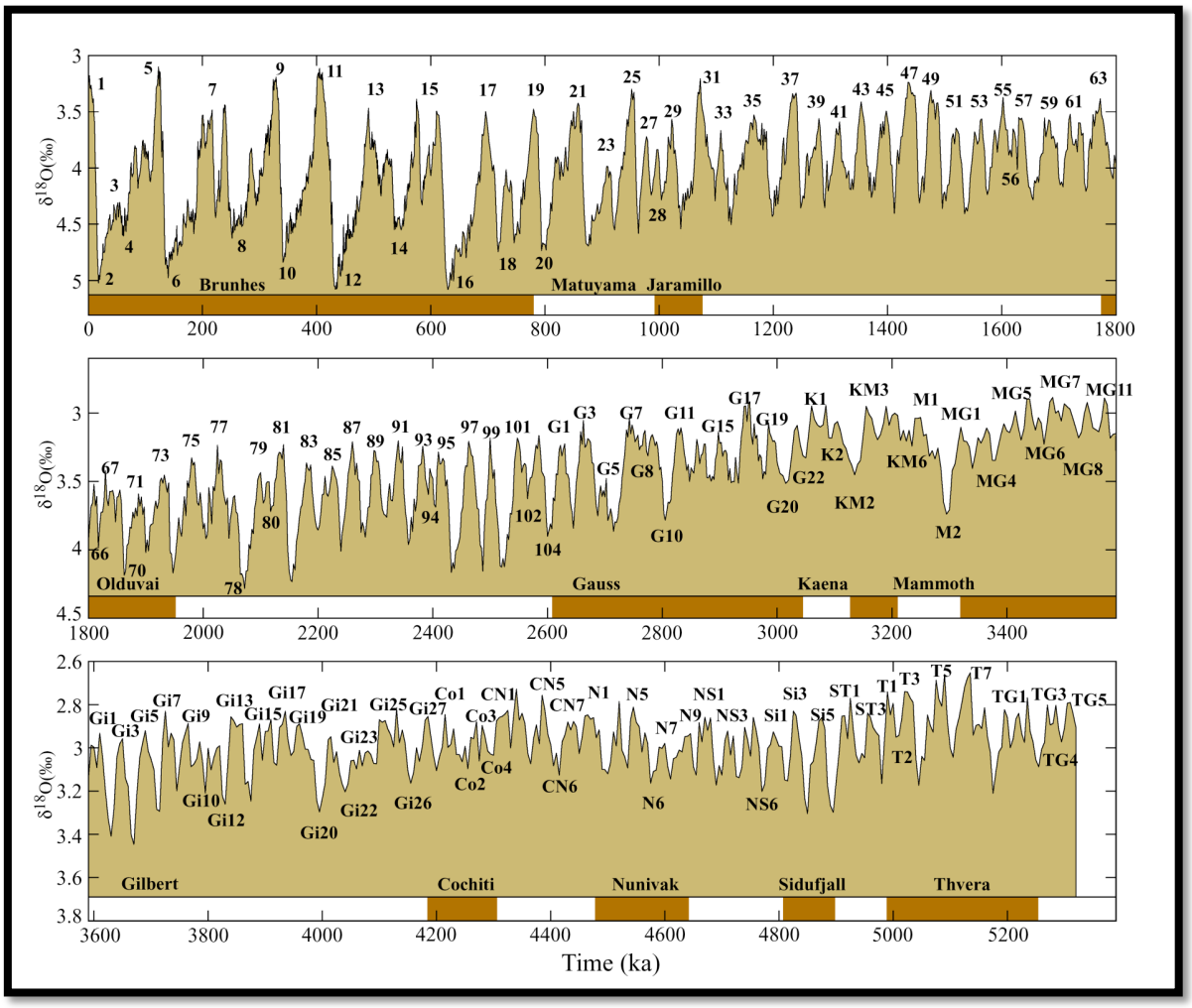

Figure 62 – A stacked record of $\delta^{18}O$ variations for the last 5.3 million years. Even numbers indicate glacial intervals, odd numbers indicate interglacials periods. After Lisiecki and Raymo (2005).

Many molluscs precipitate their shells in oxygen isotopic equilibrium with ambient water ($\delta^{18}O_w$) (Mook and Vogel, 1968; Wefer and Berger, 1991). The primary controlling factors of $\delta^{18}O$ in the carbonate of mollusk shells are the $\delta^{18}O$ of ambient seawater and ambient water temperature.

Waters of continental and marine origin usually have large different isotopic signatures, the same is true for the isotope composition of the dissolved inorganic carbon (DIC). Therefore, carbon and oxygen stable isotope composition of mollusc shells living in marginal marine environments can record the mixing between continental and marine waters (e.g. Mook and Vogel, 1968; Eisma *et al.*, 1976; Ingram *et al.*, 1976).

In the simplest case, at a given temperature, isotopic compositions of shells will describe a linear mixing trend between two end members corresponding to marine and continental environments when plotted in a $\delta^{13}C$ vs $\delta^{18}O$ diagram. Several studies have used this approach to reconstruct paleosalinity (e.g. Dodd and Stanton, 1975; Hudson *et al*., 1995) and changes in river discharge (e.g. Ingram *et al.*, 1976) in ancient marginal coastal deposits. However, local factors such as evaporation increase in the equilibration with atmospheric CO_2 reservoir, in situ decay of organic matter, and strong biological activity may alter drastically the model (e.g. Lloyd, 1964; Hendry and Kalin, 1997).

The $\delta^{13}C$ of mollusk shells primarily reflects the $\delta^{13}C$ of dissolved inorganic carbon of ambient waters, the carbon isotopic composition of organic carbon consumed by the organism, and kinetic fractionation related to growth rates and calcification (see Goman *et al*., 2008). Mollusc shell $\delta^{13}C$ variations are more difficult to interpret than $\delta^{18}O$ because ^{12}C-rich metabolically derived carbon may be incorporated into shell carbonate, obscuring variations in the carbon isotope composition of water column dissolved inorganic carbon (see references in Takesue and van Geen, 2004). Fossil mollusc shell $\delta^{13}C$ has also been used to identify past productivity events, since photosynthesis enriches surface waters in ^{13}C relative to ^{12}C (Purton and Brasier, 1997).

4.2. TRACE ELEMENTS

Trace elements in a geological context are defined as: “all elements except the eight abundant rock-forming elements: oxygen, silicon, aluminium, iron, calcium, sodium, potassium and magnesium” (Thrush *et al.*, 1968). However, for biogenic carbonates, only calcium is the major elements.

Since the molal Mg/Ca ratio of seawater is 5:1, the inorganically precipitated marine $CaCO_3$ should be high-Mg calcite (with 4-30 mol % $MgCO_3$ in the $CaCO_3$ structure according to Chave, 1954) with about 1.6-7.5% Mg or aragonite (Veizer, 1983).

The mineralogy of calcium carbonate phase is the main factor controlling the concentration of a trace element or isotope in its structure.

Carbonate minor (Mg, Sr) and trace elements may be incorporated into minerals in four ways (McIntire, 1963; Zemann, 1969; Veizer, 1983):

1) by substitution for Ca^{2+} in the calcium carbonate structure;
2) by interstitial substitution between planes
3) by substitution at lattice positions being vacant due to defects in the structure;
4) by adsorption due to remnant ionic charges.

The factors 2, 3 and 4 have a subordinate importance to that of factor 1 and, unlike the latter, are essentially random.

The reaction that expresses the incorporation of a divalent trace element (Me^{2+}) within the calcite (Cc) is (McIntire, 1963):

$$CaCO_{3(Cc)} + Me^{2+}_{(aq)} = MeCO_{3(Cc)} + Ca^{2+}_{(aq)}$$

And the equilibrium constant K is given by:

$$K = \left[\left(\frac{a_{Ca^{2+}}}{a_{Me^{2+}}}\right)_{aq}\right] \bullet \left[\left(\frac{a_{MeCO_3}}{a_{CaCO_3}}\right)_{Cc}\right]$$

where a_i is the activity of the ith component. The distribution coefficient , instead, is defined as:

$$D = \left[\left(\frac{X_{MeCO_3}}{X_{CaCO_3}}\right)_{Cc}\right] \div \left[\left(\frac{m_{Me^{2+}}}{m_{Ca^{2+}}}\right)_{aq}\right]$$

where X_i is the mo fraction of the component in calcite and m_i the total molality if the dissolved species.

At equilibrium, the distribution coefficient should be close to 1. However, reported D values of bivalve shells, gastropods and otoliths deviate from this value (e.g. Gillikin *et al.,* 2005; Freitas *et al.,* 2006).

D and K are related by the equation:

$$D = K \bullet \left[\left(\frac{\gamma_{CaCO_3}}{\gamma_{MeCO_3}} \right)_{Cc} \right] \bullet \left[\left(\frac{\gamma'_{Me^{2+}}}{\gamma'_{Ca^{2+}}} \right)_{aq} \right]$$

where γ_i is the activity coefficient of the respective component in calcite and γ_i' is the total activity coefficient accounting for complexing of that aqueous species. The latter equation is also expressed as:

$$\left[M_{Me} / M_{Ca} \right]_s = D \left[M_{Me} / M_{Ca} \right]_{aq}$$

where M means molar concentrations and the subscripts s and aq indicate the solid phase (i.e. calcite) and the aqueous phase.

When the trace element distribution coefficient (D) for calcite and aragonite (Fig. 63) is greater than 1, the precipitated solid phase will contain, relative to Ca, higher Me concentrations than the water with which the solid phase was in equilibrium. On the contrary, for trace elements with D<1 the precipitated solid phase will have lower Me concentrations.

The cell of aragonite incorporates preferentially cations larger than Ca (e.g. Sr, Na, Ba, U), while the cell of calcite, smaller, tends to incorporate smaller cations (e.g. Mg, Fe, Mn, Zn, Cu, Cd).

Non marine carbonates, due to the different composition of meteoric waters, are usually depleted in Mg, Sr, Na, Ba, U and enriched in Zn, Fe, Co and Cu (Veizer, 1983).

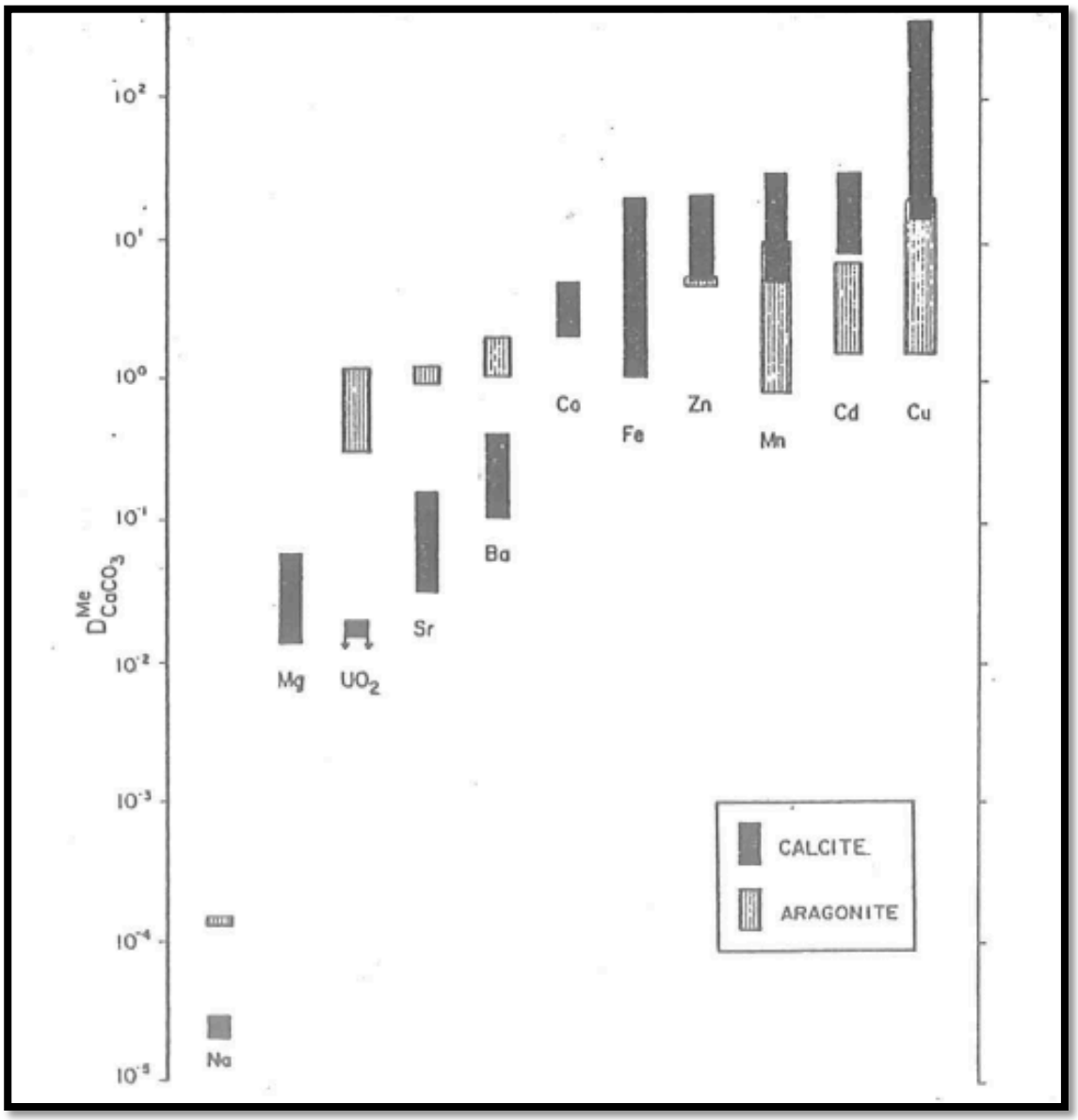

Figure 63 – Approximate trace element distribution coefficients for calcite and aragonite (Veizer, 1983).

Carbonate precipitation today is mainly related to direct (skeletal) or indirect (variations in environmental parameters, as pH) biogenic factors. Biogenic fractionations, due to the disequilibrium in which some phyla precipitate their skeletons with the seawater in which they live, can in some cases increase, in other cases reduce, the concentrations of trace elements in calcium carbonates (e.g. Dodd, 1967; Milliman, 1974; Klein *et al.*, 1996).

The element composition of marine and freshwater mollusc shells has been shown to be connected to environmental parameters (Dodd, 1965; Lorens and Bender, 1980; Bourgoin, 1990; Pitts and Wallace; 1994; Klein *et al.*, 1996; Van der Putten, 2000; Takesue and van Geen, 2004).

Past water temperatures have been reconstructed from Sr/Ca and Mg/Ca ratios of many taxonomic groups, such as brachiopods (Lowenstam, 1961; Powell *et al.,* 2009), corals (Beck *et al.,* 1992; Mitsuguchi *et al.,* 1996; Goodkin *et al.,* 2007), foraminifers (Nürnberg *et al.,* 1996), ostracods (Corrège, 1993), echinoids (Pilkey and Hower, 1960), sclerosponges (Rosenheim *et al.,* 2004), belemnites (McArthur *et al.,* 2007), gastropods (Sosdian *et al.,* 2006) and bivalves (Dodd, 1965, 1967; Sch öne *et al.,* 2011, among the others). Furthermore, the Sr/Ca and Mg/Ca ratios of artificial aragonite decrease with increasing temperature.

It has been proven as the Mg/Ca and Sr/Ca ratios are temperature-dependent, but published results on the relationship between Mg/Ca and Sr/Ca ratios of bivalve shells and calcification temperature are highly ambiguous. Shell Mg/Ca and Sr/Ca ratios vary significantly among different bivalve species and even among conspecific and contemporaneous specimens from one locality (Gillikin *et al.,* 2005; Lorrain *et al.*, 2005; Freitas *et al.*, 2008). Several researches on Sr/Ca on different specimens revealed that Sr uptake reflect not only thermodynamic substitution but kinetic effects too (Stecher *et al.*, 1996; Gillikin *et al.,* 2005). A large negative temperature dependence has been pointed out in some species (Dodd, 1965; Surge and Walker, 2006) and a negative correlation between Sr/Ca ratios and the sea surface temperature is also observed in *Arctica islandica* (Schöne *et al.,* 2011), which also show a trend towards increasing Sr/Ca with ontogeny. Gillikin *et al.* (2005) indicated that the Sr/Ca ratio and the intra-annual shell growth rate were positively correlated in butter clam *Saxidomus giganteus,* but not in hard clam *Mercenaria mercenaria,* and supposed that Sr/Ca was indirectely affected by temperature, via salinity, metabolism or food supply. Various authors, besides, noted a correlation of Mg and Sr content with growth rate (Swan, 1956; Takesue and van Geen, 2004; Gillikin *et al.,* 2005; Lorrain *et al.*, 2005) or ontogenetic age (Palacios *et al.*, 1994; Freitas *et al.*, 2005).

The parameters controlling Mg incorporation into aragonite shells are also controversial. In *Protothaca staminea,* the relationship between water temperature and Mg/Ca shows interspecimen variations, suggesting that the temperature control of Mg/Ca can be more complex than that of Sr/Ca (Takesue and van Geen, 2004; Izumida *et al.,* 2011). In *Arctica islandica* large inter- and intraspecific differences of Mg/Ca have been reported, indicating that in this species Mg is not incorporated within the aragonite crystal lattice but occurs in in organic material or in disordered

phases similar to amorphous calcium carbonate (Foster *et al.,* 2008). Always in this species Schöne *et al.* (2010; 2011) reported the close relationship between shell Mg/Ca ontogeny and Mg-bearing organic material for ontogenetically old specimens. Ba/Ca ratios in marine biogenic carbonates are largely used as a proxy for paleoproductivity, for the association of oceanic barite with areas with high productivity. Moreover, Ba concentrations are usually higher in river and lakes than in seawater due to chemical weathering occurring in their catchment. For this reason, freshwater discharges have been recognized as important sources of Ba in seawater (Martin and Meyback, 1979). Ba concentration in shells can also reflect dissolved or particulate Ba concentrations in the water (Van der Putten *et al.*, 2000; *Lazareth et al.*, 2003) or the ingestion of Ba-rich phytoplankton by the organism (Stecher *et al.*, 1996). Thus, marine molluscs could record episodic riverine or upwelling inputs of barium in the coastal areas (Torres *et al.,* 2001; Elliot *et al.*, 2009 among the others).

U/Ca ratios have been suggested as a proxy of oceanic $\left[CO_3^{2-}\right]$ in aragonitic corals (Min *et al.*, 1995; Shen and Dunbar, 1995; Anagnostou *et al.*, 2011) and calcitic foraminifera (Russell *et al.*, 2004). Shallow water coral also show a strong temperature control on skeletal U/Ca ratios (Min *et al.*, 1995; Shen and Dunbar, 1995). In addition, according to some studies (Kitano and Oomori, 1971; Chung and Swart, 1990), U content seems to be related to pH in inorganic aragonite and calcite: at higher pH less U is available to be incorporated in shell carbonate, because in aqueous solutions the carbonate ion complexes with the uranyl ion (UO_2^{2+}) (Langmuir, 1978).

Nevertheless, several papers reported strong diagenetic trends in fossil and recent shells that can mask the results (e.g. Kaufman *et al.*, 1971; 1996; McLaren and Rowe 1996; Labonne and Hillaire-Marcel, 2000).

4.3. DIAGENESIS OF SKELETAL CARBONATES

Diagenesis is defined as “all those changes that take place in a sediment near the earth’s surface at low temperature and pressure and without crustal movement being directly involved” (Taylor, 1964).

The original carbonate phase, upon exposure to meteoric water, will dissolve partially or totally, will exchange and mix its trace elements and stable isotopes with those into the interstitial water and will diagenetically transformed into low-Mg calcite. High-Mg calcite, aragonite and low-Mg calcite, in fact, are apparently stable in the original depositional marine environment (Winland,1969; Bathurst, 1975; Möller and Kubanek, 1976; Brand and Veizer, 1980). However, in diagenetic meteoric environment high-Mg calcite and aragonite are metastable and undergo rapid alteration to the stable phase low-Mg calcite (Land, 1967; Schroeder, 1969; Bathurst, 1975).

The interstitial meteoric water, generally, contains lower values of Sr^{2+}, Na^{+}, Mg^{2+}, $\delta^{13}C$ and $\delta^{18}O$, and more Mn^{2+}, Fe^{2+} and Zn^{2+} than seawater (Turekian, 1972; Brand and Veizer, 1980; Morrison and Brand, 1986; 1988). For this reason, a decrease in strontium, sodium and possibly magnesium (depending on the mineralogy of the original carbonate phase) and an increase in manganese, iron and zinc in progressively alterated carbonates should occur. In contrast, Cross and Cross (1983) indicated an apparent increase in Sr content with decrease of Mg, and no change in U and mineralogy with early diagenesis of aragonitic corals.

During the diagenesis, according to Brand (1989), no significant changes in chemical concentrations occurred fir Ba, Cu, Ni and Pb.

Furthermore, taking into account the distribution coefficient (D) of the various elements, open or partly closed diagenetic systems will lead to a decrease of concentrations for elements with $D_{calcite\text{-}water} < 1$ (Sr^{2+}, Na^{+}, Mg^{2+}) and to an increase for elements with $D > 1$ (Mn^{2+}, Fe^{2+} and Zn^{2+}).

Several papers, lastly, reported strong diagenetic trends and a secondary uranium uptake in fossil and recent shells (e.g. Kaufman *et al.*, 1971; 1996; McLaren and Rowe 1996; Labonne and Hillaire-Marcel, 2000). Broecker (1963) and Blanchard *et al.* (1967) showed that fossil marine mollusks typically have much more uranium than do living ones. By comparing the uranium concentrations of fossils of various ages it was concluded that the uranium addition ended a relatively short time after death.

5. MATERIALS AND METHODS

5.1. SITE SELECTION, FIELD CAMPAIGNS AND SAMPLING METHODS

The study area was selected collecting and collating remote sensing (mainly satellite images) and literature data. The criteria for the selection of the area were:
i) Occurrence of several orders of terraces, for which we can suppose the presence of at least Holocene, MIS5, MIS7, MIS 9 and MIS 11 successions;
ii) Availability of stratigraphic and morphological preliminary data;
iii) Availability of a basic set of robustly dated units with ^{14}C, U/Th and ESR, which reduces the cost of dating for some selected stratigraphic units;
iv) Selection of an area for which a large influence of freshwater input can be neglected. This makes it possible to select samples, which give real information on sea conditions not complicated by mixing processes;
v) Availability of local geodetic station to anchor elevation data and that can offer the opportunity to implement local topography thanks to GPS systems. The preliminary work allowed to selected the Golfo San Jorge area (Chubut and Santa Cruz Provinces) between Cabo Raso and Puerto Deseado, which includes all the required criteria listed above.

In 2009, 2010 and 2011 three field work campaigns, lasting about a month each, were held for mapping and sampling the Pleistocene, Holocene and modern coastal deposits along the Golfo San Jorge area, in Chubut and Santa Cruz Provinces (Fig. 64). The main stops were the areas of Cabo Raso, Bahia Camarones, Bahia Bustamante, Bahia Solano, Caleta Olivia and Puerto Deseado. These places allowed to visit and collect samples of the most important successions described in the older and recent literature (especially those sections containing robust chronological control and fossil accumulation are documented). In addition, new outcrops and sections were identified and sampled.

Figure 64 – Study area with main sampling localities.

During the field work about 500 samples of fossils and sediment were collected for different analyses (stable isotopes and trace element analyses; U/Th, ^{14}C and OSL dating; sedimentological and paleontological analyses).

During the field observations particular attention was placed on the sediment grain size and composition, physical and biogenic sedimentary structures and fossiliferous content.

Shell beds were sampled after the observation of the stratigraphic geometry, taphonomy and faunal composition.

Specimens of *Ameghinomya antiqua*, bivalves belonging to the Mytilidae Family (e.g. *Mytilus edulis* and *Aulacomya atra*) and *Nacella deaurata* specimens, representing the dominant molluscan species in these deposits, were chosen for the analyses. In order to decrease the possibility that shells were reworked from older beds, articulated shells collected within the deposits were preferred for the analyses (Figs. 65-66).

Figure 65 – Shell bed in a Pleistocene beach ridge. Articulated shells of *Ameghinomya antiqua.* This represents a storm accumulation.

Figure 66 – Articulated Mytilidae shells in a Pleistocene beach ridge.

Mollusc specimens from the active beaches as effect of storm activity were collected for using them as reference for fossil counterpart. To be sure that the samples were from the modern beach and not reworked from older layers, were chosen only bivalve specimens still having the ligament, an elastic fibrous multilayered structure which allow to the valves to be joined together (Fig. 67).

Figure 67 – Modern active beach with *Ameghinomya antiqua* specimens preserving the ligament.

Any section and sampling point were positioned by using a GPS (GPSmap60CSx Garmin) equipped with a high precision barometric altimeter (Fig. 68). Data were regularly tested at sea level and corrected by tide effect using the “tablas de marea, Servicio de Hidrografia Naval, Buenos Aires”, available on line and using local geodetic points.

Figure 68– GPS used in the field work for samples positioning.

The samples were collected in bags and classified with the number taken from the GPS (e.g. WP 1, WP 2). If for every sampling station (WP), the number of samples was superior to 1, at the station number a letter to distinguish different types of sample was added (e.g. WP 1A, WP 1B).

5.2. CONSTRUCTION OF A GEOGRAPHICAL DATABASE OF SAMPLING POINTS

During the field work campaigns in Patagonia about 1400 control and sampling points were acquired with a GPS (Fig. 68).

These sampling points were converted to shapefile format and imported in ArcMap of ESRI ArcGIS platform.

The geographic database, called wp_tot_20n, is constituted from the fields directly imported from the GPS (Fig. 69) and new fields that were added to make the database as complete as possible.

Attributes of wp_tot_20n

FID	Shape *	GM_LAYER	ELEVATION	VISIBLE	NAME	DESCRIPTIO	TYPE	POSITION	ALTITUDE
0	Point	WptAttribs	3,25012	001	001	13-GEN-09 14:03:29	User Waypoint	S40 42.565 W64 52.082	3 m
1	Point	WptAttribs	7,09534	002	002	14-GEN-09 1:36:23	User Waypoint	S44 20.375 W65 14.972	7 m
2	Point	WptAttribs	29,68628	003	003	14-GEN-09 11:39:50	User Waypoint	S44 15.559 W65 19.163	30 m
3	Point	WptAttribs	9,01794	004	004	14-GEN-09 13:10:53	User Waypoint	S44 16.740 W65 16.454	9 m
4	Point	WptAttribs	9,2583	005	005	14-GEN-09 14:19:23	User Waypoint	S44 16.571 W65 16.429	9 m
5	Point	WptAttribs	7,57605	006	006	14-GEN-09 15:06:08	User Waypoint	S44 16.366 W65 16.747	8 m
6	Point	WptAttribs	8,297	007	007	14-GEN-09 15:31:10	User Waypoint	S44 16.208 W65 16.923	8 m
7	Point	WptAttribs	7,57605	008	008	14-GEN-09 15:37:33	User Waypoint	S44 16.120 W65 16.738	8 m
8	Point	WptAttribs	7,09534	009	009	14-GEN-09 15:55:28	User Waypoint	S44 16.281 W65 16.810	7 m
9	Point	WptAttribs	4,21143	010	010	14-GEN-09 16:15:35	User Waypoint	S44 16.713 W65 16.620	4 m
10	Point	WptAttribs	4,45178	012	012	14-GEN-09 15:57:29	User Waypoint	S44 18.446 W65 15.646	4 m
11	Point	WptAttribs	-2,27734	013	013	14-GEN-09 16:00:23	User Waypoint	S44 18.454 W65 15.656	-2 m
12	Point	WptAttribs	0,60657	014	014	14-GEN-09 16:08:41	User Waypoint	S44 18.481 W65 15.684	1 m
13	Point	WptAttribs	4,69214	015	015	14-GEN-09 16:18:45	User Waypoint	S44 18.513 W65 15.727	5 m
14	Point	WptAttribs	1,56787	016	016	14-GEN-09 16:34:08	User Waypoint	S44 18.496 W65 15.819	2 m
15	Point	WptAttribs	16,7085	017	017	14-GEN-09 17:05:20	User Waypoint	S44 19.733 W65 16.502	17 m
16	Point	WptAttribs	16,7085	018	018	14-GEN-09 17:16:31	User Waypoint	S44 19.755 W65 16.498	17 m
17	Point	WptAttribs	60,44824	019	019	14-GEN-09 17:43:56	User Waypoint	S44 19.881 W65 18.649	60 m
18	Point	WptAttribs	38,09766	020	020	14-GEN-09 18:33:56	User Waypoint	S44 20.021 W65 17.240	38 m
19	Point	WptAttribs	32,57019	021	021	14-GEN-09 18:45:44	User Waypoint	S44 19.817 W65 17.321	33 m
20	Point	WptAttribs	5,8938	022	022	14-GEN-09 19:41:07	User Waypoint	S44 20.128 W65 16.323	6 m
21	Point	WptAttribs	13,82458	023	023	14-GEN-09 20:05:54	User Waypoint	S44 20.214 W65 15.809	14 m
22	Point	WptAttribs	43,38477	024	024	15-GEN-09 6:46:19	User Waypoint	S44 20.707 W65 14.142	43 m
23	Point	WptAttribs	8,297	025	025	15-GEN-09 7:09:10	User Waypoint	S44 20.338 W65 13.605	8 m
24	Point	WptAttribs	3,25012	026	026	15-GEN-09 7:13:18	User Waypoint	S44 20.322 W65 13.486	3 m
25	Point	WptAttribs	4,69214	027	027	15-GEN-09 7:26:27	User Waypoint	S44 20.517 W65 13.517	5 m
26	Point	WptAttribs	13,10364	028	028	15-GEN-09 7:45:29	User Waypoint	S44 20.258 W65 13.888	13 m
27	Point	WptAttribs	9,2583	029	029	15-GEN-09 7:48:04	User Waypoint	S44 20.229 W65 13.980	9 m
28	Point	WptAttribs	0,36621	030	030	15-GEN-09 7:55:02	User Waypoint	S44 20.198 W65 14.168	0 m
29	Point	WptAttribs	3,25012	031	031	15-GEN-09 9:09:00	User Waypoint	S44 20.457 W65 14.679	3 m
30	Point	WptAttribs	42,18323	032	032	15-GEN-09 9:51:26	User Waypoint	S44 20.706 W65 14.144	42 m
31	Point	WptAttribs	38,33801	033	033	15-GEN-09 9:56:31	User Waypoint	S44 20.681 W65 14.191	38 m
32	Point	WptAttribs	25,12	034	034	15-GEN-09 10:00:34	User Waypoint	S44 20.592 W65 14.348	25 m
33	Point	WptAttribs	9,97925	035	035	15-GEN-09 10:05:14	User Waypoint	S44 20.508 W65 14.568	10 m
34	Point	WptAttribs	4,93237	036	036	15-GEN-09 10:07:37	User Waypoint	S44 20.464 W65 14.662	5 m
35	Point	WptAttribs	2,28882	037	037	15-GEN-09 10:08:33	User Waypoint	S44 20.453 W65 14.677	2 m
36	Point	WptAttribs	5,17273	038	038	15-GEN-09 10:09:21	User Waypoint	S44 20.434 W65 14.664	5 m
37	Point	WptAttribs	3,97119	039	039	15-GEN-09 10:11:26	User Waypoint	S44 20.462 W65 14.724	4 m
38	Point	WptAttribs	4,45178	040	040	15-GEN-09 10:16:07	User Waypoint	S44 20.360 W65 14.567	4 m
39	Point	WptAttribs	6,61475	041	041	15-GEN-09 11:20:08	User Waypoint	S44 20.367 W65 14.806	7 m
40	Point	WptAttribs	9,97925	042	042	15-GEN-09 11:53:08	User Waypoint	S44 20.468 W65 14.803	10 m

Figure 69 – The default fields imported from the GPS.

Specifically, the fields were added:
• DESCR: to describe the point where it was acquired (e.g. in a beach ridge, on an active beach, in a quarry);
• LOCALITY: to indicate the location in which the point was carried out;
• TYPE: to show the type of sample collected at that point (sediment, shells, paleosoil);
• NOTE: for more descriptive notes;
• DATING: dating obtained on the samples were inserted.

Furthermore, during the field work a lot of pictures were made. The pictures were acquired and placed in one folder, to use them to hyperlinks through the ArcGIS geographic database (Fig. 70). In fact, in ArcMap by clicking on the point corresponding to the sampling point, you see the picture of the sample.

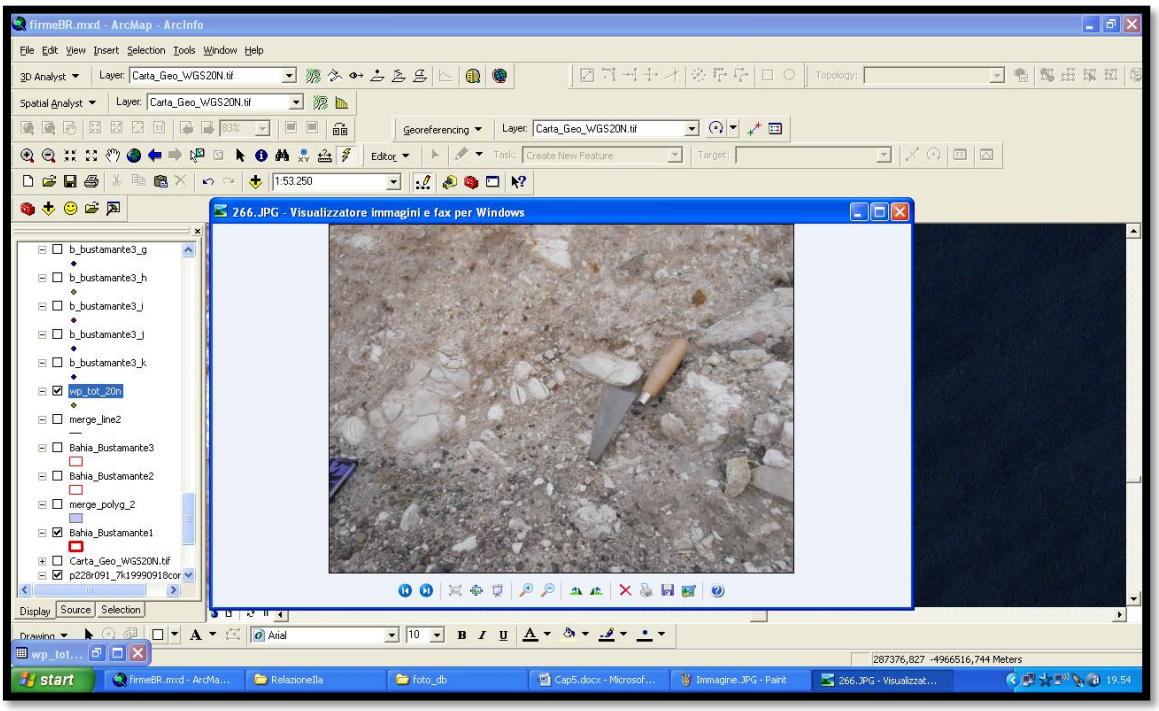

Figure 70 - Hyperlink to a photo database using ArcMap.

5.3. ECOLOGY AND DISTRIBUTION OF THE ANALYZED SPECIES

The species analyzed in this study were selected based on their abundance in the studied deposits and their degree of preservation. On the basis of these characteristics, the selected species are: *Ameghinomya antiqua, Mytilus edulis, Aulacomya atra* and *Nacella deaurata.*

Below are the main characteristics in terms of ecology and geographical distribution of these species.

5.3.1. *Ameghinomya antiqua*

Ameghinomya antiqua is a marine bivalve species belonging to the family Veneridae. This species has a generic and subfamiliar assignment still debated. Some authors include it in *Venus* (Fisher-Piette, 1975; Fisher-Piette & Vukadinovich, 1977; Osorio *et al*., 1983; Stead *et al*., 1997; Reid & Osorio, 2000; Gordillo *et al.,* 2008), in *Protothaca* (Carcelles, 1950; Feruglio, 1950; Castellanos; 1967; Herm, 1969; Rìos; 1975, 1994, Figueiras & Sicardi, 1979; Aguirre & Farinati, 2000), in *Chione* (Frizzel, 1936; Carcelles, 1944) or in *Ameghinomya* (Ihering, 1907; Soot-

Ryen,1959; Figueiras & Sicardi, 1969; Osorio & Bahamonde, 1970; Osorio *et al.*, 1979; Bernard, 1983; Beu, 2004; Huber, 2010; Pérez *et al.,* 2013). According to Gordillo *et al.* (2008), it differs from species of *Protothaca* in its shape and in the prominence of its external sculpture (Beu, 2004) and it is distinguished from species of *Ameghinomya* for the presence of a nodular anterior lateral tooth in the left valve (Osorio *et al*., 1983).

Moreover, in a molecular analysis within the family Veneridae, Kappner and Bieler (2006) found that this morphotype (*i.e.*, with a lateral tooth) falls into the Venerinae *s. novo clade*.

In a recent work Pérez *et al.* (2013), based on morphological characteristics and phylogenetic analysis, include the species *Venus antiqua* in the genus *Ameghinomya* Ihering, 1907.

In the light of this new work within this thesis I refer to this species as *Ameghinomya*. *Ameghinomya antiqua* shows a thick medium to large shell, subcircular, inequilateral. The umbo is prosogyrate and the lunule is lanceolate. The external surface is ornamented with concentric lamellae more prominent towards the ventral edge, which give the shell a reticulated appearance (Fig. 71). The periostracum is absent. The hinge is characterized by three cardinal teeth in each valve and a small tooth front side of the valve left (Guzman *et al.*, 1978). The inner edge results finely striated and the pallial line is separated from the edge showing a short triangular sinus (Fig. 72). This species, like all the specimens belonging to the family Veneridae, presents aragonite shell (Taylor *et al.,* 1973; Carter *et al.,* 1990; Takesue and van Geen, 2004; Foster *et al*., 2008).

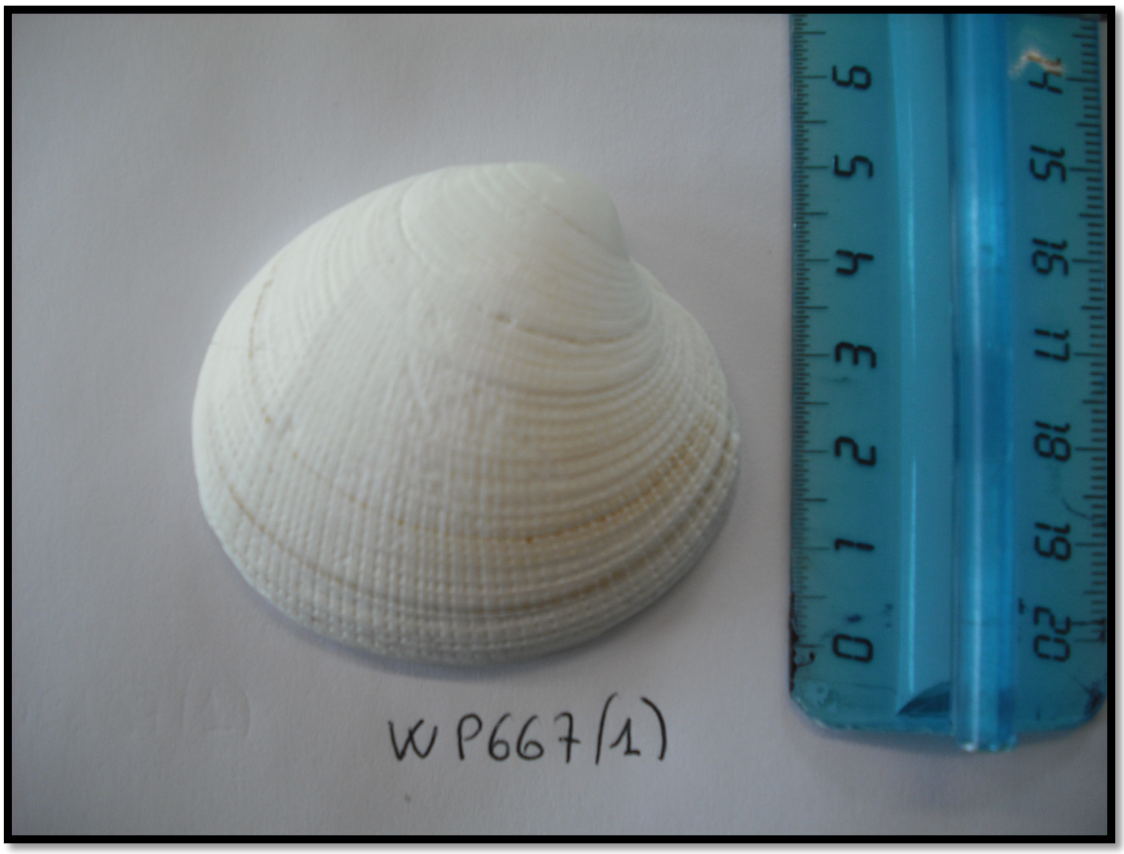

Figure 71 – Modern specimen of *Ameghinomya antiqua*. Exterior view.

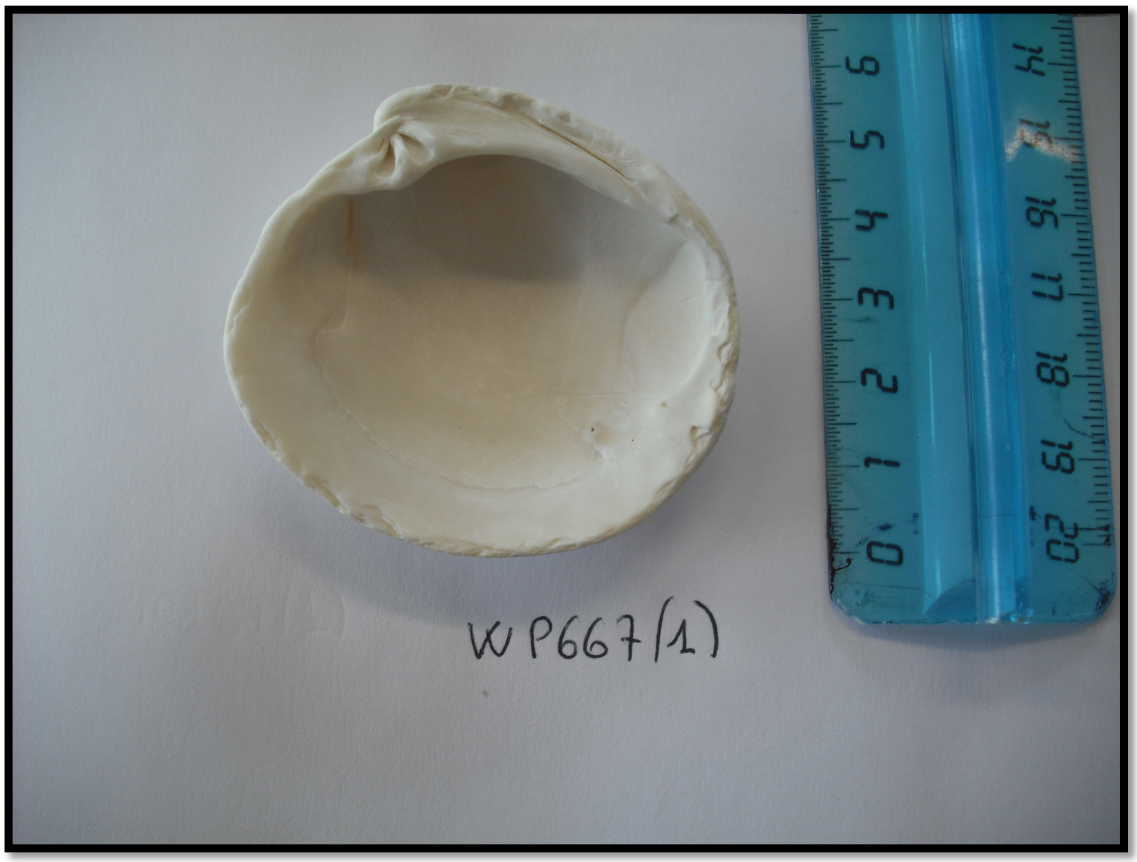

Figure 72 - Modern specimen of *Ameghinomya antiqua*. Interior view.

Ameghinomya antiqua is a semi-infaunal or infaunal filter feeder living on silty-sand to gravelly sand bottoms from the lower half of the intertidal zone to 40 m in depth (Ramorino, 1968; Clasing *et al.,* 1994; Urban, 1994a; Urban and Tesch, 1996; (Stead *et al.*, 1997; Reid and Osorio, 2000; Aguirre, 2003; Gordillo *et al.,* 2008). This species feeds on plankton and organic detritus, and also exhibits annual reproductive cycles with long spawning (Verdinelli and Schuldt, 1976; Lozada and Bustos, 1984), displaying variations in their reproductive cycles, which can be associated with variations in salinity and temperature affecting the coastal areas (Stead *et al.*, 1997). *Ameghinomya antiqua* may develop under normal to lower salinity (21-27‰ according to Reid and Osorio, 2000) and tolerates a temperature range from 4º to 20ºC (Urban, 1994b).

Ameghinomya antiqua is a dominant member of the shallow-water, soft bottom communities of the south central part of South America coast zone, also inhabiting the Beagle Channel (Fig. 73), and can be found up to Callao (northern Peru) on the Pacific side, while on the Atlantic side can be observed up to the coasts of Uruguay (Urban, 1996; Osorio *et al.,* 1983; Reid & Osorio, 2000; Gordillo *et al.,* 2008).

Ameghinomya antiqua is a typical element of the Magellanic Province, but also penetrates the Argentinean Province (Aguirre *et al*., 2008).

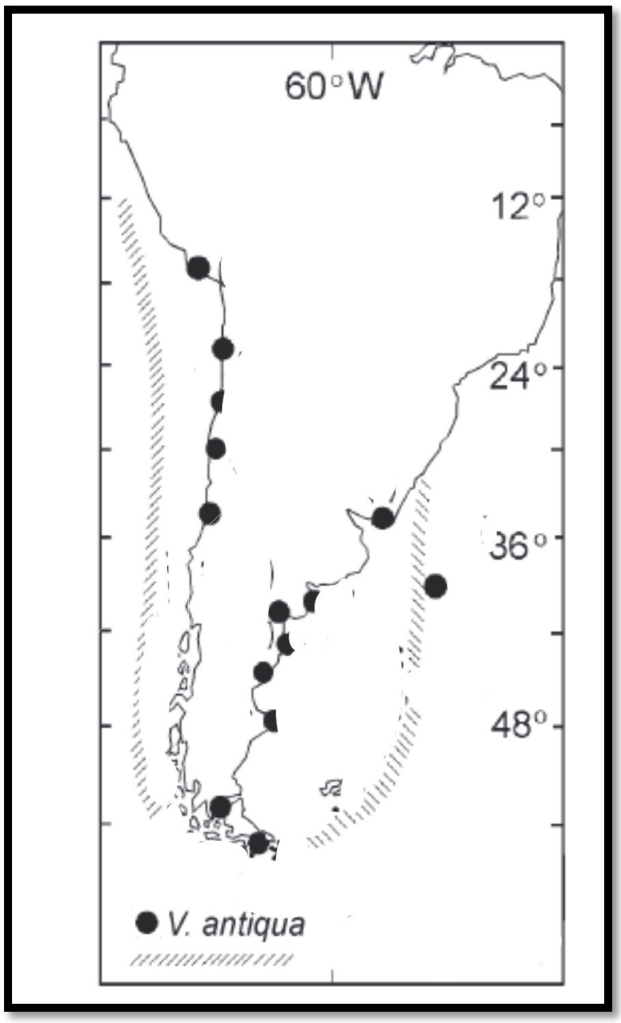

Figure 73 – Living distribution (slashed line) and locations of fossil records (dots) of *Ameghinomya antiqua* (*Venus antiqua* in the paper*)* from Gordillo et al. (2008).

The maximum northward extension of fossils *Ameghinomya antiqua* corresponds to a middle Pleistocene interglacial episode dated to the Marine Isotopic Stage 11 (Ortlieb *et al.,* 2003).

In the San Jorge gulf and the surrounding areas (e.g. Bahia Vera and Bahia Camarones) the oldest deposits containing *Ameghinomya antiqua* are dated to the Marine Isotopic Stage 9 (see Chapter 2 and references therein).

Ameghinomya antiqua, thanks to its stratigraphic distribution, the good state of preservation in fossil deposits and the high frequency both in the fossil levels both in current deposits, is one of the best species to be analyzed to reconstruct the paleoclimatic and paleoenvironmental conditions of the Atlantic coast of Argentine Patagonia.

5.3.2. *Mytilus edulis*

Mytilus edulis, also known as blue mussel, is a medium-sized marine bivalve mollusc of the family Mytilidae. This species is characterized by a smooth inequilateral shell, usually purple, blue, or dark brown, which features concentric growth lines emanating from the hinge (Fig. 74). The interior of the shell is pearl-white (Fig. 75). Internally the mantle has a whitish/yellow color, with a posterior adductor scar significantly larger than its anterior adductor scar. Extending from the closed shell are fibrous brown byssal threads for attachment to a surface. The outer surface of the shell is covered by the periostracum which when eroded, exposes the colored prismatic calcitic layer.

Figure 74 – Modern *Mytilus edulis.* Exterior view after cleaning of the shell and periostracum removal.

Figure 75 – Modern *Mytilus edulis.* Interior view.

The shell of *M. edulis* consists of biogenically produced calcium carbonate and proteins. The calcium carbonate is constituted by calcite and aragonite, which form a thick prism outer and a thin inner nacre layer respectively. Moreover, a resistant outer organic layer, the periostracum, overlay the calcitic layer (Wilbur, 1972). Organic material is also present within single crystals as well as providing a framework for the mineralized component.

The specimens belonging to this species are semi-sessile, having the ability to detach and reattach to a surface allowing the mollusk to reposition itself relative to the water position.

Mytilus edulis is an epifaunal suspension feeder species found in intertidal up to subtidal environment (it has been reported up to 25 m in depth) attached to rocks and other hard substrates (Seed and Suchanek, 1992) by strong thread-like structures called byssal threads, secreted by byssal glands located in the foot of the mussel, or as loose beds on sandy substrata (Lozan *et al.,* 1996).

Mytilus edulis is highly tolerant to a wide range of environmental conditions. This species is eurythermal and is able to withstand freezing conditions for several months. Blue mussels are well acclimated to a 5 to 20 °C temperature range, with

an upper sustained thermal tolerance limit of about 29 °C for adults Almada-Villela *et al.*, 1982). Blue mussels do not thrive in salinities of less than 15‰.

Mytilus edulis is the most widely distributed species within the genus and according to Aguirre & Farinati (2000), Aguirre (2003) and Aguirre *et al.* (2009) belongs to the group I, in which eurythermal or cosmopolitan species are included (Fig. 76).

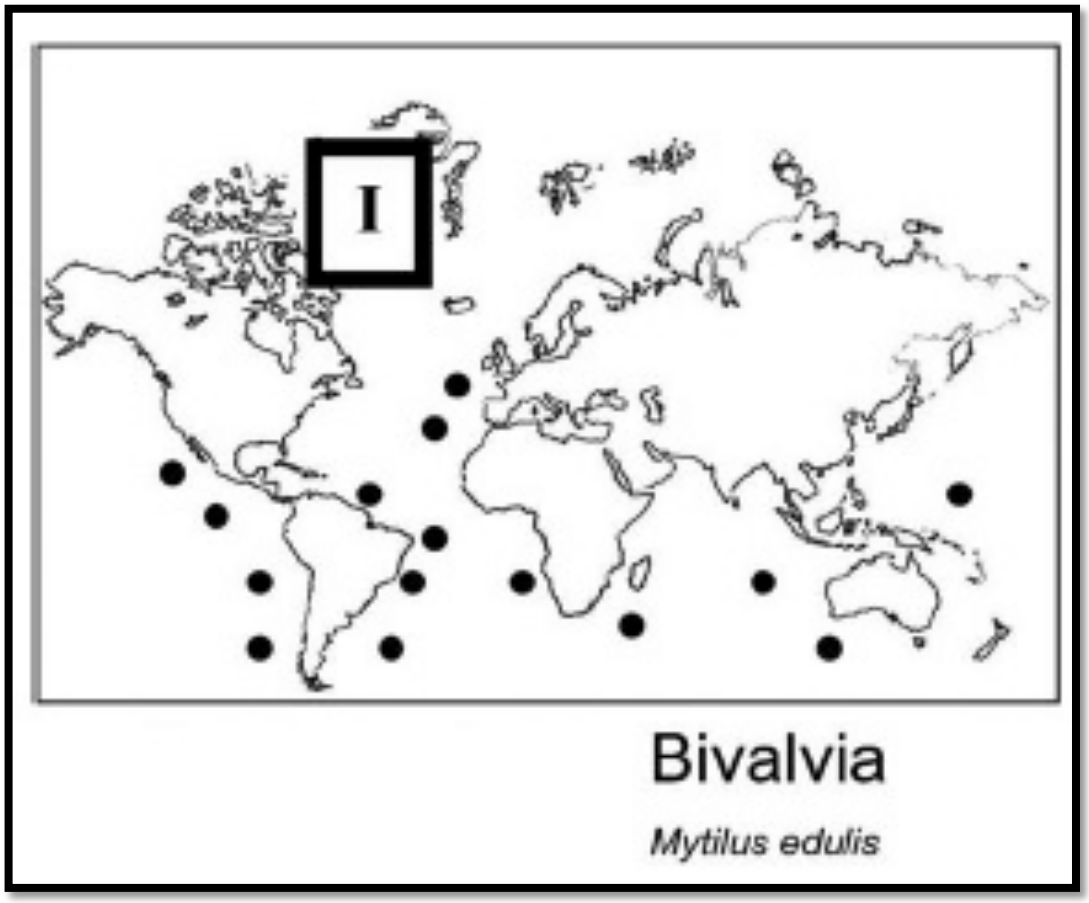

Figure 76 – *Mytilus edulis* modern distribution (Aguirre *et al.*, 2009).

Mytilus edulis represents one of the most abundant species within the marine Holocene deposits of the Patagonia Atlantic coast, but it is also present in the Pleistocene successions (Aguirre & Farinati, 2000; Aguirre, 2003; Aguirre et al., 2005; 2006; 2008; 2009; Ribolini *et al.,* 2011; Zanchetta *et al.,* 2012).

5.3.3. *Aulacomya atra*

Aulacomya atra also belongs to the family Mytilidae (Soot-Ryen, 1959). This species has big shell usually purple, blue in adult specimens or light brown in juvenile, equivalve and inequilateral. The umbo, as in *Mytilus,* is prosogirate. The hinge presents interlocking folds, at the left valve forms a tooth, which is inserted into a depression on the right. The external surface shows well differentiated radial,

weakly anastomosing costae (Fig. 77). The interior of the shell is nacreous (Fig. 78).

Figure 77 – Modern *Aulacomya atra.* Exterior view after periostracum removal.

The shell microstructure is constituted by an outer calcitic fibrous prismatic layer and an aragonitic inner nacreous layer (Fig. 78). The outer calcitic layer is covered by the periostracum.

Figure 78 – Modern *Aulacomya atra.* Interior view.

Aulacomya atra is an epifaunal suspension feeder species living in intertidal up to subtidal environment generally up to 30/40 m in depth, but occasionally it has been found up to 85 m along the Malvinas Islands coasts (Zaixso, 1999), attached to rocks and other hard substrates. Along the Argentinean Patagonia coasts this species forms shoals whose maximum concentration is between 3 and 12 m depth (Zaixso, 1999).

Aulacomya atra is linked to environments with high hydrodynamic (currents, waves) and is considered to affinity cold (Group IV belonging to the Magellanic Province according to Aguirre & Farinati, 2000 and Aguirre *et al*., 2009; Fig. 79). Being also a form intertidal is certainly euryhaline with ability to withstand values higher or lower than those typical marine. In these environments is also reported in pools with low salinity (15-20 ‰).

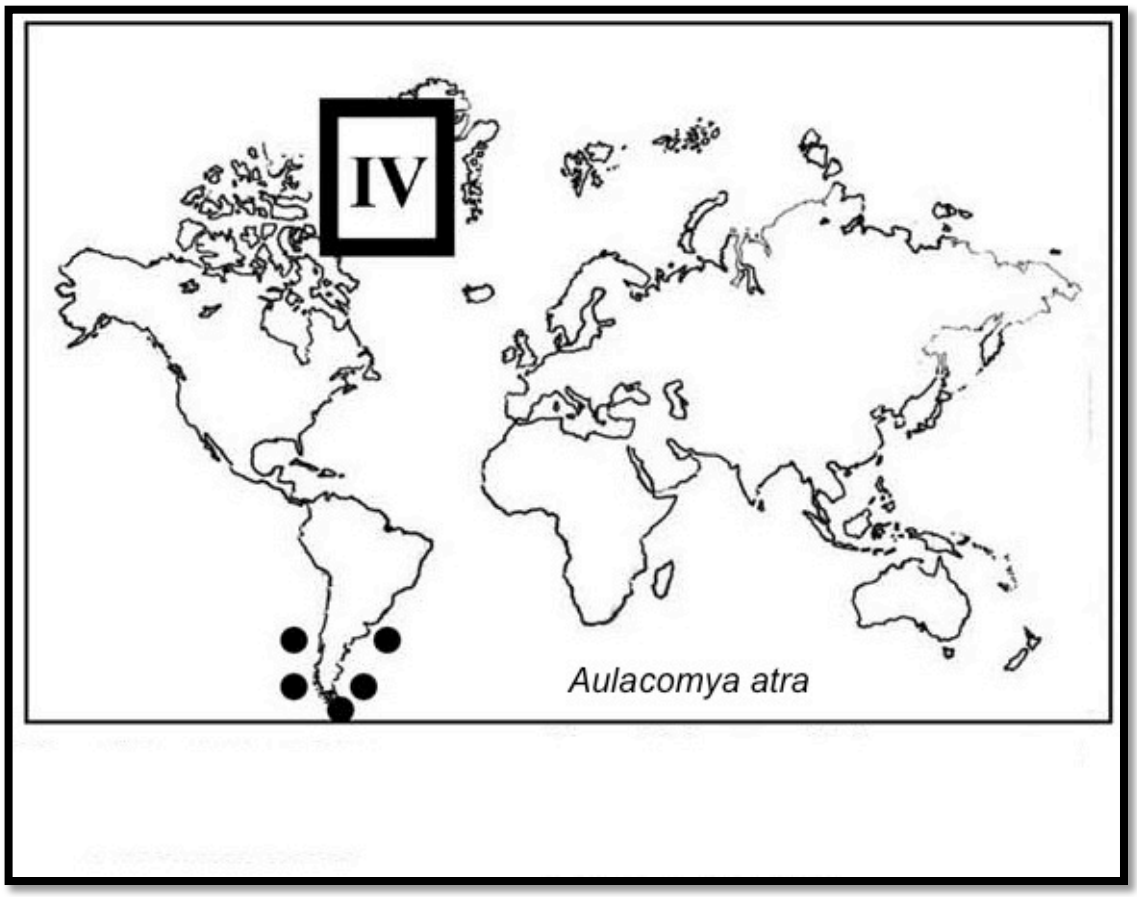

Figure 79 – Geographical distribution of *Aulacomya atra* in South America (Aguirre *et al.*, 2009).

Aulacomya atra presents a geographical distribution between El Callao (12° S) in Peru and the Strait of Magellan along the Pacific coast, and it reaches the southern areas of Brasil along the Atlantic coast (Osorio *et al.*, 1979; Pìa Mena *et al*., 2001). This species is also found on the coast of New Zealand and Southern Africa, from Namibia to Port Alfred, South Africa (Branch *et al.,* 2005).

Together with *Mytilus edulis, Aulacomya atra* is one of the most abundant species within the Holocene marine deposits outcropping along the Patagonian Atlantic coast (Aguirre & Farinati, 2000; Aguirre, 2003; Aguirre et al., 2005; 2006; 2008; 2009; Ribolini *et al.,* 2011; Zanchetta *et al.,* 2012).

5.3.4. *Nacella (Patinigera) deaurata*

The species *Nacella (Patinigera) deaurata* belongs to the family Nacellidae, marine gastropods molluscs.

The grayish-brown shell is conical, oblique, thick and relatively translucent (Fig. 80). Numerous broad rounded radial ribs and well-defined concentric growth lines from

the central zone towards the margin are present. Primary ribs are dark brown colored and bifurcate towards the margin, the interspace is white. The interior of the shell is nacreous, with a brown spot corresponding to the animal body impression and shows radial dark brown lines and white interspaces which are the equivalent to the exterior color pattern (Fig. 81).

Figure 80 – Fossil *Nacella (Patinigera) deaurata*. Exterior view.

Figure 81 – Fossil *Nacella (Patinigera) deaurata*. Interior view.

The specimens belonging to the genus *Nacella* have a predominantly foliated calcitic shell structure, with a small amount of aragonite (Mac-Clintock, 1976).

These limpets are epibenthic, sessile grazer feeder, found on rocky shores of supralittoral, intertidal and sublittoral environments up to 30 m depth (Morriconi, 1999; Gonzáles-Wevar *et al.,* 2011).

N. deaurata are cold-water limpets found in the Antarctic and sub-Antarctic waters, very common on rocky-shores of Patagonia coasts and of the Beagle Channel (Morriconi, 1999; Aguirre & Farinati, 2000; Malanga *et al*., 2004; Aguirre *et al.,* 2009) and in archaeological sites of this region (Orquera and Piana, 2001, 2002; Verdún, 2010; Verdún *et al.*, 2010; Colonese *et al.*, 2011, 2012), having their center of distribution in the Magellanic Province of South America.

No data has been found on the salinity tolerance of this species. However, being a form also intertidal, is certainly euryhaline with ability to withstand different values from those typical marine.

Specimens of *Nacella (Patinigera) deaurata* were found in both the Holocene and Pleistocene deposits outcropping in the study area (Aguirre & Farinati, 2000; Aguirre, 2003; Aguirre et al., 2005; 2006; 2008; 2009; Zanchetta *et al.,* 2012).

5.4. ANALYTICAL METHODS

5.4.1. Sample preparation

One to ten whole and well preserved shells were analyzed for each layer.

The shells were rinsed several times with deionized water and hydrogen peroxide and cleaned in an ultrasonic bath. If some part of shells was still dirty, it was cleaned manually with a drill to ensure complete removal of all detrital material. The shells were transferred again to the ultrasonic bath and cleaned using deionized water and then dried in an oven at 60°C. Each valve of *Ameghynomia antiqua* was cut using a rock saw along the axis of maximum growth along to anterior to the posterior line of section (Fig. 82) and then a half valve was powdered using a mill in agate rings (Fig. 83) for XRD, stable isotope and trace element analyses, whereas for specimens belonging to the Mytilidae Family and *Nacella deaurata* a whole valve was powdered. The remaining half valve of *A. antiqua* not powdered, and the other valve of *Mytilus edulis* or *Aulacomya atra,* in the case of samples with articulated shells, were used for radiocarbon and U/Th dating.

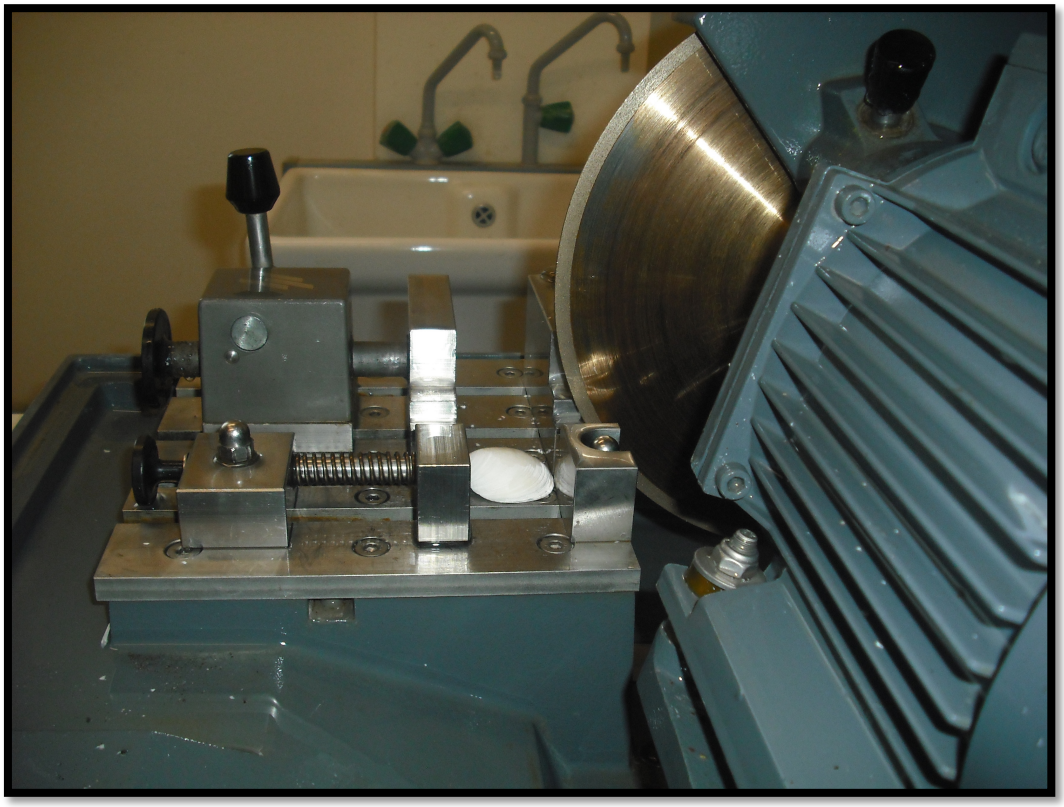

Figure 82 – Rock saw cutting an *Ameghynomia antiqua* shell along the axis of maximum growth.

Figure 83 – *Ameghinomya antiqua* shell powdered with a ring mill.

5.4.2. Powder X-ray diffraction analysis

Aragonite, forming totally or partially the shell of the bivalves analyzed, is the least-stable calcium carbonate phase at the Earth's surface (Fig. 84) and is diagenetically transformed into low-Mg calcite (Land, 1967; Brand and Veizer, 1980).

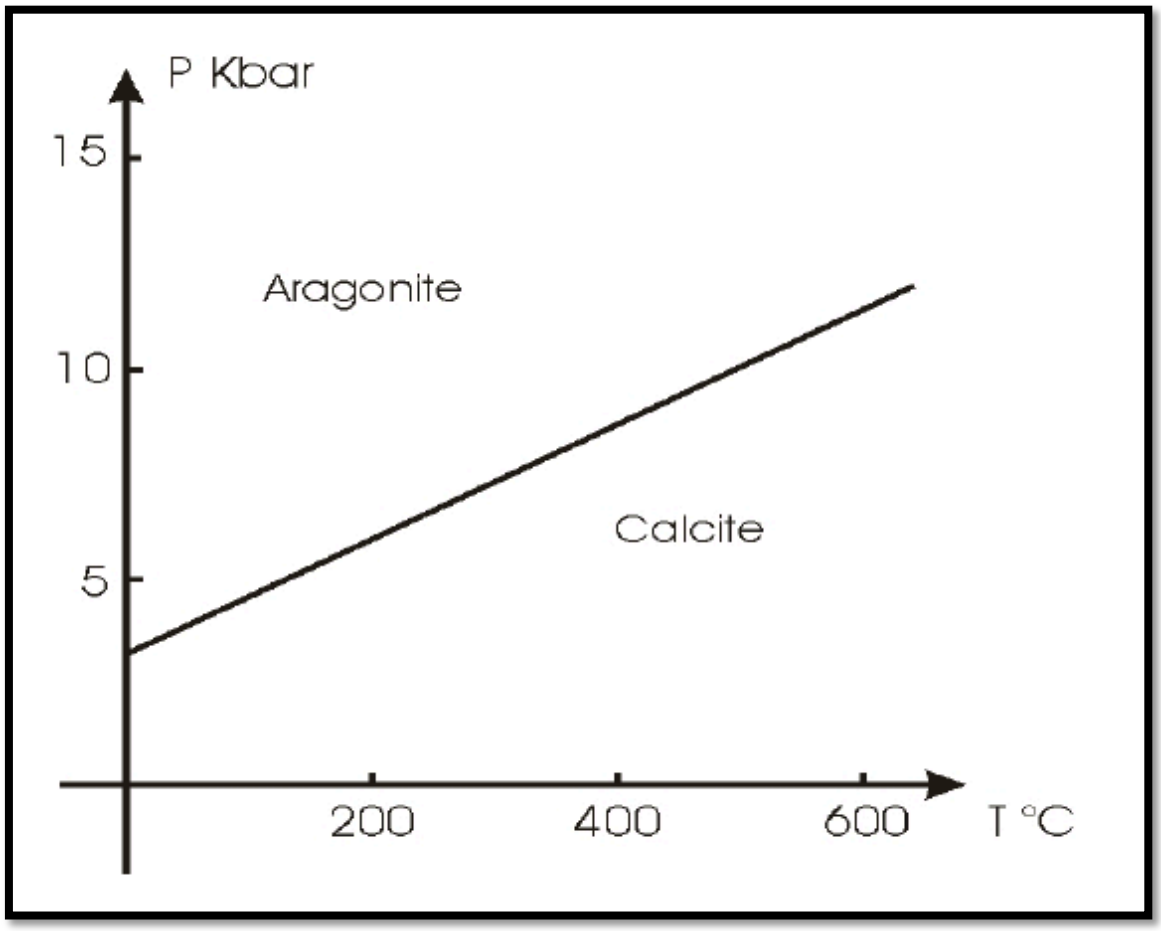

Figure 84 – Stability fields of calcite and aragonite (Clark, 1957).

It has been demonstrated that the transformation of aragonite in calcite causes variations in the isotopic composition and concentration of trace elements in the shells carbonate (Fig. 85 and Chapter 4.3).

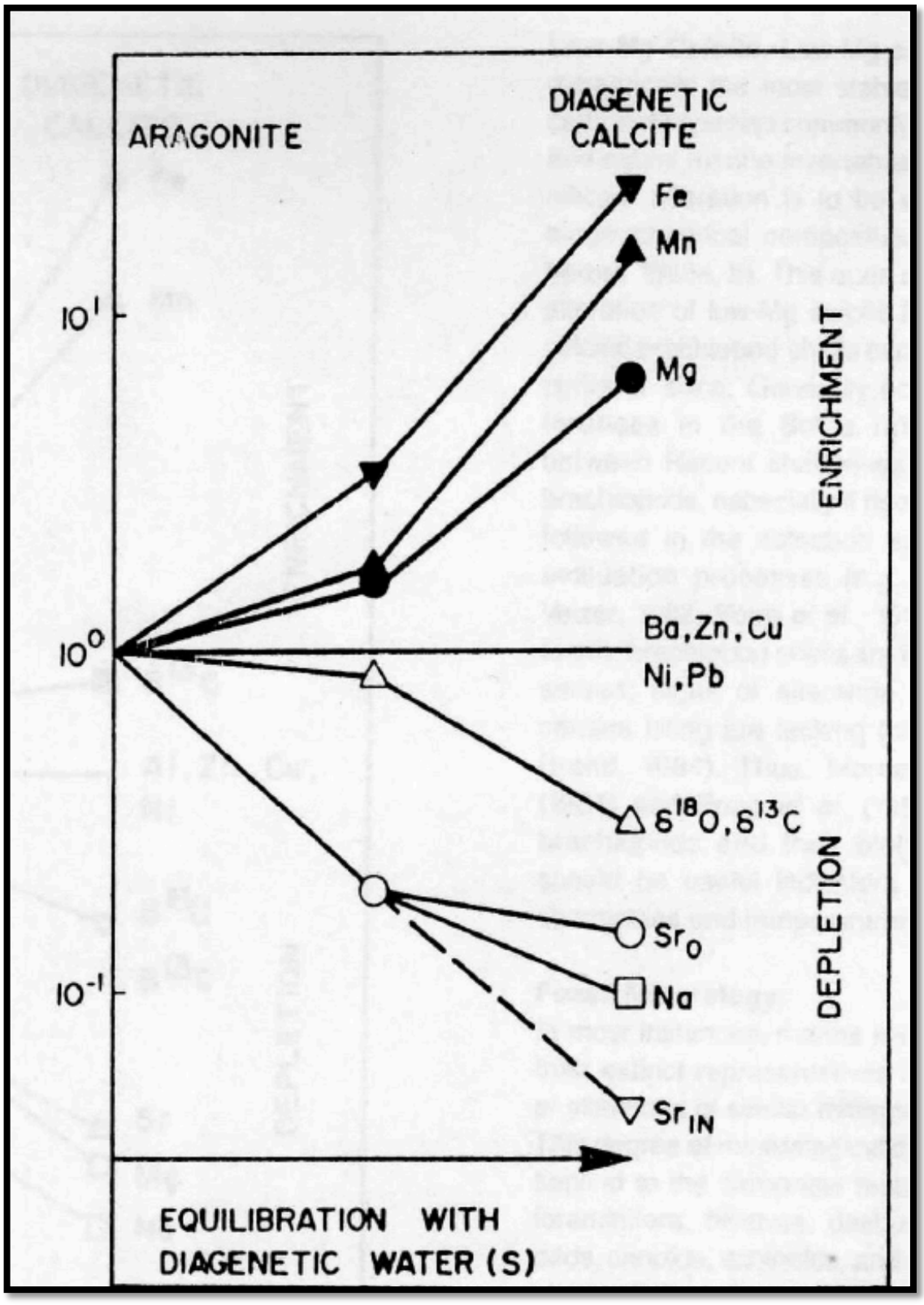

Figure 85 – Trace element and stable isotopes diagenetic trends (Brand & Morrison, 1987)

X-ray diffraction provides an easy way to distinguish between the two polymorphs of $CaCO_3$, aragonite and calcite.

For this reason several shell mineralogical analyses determined by qualitative X-Ray powder Diffraction (XRD) of random samples were carried out to indicate whether diagenetic mineral transformation had occurred.

The powder diffraction is the general method used in the study of sedimentary materials.

The sample powdered (1-50 micron particle size) is introduced in the diffractometer. The direction of the primary beam of XR remains constant because the sample rotates around an axis normal to the primary beam. The diffracted beams that arrive at the detector, in solidarity with a goniometer, are reported as peaks on a paper. The diffractometer is designed so that the arm of the goniometer and the detector integrated with it, rotate the double compared to the direction of the sample (Fig. 86). So while the sample rotates by an angle θ, the detector wheel angle 2θ, which is thus the angle read from the protractor.

The geometry of the diffractometer is such that only the grains of the mineral whose lattice planes are parallel to the surface of the sample holder will contribute to the beam secondary reflection that will arrive at the detector.

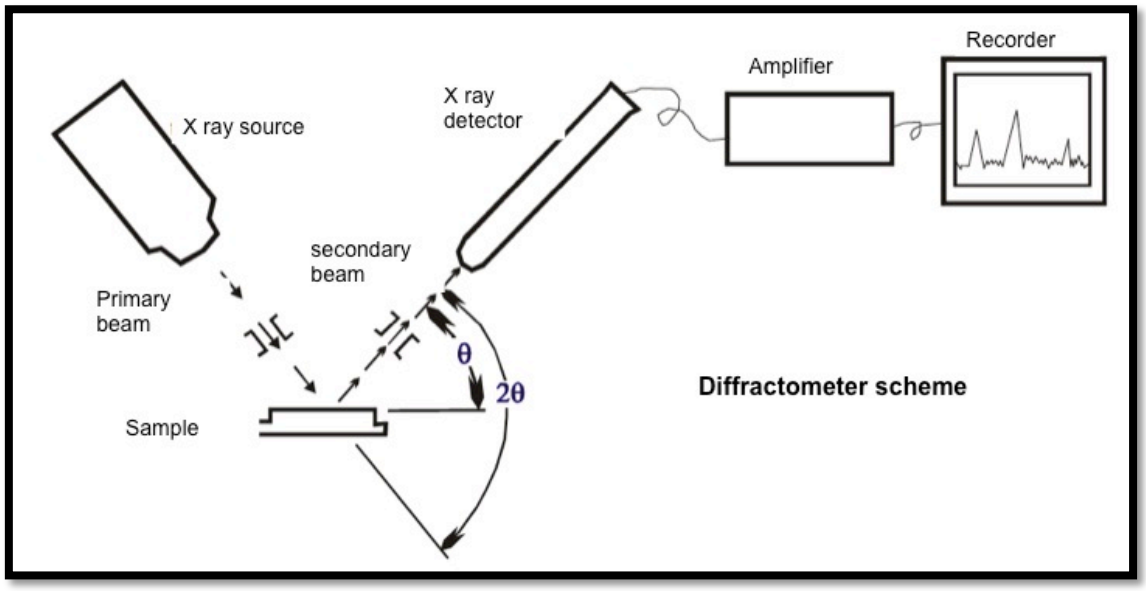

Figure 86 – Diffractometer scheme.

Each angle is relative to a crystal lattice that has a distance "d" between the different floors. Every mineral has a particular number of lattice, then the diffraction produces a single set of reflections (peaks) on the strip named diffractogram. This characteristic is due to the position of each measured reflection with the angle 2θ

and with the intensity of each reflection. The "relative intensity" (I/I_1) is equal to the intensity of a particular reflection as ratio with the stronger reflection.

Calcite and aragonite have their highest-intensity peaks at different positions, and the general look of the two patterns is different. Aragonite has its greatest peak (111) at relatively small °2θ and has several lesser peaks, whereas calcite has a booming 104 peak a bit to the right of the aragonite large peak, and few and comparatively small other peaks (Fig. 87).

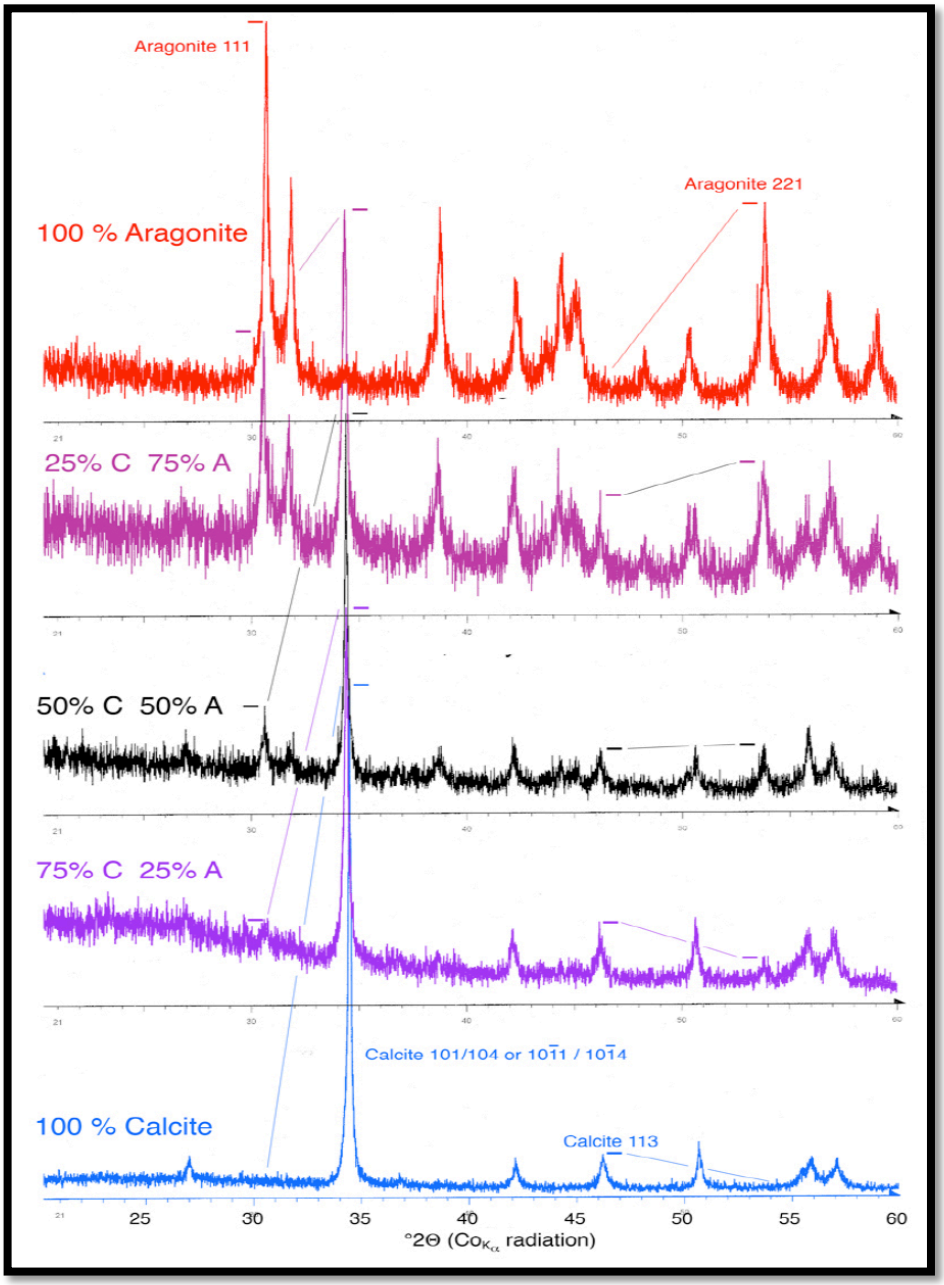

Figure 87 – Calcite (C) and aragonite (A) mixtures diffractograms (Railsback, 2012).

XRD analyses were performed at the Earth Science Department in Pisa, using a diffractometer equipped with a Philips PW 1830 generator, a Philips PW1050725 goniometer and an acquisition system of the diffractions Philips PW1710. The profile-analysis of x-ray reflections and the phase identification was made using the Winfit program.

The mineralogical composition of fossil shells was compared with the mineralogical composition of modern shells (Appendix A).

To identify the limits of detection of calcite in a mixture with a predominantly aragonitic composition, some mixtures of known composition of calcite and aragonite were prepared. Specifically, the XRD analyses were performed on powders with a percentage of 1%, 3.5%, 5% and 10% of calcite in aragonitic samples.

XRD analysis was carried out also on 11 paleosols sampled in the study area.

5.4.3. Petrographic analysis

Thin sections of the shell of modern, Holocene and Plestocene specimens of *Ameghinomya antiqua* were performed to observe the structure of the shell and possible recrystallization and alteration.

The shells were cut with a rock saw along to anterior to the posterior line of section and embedded in epoxy resin.

Thin sections were then observed with a petrographic microscope.

5.4.4. Dating methods

5.4.4.1. Radiocarbon dating

Almost 50 samples of shells and sediments from Holocene deposits were dated using the radiocarbon dating (Appendix A) for improving the stratigraphy of Holocene beach-ridges successions.

Selected shell samples for radiocarbon dating were firstly cleaned mechanically, then cleaned in ultrasonic bath with addition of oxygen peroxide and gently etched with dilute HCl.

The ^{14}C dating was performed in collaboration with the Centre for Isotopic Research

on Cultural and Environmental heritage (CIRCE) of Caserta (Director Prof. Terrasi) trough AMS facility (Tandem acceleration Pelletron 3 MV). From the selected samples, CO_2 is produced in muffle at 920°C for 6 hours, inside a sealed quartz tube and then purified in a cryogenic line. The purified CO_2 is then converted to graphite by the Bosch reaction in a multisamples graphitization line controlled by a Lab View interface (Passariello *et al.,* 2007). The graphite samples are pressed into an aluminium cathode and then measured with the AMS system (Terrasi *et al.,* 2008).

Radiocarbon data are reported as Fraction Modern (FM), the ratio $^{14}C/^{12}C$ in the sample, corrected for isotopic fractionation, with respect to a "Modern" sample defined as the 95% activity (in AD 1950) of NBS Oxalic Acid I normalized to $\delta^{13}C$ =-19 ‰ PDB (Olsson, 1970). Conventional radiocarbon age is always reported without adjustment for differences in ^{14}C specific activity of reservoirs, i.e. the difference between the atmospheric ^{14}C content and the local ^{14}C content of ocean surface water.

Schellmann & Radtke (2010) observed that the estimate reservoir effects, on the whole, are relatively close to the average value for the mean ocean (about 400 years according to Hughen *et al.*, 2004). Nevertheless, they suggested care in using calibrated chronologies.

Data estimating reservoir marine correction for the sector studied of Patagonian coast, in fact, are very few. In particular, for present day reservoir effect Cordero *et al.* (2003) reported ^{14}C offset values from different localities between ca. 42° and 50°S for surface waters ranging between ca. 180 and 530 yr. Surface water of the Falkland current has a ^{14}C reservoir value of about 560 to 600 years, corrected for atmospheric atomic testing (Broecker and Olson, 1961). For the past, Butzin *et al.* (2005) use a 3-D ocean circulation model to asses reservoir age differences in Southern Ocean since LGM. Reservoir Age Model Estimates for this area are around 500 yr (http://www.radiocarbon.ldeo.columbia.edu).

A living shell of *Aulacomya atra* collected in the studied area gave an apparent age of –390±50 yr BP.

For this reason, conventional radiocarbon ages are firstly reported and discussed without reservoir marine correction.

For completeness, however, corrections and calibrations are performed using the marine calibration curve Marine13 curve in CALIB 7.0 (Reimer *et al.*, 2013). All

calibrated data were presented using 2 sigma uncertainty term (95% degree of confidence).

5.4.4.2. U/Th dating

The U–Th decay scheme is a highly robust dating method for carbonate materials up to half a million years in age even if application to shell is still challenging (Broecker, 1963; Blanchard *et al.,* 1967; Kaufman *et al.,* 1971; 1996; McLaren and Rowe, 1996; Labonne and Hillaire-Marcel, 2000).

Small chunks of solid and pristine shell material were extracted from 8 *Ameghinomya antiqua* specimens coming from Pleistocene outcrops in order to apply the α-spectrometric $^{230}Th/^{234}U$ dating method. Almost all of the samples were from outcrops dated in prior to Schellmann & Radtke (1997, 2000; 2003) so as to compare the age obtained by this method with those obtained by the method of ESR.

Bearing in mind the problem of a secondary uranium uptake in fossil and modern shell (Chapter 4.3) and having observed through the thin sections (Chapter 6) that major alterations of the shell take place in the outer layer of the shell, the samples of *A. antiqua* were then prepared for U/Th dating abrading with a drill the inner and the outer surfaces of the shell and keeping only the core of the inner layer.

The U/Th ages were determined using a multicollector inductively coupled plasma mass spectrometer (MC-ICP-MS) at the School of Earth Sciences at University of Melbourne following the method of Hellstrom (2003, 2006).

Uranium and thorium are separated using ion-exchange resins and liquid-liquid extraction techniques and counted using an alpha spectrometer equipped with silicon-barrier detectors. The age of the pedogenic carbonate is calculated measuring the ($^{230}Th/^{232}Th$), ($^{234}U/^{232}Th$) and ($^{238}U/^{232}Th$) activity ratios of four coeval sub-samples, in order to obtain the value of ($^{230}Th/^{234}U$) and ($^{234}U/^{238}U$) activity ratios in the pure carbonate fraction. Such values are respectively calculated from the slopes of the regression lines in ($^{230}Th/^{232}Th$) vs ($^{234}U/^{232}Th$) and ($^{234}U/^{232}Th$) vs ($^{238}U/^{232}Th$) isochron plots.

5.4.5. Strontium isotope analysis

For selected samples $^{87}Sr/^{86}Sr$ analyses for characterizing past local seawater composition and/or possible mixing with local freshwater were performed.

Sr isotopic analyses were carried out on 7 specimens of *A. antiqua* collected from active beach and Holocene and Pleistocene beach ridges in Camarones and Bahia Bustamante area and on 7 Mytilidae shells sampled on the modern beach and in Holocene ridges of different ages outcropping in Camarones area (Fig. 64).

The Sr isotope ratios act as an independent indicator of water source, i.e., continental versus marine, and therefore indirectly as indicators of salinity. Deviation away from typical marine values reflects the contribution of non seawater Sr. In the present setting, and in the absence of post-depositional and diagenetic alterations, values lower than typical marine Sr are thought to represent large additions of fresh water which contain Sr from rock weathering of the rocks which forming the catchment.

The Sr isotopic composition of the main Patagonian rivers (Chubut and Deseado rivers) that flow in the study area is comprised between 0.706340 and 0.706821 (Brunet *et al.,* 2005).

North Atlantic seawater standard currently used at NIGL gives 0.70916 ± 0.00011.

The $^{87}Sr/^{86}Sr$ ratios were measured by thermal ionization mass spectrometry (TIMS) at the laboratories of the Department of Mathematics and Geosciences, University of Trieste. The powdered samples were dissolved in ultrapure HCl; separation of Sr from the matrix was performed by ion exchange chromatography, using Bio-Rad resins Dowex AG50W X -8, 200-400 mesh, H + form. The eluate was appropriately transferred on a tungsten filament for the subsequent ionization of the element, after conversion to form nitrate and using TaCL5 as emitter.

The isotopic composition of Sr was obtained through a mass spectrometer VG 54; $^{87}Sr/^{86}Sr$ ratios were normalized to the ratio $^{86}Sr/^{88}Sr = 0.1194$ for the correction of the splitting. Repeated analysis of the isotopic standard NIST -SRM 987 gave a mean value of 0.71024 ± 0.00002 (n = 12), in agreement with literature data, was therefore not applied any correction to the measured ratios for any instrument drifts.

The errors associated with the $^{87}Sr/^{86}Sr$ ratios represent the counting statistics "in -run", expressed as 2-σ including the contribution of the dispersion relations.

5.4.6. Carbon and oxygen isotope analysis

In this thesis the research had focused on the study of the trace elements (about 150 analyses) and stable isotopes ($\delta^{18}O$ and $\delta^{13}C$, about 500 analyses) on the mollusc shells collected from middle Pleistocene to Holocene beach ridges and modern beach deposits (Appendix A).

5.4.6.1. Mass spectrometry

Mass spectrometry is an analytical technique used for both the identification of unknown substances both for the analysis of trace substances.
A mass spectrometer separates charged atoms and molecules on the basis of their masses and motions in magnetic and/or electric fields.
The methods of mass spectrometry are those far more effective to measure and quantify the relative isotopic abundances of constituents of a material (Hoefs, 2009). These methods are implemented through the use of mass spectrometers with which determine isotope ratios (Isotopic Ratio Mass Spectrometers, IRMS).
The functions of a mass spectrometer are substantially the following:

1. produce positive ions from the molecules;
2. separate the ions produced in function of their mass / charge ratio;
3. measure the relative abundance of each ion.

In general, the main constituents of an IRMS mass spectrometer (Fig. 88) are: a) the analyser (ion source, flight tube and collector system); b) a differential pumping system to maintain a vacuum within the analyser; c) the dual inlet; d) a carbonate preparation apparatus to generate CO_2 for analysis.

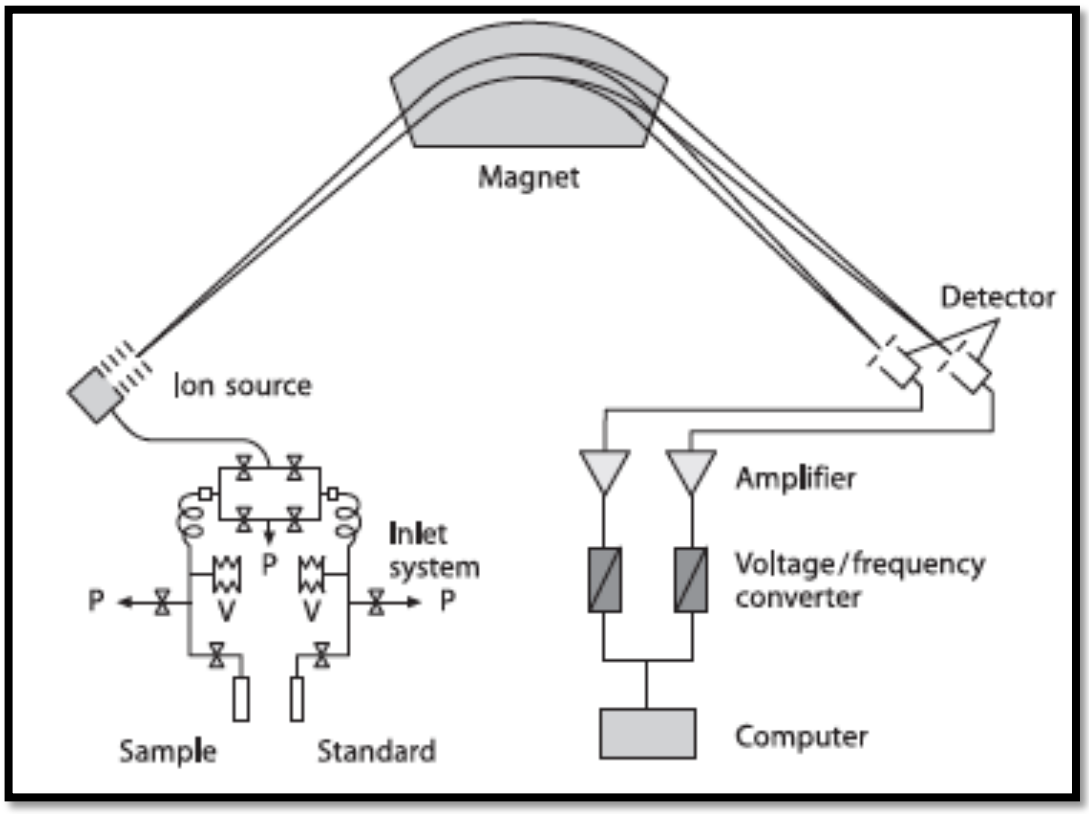

Figure 88 – Schematic representation of a gas-source mass spectrometer for stable isotopes analysis (Hoefs, 2009).

The analyser is constituted by an ion source producing a beam of mono-energetic ions from the sample gas, a flight path that passes through a permanent magnetic field, and a collector system collecting spatially separated components of the beam. The ion source impart energy to the maximum number of incoming neutral gas molecules, which are first given an electric charge by stripping them of single electron (are ionised) and then the charged molecules are given an exact amount of energy by an electric field, and shot into a magnetic field, where they follow curved paths dependent on their mass. After passing through the magnetic field, the separated beams of molecules are collected in Faraday "bucket" collectors. By collecting two or three ion beams of the isotopes (in the case of carbon dioxide, the isotopes collected are of masses 44, 45 and 46 amu) simultaneously, the ratio of the currents can be measured directly, obtaining greater precision. The ratios are calculated by the software controlling the IRMS.

The differential pumping system is constituted by a turbo-molecular pump, which provides the ultimate vacuum to the analyser, coupled with a mechanical rotary pump two-stage.

The dual inlet ensures that both sample and reference gases are presented to the analyser at the same pressure and handled in the same way while one is flowing into the ion source, the same amount of the other is being pumped to waste, ensuring that flow conditions remain the same for both sample and reference. The ion currents of sample and standard are balanced by varying the size of the gas reservoirs using stepper motors.

5.4.6.2. Bulk isotopic analysis

The isotopic analyses were carried out at Istituto di Geoscienze e Georisorse (IGG) at CNR in Pisa.

After the shells were cleaned and reduced to powder, amount of powder between 10 and 15 mg of the whole shell were weighed using a digital precision balance.

The samples were, then, introduced in glass reaction tube-shaped y, which are specially built to keep separate the sample and the phosphoric acid. 0.6 ml of 100% phosphoric acid with a disposable dropper were added to the other partitioned chamber of each reaction tube, making sure to do not drip any acid on the sample (Fig. 89).

Figure 89 – Reactions tubes containing powdered shell samples and phosphoric acid.

The tubes were connected, by means of a coupling with a stopcock, to a high vacuum line where both the acid that the powder underwent a degassing until a pressure of 10^{-3} mbar, in order to eliminate atmospheric CO_2 and other gases that would, otherwise, have gone to interfere final analysis (Fig. 90).

Figure 90 – CO_2 purification and extraction line used for the carbonate isotopic analysis.

The tube and the joint were then immersed in a thermostatic bath at a temperature of 70 °C; here, once the sample and the phosphoric acid reached equilibrium with the water temperature, were put in contact and left to react for one hour (Fig. 91).

The CO_2 is produced by reaction of the carbonate with phosphoric acid:

$$3CaCO_3 + 2H_3PO_4 \Leftrightarrow Ca_3(PO_4)_2 + 3CO_2 + 3H_2O$$

Figure 91 - Thermostatic bath.

The carbon dioxide released by the reaction between the phosphoric acid and the carbonate powder was purified on the high vacuum line using liquid nitrogen (T = -196 °C) and a cryogenic mixture (T = -80 °C) formed by ethyl alcohol and liquid nitrogen (Fig. 92).

Figure 92 – Extraction of carbon dioxide.

At the end of the purification process the CO_2 devoid of extraneous condensable components in liquid nitrogen was collected in special sample holder for the final analysis to the mass spectrometer.

The stable isotope composition of carbon and oxygen was analysed by mass spectrometric determination of the mass ratios of carbon dioxide (CO_2) using a Varian Mat 252 mass spectrometer (Fig. 93).

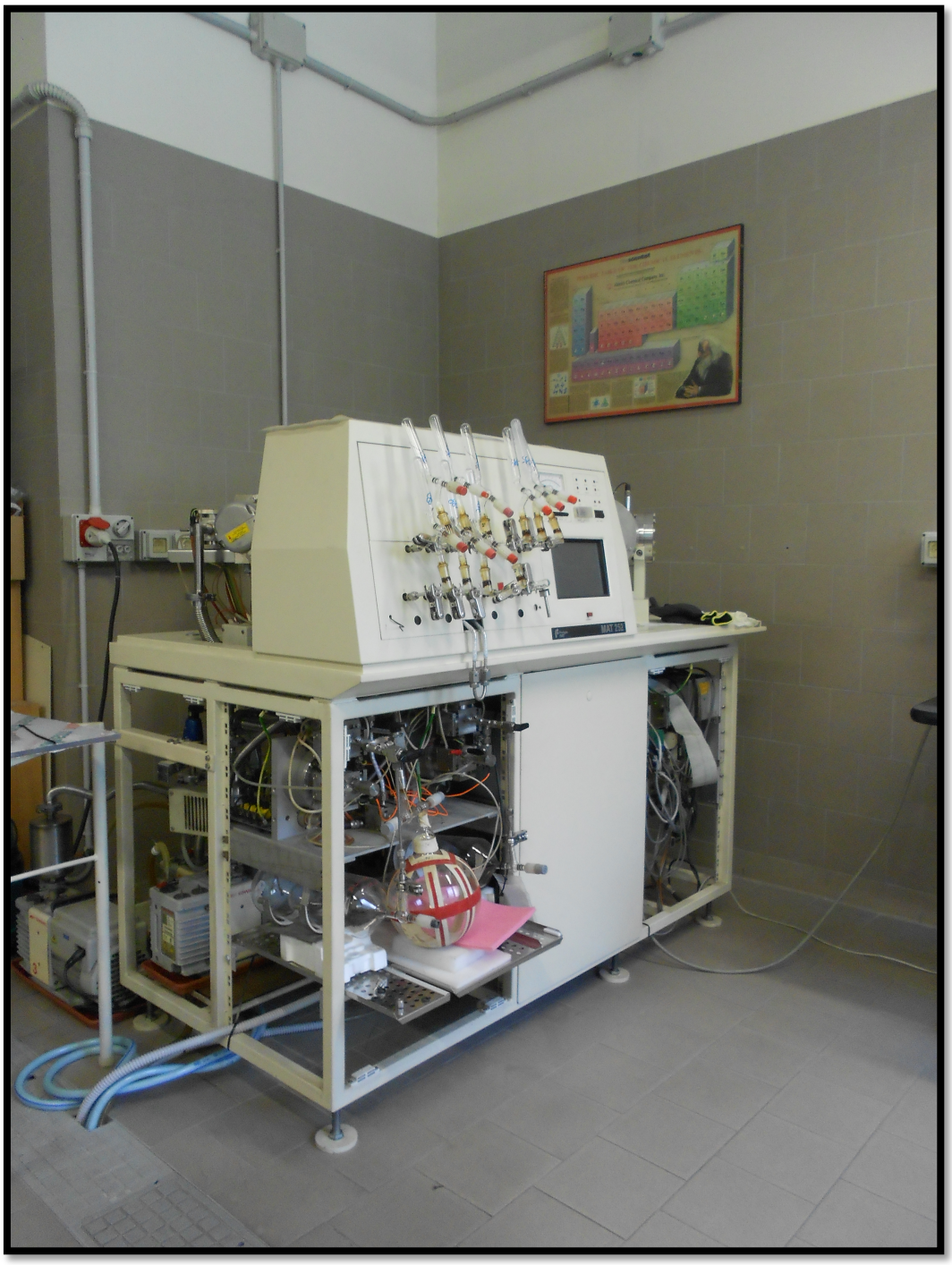

Figure 93 – Varian Mat 252 mass spectrometer used for the isotopic analysis.

The IRMS measures two ratios: the mass 45/44 ratio and the mass 46/44 ratio, these being the three isotopic masses collected and measured in the analyser. Mass ratios 45/44 and 46/44 were used to calculate $\delta^{13}C$ and $\delta^{18}O$ respectively. Corrections were applied using the method prescribed by Craig (1957) accounting the presence of ^{17}O and other interference in the system.

Isotopic results were reported using the conventional δ‰ notation, with reference to the Vienna Pee Dee Belemnite (VPDB) international standard (Coplen, 1995; Gonfiantini *et al.*, 1995). Precision of each analysis was calculated through addition of internal laboratory marbles (MAB, MOM and MS) standards. The internal laboratory standards were tested during the analysis against the International Atomic Energy Agency (IAEA) intercomparison material, NBS-18, NBS-19, NBS-20, producing acceptable values for the respective known composition of the standard. For each batch of analyses, reproducibility between MAB, MOM and MS standards for both $^{18}O/^{16}O$ and $^{13}C/^{12}C$ better than 0.1‰ was required to ensure accuracy.
The analytical reproducibility for the samples analyzed was <0.1‰ for both the values of the $\delta^{13}C$ than for $\delta^{18}O$.
Variability between replicates analyses was, on average, <0.2‰. Where the reproducibility of the analysis was >0.2‰ the analysis was replicated. Higher incidences of variability in some sample replicates were attributed to possible remaining organic matter (for modern samples), contamination within the shell structure, slight contamination between samples and occasional sample heterogeneity.

5.4.7. Trace element analysis

Trace element analysis was carried out on shells and also on paleosols outcropping in the study area to observe if marine molluscs had undergone alteration by meteoric waters.

5.4.7.1. Sample preparation for trace element analysis

The extracting solutions from the powdered shells were prepared by using concentrated high purity acids (Carlo Erba Suprapur HCl and HNO3) and Milli-Q water (Millipore) with a resistivity of 18.2 MΩ cm. All the containers and glassware used were previously cleaned with nitric acid and rinsed carefully with Milli-Q water.
Aliquots of about 1-2 g of samples (shells and soils) were digested with a 5 ml of a mixture of HCl and HNO_3 (3:2) in closed Teflon PFA vessels. The vessels were tightly closed and placed into the microwave system. The heating program was: 2 min at 150°C (75% of 800 W), 10 min at 180°C (100% 800 W). Blank assays were carried out.

Metals were extracted using a CEM Mars 5 Accelerated Reaction System (Matthews, NC, USA) equipped with temperature and pressure regulation via a sensor vessel.

After the reactions, once the vessels cooled down, the solutions were filtered using glass microfiber filters (Whatman® Grade GF/A - 1.6 µm) into glass vessell and diluted to 20 ml with Milli-Q water. The extracts were stored at 4 °C inPET-HD flasks previously cleaned with nitric acid.

After the digestions samples were diluted several times for the ICP-OES analysis. Standards with known dilution were used for each element analyzed.

5.4.7.2. ICP-OES

The Optical Emission Spectrometry (OES) is an emission spectroscopic technique used in chemical analysis.

The plasma is a particular state of matter in which a highly ionized system composed by ions, electrons and neutral particles at high energy is characterized by its tendency to electrical neutrality with respect to the surrounding environment. The plasma is usually produced by applying energy to a common rarefied gas (plasmagen gas, generally argon) until obtaining the ionization of atoms. The ionization can be obtained by the action of a strong electric field generated directly or by means of electric or magnetic induction.

In the case of the ICP plasma is inductively coupled with radiofrequency.

In ICP systems, the variable magnetic field is obtained by applying a high frequency current to an induction coil within which the ionized gas flows. The electric field is generated from the periodic oscillation of the magnetic flux and is directed along circular lines of force lying in a plane perpendicular to the flow direction of the magnetic field. How plasmagen gas is generally used argon. The ionized gas flowing through a quartz tube, or other refractory material transparent to a wide spectrum of the emitted radiation, the upper end of which is inserted in the coil connected to the high frequency generator. The ionization process is triggered by dispersing gas in the livelihood of the free electrons produced for thermoelectric effect by a small rod of graphite inserted in the electric field or by means of a discharge Tesla. The electrons and ions formed are then accelerated by the induced magnetic field resulting in heating by Joule effect due to the resistance of

the support gas. Once triggered, the source plasma is self-perpetuating assuming the form of a luminous flame emerging from the top of the coil. The temperature of the plasma is maintained on average about 6000 ° K and, locally, may even reach 10,000 ° K. The region useful for analytical purposes, however, is the "tail" between 5000 and 6000 ° K; in this area is placed the sample solution to be analyzed atomized in argon.

The ICP-OES spectrometer is composed of the following main parts:

• System of atomization and excitation: it is constituted mainly by a radiofrequency generator, a circuit impedance adapter, a coil and torch, a unit of introduction and transport of the sample to the torch itself. The RF generator provides the high frequency current to the coil and includes a free or fixed frequency oscillator.

• Dispersive optical system (monochromator or polychromator): allows the transfer, dispersion and the selection of electromagnetic radiation and typically includes:

1) a system of lenses and / or mirrors;

2) a monochromator.

• Detector (photomultiplier) is usually employed a photomultiplier which converts the intensity of electromagnetic radiation into an electrical signal. It consists of a photodetector and an amplification system enclosed in a glass tube in which is practiced a high vacuum.

• Control system, data acquisition and data processing: the data acquisition and processing system is typically made up of a unit controlled by the computer which also controls the spectrometer parameters and in certain configurations, even those of the torch, and the generator of 'introduction unit. The system provides for the acquisition and processing of the measured values from the detector and to the storage of all data and operating variables.

The metal concentrations (Ba, Sr, Mn and Fe) in the extracts were determined by Inductively Coupled Plasma Optical Emission Spectrometer (ICP-OES Optima 2000, Perkin Elmer, Fig. 94) in the IGG-CNR laboratory in Pisa with which, thanks to a specific software, can be directly constructed calibration curves from which date back the concentrations of trace analytes.

Digested samples are aspirated into the plasma where a portion of the sample is excited. The excited elements emit light (UV/VIS) at characteristic wavelengths. The computer compares the intensity of a sample to the intensity of a known standard.

The analytical reproducibility (RSD) is 2% for the measurement of trace metals.

Figure 94 – ICP-OES used for trace element anaylisis.

Magnesium and Calcium were analysed by flame atomic absorption spectrometry (Perkin Elmer mod. 3110) and by Dionex 100 Ion chromatograph. Uranium contents were analysed by ICP-MS Perkin Elmer modello ELAN 5000 at the Eurolab s.r.l. laboratory (Nichelino, Torino).

5.4.7.3. Trace elements results

Measurements were corrected for “blank” subtraction. The metal contents are expressed in ppm and then converted in ratio Metal/Ca given in molar ratio.

6. RESULTS

6.1. XRD POWDER ANALYSIS

To identify the limits of detection of calcite in a mixture with a predominantly aragonitic composition, some mixtures of known proportion of calcite and aragonite were prepared.

The XRD analysis performed on mixtures of known composition of calcite and aragonite (1%, 3.5%, 5% and 10% of calcite in mainly aragonite samples) produced the following diffractograms (Figs. 95 to 98, respectively). For each diffractogram, on the horizontal axis can be read the angle 2θ expressed in degrees while the ordinate axis indicates the counts per second. The position of the peak of maximum relative intensity (I/I_1 = 100) of calcite is located at 2θ = 29.5 (d = 3.035 Å).

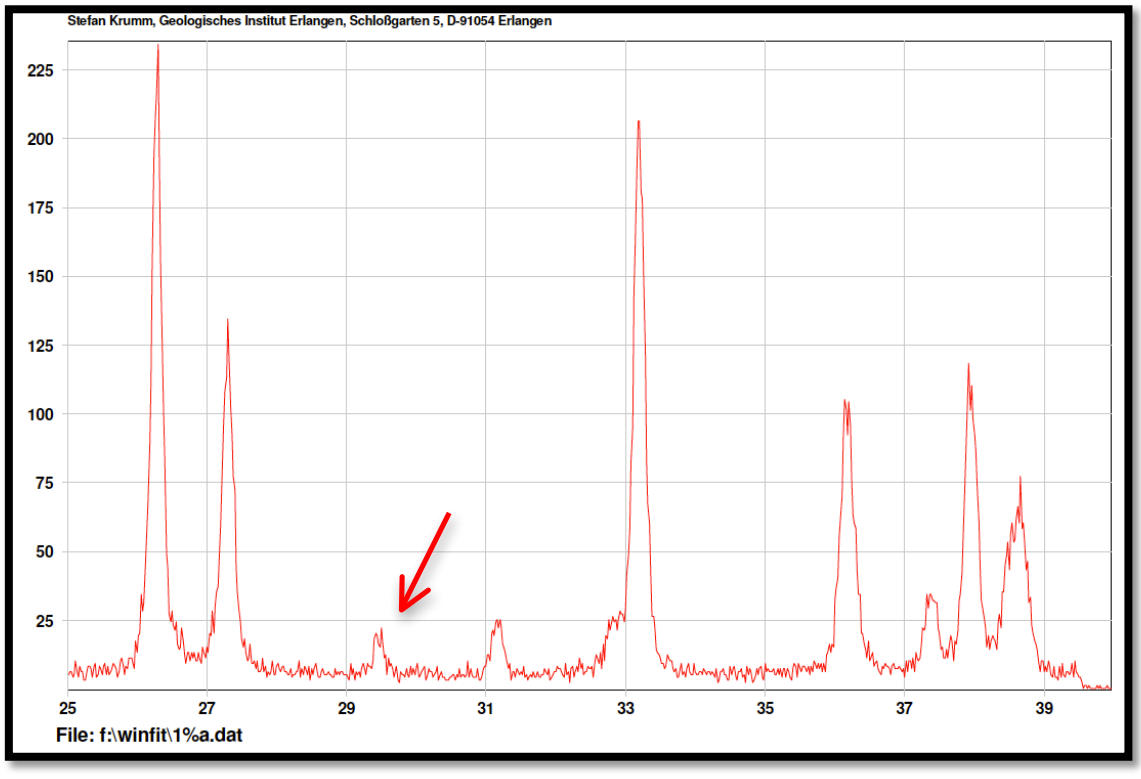

Figure 95 – Mixture of calcite 1% and aragonite 99%. The arrow indicates the maximum intensity peak of calcite. The other peaks belong to aragonite.

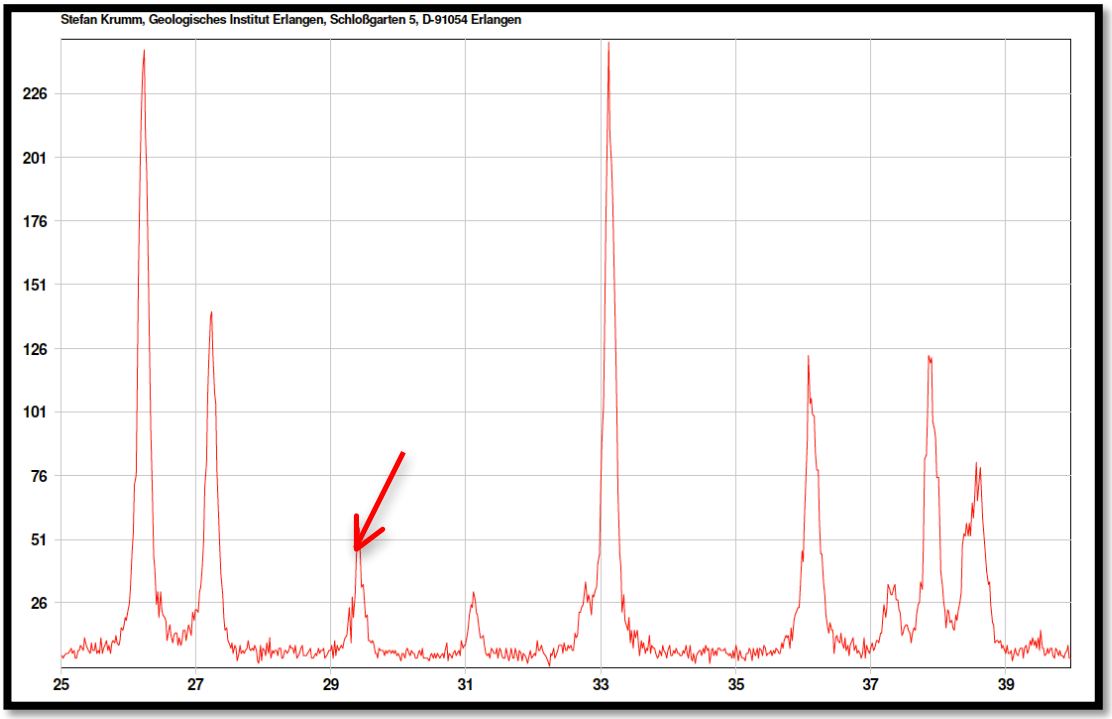

Figure 96 – Mixture of calcite 3.5% and aragonite 96.5%. The arrow indicates the maximum intensity peak of calcite. The other peaks belong to aragonite.

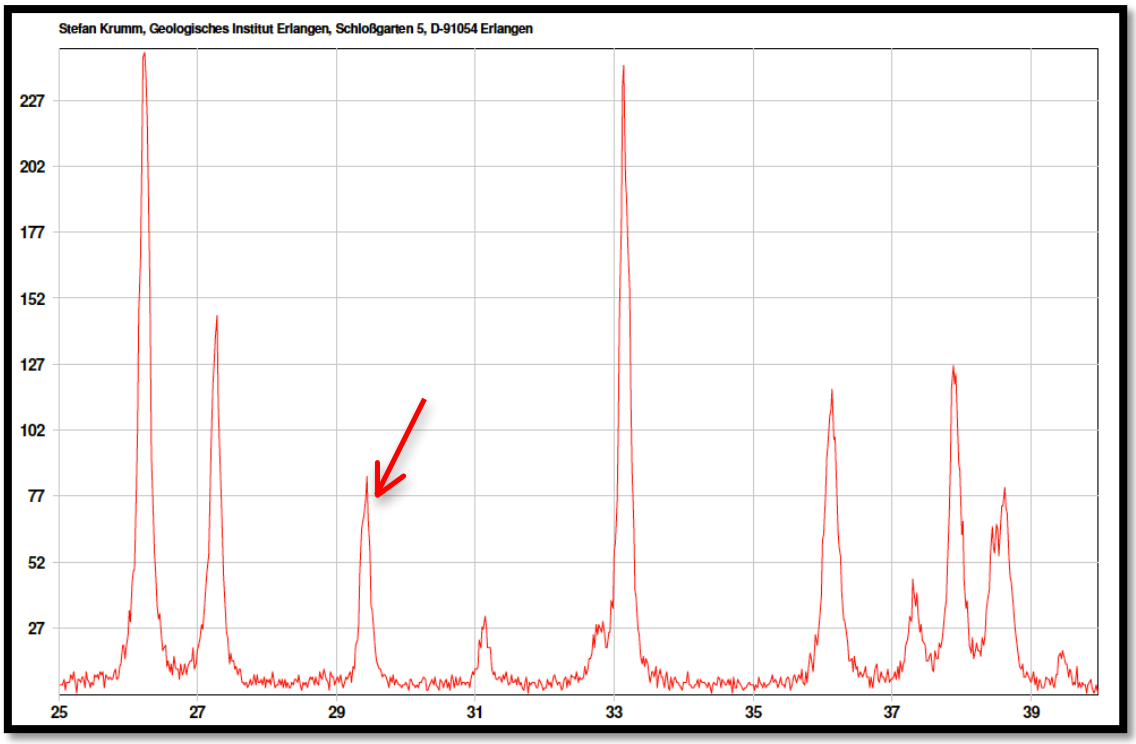

Figure 97 – Mixture of calcite 5% and aragonite 95%. The arrow indicates the maximum intensity peak of calcite. The other peaks belong to aragonite.

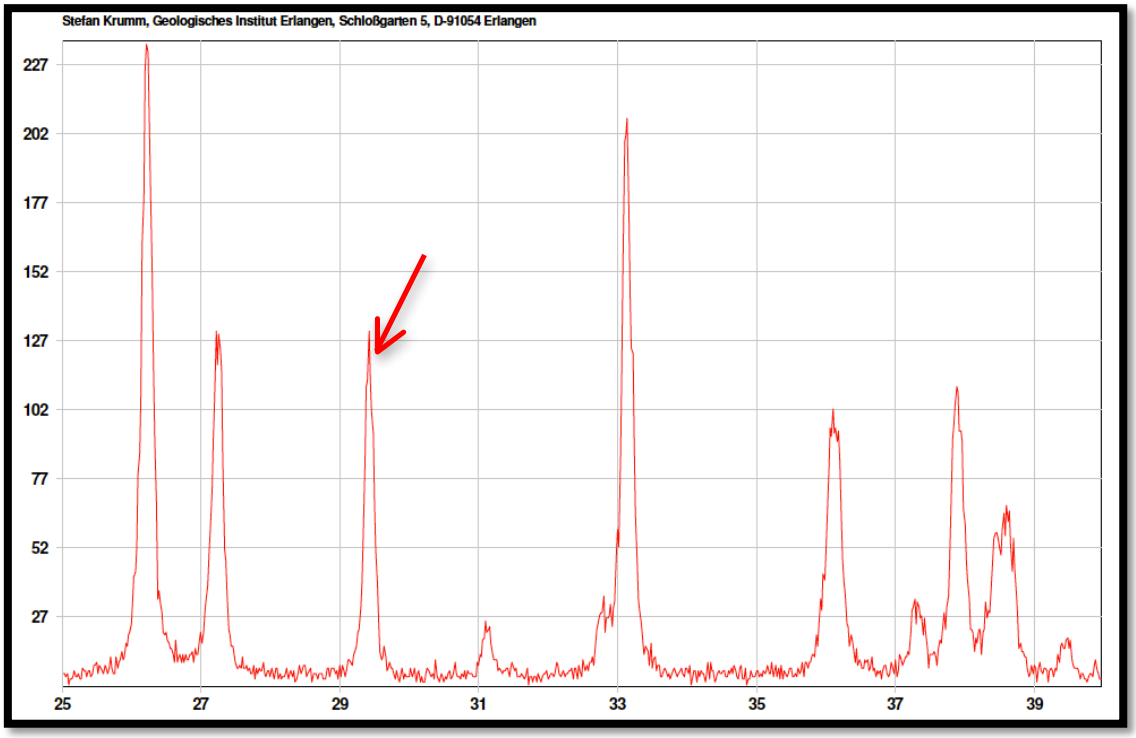

Figure 98 – Mixture of calcite 10% and aragonite 90%. The arrow indicates the maximum intensity peak of calcite. The other peaks belong to aragonite.

6.1.1. XRD powder analysis on *Ameghinomya antiqua*

According to calibration with mixtures of calcite standards and shell aragonite, results indicate that all modern and fossil shells were largely composed of aragonite (>99%).

In Figures 99, 100 and 101 are shown diffractograms of specimens of *A. antiqua* collected, respectively, from modern beach, Holocene and Pleistocene beach ridges. Table 5 compares all the XRD analyses carried out on samples of *A. antiqua* of different age and the presence of calcite in each sample (for the other diffractograms see Appendix A).

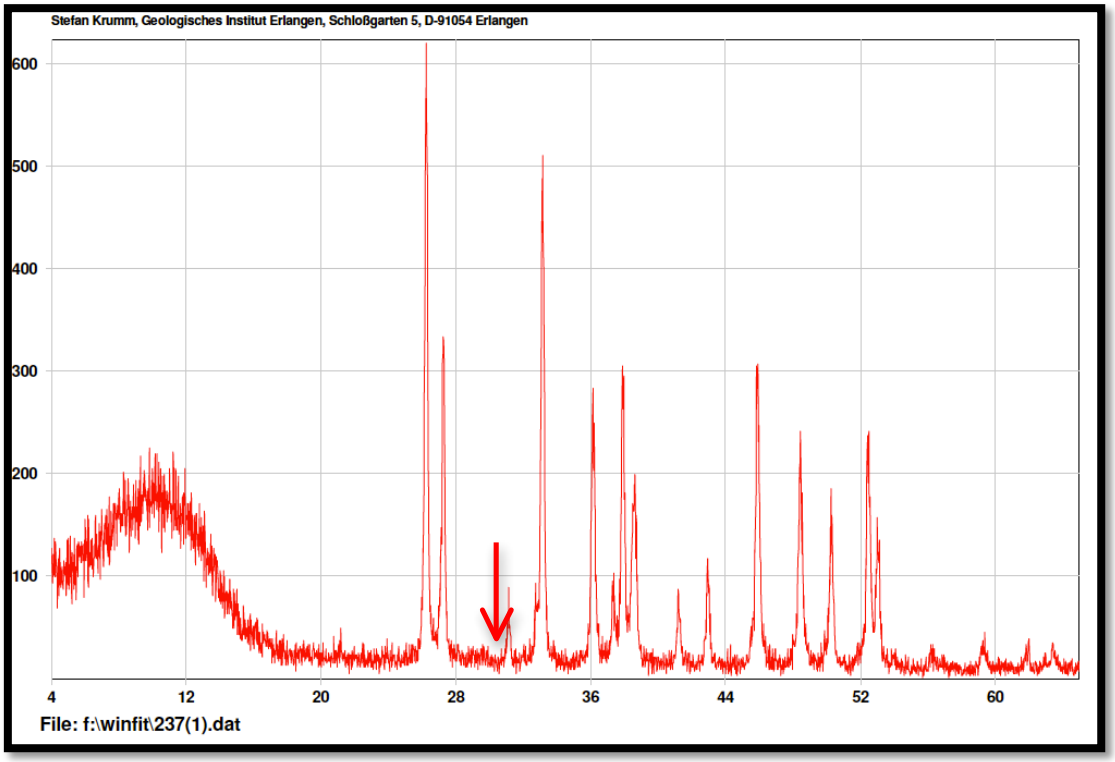

Figure 99 – Diffractogram of a modern specimen of *Ameghinomya antiqua*. The arrow indicates where the maximum intensity peak of calcite should be located.

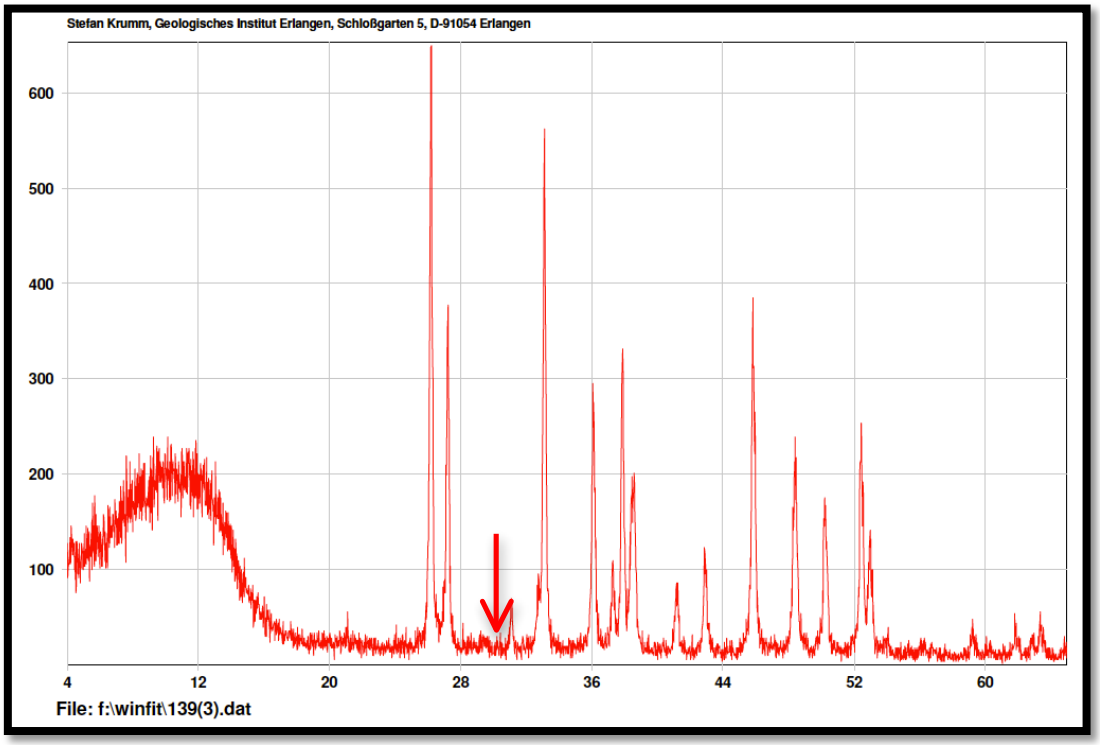

Figure 100 – Diffractogram of *A. antiqua* sampled in a Holocene beach ridge. The arrow indicates where the maximum intensity peak of calcite should be located.

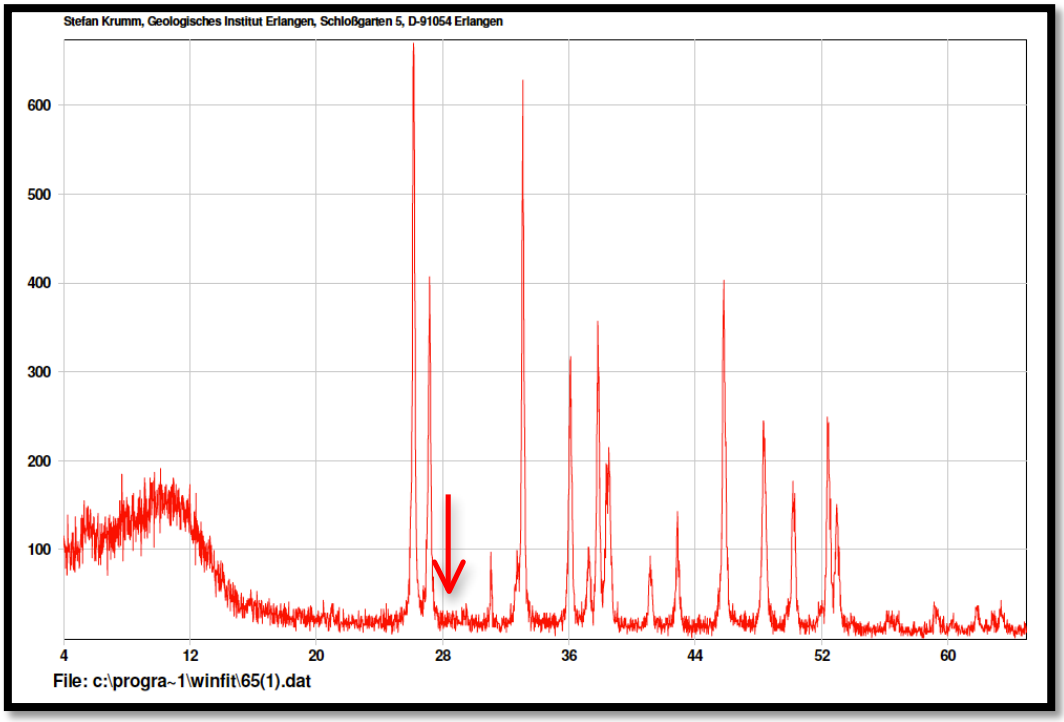

Figure 101 – Diffractogram of a Pleistocene specimen of *A. antiqua.* The arrow indicates where the maximum intensity peak of calcite should be located.

WP 237(1)	MODERN	ABSENT	BAHIA BUSTAMANTE
WP 237(3)	MODERN	ABSENT	BAHIA BUSTAMANTE
WO 104A(1)	HOLOCENE	ABSENT	CAMARONES
WP 138(1)	HOLOCENE	ABSENT	BAHIA BUSTAMANTE
WP 23(3)	PLEISTOCENE	ABSENT	CABO RASO
WP 64A(3)	MIS 5 (PLEISTOCENE)	LESS THAN 1%	CAMARONES
WP 64B(1)	MIS 5 (PLEISTOCENE)	ABSENT	CAMARONES
WP 65(3)	MIS 5 (PLEISTOCENE)	ABSENT	CAMARONES
WP 65(4)	MIS 5 (PLEISTOCENE)	LESS THAN 1%	CAMARONES
WP 65(2)	MIS 5 (PLEISTOCENE)	LESS THAN 1%	CAMARONES
WP 68(1)	PLEISTOCENE	ABSENT	CAMARONES
WP 70(A)	PLEISTOCENE	ABSENT	CAMARONES
WP 70(B)	PLEISTOCENE	LESS THAN 1%	CAMARONES
WP 92A(2)	PLEISTOCENE (MIS 7?)	ABSENT	CAMARONES
WP 97(1)	MIS 11 (PLEISTOCENE)	ABSENT	CAMARONES
WP 148(3)	MIS 5 (PLEISTOCENE)	ABSENT	BAHIA BUSTAMANTE
WP 154A(2)	MIS 5 (PLEISTOCENE)	LESS THAN 1%	BAHIA BUSTAMANTE
WP 168(1)	MIS 5 (PLEISTOCENE)	ABSENT	BAHIA BUSTAMANTE
WP 175A(4)	MIS 7 (PLEISTOCENE)	ABSENT	BAHIA BUSTAMANTE
WP 197	PLEISTOCENE	ABSENT	BAHIA BUSTAMANTE
WP 199(2)	PLEISTOCENE	ABSENT	BAHIA BUSTAMANTE
WP 455(7)	PLEISTOCENE	ABSENT	CALETA OLIVIA
WP 479B(2)	MIS 9 (PLEISTOCENE)	ABSENT	CALETA OLIVIA
WP 506(2)	PLEISTOCENE	ABSENT	CALETA OLIVIA

Table 5 – XRD powder analysis on *A. antiqua.*

6.1.2. XRD powder analysis on *Mytilus edulis*

The shell of *Mytilus edulis* has a mixed composition consisting of calcite and aragonite.

XRD powder analysis carried out on modern shells of *M. edulis* sampled in the study area show a mainly calcitic composition (Fig. 102 and Appendix A for other diffractograms).

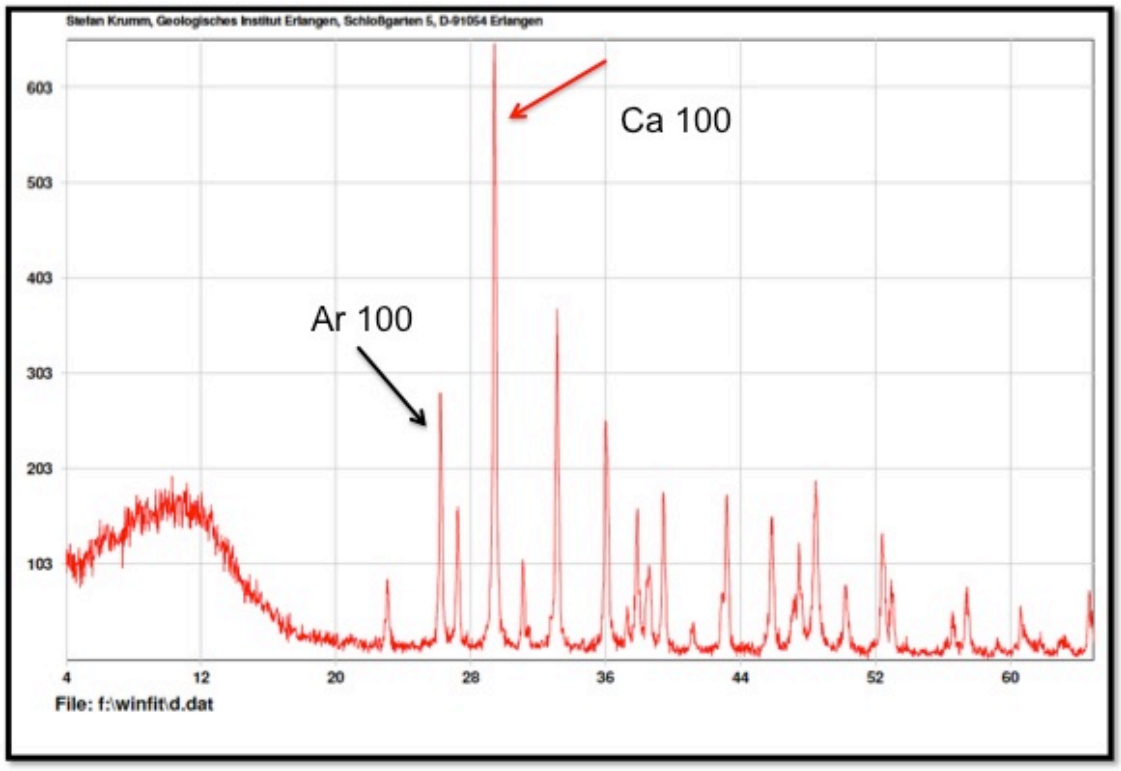

Figure 102 – Powder diffractogram of a modern *Mytilus edulis* shell. The red arrow indicates the maximum intensity peak of calcite (Ca 100), the black arrow indicates the maximum intensity peak of aragonite.

From the powder diffractogram of a Holocen *Mytilus edulis* is possible to observe that the aragonite/calcite ratio remains essentially unchanged compared to the modern sample (Fig. 103).

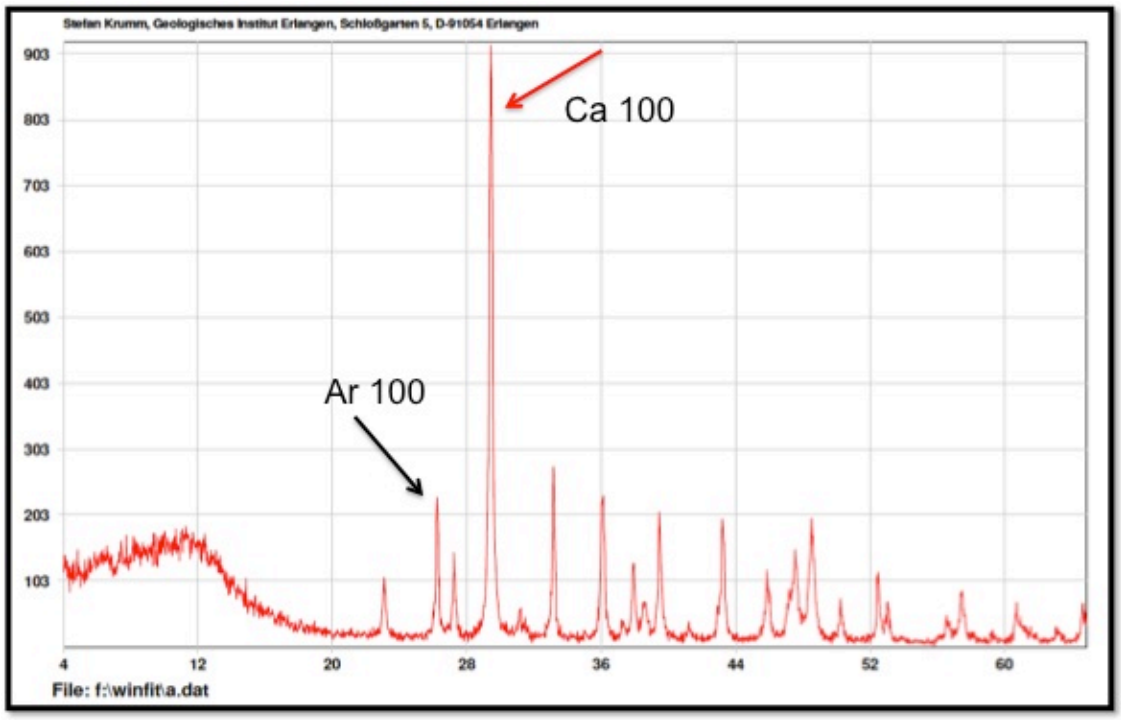

Figure 103 – Powder diffractogram of a Holocene *Mytilus edulis* shell. The red arrow indicates the maximum intensity peak of calcite (Ca 100), the black arrow indicates the maximum intensity peak of aragonite.

The predominant composition of calcite shell of modern and Holocene *M. edulis* contrasts with what has been observed in the literature by Panarello (1987) for specimens of *Mytilus edulis* of Tierra del Fuego, which reports a calcite/aragonite ratio equivalent to 5/95 for modern specimens and equal to 15/85 for Holocene samples.

It is possible that this discrepancy is due to the partial removal, during the phases of mechanical cleaning with the drill, of the inner aragonite layer of the shell or abrasion of shells during natural processes.

6.1.3. XRD powder analysis on *Aulacomya atra*

The shell of *Aulcomya atra,* like other mussels, has a mixed composition consisting of calcite and aragonite, however, contrary to *Mytilus edulis*, the composition is predominantly aragonitic instead calcitic (Fig. 104).

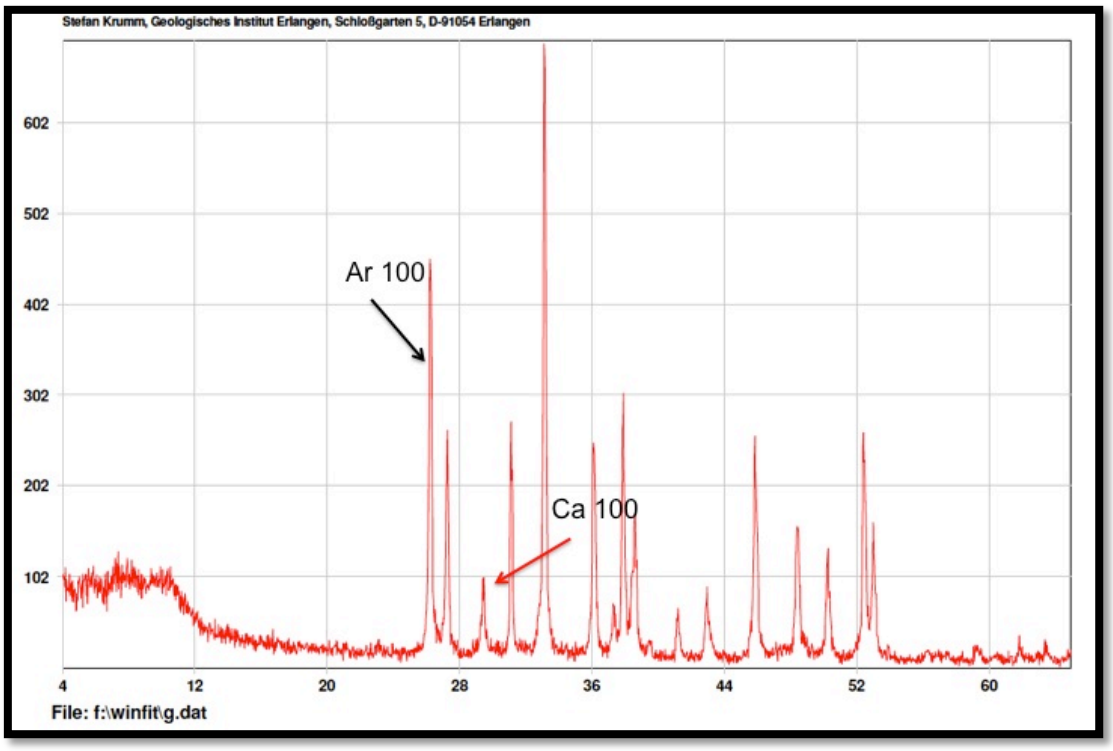

Figure 104 – Powder diffractogram of a modern *Aualcomya atra* shell. The red arrow indicates the maximum intensity peak of calcite (Ca 100), the black arrow indicates the maximum intensity peak of aragonite.

Also the fossils of *A. atra*, although only Holocene samples were analyzed, do not appear to have varied in mineralogy of the shells (Fig. 105; see Appendix A for other diffractograms).

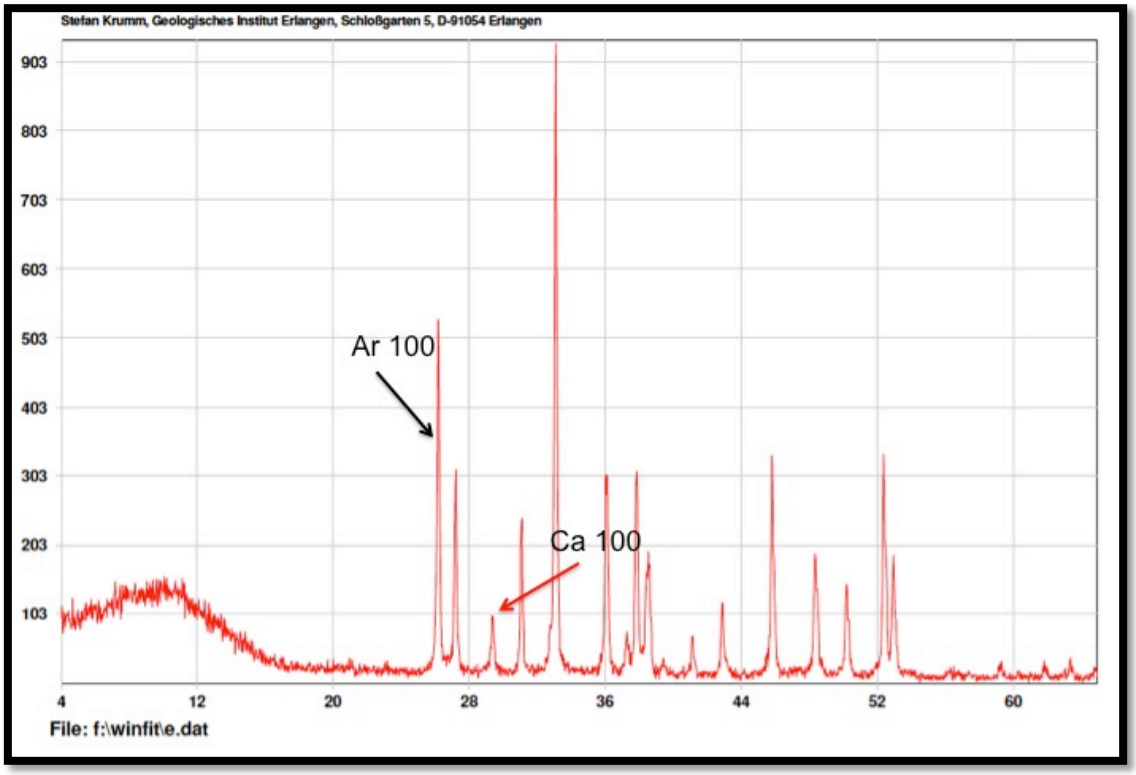

Figure 105 – Powder diffractogram of a Holocene *Aualcomya atra* shell. The red arrow indicates the maximum intensity peak of calcite (Ca 100), the black arrow indicates the maximum intensity peak of aragonite.

6.1.4. XRD powder analysis on paleosols

Diffractometric analysis on paleosols sampled in different localities allowed to distinguish 3 types of paleosols with different mineralogical composition of the concretions: paleosols mainly constituted by calcite and in much less quantity by quartz and feldspar, corresponding to carbonate-enriched soil horizons (Bk) (Fig. 106), paleosols with a mainly quartz composition (Fig. 107) and paleosols consisting of gypsum (By-type horizon, Fig. 108).

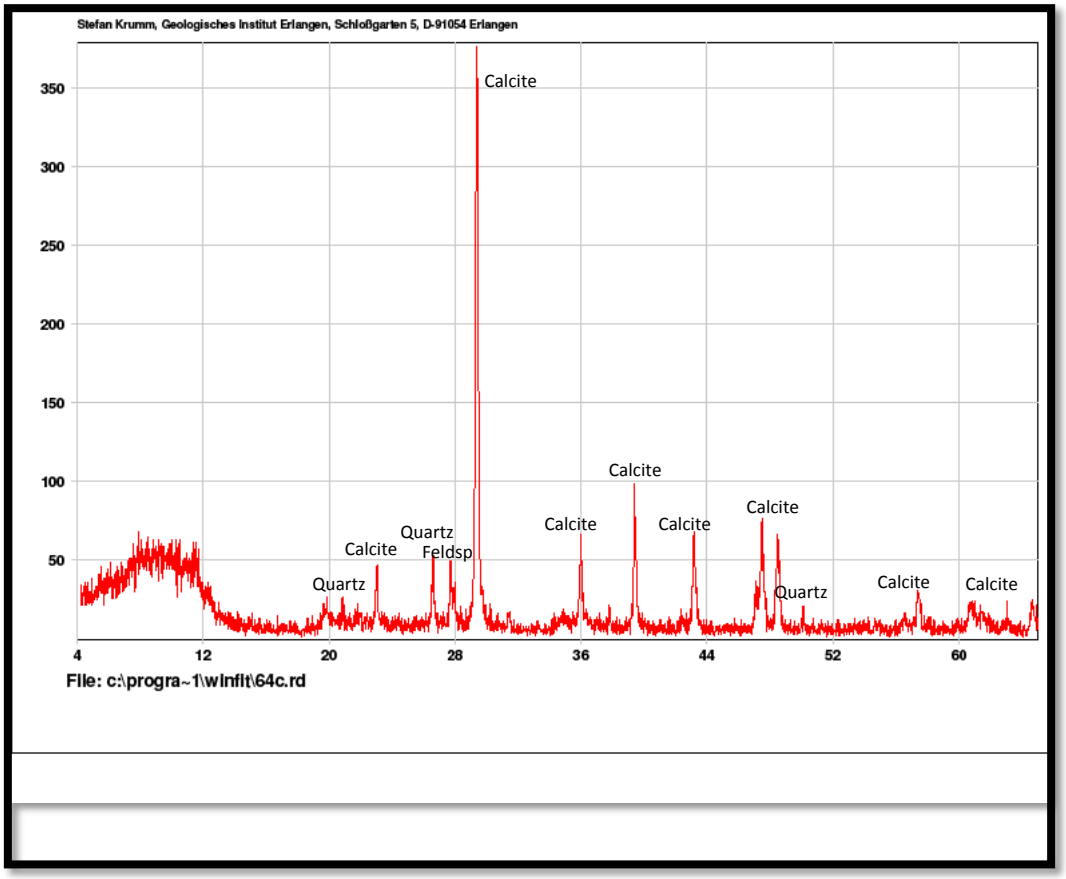

Figure 106 – Powder diffractogram of a carbonate paleosol.

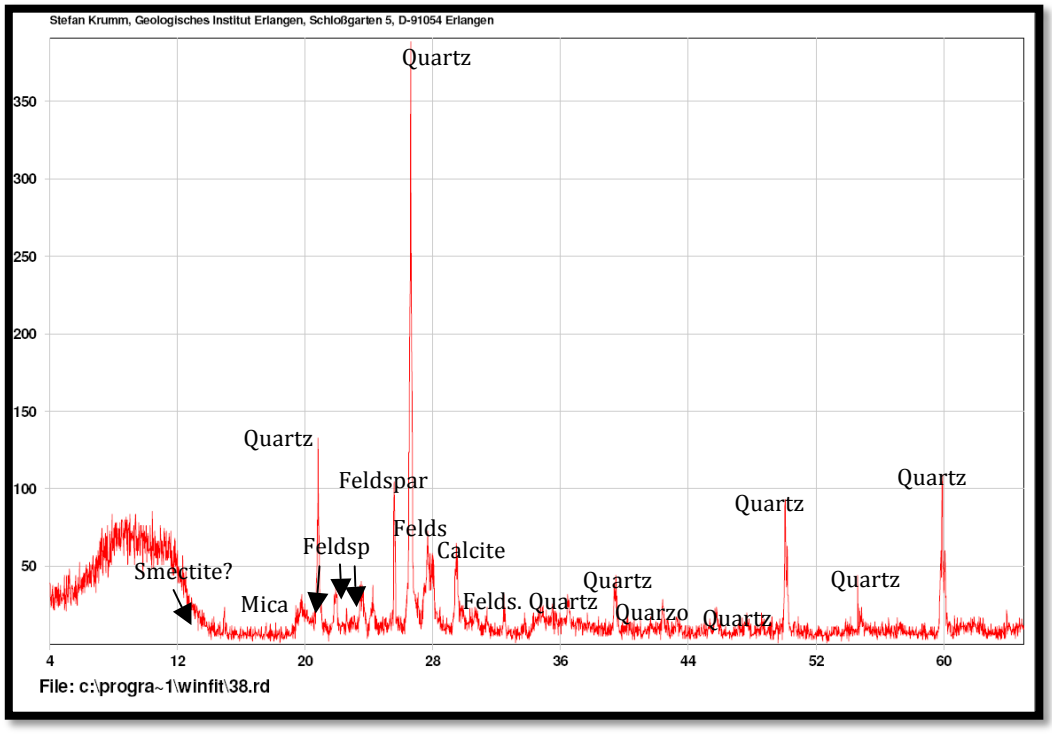

Figure 107 – Powder diffractogram of a paleosol mainly constituted by quartz.

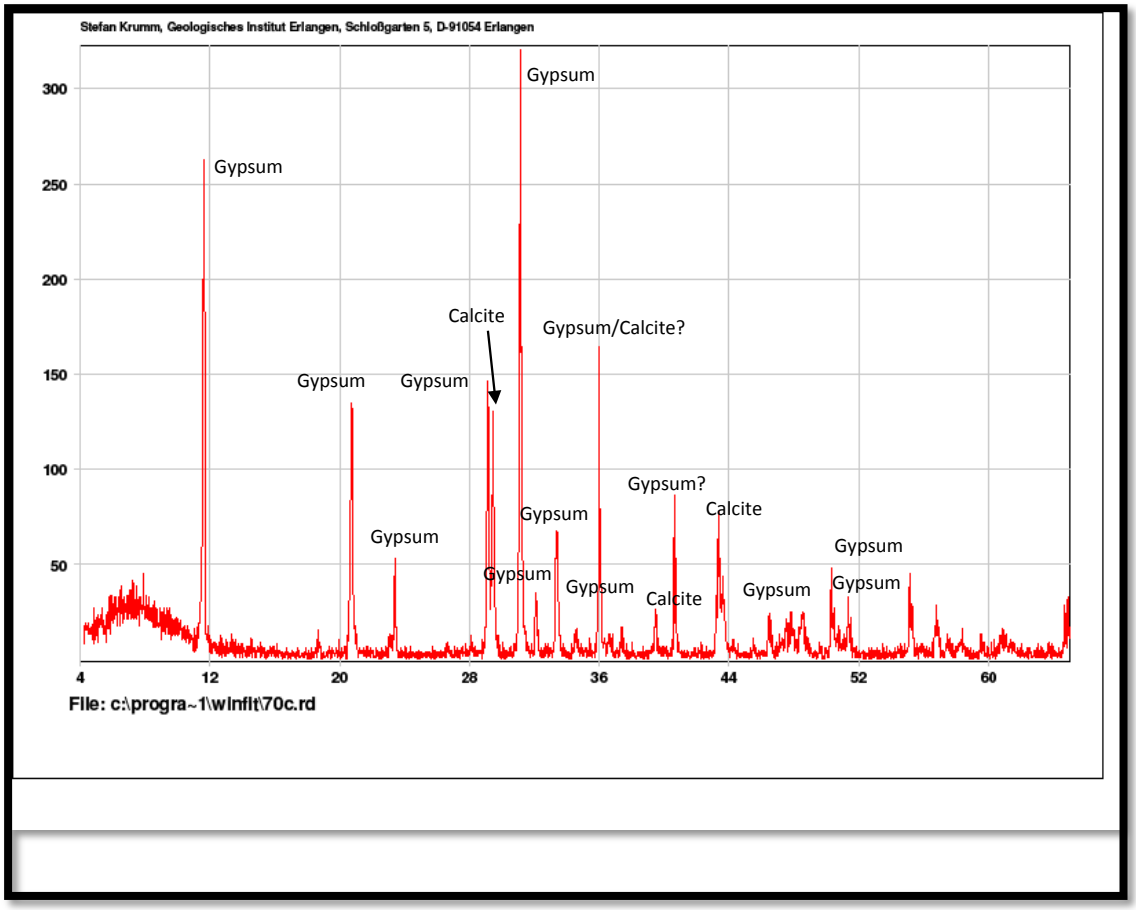

Figure 108 – Powder diffractogram of a paleosol mainly constituted by gypsum.

6.2. PETROGRAPHIC ANALYSIS

Thin sections performed on *Ameghinomya antiqua* shells indicate that the shells consist of two aragonitic layers (Figs. 109 and 110): an external layer (Fig. 111) and internal layer (Fig. 112).

The outer layer, according to Takesue & van Geen (2004) and Carter (1990) show a prismatic microstructure, while the inner layer is nacreous. The brown layer, between the internal and the external layer and darker than calcium carbonate under reflected light, should represent an organic-rich layer (Figs. 109 and 110).

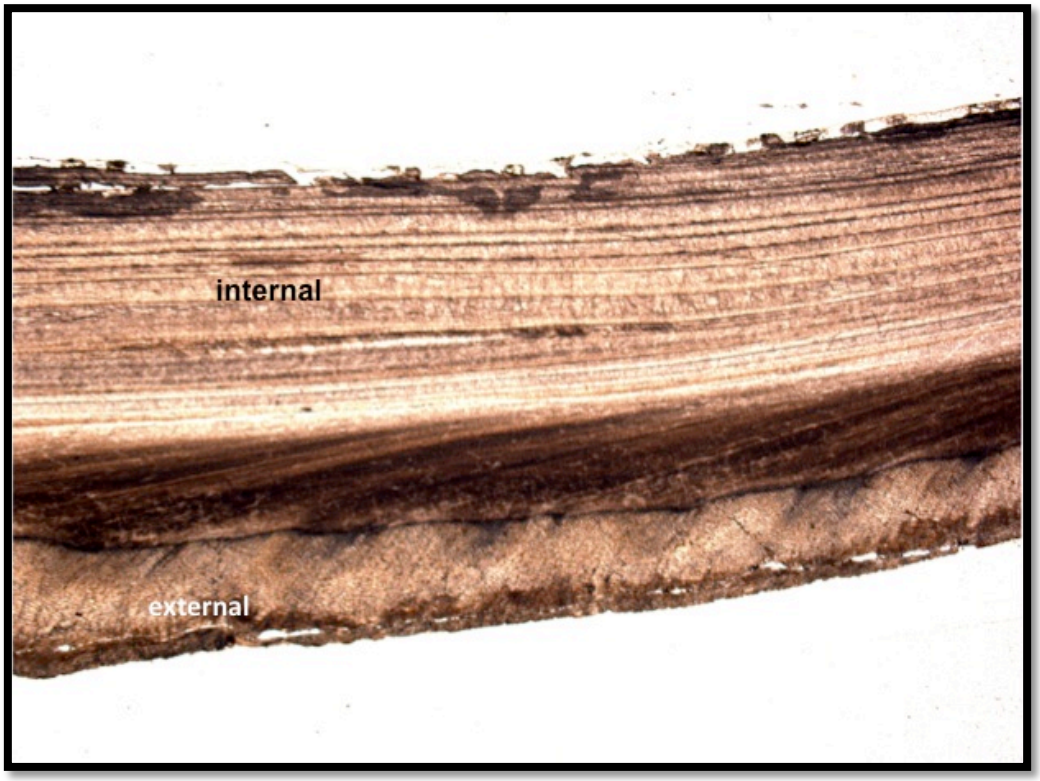

Figure 109 – Thin section of a modern *Ameghinomya antiqua* shell (parallel Nicols, magnification 2.5X).

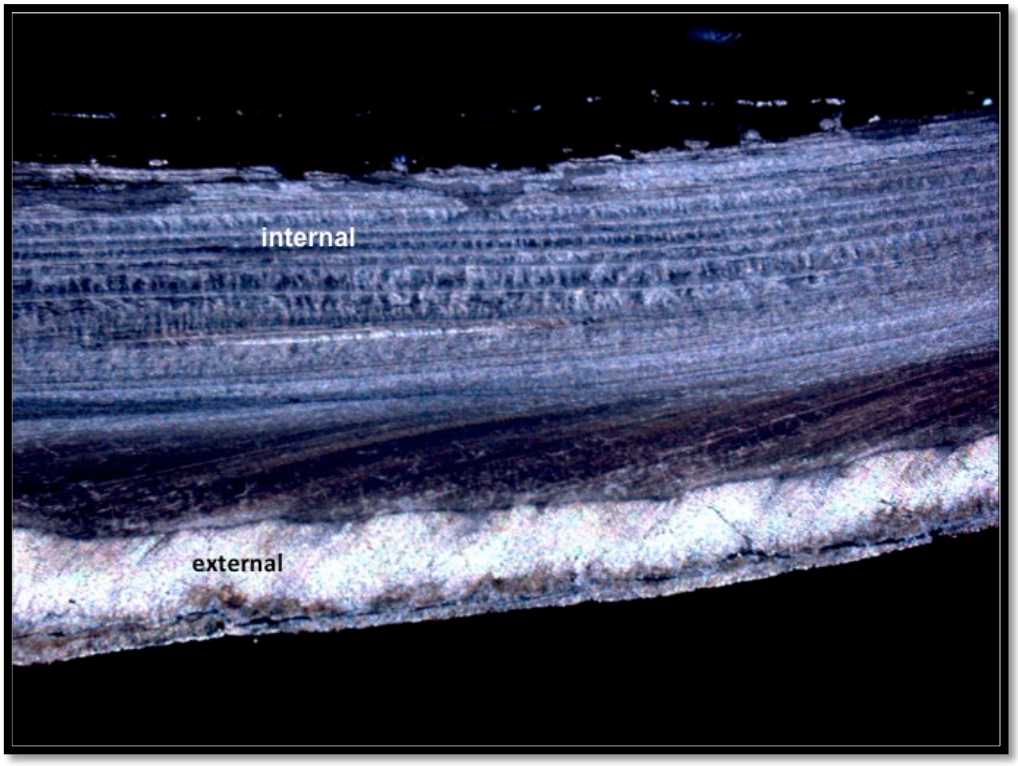

Figure 110 – Thin section of a modern *Ameghinomya antiqua* shell (crossed Nicols, magnification 2.5X).

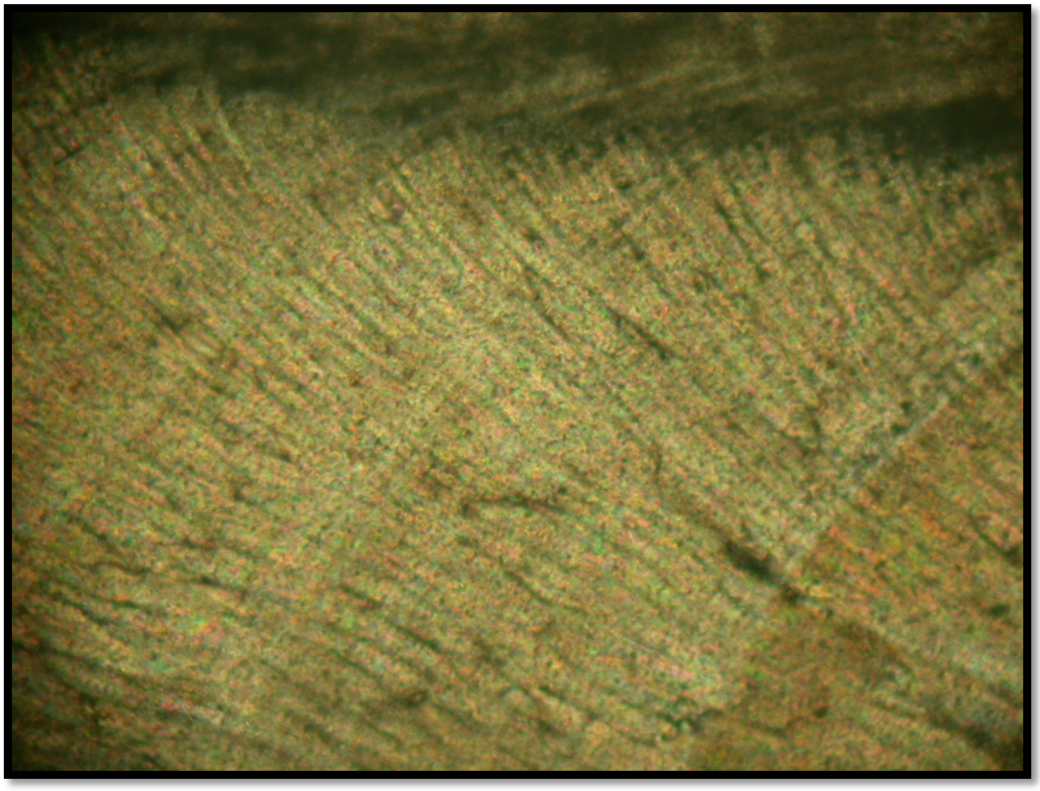

Figure 111 – Detail of the external layer in modern *A. antiqua* shell (crossed Nicols, magnification 10X).

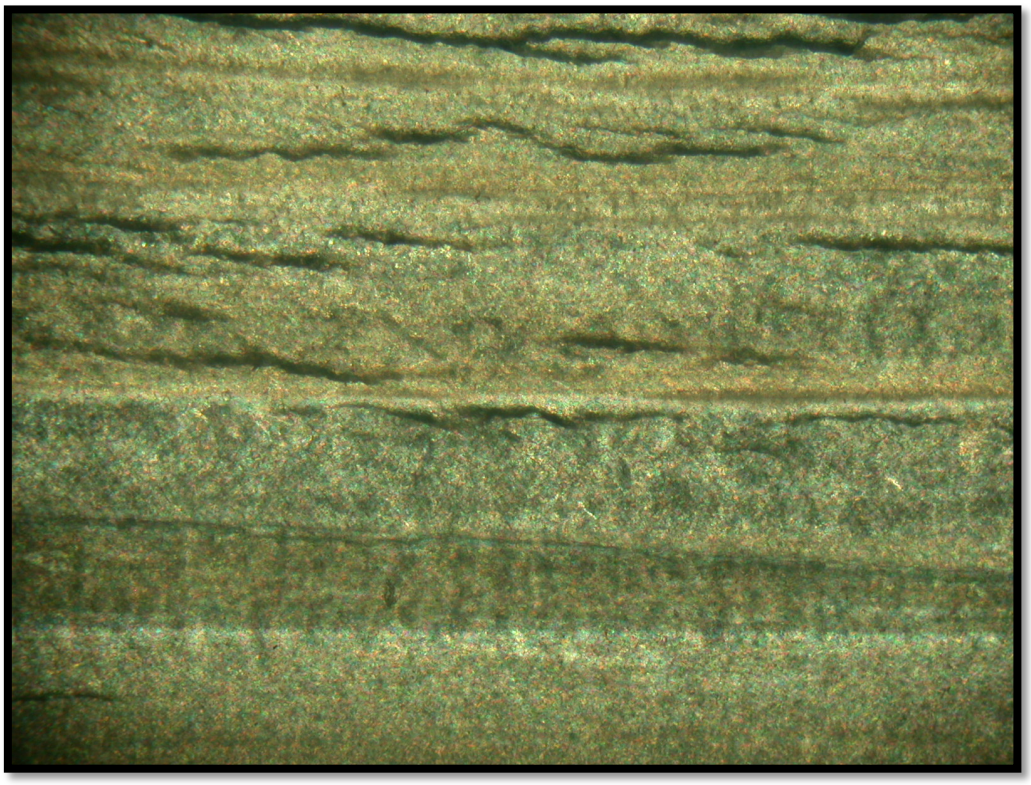

Figure 112 – Detail of the internal layer in modern *A. antiqua* (crossed Nicols, magnification 10X).

Only in a Pleistocene specimen (WP 154A(2)) a partial recrystallization of the external layer of the shell was observed (Fig. 113). However, the analysis of the powder X-ray diffraction of the sample indicates the presence of calcite less than 1% (Table 5).

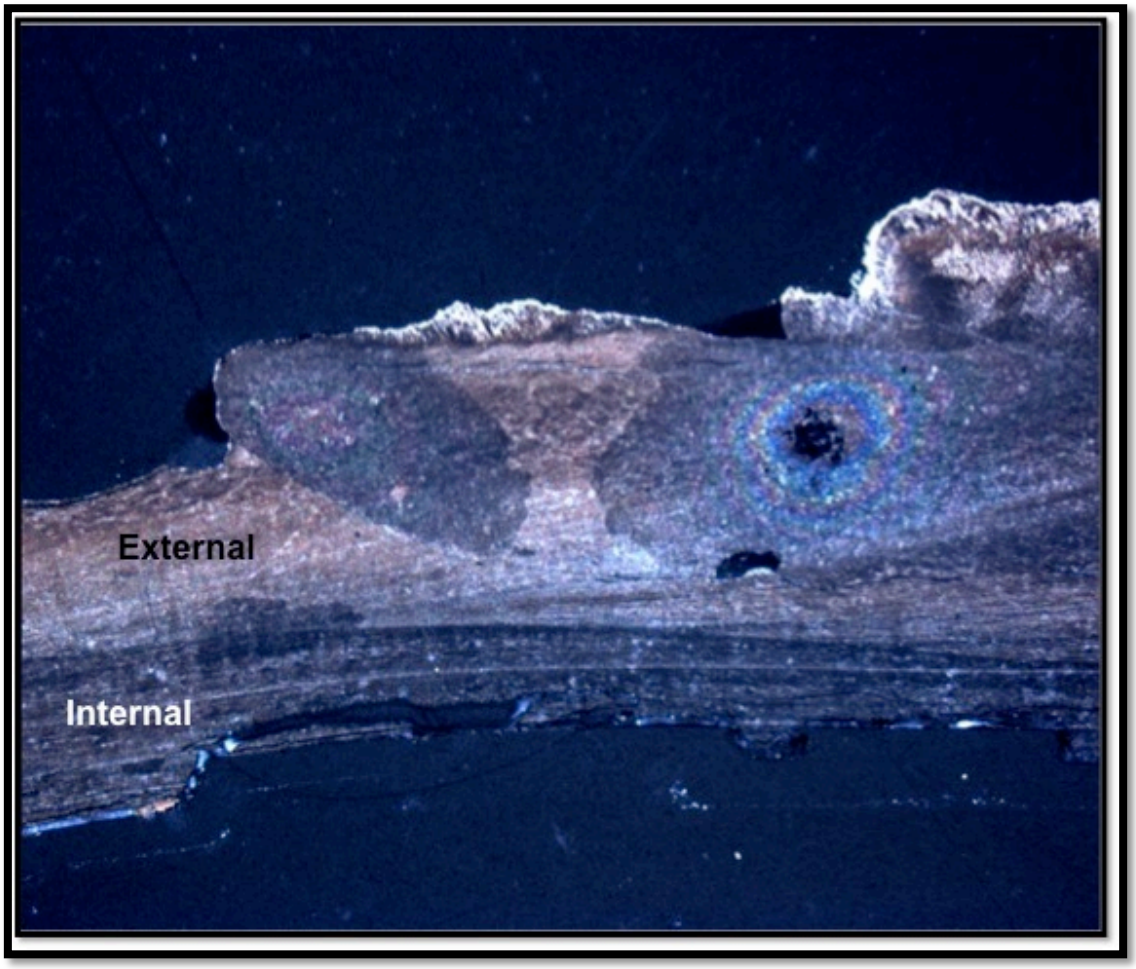

Figure 113 – Partial recrystallization of a Pleistocene *Ameghinomya antiqua* shell.

6.3. STABLE ISOTOPE (oxygen and carbon) COMPOSITION OF MARINE SHELLS

6.3.1. Stable isotope composition of modern marine shells

Oxygen and carbon isotope analyses of modern shells were performed on *Ameghynomia antiqua, Mytilus edulis* and *Aulacomya atra.*

6.3.1.1. *Ameghinomya antiqua* shells

Modern specimens of *Ameghinomya antiqua* were collected from the active beach in various localities along the Atlantic coast of Patagonia shown in figure 64 (Chapter 5).

Ameghinomya antiqua exhibits $\delta^{18}O$ mean values ranging from +0.22±0.14‰ for Bahia Bustamante samples to +0.71±0.23‰ of Bahia Langara specimens and $\delta^{13}C$ mean values are between -0.27±0.20‰ of Bahia Bustamante shells and 0.87±0.4‰ of Cabo Raso and Bahia Langara (Tab. 6). The intra-specific variability for each locality is always higher for the $\delta^{13}C$ ($\Delta\delta^{13}C$ from 0.39‰ to 0.92‰) than for the $\delta^{18}O$ ($\Delta\delta^{18}O$ from 0.16‰ to 0.47‰) (Tab. 7).

SAMPLE	LOCALITY	LATITUDE (°S)	Number of samples	$\delta^{13}C$‰ (mean value)	st. dev.	$\delta^{18}O$‰ (mean value)	st. dev.
WP667	Puerto Lobos	42.1	5	**0.63**	0.30	**0.23**	0.18
WP04	Cabo Raso	44.16	5	**0.87**	0.38	**0.68**	0.12
WP54	Bahia S. Sebastian	44.34	6	**0.07**	0.26	**0.25**	0.11
WP60BBIS+WP623BIS	Camarones North	44.41	8	**0.22**	0.48	**0.33**	0.12
WP95+WP110	Camarones South	44.5	4	**0.69**	0.14	**0.32**	0.06
WP237+WP613	Bahia Bustamante	45.08	10	**0.00**	0.28	**0.22**	0.14
WP271	Bahia Solano	45.4	6	**-0.27**	0.20	**0.28**	0.06
WP473B	Caleta Olivia	46.23	4	**0.25**	0.19	**0.69**	0.14
MPA3	Bahia Langara	46.39	3	**0.87**	0.38	**0.71**	0.23

Table 6 – Carbon and oxygen isotopic composition (mean value and standard deviation) of modern *Ameghinomya antiqua* shells for each locality.

SAMPLE	LOCALITY	$\delta^{13}C$‰	$\Delta\delta^{13}C$‰	$\delta^{18}O$ ‰	$\Delta\delta^{18}O$ ‰
WP667(1)	PUERTO LOBOS	1.01	0.76	0.45	0.44
WP667(2)	PUERTO LOBOS	0.61		0.14	
WP667(3)	PUERTO LOBOS	0.25		0.01	
WP667(4)	PUERTO LOBOS	0.82		0.39	
WP667(5)	PUERTO LOBOS	0.44		0.15	
WP04(1)	CABO RASO/BAHIA VERA	1.13	0.85	0.71	0.33
WP04(2)	CABO RASO/BAHIA VERA	1.40		0.70	
WP04(3)	CABO RASO/BAHIA VERA	0.68		0.51	
WP04(4)	CABO RASO/BAHIA VERA	0.55		0.62	
WP04(5)	CABO RASO/BAHIA VERA	0.57		0.84	
WP54(1)	BAHIA SAN SEBASTIAN	-0.33	0.73	0.08	0.35
WP54(2)	BAHIA SAN SEBASTIAN	0.18		0.25	
WP54(3)	BAHIA SAN SEBASTIAN	0.12		0.43	
WP54(4)	BAHIA SAN SEBASTIAN	0.40		0.20	
WP54(5)	BAHIA SAN SEBASTIAN	0.24		0.28	
WP54(6)	BAHIA SAN SEBASTIAN	-0.08		0.28	
WP60BBIS(1)	CAMARONES NORTH	0.11	0.92	0.07	0.46
WP60BBIS(2)	CAMARONES NORTH	0.49		0.40	
WP623BIS(1)	CAMARONES NORTH	0.07		0.42	
WP623BIS(3)	CAMARONES NORTH	0.36		0.33	
WP623BIS(4)	CAMARONES NORTH	0.30		0.23	
WP623BIS(5)	CAMARONES NORTH	-0.09		0.39	
WP623BIS(6)	CAMARONES NORTH	-0.43		0.37	
WP95(2)	CAMARONES SOUTH	0.59	0.69	0.38	0.13
WP95(3)	CAMARONES SOUTH	0.62		0.30	
WP95(4)	CAMARONES SOUTH	0.89		0.35	
WP110(2)	CAMARONES SOUTH	0.65		0.25	
WP237(1)	BAHIA BUSTAMANTE	-0.24	0.77	0.02	0.47
WP237(2)	BAHIA BUSTAMANTE	-0.06		0.16	
WP237(3)	BAHIA BUSTAMANTE	0.41		0.27	
WP237(4)	BAHIA BUSTAMANTE	-0.36		0.23	
WP237(5)	BAHIA BUSTAMANTE	-0.21		-0.03	
WP613(1)	BAHIA BUSTAMANTE SOUTH	-0.15		0.28	
WP613(2)	BAHIA BUSTAMANTE SOUTH	0.35		0.27	
WP613(3)	BAHIA BUSTAMANTE SOUTH	-0.22		0.23	
WP 613(4)	BAHIA BUSTAMANTE SOUTH	0.24		0.44	
WP 613 (5)	BAHIA BUSTAMANTE SOUTH	0.23		0.36	
WP271(1)	BAHIA SOLANO	-0.14	0.46	0.17	0.16
WP271(2)	BAHIA SOLANO	-0.39		0.26	
WP271(3)	BAHIA SOLANO	-0.38		0.32	
WP271(4)	BAHIA SOLANO	-0.45		0.27	
WP271(5)	BAHIA SOLANO	0.01		0.33	
WP473B(1)	CALETA OLIVIA	0.06	0.39	0.71	0.32
WP473B(2)	CALETA OLIVIA	0.45		0.81	
WP473B(4)	CALETA OLIVIA	0.37		0.75	
WP 473B(6)	CALETA OLIVIA	0.12		0.49	
MPA3(1)	BAHIA LANGARA	0.43	0.70	0.62	0.42
MPA3(3)	BAHIA LANGARA	1.13		0.97	
MPA3(4)	BAHIA LANGARA	1.04		0.55	

Table 7 – Carbon and oxygen isotopic composition and range values of modern shells of *Ameghinomya antiqua* from the Atlantic coast of Patagonia.

By analyzing the oxygen isotope composition of the shells of modern *Ameghinomya antiqua* to vary the latitude, it is possible to observe that the oxygen isotopic composition tends to increase down south from Puerto Lobos to Cabo Raso, before declining in the area between Bahia San Sebastian and Bahia Solano, where there are the lowest values. In the area of Bahia Langara and Caleta Olivia, instead, the values increase again (Fig. 114).

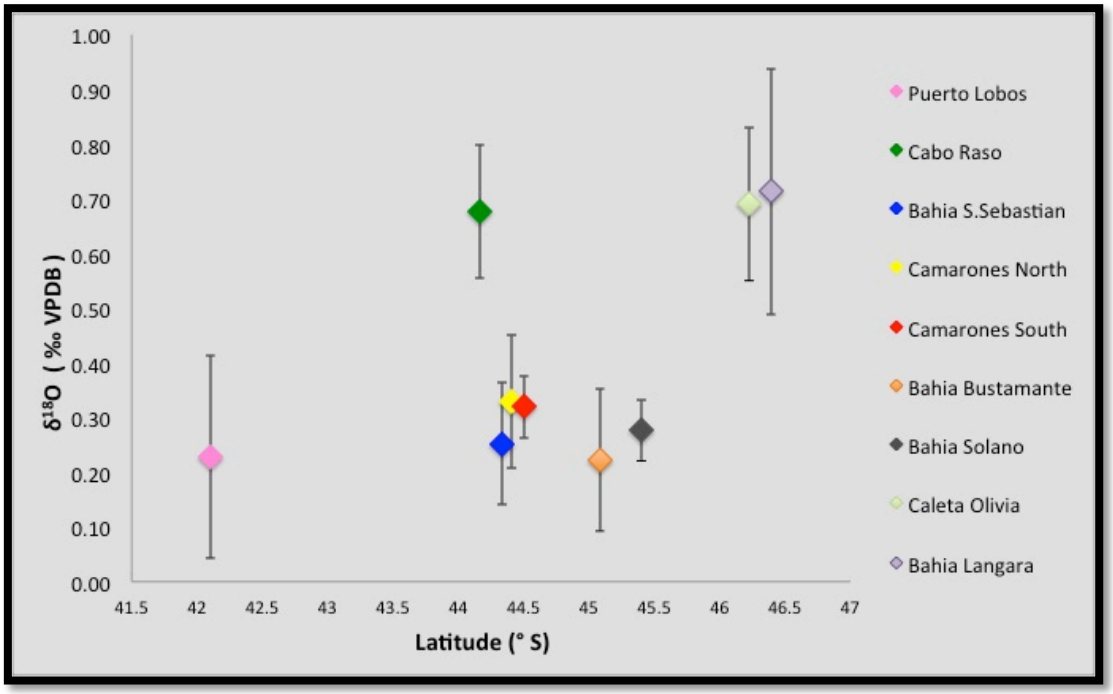

Figure 114 – Oxygen isotope composition of modern *A. antiqua* to vary the latitude.

$\delta^{13}C$ values are higher at the edges of the study area and have similar values in the localities of Puerto Lobos, Cabo Raso and Bahia Langara (Fig. 115).

The carbon isotopic composition decreases in the vicinity of the upper part of the Gulf of San Jorge (localities of Bahia San Sebastian, Camarones, Bahia Bustamante and Bahia Solano).

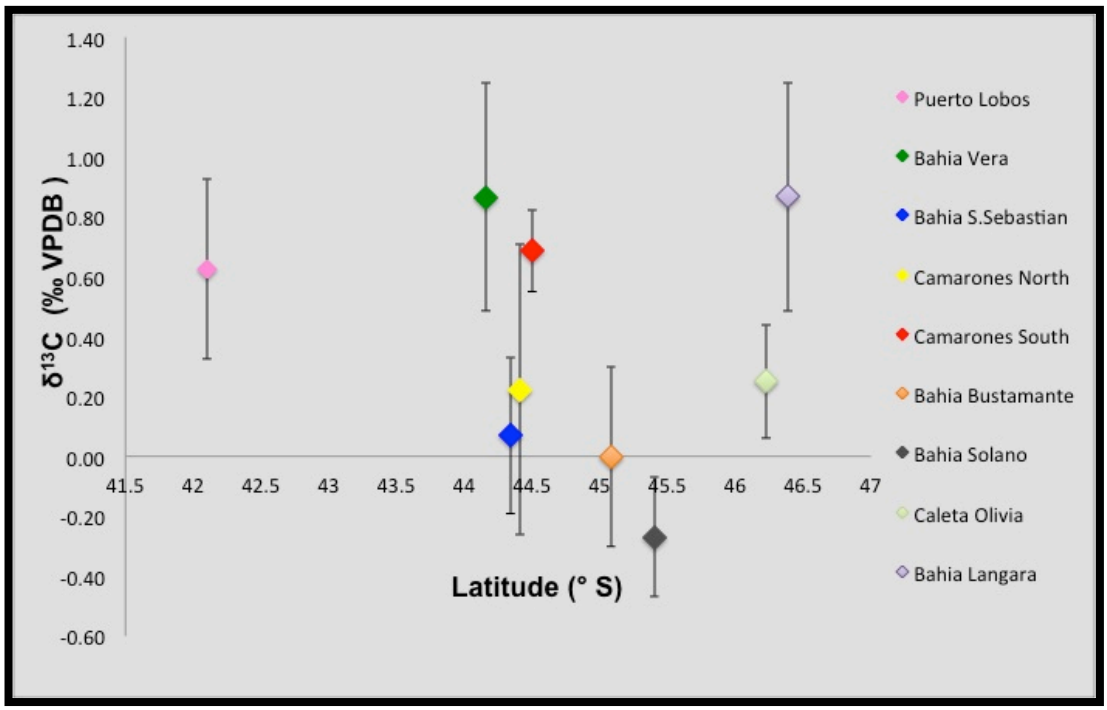

Figure 115 – Carbon isotope composition of modern *A. antiqua* to vary the latitude.

6.3.1.2. *Mytilus edulis* shells

Mytilus edulis shells show mean values of $\delta^{13}C$ from 0.96‰ for Puerto Lobos samples to 1.62±0.1‰ for specimens collected in Bahia Bustamante active beach (Tab. 8). Mean values of oxygen isotopic composition are between 0.52 of Puerto Lobos shells and 1.46±0.25‰ for Puerto Deseado mussels (Tab. 8).

Modern individuals of *Mytilus edulis* show for each locality sampled an intra-specific variability for the $\delta^{13}C$ ranging from 0.0‰ to 1.09‰ and for the $\delta^{18}O$ from 0.1‰ to 0.76‰ (Tab. 9).

SAMPLE	LOCALITY	LATITUDE (°S)	Number of samples	$\delta^{13}C$‰ (mean value)	st. dev.	$\delta^{18}O$‰ (mean value)	st. dev.
WP667	PUERTO LOBOS	42.1	1	**0.96**		**0.52**	
WP95	CAMARONES SOUTH	44.5	2	**1.37**	0.0	**1.03**	0.21
WP191	BAHIA BUSTAMANTE	45.04	4	**1.62**	0.10	**0.91**	0.08
WP271	BAHIA SOLANO	45.4	3	**1.59**	0.14	**1.24**	0.42
MPA3	RADA TILLY	45.55	3	**1.45**	0.25	**1.13**	0.11
WP330	PUERTO DESEADO	47.45	5	**1.40**	0.43	**1.46**	0.25

Table 8 – Mean values and standard deviation of $\delta^{13}C$ and $\delta^{18}O$ of modern *Mytilus edulis.*

SAMPLE	LOCALITY	$\delta^{13}C$‰	$\Delta\delta^{13}C$‰	$\delta^{18}O$ ‰	$\Delta\delta^{18}O$ ‰
WP667(7)	PUERTO LOBOS	**0.96**		**0.52**	
WP95(6)	CAMARONES SOUTH	**1.37**	0	**0.88**	0.3
WP95(7)	CAMARONES SOUTH	**1.37**		**1.18**	
WP191(5)	BAHIA BUSTAMANTE	**1.71**	0.23	**0.91**	0.1
WP191(6)	BAHIA BUSTAMANTE	**1.66**		**0.98**	
WP191(7)	BAHIA BUSTAMANTE	**1.63**		**0.96**	
WP191(8)	BAHIA BUSTAMANTE	**1.48**		**0.81**	
WP271M(3)	BAHIA SOLANO	**1.64**	0.25	**1.72**	0.76
WP271M(4)	BAHIA SOLANO	**1.43**		**0.96**	
WP271M(5)	BAHIA SOLANO	**1.69**		**1.03**	
MPA2(11)	RADA TILLY	**1.75**	0.45	**1.15**	0.22
MPA2(12)	RADA TILLY	**1.30**		**1.01**	
MPA2(13)	RADA TILLY	**1.31**		**1.23**	
WP330(1)	PUERTO DESEADO	**1.06**	1,09	**1.43**	0.59
WP330(2)	PUERTO DESEADO	**1.98**		**1.89**	
WP330(3)	PUERTO DESEADO	**1.61**		**1.30**	
WP330(4)	PUERTO DESEADO	**1.45**		**1.31**	
WP330(5)	PUERTO DESEADO	**0.89**		**1.35**	

Table 9 – Carbon and oxygen isotopic composition and range values of modern shells of *Mytilus edulis* for each locality.

Modern shells of *Mytilus edulis* show oxygen isotopic compositions progressively more positive moving southward (Fig. 116 and Fig. 117), with a $\Delta\delta^{18}O$=0.94‰ from north to south. The samples from the central part of the study area show similar isotopic values. The correlation coefficient between oxygen isotopic composition and latitude is r^2 = 0.92.

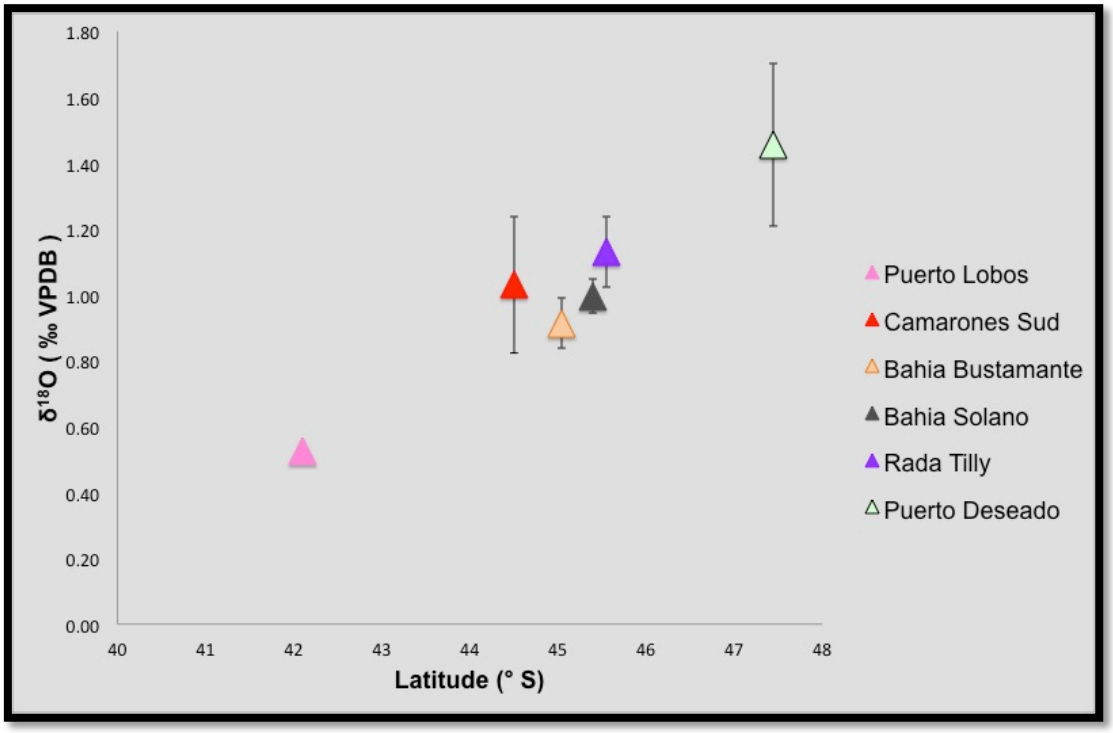

Figure 116 – Oxygen isotope composition of modern *M. edulis* to vary the latitude.

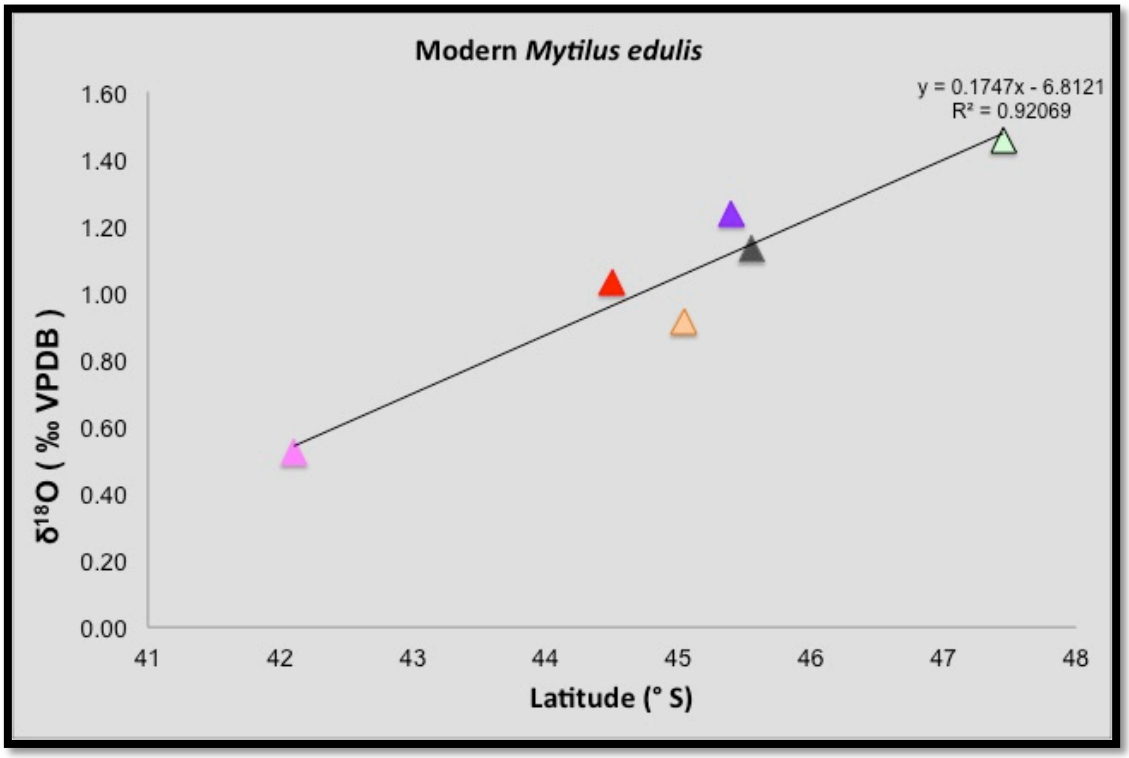

Figure 117 – Oxygen isotope composition of modern *M. edulis* to vary the latitude, with regression line and relative R^2.

A similar trend can also be observed for the $\delta^{13}C$ (Fig. 118). The sample collected in the most northern beach of the study area shows an isotopic composition of carbon lower than that of specimens sampled further south.

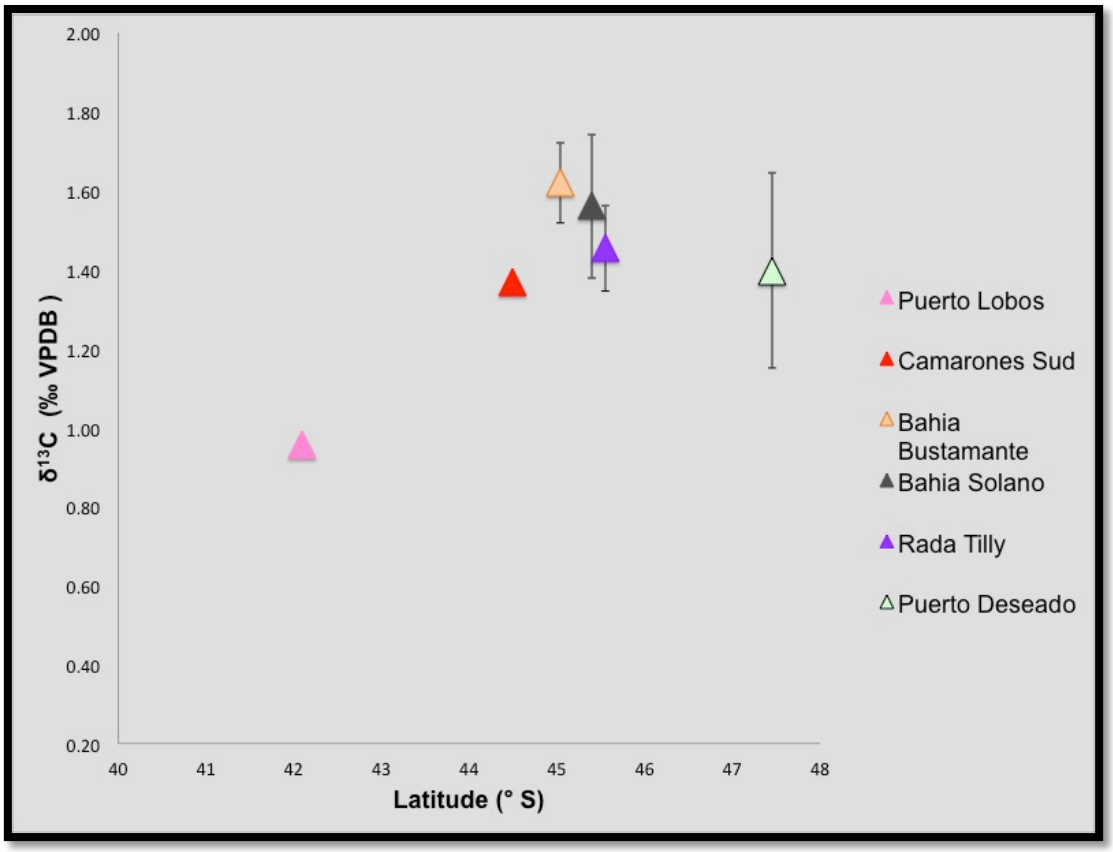

Figure 118 – Carbon isotope composition of *Mytilus edulis* to vary the latitude.

6.3.1.3. *Aulacomya atra* shells

Modern specimens of *Aulacomya atra* show $\delta^{13}C$ mean values ranging from 1.26 for Puerto Lobos samples to 2.10±0.29‰ for Rada Tilly shells. Small differences in oxygen isotopic composition are observed, with values between 1.27 for Puerto Lobos specimens and 1.55±0.13‰ in Rada Tilly area (Tab. 10).

SAMPLE	LOCALITY	LATITUDE	Number of sample	$\delta^{13}C$‰ (mean value)	st. dev.	$\delta^{18}O$‰ (mean value)	st. dev.
WP667	PUERTO LOBOS	42.1	1	**1.26**		**1.27**	
WP60B	CAMARONES NORTH	44.41	5	**1.73**	0.32	**1.28**	0.15
WP95	CAMARONES SOUTH	44.5	4	**1.50**	0.31	**1.43**	0.07
WP191+WP613	BAHIA BUSTAMANTE	45.08	9	**1.66**	0.18	**1.42**	0.17
WP271	BAHIA SOLANO	45.4	2	**1.68**	0.05	**1.29**	0.32
MPA2	RADA TILLY	45.55	3	**2.10**	0.29	**1.40**	0.13
WP473B	CALETA OLIVIA	46.23	6	**1.65**	0.17	**1.55**	0.13

Table 10 – Mean values and standard deviation of $\delta^{13}C$ and $\delta^{18}O$ of modern *Aulacomya atra* shells.

Intra-specific variability of each locality ranges between 0.07‰ and 0.76‰ for $\delta^{13}C$ and between 0.15‰ and 0.46‰ for $\delta^{18}O$ (Tab. 11).

SAMPLE	LOCALITY	$\delta^{13}C$‰	$\Delta\delta^{13}C$‰	$\delta^{18}O$ ‰	$\Delta\delta^{18}O$ ‰
WP667	PUERTO LOBOS	**1.26**		**1.27**	
WP60B(2)	CAMARONES NORTH	**1.80**	0.76	**1.39**	0.41
WP60B(3)	CAMARONES NORTH	**1.88**		**1.01**	
WP60B(4)	CAMARONES NORTH	**2.04**		**1.29**	
WP60B(5)	CAMARONES NORTH	**1.37**		**1.30**	
WP60B(6)	CAMARONES NORTH	**2.00**		**1.24**	
WP60B(10)	CAMARONES NORTH	**1.28**		**1.42**	
WP95(3)	CAMARONES SOUTH	**1.13**	0.74	**1.41**	0.15
WP95(4)	CAMARONES SOUTH	**1.43**		**1.49**	
WP95(8)	CAMARONES SOUTH	**1.57**		**1.34**	
WP95(10)	CAMARONES SOUTH	**1.87**		**1.48**	
WP191(1)	BAHIA BUSTAMANTE	**1.32**	0.5	**1.28**	0.42
WP191(2)	BAHIA BUSTAMANTE	**1.82**		**1.22**	
WP191(3)	BAHIA BUSTAMANTE	**1.75**		**1.42**	
WP191(4)	BAHIA BUSTAMANTE	**1.79**		**1.24**	
WP613(6)	BAHIA BUSTAMANTE	**1.78**		**1.33**	
WP613(7)	BAHIA BUSTAMANTE	**1.78**		**1.63**	
WP613(8)	BAHIA BUSTAMANTE	**1.44**		**1.39**	
WP613(9)	BAHIA BUSTAMANTE	**1.61**		**1.64**	
WP613(10)	BAHIA BUSTAMANTE	**1.68**		**1.60**	
WP271M(1)	BAHIA SOLANO	**1.72**	0.07	**1.52**	0.46
WP271M(2)	BAHIA SOLANO	**1.65**		**1.06**	
MPA2(7)	RADA TILLY	**2.21**	0.62	**1.39**	0.28
MPA2(8)	RADA TILLY	**2.21**		**1.22**	
MPA2(9)	RADA TILLY	**1.68**		**1.47**	
MPA2(10)	RADA TILLY	**2.30**		**1.50**	
WP473B(7)	CALETA OLIVIA	**1.50**	0.39	**1.46**	0.34
WP473B(8)	CALETA OLIVIA	**1.66**		**1.51**	
WP473B(9)	CALETA OLIVIA	**1.85**		**1.73**	
WP473B(10)	CALETA OLIVIA	**1.87**		**1.68**	
WP473B(11)	CALETA OLIVIA	**1.48**		**1.53**	
WP473B(12)	CALETA OLIVIA	**1.56**		**1.39**	

Table 11 - Carbon and oxygen isotopic composition and range values of modern shells of *Aulacomya atra* for each locality.

Contrary to what was observed for specimens of modern *Mytilus edulis,* the oxygen isotopic composition of modern *Aulacomya atra* shells is fairly homogeneous in all the study area (Fig. 119), with small differences substantially overlapping. $\delta^{13}C$,

instead, shows a larger range of values progressively and slightly more positive towards south (Fig. 120).

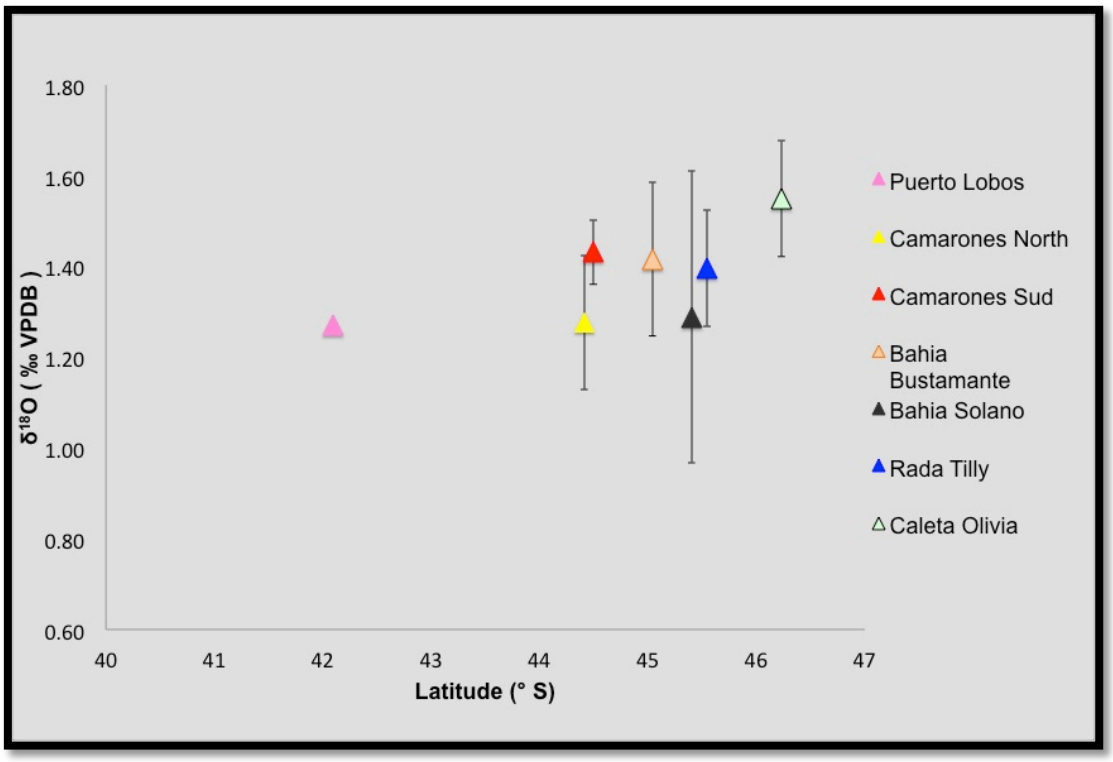

Figure 119 – Oxygen isotopic composition of modern *Aulacomya atra* from north to south.

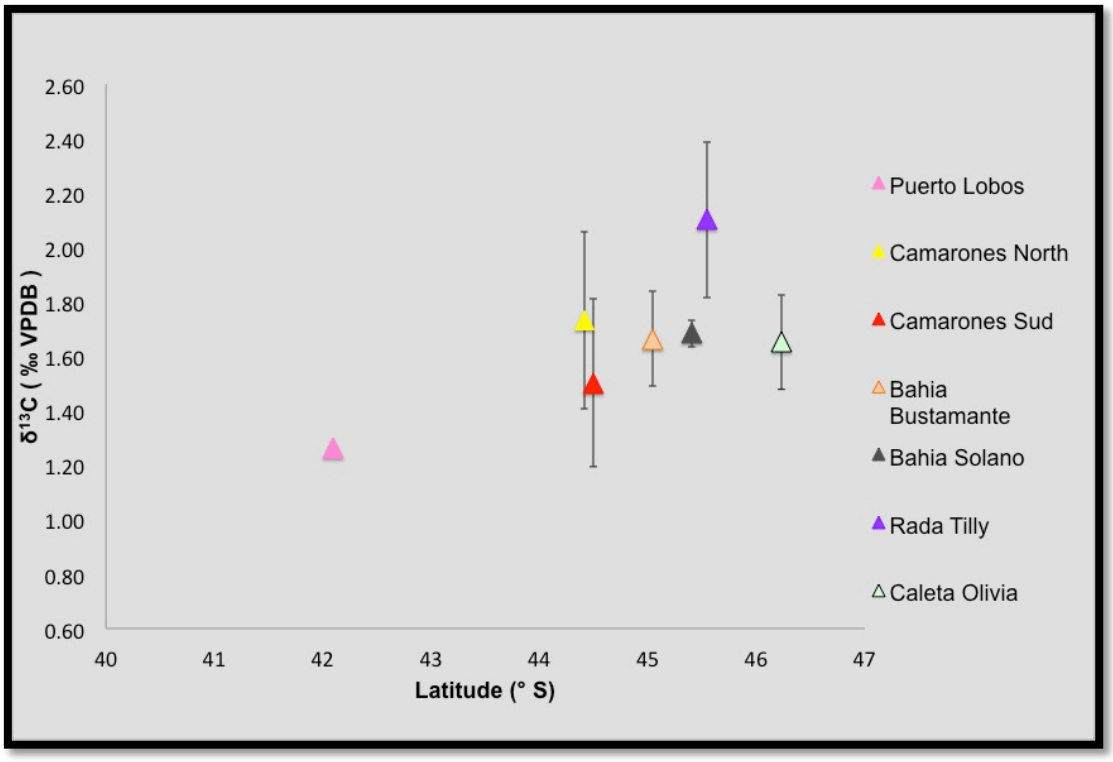

Figure 120 – Carbon isotopic composition of modern *Aulacomya atra* from north to south.

6.3.2. Stable isotope composition of Holocene marine shells

Oxygen and carbon isotope analyses of Holocene shells were carried out on *Ameghynomia antiqua, Mytilus edulis*, *Aulacomya atra* and *Nacella (Patinigera) deaurata* specimens sampled from beach deposits in different localities on the Atlantic coast of Patagonia (Fig. 121). For all the localities the Holocene beach deposits represent storm accumulation.

Figure 121 – Localities of the Patagonia Atlantic coast where Holocene beach ridges were sampled.

The results of stable isotope analyses on Holocene shells are presented by species analyzed and locality and compared with specimens collected in the modern beach of the same locality.

Where possible radiocarbon ages performed within this study were used (for all dating see Appendix A). Otherwise dating from the works of Schellmann & Radtke (indicated with the words LIT in tables), or the age deduced from stratigraphic considerations on the field was used.

6.3.2.1. Stable isotope composition of Holocene Mytilidae shells in Camarones North

Holocene shells belonging to the family Mytilidae come from a section located North of the village of Camarones (Fig. 121). The shells were collected from two Holocene beach ridges, never studied before and dated specifically for this project, and from a local shell midden, due to the accumulation performed by native population in the past (Fig. 122). Detailed stratigraphy is proposed in Zanchetta *et al.* (2012).

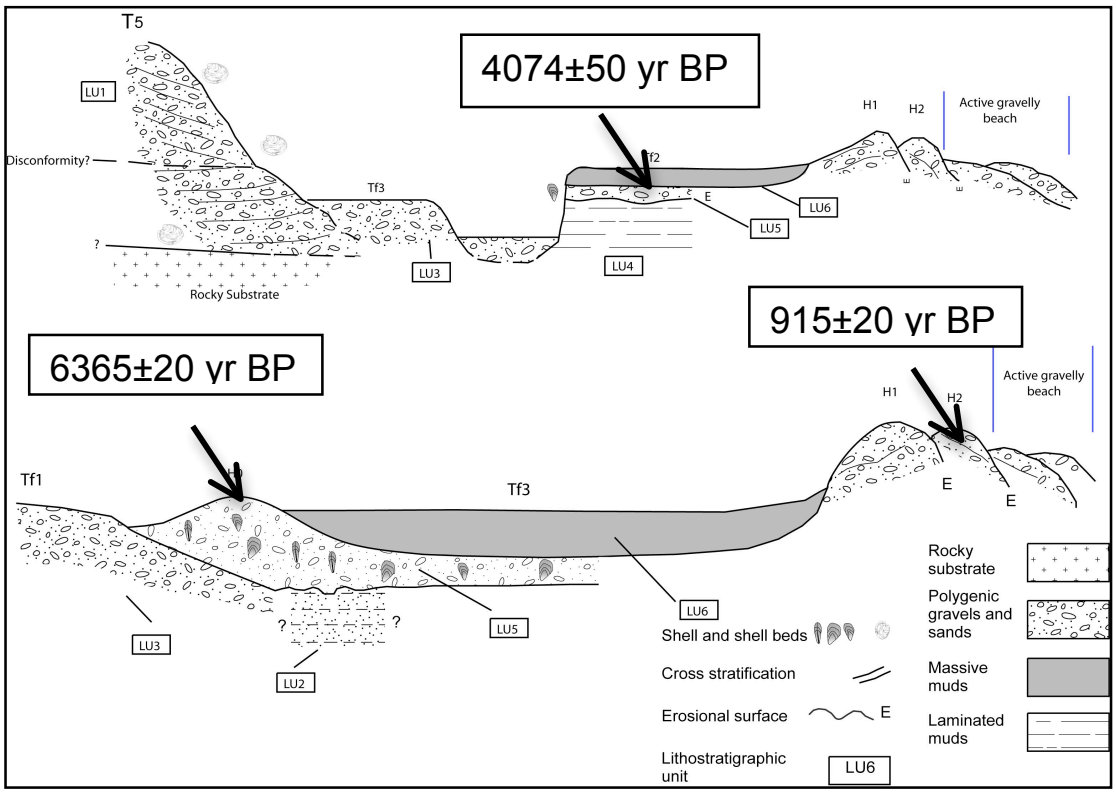

Figure 122 - Sketch of the relations between litostratigraphic units (LU) and morphostratigraphic units (MU) (not in scale) (after Zanchetta *et al*., 2012).

As in the older beach ridge were missing specimens of *Aulacomya atra* shells to be compared with the more recent specimens, the stable isotope (oxygen and carbon) composition of modern shells of *Aulacomya atra* and *Mytilus edulis* collected from San Jorge Gulf area was compared (for the samples see Tabs 8-11), in order to understand if the two species can be used interchangeably for the reconstruction of past coastal conditions (Fig. 123).

Modern shells of *Mytilus edulis* and *Aulacomya atra* show overall small differences in isotopic composition substantially overlapping in terms of carbon isotope composition (Fig. 123) and to lesser extent with oxygen. $\delta^{18}O$ of *Aulacomya atra* shells tends to be more weakly positive than in *Mytilus edulis.* This is in agreement

with the more aragonitic content of *A. atra* compared to *M. edulis*. Aragonite is usually more ^{18}O-enriched compared to the coexisting calcite (Grossman & Ku, 1986). However the difference is small and on the basis of these results it was decided to compare the isotopic composition of *Aulacomya atra* and *Mytilus edulis* shells from different Holocene beach ridges.

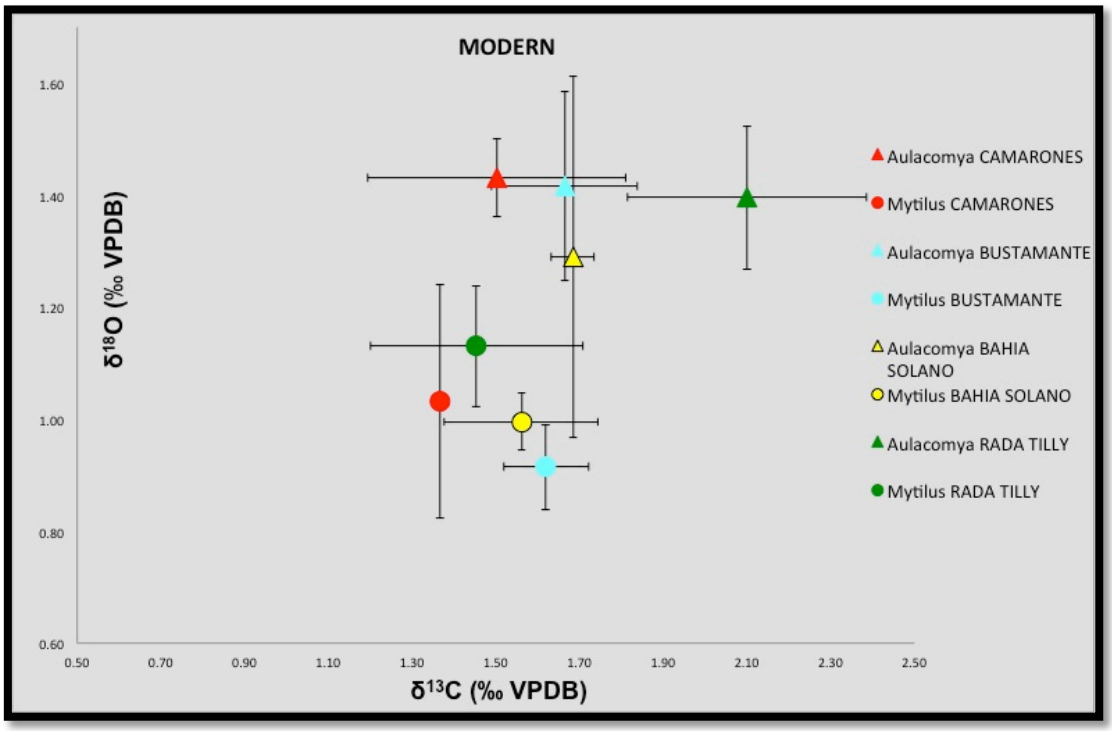

Figure 123 - $\delta^{13}C$ vs $\delta^{18}O$ mean values of modern *Aulacomya atra* and *Mytilus edulis* from San Jorge Gulf area.

The layer dated to 6365±20 yr BP shows the highest oxygen isotopic composition, which ranges from 2.16 to 2.69‰ (mean $\delta^{18}O$ value of 2.39±0.19‰ and $\Delta\delta^{18}O$ = 0.53‰). The layer dated to ca. 4000 yr BP, related to a shell midden accumulation, has a narrower range of $\delta^{18}O$ (from 1.15 to 1.18‰) with a mean value of 1.15±0.02‰ ($\Delta\delta^{18}O$ = 0.05‰) and the beach deposit dated to 915±20 yr BP ranges from 0.99 to 1.6‰, showing a mean value of 1.36±0.18‰ and $\Delta\delta^{18}O$ = 0.58‰ (Tab. 12). The isotopic data obtained from *Aulacomya atra* shells coming from the shell midden at 4074 yr BP were also added the results obtained from two specimens of *Nacella (Patinigera) deaurata* (Tab. 12 and Fig. 124). Carbon isotope composition of the specimens from the older beach ridge shows the highest values (from 1.75 to 2.65‰, with a mean value of 2.19±0.29‰ ($\Delta\delta^{13}C$ = 0.90‰). The shells collected

from the layer at 4074±50 yr BP show $\delta^{13}C$ values from 1.15 to 1.84‰ and mean value of 1.58±0.26‰ ($\Delta\delta^{13}C$ = 0.60‰). The Mytilidae individuals sampled in the beach deposit dated to 915 yr BP show carbon isotope values ranging from 1.51 to 2.71, with $\delta^{13}C$ mean value of 2.11±0.36‰ ($\Delta\delta^{13}C$ = 1.2‰).

SAMPLE	Species	^{14}C AGE (uncalibrated)	^{14}C cal BP 2 sigma	$\delta^{13}C$‰	$\delta^{18}O$‰	$\delta^{13}C$‰ (mean value)	st. dev.	$\Delta\delta^{13}C$‰	$\delta^{18}O$‰ (mean value	st. dev.	$\Delta\delta^{18}O$ ‰
WP60B(2)	*A.atra*	-390±20		**1.80**	**1.39**	**1.73**	0.32	0.76	**1.28**	0.15	0.41
WP60B(3)	*A.atra*	-390±20		**1.88**	**1.01**						
WP60B(4)	*A.atra*	-390±20		**2.04**	**1.29**						
WP60B(5)	*A.atra*	-390±20		**1.37**	**1.30**						
WP60B(6)	*A.atra*	-390±20		**2.00**	**1.24**						
WP60B(10)	*A.atra*	-390±20		**1.28**	**1.42**						
WP60A(1)	*A.atra*	915±20	477-560	**2.16**	**1.41**	**2.11**	0.36	1.2	**1.36**	0.18	0.58
WP60A(2)	*A.atra*	915±20	477-560	**2.71**	**1.55**						
WP60A(3)	*A.atra*	915±20	477-560	**2.25**	**1.20**						
WP60A(4)	*A.atra*	915±20	477-560	**2.27**	**1.34**						
WP60A(5)	*A.atra*	915±20	477-560	**2.10**	**0.99**						
WP60A(7)	*A.atra*	915±20	477-560	**1.65**	**1.36**						
WP60A(8)	*A.atra*	915±20	477-560	**2.33**	**1.39**						
WP60A(9)	*A.atra*	915±20	477-560	**1.51**	**1.42**						
WP60A(10)	*A.atra*	915±20	477-560	**2.02**	**1.57**						
G001(1)	*A.atra*	4074±50	3948-4271	**1.84**	**1.13**	**1.58**	0.26	0.69	**1.15**	0.02	0.05
G001(4)	*A.atra*	4074±50	3948-4271	**1.65**	**1.18**						
G001(5)	*A.atra*	4074±50	3948-4271	**1.15**	**1.14**						
G001(6)	*A.atra*	4074±50	3948-4271	**1.64**	**1.17**						
G001(7)	*A.atra*	4074±50	3948-4271	**1.64**	**1.14**						
G001(2)	*N. deaurata*	4074±50	3948-4271	**1.14**	**1.37**						
G001(3)	*N. deaurata*	4074±50	3948-4271	**1.18**	**1.17**						
WP63B(1)	*M.edulis*	6365±20	6750-6913	**2.08**	**2.50**	**2.19**	0.29	0.9	**2.39**	0.19	0.53
WP63B(2)	*M.edulis*	6365±20	6750-6913	**2.07**	**2.35**						
WP63B(3)	*M.edulis*	6365±20	6750-6913	**2.65**	**2.51**						
WP63B(4)	*M.edulis*	6365±20	6750-6913	**2.23**	**2.19**						
WP63B(5)	*M.edulis*	6365±20	6750-6913	**1.75**	**2.23**						
WP63B(6)	*M.edulis*	6365±20	6750-6913	**2.24**	**2.50**						
WP63B(7)	*M.edulis*	6365±20	6750-6913	**1.99**	**2.16**						
WP63B(8)	*M.edulis*	6365±20	6750-6913	**2.53**	**2.69**						

Table 12 – Carbon and oxygen isotopic composition, mean, standard deviation and range values of modern and Holocene shells of *Aulacomya atra, Mytilus edulis* and *Nacella (Patinigera) deaurata* from Camarones North section.

The most interesting and relevant feature of the isotopic data is the highest $\delta^{18}O$ values showed by the layer dated to 6365±20 yr BP, whereas its carbon isotope composition overlaps the values of the shells found at 915 yr BP and the modern specimens (Figs. 123-125). Instead, the modern samples, those dated at ca 4000 yr

BP and the more recent Holocene individuals have very similar $\delta^{18}O$ values (Fig. 124) but different or partially overlapping $\delta^{13}C$ (Figs. 124-126).

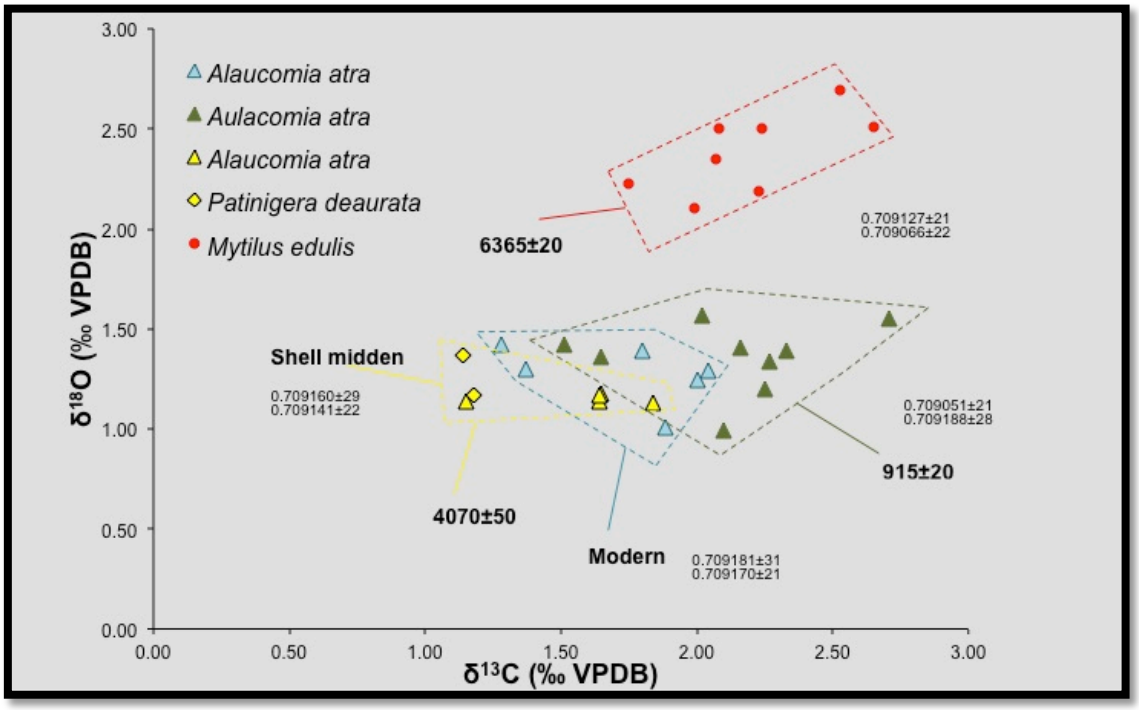

Figure 124 - $\delta^{13}C$ vs $\delta^{18}O$ of modern and Holocene *Aulacomya atra, Nacella deaurata* and *Mytilus edulis* from Camarones North area. In the diagram Sr isotopic data for each layer are reported.

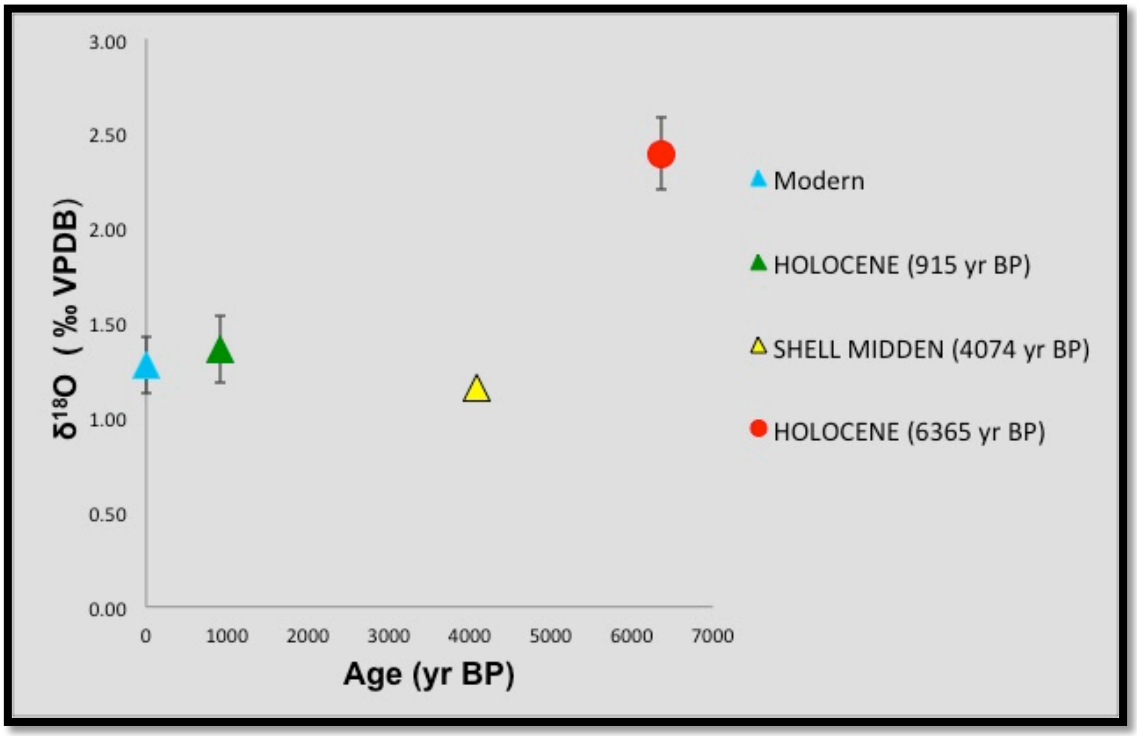

Figure 125 – Oxygen isotope mean values and standard deviation vs age of Holocene and modern Mytilidae shells sampled in Camarones North area.

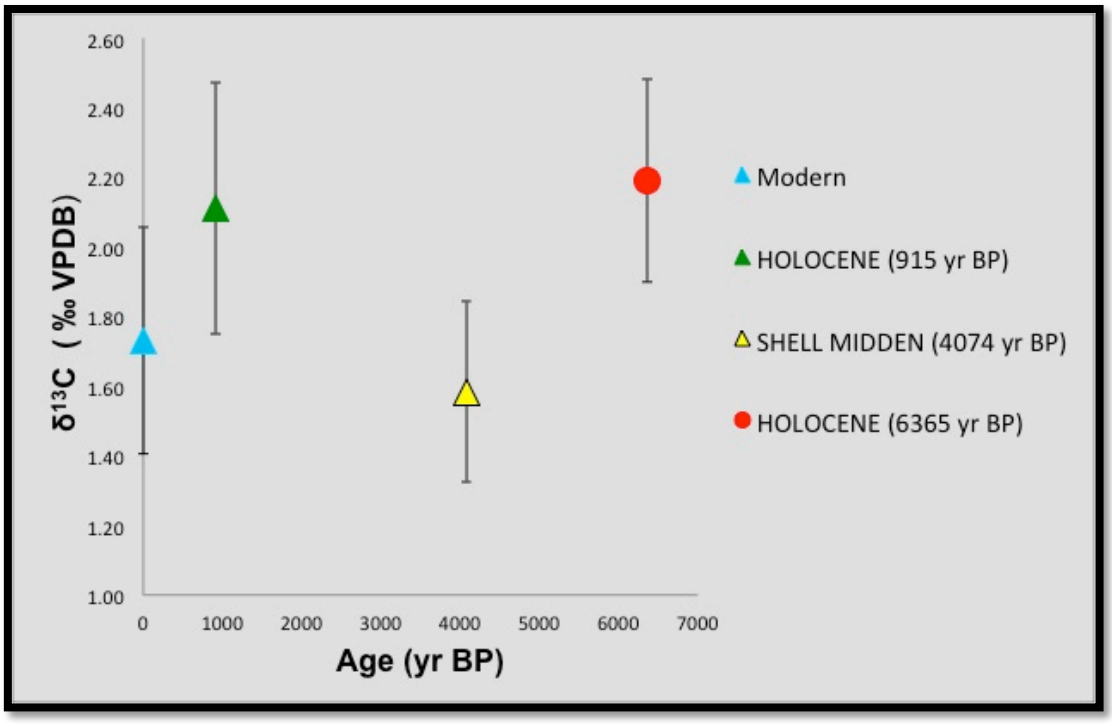

Figure 126 – Carbon isotope mean values and standard deviation vs age of Holocene and modern Mytilidae shells sampled in Camarones North area.

6.3.2.2. Stable isotope composition of Holocene *Ameghinomya antiqua* shells in Camarones South

Oxygen and carbon isotope analysis was carried out on four Holocene beach ridges (Fig. 127) outcropping in Camarones South area, 3 of which (indicated with the word LIT in Tab. 13) were dated by Schellmann (1998; 2007) and Schellmann & Radtke (2003; 2010) and one dated within this project (Tab.13).

The older layers dated to 5800±51 yr BP and 6620±65 yr BP have the highest oxygen isotopic composition, which ranges from 0.75 to 0.82‰ (mean $\delta^{18}O$ value of 0.79±0.0.5‰ and $\Delta\delta^{18}O$ = 0.07‰) and from 0.77 to 0.83‰ (mean $\delta^{18}O$ value of 0.79±0.0.3‰ and $\Delta\delta^{18}O$ = 0.06‰) respectively (Tab. 13 and Fig. 128), similarly to what observed in Camarones North. The layer dated to 5675 yr BP show a range of $\delta^{18}O$ from 0.33 to 0.64‰ with a mean value of 0.50±0.13‰ ($\Delta\delta^{18}O$ = 0.31‰) and the beach deposit dated to 5754±62 yr BP ranges from 0.38 to 0.58‰, showing a mean value 0.50±0.09‰ and $\Delta\delta^{18}O$ = 0.2‰ (Tab. 13). Carbon isotope composition of the specimens from the older beach ridge shows the highest values (from 1.56 to 1.83‰, with a mean value of 1.71±0.14‰ and $\Delta\delta^{13}C$ = 0.27‰). The samples

collected from the layer at 5800±51 yr BP show $\delta^{13}C$ values from 0.93 to 1.10‰ and mean value of 11.01±0.12‰ ($\Delta\delta^{13}C$ = 0.17‰). The Mytilidae shells sampled in the beach deposits dated to 5675 and 5754 yr BP show carbon isotope values ranging from 0.59 to 1.08‰, with $\delta^{13}C$ mean value of 0.66±0.27‰ ($\Delta\delta^{13}C$ = 0.70‰) and from 0.92 to 1.35 with mean $\delta^{13}C$ value of 1.14±0.21‰ ($\Delta\delta^{13}C$ = 0.43‰) respectively (Tab. 13 and Fig. 128).

Figure 127 – Holocene and modern beach ridges sampled and analyzed (for *Ameghinomya antiqua)* in Camarones South area.

SAMPLE	^{14}C AGE (uncalibrated)	^{14}C cal BP 2 sigma	$\delta^{13}C$‰	$\delta^{18}O$‰	$\delta^{13}C$‰ (mean value)	st. dev	$\Delta\delta^{13}C$‰	$\delta^{18}O$‰ (mean value)	st. dev.	$\Delta\delta^{18}O$ ‰
WP95(2)	modern beach ridge		0.59	0.38	**0.69**	0.14	0.30	**0.32**	0.06	0.13
WP95(3)	modern beach ridge		0.62	0.3						
WP95(4)	modern beach ridge		0.89	0.35						
WP110(2)	modern beach ridge		0.65	0.25						
WP104A(1)	5675±45 BP	5947-6196	0.59	0.64	**0.66**	0.27	0.70	**0.50**	0.13	0.31
WP104A(2)	5675±45 BP	5947-6196	0.74	0.33						
WP104A(3)	5675±45 BP	5947-6196	0.38	0.58						
WP104A(4)	5675±45 BP	5947-6196	1.08	0.54						
WP104A(5)	5675±45 BP	5947-6196	0.50	0.39						
WP 108A(1)	LIT 5754±62 BP	5955-6286	1.29	0.49	**1.14**	0.21	0.43	**0.50**	0.09	0.2
WP108A(2)	LIT 5754±62 BP	5955-6286	1.01	0.54						
WP108A(3)	LIT 5754±62 BP	5955-6286	1.35	0.38						
WP108A(4)	LIT 5754±62 BP	5955-6286	0.92	0.58						
WP94B(1)	LIT.5800±51 BP	6090-6333	1.10	0.82	**1.01**	0.12	0.17	**0.79**	0.05	0.07
WP94B(2)	LIT.5800±51 BP	6090-6333	0.93	0.75						
WP 114(1)	LIT. 6620±65 BP	6970-7281	1.56	0.77	**1.71**	0.14	0.27	**0.79**	0.03	0.06
WP114(2)	LIT. 6620±65 BP	6970-7281	1.75	0.83						
WP114(3)	LIT. 6620±65 BP	6970-7281	1.83	0.79						

Table 13 – Carbon and oxygen isotopic composition, mean, standard deviation and range values of modern and Holocene shells of *Ameghinomya antiqua* from Camarones South area. The words LIT before the ^{14}C ages indicate that the dating come from the work of Schellmann (1998) and Schellmann and Radtke (2010).

Almost all the shells from the Holocene beach ridges are enriched in ^{18}O and ^{13}C, except some samples from the beach ridge dated to 5675 yr BP, compared to specimens collected in the active beach (Fig. 128).

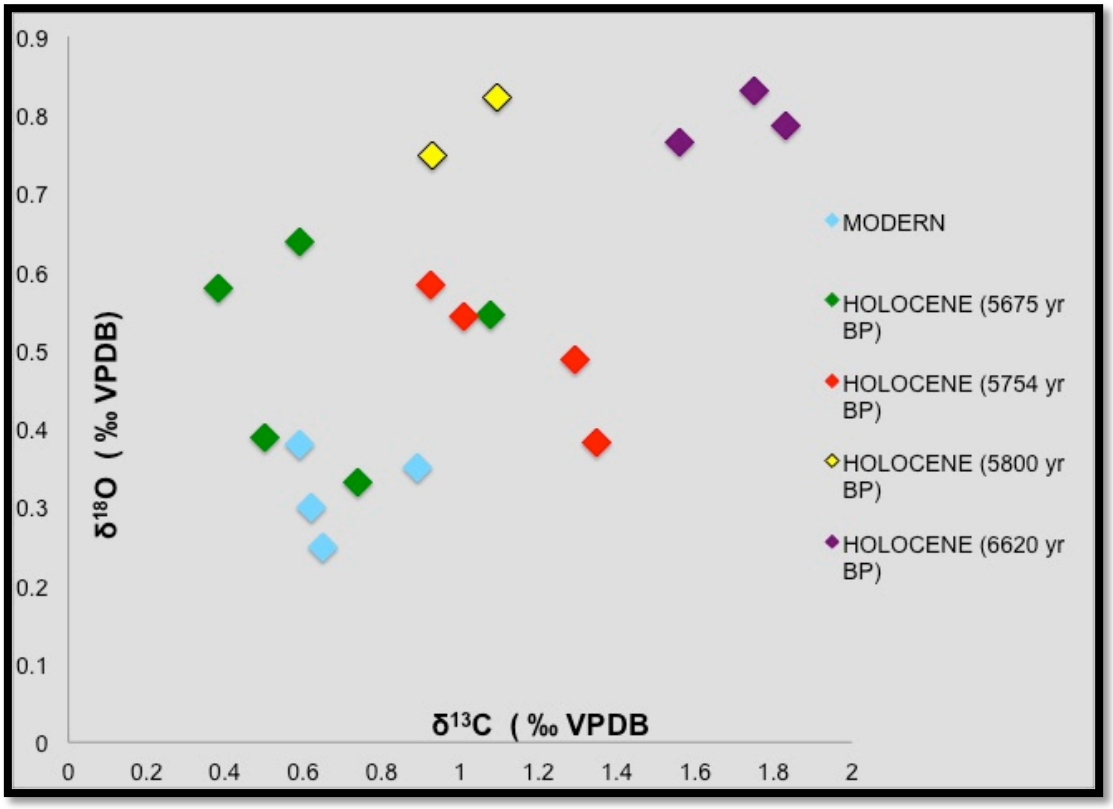

Figure 128 - $\delta^{13}C$ vs $\delta^{18}O$ of Holocene and modern *Ameghinomya antiqua* from Camarones South area.

Shells from beach ridges dated to 5675±45 yr BP and 5754±62 yr BP are slightly ^{18}O enriched (by 0.20‰) compared to modern specimens. The relatively older Holocene shells, on the other hand, show more positive $\delta^{18}O$ values than modern and more recent Holocene individuals (Fig. 129).

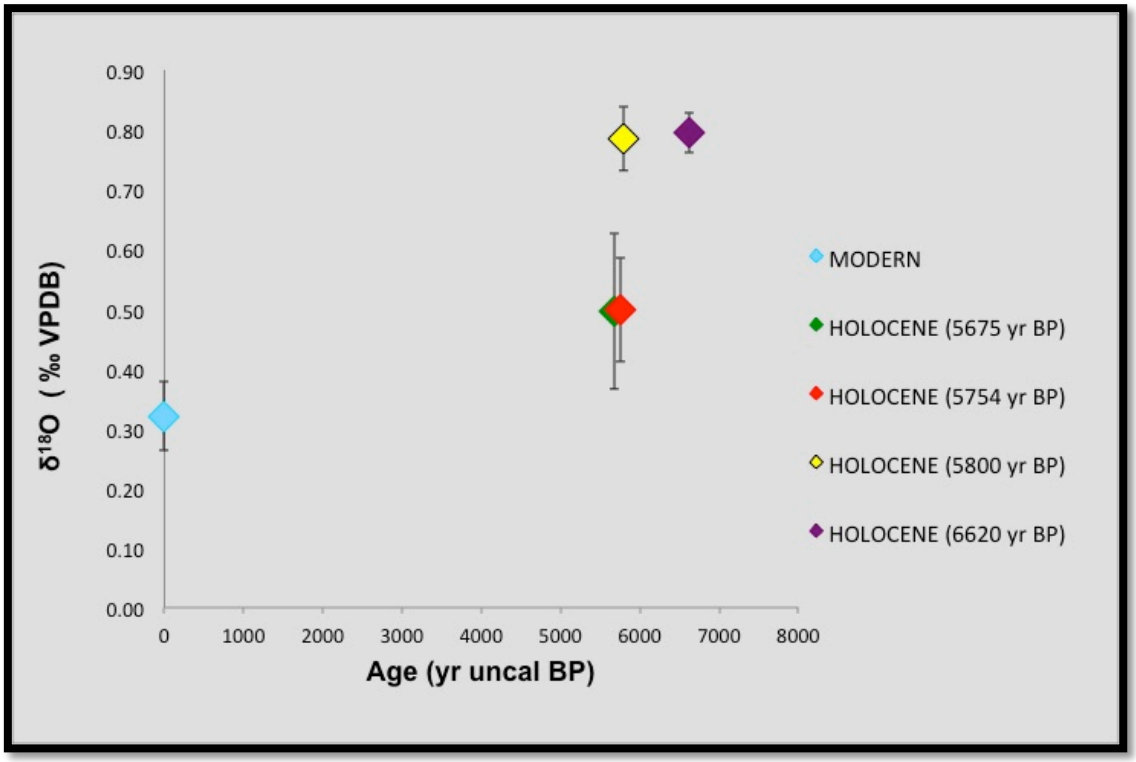

Figure 129 – Oxygen isotope mean values and standard deviation vs age of Holocene and modern *Ameghinomya antiqua* shells sampled in Camarones South area.

Holocene mean $\delta^{13}C$ values are more positive than modern mean values from 5754±62 yr BP and are significantly higher for the shells collected in the beach ridge dated to 6620±62 yr BP, with a difference of 1.02‰ compared to the modern counterpart (Fig. 130).

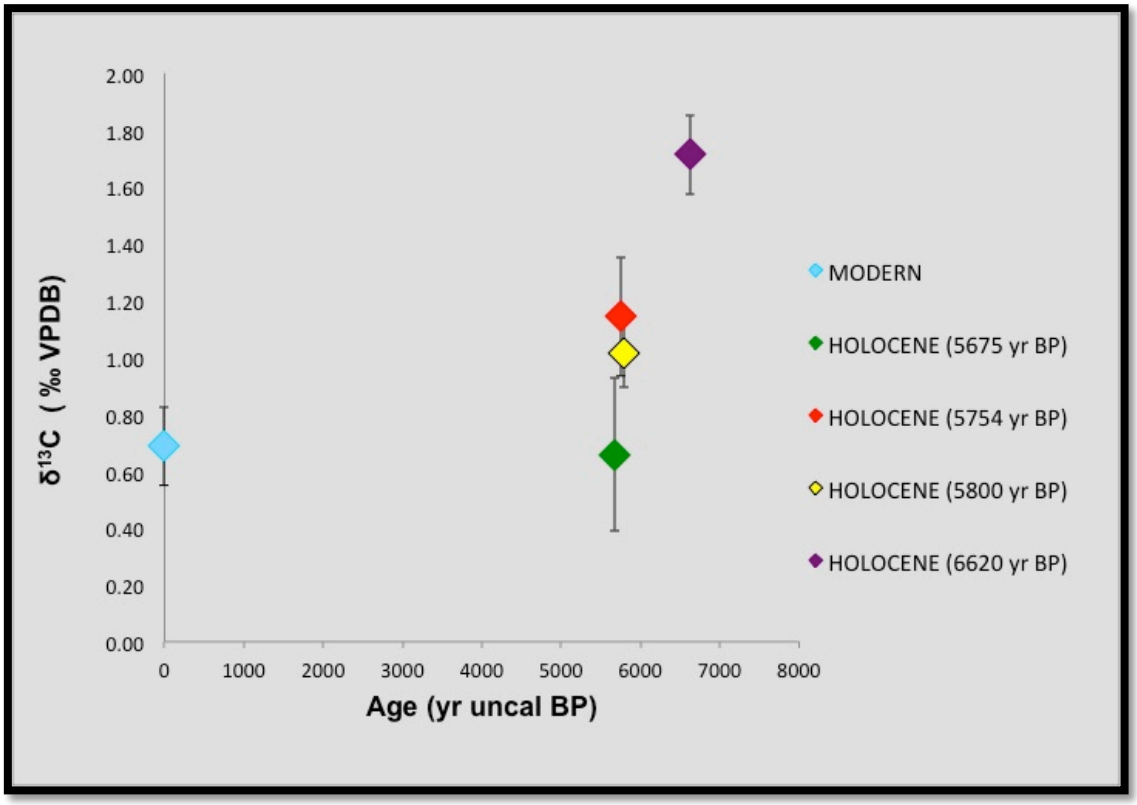

Figure 130 – Carbon isotope mean values and standard deviation vs age of Holocene and modern *Ameghinomya antiqua* shells sampled in Camarones South area.

6.3.2.3. Stable isotope composition of *Holocene Mytilus* edulis shells in Camarones South

Holocene *Mytilus edulis* specimens from Camarones South area come from the two younger beach ridges sampled also for *Ameghinomya antiqua* (WP 104 and WP 108, Fig. 127) and from two beach deposits (WPi 436 and AO 154) dated within this project with the radiocarbon dating to 5562±43 yr BP and 5132±67 yr BP respectively (Fig. 131).

Figure 131 – Holocene and modern beach ridges sampled and analyzed (for *Mytilus edulis)* in Camarones South area.

Middle Holocene shells from AO154D (n = 2; 5132±67 yr BP) exhibit $\delta^{18}O$ values from 1.26 to 1.29‰ and mean $\delta^{18}O$ value of 1.28±0.02‰ ($\Delta\delta^{18}O$ = 0.03‰), the specimens collected in WPi436 (n = 2; 5562±43 yr BP) show $\delta^{18}O$ values from 1.19 to 1.22‰ with mean $\delta^{18}O$ value of 1.20±0.02‰ ($\Delta\delta^{18}O$ = 0.03‰). *Mytilus edulis* shells sampled from WP104B (n = 4; 5675±45 yr BP uncalibrated) and from WP 108B (n = 5; 5754±62 yr BP uncalibrated) have oxygen isotopic values ranging from 1.07 to 1.46‰ with mean value of 1.27±0.16‰ ($\Delta\delta^{18}O$ = 0.39‰) and from 1.07 to 1.24‰ with mean value of 1.17±0.05‰ ($\Delta\delta^{18}O$ = 0.13‰) respectively (Tab. 14).
The same specimens show $\delta^{13}C$ values between 1.71 and 1.72‰ (mean $\delta^{13}C$ value of 1.72±0.01‰ and $\Delta\delta^{13}C$ = 0.01‰), between 1.86 and 1.87‰ (mean $\delta^{13}C$ value of 1.87±0.01‰ and $\Delta\delta^{13}C$ = 0.01‰), between 2.38 and 2.82‰ (mean $\delta^{13}C$ value of 2.63±0.19‰ and $\Delta\delta^{13}C$ = 0.44‰) and between 1.90 and 2.61‰ with mean value of 2.23±0.29‰ and $\Delta\delta^{13}C$ = 0.71‰ respectively (Tab. 14).

SAMPLE	^{14}C AGE (uncalibrated)	^{14}C cal BP 2 sigma	$\delta^{13}C$‰	$\delta^{18}O$‰	$\delta^{13}C$‰ (mean value)	st. dev.	$\Delta\delta^{13}C$‰	$\delta^{18}O$‰ (mean value)	st. dev.	$\Delta\delta^{18}O$ ‰
WP95(6)	modern beach ridge		1.37	0.88	1.37	0.0	0	1.03	0.21	0.2
WP95(7)	modern beach ridge		1.37	1.18						
AO 154D	5132±67	5313-5608	1.72	1.29	1.72	0.01	0.01	1.28	0.02	0.03
AO 154D	5132±67	5313-5608	1.71	1.26						
WPi 436	5562±43	5861-6092	1.86	1.19	1.87	0.00	0.01	1.20	0.02	0.03
WPi 436	5562±43	5861-6092	1.87	1.22						
WP104B(1)	5675±45 BP	5947-6196	2.58	1.32	2.63	0.19	0.44	1.27	0.16	0.39
WP104B(2)	5675±45 BP	5947-6196	2.75	1.46						
WP104B(3)	5675±45 BP	5947-6196	2.38	1.07						
WP104B(4)	5675±45 BP	5947-6196	2.82	1.24						
WP108B(1)	LIT 5754±62 BP	5955-6286	2.35	1.13	2.23	0.29	0.71	1.17	0.05	0.13
WP108B(2)	LIT 5754±62 BP	5955-6286	2.29	1.17						
WP108B(3)	LIT 5754±62 BP	5955-6286	2.61	1.19						
WP108B(4)	LIT 5754±62 BP	5955-6286	1.99	1.11						
WP108B(5)	LIT 5754±62 BP	5955-6286	1.90	1.24						

Table 14 – Carbon and oxygen isotopic composition, mean, standard deviation and range values of modern and Holocene shells of *Mytilus edulis* from Camarones South area. The words LIT before the uncalibrated ^{14}C ages indicate that the dating come from the works of Schellmann and Radtke.

Holocene shells compared to modern specimens show similar values of $\delta^{18}O$, but higher values of carbon isotope composition (Fig. 132), in particular for the *Mytilus edulis* coming from the two older middle Holocene beach ridges dated to 5675±45 yr BP and to 5754±62 yr BP, which show $\delta^{13}C$ values more positive of at least 1‰ (up to ca 1.51‰).

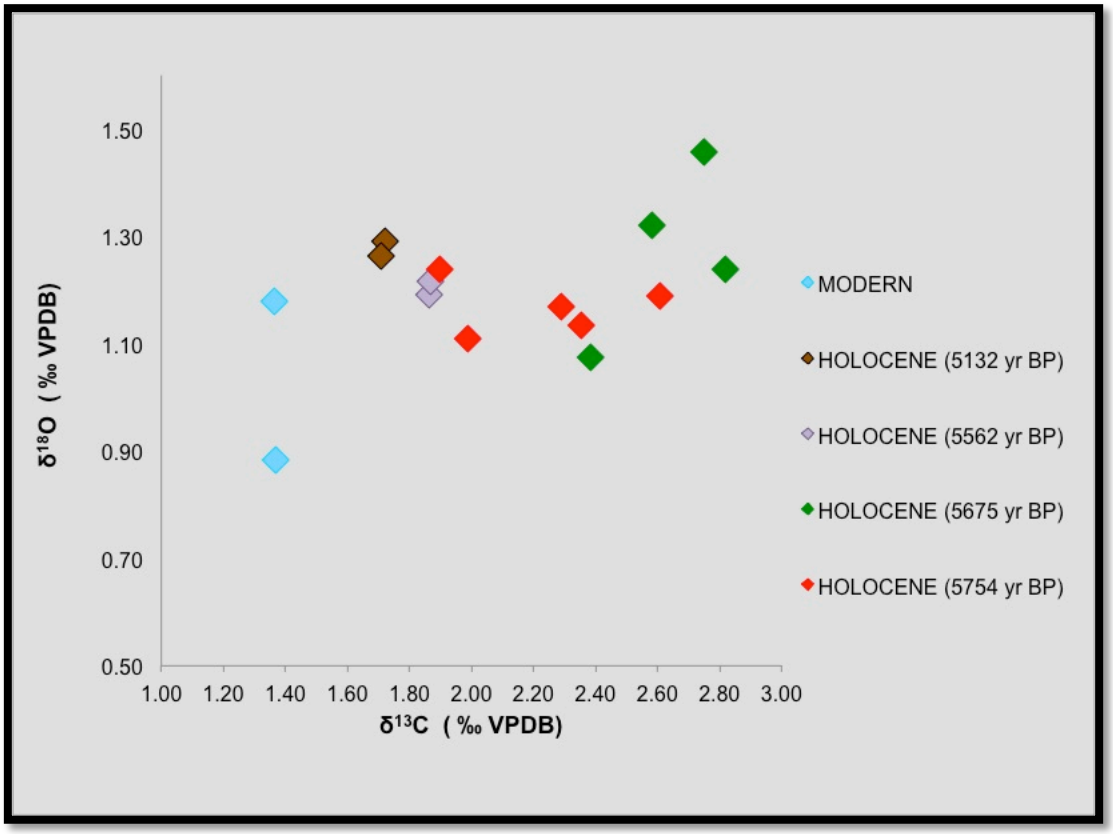

Figure 132 - $\delta^{13}C$ vs $\delta^{18}O$ of Holocene and modern *Mytilus edulis* from Camarones South area.

The mean oxygen isotope values of Holocene specimens are very similar with respect to the modern $\delta^{18}O$ values and are overlapping (Fig. 133) while the $\delta^{13}C$ mean values progressively increase in the older beach ridges up to reach a difference of 1‰ respect to the modern samples (Fig. 134).

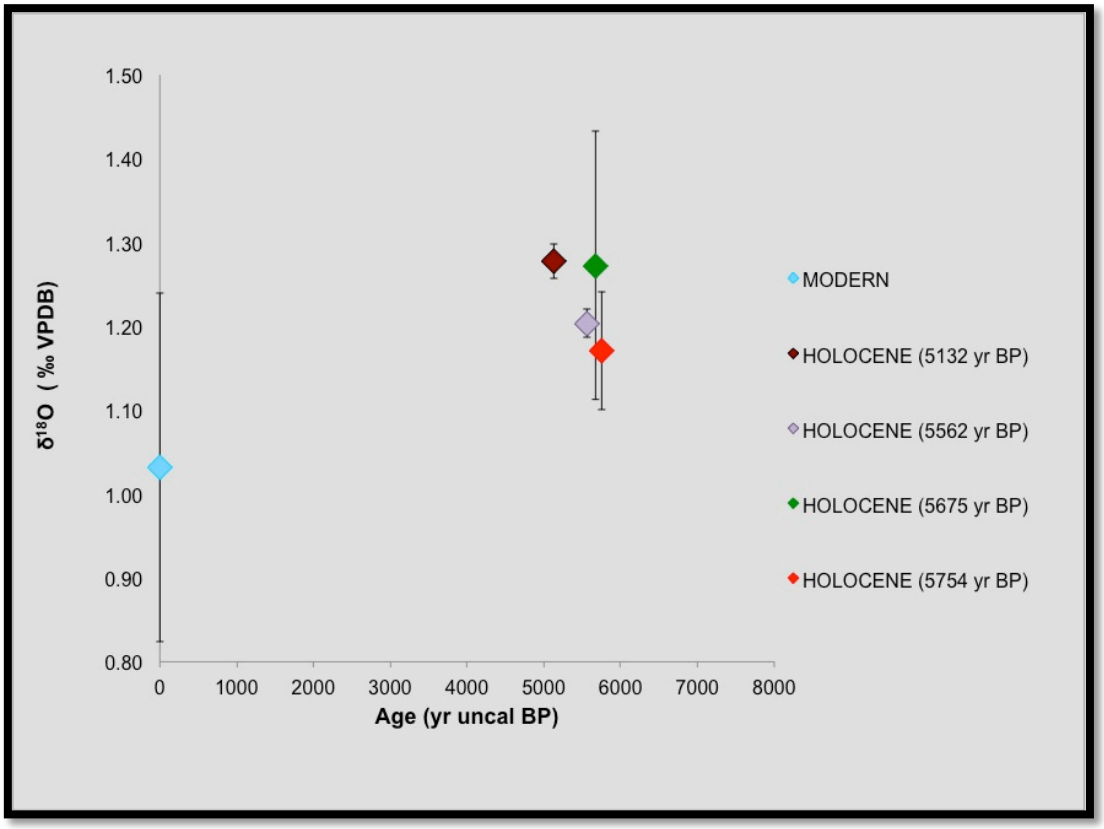

Figure 133 – Oxygen isotope mean values and standard deviation vs age of Holocene and modern *Mytilus edulis* shells sampled in Camarones South area.

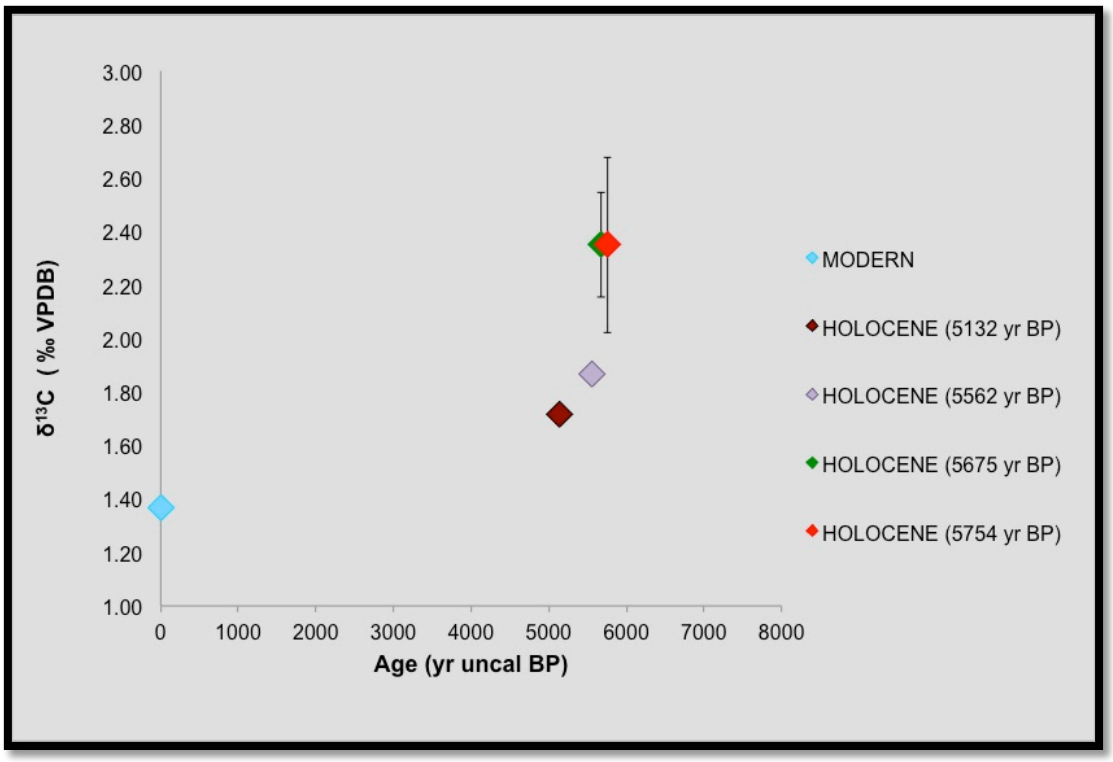

Figure 134 – Carbon isotope mean values and standard deviation vs age of Holocene and modern *Mytilus edulis* shells sampled in Camarones South area.

6.3.2.4. Stable isotope composition of Holocene *Ameghinomya antiqua* shells in Bahia Bustamante

Ameghinomya antiqua shells from three Holocene beach ridges outcropping in Bahia Bustamante (Figs. 135-136) were sampled to perform stable isotope studies (Tab.15). All the beach ridges were dated within this project by using the radiocarbon dating method (Tab. 15). Isotopic results were then compared with the oxygen and carbon isotopic composition of modern shells collected from the active beach in the same area. The beach ridge that was assigned the WP138 is, according to data from remote sensing and field data, is the same beach ridge of WP 139, on which was carried out a radiocarbon dating. For this reason, the isotopic results of the shells from the two WP were combined.

Figure 135 – Holocene and modern beach ridges sampled and analyzed in Bahia Bustamante area.

Figure 136 – Sampling of the shells from the beach ridge dated to 5276±47 yr BP.

Holocene shells from WP 256, the beach deposit dated to 4138±41 yr BP have oxygen isotopic composition ranging from 0.43 to 0.88‰ and mean $\delta^{18}O$ value of 0.59±0.20‰ ($\Delta\delta^{18}O$ = 0.46‰), the specimens sampled from WP 144 dated to 4693±59 yr BP show $\delta^{18}O$ values between 0.39 and 0.65‰ with mean $\delta^{18}O$ value of 0.56±0.14‰ and $\Delta\delta^{18}O$ = 0.26‰ (Tab. 15). The $\delta^{18}O$ values of *Ameghinomya antiqua* individuals collected from WP 138-139 beach ridges (5276±47 yr BP uncalibrated) ranges from 0.25 to 0.59‰ and show mean $\delta^{18}O$ value of 0.37±0.11‰ with $\Delta\delta^{18}O$ = 0.34‰ (Tab. 15).

The same specimens show carbon isotope composition values ranging from 0.88 to 1.59 ‰ (mean $\delta^{13}C$ values of 1.36±0.32‰ and $\Delta\delta^{13}C$ = 0.71‰), from 0.69 to 1.38‰ (mean $\delta^{13}C$ values of 1.01±0.35‰ and $\Delta\delta^{13}C$ = 0.69‰) and from 0.36 to 1.01 (mean $\delta^{13}C$ values of 0.70±0.24‰ and $\Delta\delta^{13}C$ = 0.75‰) respectively (Tab. 15).

SAMPLE	^{14}C AGE (uncalibrated)	^{14}C cal BP 2 sigma	δ^{13}C‰	δ^{18}O‰	δ^{13}C‰ (mean	st. dev.	$\Delta\delta^{13}$C‰	δ^{18}O‰ (mean va	st. dev	$\Delta\delta^{18}$O ‰
WP237(1)			**-0.24**	**0.02**	**0.00**	0.28	0.77	**0.22**	0.14	0.47
WP237(2)			**-0.06**	**0.16**						
WP237(3)			**0.41**	**0.27**						
WP237(4)			**-0.36**	**0.23**						
WP237(5)			**-0.21**	**-0.03**						
WP613(1)			**-0.15**	**0.28**						
WP613(2)			**0.35**	**0.27**						
WP613(3)			**-0.22**	**0.23**						
WP 613(4)			**0.24**	**0.44**						
WP 613 (5)			**0.23**	**0.36**						
WP256A(1)	4138 ± 41	4074-4352	**1.58**	**0.72**	**1.36**	0.32	0.71	**0.59**	0.20	0.46
WP256A(2)	4138 ± 41	4074-4352	**1.57**	**0.88**						
WP256A(3)	4138 ± 41	4074-4352	**1.17**	**0.42**						
WP256A(4)	4138 ± 41	4074-4352	**0.88**	**0.43**						
WP256B	4138 ± 41	4074-4352	**1.59**	**0.51**						
WP144(1)	4693 ± 59	4764-5047	**0.95**	**0.65**	**1.01**	0.35	0.69	**0.56**	0.14	0.26
WP144(3)	4693 ± 59	4764-5047	**1.38**	**0.39**						
WP144(4)	4693 ± 59	4764-5047	**0.69**	**0.63**						
WP138(1)	5276 ± 47	5955-6183	**0.95**	**0.59**	**0.70**	0.24	0.75	**0.367**	0.11	0.34
WP138(2)	5276 ± 47	5955-6183	**0.75**	**0.27**						
WP138(3)	5276 ± 47	5955-6183	**0.96**	**0.31**						
WP138(4)	5276 ± 47	5955-6183	**0.74**	**0.34**						
WP139(1)	5276 ± 47	5955-6183	**0.36**	**0.26**						
WP139(2)	5276 ± 47	5955-6183	**0.41**	**0.25**						
WP139(3)	5276 ± 47	5955-6183	**0.58**	**0.38**						
WP139(4)	5276 ± 47	5955-6183	**0.54**	**0.45**						
WP139BIS(2	5276 ± 47	5955-6183	**1.01**	**0.45**						

Table 15 – Carbon and oxygen isotopic composition, mean values, standard deviation and range values of modern and Holocene shells of *Ameghinomya antiqua* from Bahia Bustamante area.

Comparing the Holocene and the modern shell isotopic composition it is possible to observe that the shells sampled from the beach ridge dated to 4138±41 yr BP show the values of the oxygen isotopic composition similar to the values of the modern individuals, while for the specimens from the older Holocene beach ridges the values are slightly more positive (Fig. 137). The carbon isotope composition results, except for two samples, always more positive for Holocene shells than for the modern specimens (Fig. 137).

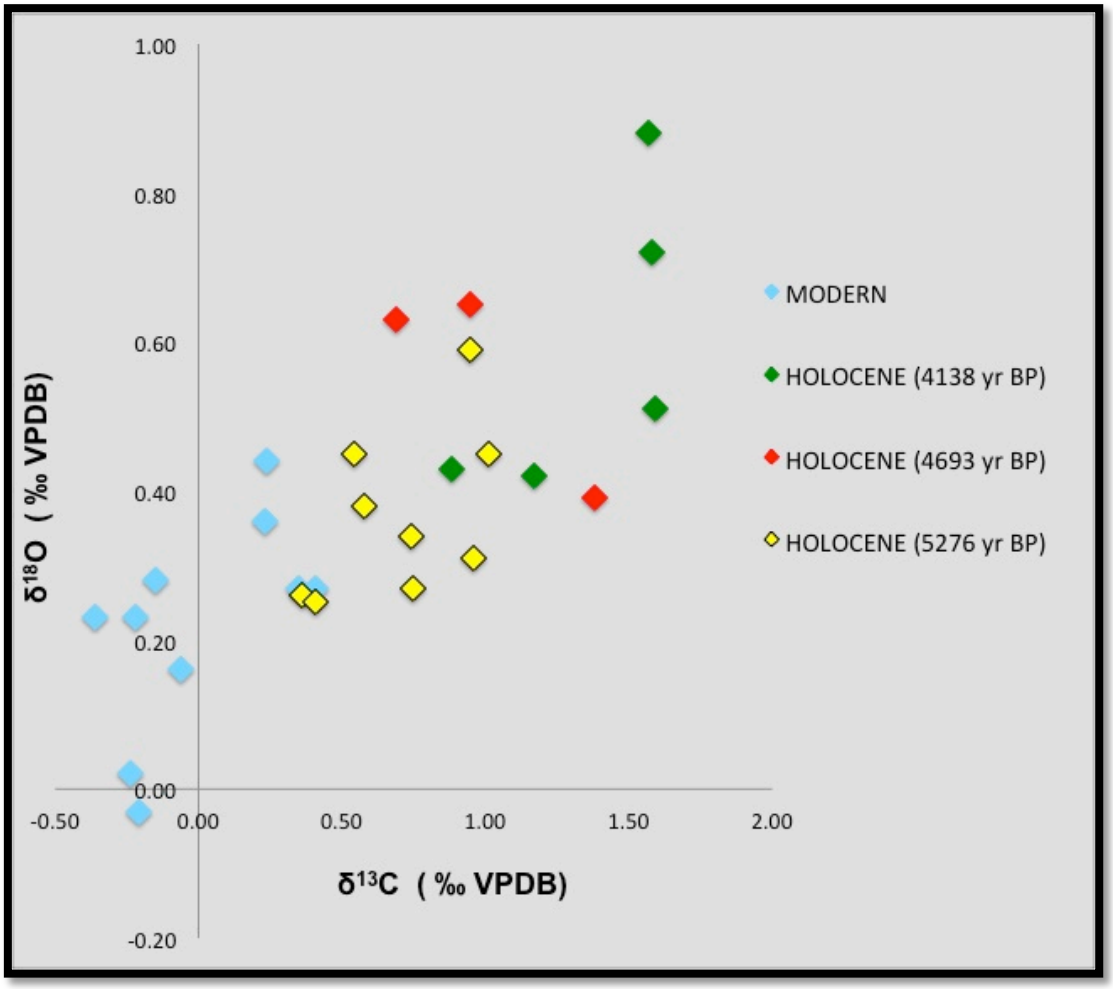

Figure 137 - $\delta^{13}C$ vs $\delta^{18}O$ of Holocene and modern *Ameghinomya antiqua* from Bahia Bustamante area.

Mean values of $\delta^{18}O$ for each layer indicate that all the Holocene shells are slightly ^{18}O-enriched (by maximum 0.40‰) compared to modern specimens (Fig. 138).

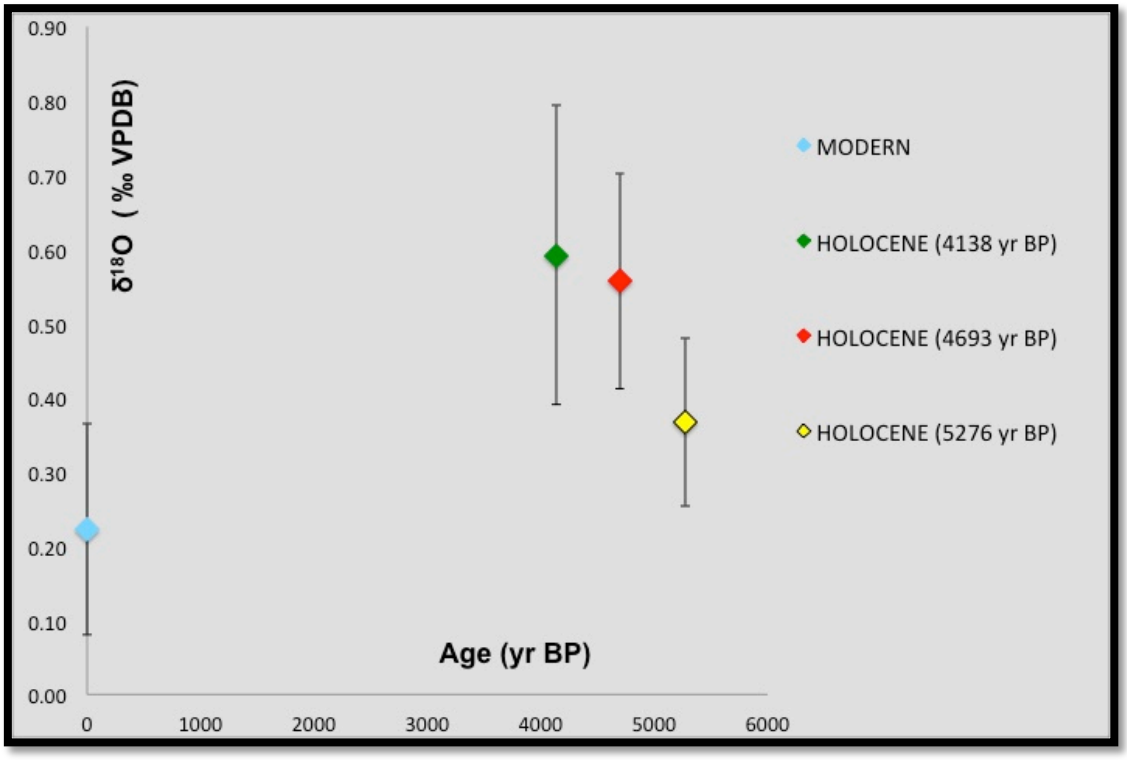

Figure 138 - Oxygen isotope mean values and standard deviation vs age of Holocene and modern *Ameghinomya antiqua* shells sampled in Bahia Bustamante area.

The Holocene shells, furthermore, also show mean $\delta^{13}C$ values more positive than modern samples. Higher value is found for the more recent Holocene beach ridge, while for the two oldest beach ridge the carbon isotopic composition tends to decrease, but remains higher than in specimens of the modern beach (Fig. 139).

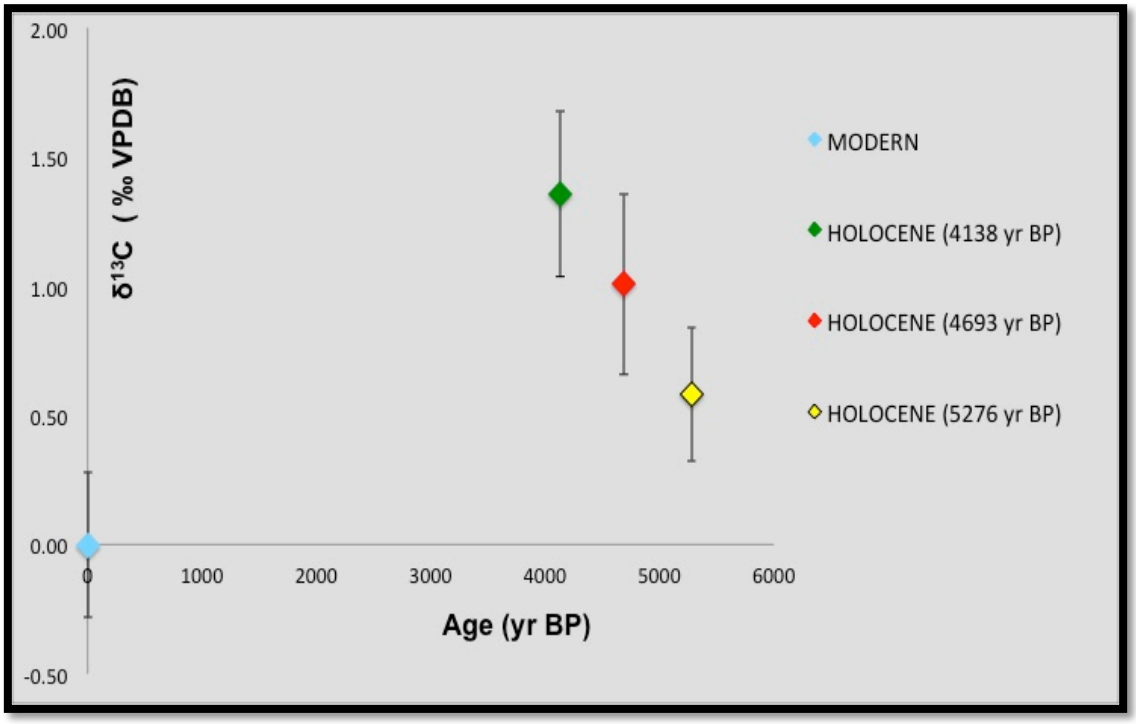

Figure 139 - Carbon isotope mean values and standard deviation vs age of Holocene and modern *Ameghinomya antiqua* shells sampled in Bahia Bustamante area.

6.3.2.5. Stable isotope composition of Holocene *Ameghinomya antiqua* shells in Bahia Solano

In Bahia Solano the stable isotope composition was studied on shells sampled from three Holocene levels (Fig. 140) outcropping along the Cañadon Celeste, a very small river. Two levels were dated with the radiocarbon dating method (Tab. 16).

Figure 140 - Localization of Holocene deposits sampled and analyzed in Bahia Solano.

The shells coming from WP 274A and WP 274C were sampled from an outcrop, whose upper part (WP 275A) was dated to 2133±62 yr BP (Fig. 141). The shells sampled in WP 278 are from a Holocene beach ridge located further upstream. Codignotto (1990) in Bahia Solano, a couple of km from our sampling area, recognized and dated three Holocene systems of littoral successions progressively older going inwards.

Based on the stratigraphy of Codignotto (1990) and on the field work data, it is possible to hypothesize that the beach ridge at WP 278 is older than the beach ridges at WP 272 and WP 274.

Figure 141 – Holocene beach ridges sampled at WP 274 and WP 275.

Holocene shells from WP 272 (n = 6; 1930±24 yr BP), WP 274A (n = 6; younger than 2133±62 yr BP), WP 274C (n = 6; younger than 2133±62 yr BP) and WP 278 (n = 6; undetermined Holocene) show oxygen isotopic values between 0.28 and 0.55‰ for the younger Holocene deposit, between 0.08 and 0.77‰ and between 0.13 and 0.51‰ for the layers younger than 2133±62 yr BP and between 0.37 and 0.75‰ for the older beach ridge (Tab. 16 and Fig. 141). These shells show mean $\delta^{18}O$ values of 0.46±0.10‰ ($\Delta\delta^{18}O$ = 0.27‰), 0.40±0.29‰ ($\Delta\delta^{18}O$ = 0.69‰), 0.34±0.16‰ ($\Delta\delta^{18}O$ = 0.38‰) and 0.50±0.17‰ ($\Delta\delta^{18}O$ = 0.38‰) respectively (Tab. 16).

The same *Ameghinomya antiqua* shells show carbon isotope composition values ranging from 0.50 to 0.86 ‰ (mean $\delta^{13}C$ value of 0.52±0.28‰ and $\Delta\delta^{13}C$ = 0.70‰), from 0.10 to 1.62‰ (mean value of 0.72±0.52‰ and $\Delta\delta^{13}C$ = 1.51‰), from 0.29 to 0.86‰ (mean $\delta^{13}C$ value of 0.53±0.25‰ and $\Delta\delta^{13}C$ = 0.57‰) and from 0.0.64 to 1.26‰ (mean $\delta^{13}C$ value of 0.96±0.26‰ and $\Delta\delta^{13}C$ = 0.62‰) respectively (Tab. 16).

SAMPLE	^{14}C AGE (uncalibrated)	^{14}C cal BP 2 sigma	$\delta^{13}C$‰	$\delta^{18}O$‰	$\delta^{13}C$‰ (mean value)	st. dev.	$\Delta\delta^{13}C$‰	$\delta^{18}O$‰ (mean value)	st. dev.	$\Delta\delta^{18}O$ ‰
WP271(1)	MODERN		**-0.14**	**0.17**	**-0.27**	0.20	0.46	**0.27**	0.06	0.16
WP271(2)	MODERN		**-0.39**	**0.26**						
WP271(3)	MODERN		**-0.38**	**0.32**						
WP271(4)	MODERN		**-0.45**	**0.27**						
WP271(5)	MODERN		**0.01**	**0.33**						
WP272A	1930±24	1394-1548	**0.55**	**0.28**	**0.52**	0.28	0.7	**0.46**	0.10	0.27
WP272B(1)	1930±24	1394-1548	**0.50**	**0.54**						
WP272B(2)	1930±24	1394-1548	**0.16**	**0.52**						
WP272B(3)	1930±24	1394-1548	**0.80**	**0.55**						
wp272B(4)	1930±24	1394-1548	**0.86**	**0.40**						
WP272B(5)	1930±24	1394-1548	**0.28**	**0.49**						
WP274A(1)	<2133±62 upper layer	<1558-1865	**1.62**	**0.08**	**0.72**	0.52	1.51	**0.40**	0.29	0.69
WP274A(2)	<2133±62 upper layer	<1558-1865	**0.37**	**0.61**						
WP274A(3)	<2133±62 upper layer	<1558-1865	**0.10**	**0.54**						
WP274A(4)	<2133±62 upper layer	<1558-1865	**0.78**	**0.77**						
WP274A(5)	<2133±62 upper layer	<1558-1865	**0.82**	**0.10**						
WP274A(6)	<2133±62 upper layer	<1558-1865	**0.62**	**0.30**						
WP274C(1)	<2133±62 lower layer	<1558-1865	**0.45**	**0.13**	**0.53**	0.25	0.57	**0.34**	0.13	0.38
WP274C(2)	<2133±62 lower layer	<1558-1865	**0.30**	**0.27**						
WP274C(3)	<2133±62 lower layer	<1558-1865	**0.48**	**0.51**						
WP274C(4)	<2133±62 lower layer	<1558-1865	**0.86**	**0.40**						
WP274C(5)	<2133±62 lower layer	<1558-1865	**0.29**	**0.39**						
WP274C(6)	<2133±62 lower layer	<1558-1865	**0.82**	**0.35**						
WP278(1)	HOLOCENE		**0.95**	**0.75**	**0.96**	0.26	0.62	**0.50**	0.17	0.38
WP278(2)	HOLOCENE		**0.64**	**0.37**						
WP278(3)	HOLOCENE		**1.00**	**0.40**						
WP278(4)	HOLOCENE		**1.26**	**0.49**						

Table 16 – Carbon and oxygen isotopic composition, mean values, standard deviation and range values of modern and Holocene shells of *Ameghinomya antiqua* from Bahia Solano area.

The stable isotope composition of Holocene shells was compared, as for the other localities, with the isotopic values of modern specimens (Figs. 142-143).

Lacking the age of the beach ridge located more in the interior and even the exact age of beach ridges placed at the WP 274, it was not possible to plot the results of the isotopic composition versus the age. However, it is possible to observe that Holocene shells show more positive values of $\delta^{13}C$ with a large range of values, while the $\delta^{18}O$ values are extremely variable (Fig. 142).

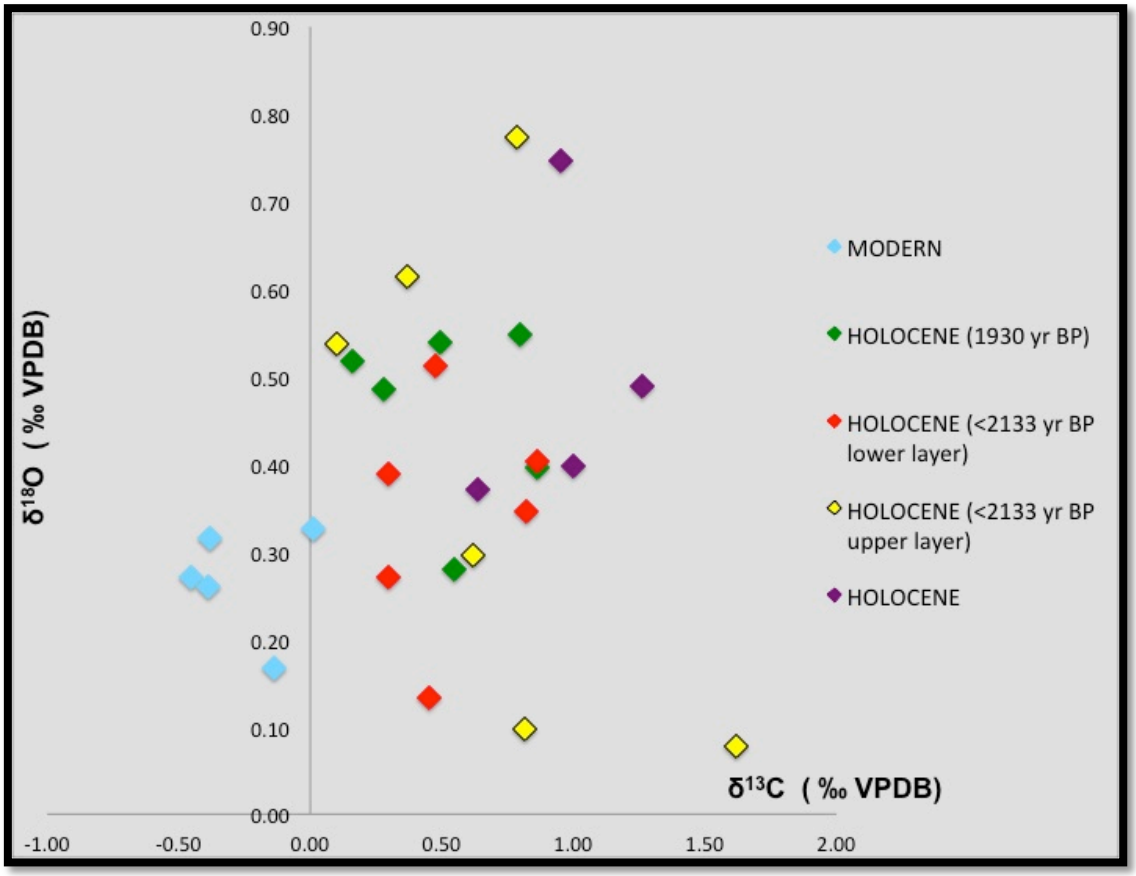

Figure 142 – Oxygen vs carbon isotopic composition of Holocene and modern shells from Bahia Solano beach deposits.

In these samples, in fact, the standard deviation from the mean value, especially for the oxygen, is particularly high and causes the values overlap. For the carbon isotopic composition, however, the average values are decidedly more positive than the mean value of the modern shells, while there are not big differences between the mean values of the Holocene specimens (Fig. 143).

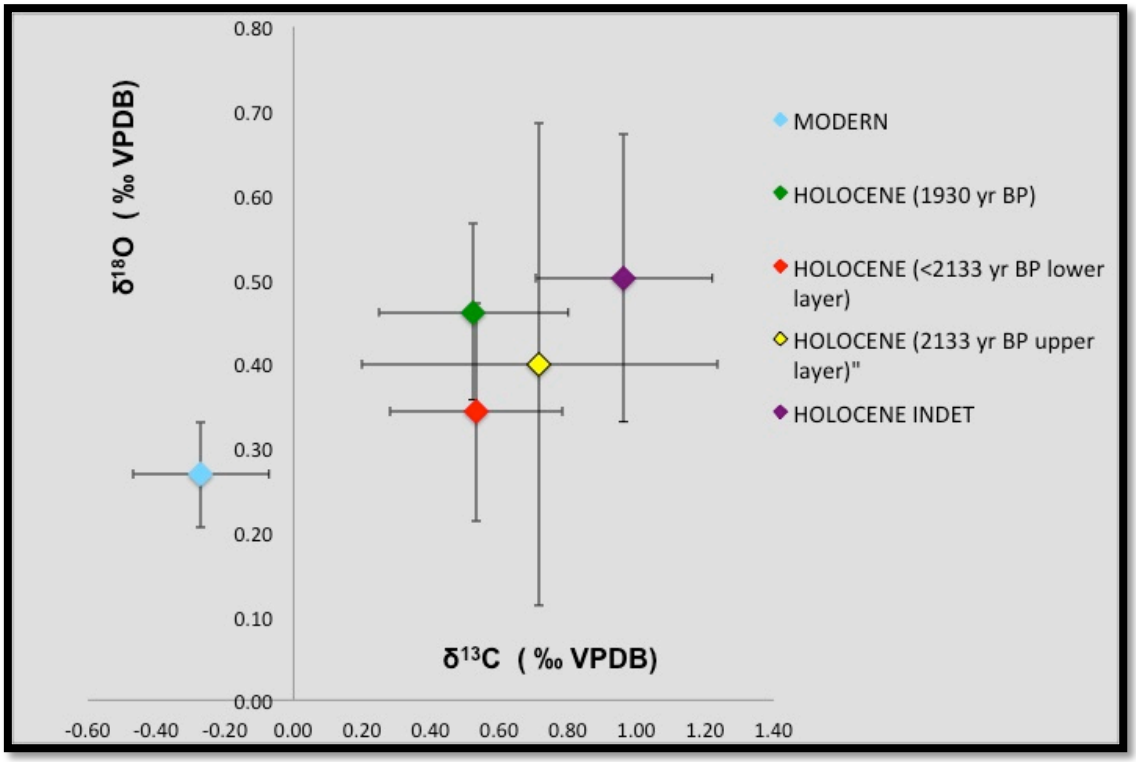

Figure 143 – $\delta^{13}C$ and $\delta^{18}O$ mean values and standard deviation of modern and Holocene shells from Bahia Solano area.

6.3.2.6. Stable isotope composition of Holocene *Ameghinomya antiqua* shells in Caleta Olivia

Stable isotope (carbon and oxygen) analyses were performed on *Ameghinomya antiqua* shells sampled within three Holocene beach ridges located in Caleta Olivia area (Fig. 144). The beach ridge at WP 468A (Fig. 145) was dated with the ^{14}C dating within this project, the radiocarbon ages of the other two beach ridges were obtained from Schellmann and Radtke (2003; 2010).

Figure 144 – Localization of Holocene and modern beach deposits sampled and analyzed.

Figure 145 – The more recent Holocene beach ridge with *A. antiqua* articulated shell.

Holocene *Ameghinomya antiqua* specimens from WP 468A (n = 4; 539±38 yr BP), WP 475B (n = 3; 4074±34 yr BP) and WP 523 (n = 3; 5450±100 yr BP) show $\delta^{18}O$ values ranging from 0.92 to 1.08‰, from 0.66 to 1.34‰ and from 0.43 to 0.85‰ and present mean $\delta^{18}O$ values of 0.99±0.07‰ ($\Delta\delta^{18}O$ = 0.16‰), 0.93±0.36‰ ($\Delta\delta^{18}O$ = 0.68) and 0.85±0.23‰ ($\Delta\delta^{18}O$ = 0.42‰) respectively (Tab. 17).

The same shells have $\delta^{13}C$ values between 0.56 and 1.23‰, between 0.23 and 0.47‰ and between -0.35 and 0.52‰ and show mean $\delta^{13}C$ values of 0.86±0.28‰ ($\Delta\delta^{13}C$ = 0.67‰), 0.32±0.13‰ ($\Delta\delta^{13}C$ = 0.24‰) and 0.11±0.43‰ ($\Delta\delta^{13}C$ = 0.87‰) respectively (Tab. 17).

SAMPLE	^{14}C AGE (uncalibrated)	^{14}C cal BP 2 sigma	$\delta^{13}C$‰	$\delta^{18}O$‰	$\delta^{13}C$‰ (mean value)	st. dev.	$\Delta\delta^{13}C$‰	$\delta^{18}O$‰ (mean value)	st. dev.	$\Delta\delta^{18}O$ ‰
WP473B(1)	MODERN		**0.06**	**0.71**	**0.25**	0.19	0.39	**0.69**	0.14	0.32
WP473B(2)	MODERN		**0.45**	**0.81**						
WP473B(4)	MODERN		**0.37**	**0.75**						
WP 473B(6)	MODERN		**0.12**	**0.49**						
WP468A(1)	539±38	509-564	**0.56**	**1.08**	**0.86**	0.28	0.67	**0.99**	0.07	0.16
WP468A(2)	539±38	509-564	**0.86**	**0.92**						
WP468A(3)	539±38	509-564	**0.80**	**0.99**						
WP468A(4)	539±38	509-564	**1.23**	**0.99**						
WP475B(1)	LIT 4074±34	3983-4226	**0.47**	**1.34**	**0.32**	0.13	0.24	**0.93**	0.36	0.68
WP475B(2)	LIT 4074±34	3983-4226	**0.28**	**0.78**						
WP475B(4)	LIT 4074±34	3983-4226	**0.23**	**0.66**						
WP523(1)	LIT 5450±100	5592-6054	**0.52**	**0.85**	**0.11**	0.43	0.87	**0.85**	0.23	0.42
WP523(2)	LIT 5450±100	5592-6054	**0.15**	**0.48**						
WP523(3)	LIT 5450±100	5592-6054	**-0.35**	**0.43**						

Table 17 – Carbon and oxygen isotopic composition, mean values, standard deviation and range values of modern and Holocene shells of *Ameghinomya antiqua* from Caleta Olivia area.

Comparing the isotopic results of the Holocene shells with the modern individuals it is possible to observe that the shells collected from the beach ridges dated to 4074±34 yr BP and 5450±100 yr BP show similar oxygen and carbon isotopic values with respect to the modern specimens (Figs. 146). The shells from the late

Holocene beach deposit, instead, have slightly more positive values of $\delta^{18}O$ and $\delta^{13}C$ (Fig. 146).

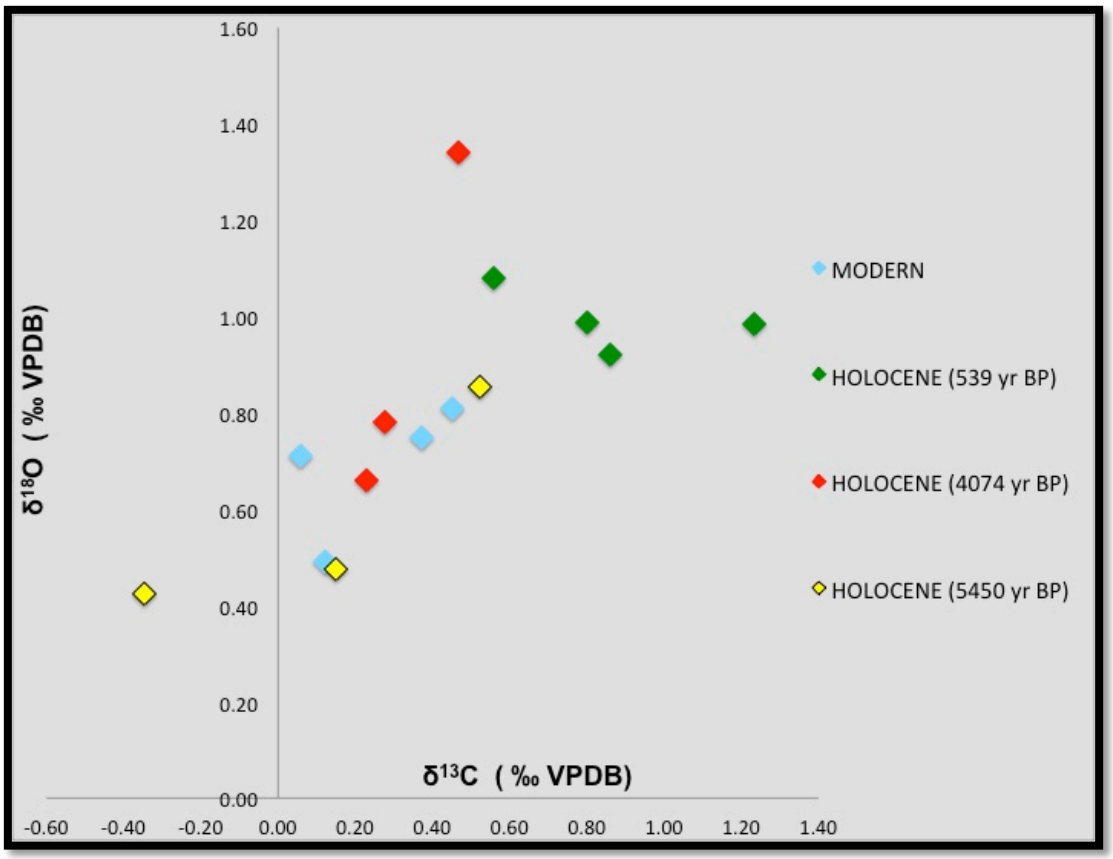

Figure 146 – Oxygen vs carbon isotopic composition of Holocene and modern shells from Caleta Olivia beach deposits.

No significant difference was observed for $\delta^{18}O$ (Fig. 147) and $\delta^{13}C$ (Fig. 148) mean values between modern and middle Holocene specimens. On the other hand, late Holocene shells were slightly ^{18}O- and ^{13}C-enriched.

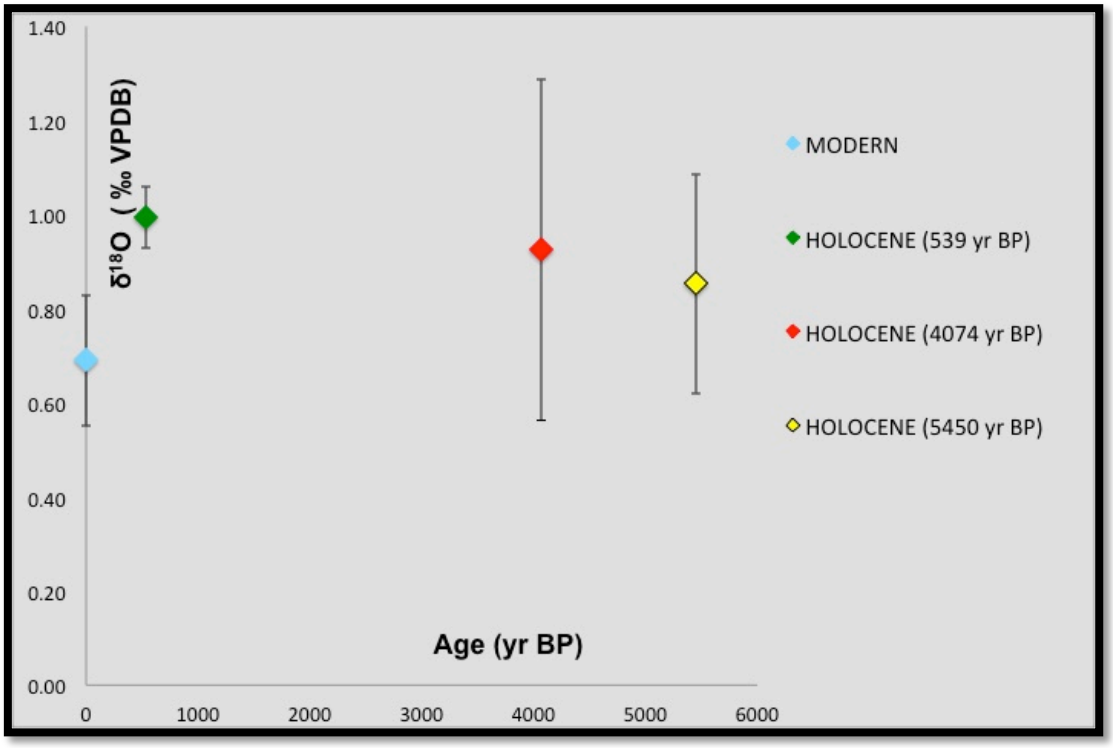

Figure 147 - Oxygen isotope mean values and standard deviation vs age of Holocene and modern *Ameghinomya antiqua* shells sampled in Caleta Olivia area.

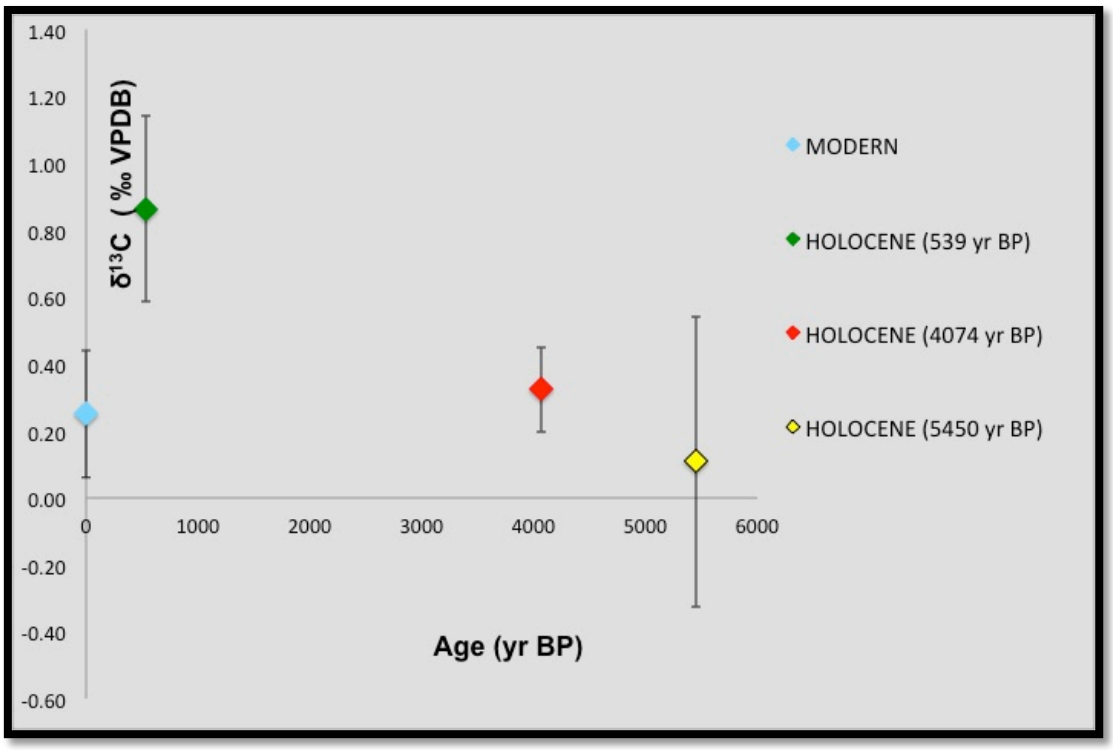

Figure 148 - Carbon isotope mean values and standard deviation vs age of Holocene and modern *Ameghinomya antiqua* shells sampled in Caleta Olivia area.

6.3.3. Stable isotope composition of Pleistocene marine shells

Stable isotope analyses were carried out only on *Ameghinomya antiqua* shells, because the shells belonging to the family Mytilidae are much less abundant in Pleistocene deposits. The shells analyzed come from different beach ridges outcropping in three localities (Camarones, Bahia Bustamante and Caleta Olivia, Fig. 121) and deposited during different Marine Isotope Stages ("MIS"). The oldest beach deposits date back to the MIS 11, the interglacial period between 424,000 and 374,000 years ago (Lisiecki, 2005), while most recent Pleistocene deposits analyzed were dated to MIS 5, the interglacial stage between 130,000 and 71,000 years ago (Lisiecki, 2005).

Where possible U/Th ages performed within this study were used (for all dating see Appendix A). Otherwise ESR dating from the works of Schellmann & Radtke (indicated with the words LIT in tables), or the age deduced from stratigraphic considerations on the field was used.

The oxygen and carbon isotopic composition of Pleistocene *Ameghinomya antiqua* shells were compared with specimens collected from the active beach of the same locality.

6.3.3.1. Stable isotope composition of Pleistocene *Ameghinomya antiqua* shells in Camarones area

In Camarones area five raised beach systems were referred to Holocene, MIS 5, 7, 9 and 11 (Schellmann, 1998; 2007; Schellmann & Radtke, 2003; Zanchetta *et al*., 2012; Pappalardo *et al*., 2013).

In the coastal tract north of Camarones village, in the same area were Holocene Mytilidae shells were collected (see chapter 6.3.2.1.), a beach ridge system dated to MIS 5 was mapped and sampled (Fig. 149). Within this system four beach ridges (two of which was also dated by Schellmann, 1998) were sampled, dated with the U/Th dating method and analyzed for stable isotope composition (Fig. 149 and Tab. 18). The two U/Th ages obtained from the beach ridges dated formerly by Schellmann (1998) are in perfect agreement with ESR dating.

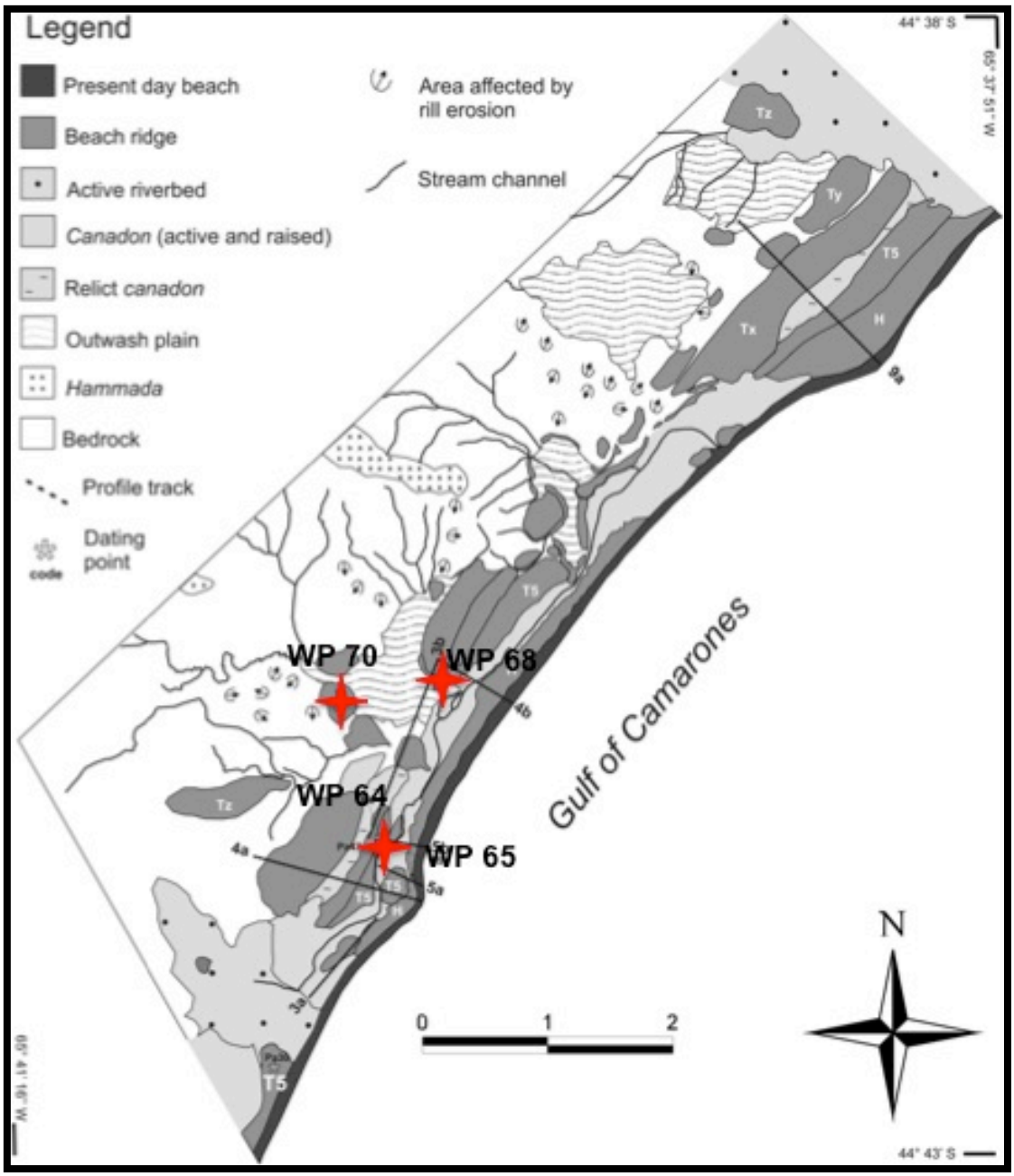

Figure 149 – Sketch map of the coast tract north of Camarones village where *Ameghinomya antiqua* shells were collected from beach ridges dated at MIS 5 (from Pappalardo *et al.,* 2013).

South of the village of Camarones two Pleistocene beach deposits were sampled and dated with the U/Th dating (Fig. 150): the beach ridge sampled at WP92 yielded an U/Th age of 92±0.6 ka BP and the beach ridge at WP97 an age consistent with a deposition during MIS 11 (414±16 ka BP).

These beach deposits were dated with ESR dating method by Schellmann (1998) at MIS 7 and MIS 9 respectively.

However, since the section at WP 92, from which specimens of *A. antiqua* were

sampled for dating and for the isotopic analysis, is constituted by two stratigraphic units separated by an unconformity and since from the Schellmann work is not clear in which unit the shells were sampled, in this thesis our U/Th dating was used.

Figure 150 – Sampling locations of Pleistocene beach ridges south of Camarones village.

Ameghinomya antiqua shells sampled from beach ridges outcropping in the northern sector of Camarones show oxygen isotopic values ranging from 0.22 to 0.70‰ for the beach deposit dated to 121000±900 yr BP, with mean $\delta^{18}O$ value of 0.40± 0.16‰ and $\Delta\delta^{18}O$ = 0.32‰, from 0.20 to 0.74‰ (mean $\delta^{18}O$ value of 0.50±0.18‰ and $\Delta\delta^{18}O$ = 0.54‰) for the beach ridge dating back to 127000±1200 yr BP, from 0.26 to 0.91‰ (mean $\delta^{18}O$ value of 0.57± 0.27‰ and $\Delta\delta^{18}O$ = 0.65‰) for the shells sampled from the beach ridge with an age of 130±2.5 ka BP and $\delta^{18}O$ values between 0.37 and 0.70‰, with mean $\delta^{18}O$ value of 0.53± 0.13‰ and $\Delta\delta^{18}O$ = 0.33‰ for the beach deposit dated to 131±1.1 ka BP (Tab. 18 and Fig. 151).

The same *A. antiqua* specimens have $\delta^{13}C$ values between 0.65 and 1.01‰, between 0.19 and 1.61‰, between -0.05 and 0.83‰ and between 0.19 and 0.93‰ and show mean $\delta^{13}C$ values of 0.87±0.12‰ ($\Delta\delta^{13}C$ = 0.46‰), 0.77±0.51‰ ($\Delta\delta^{13}C$ = 1.42‰), 0.29±0.30‰ ($\Delta\delta^{13}C$ = 0.88‰) and 0.58±0.36‰ ($\Delta\delta^{13}C$ = 0.74‰) respectively (Tab. 18 and Fig. 151).

The shells from the two Pleistocene beach ridges deposited south to the village of Camarones show narrower $\delta^{18}O$ values ranging from 0.51 to 0.71‰ with mean oxygen isotopic value of 0.60±0.07‰ and $\Delta\delta^{18}O$ = 0.2‰ for the layer dated at MIS 5 and from 0.18 to 0.37‰ (mean $\delta^{18}O$ value of 0.28± 0.07‰ and $\Delta\delta^{18}O$ = 0.19‰) for the beach ridge deposited during the MIS 11 (Tab. 18 and Fig. 151). Carbon isotopic values for the same shells ranges from 0.55 to 1.01‰ (mean $\delta^{13}C$ values of 0.83±0.28‰ and $\Delta\delta^{13}C$ = 0.57‰) and from 0.32 to 1.14‰, with mean $\delta^{13}C$ values of 0.65±0.32‰ ($\Delta\delta^{13}C$ = 0.82‰).

SAMPLE	AGE (yr BP)	$\delta^{13}C$‰	$\delta^{18}O$‰	$\delta^{13}C$‰ (mean value)	st. dev.	$\Delta\delta^{13}C$‰	$\delta^{18}O$‰ (mean value)	st. dev.	$\Delta\delta^{18}O$ ‰
WP60BBIS(1)	modern beach	**0.11**	**0.07**	**0.32**	0.38	1.32	**0.32**	0.10	0.35
WP60BBIS(2)	modern beach	**0.49**	**0.40**						
WP623BIS(1)	modern beach	**0.07**	**0.42**						
WP623BIS(3)	modern beach	**0.36**	**0.33**						
WP623BIS(4)	modern beach	**0.30**	**0.23**						
WP623BIS(5)	modern beach	**-0.09**	**0.39**						
WP623BIS(6)	modern beach	**-0.43**	**0.37**						
WP95(2)	modern beach	**0.59**	**0.38**						
WP95(3)	modern beach	**0.62**	**0.30**						
WP95(4)	modern beach	**0.89**	**0.35**						
WP110(2)	modern beach	**0.65**	**0.25**						
WP64A(2)	121000±900	**0.87**	**0.22**	**0.87**	0.12	0.46	**0.40**	0.16	**0.32**
WP64A(3)	121000±900	**0.91**	**0.31**						
WP64A(4)	121000±900	**0.75**	**0.44**						
WP64A(7)	121000±900	**1.01**	**0.54**						
WP64B(2)	121000±900	**0.82**	**0.37**						
WP64B(3)	121000±900	**0.65**	**0.28**						
WP64B(4)	121000±900	**0.96**	**0.30**						
WP64B(7)	121000±900	**0.97**	**0.70**						
WP70A(1)	127000±1200	**0.19**	**0.20**	**0.77**	0.51	1.42	**0.50**	0.18	0.54
WP70A(2)	127000±1200	**1.12**	**0.39**						
WP70A(3)	127000±1200	**0.25**	**0.44**						
WP70A(4)	127000±1200	**0.64**	**0.43**						
WP70A(5)	127000±1200	**0.54**	**0.59**						
WP70A(6)	127000±1200	**1.02**	**0.74**						
WP70B	127000±1200	**1.61**	**0.67**						
WP65(1)	130000±2500	**0.06**	**0.40**	**0.29**	0.30	0.88	**0.57**	0.27	0.65
WP65(2)	130000±2500	**-0.05**	**0.26**						
WP65(3)	130000±2500	**0.83**	**0.47**						
WP65(6)	130000±2500	**0.28**	**0.91**						
WP65(7)	130000±2500	**0.30**	**0.88**						
WP65(8)	130000±2500	**0.34**	**0.46**						
WP68(1)	131000±1100	**0.23**	**0.70**	**0.58**	0.359	0.74	**0.53**	0.13	0.33
WP68(2)	131000±1100	**0.85**	**0.63**						
WP68(3)	131000±1100	**0.19**	**0.52**						
WP68(4)	131000±1100	**0.33**	**0.37**						
WP 68(5)	131000±1100	**0.93**	**0.51**						
WP 68(6)	131000±1100	**0.92**	**0.43**						
WP92A(1)	92000±600	**1.10**	**0.61**	**0.83**	0.28	0.57	**0.60**	0.07	0.2
WP92A(2)	92000±600	**0.55**	**0.51**						
WP92A(3)	92000±600	**0.87**	**0.62**						
WP92A(4)	92000±600	**0.53**	**0.57**						
WP92A(5)	92000±600	**1.10**	**0.71**						
WP97(1)	414000±16000	**0.43**	**0.23**	**0.65**	0.32	0.82	**0.28**	0.07	0.19
WP97(2)	414000±16000	**0.57**	**0.18**						
WP97(3)	414000±16000	**1.14**	**0.29**						
WP97(4)	414000±16000	**0.76**	**0.37**						
WP97(5)	414000±16000	**0.32**	**0.30**						

Table 18 – Carbon and oxygen isotopic composition, mean values, standard deviation and range values of modern and Pleistocene shells of *Ameghinomya antiqua* from Camarones area.

The stable isotope composition of Pleistocene shells is similar to composition of modern specimens for both oxygen and carbon values, though some individuals sampled from beach ridges dated to MIS 5 show slightly more positive values of $\delta^{18}O$ (Fig. 151).

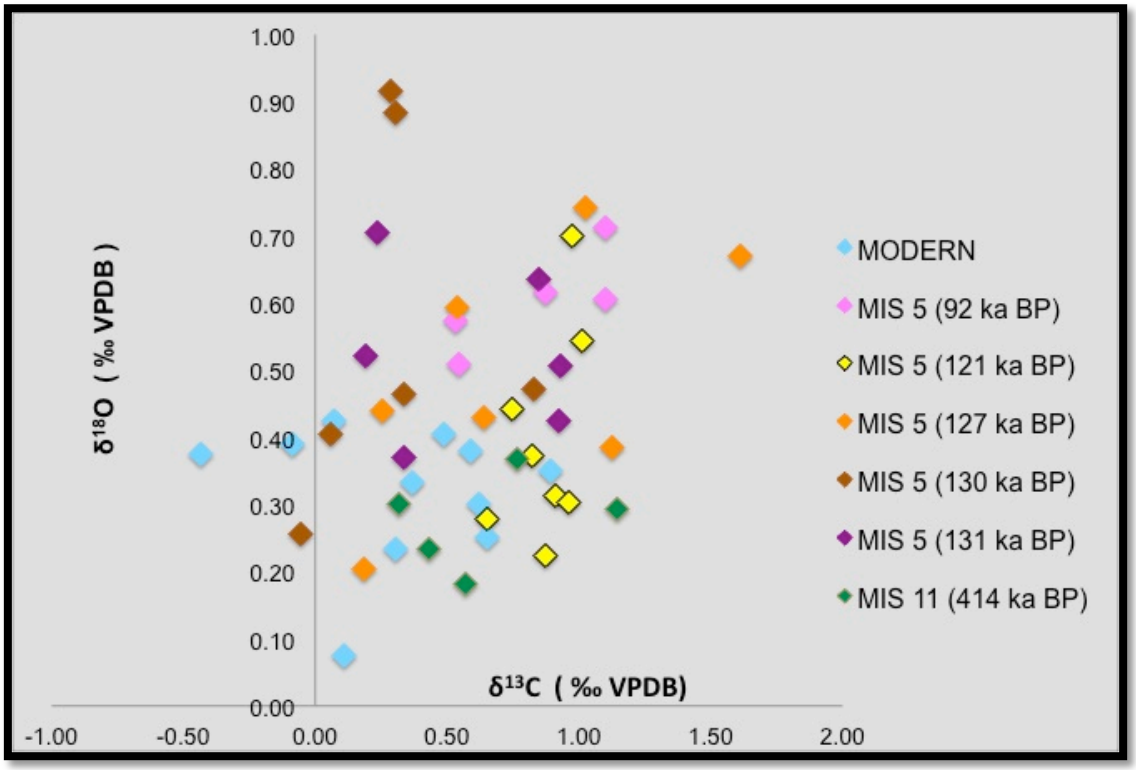

Figure 151 – Oxygen and carbon composition of *Ameghinomya antiqua* shells sampled from Pleistocene and modern beach ridges in Camarones area.

Comparing the $\delta^{18}O$ mean values of Pleistocene specimens with modern ones it is possible to observe that Pleistocene *Ameghinomya antiqua* shells have more positive values, but the high standard deviations from the mean values make that the values overlap (Fig. 152). The specimens from the beach deposit with an U/Th age of 92±0.6 ka BP show higher $\delta^{18}O$ mean value than modern shells. The shells dated at MIS 11 and the modern individuals have very similar oxygen isotopic mean values.

Similar results were also obtained for the $\delta^{13}C$ mean values: also in this case mean values of the Pleistocene shells are slightly higher than modern ones (Fig. 153).

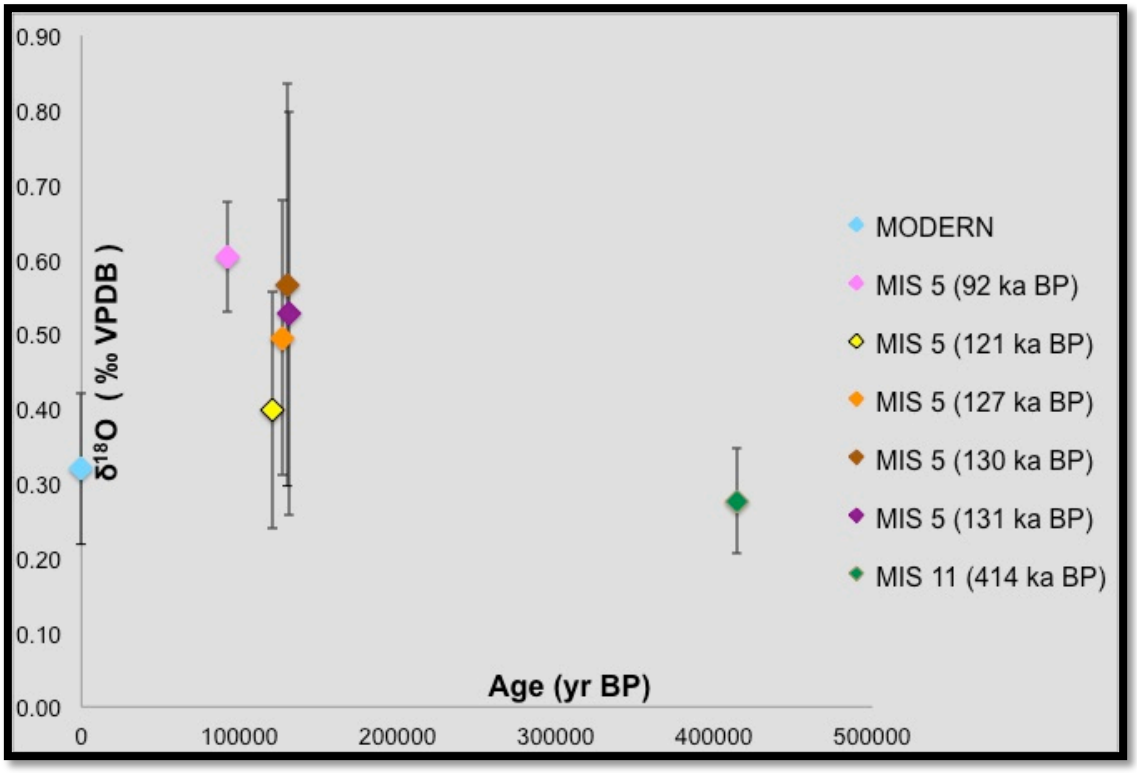

Figure 152 - Oxygen isotope mean values and standard deviations vs age of Pleistocene and modern *Ameghinomya antiqua* shells sampled in Camarones area.

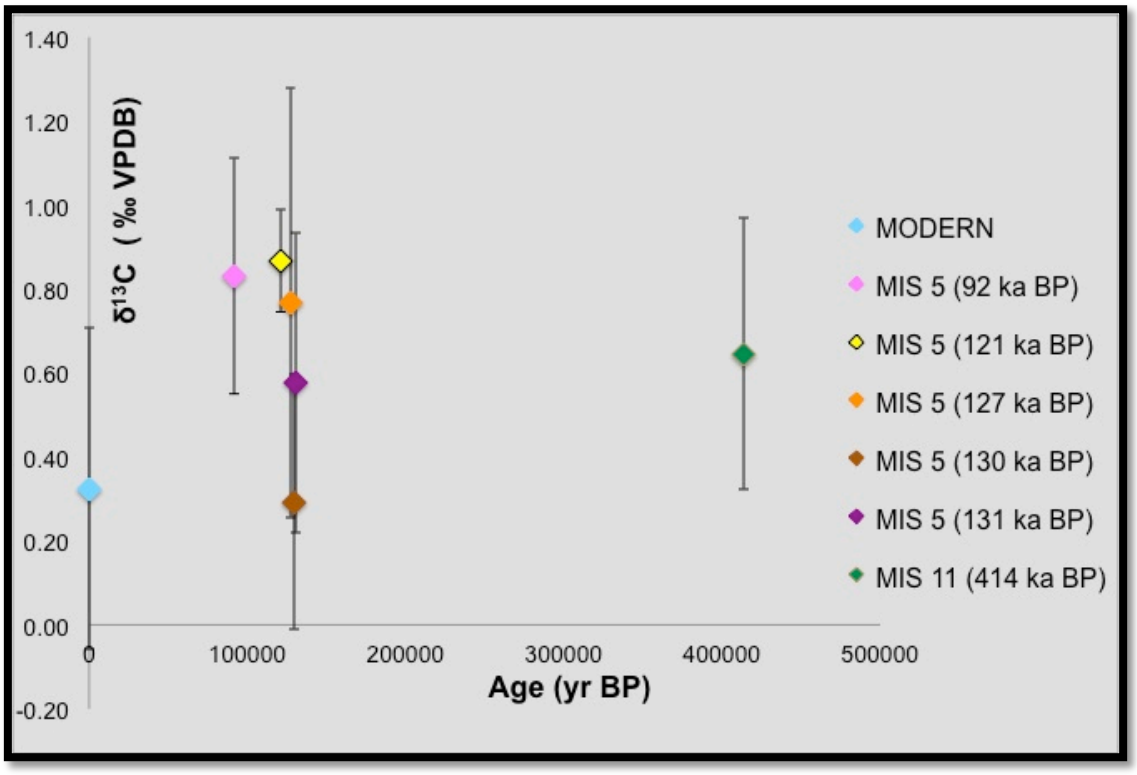

Figure 153 - Carbon isotope mean values and standard deviations vs age of Pleistocene and modern *Ameghinomya antiqua* shells sampled in Camarones area.

6.3.3.2. Stable isotope composition of Pleistocene *Ameghinomya antiqua* shells in Bahia Bustamante area

In Bahia Bustamante area *Ameghinomya antiqua* shells were collected from several Pleistocene beach deposits (Fig. 154 and Tab. 19). The assignment of the various beach ridges mapped and sampled at different Marine Isotope Stages was carried out through field survey (Isola *et al.,* 2011) confirming the stratigraphy inferred from the work of Schellmann (1998, 2007) and Schellmann & Radtke (2000, 2003). On the basis of these assumptions shells used for isotopic analysis come from beach deposits attributed to the MIS 5, MIS 7 and MIS 9 (Fig. 154 and Tab. 19). Two U/Th dating were performed on *Ameghinomya antiqua* shells taken by two beach deposits dated also by Schellmann (1998) with the ESR method. The first U/Th dating, yielding an age of 89±0.9 ka BP, is in agreement with Schellmann (1998) dating, the second dating yielded an age of 82±0.5 ka BP, attributing to MIS 5 a beach ridge that according to the dating of Schellmann (1998) and according to our field observations would be deposited during the MIS 7. For this reason, the second dating carried out within this project was rejected and the deposit was attributed to MIS 7.

Schellmann (1998) identifies in this area different levels (“terraces”) of beach ridges within the various MIS (called T1, T2, T3). For the area of Bahia Bustamante in this thesis the same classification is followed (Fig. 154 and Tab. 19). The beach ridges dated at MIS 5 from which the shells were removed for the analysis belong to two different levels, here called T1 and T3. On the contrary the shells sampled from MIS 7 and MIS 9 beach deposits come from the same level.

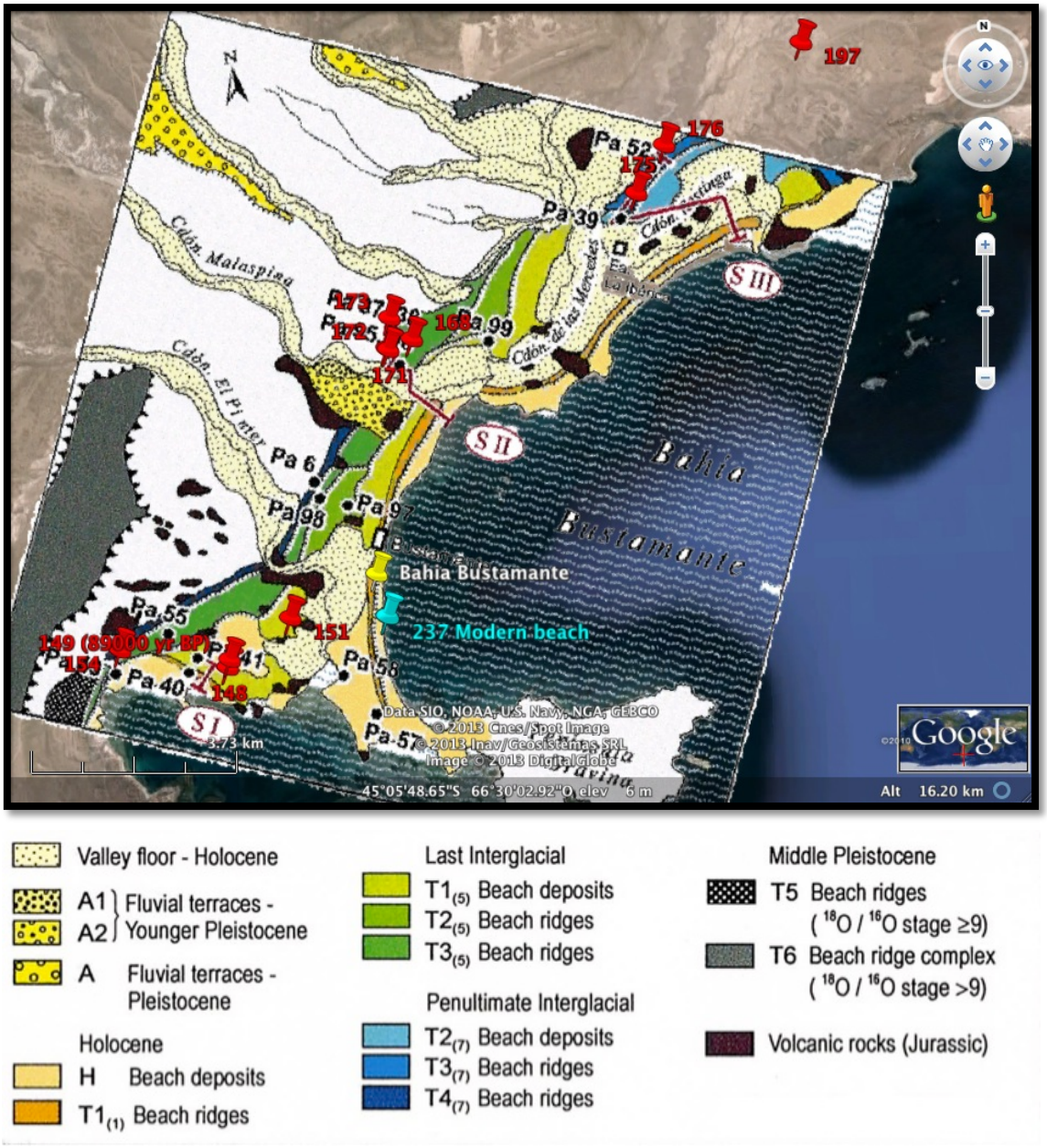

Figure 154 – Distribution of marine beach deposits at Bahia Bustamante. The points in red represent the Pleistocene beach ridges sampled for the analyses (modified from Schellmann & Radtke, 2000).

Shells collected from Pleistocene beach ridges deposited in Bahia Bustamante area show oxygen isotopic values ranging from 0.08 to 0.58‰ and from 0.11 to 0.63‰ for the beach deposit attributed to MIS 5, with mean $\delta^{18}O$ value of 0.34± 0.13‰ and $\Delta\delta^{18}O$ = 0.5‰ and 0.34± 0.13‰ and $\Delta\delta^{18}O$ = 0.52‰ respectively, from -0.19 to 0.42‰ (mean $\delta^{18}O$ value of 0.15±0.23‰ and $\Delta\delta^{18}O$ = 0.61‰) for the beach ridges deposited during MIS 7 and from 0.18 to 0.24‰ (mean $\delta^{18}O$ value of 0.21± 0.04‰ and $\Delta\delta^{18}O$ = 0.06‰) for the shells sampled from the MIS 9 beach ridge (Tab. 19 and Fig. 155).

The same *A. antiqua* specimens have $\delta^{13}C$ values between -0.08 and 1.52‰, between -0.54 and 1.02‰, between -0.55 and 1.00‰ and between 0.22 and 0.72‰ and show mean $\delta^{13}C$ values of 0.82±0.45‰ ($\Delta\delta^{13}C$ = 1.6‰), 0.36±0.47‰ ($\Delta\delta^{13}C$ = 1.56‰), 0.22±0.49‰ ($\Delta\delta^{13}C$ = 1.55‰) and 0.47±0.36‰ ($\Delta\delta^{13}C$ = 0.5‰) respectively (Tab. 19 and Fig. 155).

SAMPLE	AGE (yr BP)	$\delta^{13}C$‰	$\delta^{18}O$‰	$\delta^{13}C$‰ (mean value)	st. dev.	$\Delta\delta^{13}C$‰	$\delta^{18}O$‰ (mean value)	st. dev.	$\Delta\delta^{18}O$ ‰
WP237(1)	modern beach	**-0.24**	**0.02**	**0.00**	0.28	0.77	**0.22**	0.14	0.47
WP237(2)	modern beach	**-0.06**	**0.16**						
WP237(3)	modern beach	**0.41**	**0.27**						
WP237(4)	modern beach	**-0.36**	**0.23**						
WP237(5)	modern beach	**-0.21**	**-0.03**						
WP613(1)	modern beach	**-0.15**	**0.28**						
WP613(2)	modern beach	**0.35**	**0.27**						
WP613(3)	modern beach	**-0.22**	**0.23**						
WP 613(4)	modern beach	**0.24**	**0.44**						
WP 613 (5)	modern beach	**0.23**	**0.36**						
WP149(1)	T1 MIS 5 89000 ± 800	**0.84**	**0.29**	**0.82**	0.45	1.6	**0.34**	0.13	0.5
WP149(2)	T1 MIS 5 89000 ± 800	**0.01**	**0.27**						
WP149(3)	T1 MIS 5 89000 ± 800	**1.17**	**0.37**						
WP149(5)	T1 MIS 5 89000 ± 800	**1.13**	**0.36**						
WP149(6)	T1 MIS 5 89000 ± 800	**0.98**	**0.27**						
WP149(7)	T1 MIS 5 89000 ± 800	**1.52**	**0.35**						
WP148(1)	T1 MIS 5	**0.50**	**0.31**						
WP148(2)	T1 MIS 5	**1.22**	**0.08**						
WP148(3)	T1 MIS 5	**1.08**	**0.56**						
WP148(4)	T1 MIS 5	**0.51**	**0.29**						
WP151(1)	T1 MIS 5	**1.22**	**0.37**						
WP151(2)	T1 MIS 5	**0.65**	**0.33**						
WP151(3)	T1 MIS 5	**0.62**	**0.48**						
WP151(4)	T1 MIS 5	**0.87**	**0.22**						
WP151(5)	T1 MIS 5	**-0.08**	**0.58**						
WP154A(1)	T3 MIS 5	**0.06**	**0.33**	**0.36**	0.47	1.56	**0.36**	0.13	0.52
WP154A(2)	T3 MIS 5	**0.91**	**0.47**						
WP154B(1)	T3 MIS 5	**-0.29**	**0.34**						
WP154B(2)	T3 MIS 5	**0.05**	**0.26**						
WP154B(3)	T3 MIS 5	**-0.28**	**0.33**						
WP154B(4)	T3 MIS 5	**-0.54**	**0.11**						
WP168(1)	T3 MIS 5	**0.40**	**0.31**						
WP168(2)	T3 MIS 5	**-0.09**	**0.25**						
WP168(3)	T3 MIS 5	**0.74**	**0.19**						
WP168(4)	T3 MIS 5	**1.02**	**0.36**						
WP171A	T3 MIS 5	**0.61**	**0.63**						
WP172(1)	T3 MIS 5	**0.56**	**0.53**						
WP172(2)	T3 MIS 5	**0.44**	**0.38**						
WP172(3)	T3 MIS 5	**0.97**	**0.59**						
WP172(4)	T3 MIS 5	**0.51**	**0.29**						
WP172(5)	T3 MIS 5	**0.55**	**0.42**						
WP173A(1)	T3 MIS 5	**0.05**	**0.26**						
WP173A(2)	T3 MIS 5	**0.89**	**0.40**						
WP175A(1)	MIS7	**0.34**	**0.15**	**0.22**	0.49	1.55	**0.15**	0.23	0.61
WP175A(2)	MIS7	**0.52**	**0.34**						
WP175A(3)	MIS7	**0.55**	**0.29**						
WP175A(5)	MIS7	**1.00**	**0.27**						
WP176BIS(1)	MIS7	**0.59**	**0.42**						
WP176BIS(2)	MIS7	**-0.17**	**-0.01**						
WP176BIS(3)	MIS7	**-0.55**	**-0.19**						
WP176BIS(4)	MIS7	**0.37**	**0.41**						
WP176BIS(5)	MIS7	**-0.02**	**-0.02**						
WP176BIS(6)	MIS7	**-0.39**	**-0.13**						
WP197(1)	MIS 9	**0.22**	**0.18**	**0.47**	0.36	0.5	**0.21**	0.04	0.06
WP197(2)	MIS 9	**0.72**	**0.24**						

Table 19 – Carbon and oxygen isotopic composition, mean values, standard deviation and range values of modern and Pleistocene shells of *Ameghinomya antiqua* from Bahia Bustamante area.

Pleistocene shells collected from different beach deposits attributed to MIS 5 show similar oxygen isotope composition, while some specimens coming from the MIS 5 Terrace 1 have highest values of $\delta^{13}C$ (Fig. 155). Some samples from beach ridges dated at MIS 7 show negative values of both oxygen and carbon. The *Ameghinomya antiqua* individuals collected from the oldest beach ridge, attributed to MIS 9, have oxygen isotopic values similar to shells collected on the active beach (Fig. 155).

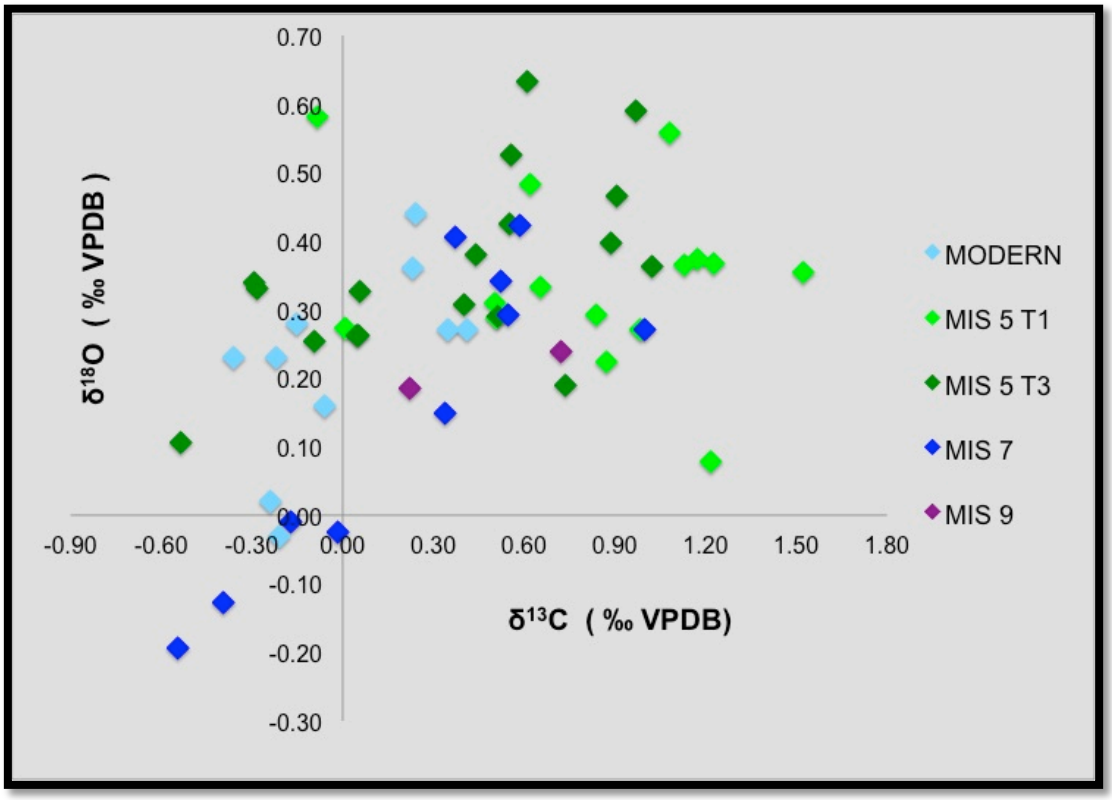

Figure 155 – Oxygen vs carbon isotopic composition of Pleistocene and modern *Ameghinomya antiqua* shells from Bahia Bustamante area.

Comparing the $\delta^{18}O$ mean values of Pleistocene and modern shells it is possible to observe that the specimens sampled from beach deposits dated at MIS 5 show oxygen mean values slightly higher than modern and older Pleistocene shells, which instead are quite similar. However, standard deviations from mean values do not allow differentiating them (Fig. 156). All Pleistocene shells $\delta^{13}C$ mean values are more positive than the modern shell mean value, but even in this case the high standard deviations from mean values make that the values overlap (Fig. 157).

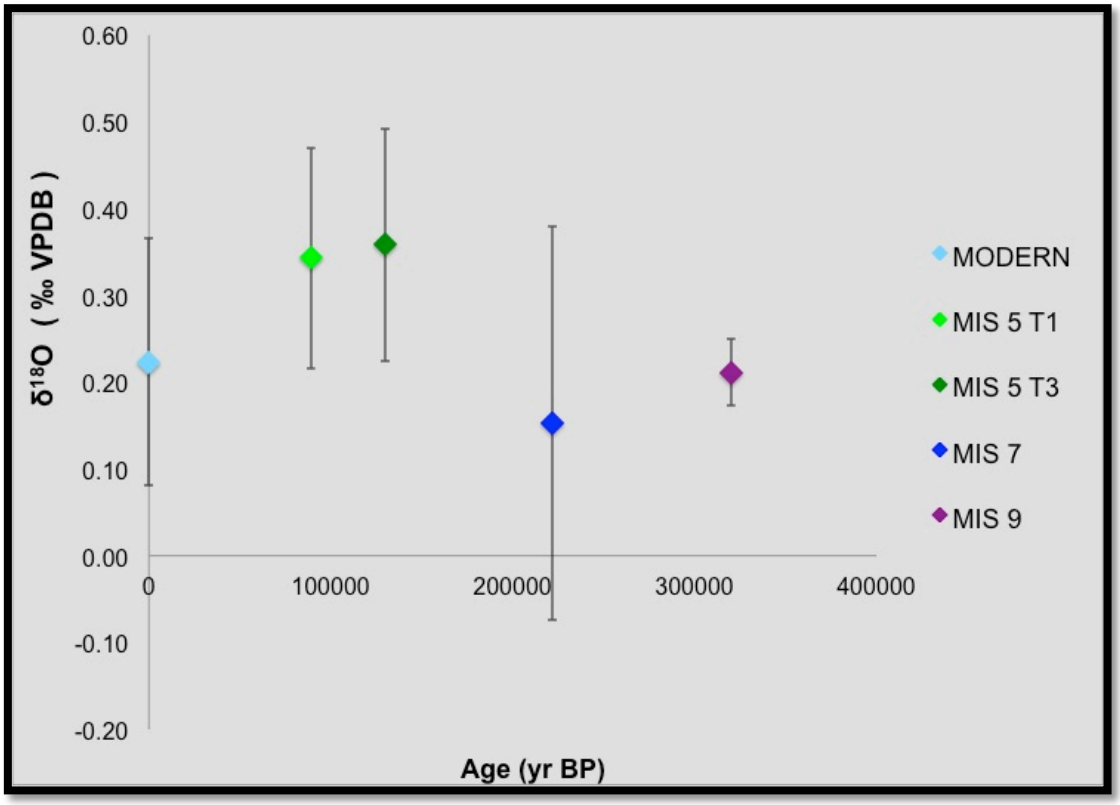

Figure 156 - Oxygen isotope mean values and standard deviations vs age have Pleistocene and modern *Ameghinomya antiqua* shells sampled in Bahia Bustamante area.

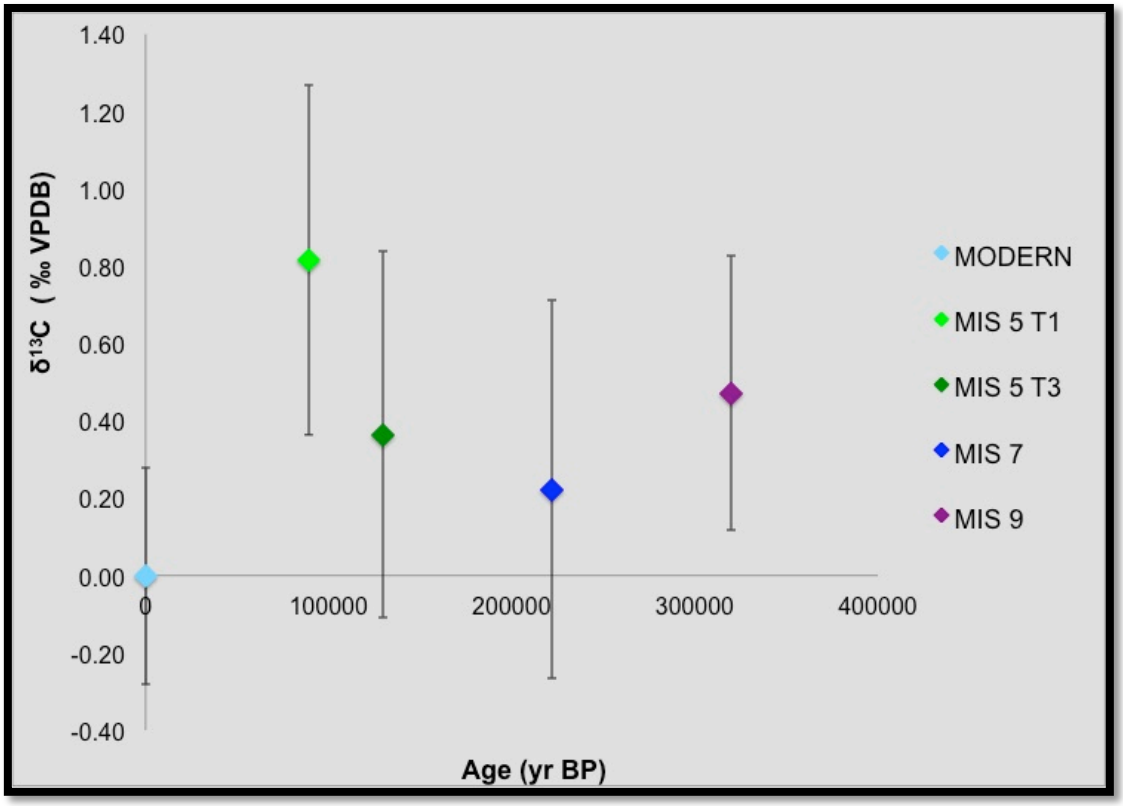

Figure 157 - Carbon isotope mean values and standard deviations vs age of Pleistocene and modern *Ameghinomya antiqua* shells sampled in Bahia Bustamante area.

6.3.3.3. Stable isotope composition of Pleistocene *Ameghinomya antiqua* shells in Caleta Olivia area

In Caleta Olivia area *Ameghinomya antiqua* shells were collected from Pleistocene beach deposits (Fig. 158) whose attribution to the different Marine Isotope Stages was established through field observations, which confirmed or not the previous works in the area (Schellmann, 1998; 2007; Schellmann & Radtke 2000; 2003). On the basis of these assumptions shells used for isotopic analysis come from beach deposits attributed to the MIS 5 (Fig. 159), MIS 7 and MIS 9 (Fig. 160) (Tab. 20).

Figure 158– Distribution of Pleistocene beach deposits at Caleta Olivia sampled for the stable isotope analysis.

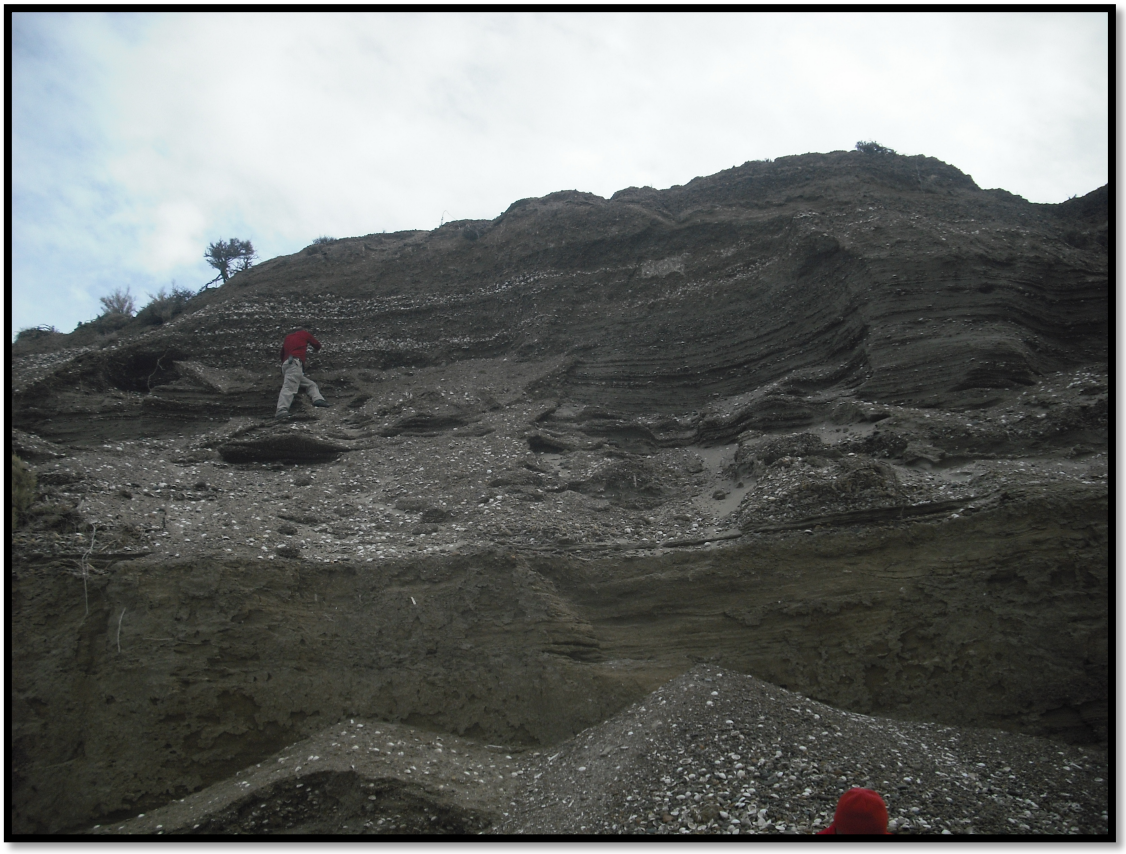

Figure 159 – Pleistocene beach ridge attributed to Marine Isotope Stage 5.

Figure 160 – Ameghinomya antiqua shells in a Pleistocene beach deposit attributed to Marine Isotope Stage 9.

Ameghinomya antiqua specimens sampled from Pleistocene beach deposits outcropping in Caleta Olivia area show oxygen isotopic composition between 0.32 and 0.77‰ (mean value of 0.59±0.12‰ and $\Delta\delta^{18}O$ = 0.45‰) for the beach ridges attributed to MIS 5, from 0.25 and 1.03‰, with mean $\delta^{18}O$ value of 0.72±0.32‰ and $\Delta\delta^{18}O$ = 0.78‰) for the beach ridges deposited during MIS 7 and between 0.34 and 1.11‰ (mean $\delta^{18}O$ value of 0.67± 0.21‰ and $\Delta\delta^{18}O$ = 0.79‰) for the shells sampled from the MIS 9 beach ridge (Tab. 20 and Fig. 160). The same shells have $\delta^{13}C$ values ranging from -0.57 and 0.84‰, from -0.69 to 0.40‰ and from -0.88 to 1.01‰ and show mean $\delta^{13}C$ values of 0.07±0.39‰ ($\Delta\delta^{13}C$ = 1.06‰), 0.02±0.38‰ ($\Delta\delta^{13}C$ = 1.09‰) and 0.24±0.48‰ ($\Delta\delta^{13}C$ = 1.89‰) respectively (Tab. 20 and Fig. 161).

SAMPLE	AGE (	$\delta^{13}C$‰	$\delta^{18}O$‰	$\delta^{13}C$‰ (mean value)	st. dev.	$\Delta\delta^{13}C$‰	$\delta^{18}O$‰ (mean value)	st. dev.	$\Delta\delta^{18}O$ ‰
WP473B(1)		**0.06**	**0.71**	**0.25**	0.19	0.39	**0.69**	0.14	0.32
WP473B(2)		**0.45**	**0.81**						
WP473B(4)		**0.37**	**0.75**						
WP 473B(6)		**0.12**	**0.49**						
WP446(1)	MIS 5	**0.30**	**0.58**	**0.07**	0.39	1.06	**0.59**	0.12	0.45
WP446(2)	MIS 5	**-0.19**	**0.57**						
WP447B(1)	MIS 5	**-0.13**	**0.61**						
WP447B(2)	MIS 5	**-0.57**	**0.70**						
WP447B(3)	MIS 5	**-0.08**	**0.54**						
WP447B(4)	MIS 5	**-0.22**	**0.53**						
WP455(1)	MIS 5	**0.84**	**0.32**						
WP455(2)	MIS 5	**0.19**	**0.77**						
WP455(4)	MIS 5	**0.60**	**0.75**						
WP455(5)	MIS 5	**0.23**	**0.63**						
WP455(6)	MIS 5	**-0.18**	**0.55**						
WP455(7)	MIS 5	**0.10**	**0.54**						
WP447C(1)	MIS 7	**0.00**	**0.47**	**0.02**	0.38	1.09	**0.72**	0.32	0.78
WP447C(2)	MIS 7	**-0.69**	**0.25**						
WP447C(4)	MIS 7	**-0.02**	**0.64**						
WP454A(1)	MIS 7	**0.20**	**0.93**						
WP454A(2)	MIS 7	**0.23**	**1.01**						
WP454A(3)	MIS 7	**0.40**	**1.03**						
WP471(1)	MIS 9	**-0.88**	**0.52**	**0.24**	0.48	1.89	**0.67**	0.21	0.77
WP471(2)	MIS 9	**1.01**	**0.63**						
WP471(3)	MIS 9	**0.93**	**1.11**						
WP479A(1)	MIS 9	**0.87**	**1.08**						
WP479A(2)	MIS 9	**0.80**	**0.71**						
WP479A(3)	MIS 9	**0.00**	**0.51**						
WP479B(1)	MIS 9	**0.02**	**0.34**						
WP479B(2)	MIS 9	**0.18**	**0.69**						
WP479B(3)	MIS 9	**0.75**	**0.80**						
WP479B(4)	MIS 9	**0.41**	**0.57**						
WP481(1)	MIS 9	**0.37**	**0.80**						
WP481(2)	MIS 9	**0.12**	**0.87**						
WP481(3)	MIS 9	**-0.19**	**0.90**						
WP481(4)	MIS 9	**0.06**	**0.52**						
WP481(5)	MIS 9	**0.11**	**0.64**						
WP481(6)	MIS 9	**-0.04**	**0.38**						
WP506(1)	MIS 9	**0.24**	**0.64**						
WP506(2)	MIS 9	**-0.43**	**0.44**						
WP506(3)	MIS 9	**0.27**	**0.68**						

Table 20– Carbon and oxygen isotopic composition, mean values, standard deviation and range values of modern and Pleistocene shells of Ameghinomya antiqua from Caleta Olivia area.

Ameghinomya antiqua shells from Pleistocene beach ridges show a large isotopic variability for carbon isotope ratio, >1 ‰ (almost 2‰ for the samples collected from the beach ridges deposited during MIS 9) for all the Marine Isotope Stages and narrower range of values for oxygen isotope composition (Fig. 161).

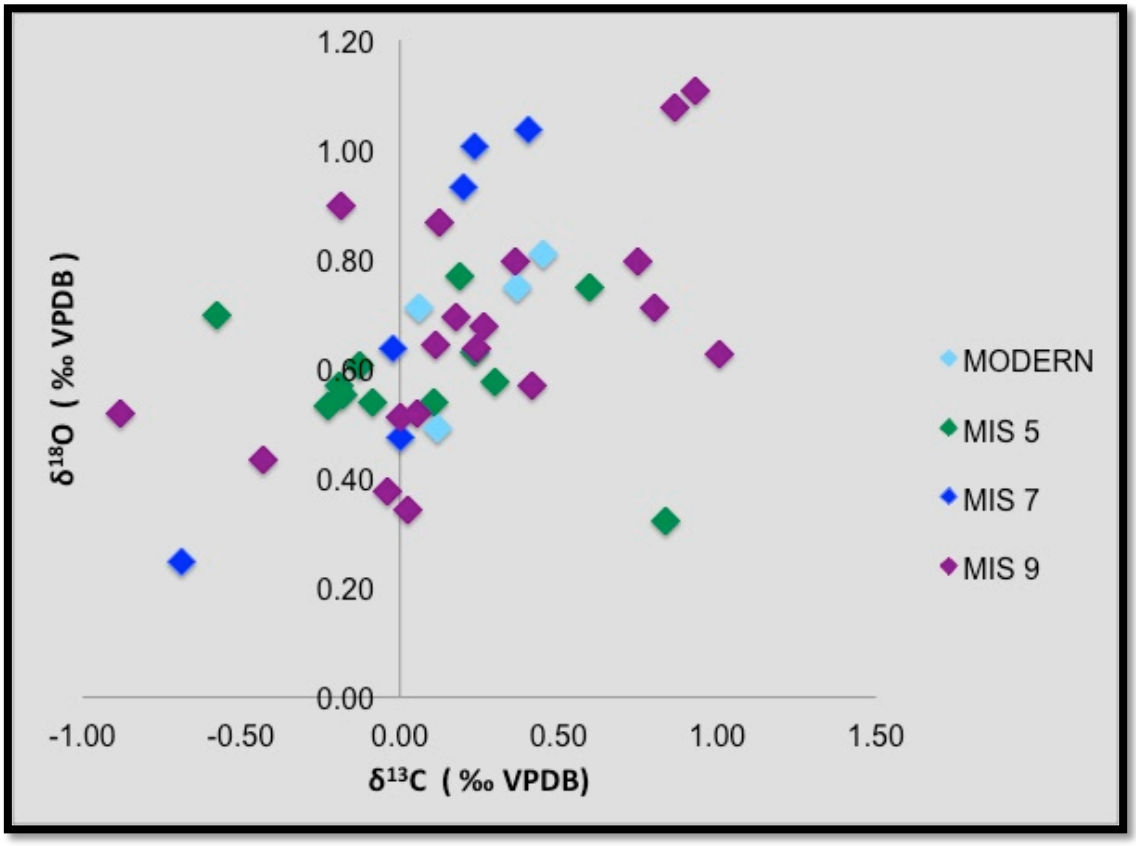

Figure 161 – Oxygen vs carbon isotope composition of Pleistocene and modern *Ameghinomya antiqua* shells from Caleta Olivia area.

Samples from Pleistocene beach deposits belonging to different MIS show mean values of the isotopic composition rather homogeneous both for oxygen both for carbon and substantially overlapping with the mean values of modern *Ameghinomya antiqua* shells (Fig. 162 and Fig. 163).

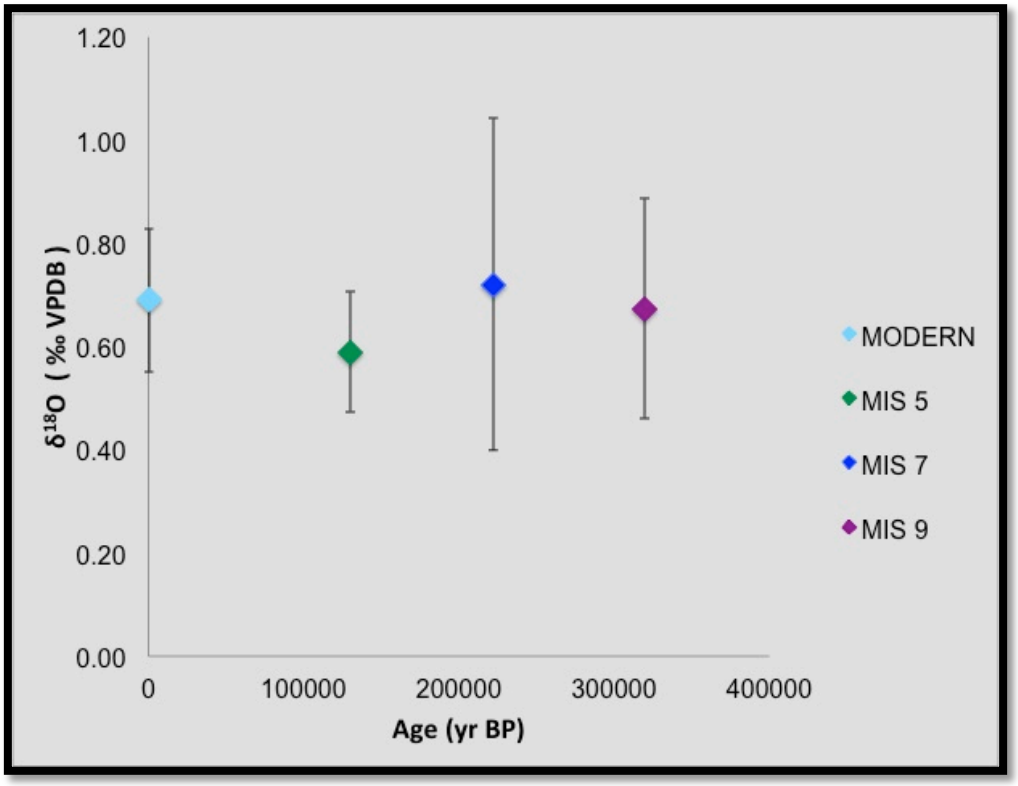

Figure 162 - Oxygen isotope mean values and standard deviations vs age have Pleistocene and modern *Ameghinomya antiqua* shells sampled in Caleta Olivia area.

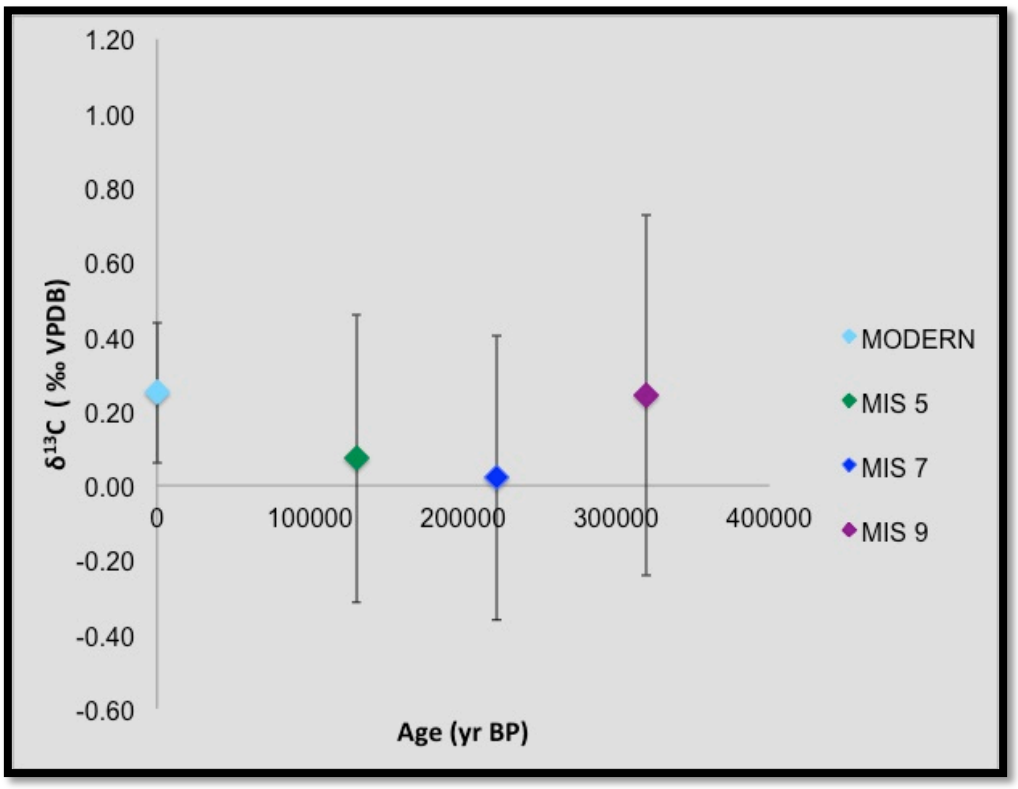

Figure 163 - Oxygen isotope mean values and standard deviations vs age have Pleistocene and modern Ameghinomya antiqua shells sampled in Caleta Olivia area.

6.4. TRACE ELEMENT ANALYSIS OF MARINE SHELLS

6.4.1. Preservation state of marine shells

Trace element concentrations of marine shells were used to infer the degree of preservation (e.g. Mn content) of shells comparing modern shells and fossils. In addition, concretions in soil/paleosol carbonate of the area were analyzed assuming that these concretions have been formed from the same potentially alterating solution of fossil shells.

6.4.1.1. Manganese content

When meteoric water alters marine carbonate, manganese (Mn) concentrations may increase (Brand and Veizer, 1980) because meteoric water contains ca. 40 times more Mn than seawater (Drever, 1997). For this reason Mn concentrations in Holocene and Pleistocene shells were compared to Mn content in modern samples and to the Mn concentration of paleosols as a relative indicator of diagenetic trace element exchange (Fig. 164).

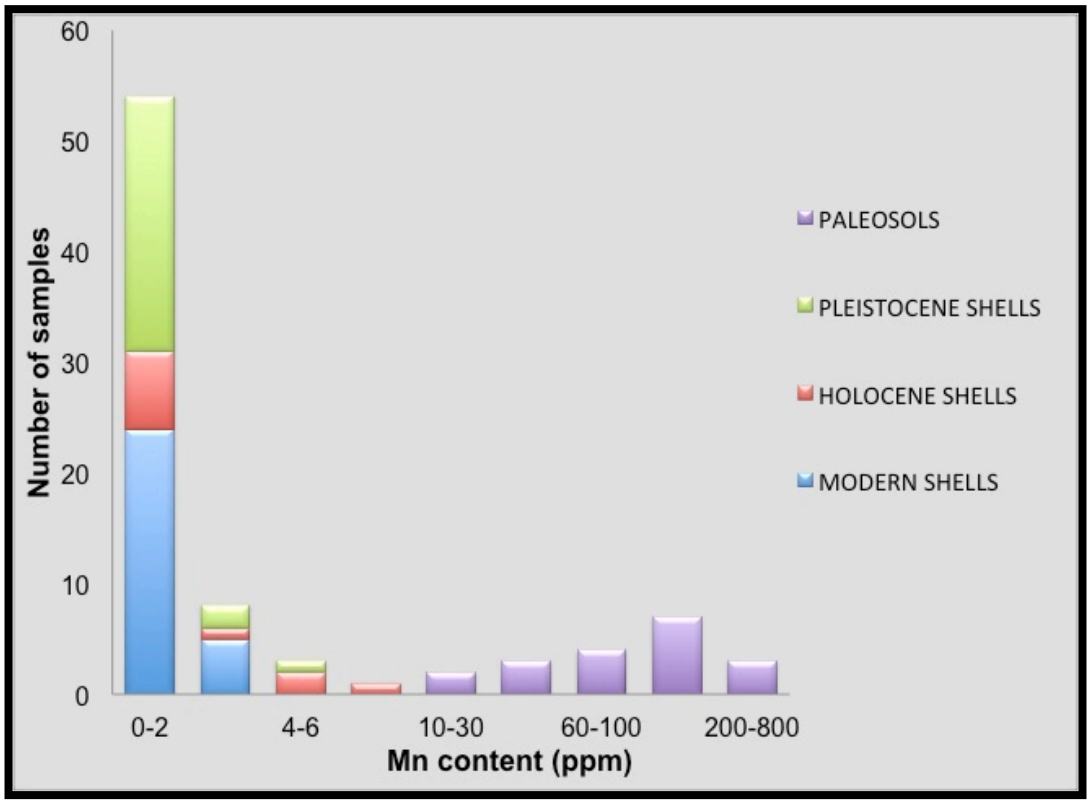

Figure 164 – Manganese concentrations in modern and fossil *A. antiqua* shells and in paleosols.

The manganese content in fossil shells is within the variability of modern specimen concentrations. This data confirms the absence of significant shell alterations by meteoric waters for *Ameghinomya antiqua* specimens, as already showed by XRD analyses.

6.4.1.2. Uranium content and U/Th dating method applied to marine molluscs

Despite Late Quaternary marine molluscs can be potentially dated with U/Th, so offering a robust chronological support to geochemical proxies, the applicability of this method is still a challenge owing to the postmortem migration of uranium into mollusc shells (Kaufman *et al.*, 1971; 1996; McLaren & Rowe, 1996; Labonne & Hillaire-Marcel, 2000).
U concentration shows higher values in older samples (up to 4 ppm) above the values measured on modern specimens (Fig. 165).

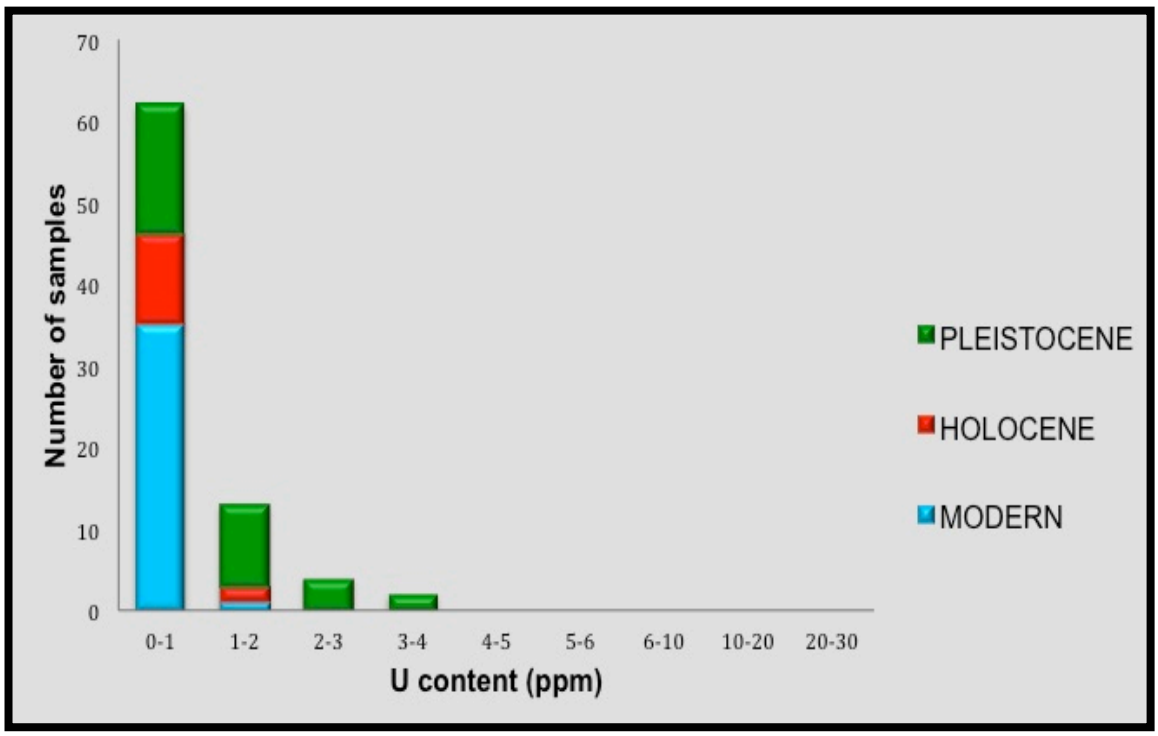

Figure 165 – Uranium content in modern and fossil *A. antiqua* shells.

Therefore, U content could indicate which samples can be selected for U/Th dating. Where possible, our U/Th ages were compared with the age obtained from Schellmann (1998) for the same beach deposits (Tab. 21 and Fig. 166). It is

possible to observe that, although the data available are very few to draw any conclusions, low uranium content is not a discriminating factor to obtain reliable U/Th dating (Tab. 21).

Sample	Species analyzed	U/Th age yr BP (our data)	Locality	Schellmann (1998) ESR age yr BP	U (ppm)
WP 64A(3)	*A. antiqua*	121000±900	Camarones N	102000±10000	2.21
WP 65(1)	*A. antiqua*	130000±2500	Camarones N	129000±15750	1.44
WP 92A(3)	*A. antiqua*	92000±600	Camarones S	198000±23000	0.79
WP 97(1)	*A. antiqua*	41400±16000	Camarones S	370000±48200	1.94
WP 149(1)	*A. antiqua*	89000±800	B.Bustamante	119000±16000	0.2
WP176BIS(1)	*A. antiqua*	82500±500	B.Bustamante	215000±24500	1.6

Table 21 – U/Th (our data) and ESR (Schellmann, 1998) dating and U content of *Ameghinomya antiqua* from Pleistocene beach deposits.

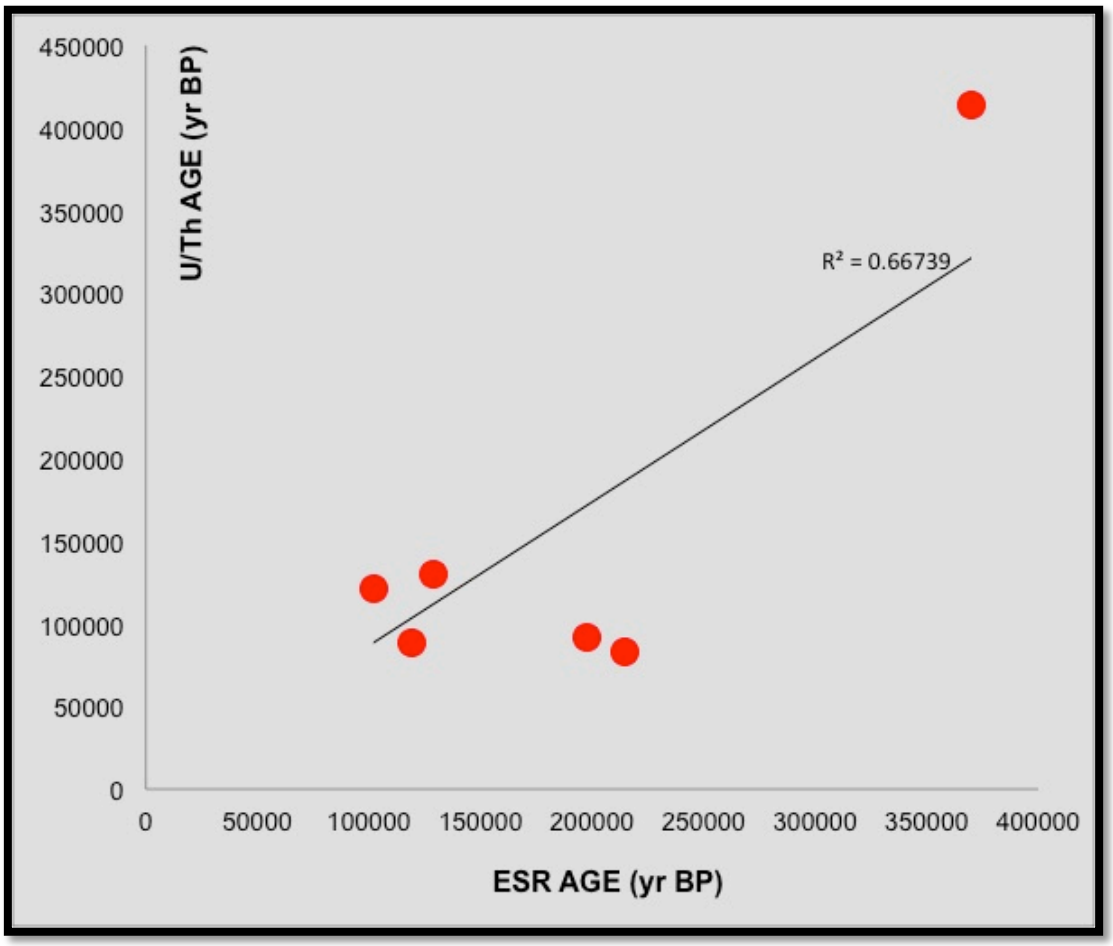

Figure 166 – Comparison between U/Th and ESR ages on *Ameghinomya antiqua* specimens sampled from the same Pleistocene beach ridges.

6.4.1.3. Barium content

During diagenesis no significant variations in chemical concentration occur for Ba for its tendency to be immobile (Brand & Morrison, 1987; Brand, 1989). The barium concentration in fossil shells is within the variability of modern specimen concentrations (Fig. 167). Moreover, the Ba content in most of paleosols is considerably higher than that in the marine shells.

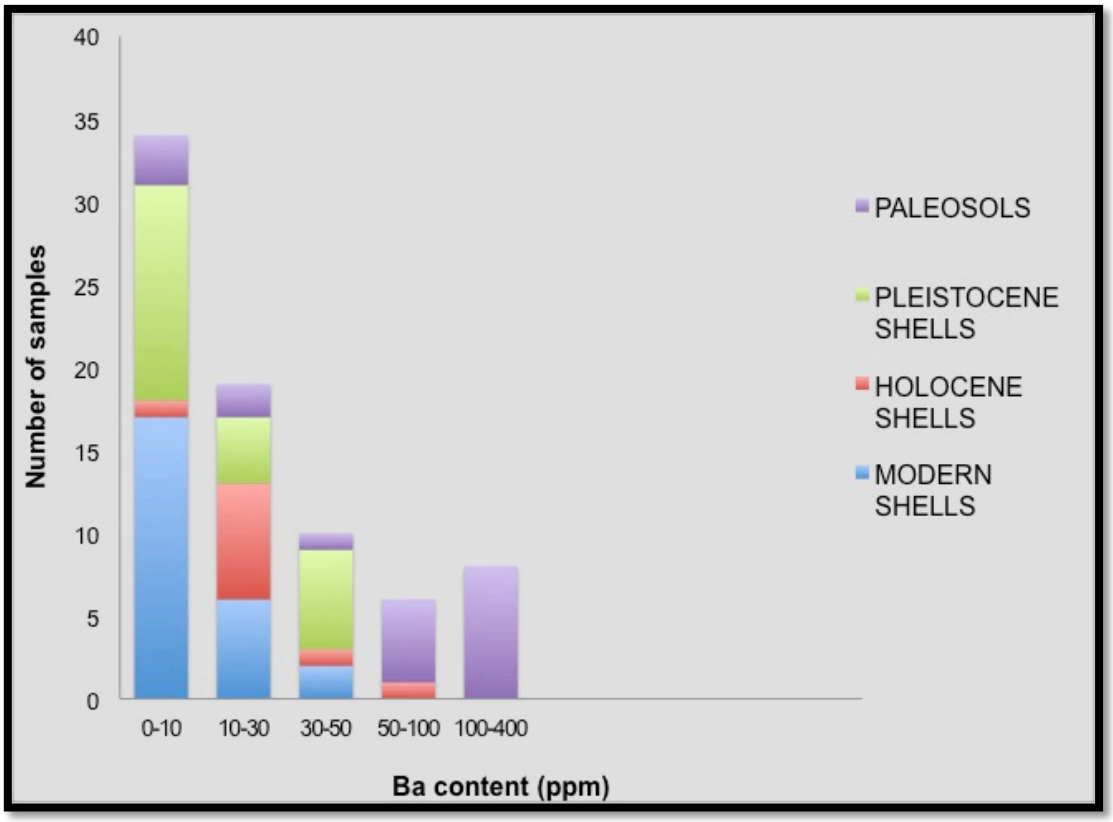

Figure 167 – Barium content in modern and fossil *A. antiqua* shells and in paleosols.

6.4.1.4. Iron content

Meteoric waters contain, generally, more Fe than seawater (Brand & Veizer, 1980; Brand & Morrison, 1987). The paleosols sampled in the study area show very high values of Fe, usually two orders of magnitude higher than marine shells selected from the same study area (Fig. 168).

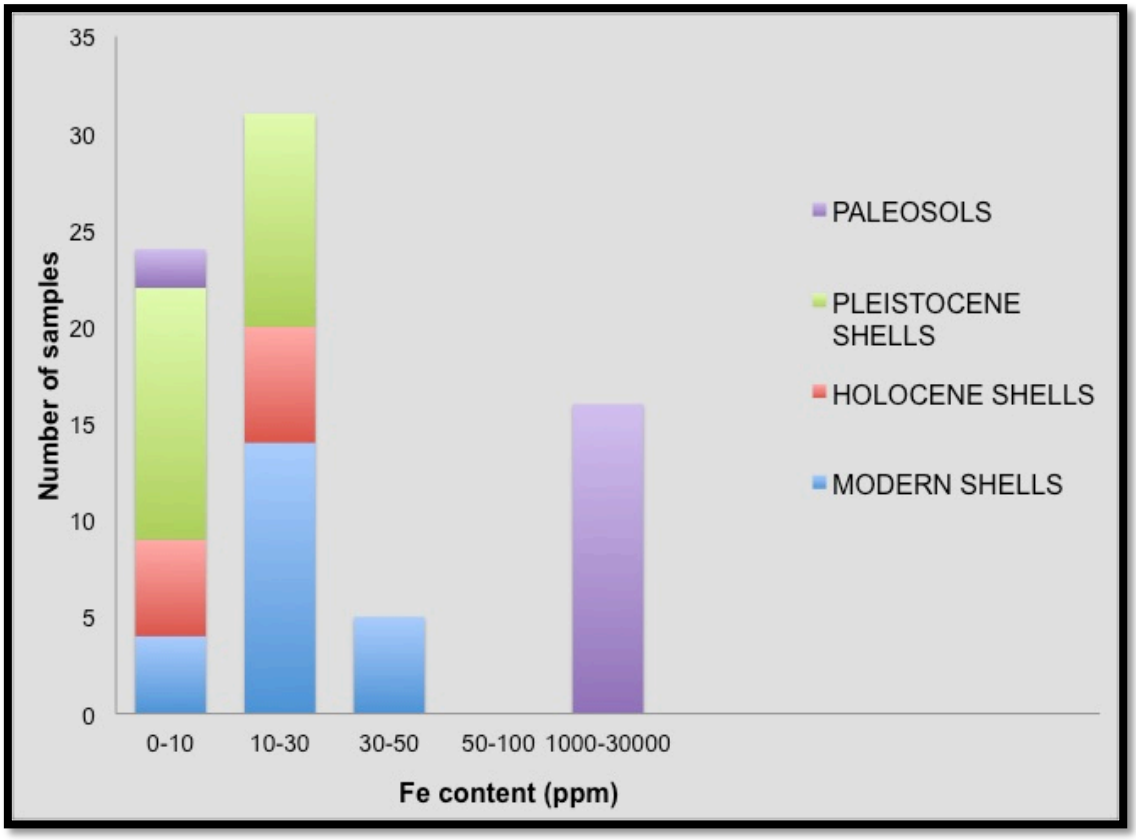

Figure 168 – Iron content in modern and fossil *A. antiqua* shells and in paleosols.

6.4.1.5. Magnesium and strontium content

The meteoric water, generally, contains lower concentrations of Mg and Sr than seawater (Turekian, 1972; Brand & Veizer, 1980; Brand and Morrison, 1987). However, in the case of equilibration by aragonitic shells with diagenetic waters, it is observed an enrichment in the content of Mg, while in calcitic shells is observed a depletion (Brand and Morrison, 1987).

Paleosols from Atlantic coast of Patagonia have higher values of magnesium than fossil and modern marine shells (Fig. 169).

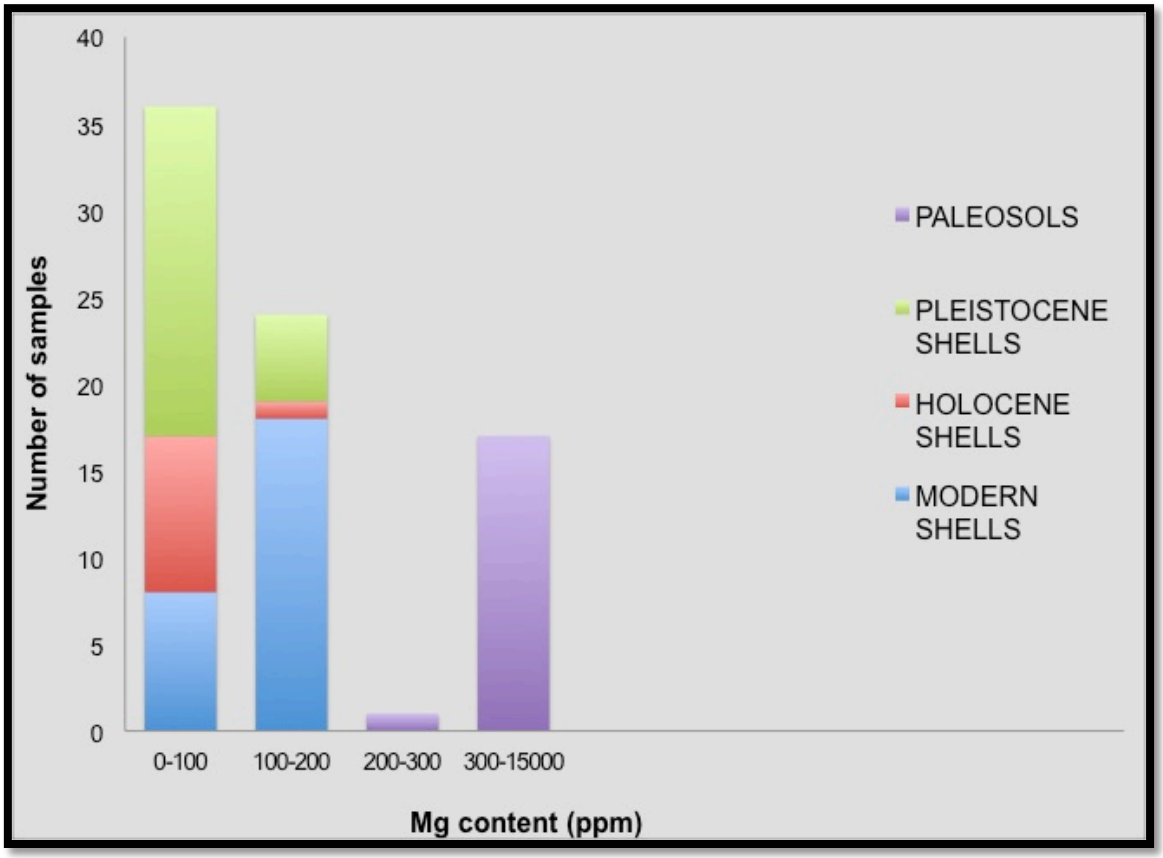

Figure 169 – Magnesium concentration in modern and fossil *A. antiqua* shells and in paleosols.

The strontium concentration in paleosols, on the contrary, is lower than in modern and fossil marine shells (Fig. 170).

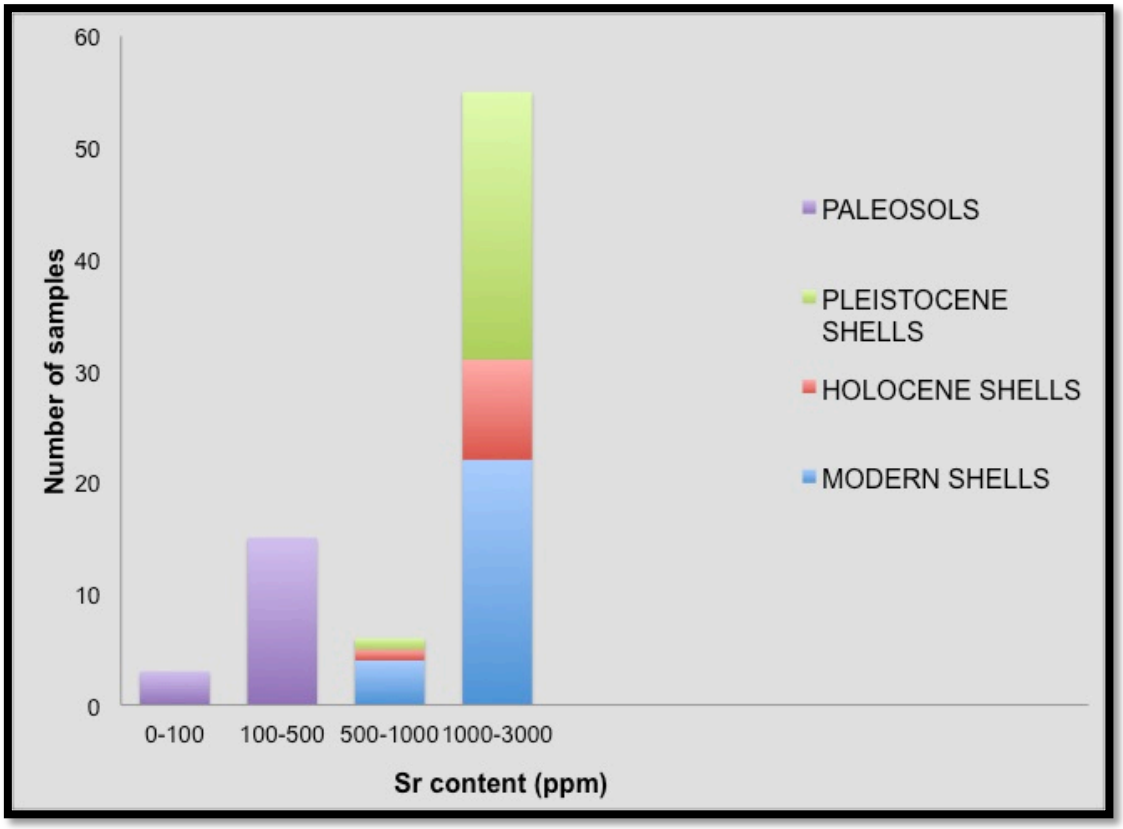

Figure 170 – Strontium concentration in modern and fossil *A. antiqua* shells and in paleosols.

6.4.2. Trace element concentration on modern marine shells

6.4.2.1. Trace element analysis of the modern shells *Ameghynomia antiqua*

Modern shells of *Ameghinomya antiqua* were collected from the active beach in different localities along the Atlantic coast of Patagonia (figure 64, Chapter 5). All the metal/Ca ratios, expressed in molar ratio, are shown in Tab. 22.

SAMPLE	LATITUDE (°S)	LOCALITY	Ba/Ca (µmol/mol)	Fe/Ca (µmol/mol)	Mg/Ca (µmol/mol)	Mn/Ca (µmol/m	Sr/Ca (mmol/mol)*10	U/Ca (µmol*10/mol)
WP667(1)	42.1	PUERTO LOBOS	4.86		549.65	0.14	18.62	0.77
WP667(2)	42.1	PUERTO LOBOS	4.27	40.42	670.03	0.00	15.69	0.36
mean value			**4.57**		**609.84**	**0.07**	**17.16**	**0.57**
standard deviation			**0.42**		**85.12**	**0.10**	**2.07**	**0.29**
WP04(1)	44.16	CABO RASO	2.73	24.52	609.11	1.92	15.69	0.71
WP04(2)	44.16	CABO RASO	22.32	30.85	459.67	3.35	19.69	1.07
WP04(3)	44.16	CABO RASO	0.35	11.75	531.93	6.79	17.88	0.05
mean value			**8.47**	**22.37**	**533.57**	**4.02**	**17.75**	**0.61**
standard deviation			**12.05**	**9.73**	**74.74**	**2.50**	**2.00**	**0.52**
WP54(2)	44.34	BAHIA S.SEBASTIAN	0.04	58.14	459.55	2.92	16.82	0.04
WP54(3)	44.34	BAHIA S.SEBASTIAN	3.37	78.95	565.00	0.00	15.09	0.47
WP54(4)	44.34	BAHIA S.SEBASTIAN	1.99	60.15	568.76	0.00	13.45	0.54
mean value			**1.80**	**65.75**	**531.10**	**0.97**	**15.12**	**0.35**
standard deviation			**1.67**	**11.48**	**61.99**	**1.69**	**1.68**	**0.27**
WP60BBIS(1)	44.41	CAMARONES NORTH	4.23	29.10	557.23	0.74	17.47	0.67
WP60BBIS(2)	44.41	CAMARONES NORTH	2.01	68.46	547.59	4.92	9.14	0.68
WP60BBIS(3)	44.41	CAMARONES NORTH	26.40	56.15	537.92	3.33	17.06	0.00
WP623BIS(1)	44.41	CAMARONES NORTH	18.94	52.49	429.04	2.90	17.76	1.54
WP623BIS(2)	44.41	CAMARONES NORTH	22.95	19.06	380.36	2.08	17.58	1.84
mean value			**14.91**	**45.05**	**490.43**	**2.80**	**15.80**	**0.95**
standard deviation			**11.11**	**20.35**	**80.42**	**1.55**	**3.73**	**0.74**
WP95(1)	44.5	CAMARONES SOUTH			485.25	0.28		
WP95(2)	44.5	CAMARONES SOUTH	4.28	27.22	767.34	2.51	10.64	0.98
WP95(3)	44.5	CAMARONES SOUTH	19.97	46.95	536.43	4.06	18.35	0.35
WP110(1)	44.5	CAMARONES SOUTH	10.09	53.74	281.84	1.62	11.67	5.58
WP110(2)	44.5	CAMARONES SOUTH	3.94	37.23	211.19	1.07	15.48	0.68
mean value			**9.57**	**41.28**	**456.41**	**1.91**	**14.04**	**1.90**
standard deviation			**7.48**	**11.57**	**220.52**	**1.45**	**3.55**	**2.47**
WP237(1)	45.08	BAHIA BUSTAMANTE	2.73	15.43	530.80	0.00	15.69	0.35
WP237(2)	45.08	BAHIA BUSTAMANTE	3.82	21.96	416.98	0.25	14.46	0.42
WP237(4)	45.08	BAHIA BUSTAMANTE	27.46	16.31	451.72	1.50	25.82	0.63
mean value			**11.34**	**17.90**	**466.50**	**0.58**	**18.66**	**0.47**
standard deviation			**13.97**	**3.55**	**58.33**	**0.80**	**6.23**	**0.14**
WP271(1)	45.4	BAHIA SOLANO	37.11	17.89	414.89	1.52	16.19	0.50
WP271(3)	45.4	BAHIA SOLANO	9.15	56.21	445.50	3.57	30.35	1.95
mean value			**23.13**	**37.05**	**430.19**	**2.55**	**23.27**	**1.23**
standard deviation			**19.77**	**27.10**	**21.65**	**1.45**	**10.01**	**1.02**

Table 22 – Metal/Ca ratios in modern *Ameghinomya antiqua* from the Atlantic coast of Patagonia.

Ameghinomya antiqua modern shells show Ba/Ca ratios ranging from 0.04 for a Bahia San Sebastian specimen to 37.11 µmol/mol for Bahia Solano sample, with mean values between 1.80±1.67 µmol/mol of Bahia San Sebastian specimens and 23.13±19.77 µmol/mol of Bahia Solano shells (Tab. 22).

Modern samples collected at different localities show a large intra-specific variability even within the same sampled beach (e.g. for the localities of Cabo Raso, Camarones North, Camarones South, Bahia Bustamante and Bahia Solano, Fig. 171).

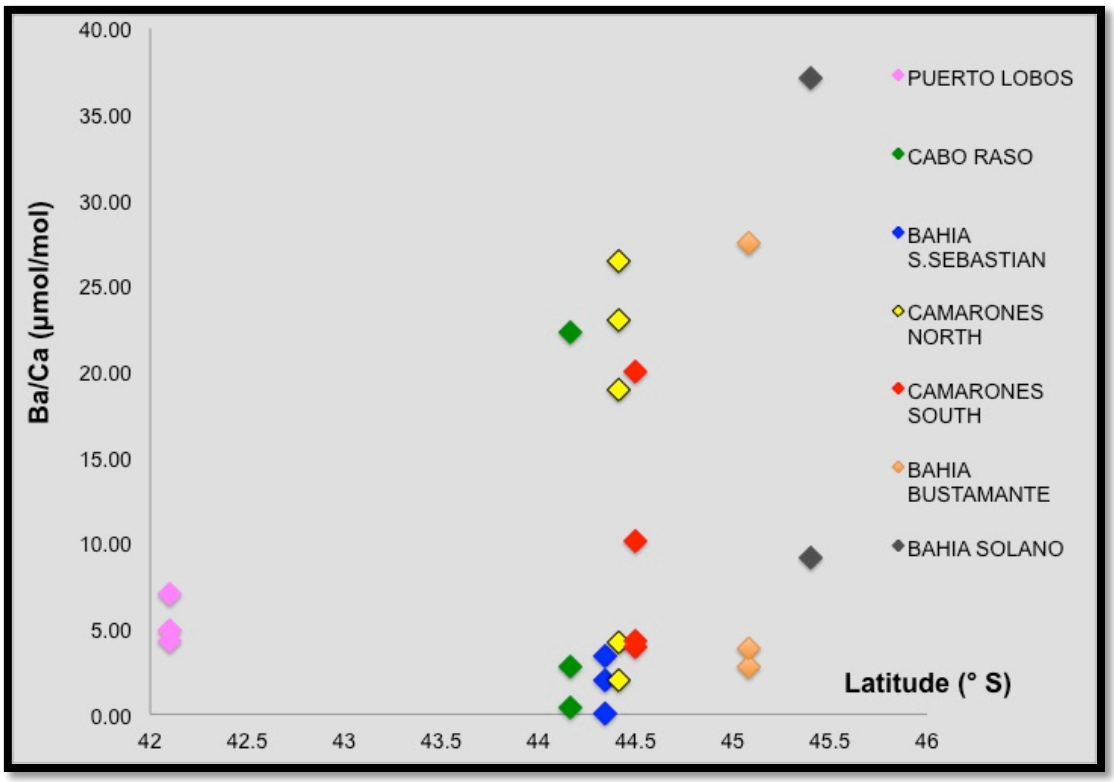

Figure 171 – Ba/Ca ratios of modern *A. antiqua* shells along the Patagonia Atlantic coast.

By analyzing the mean values of Ba/Ca ratio of the shells of modern *Ameghinomya antiqua* to vary the latitude, it is possible to observe that owing to the very large variability no trends is observed when samples are plotted against latitude (Fig. 172).

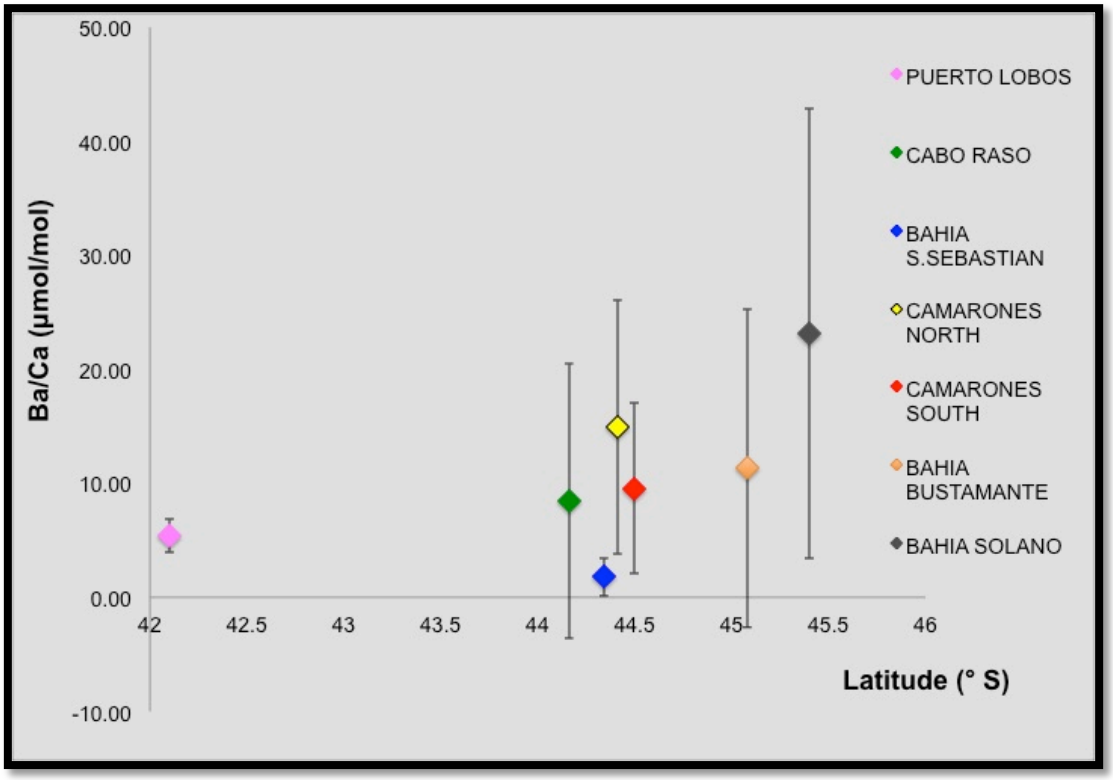

Figure 172 – Mean values and standard deviations of Ba/Ca ratios of modern *A. antiqua* shells to vary the latitude.

Modern specimens of *Ameghinomya antiqua* collected at different localities have Fe/Ca ratios between 11.75 and 90.73 µmol/mol obtained respectively from a Cabo Raso and a Puerto Lobos sample (Tab. 22). Mean values ranges from 17.90±3.55 µmol/mol of Bahia Bustamante specimens and 65.75±11.48 µmol/mol of Bahia San Sebastian samples (Tab. 22).

A large intra-specific variability within the same sampled beach is found for the shells collected from Puerto Lobos, Camarones North and Bahia Solano beaches (Fig. 173).

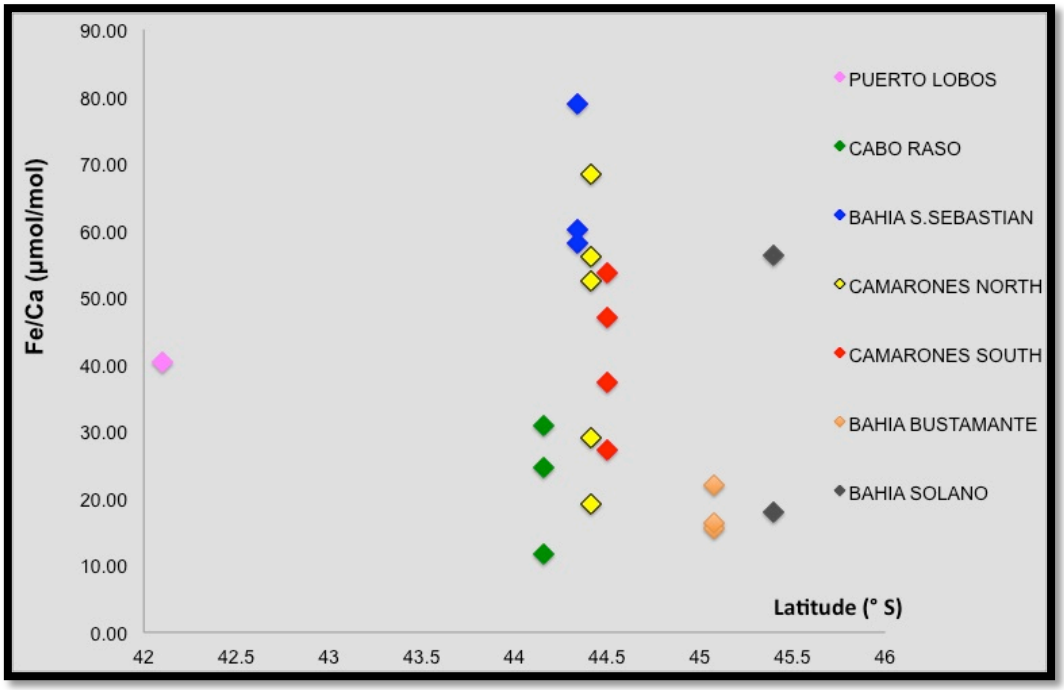

Figure 173 – Fe/Ca ratios of modern *A. antiqua* shells along the Patagonia Atlantic coast.

In the central part of the study area, from Bahia San Sebastian, where the Fe/Ca ratio is higher, to Bahia Bustamante, the mean values slightly decrease (Fig. 174). Nevertheless, no particular trend is observed also for Fe/Ca content in modern shells from north to south.

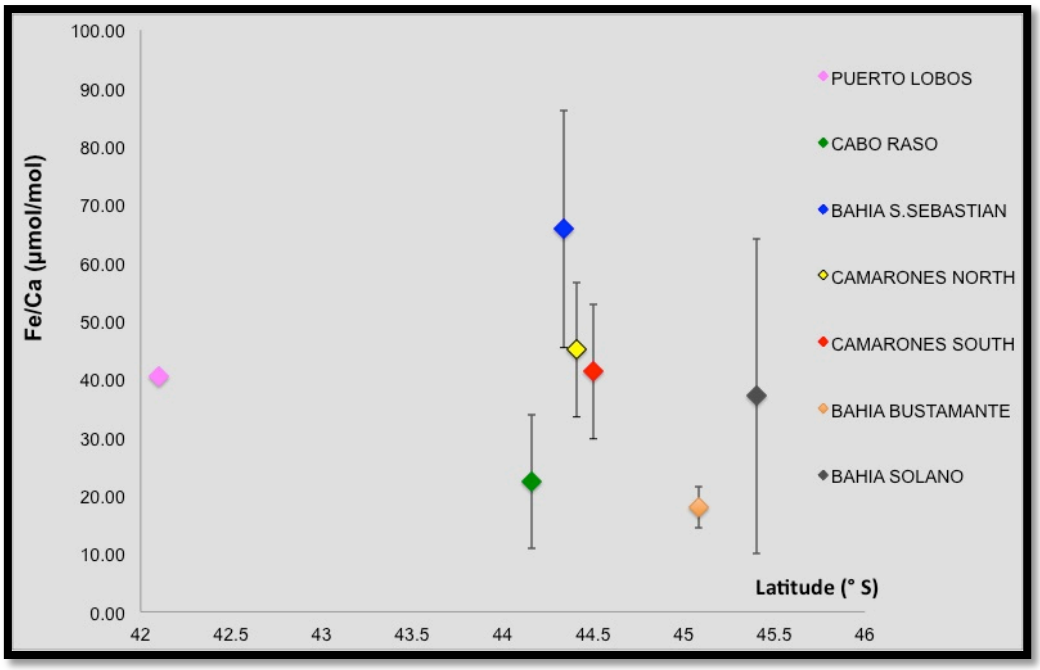

Figure 174 – Mean values and standard deviations of Fe/Ca ratios of modern *A. antiqua* shells to vary the latitude.

Mg/Ca varies in modern *A. antiqua* shells from 211.19 to 767.34 µmol/mol in Camarones South samples, which show the highest intra-specific variability within the same beach (Tab. 22 and Fig. 175). Mean values ranges from 430.19±21.65 µmol/mol of specimens collected from the beach sampled further south (Bahia Solano) and 570.06±91.48 µmol/mol of the northernmost Puerto Lobos samples (Tab. 22). Except for the shells sampled at Camarones South, the samples have a narrow compositional variability within the same beach (Tab. 22 and Fig. 175).

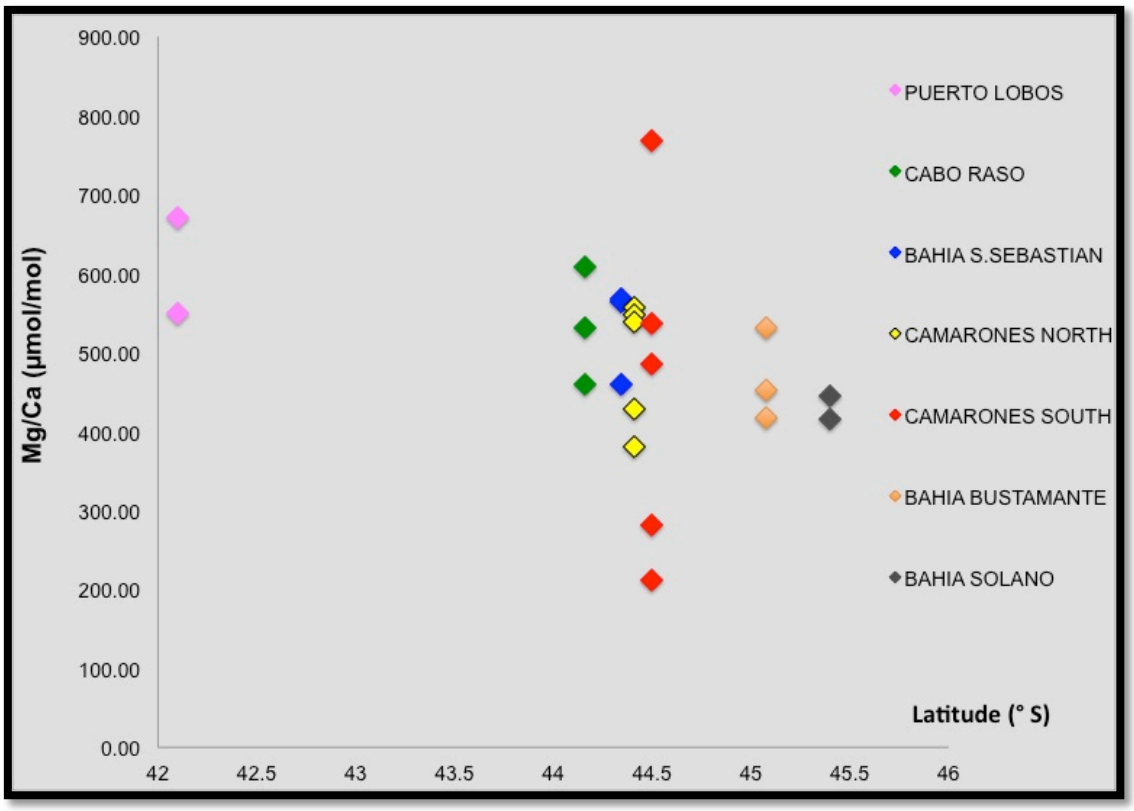

Figure 175 – Mg/Ca ratios of modern *A. antiqua* shells along the Patagonia Atlantic coast.

Mean values of Mg/Ca ratio are progressively lower from north to south (Fig. 176).

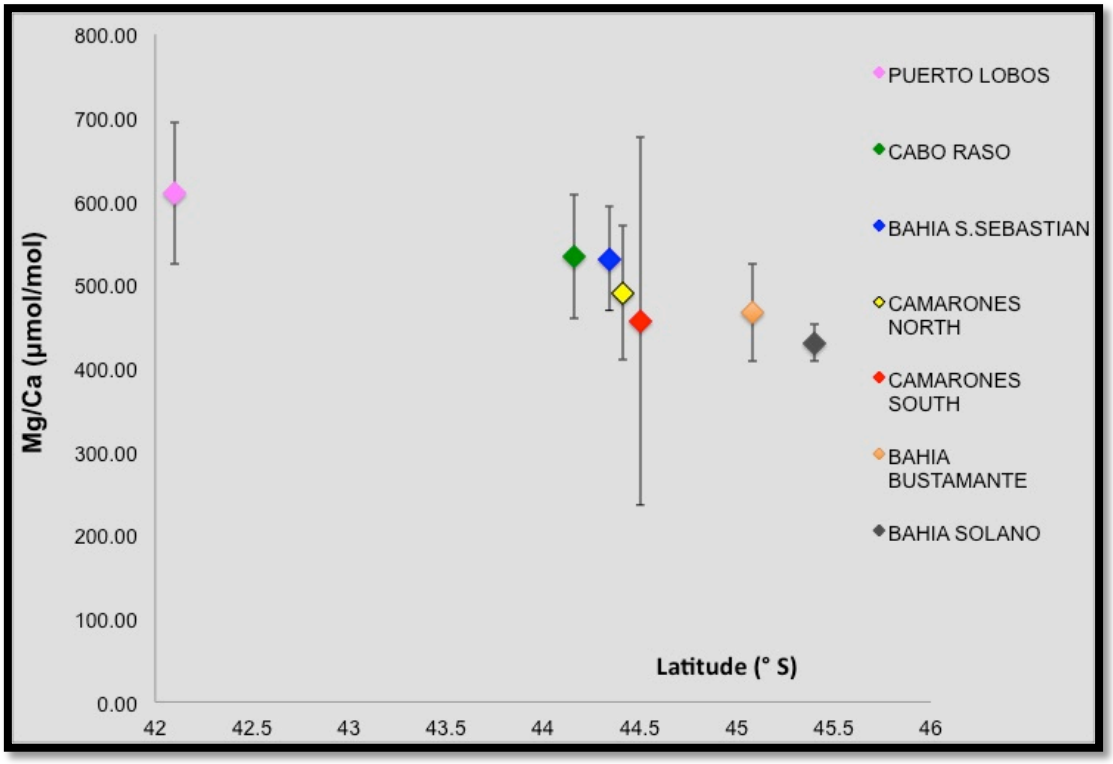

Figure 176 – Mean values and standard deviations of Mg/Ca ratios of modern *A. antiqua* shells to vary the latitude.

Mn/Ca ratios of *Ameghinomya antiqua* specimens collected from active beaches ranges from 0 in shells from Puerto Lobos, Bahia San Sebastian and Bahia Bustamante up to 6.79 µmol/mol for a Cabo Raso sample (Tab. 22), with mean values between 0.58±0.80 µmol/mol of Bahia Bustamante individuals and 2.80 ±1.55 µmol/mol of Camarones shells (Tab. 22 and Fig. 177).

Mean values, as for Fe/Ca, show a decrease in terms of Mn/Ca ratio between Camarones and Bahia Bustamante, even if the differences between the various localities are substantially overlapping (Fig. 178). The mean value in shells from the northern beach is lower than the mean values in shells collected further south.

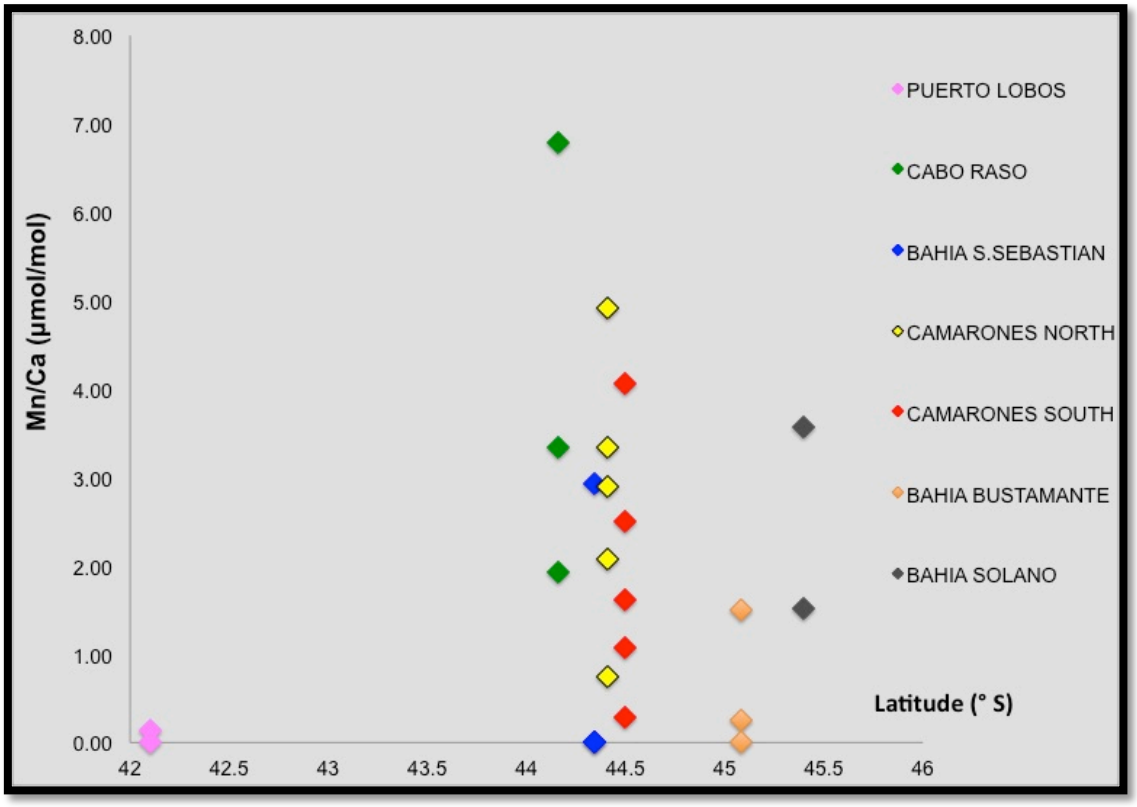

Figure 177 – Mn/Ca ratios of modern *A. antiqua* shells along the Patagonia Atlantic coast.

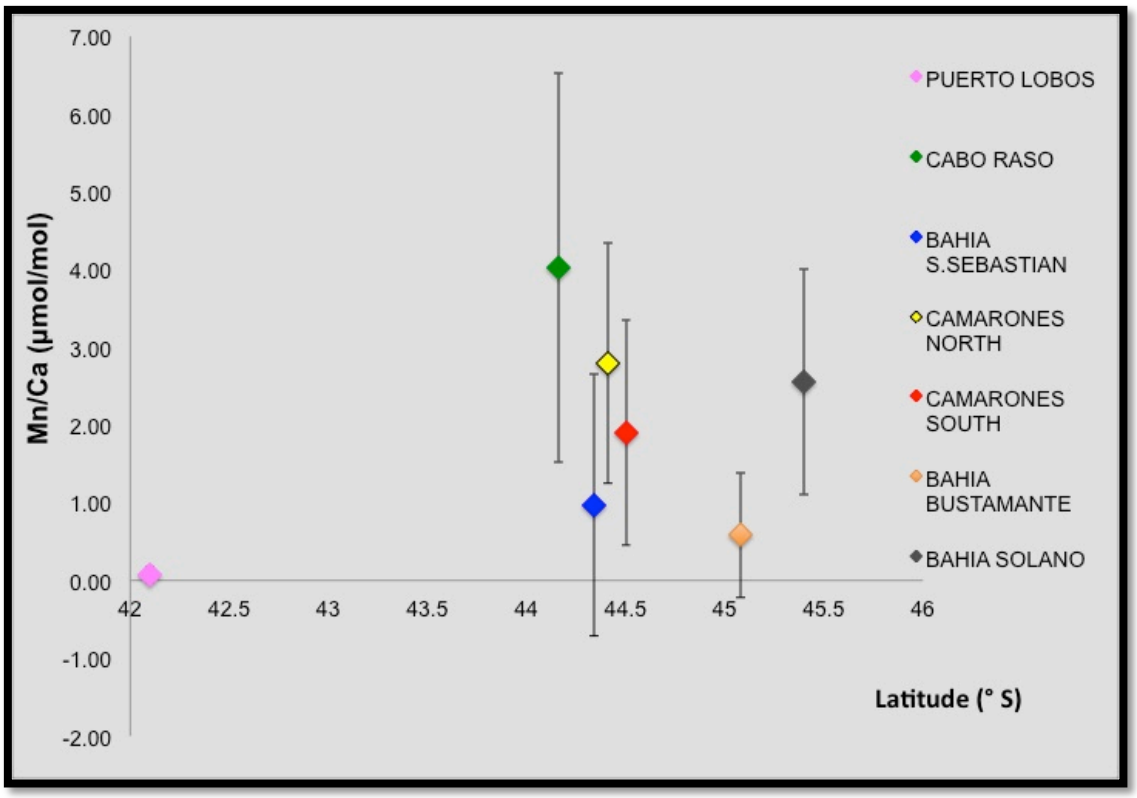

Figure 178 – Mean values and standard deviations of Mn/Ca ratios of modern *A. antiqua* shells to vary the latitude.

Modern *Ameghinomya antiqua* shells show the lower Sr/Ca ratio (9.14 mmol*10/mol) in a specimen coming from the beach of Camarones North and the higher ratio (41.78 mmol*10/mol) in a sample collected from Puerto Lobos beach (Tab. 22). Mean values vary from 14.04±3.55 mmol*10/mol of Camarones South individuals and 25.37±14.29 mmol*10/mol of Puerto Lobos shells (Tab. 22 and Fig. 179).

Compared to other metal/Ca ratios the values of Sr/Ca, except for a few, are fairly homogeneous in all the study area (Fig. 179) and the mean values show very small differences, in particular in the central part of the study area, substantially overlapping (Fig. 180).

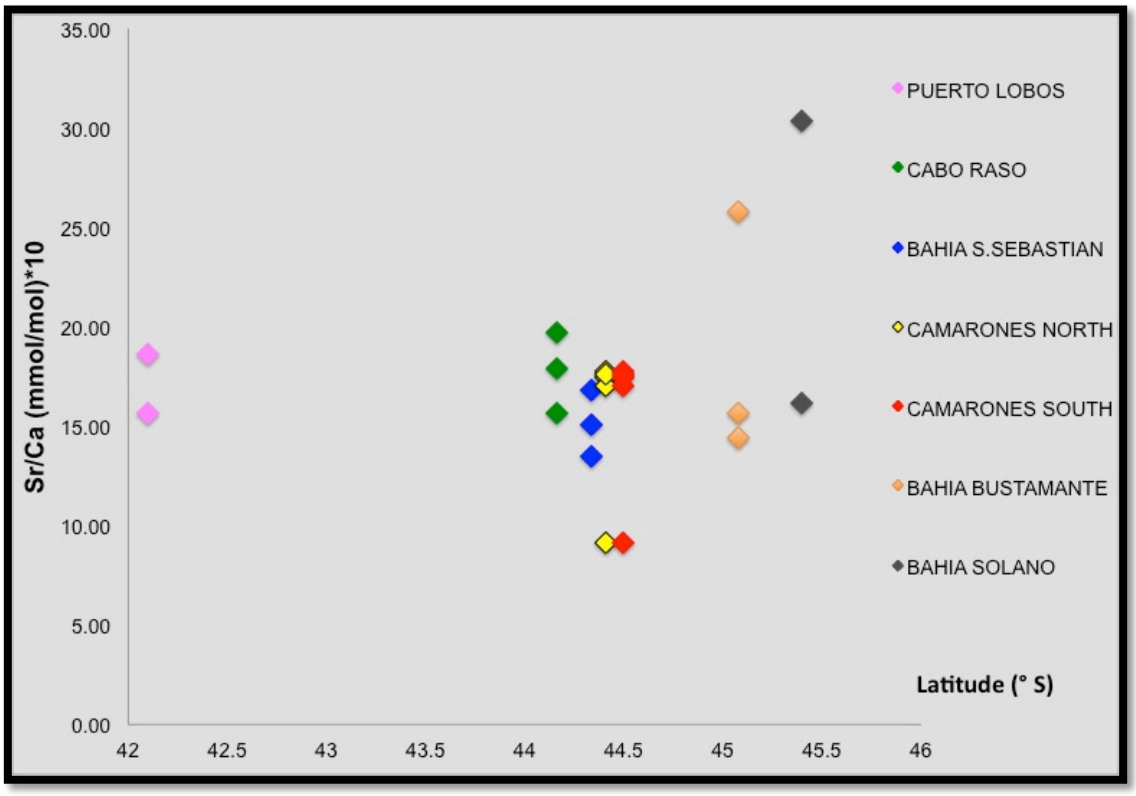

Figure 179 - Sr/Ca ratios of modern *A. antiqua* shells along the Patagonia Atlantic coast.

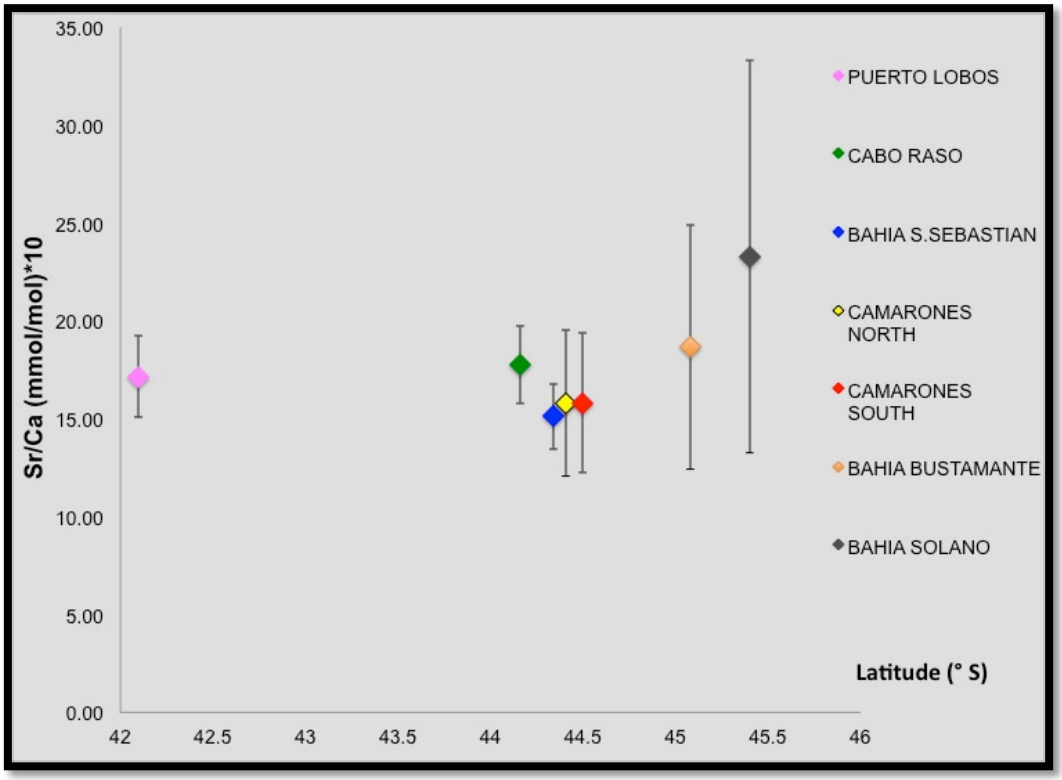

Figure 180 – Sr/Ca mean values and standard deviations of modern *A. antiqua* shells to vary the latitude.

U/Ca ratios in *Ameghinomya antiqua* modern shells coming from modern beaches of the Atlantic coast of Patagonia are between 0.04 µmol*10/mol (sample from Bahia San Sebastian beach) and 5.58 µmol*10/mol (specimen from Camarones South active beach). Mean values range from 0.35±0.27 µmol*10/mol of Bahia San Sebastian samples and 1.90±2.47 µmol*10/mol of Camarones South specimens (Tab. 22 and Fig. 181).

As for the ratio Sr/Ca, also U/Ca does not show any gradient and has similar values in all the study area (except for the high value found in a Camarones South sample) (Fig. 181 and Fig. 182).

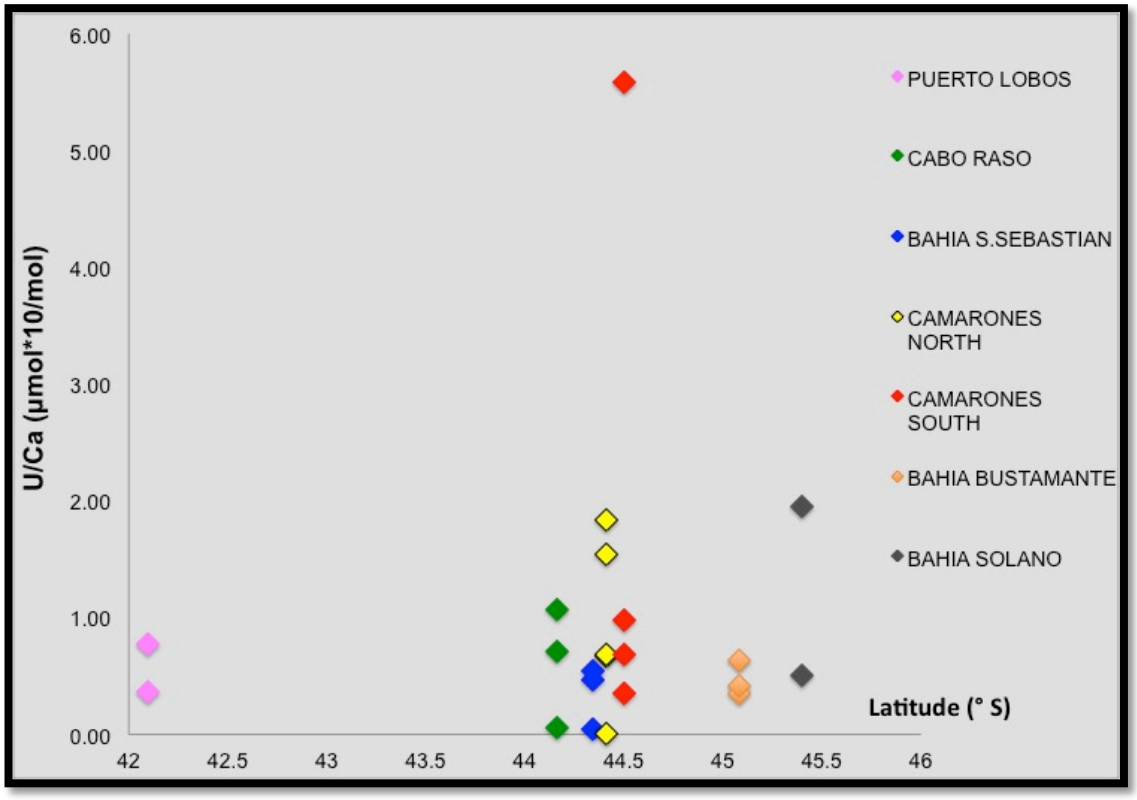

Figure 181 - U/Ca ratios of modern *A. antiqua* shells along the Patagonia Atlantic coast.

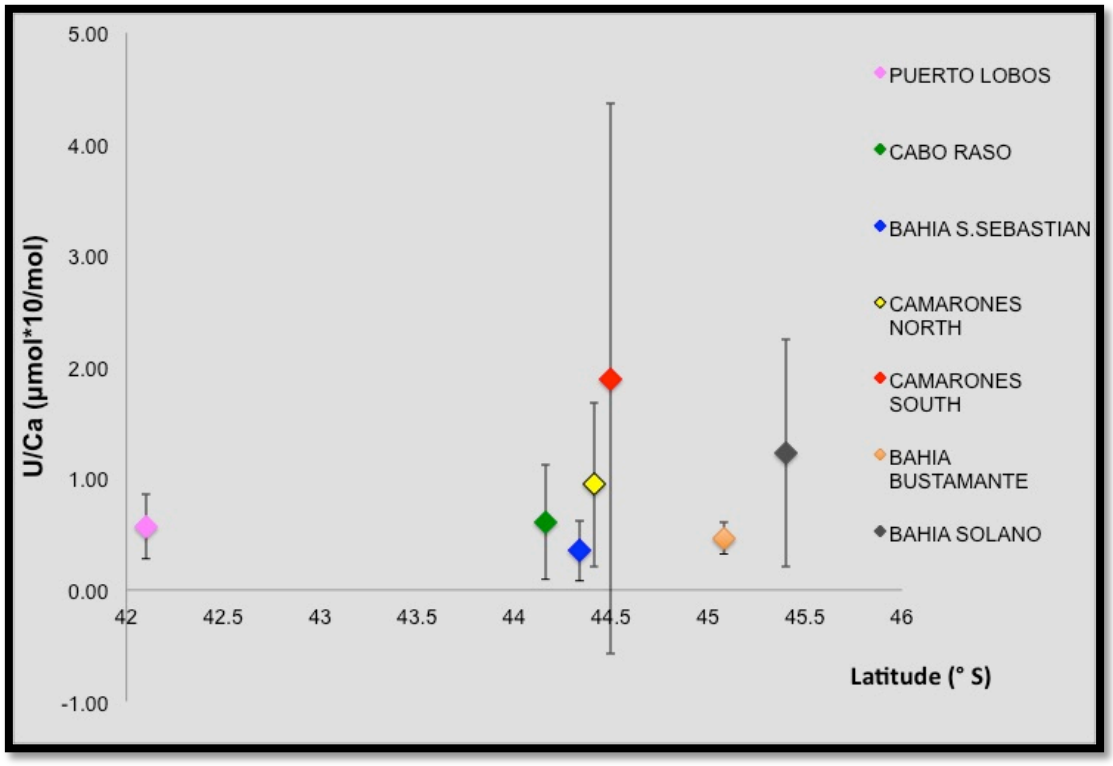

Figure 182 – U/Ca mean values and standard deviations of modern *A. antiqua* shells to vary the latitude.

In summary, no trend along the Patagonia Atlantic coast is observable for Ba/Ca, Fe/Ca, U/Ca and Sr/Ca ratios, showing similar values in all the study area. Mg/Ca tends to slightly decrease moving southward. Finally, Mn/Ca show lower values in the northern part of the study area,

6.4.3. Trace element concentration on fossil marine shells

Trace element analysis was carried out on part of the shells of *A. antiqua, Aulacomya atra* and *M. edulis* on which stable isotope analysis was performed (Chapter 6.3). Holocene and Pleistocene shells analyzed for the trace element concentrations are from beach deposits outcropping in the north and south of the village of Camarones and in the Bahia Bustamante area (Fig. 121).
Since the samples analyzed for trace elements are fewer than those analyzed for stable isotopes, the results of Holocene and Pleistocene samples are combined in a single graph. The trace element contents of fossil shells were compared with specimens collected from the modern beach of the same locality.

6.4.3.1. Trace element composition of Holocene Mytilidae shells in Camarones North

The analyses were made on some of the shells also analyzed for the stable isotopes selected from the section located North of the village of Camarones and previously described (Fig. 122). The results of trace element analysis on modern and Holocene Mytilidae shells are shown in Tab. 23.

SAMPLE	Species	^{14}C AGE (uncalibrated) yr BP	^{14}C cal BP 2 sigma	Ba/Ca (µmol/mol)	Fe/Ca (µmol/mol)	Mg/Ca (µmol/mol)	Mn/Ca (µmol/mol)	Sr/Ca (mmol/mol)*10
WP 60B(1)	*A.atra*	-390±20		92.55	19.03	636.83	20.80	5.79
WP 60B(4)	*A.atra*	-390±20		63.03	19.98	871.83	20.82	5.99
WP 60B(10)	*A.atra*	-390±20		35.98	23.19	705.70	33.01	7.81
mean value				**63.85**	**20.73**	**738.12**	**24.88**	**6.53**
standard dev.				28.29	2.18	120.81	7.04	1.11
WP 60A(4)	*A.atra*	915±20	477-560	61.19	18.35	858.28	25.63	5.39
WP 60A(7)	*A.atra*	915±20	477-560	57.92	58.77	872.07	14.38	10.17
WP 60A(9)	*A.atra*	915±20	477-560	49.88	18.61	961.56	16.26	8.53
mean value				**56.33**	**31.91**	**897.30**	**18.76**	**8.03**
standard dev.				5.82	23.26	56.07	6.03	2.43
G001(1)	*A.atra*	4074±50	3948-4271	49.67	60.46	1665.14	22.88	9.78
G001(6)	*A.atra*	4074±50	3948-4271	37.80	83.11	650.72	14.48	6.56
G001(7)	*A.atra*	4074±50	3948-4271	43.99	102.59	968.61	17.83	10.76
mean value				**43.82**	**82.06**	**1094.82**	**18.40**	**9.03**
standard dev.				5.94	21.08	518.85	4.23	2.20
WP 63B(2)	*M.edulis*	6365±20	6750-6913	78.29	80.71	3941.54	100.72	10.61
WP 63B(5)	*M.edulis*	6365±20	6750-6913	49.71	96.83	4843.72	88.82	2.05
WP 63B(7)	*M.edulis*	6365±20	6750-6913	47.65	66.48	4466.77	140.01	4.45
mean value				**58.55**	**81.34**	**4417.34**	**109.85**	**5.70**
standard dev.				17.13	15.19	453.11	26.79	4.42

Table 23 – Metal/Ca ratios, mean values and standard deviations of modern and Holocene shells of *Aulacomya atra* and *Mytilus edulis* from Camarones North section.

Modern shells show a great variability for the Ba/Ca ratio with values ranging from 35.98 µmol/mol to 92.55 µmol/mol and mean value of 63.85±28.29 µmol/mol. These values are the lower and the higher values of Ba/Ca respectively between all the Mytilidae shells analyzed and the Ba/Ca ratios of the Holocene specimens are between these two values (Tab. 123 and Fig. 183). The Ba/Ca ratios of the Holocene specimens for each sampled level show a narrower variability than modern ones, with concentrations between 49.88 and 61.87 µmol/mol and mean value of 56.33±5.82 µmol/mol for the shells from the beach ridge dated to 915±20 yr BP, between 37.80 and 49.67 µmol/mol with mean value of 43.82±5.94 µmol/mol for the samples collected from the shell middden which gave an age of 4074±50 yr BP and between 47.75 and 78.29 µmol/mol (mean value of 58.55±17.13 µmol/mol) for the specimens sampled from the older beach deposit dated at 6365±20 yr BP (Tab. 23).

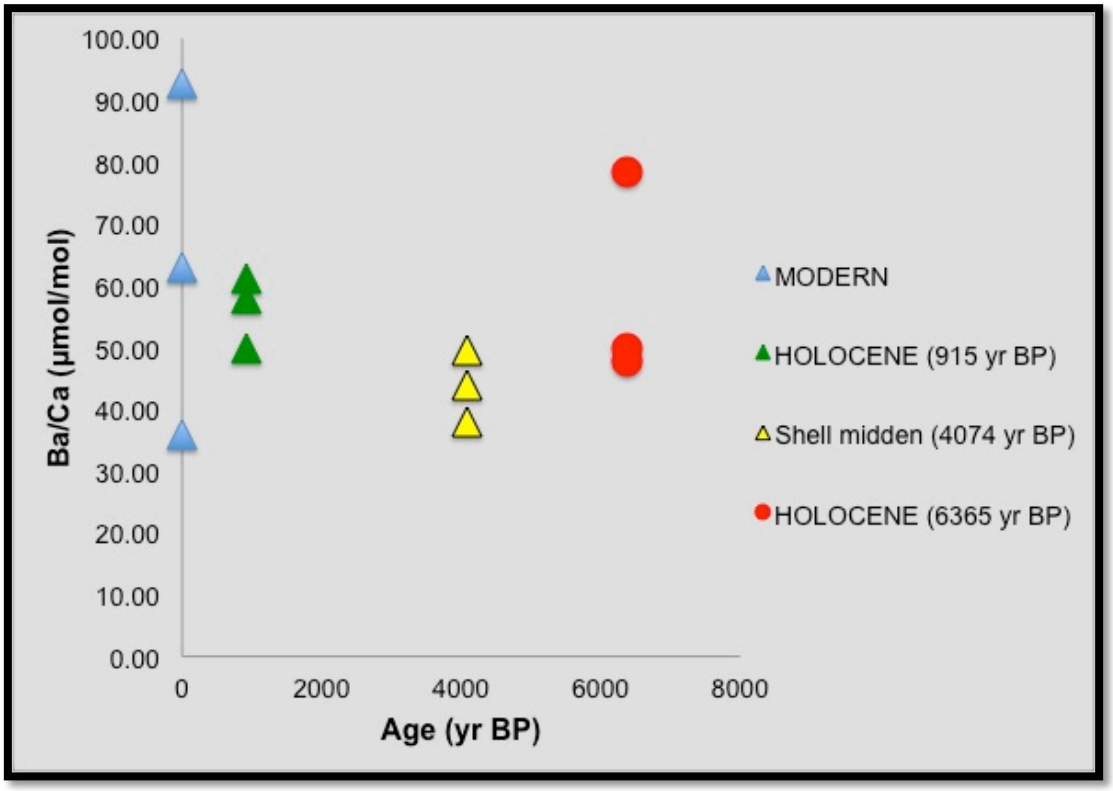

Figure 183 – Ba/Ca ratios of modern and Holocene Mytildae shells from Camarones North section.

Ba/Ca mean values of specimens sampled from all the three Holocene layers are rather homogeneous and substantially overlapping with the mean value of modern *Aulacomya atra* shells (Fig. 184).

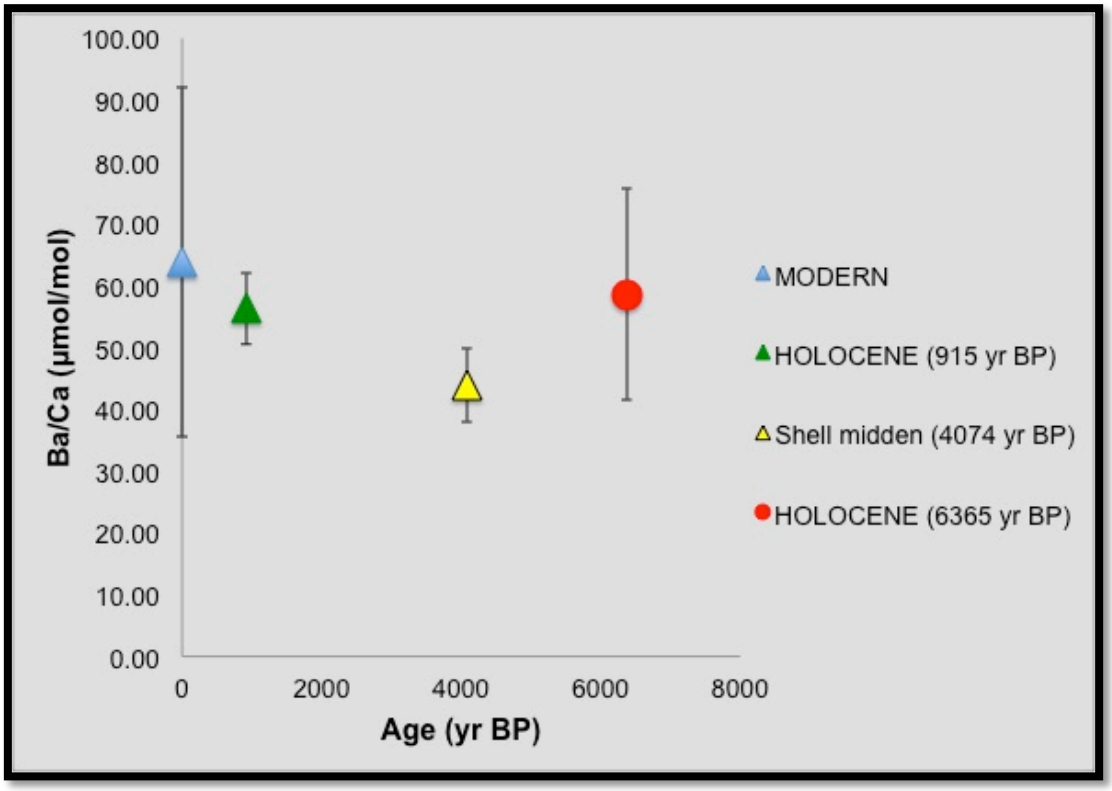

Figure 184 – Ba/Ca mean values and standard deviations of modern and Holocene *Aulacomya atra* and *Mytilus edulis* from Camarones North area.

Lower Fe/Ca contents are found in *Aulacomya atra* shells selected from the more recent Holocene beach ridge (ca. 18 µmol/mol) while the higher value was measured in a sample from the Holocene shell midden (102.59. µmol/mol). *Aulacomya atra* modern specimens present Fe/Ca ratios variable between 19.03 and 23.19 µmol/mol and mean value of 20.73±2.18 µmol/mol, the Holocene shells from the beach ridges dated to 915±20 yr BP have Fe/Ca ranging from 18.35 to 58.77 µmol/mol (mean value of 31.91±23.26 µmol/mol), from 60.46 to 102.59 µmol/mol, with mean value of 82.06±21.08 µmol/mol, for the specimens from the shell midden and from 66.48 to 96.83 µmol/mol (mean value of 81.34±15.19 µmol/mol) for the samples selected from the layer deposited 6365 years ago (Tab. 23 and Fig. 185).

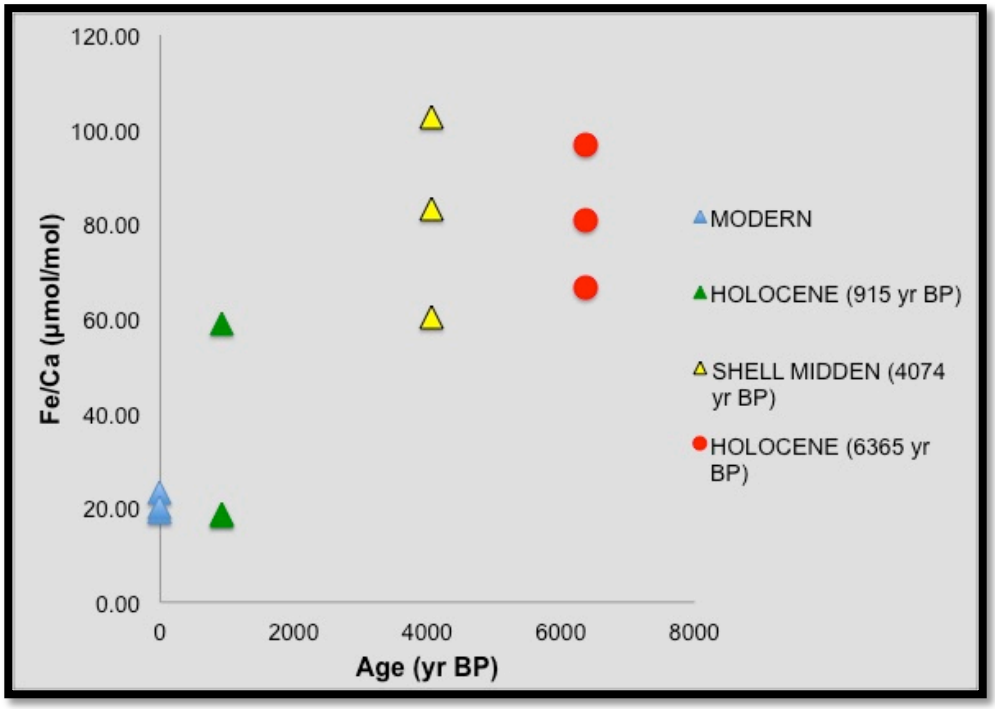

Figure 185 – Fe/Ca values of modern and Holocene Mytildae shells from Camarones North section.

Almost all the Holocene shells have higher Fe/Ca values than modern samples (Fig. 185 and Fig. 186). The mean values of the two older Holocene deposits are substantially the same (Fig. 186).

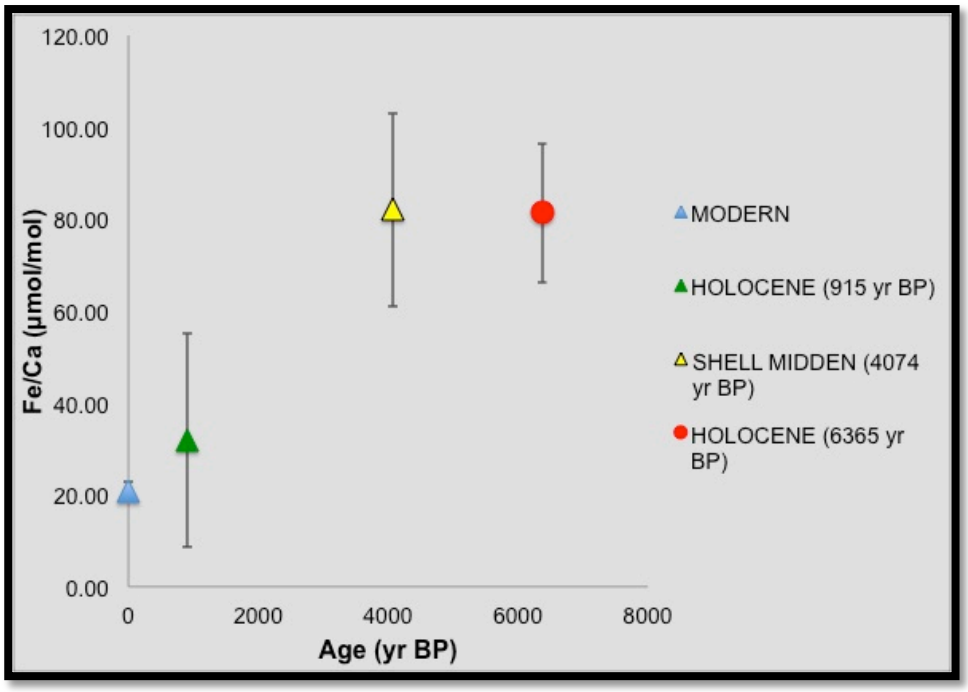

Figure 186 – Fe/Ca mean ratios and standard deviations of modern and Holocene *Aulacomya atra* and *Mytilus edulis* from Camarones North area.

Mytilus edulis shells selected from the beach ridge dated to 6365±20 yr BP show the higher Mg/Ca ratios, having values between 3941.54 and 4843.72 µmol/mol and mean value of 4417.34±453.11 µmol/mol (Tab. 23 and Figs. 187-188).

The more recent Holocene shells and the modern individuals present similar Mg/Ca content with values from 636.83 to 871.83 µmol/mol (mean value of 738.12±120.81 µmol/mol) for modern shells, from 858.28 and 961.56 µmol/mol (mean value of 897.30±56.07 µmol/mol) for the samples collected from the early Holocene beach ridge and from 650.72 to 1665.82 µmol/mol with mean value of 1094.82±518.85 µmol/mol for the shell midden dated to ca. 4070 yr BP (Tab. 23 and Figs. 187-188).

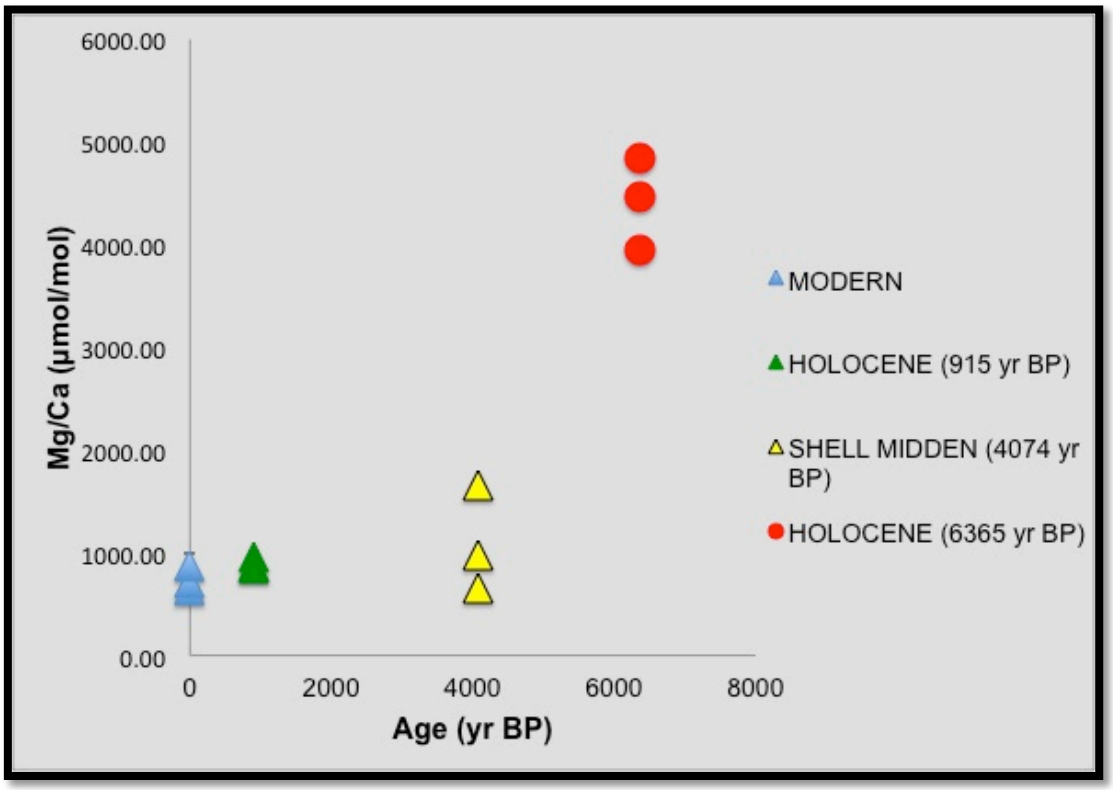

Figure 187 – Mg/Ca values of modern and Holocene Mytildae shells from Camarones North section.

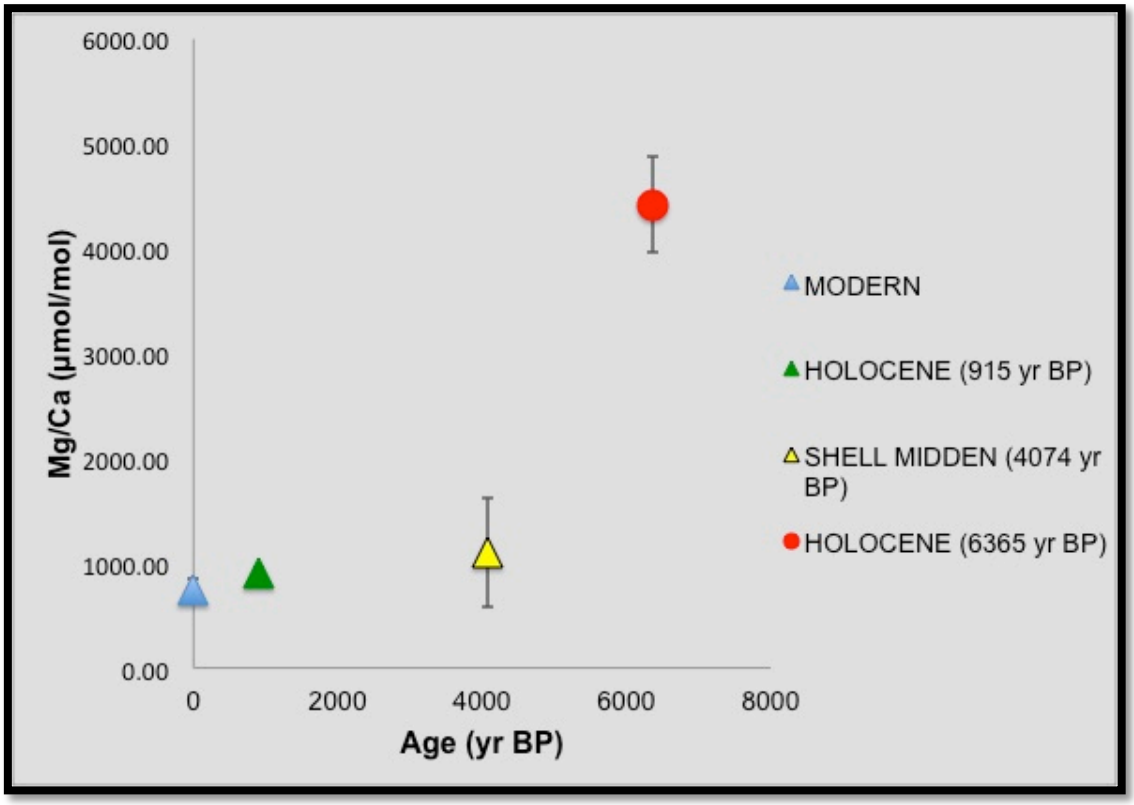

Figure 188 – Mg/Ca mean ratios and standard deviations of modern and Holocene *Aulacomya atra* and *Mytilus edulis* from Camarones North area.

The same trend observed for Mg/Ca is shown also for Mn/Ca ratios (Fig. 189 and Fig. 190).

In fact the modern and the younger Holocene deposits have the lower values of Mn/Ca, with ratios variable from 20.80 to 33.01 µmol/mol (mean value of 24.88±7.04 µmol/mol) measured in modern specimens, from 14.38 to 25.63 µmol/mol (mean value of 18.76±6.03 µmol/mol) for the *A. atra* samples coming from the beach ridge deposited ca. 900 years ago and from 14.4 to 22.88 µmol/mol (mean value of 18.40±4.23 µmol/mol) for the shells collected from the shell midden (Tab. 23). The Mn/Ca values obtained from the shells which yielded a radiocarbon age of 6365±20 yr BP, on the contrary, are up to ten times greater than the other Holocene and modern samples (Tab. 23), with ratios ranging from 88.82 to 140.01 µmol/mol and mean value of 109.85±28.79 µmol/mol (Fig. 189 and Fig. 190).

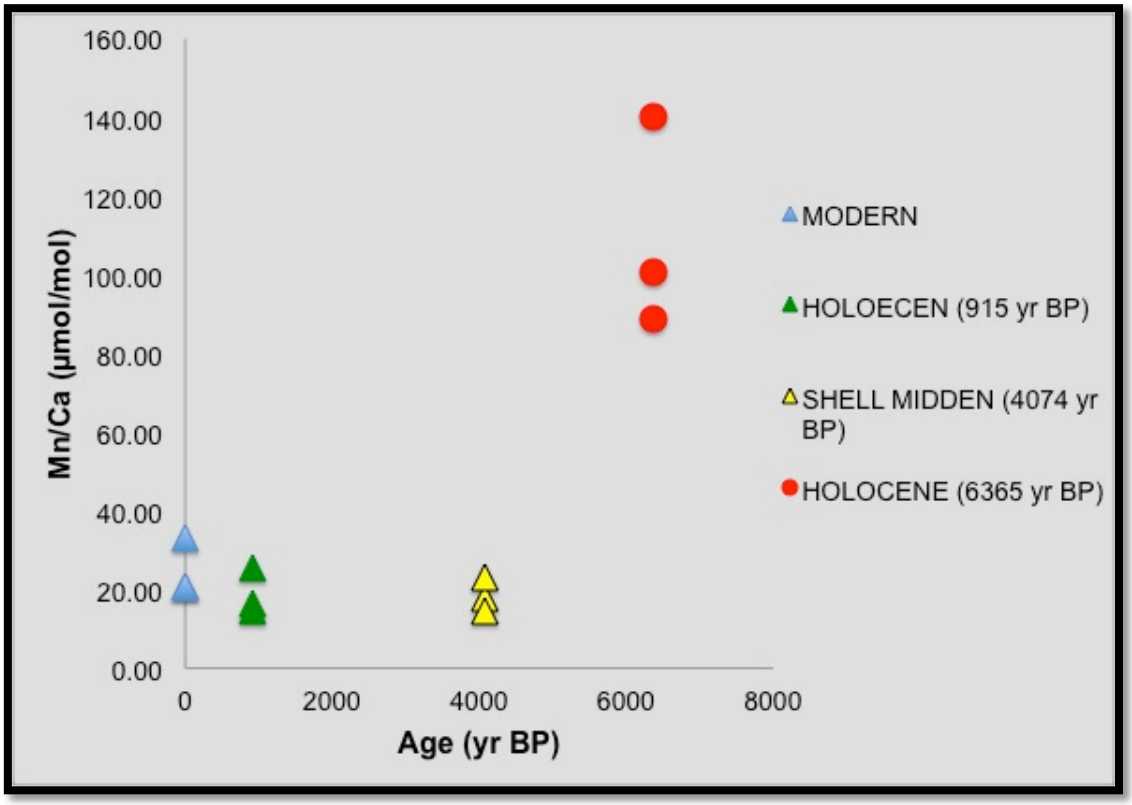

Figure 189 – Mn/Ca values of modern and Holocene Mytildae shells from Camarones North section.

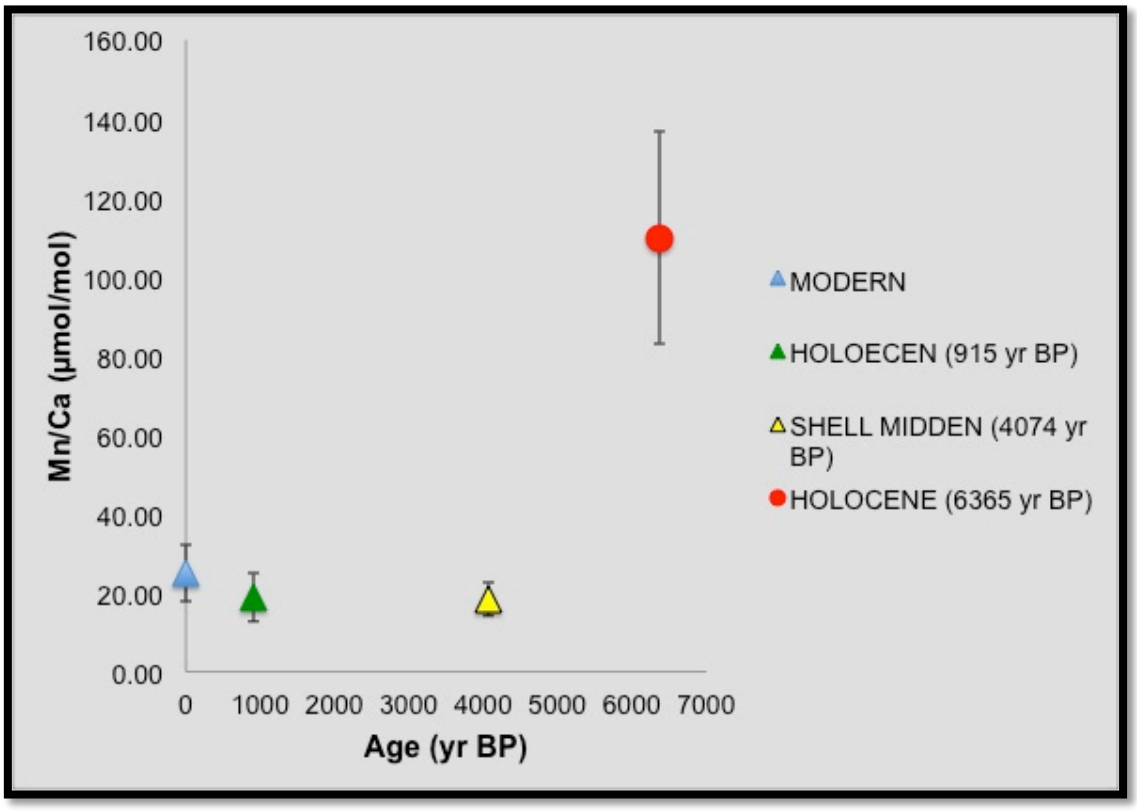

Figure 190 – Mn/Ca mean ratios and standard deviations of modern and Holocene *Aulacomya atra* and *Mytilus edulis* from Camarones North area.

Finally, modern shells of *Aulacomya atra* show Sr/Ca ratio between 5.79 and 7.81 mmol*10/mol (mean value of 6.53±1.1 mmol*10/mol), while Holocene specimens have values ranging from 5.39 to 10.17 mmol*10/mol (mean value of 8.03±2.43 mmol*10/mol), from 6.56 to 10.76 mmol*10/mol (mean value of 9.03±2.20 mmol*10/mol) and from 2.05 to 10.61 mmol*10/mol (mean value of 5.70±4.42 mmol*10/mol) respectively, going from the more recent to the older beach deposit, which show the large strontium variability (Tab. 23 and Fig. 191).

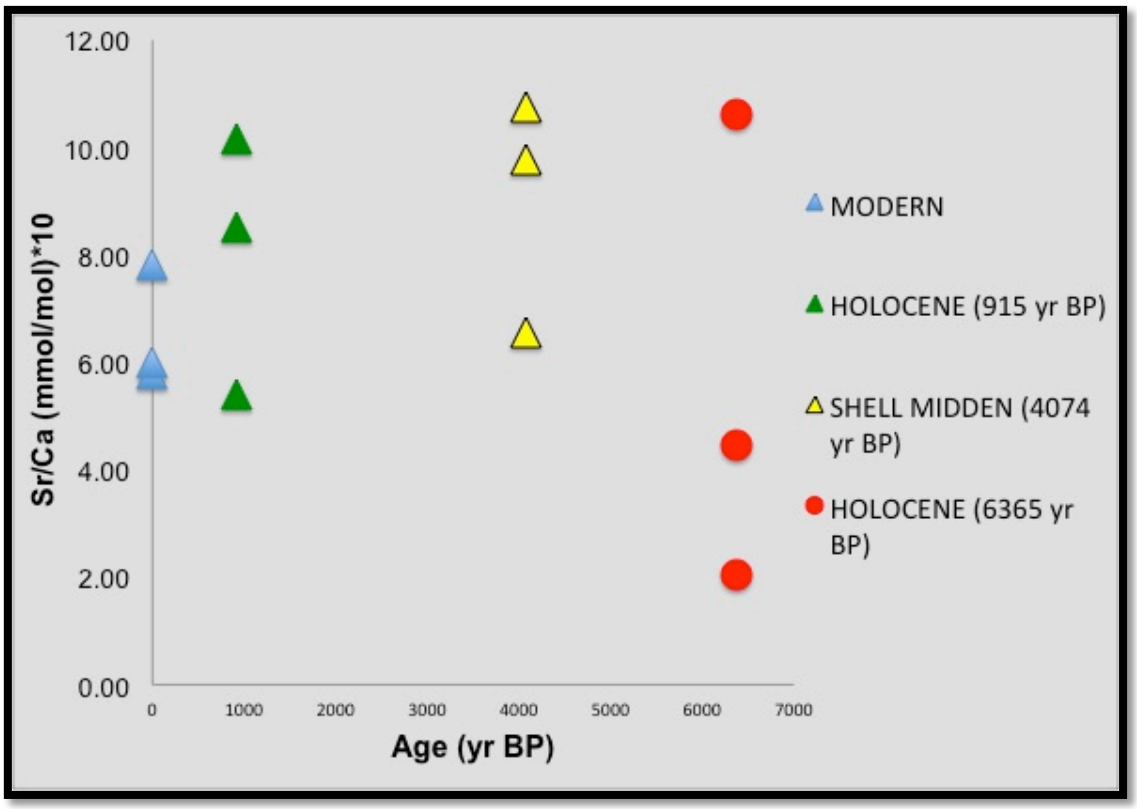

Figure 191 – Sr/Ca ratios of modern and Holocene Mytildae shells from Camarones North section.

No significant variation was observed comparing modern and Holocene shells belonging to the Mytilidae family as regards the strontium concentration (Fig. 192).

Figure 192 – Sr/Ca mean values and standard deviations of modern and Holocene *Aulacomya atra* and *Mytilus edulis* from Camarones North area.

6.4.3.2. Trace element composition of fossil *Ameghinomya antiqua* shells in Camarones area

In Camarones area trace element analysis was carried out on modern and fossil *Ameghinomya antiqua* shells (Tab. 24). The fossil samples come from a Middle Holocene beach ridge dated to 5676±45 yr BP and deposited south of Camarones village (WP 104, Fig. 127) and from four Pleistocene beach deposits, three of which were dated to MIS 5 (WP 64, WP 65 and WP 92) and one to MIS 11 (WP 97; see Chapter 6.3.3.1. and Figs. 149-150 for the location of the beach ridges).

SAMPLE	AGE (yr BP)	Ba/Ca (µmol/mol)	Fe/Ca (µmol/mol)	Mg/Ca (µmol/mol)	Mn/Ca (µmol/mol)	Sr/Ca (mmol/mol)*10	U/Ca (µmol*10/mol)
WP60BBIS(1)	modern beach	4.23	29.10	557.23	0.74	17.47	0.67
WP60BBIS(2)	modern beach	2.01	68.46	547.59	4.92	9.14	0.68
WP60BBIS(3)	modern beach	26.40	56.15	537.92	3.33	17.06	0.00
WP623BIS(1)	modern beach	18.94	52.49	429.04	2.90	17.76	1.54
WP623BIS(2)	modern beach	22.95	19.06	380.36	2.08	17.58	1.84
WP95(2)	modern beach	4.28	27.22	767.34	2.51	10.64	0.98
WP95(3)	modern beach	19.97	46.95	536.43	4.06	18.35	0.35
WP110(1)	modern beach	10.09	53.74	281.84	1.62	11.67	5.58
WP110(2)	modern beach	3.94	37.23	211.19	1.07	15.48	0.68
mean value		**12.53**	**43.38**	**472.11**	**2.58**	**15.02**	**1.37**
standard deviation		9.52	16.16	167.01	1.38	3.55	1.68
WP104A(2)	5675±45	12.43	5.91	203.70	1.46	20.08	7.16
WP104A(3)	5675±45	5.94	5.10	225.80	1.23	19.05	4.87
WP104A(4)	5675±45	9.31	9.23	192.73	1.75	17.40	5.30
mean value		**9.23**	**6.74**	**207.41**	**1.48**	**18.84**	**5.78**
standard deviation		3.25	2.19	16.84	0.26	1.35	1.21
WP92A(1)	92000±600	7.26	15.00	220.43	1.65	30.15	3.44
WP92A(2)	92000±600	5.59	8.64	182.33	0.82	33.80	3.59
WP92A(3)	92000±600	25.41	19.40	239.53	1.53	29.71	3.56
mean value		**12.76**	**14.35**	**214.10**	**1.33**	**31.22**	**3.53**
standard deviation		10.99	5.41	29.12	0.45	2.24	0.08
WP64B(1)	121000±900	36.80	13.95	341.18	1.56	27.41	2.74
WP64B(2)	121000±900	31.52	13.05	911.85	1.13	25.39	1.41
WP64B(3)	121000±900	30.52	8.19	190.86	0.93	23.56	1.22
mean value		**32.95**	**11.73**	**481.29**	**1.21**	**25.45**	**1.79**
standard deviation		3.37	3.10	380.37	0.32	1.92	0.83
WP65(2)	130000±2500	11.54	15.66	278.35	1.54	24.11	10.69
WP65(3)	130000±2500	29.05	34.88	270.13	10.88	32.01	10.22
WP65(4)	130000±2500	42.79	44.82	268.47	3.65	24.96	8.10
mean value		**27.79**	**31.79**	**272.32**	**5.35**	**27.03**	**9.67**
standard deviation		15.66	14.83	5.29	4.90	4.33	1.38
WP97(1)	414000±16000	3.80	12.86	216.04	1.82	27.25	7.61
WP97(2)	414000±16000	0.81	5.98	149.71	0.83	19.22	8.69
WP97(3)	414000±16000	22.25	5.34	162.10	0.84	18.50	8.58
mean value		**8.95**	**8.06**	**175.95**	**1.16**	**21.65**	**8.29**
standard deviation		11.61	4.17	35.27	0.57	4.85	0.60

Table 24 – Metal/Ca ratios, mean values and standard deviations of modern and fossil shells of *Ameghinomya antiqua* from Camarones area.

Ba/Ca is the metal/Ca ratio showing the greater variability in modern and fossil shells from Camarones area (Tab. 24). Modern samples, in fact, have Ba/Ca values ranging from 2.01 to 26.40 µmol/mol and a mean value of 12.53±9.52 µmol/mol. Ba/Ca in Holocene shells is between 5.94 and 12.43 µmol/mol, with a mean value of 9.23±3.35 µmol/mol. The Pleistocene specimens collected to beach ridges dated to MIS 5 show values variable between 5.59 and 25.41 µmol/mol (mean value of 12.76±10.99 µmol/mol), between 30.52 and 36.80 µmol/mol (mean value of 32.95±3.37µmol/mol) and between 11.54 and 42.79 µmol/mol (mean value of 27.79±15.66 µmol/mol). The Ba/Ca of shells from the older Pleistocene beach ridge

deposited during MIS 11 ranges from 0.81 to 22.25 µmol/mol, with a mean value of 8.95±11.61 µmol/mol (Tab. 24 and Figs. 193-194).

Almost all the Ba/Ca ratios of the fossil shells fall within the range of values of the modern samples (Fig. 189), but the specimens selected from the deposit dated at 121 ka BP show slightly higher values than the modern ones (Fig. 194).

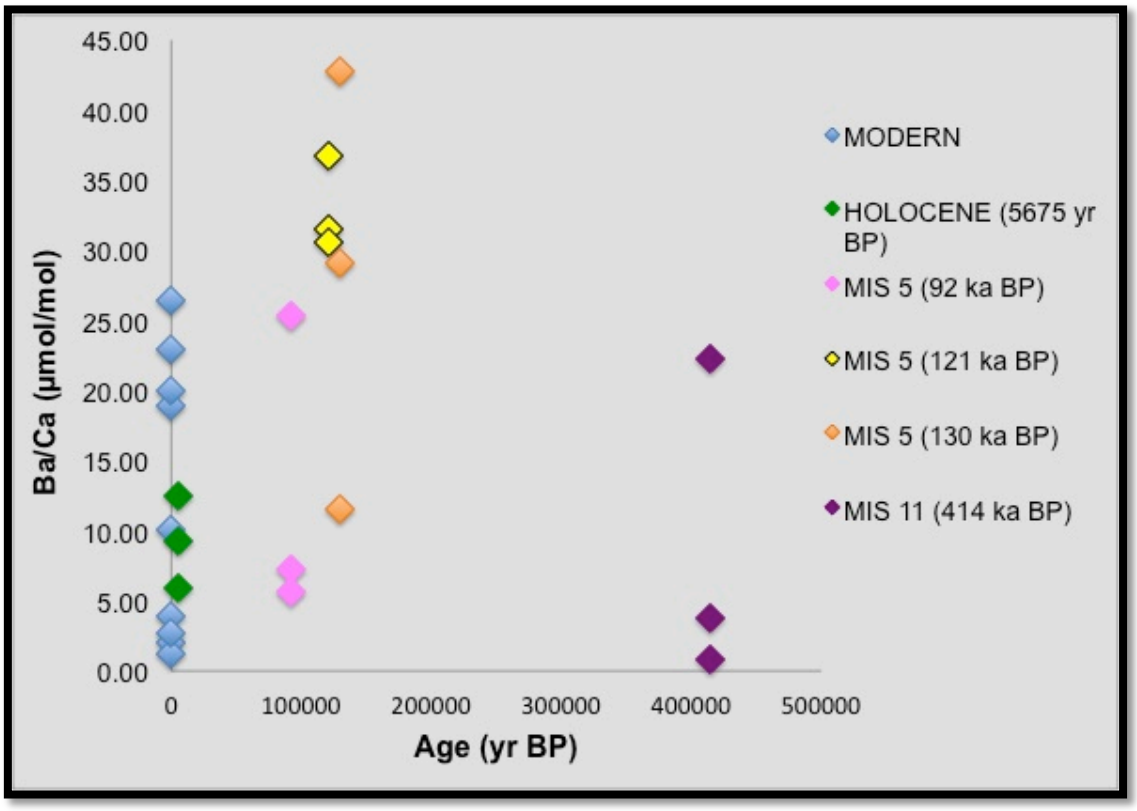

Figure 193 – Ba/Ca ratios of modern and fossil *A. antiqua* shells from Camarones area.

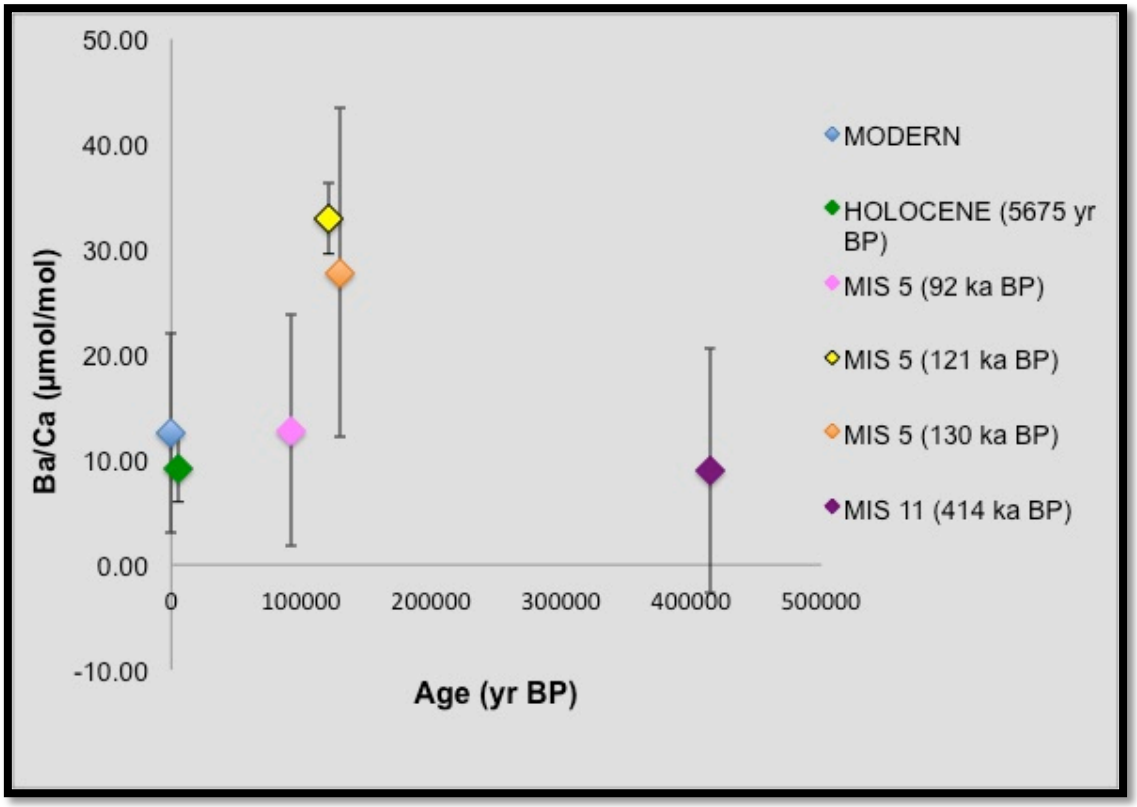

Figure 194 – Ba/Ca mean values and standard deviations of modern and fossil *Ameghinomya antiqua* shells from Camarones area.

The shells collected from the top active beach (modern) show the higher Fe/Ca ratios compared to the fossil specimens (Tab. 24 and Figs. 195-196), having values between 19.06 and 68.46 µmol/mol (mean value of 43.38±16.16 µmol/mol). The fossil samples, going from the youngest to the oldest deposit, show Fe/Ca values between 5.10 and 9.23 µmol/mol (mean value of 6.74±2.19 µmol/mol), between 8.64 and 19.40 µmol/mol (mean value of 14.35±5.41 µmol/mol), between 8.19 and 13.95 µmol/mol (mean value of 11.63±3.10 µmol/mol), between 15.66 and 44.82 µmol/mol (mean value of 31.79±14.83 µmol/mol) and between 5.34 and 12.86 µmol/mol (mean value of 8.06±4.17 µmol/mol) respectively (Fig. 195).

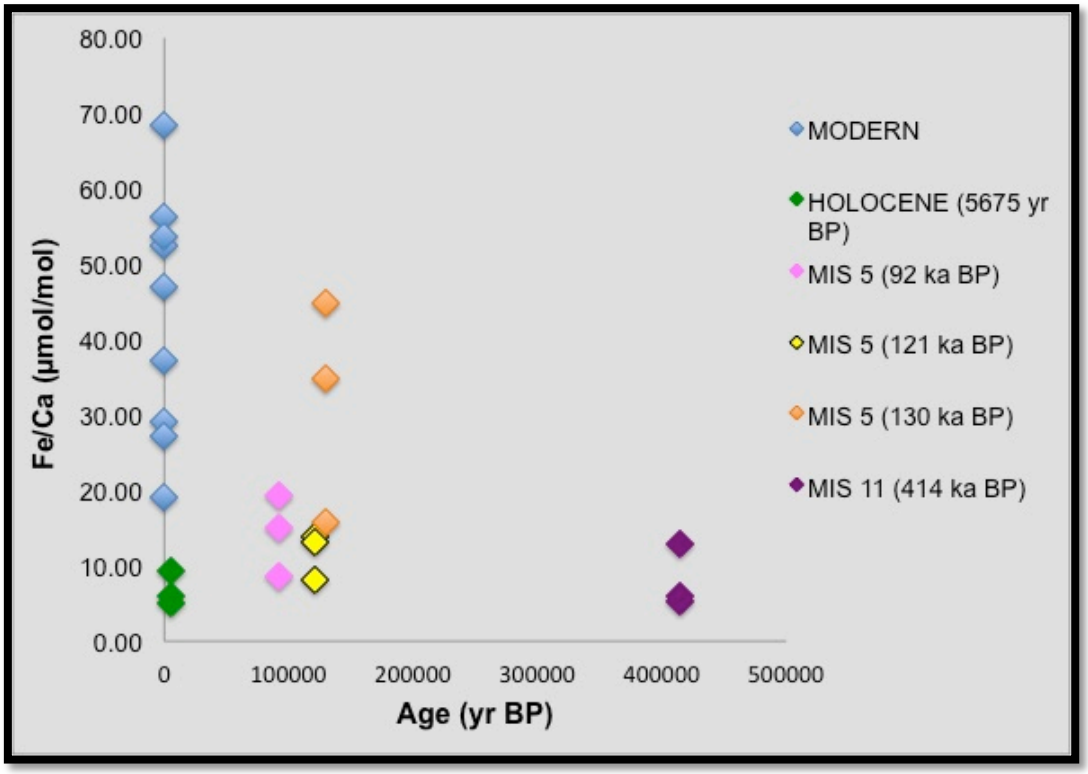

Figure 195 – Fe/Ca ratios of modern and fossil *A. antiqua* shells from Camarones area.

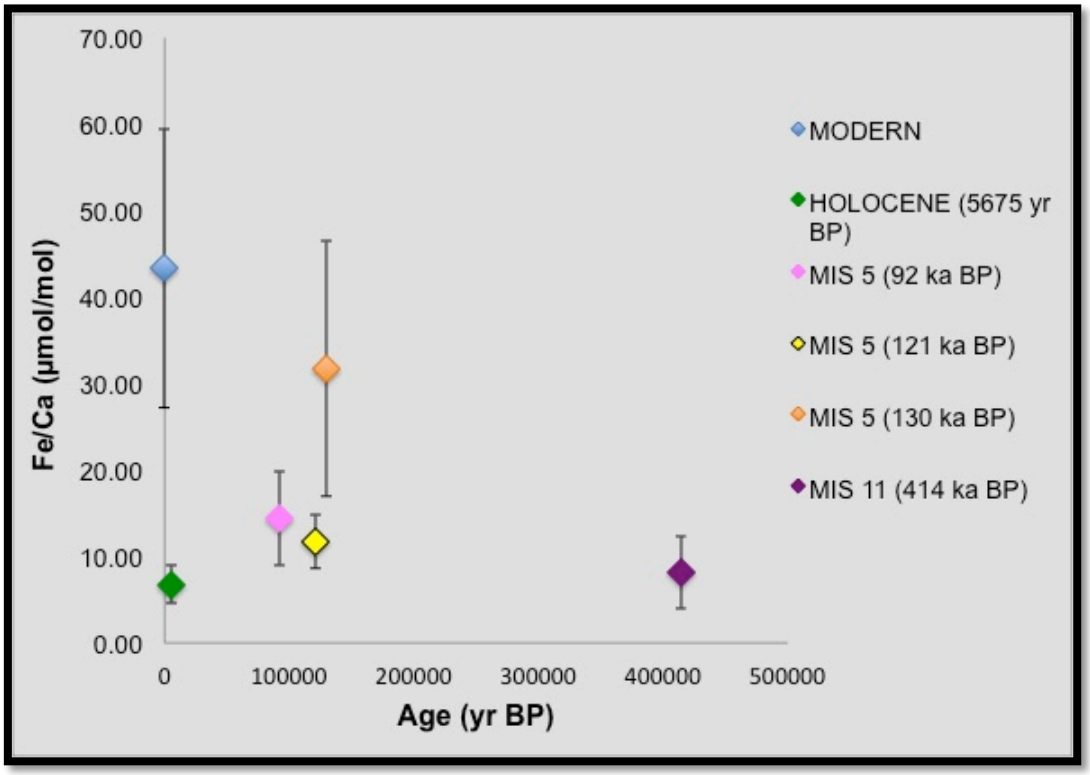

Figure 196 – Fe/Ca mean values and standard deviations of modern and fossil *Ameghinomya antiqua* shells from Camarones area.

Modern *A. antiqua* samples with respect to fossil shells also have a content slightly higher Mg/Ca content, with the exception of a specimen collected from the beach ridge dated at 121 ka BP (Fig. 197).

Modern samples, in fact, show Mg/Ca values ranging from 211.19 to 767.34 µmol/mol and a mean value of 472.11±167.01 µmol/mol. Mg/Ca in the Holocene shells is between 192.73 and 225.80 µmol/mol, with a mean value of 207.41±16.84 µmol/mol. The Pleistocene specimens collected in beach ridges dated to MIS 5 show values variable between 182.33 and 239.53 µmol/mol (mean value of 214.10±29.12 µmol/mol), between 190.86 and 911.85 µmol/mol (mean value of 481.29±380.37µmol/mol) and between 268.47 and 278.35 µmol/mol (mean value of 272.32±5.29 µmol/mol). The Mg/Ca values of shells from the older Pleistocene beach ridge deposited during MIS 11 ranges from 149.71 to 216.04 µmol/mol, with a mean value of 175.95±35.27 µmol/mol (Tab. 24 and Figs. 197-198).

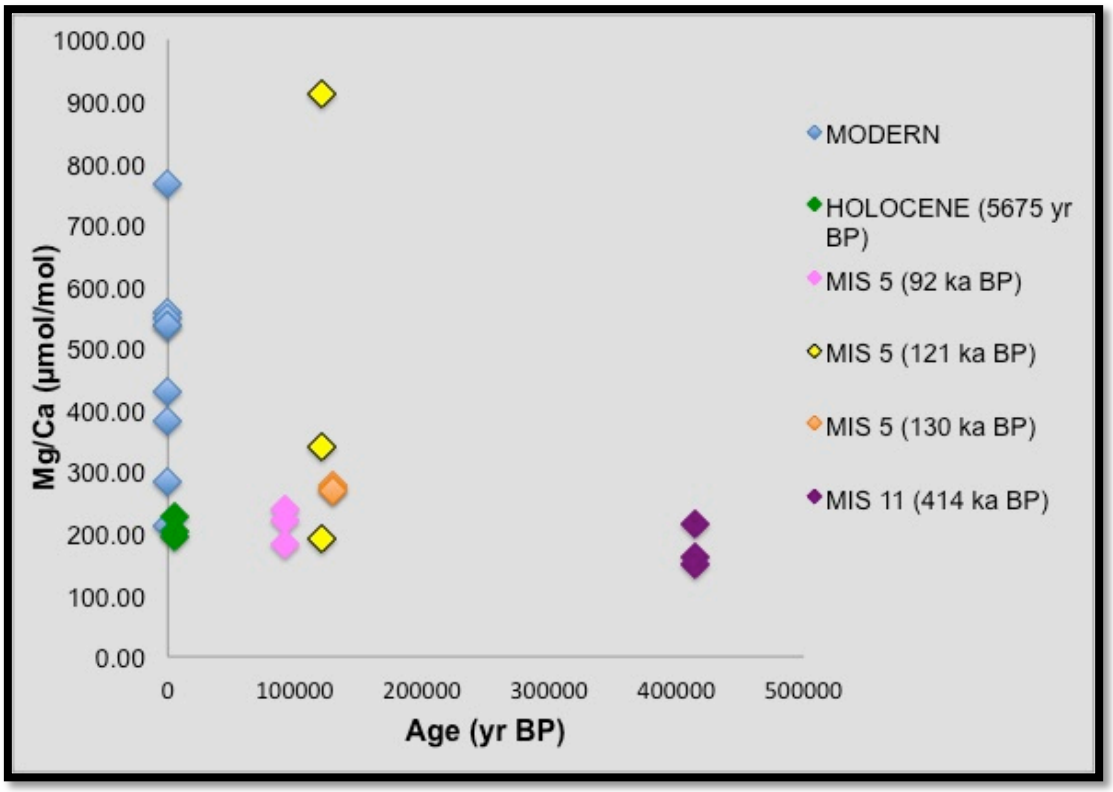

Figure 197 – Mg/Ca ratios of modern and fossil *A. antiqua* shells from Camarones area.

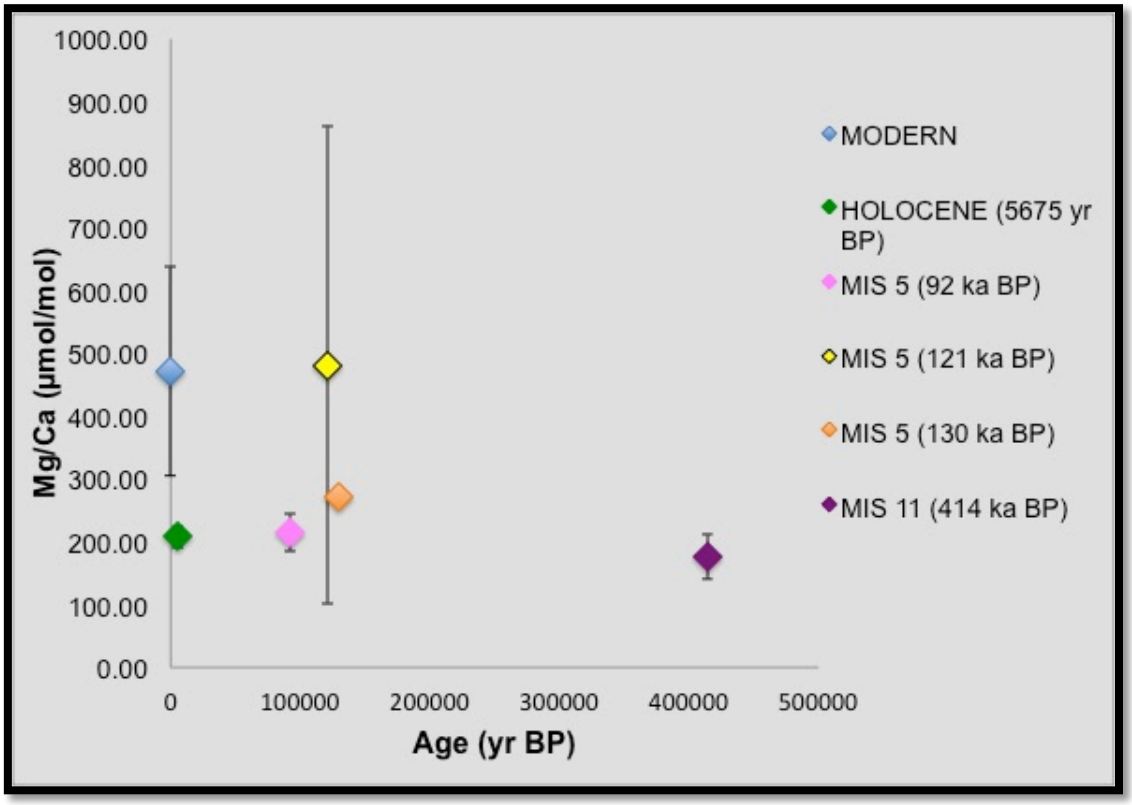

Figure 198 – Mg/Ca mean values and standard deviations of modern and fossil *Ameghinomya antiqua* shells from Camarones area.

Ameghinomya antiqua shells sampled from the modern beach show Mn/Ca ratios between 0.74 and 4.92 µmol/mol, with a mean value of 2.58±1.38 µmol/mol. Mn/Ca in the Holocene samples ranges between 1.23 and 1.75 µmol/mol, with a mean value of 1.48±0.26 µmol/mol. The Pleistocene specimens collected to beach ridges dated to the last interglacial period show values variable between 0.82 and 1.65 µmol/mol (mean value of 1.33±0.45 µmol/mol), between 0.93 and 1.56 µmol/mol (mean value of 1.21±0.32 µmol/mol) and between 1.54 and 10.88 µmol/mol (mean value of 5.35±4.90 µmol/mol). The Mn/Ca values of shells from the MIS 11 beach ridge ranges from 0.83 to 1.82 µmol/mol, with a mean value of 1.16±0.57 µmol/mol (Tab. 24 and Figs. 199-200).

Mn/Ca content in modern and fossil Camarones shells is fairly homogeneous in all the samples analyzed (Tab. 24 and Fig. 199), with small differences substantially overlapping (Fig. 200).

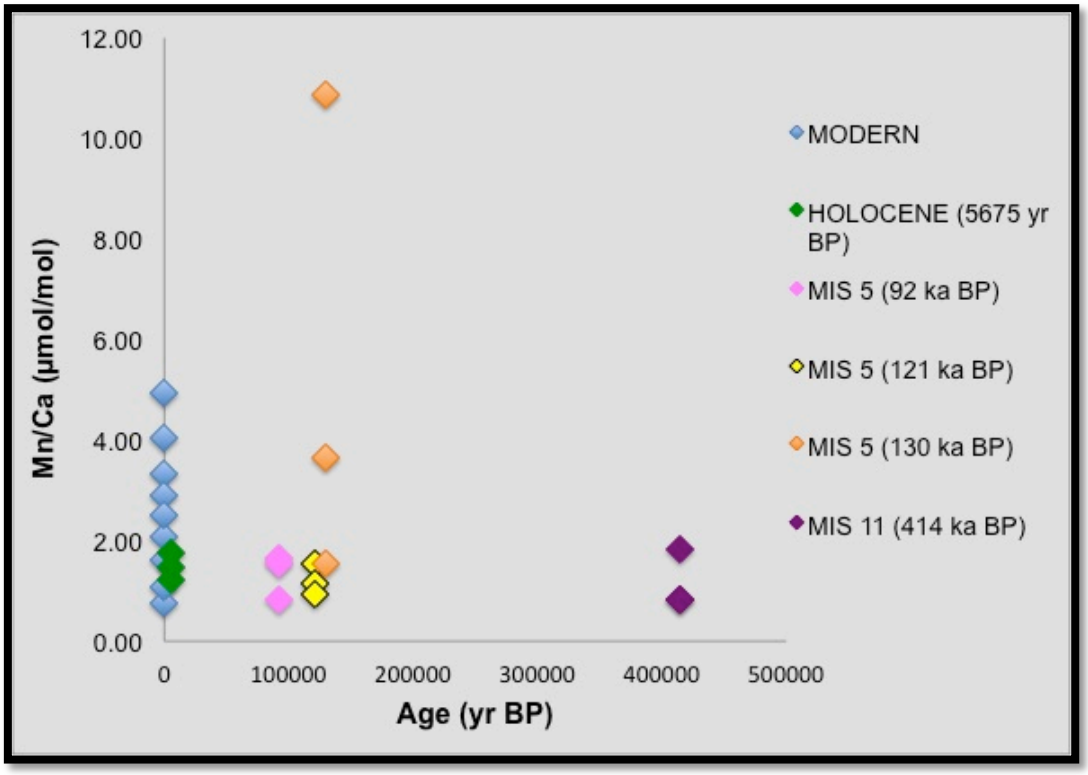

Figure 199 – Mn/Ca ratios of modern and fossil *A. antiqua* shells from Camarones area.

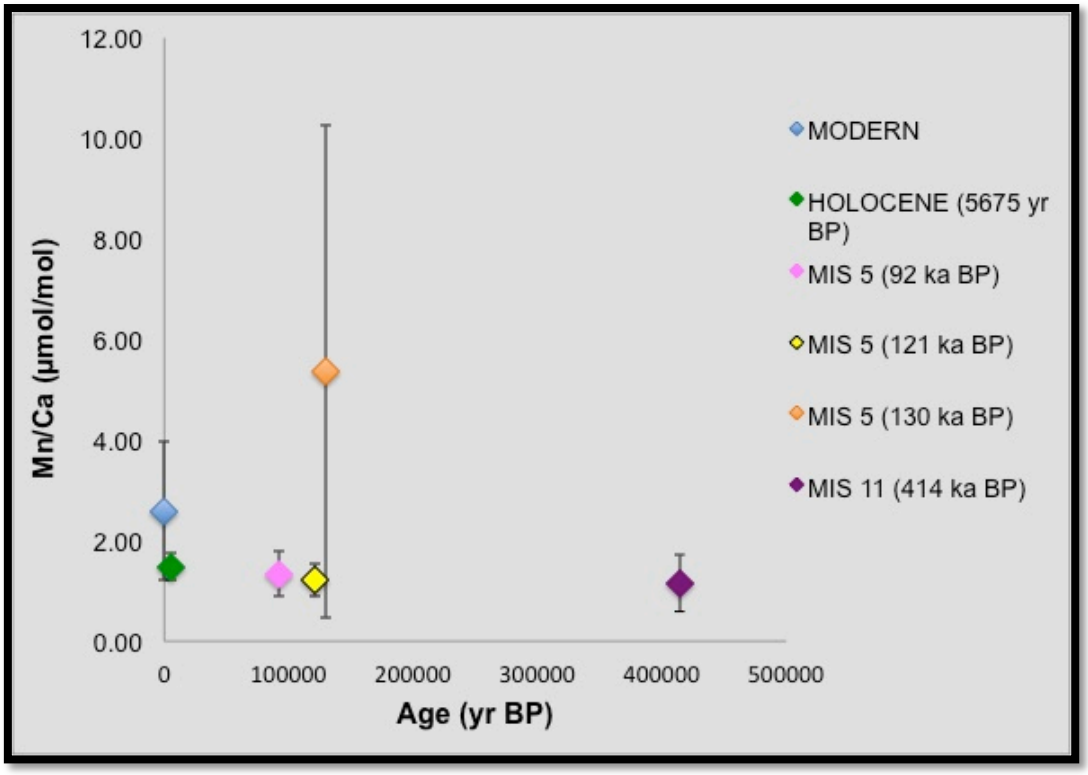

Figure 200 – Mn/Ca mean values and standard deviations of modern and fossil *Ameghinomya antiqua* shells from Camarones area.

Sr/Ca in modern shells collected in Camarones area ranges from 9.14 to 18.35 mmol*10/mol (mean value of 15.02±3.55 mmol*10/mol), in Holocene shells varies from 17.40 to 20.08 mmol*10/mol (mean value of 18.84±1.35 mmol*10/mol), in specimens dated to 92 ka BP is between 29.71 and 33.80 mmol*10/mol (mean value of 31.22±2.24 mmol*10/mol), in those dated to 121 ka BP is between 23.56 and 27.41 mmol*10/mol (mean value of 25.45±1.92 mmol*10/mol), in individuals sampled from the beach ridge dated to 130 ka BP ranges from 24.11 to 32.01 mmol*10/mol (mean value of 27.03±4.33 mmol*10/mol) and, finally, the shells from MIS 9 beach deposit have values from 18.50 to 27.25 mmol*10/mol, with a mean value of 21.65±4.85 mmol*10/mol (Tab. 24 and Figs. 201-202).

The Pleistocene shells, in particular the specimens collected from the beach ridges deposited during the Marine Isotope Stage 5, show Sr/Ca ratios higher than modern and Holocene samples (Figs. 201-202).

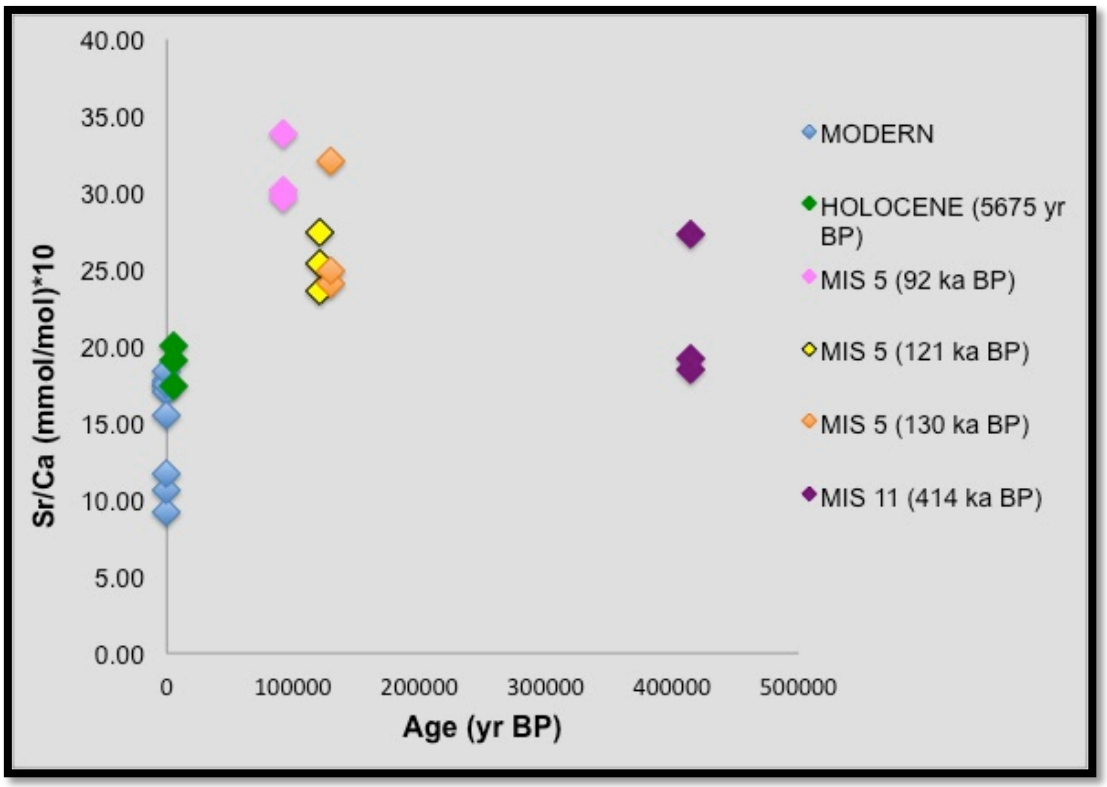

Figure 201 – Sr/Ca ratios of modern and fossil *A. antiqua* shells from Camarones area.

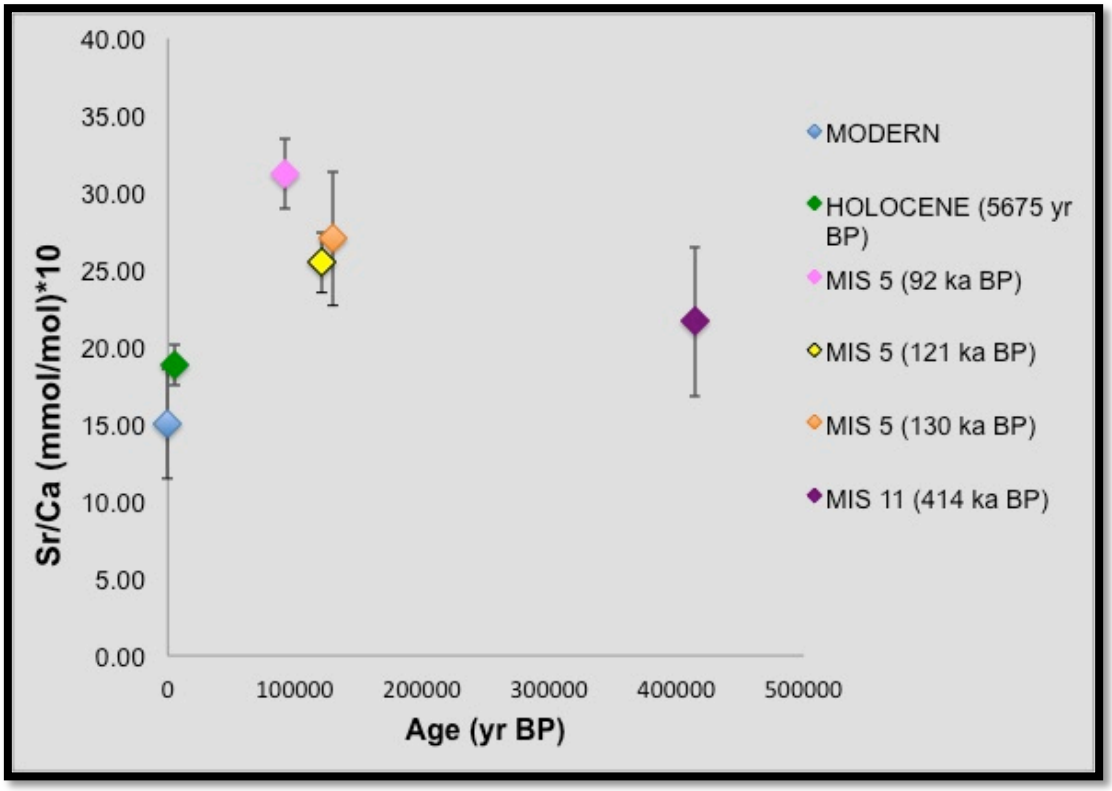

Figure 202 – Sr/Ca mean values and standard deviations of modern and fossil *Ameghinomya antiqua* shells from Camarones area.

Ameghinomya antiqua shells selectioned from the modern beach show U/Ca ratios between 0.0 and 5.58 µmol*10/mol, with a mean value of 1.37±1.68 µmol*10/mol. U/Ca in the Holocene samples increases and ranges between 4.37 and 7.16 µmol*10/mol, with a mean value of 5.78±1.21µmol*10/mol. The Pleistocene specimens collected to beach ridges dated to the last interglacial period show values variable between 3.44 and 3.59 µmol*10/mol (mean value of 3.53±0.08 µmol*10/mol), between 1.22 and 2.74 µmol*10/mol (mean value of 1.79±0.83 µmol*10/mol) and between 8.10 and 10.69 µmol*10/mol (mean value of 9.67±1.36 µmol*10/mol). The U/Ca values of shells from the MIS 11 beach ridge ranges from 7.61 to 8.69 µmol*10/mol, with a mean value of 8.29±0.60 µmol*10/mol (Tab. 24 and Figs. 203-204).

Except for the shells sampled from the Pleistocene beach ridge dated at 121 ka BP, showing values similar to the modern samples (Fig. 203), all fossil specimens have U/Ca ratios higher than the modern ones (Fig. 203 and Fig. 204).

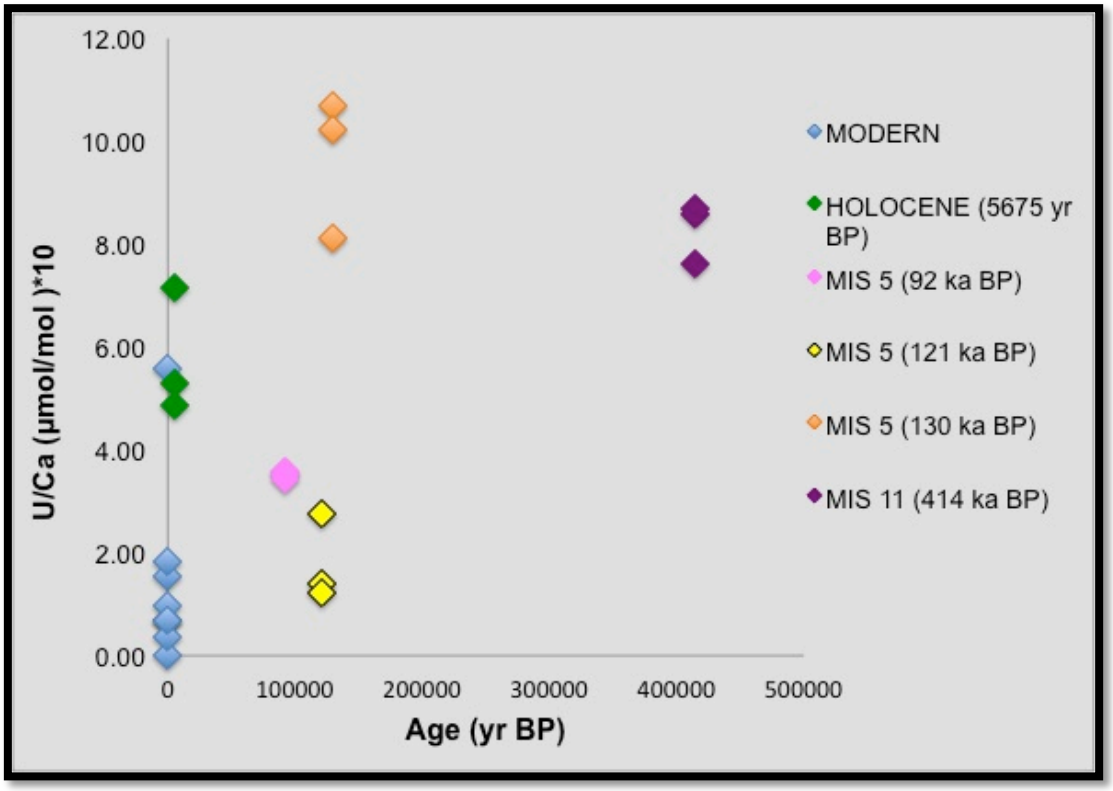

Figure 203 – U/Ca ratios of modern and fossil *A. antiqua* shells from Camarones area.

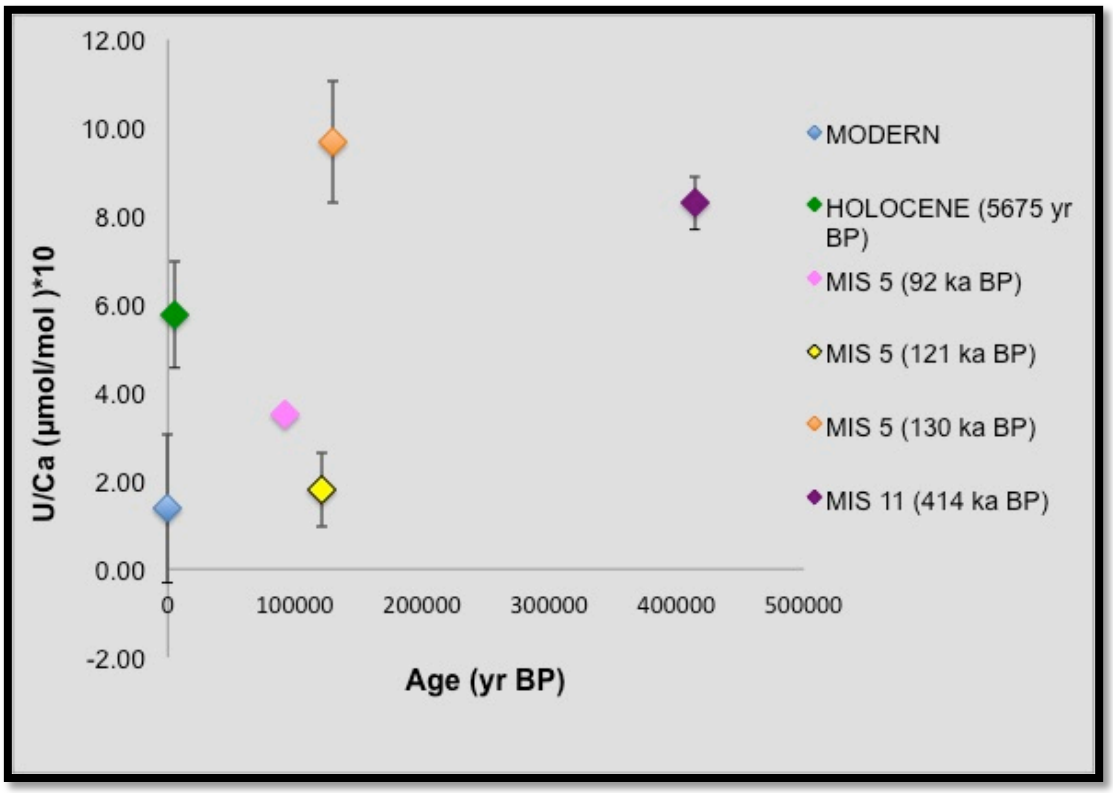

Figure 204 – U/Ca mean values and standard deviations of modern and fossil *Ameghinomya antiqua* shells from Camarones area.

6.4.3.3. Trace element composition of fossil *Ameghinomya antiqua* shells in Bahia Bustamante area

In Bahia Bustamante area trace element analysis was performed on modern and fossil *Ameghinomya antiqua* shells (Tab. 25). The fossil samples were collected from a Middle Holocene beach ridge dated to 5276±47 yr BP (WP 139, Fig. 135) and from four Pleistocene beach deposits, two of which was dated to MIS 5 (WP 149 and WP 154), one to MIS 7 (WP 176BIS) and one to MIS 9 (WP 197; see Chapter 6.3.3.2. and Fig. 154 for the location of the Pleistocene beach ridges).

SAMPLE	AGE (yr BP)	Ba/Ca (µmol/mol)	Fe/Ca (µmol/mol)	Mg/Ca (µmol/mol)	Mn/Ca (µmol/mol)	Sr/Ca (mmol/mol)*10	U/Ca (µmol*10/mol)
WP237(1)	modern beach	2.73	15.43	530.80	0.00	15.69	0.35
WP237(2)	modern beach	3.82	21.96	416.98	0.25	14.46	0.42
WP237(4)	modern beach	27.46	16.31	451.72	1.50	25.82	0.63
mean value		**11.34**	**17.90**	**466.50**	**0.58**	**18.66**	**0.47**
standard deviation		13.97	3.55	58.33	0.80	6.23	0.14
WP139(2)	5276 ± 47	15.90	26.9266	443.49		11.18	0.82
WP139(4)	5276 ± 47	13.87	16.8143	417.51	0.37	11.70	0.78
mean value		**14.88**	**21.87**	**430.50**		**11.44**	**0.80**
standard deviation		1.44	7.15	18.37		0.36	0.03
WP149(1)	T1 MIS 5 89000 ± 800	8.71	13.4411	558.18		15.37	0.87
WP149(2)	T1 MIS 5 89000 ± 800	8.00	32.3356	436.87		16.63	0.96
WP149(3)	T1 MIS 5 89000 ± 800	0.90	16.2629	525.45		21.33	0.83
mean value		**5.87**	**20.68**	**506.83**		**17.78**	**0.89**
standard deviation		4.32	10.19	62.76		3.14	0.07
WP154A(1)	T3 MIS 5	1.61	26.9541	280.58		17.96	3.83
WP154A(2)	T3 MIS 5	3.72	32.6742	231.98	0.29	14.41	5.75
mean value		**2.66**	**29.81**	**256.28**		**16.18**	**4.79**
standard deviation		1.49	4.04	34.37		2.51	1.35
WP176BIS(1)	MIS7	4.36	22.3993	297.75	0.34	17.77	6.98
WP176BIS(2)	MIS7	1.62	32.8984	319.40		14.50	6.23
WP176BIS(3)	MIS7	4.22	25.8055	347.15		21.78	4.64
mean value		**3.40**	**27.03**	**321.44**	**0.34**	**18.02**	**5.95**
standard deviation		1.54	5.36	24.76		3.64	1.19
WP197(1)	MIS 9	9.42	54.1414	279.77	0.12	12.93	0.01
WP197(2)	MIS 9	0.92	20.2764	241.13		15.78	7.60
mean value		**5.17**	**37.21**	**260.45**		**14.36**	**3.80**
standard deviation		6.01	23.95	27.32		2.01	5.37

Table 25 – Metal/Ca ratios, mean values and standard deviations of modern and fossil shells of *Ameghinomya antiqua* from Bahia Bustamante area.

Ba/Ca in modern shells selected from active beach in Bahia Bustamante area ranges from 2.73 to 27.46 µmol/mol (mean value of 11.34±13.97 µmol/mol), in Holocene samples varies from 13.97 to 15.90 µmol/mol (mean value of 14.88±1.44 µmol/mol), in specimens dated to 89 ka BP is between 0.90 and 8.71 µmol/mol (mean value of 5.87±4.32 µmol/mol), in those coming from MIS Terrace 3 is between 1.61 and 3.72 µmol/mol (mean value of 2.66±1.49 µmol/mol), in individuals sampled from the beach ridge dated to MIS 7 ranges from 1.62 to 4.36 µmol/mol (mean value of 3.40±1.54 µmol/mol) and, finally, the shells from MIS 9 beach deposit have values from 0.92 to 9.42 µmol/mol, with a mean value of 5.17±6.01 µmol/mol (Tab. 25 and Figs. 205-206).

As in the case of Camarones, even the shells of *Ameghinomya antiqua* collected in actual beach of Bahia Bustamante show a great variability in the ratio Ba/Ca (Fig. 206). The samples taken from the various fossil beach ridges instead show low Ba/Ca content more homogeneous, which is within the range of values of the specimens present (Fig. 206). Holocene shells have a slightly higher Ba/Ca ratio than the Pleistocene samples.

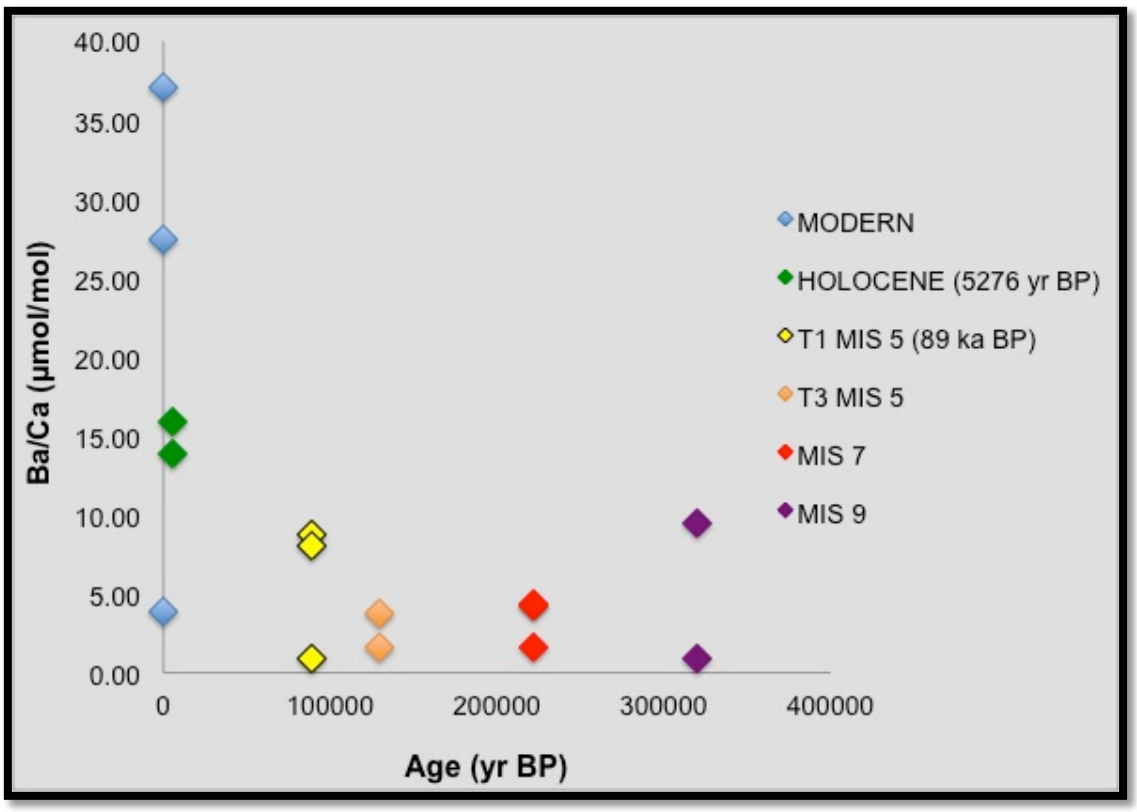

Figure 205 – Ba/Ca ratios of modern and fossil *A. antiqua* shells from Bahia Bustamante area.

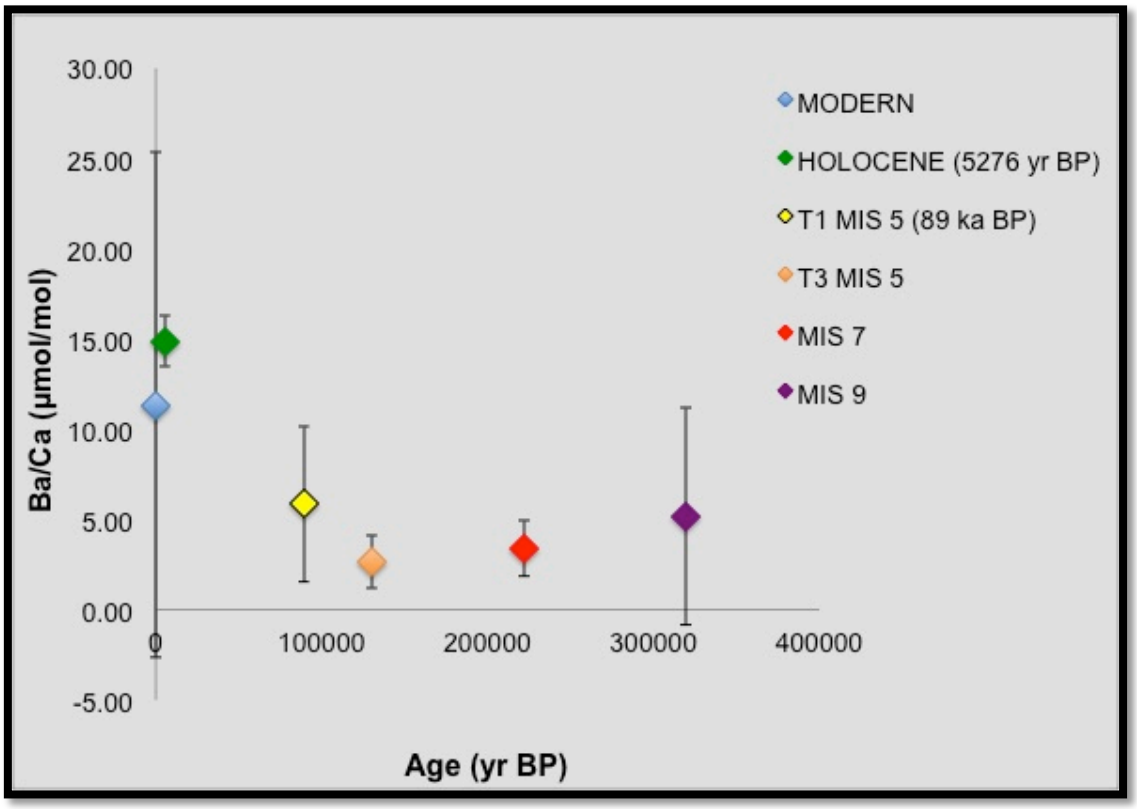

Figure 206 – Ba/Ca mean values and standard deviations of modern and fossil *Ameghinomya antiqua* shells from Bahia Bustamante area.

Fe/Ca ratio varies from 15.43 to 21.96 µmol/mol in the modern shells, which show a mean value of 17.90±3.55 µmol/mol; from 16.81 to 26.93 µmol/mol (mean value of 21.87±7.15 µmol/mol) in Holocene samples; from 13.44 to 32,34 µmol/mol and from 26.95 to 32.67 µmol/mol for the shells collected from beach ridges deposited during the Marine Isotope Stage 5, which have mean values of 20.68±10.19 µmol/mol and 29.81±4.04 µmol/mol respectively; from 22.90 to 32.90 µmol/mol (mean value of 27.03±5.36 µmol/mol) for the shells from MIS 7 deposit and from 20.28 to 54.14 for the samples selected from MIS 9 beach ridge (Tab. 25 and Fig. 207).

A. antiqua shells show overall very small differences in Fe content substantially overlapping in terms of Fe/Ca ratios (Fig. 207 and Fig. 208).

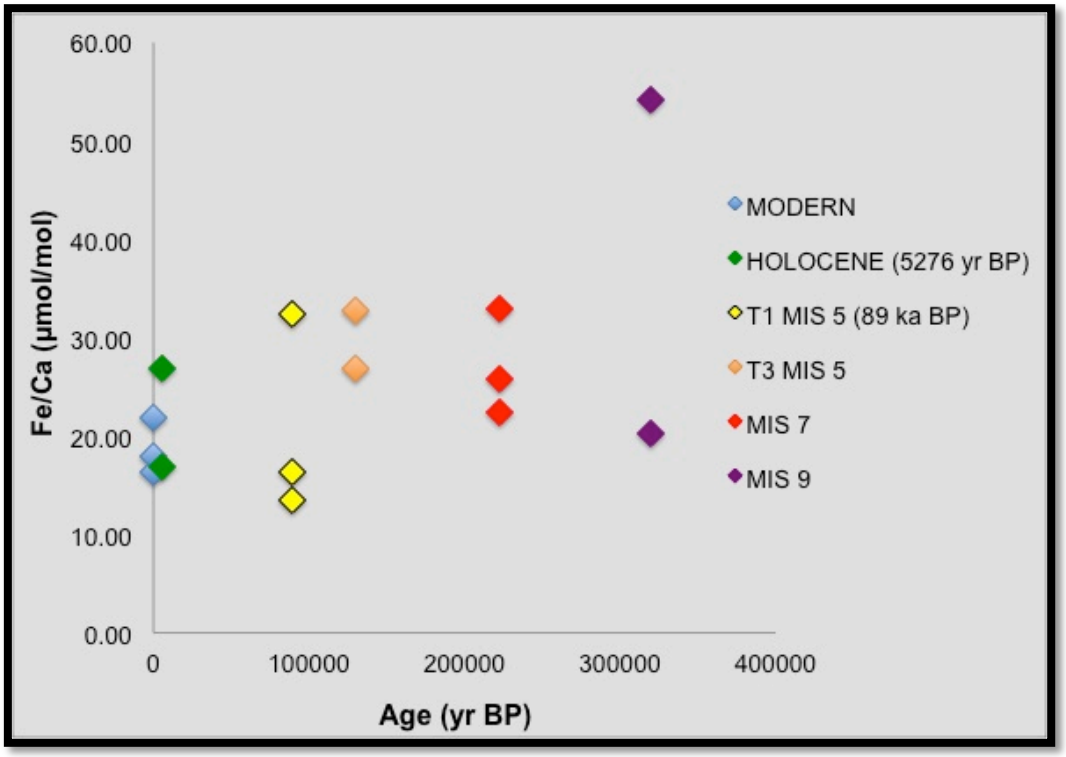

Figure 207 – Fe/Ca ratios of modern and fossil *A. antiqua* shells from Bahia Bustamante area.

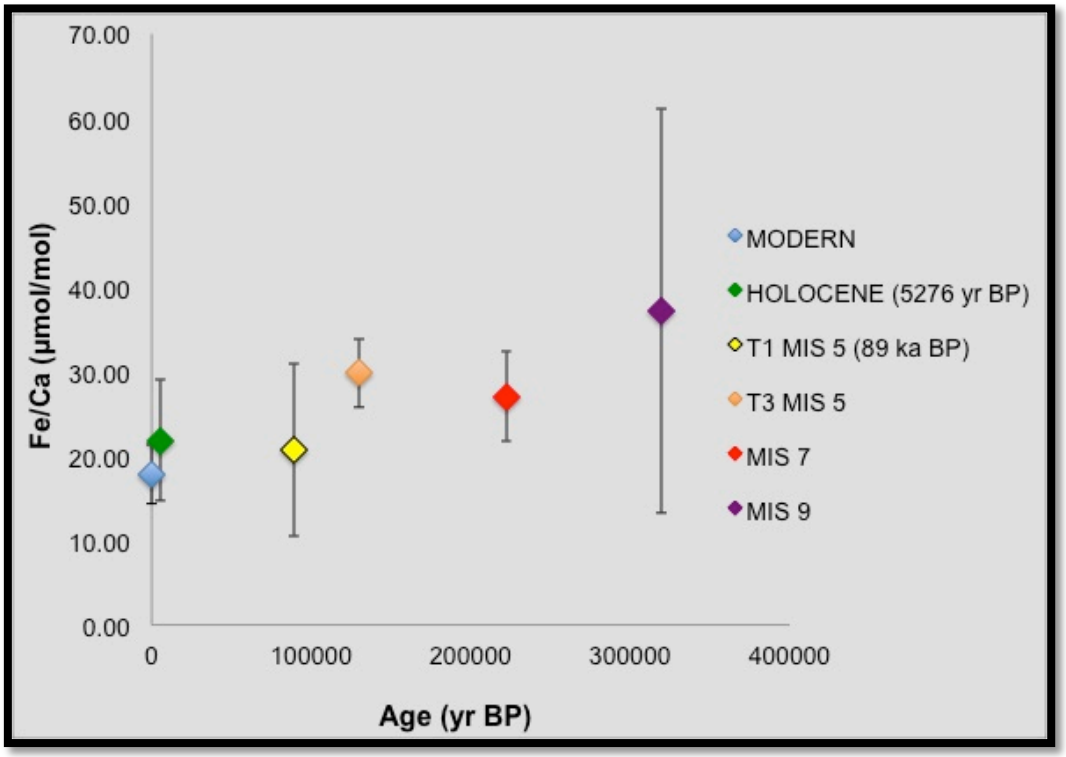

Figure 208 – Fe/Ca mean values and standard deviations of modern and fossil *Ameghinomya antiqua* shells from Bahia Bustamante area.

The same shells have Mg/Ca values ranging from 416.97 to 530.80 µmol/mol (mean value of 466.50±58.33 µmol/mol), from 417.51 to 443,49 µmol/mol (mean value of 430.50±18.37 µmol/mol), from 436.87 to 588.18 µmol/mol (mean value of 506.83±52.76 µmol/mol), from 231.98 to 280.58 µmol/mol (mean value of 256.28±34.37 µmol/mol), from 297.75 to 347.15 µmol/mol (mean value of 321.44±24.76 µmol/mol) and from 241.19 to 279.77 µmol/mol with a mean value of 260.45 ±27.32 µmol/mol.

Samples from older Pleistocene deposits have Mg/Ca low values, while the Holocene specimens and shells dated to 89 ka BP show very similar ratio to the modern specimens (Fig. 209 and Fig. 210).

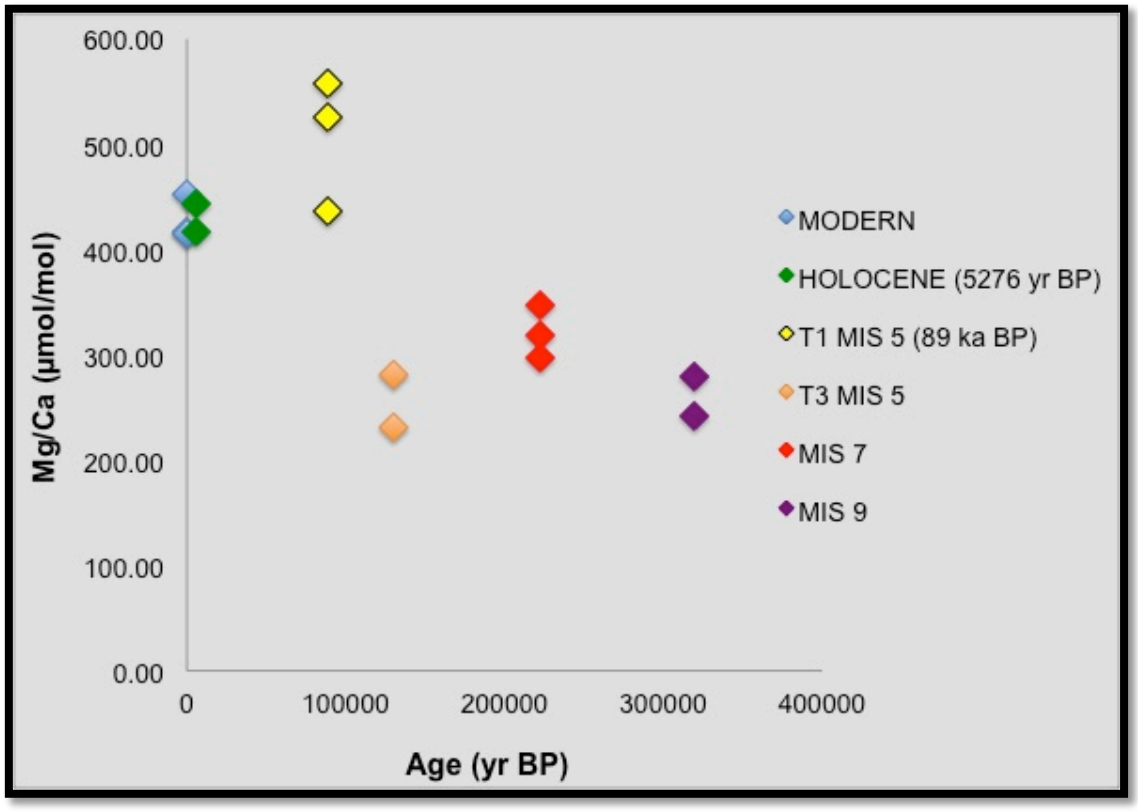

Figure 209 – Mg/Ca ratios of modern and fossil *A. antiqua* shells from Bahia Bustamante area.

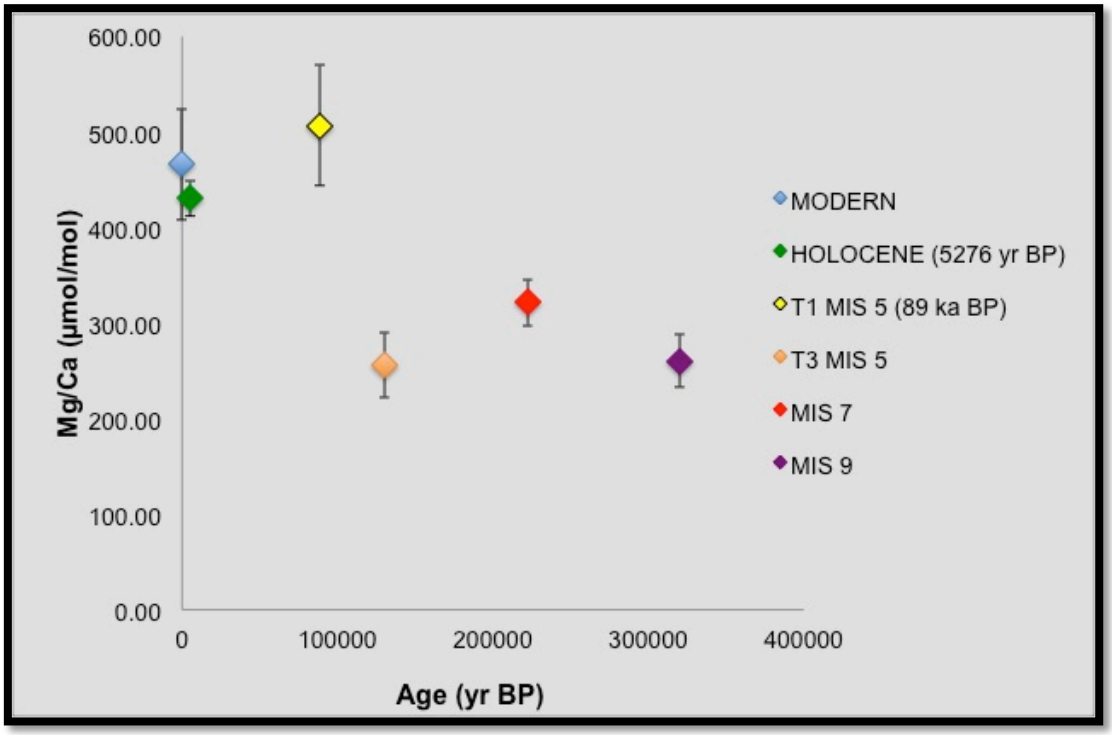

Figure 210 – Mg/Ca mean values and standard deviations of modern and fossil *Ameghinomya antiqua* shells from Bahia Bustamante area.

The opposite is observed for the ratio U/Ca. In fact, shells selected from the third order terrace (T3 according to Schellmann, 1998) deposited during the last interglacial period and from the beach ridges dated at MIS 7 and MIS 9 show higher values of U/Ca ratio compared with younger fossil shells and modern individuals (Fig. 211 and Fig. 212). Modern shells have values between 0.35 and 0.63 µmol*10/mol, with the lower mean value of 0.47±0.14 µmol*10/mol. The Holocene samples show values from 0.78 and 0.82 µmol*10/mol (mean value of 0.80±0.03 µmol*10/mol). The younger Pleistocene shells analyzed have U/Ca ratios ranging from 0.83 to 0.96 µmol*10/mol (mean value of 0.89±0.07 µmol*10/mol), while the samples collected from the T3 dated to MIS 5 from 3.83 to 5.75, with a mean value of 4.79±0.1.35 µmol*10/mol. Finally, the specimens collected from MIS 7 and MIS 9 beach deposits show values from 4.64 to 6.98 and from 0.01 to 7.60 µmol*10/mol and mean values of 5.95±1.19 and 3.805.37 µmol*10/mol (Tab. 25 and Figs. 211-212).

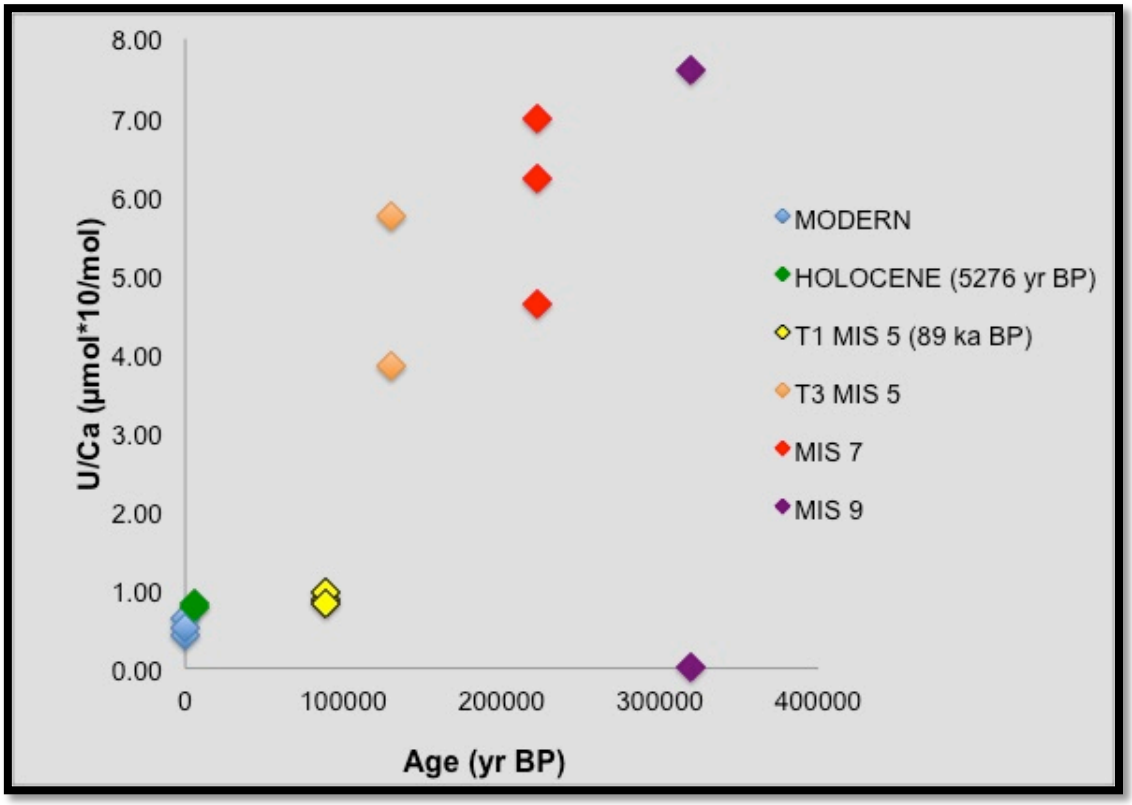

Figure 211 – U/Ca ratios of modern and fossil *A. antiqua* shells from Bahia Bustamante area.

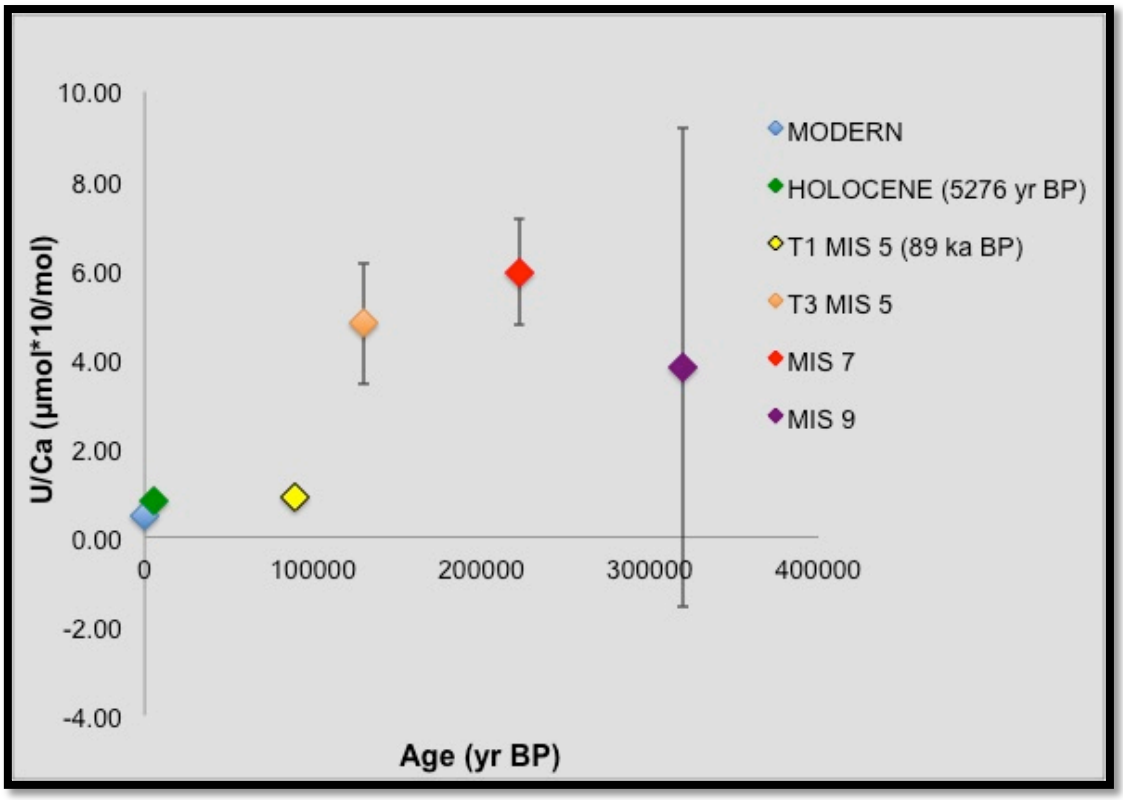

Figure 212 – U/Ca mean values and standard deviations of modern and fossil *Ameghinomya antiqua* shells from Bahia Bustamante area.

Finally, no important variation is observed between modern and fossil shell Sr/Ca ratios (Fig. 213 and Fig. 214), which vary between 11.18 and 25.82 mmol*10/mol with mean values from 11.44±0.36 to 18.02±3.64 mmol*10/mol (Fig. 213 and Fig. 214). Only the *Ameghinomya antiqua* specimens collected from the Holocene beach ridge dated to 5276±47 yr BP show very slightly lower Sr/Ca values than the modern individuals and fossils.

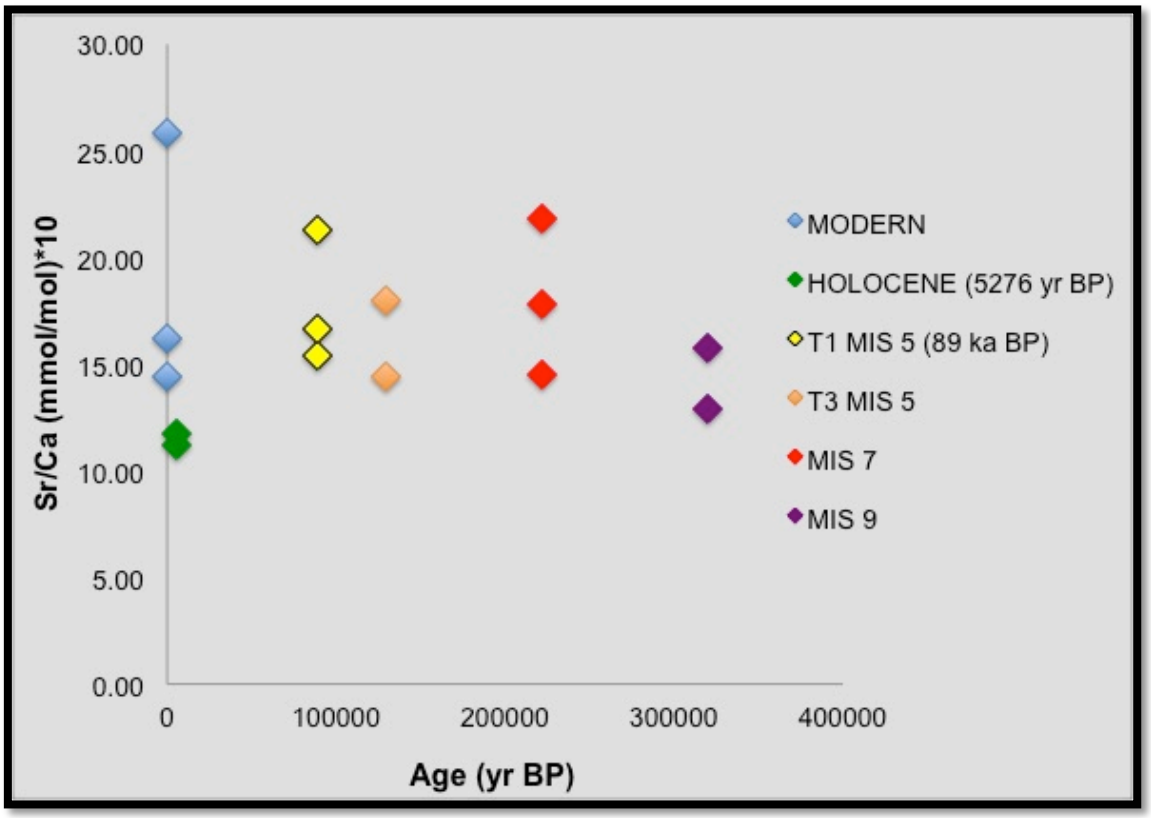

Figure 213 – Sr/Ca ratios of modern and fossil *A. antiqua* shells from Bahia Bustamante area.

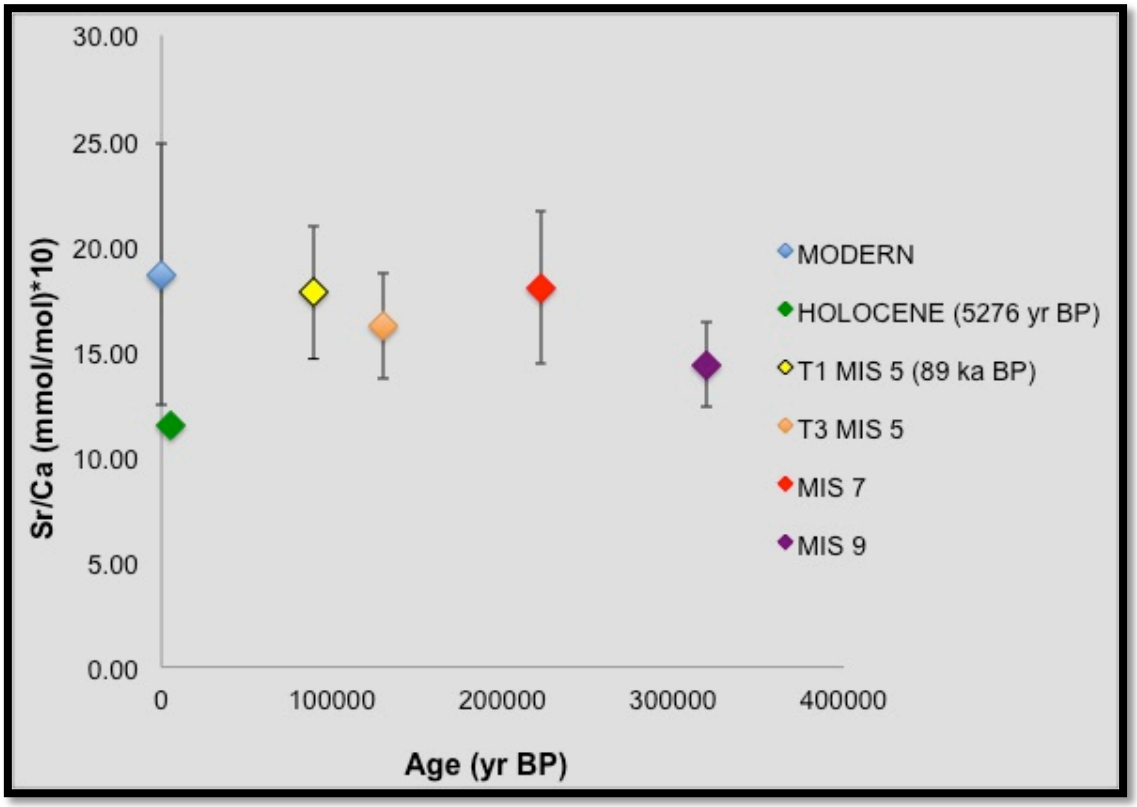

Figure 214 – Sr/Ca mean values and standard deviations of modern and fossil *Ameghinomya antiqua* shells from Bahia Bustamante area.

6.5. STRONTIUM ISOTOPIC COMPOSITION OF MARINE SHELLS

Strontium isotope analysis was performed on *Ameghinomya antiqua; Aulacomya atra* and *Mytilus edulis* shells, selected from modern, Holocene and Pleistocene beach deposits (Tab. 26). $^{87}Sr/^{86}Sr$ ratio ranges from 0.70896±24, for an *A. antiqua* specimen collected in Bahia Solano active beach to 0.709181±31 for a *Aulacomya atra* shell coming from the Camarones modern beach.

Seawater $^{87}Sr/^{86}Sr$ presently ranges from 0.70916 to 0.70923 (DePaolo and Ingram, 1985) and has not fallen below 0.70915 during the Pleistocene (Capo and DePaolo, 1990). So the values measured are within the range of marine waters, but leave the possibility of small mixing of continental waters.

It is important to note that the concentration of Sr in river waters is two orders of magnitude lower than in sea water (Bowen, 1988; Brunet *et al.* 2005) and that should complicate the recognition of freshwater input, which should be very high to be detected in the Sr isotope ratios.

sample	$^{87}Sr/^{86}Sr$	error	Age (yr BP)	Locality	Sr (ppm)	Species
WP 623BIS(3)	0.70917	21	MODERN	Camarones N	1408	*Ameghinomya antiqua*
WP 271(2)	0.70896	24	MODERN	Bahia Solano	1479	*Ameghinomya antiqua*
WP 272A	0.70905	21	1930 ± 24	Bahia Solano	1523	*Ameghinomya antiqua*
WP 139(3)	0.70917	19	5276 ± 47	Bahia Bustamante	1720	*Ameghinomya antiqua*
WP 149(1)	0.70902	23	89000 ± 800	Bahia Bustamante	1822	*Ameghinomya antiqua*
WP 176BIS (1)	0.70899	20	MIS 7	Bahia Bustamante	1693	*Ameghinomya antiqua*
WP 97(3)	0.70889	19	MIS 11	Camarones S	1571	*Ameghinomya antiqua*
WP 60B(3)	0.709181	31	MODERN	Camarones N		*Aulacomya atra*
WP 60A(7)	0.709051	21	915±20	Camarones N	750.24	*Aulacomya atra*
WP 60A(9)	0.709188	28	915±20	Camarones N	637.44	*Aulacomya atra*
G001(1)	0.709141	22	4074±50	Camarones N	625.66	*Aulacomya atra*
G001(7)	0.70916	29	4074±50	Camarones N	746.04	*Aulacomya atra*
WP 63B(1)	0.709127	21	6365±20	Camarones N		*Mytilus edulis*
WP 63B(6)	0.709066	22	6365±20	Camarones N		*Mytilus edulis*

Tab. 26 – $^{87}Sr/^{86}Sr$ ratio in modern and fossil marine shells from beach deposits of Atlantic coast of Patagonia.

7. DISCUSSION

7.1. PRESERVATION STATE OF MARINE SHELLS

The selection of suitable well-preserved samples is of paramount importance for obtaining reliable results both in chronology and paleoproxy interpretation. Marine molluscs are particularly interesting in this respect in what different radiometric methods (e.g. ^{14}C, U/Th, ESR) can be applied coupled with chemical analyses to reconstruct past environment. For this kind of material is imperative that the samples have not undergone any alteration.

Multiproxy analyses performed on marine modern and fossil (Holocene and Pleistocene) shells from Patagonia Atlantic coast show that the degree of weathering is quite variable but not enough for undermining the paleoclimatic values of the stable isotopes composition and of some trace element. Moreover, samples usually seem perfectly suitable for radiocarbon dating. Measurements performed on samples within this project (Zanchetta *et al.,* 2012; Ribolini *et al.,* 2011; 2013) confirm this after a careful cleaning and preliminary soft acid batch. However, samples older from Holocene have experienced subtle alteration (which may include also “impregnation”) at the expenses of U enough severe to make problematic the application of U/Th dating method. In fact, on the basis of XRD powder analysis, petrographic and trace element screening tests (comparison between marine shells and paleosols), a large dataset of unaltered bivalves with aragonite (*Ameghinomya antiqua* species) or mixed aragonite-calcite (*Mytilus edulis* and *Aualcomya atra* species) composition of the shells was identified for the reconstruction of paleoceanographic evolution during the Holocene and the Pleistocene of the Atlantic coast of Patagonia in the vicinity of San Jorge Gulf. Fossil *Ameghinomya antiqua* shells are preserved in their pristine aragonite mineralogy and in their biogeochemistry because the trace element contents of many samples correspond well to those recorded in unaltered recent counterparts, which show very different values compared to continental carbonates (i.e. pedogenic carbonate). In this frame pedogenic carbonate are seen as potential

counterpart of fluid potentially producing alteration.

On the contrary, in fossil *A. antiqua* specimens, post-mortem uranium migration processes are observed (Fig. 204 and Fig. 211). A secondary U uptake in fossil shells is showed also in Fig. 215, where U/Ca is compared with the Ba/Ca, which is considered immobile during diagenesis processes (Brand & Morrison, 1987; Brand, 1989).

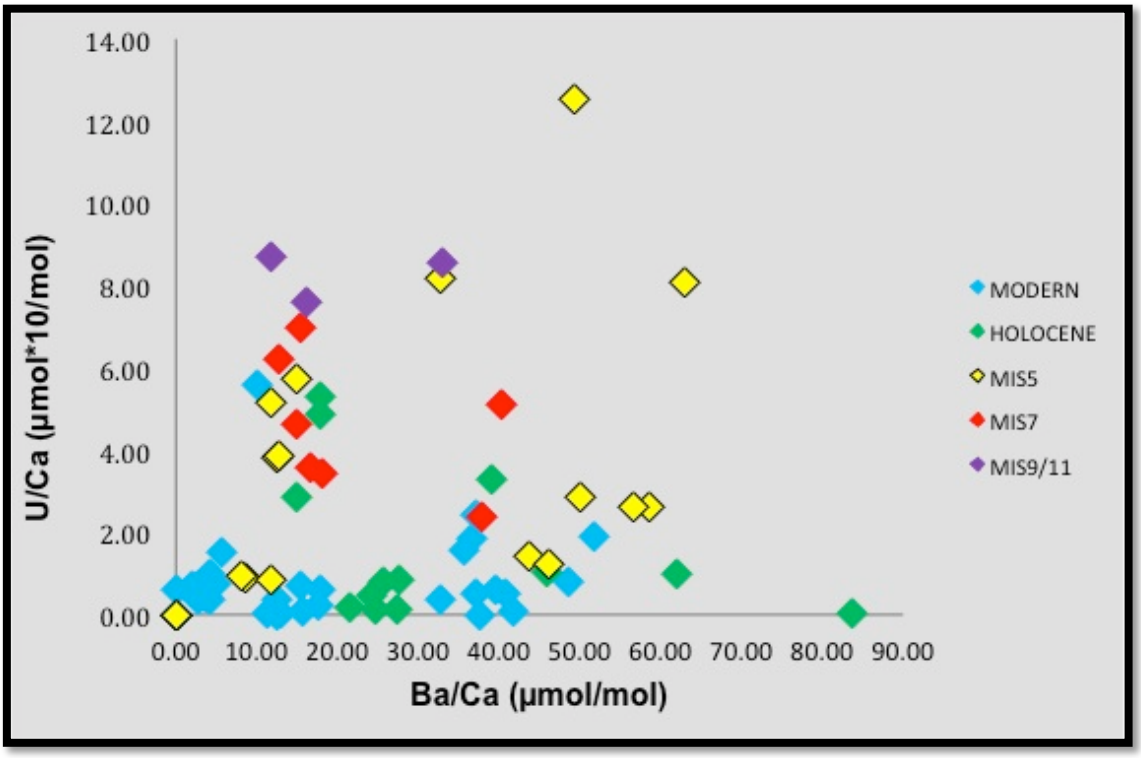

Fig. 215 – U/Ca vs Ba/Ca ratios in modern and fossil *Ameghinomya antiqua* shells.

As it is possible to see modern shells have very narrow range of values for U (0.90±1.12 µmol*10/mol), but very large variability in the Ba/Ca. This indicates (as well known, Ku *et al*., 1977; Chen *et al*., 1986; Henderson, 2002) that U concentration over the seas is quite constant but the Ba/Ca is more variable and indicator of local conditions as circulation, upwelling (Vander Putten *et al*., 2000; Gillikin *et al*., 2006).

However, some modern shells seem to have higher values, which it may suggest that locally the U concentration would be different giving more local information. This may also open the possibility that not all the high values in fossil shells are necessary indication of alteration and U uptake. Instead, Holocene shells show most values comprised (2.06±2.64 µmol*10/mol) within the modern values, but

some show an evident enrichment. This can indicate that U uptake was already present early after shell burial. Pleistocene sample show variable degrees of U uptake (from 0.01 to 10.69 µmol*10/mol) but usually far from modern samples.
At this stage, despite some encouraging trials application of the U/Th method to Patagonian shells, they appear still problematic and confirm the complexity of the problem already noted in international literature (Broecker, 1963; Blanchard *et al*., 1967; Kaufman *et al.,* 1971; 1996; McLaren and Rowe, 1996; Labonne and Hillaire-Marcel, 2000) and in particular the application of Patagonian shells (Rostami *et al*., 2000; Schellmann & Radtke, 2000; 2003). Considering the problems related to ESR dating (which it has been used as alternative methods for dating in the area, Schellmann & Radtke, 1997, 1999; Schellmann *et al*., 2004, 2008), we can conclude that chronology of Pleistocene deposits is still problematic for the Patagonian Atlantic coast.

7.2. MODERN MARINE SHELLS: STABLE ISOTOPE COMPOSITION AND TRACE ELEMENT CONCENTRATIONS

Stable isotope analyses on modern marine shells were performed on three species of bivalves: *Ameghinomya antiqua, Mytilus edulis* and *Aulacomya atra.*
Mytilus edulis shells show an increase in $\delta^{18}O$ values moving southwards (Fig. 216). The same trend is observed for the carbon isotopic composition of the same specimens (Fig. 217).

Figure 216 – Variations in modern *Mytilus edulis* $\delta^{18}O$ with latitude.

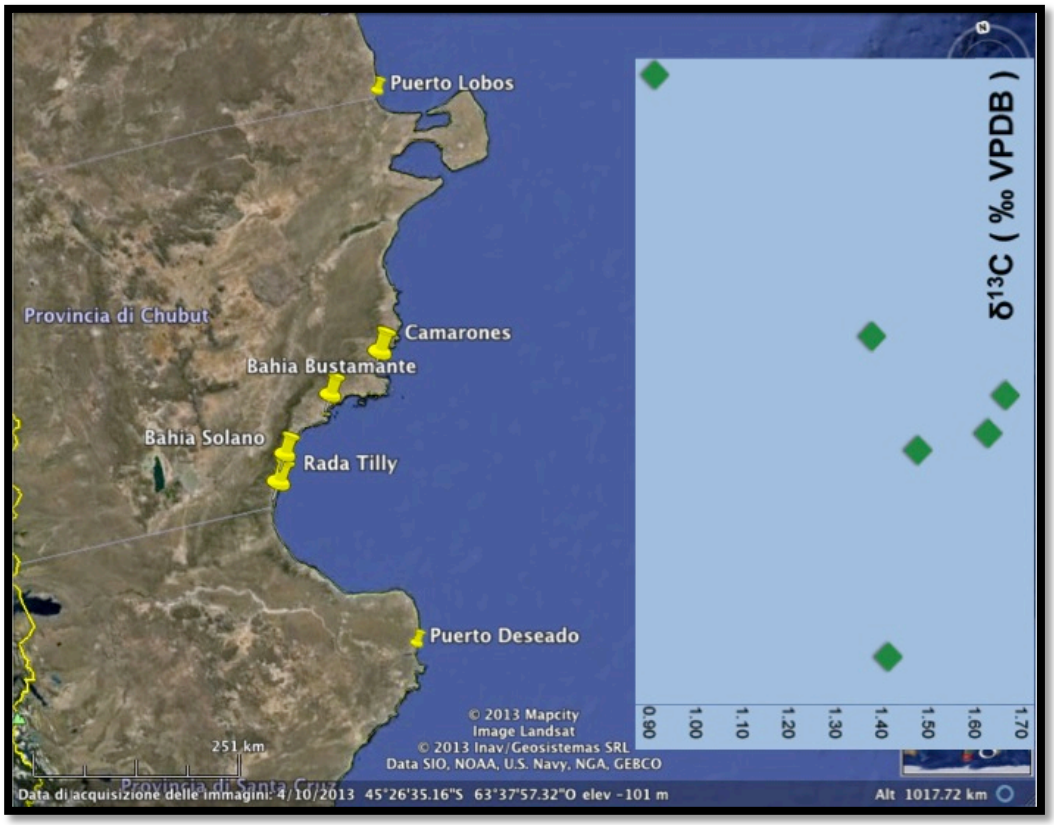

Figure 217 – Variations in modern *Mytilus edulis* $\delta^{13}C$ with latitude.

The changes in isotopic composition do not seem to be related to variations in isotopic composition of seawater. Figure 218 shows the oxygen isotopic composition of regional seawater, indicating that average values are around -0.3‰.

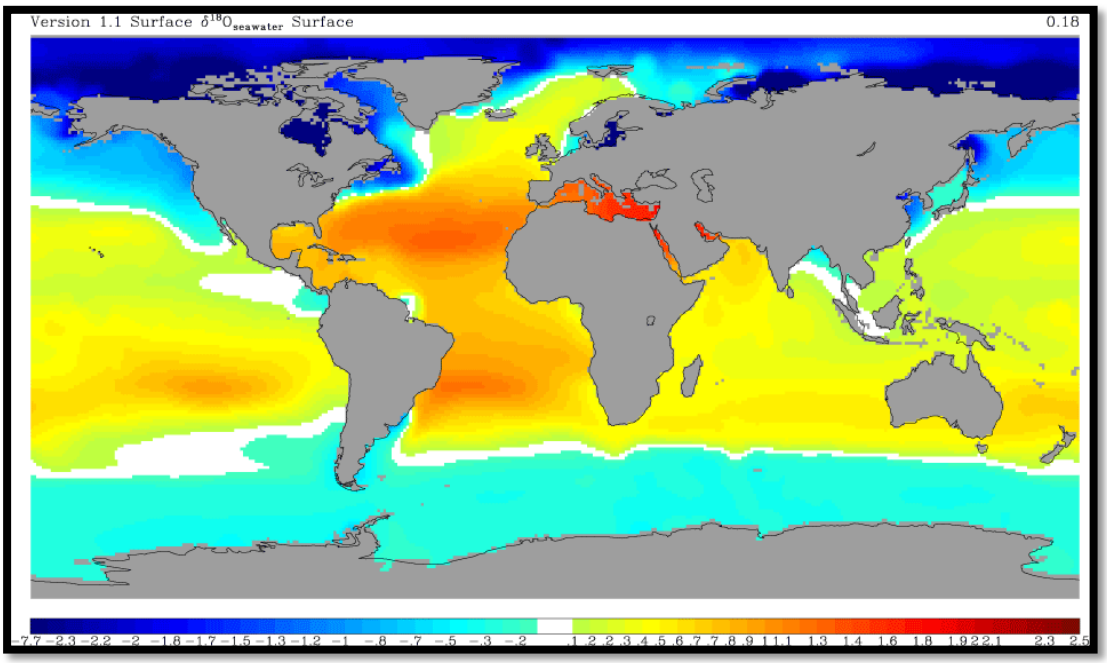

Figure 218 – Global oxygen isotopic composition of seawater (Schmidt *et al.*, 1999).

This is also visible on water salinity, since the salinity in the area of study is rather homogeneous, amounting to approximately 33‰ (Fig. 219), even if figure 219 cannot completely capture the very local, nearshore, variability. Therefore, the latitudinal gradient can probably better related to variations in seawater temperature, which from north to south of the study area equal to about 5° C (Fig. 220). This fact is of particular interest for possible paleoclimatic reconstruction.

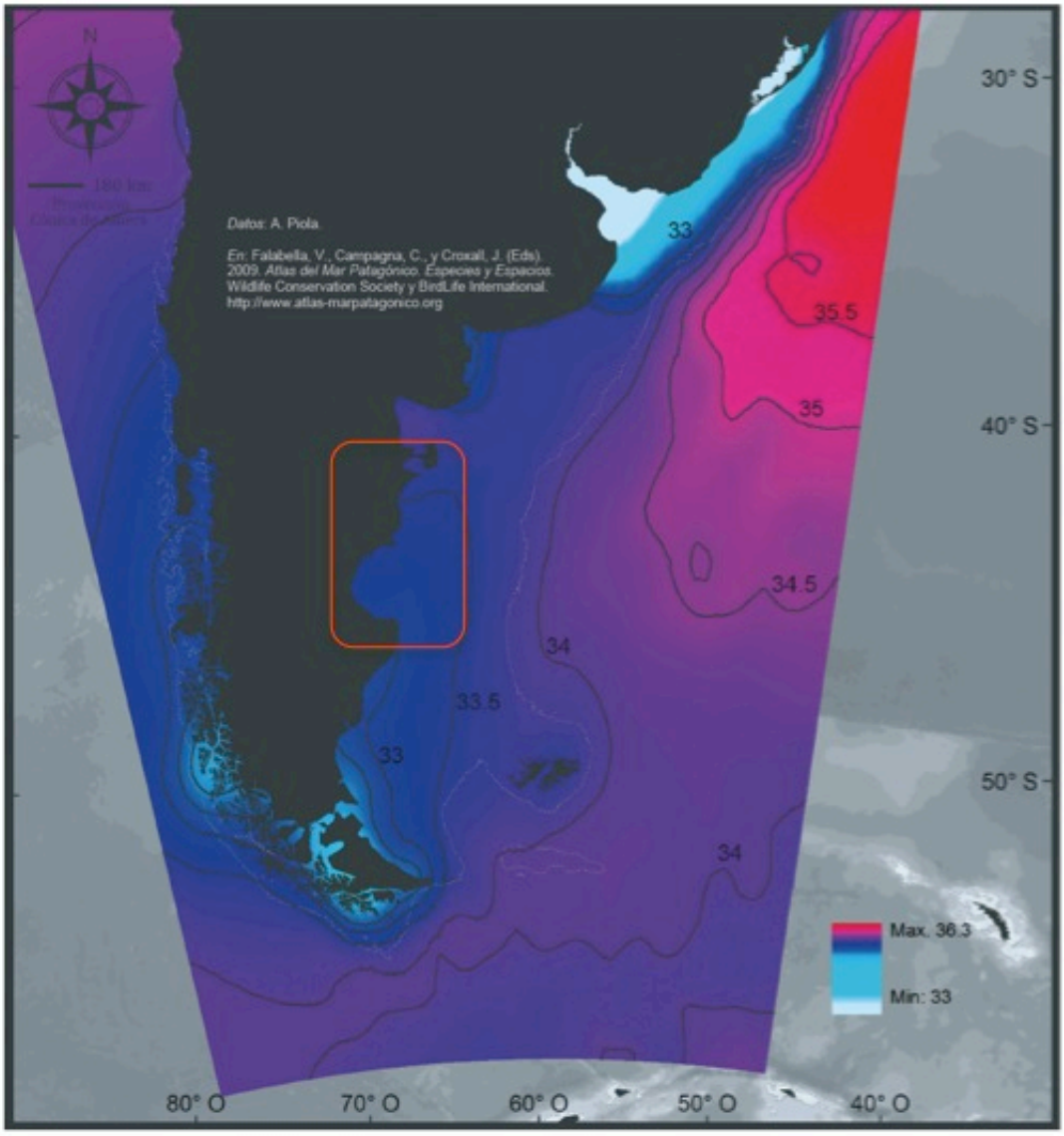

Figure 219 – Salinity of seawater along the Atlantic coast of Patagonia (from Falabella *et al.*, 2009). The red rectangle indicates the study area.

In fact, having an average $\Delta\delta^{18}O=0.94‰$ (Fig. 216) from north to south and assuming a $\Delta\delta^{18}O/\Delta T$ = -0.2‰/°C as due to isotopic fractionation (Kim & O'Neil, 1997), this changes in oxygen isotopic composition are in agreement with seawater temperature variations.

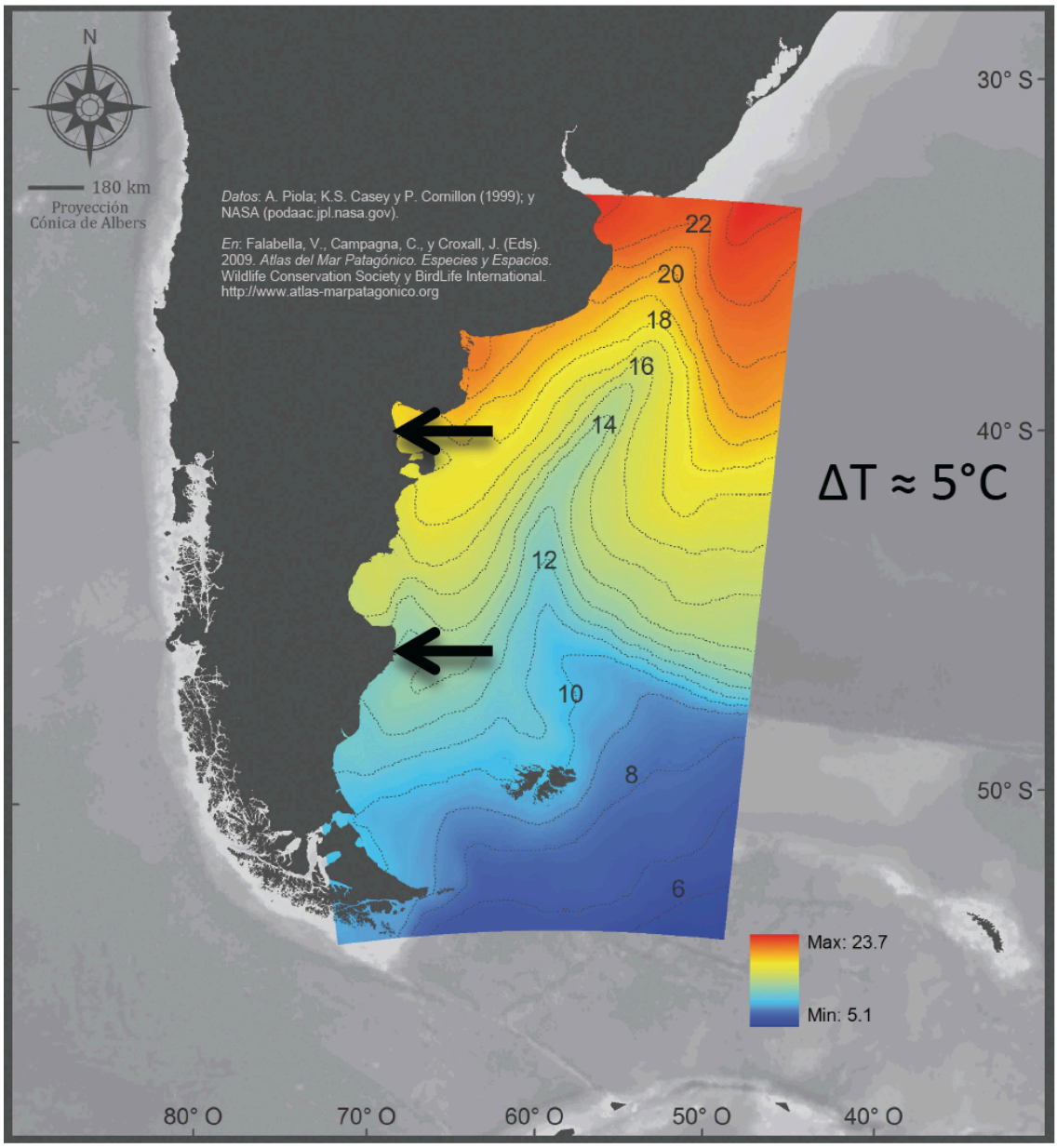

Figure 220 – Seawater temperature along the Atlantic coast of Patagonia (from Falabella *et al.*, 2009). The black arrows indicate the boundaries of the study area.

Despite, generally the oxygen and carbon isotopic compositions of modern *A. antiqua* follow a general latitudinal trend there is a clear anomaly with lower values in the Gulf of S. Jorge (Fig. 221 and Fig. 222), which is not recorded by *Mytilus edulis*.

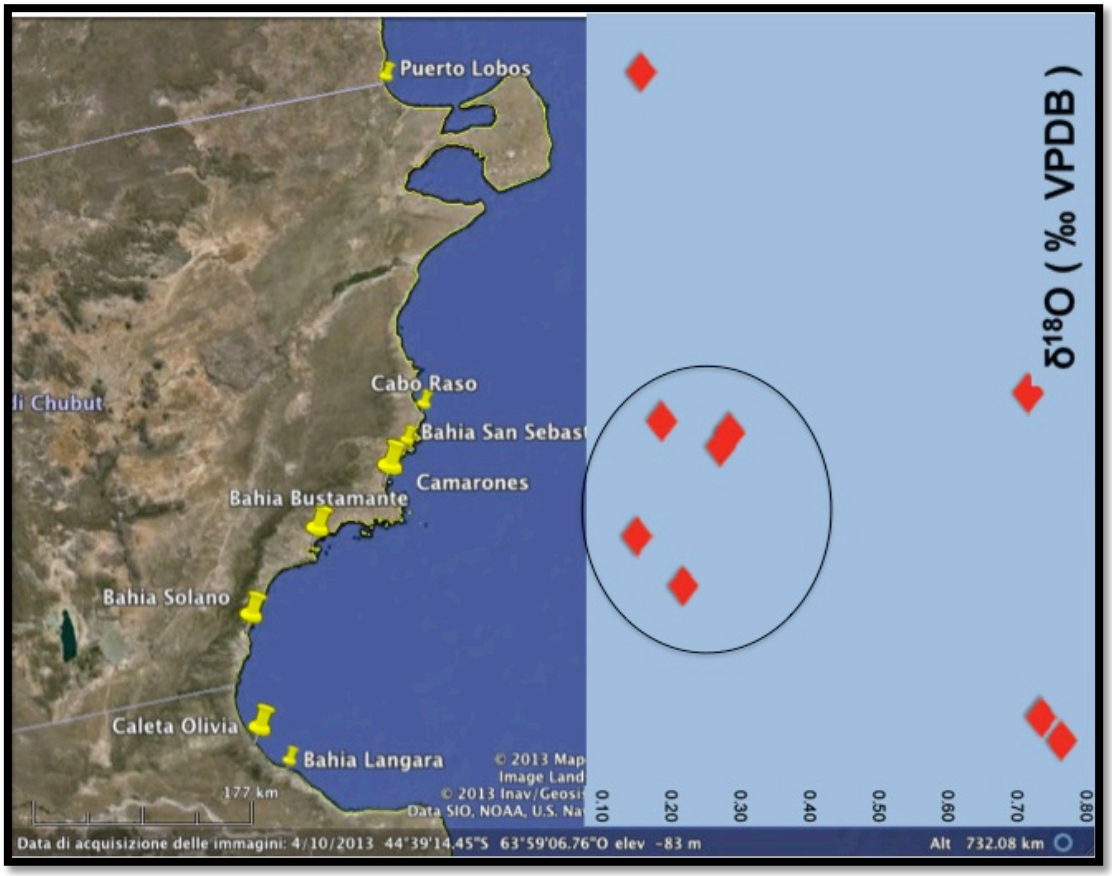

Figure 221 – Variations in modern *Ameghinomya antiqua* $\delta^{18}O$ with latitude.

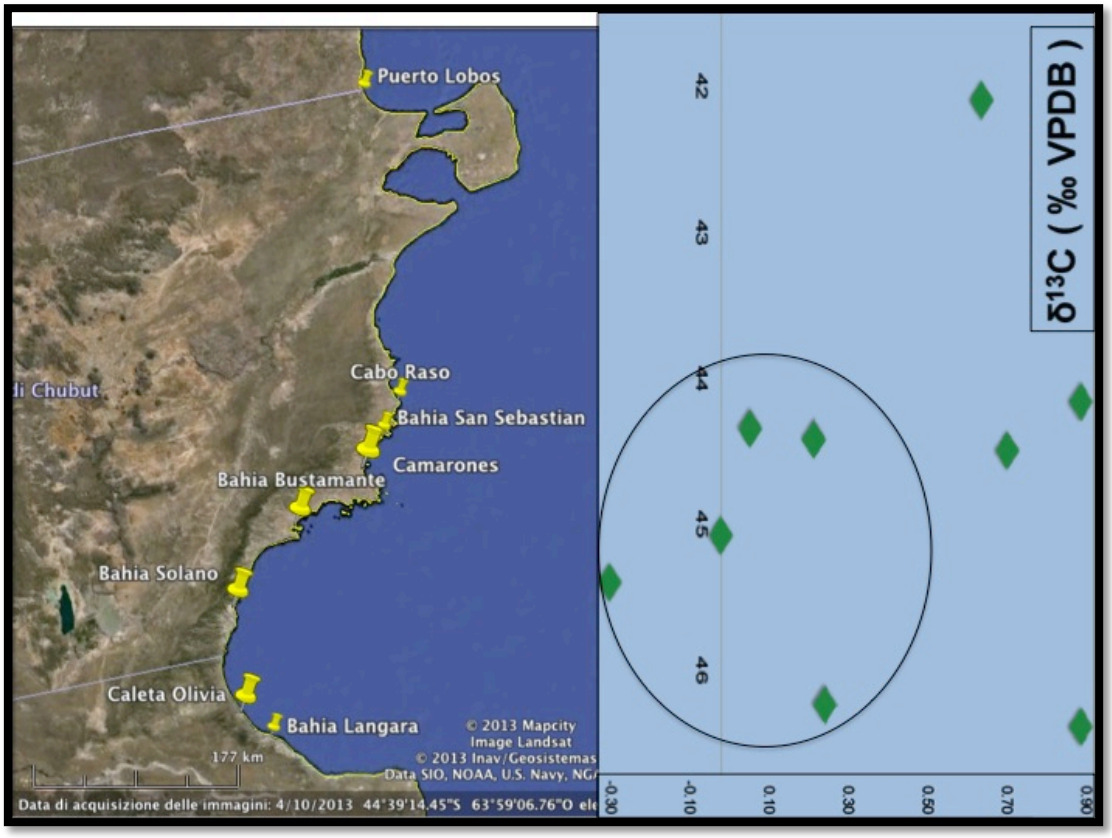

Figure 222 – Variations in modern *Ameghinomya antiqua* $\delta^{13}C$ with latitude.

Whereas *Mytilus edulis* lives in shallower waters than *Ameghinomya antiqua*, it is possible that the latter is affected much less than the surface variations in salinity and temperature of the water. It is possible, moreover, that the populations living within the Gulf are subject to anomaly of the local thermal gradient of depth that can be due to the presence of currents at low depth which does not influence the *Mytilus edulis*.

On the other hands the concentrations of trace elements indicate that there are no systematic variations with salinity and temperature and therefore the local effect is extremely important in governing their distribution within shells.

Nevertheless, the higher values of Mn/Ca (Fig. 223) are from the same area where lower carbon and oxygen isotopic compositions were found (Fig. 216 and Fig. 217).

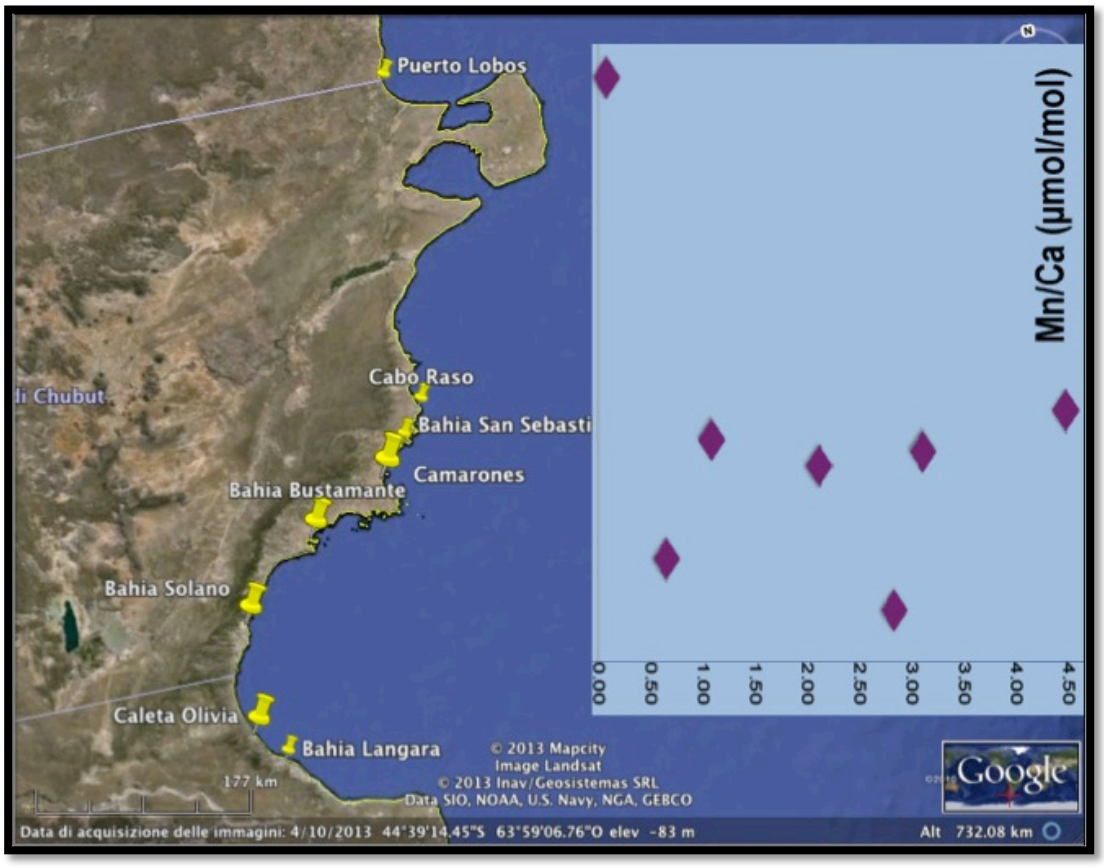

Figure 223 – Mn/Ca ratio in modern *A. antiqua* varying the latitude.

This could be explained with weak mixing between freshwater and seawater, recorded only from the trace elements that are more concentrated in freshwater (e.g. Mn) than in sea water and by small signal in oxygen and carbon isotope composition, having DIC values isotopic composition and water oxygen isotopic composition lower in freshwater than in the seawater (Mook & Tan, 1991). Indeed, along the Patagonian

coast it has been reported (Cordero *et al.,* 2003; Gomez *et al.,* 2008) of watershed and groundwater discharge of old bicarbonates in inshore zone that mix freshwater with seawater in marine environment causing anomalies in ^{14}C reservoir effect. Living the *A. antiqua* as infaunal in the sediment from which freshwaters go back and mix locally with seawater, the composition of the pore water may have different isotopic composition and content of trace elements. This would explain why these changes do not affect the specimens of *Mytilus edulis,* which is sessile, and need hard substrates and this latter show a good correlation with temperature gradient.

The absence of variations in the Sr/Ca ratio in modern shells from the Atlantic coast of Patagonia, on the contrary, is not surprising, since the Sr content in carbonate shells is closely related to the content of Sr in seawater, the concentration of which is two orders of magnitude higher than the concentration of Sr in the waters of the rivers (Bowen, 1988; Brunet *et al.,* 2005) and which cannot affected by modest mixing with water. Nevertheless, no correlation between Sr/Ca ratios and temperature was observed. However, it is interesting to note that the slight decrease of Mg/Ca of modern shells moving southward is consistent with a progressively lowering of seawater temperature (Fig. 224 and Fig. 225), suggesting a correlation between mollusc shell Mg incorporation and temperature, which has already supposed by more detailed studies (Dodd, 1965; Klein et al., 1996).

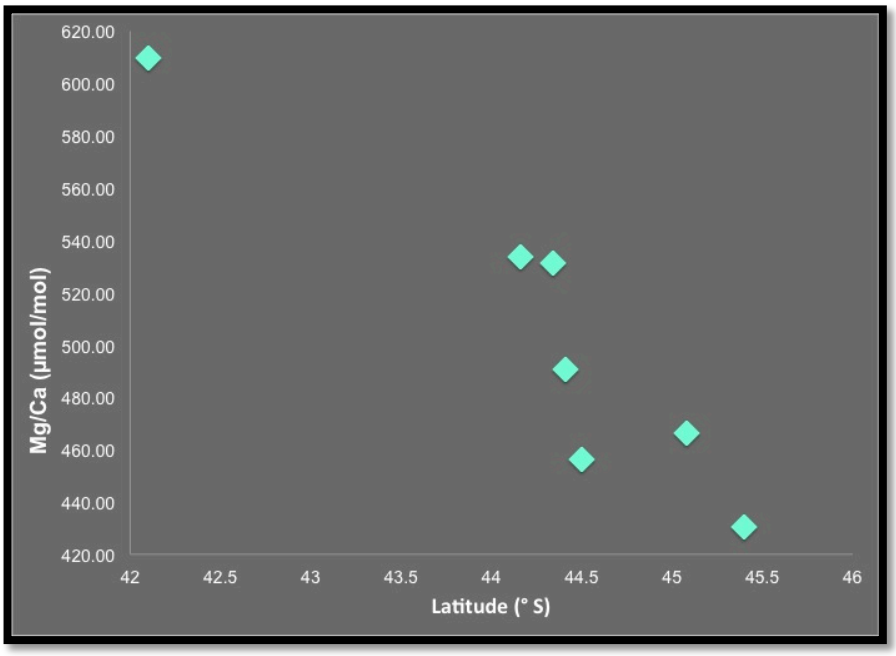

Figure 224 – Mg/Ca trend in modern *A. antiqua* shells from north to south of the study area.

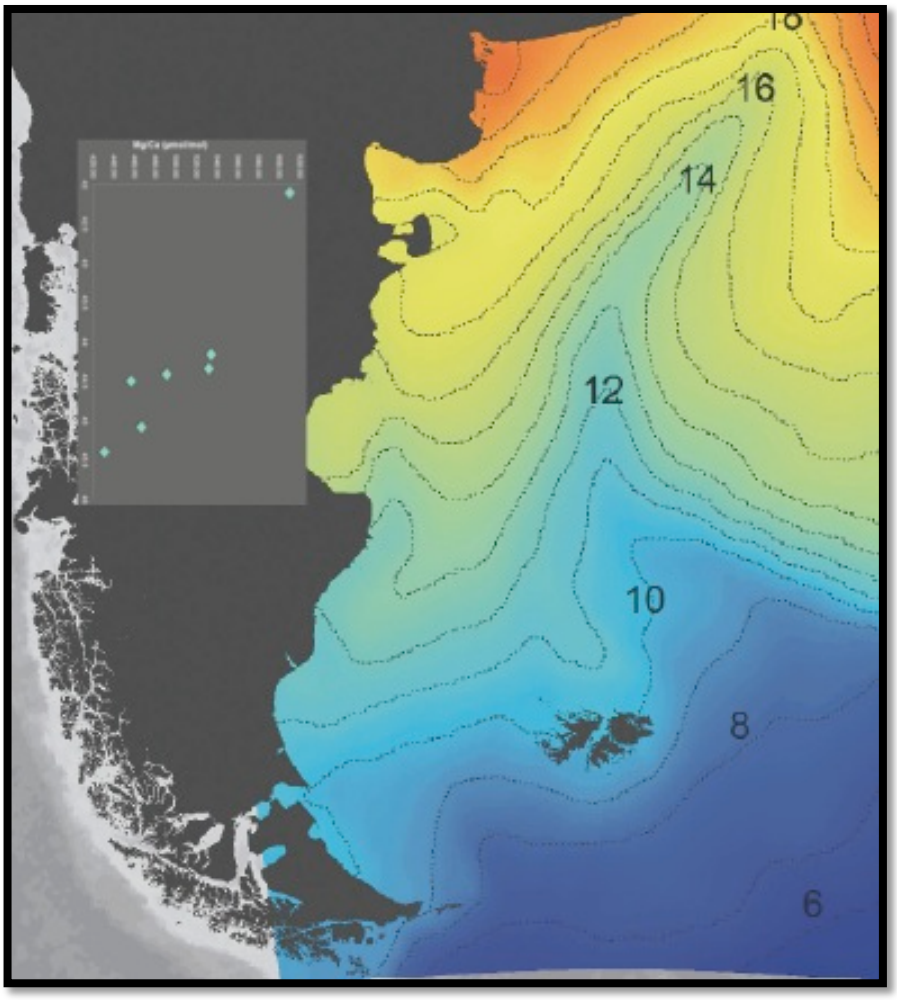

Figure 225 – Mg/Ca trend in modern *A. antiqua* shells and seawater temperature from north to south of the study area.

7.3. FOSSIL MARINE SHELLS: STABLE ISOTOPE COMPOSITION AND TRACE ELEMENT CONCENTRATIONS

7.3.1. Stable isotope composition and trace element content of Holocene Mytilidae shells in Camarones North

Based on Sr isotopic data from ca. 6000 to 900 yr BP the marine water had similar composition overlapping those of modern shell samples (Tab. 26, Fig. 124). Because the measured values are within the range of marine waters (DePaolo and Ingram, 1985), there is no evidence of mixing with freshwaters, which should alter the marine $^{87}Sr/^{86}Sr$ ratio. However, this could be a weak argument due to the large

Sr reservoir represent by the sea (about 8 ppm, Nagaya *et al*., 1971*;* de Villiers, 1999) compared to the Sr content of Patagonia river waters (about 50 ppb according to Brunet et al., 2005) and for the current absence of big river in the area even the selected sections are close to a river mouth. The substantial stable conditions of the environment similar to the present seem to be supported by the very similar isotopic composition and trace element in samples of the last 4000 yr (Fig. 226 and Fig. 227).

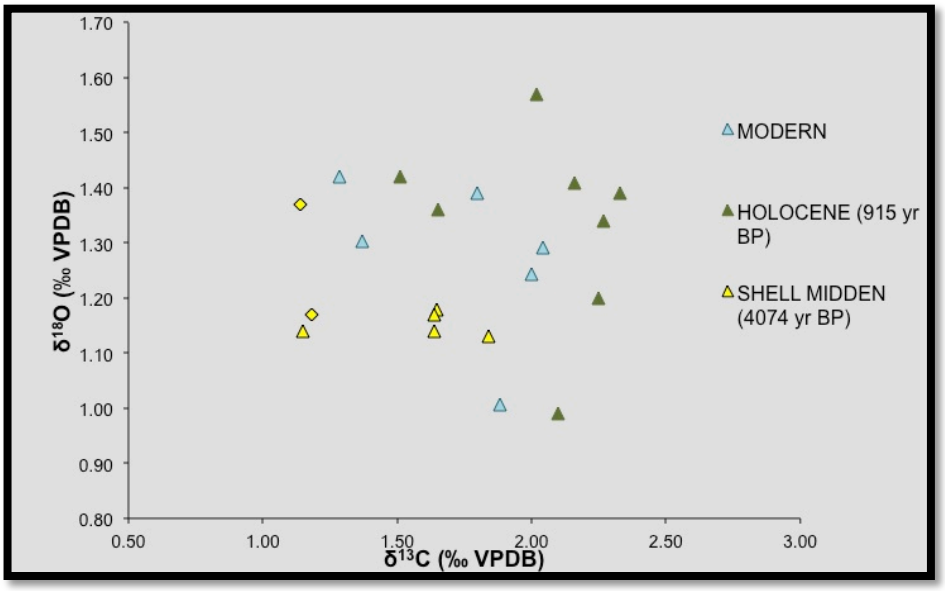

Figure 226 – Stable isotope composition of shells from the last 4000 yr.

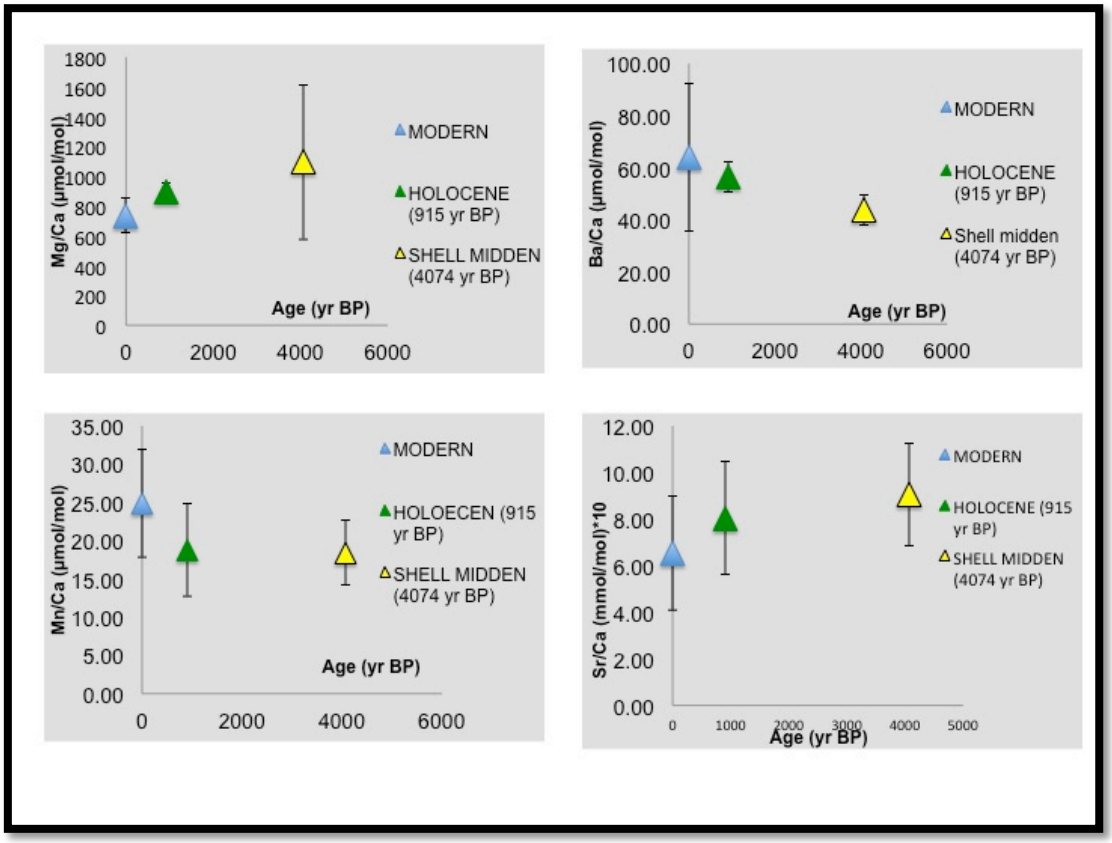

Figure 227 – Trace element concentrations of Mytilidae shells from the last 4000 yr.

High Mn and Fe throughout Middle Holocene shells dated to 6365±20 yr BP, on the contrary, could be evidence that Ca-substituting ions in the mixed calcite-aragonite lattice of some diagenetic modification. However, *Mytilus edulis* shells did not undergo major diagenetic alteration, since the shells appear extremely well preserved, and having the same mineralogical composition compared to the modern shells and oxygen and carbon do not appear to have exchanged with meteoric water for their positive values. Moreover, the radiocarbon age is in perfect agreement with the stratigraphic position of these shells at the base of the Holocene marine transgression (Zanchetta *et al.*, 2012). Provided that alteration is not occurred, high positive $\delta^{18}O$ values seem to indicate a significant change in the isotopic composition (salinity) and/or temperature of marine water in Camarones area occurring between ca. 6300 and 4000 yr BP.

If only temperature is considered, a change of ca. 1‰ from shells dated at ca. 4 ka, 0.9 ka, modern and that dated at ca. 6 ka can be explained with a decrease of temperature of ca. 5°C (assuming that the fractionation factor between water and calcium carbonate is ca. 0.2‰/°C according to Kim and O'Neil, 1997). Nevertheless, paleontological evidences from mollusc shells from the area suggest that during the

middle Holocene waters were warmer than Late Holocene and modern conditions (Aguirre *et al*., 2008), so a significant cooling should be excluded.

Therefore, an important change in salinity could be responsible for the higher oxygen isotope values at a. 6 ka, with shells of this age were living in an environment ^{18}O-enriched, and, as suggested by mollusc associations (Aguirre et al., 2008), in a warmer environment. This could be accounted by the descending influence of the Brazilian current, compared to its front position now located northward. If Mg/Ca reflect variations in ambient temperature, so with higher temperature during the deposition of the Mid-Holocene beach ridge 6000 yr-old (Fig. 187) and considering that the saltier and warmer Brazilian current shows higher oxygen isotopic composition than the Malvinas current (Schmidt *et al.,* 1999), can be assumed that a southward shift of the warm Brazilian current, likely connected with the Mid-Holocene "Climatic Optimum", occurred (Fig. 228). This conclusion, which is intriguing at this stage, is not the only one possible.

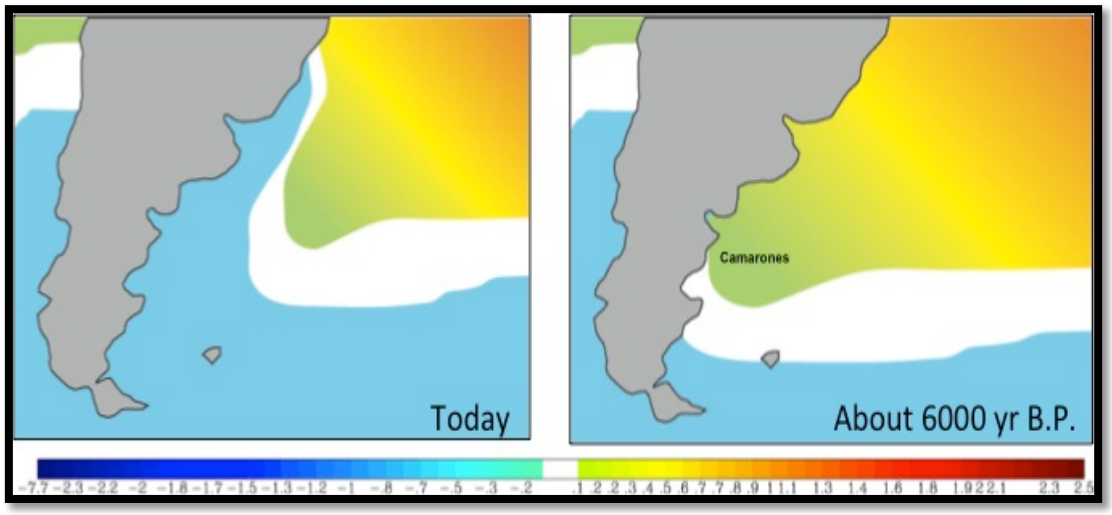

Figure 228 – Modern and Middle Holocene (ca. 6000 yr BP) tentative position of marine currents based on oxygen isotopic composition of seawater (qualitative).

High positive $\delta^{13}C$ values in the ca. 6000 yr-old shells suggest they grew in ^{12}C-depleted waters, possibly highly productive (Grossman, 1984; Purton and Braiser, 1997; Takesue and van Geen, 2004). Then, high values of $\delta^{18}O$ and $\delta^{13}C$ should suggest that *Mytilus edulis* grew in a low energy environment such as a protected embayment or lagoon, in which evaporative phenomenon can have a significant role and on which also mixing with local river waters can be detectable effect on trace elements like Fe and Mn and characterized by high eutrophy. Nevertheless, same higher values of oxygen and carbon stable isotopes are found for

Ameghinomya antiqua shells (less tolerant to changes in salinity than *Mytilus edulis* and living in strictly marine environment) collected from beach ridges deposited from 5800 yr BP south of Camarones village (Fig. 231).

Because these shells were collected in some of the most internal ridges in the area corresponding to the older phases of the Holocene marine transgression (Schellmann and Radke, 2010; Zanchetta *et al.*, 2012), these values may represent just the expression of particular conditions developed during this phase: large embayment was produced in the area at that time with possibly the presence of protected environments and lagoon (Zanchetta *et al*., 2012).

7.3.2. Stable isotope composition of Holocene Mytilidae shells in Camarones area

Integrating the isotopic data from Camarones North with the stable isotope results obtained on *Mytilus edulis* shells from Camarones South it is possible to observe that in all Camarones area no changes in oxygen isotopic composition occurred since ca. 5700 yr BP, suggesting that variations in seawater isotope composition and temperature took place between 5700 and 6300 yr BP (Fig. 229), as confirmed by stable isotopic results on Holocene *Ameghynomya antiqua* shells (Fig. 231). On the contrary, the source of dissolved inorganic carbon changed during all the Holocene (Fig. 230) but remained quite high between ca. 5700 and 6300 yr. This may suggest that was still locally characterized by high consumption of ^{12}C, possibly indicating still persistence of lagoonal conditions with restricted circulation and local high biological activity. This trend seems reasonably correlated with the progressive development of the local transgressive-regressive cycle of the Holocene. During the first part when sea-level rise was fast (faster than local glacioisostatic adjustment), the sea penetrate deep into previous incised valley producing articulate morphologies, embayment and lagoons, favorable for development of local condition of restricted circulation enhanced by the macrotidal regime of the area. When the rate of sea level was reduced and sediment supply sufficient, coastline retreated and the coast became less articulated and the general environment was more connected to the sea. In this view (which can know exceptions) the carbon isotope composition could indicate that this transition occurred in the Camarones area at ca. 5600 yr BP (Fig. 230).

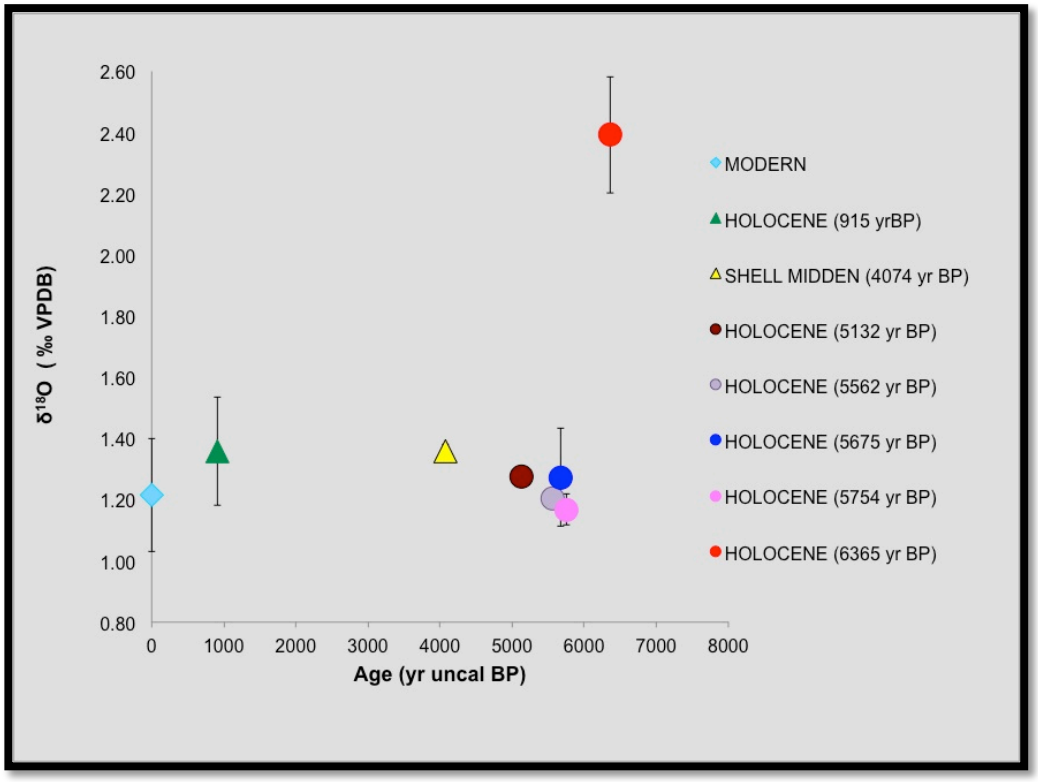

Figure 229 – Oxygen isotope composition of Holocene Mytilidae shells in Camarones area. The dots are referred to *M. edulis,* triangles to *A. atra* and diamonds to both.

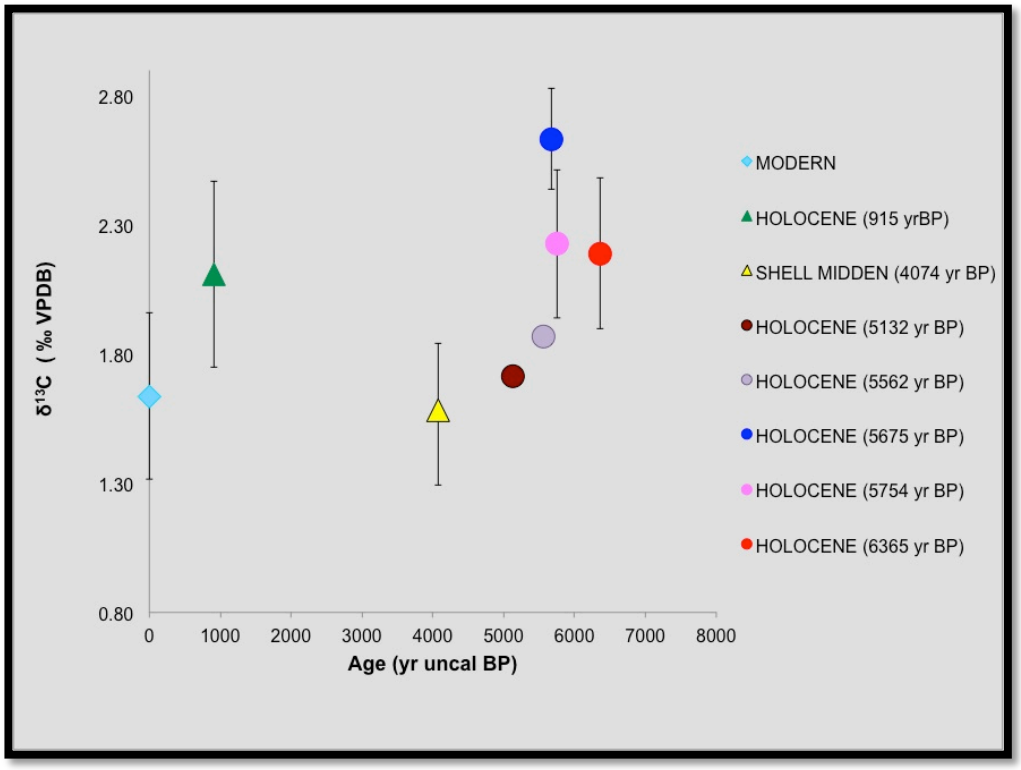

Figure 230 – Carbon isotope composition of Holocene Mytilidae shells in Camarones area. The dots are referred to *M. edulis,* triangles to *A. atra* and diamonds to both.

7.3.3. Stable isotope changes in *Ameghinomya antiqua* shells during the Holocene

Comparisons between *A. antiqua* shells selected from Holocene beach deposits outcropping along the study area reveal that, as observed for modern shells, the $\delta^{18}O$ values of Holocene specimens increase moving southward (Fig. 231). In fact, shells collected from beach ridges deposited at the same age show more positive oxygen isotopic composition for the individuals collected in the southern part of the study area (Caleta Olivia) than in the north. These results would suggest that also during the Holocene a progressive decrease of the temperature going south took place. However, Fig. 231 suggests an important point: the present gradient of ca. 0.5‰ between the northern and southern localities (Caleta Olivia) present today is progressively lost during the Holocene. Moreover, all the selected sites show ^{18}O-enriched values during the Holocene compared to the modern samples, even if some variability is present. This may indicate that today the influence of Malvinas current (fresher, colder and with lower isotopic composition, Fig. 218) is much stronger than in the past and, if the proposed interpretation for Camarones North is applicable, that during the Holocene the Brazilian current has exerted a major role southward.

So two different species with different ecological requirements (*M. edulis* more euryhaline than *A. antiqua*) point to the similar conclusion: previous ca. 5600 yr BP water appears more saline (higher $\delta^{18}O$ values) with higher $\delta^{13}C$ (more eutrophic?) and probably warmer (as suggested by paleontological data of Aguirre et al., 2008 and Mg/Ca ratio). *A. antiqua,* whose condition changed during time with period of higher $\delta^{18}O$, can support the notion that influence of Malvinas current (strong today) was less in the past or at least in some period. The chronological resolution we have cannot allow to detail where this influence stopped and if there was period much similar to present. Summing up seems that local effect can have minor role and that these values may represent genuine shift in the warmer Brazilian current. It is also possible that during warmer climate wetter condition prevailed increasing discharge of local aquifers of small rivers producing a small effect on trace element but not affecting in a particular way isotopic composition of waters changed toward generally higher isotopic values.

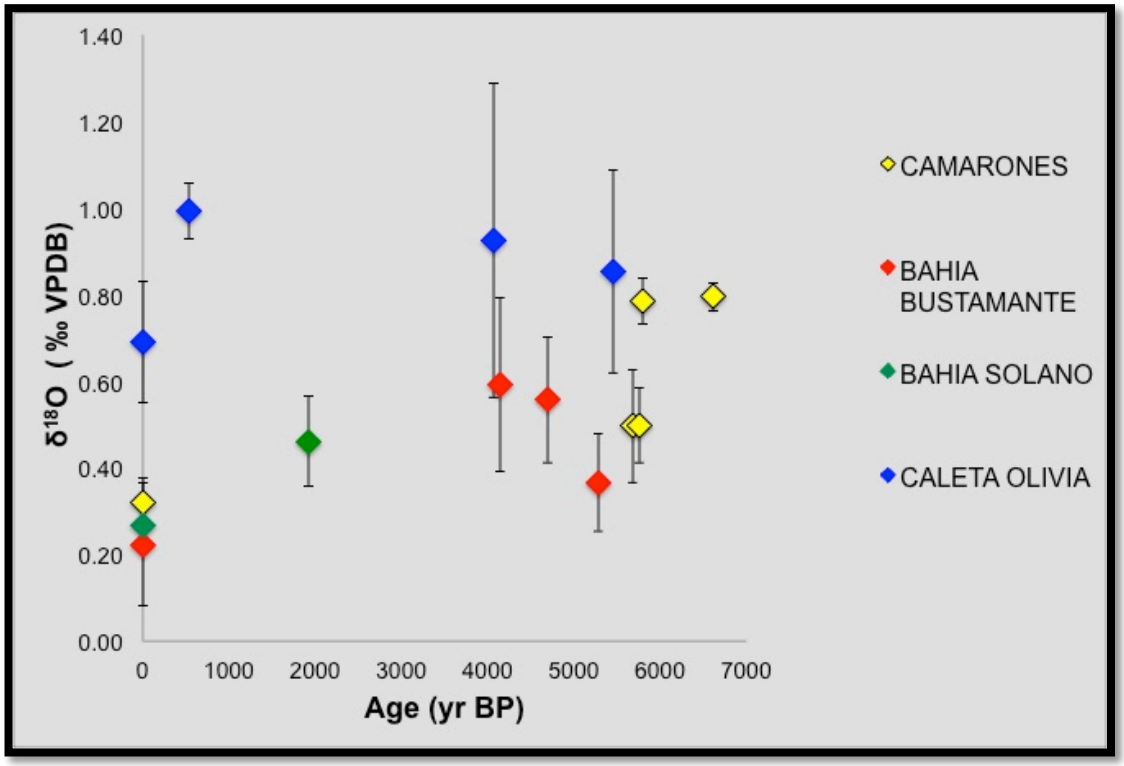

Figure 231 – Oxygen isotope composition of Holocene *Ameghinomya antiqua* shells collected from Atlantic Patagonia beach deposits.

Carbon isotopic composition of Holocene *Ameghinomya antiqua* shells results often more positive than modern specimens in all the localities studied except for Caleta Olivia, where modern and Holocene shells show similar $\delta^{13}C$ values (Fig. 232). This appears similar to what seen for Camarones for the Mytilidae specimens, in a way that may suggest that Brazilian current is not only saltier and more isotopically enriched compared to Malvinas but probably also characterized by higher $\delta^{13}C$, as indicated by the data obtained by Kroopnick, 1980.

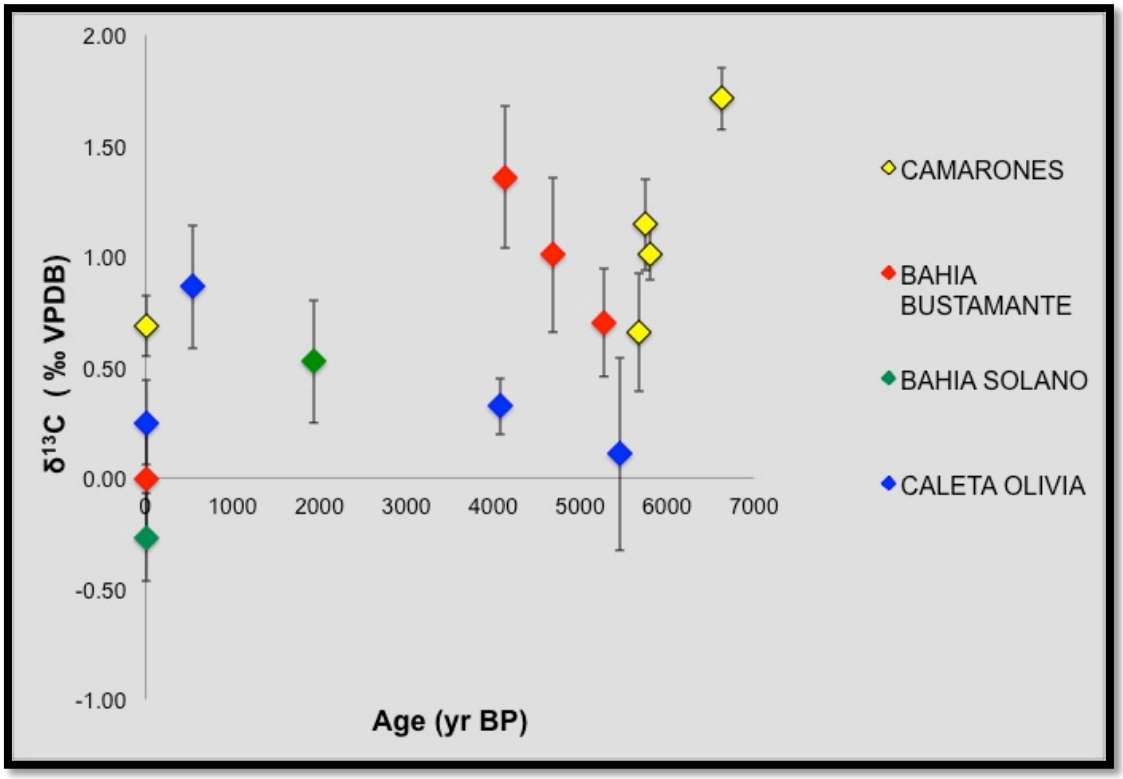

Figure 232 – Carbon isotope composition of Holocene *Ameghinomya antiqua* shells collected from Atlantic Patagonia beach deposits.

7.3.4. Stable isotope composition and trace element concentrations of Pleistocene *Ameghinomya antiqua* shells

The *A. antiqua* shells sampled from beach deposits outcropping in Camarones and Bahia Bustamante dated at MIS 5 show oxygen mean values slightly higher than modern and older Pleistocene shells, which instead are quite similar (Fig. 233). However, standard deviations from mean values do not allow differentiating them. All Pleistocene shells $\delta^{13}C$ mean values are more positive than the modern shell mean value, but even in this case the high standard deviations from mean values make that the valuesoverlap (Fig. 234). The higher values of $\delta^{18}O$ and $\delta^{13}C$ in *A. antiqua* shells from beach ridges deposited during the last interglacial in Camarones and Bahia Bustamante should indicate, as during middle Holocene, that the Brazilian current had a stronger influence down to Bahia Bustamante, while lost its influence in Caleta Olivia. In Caleta Olivia, in fact, specimens from Pleistocene beach deposits belonging to the different MIS show mean values of the isotopic composition rather homogeneous both for oxygen both for carbon and substantially

overlapping with the mean values of modern *Ameghinomya antiqua* shells, suggesting that the general conditions of the littoral environment during the Mid-Late Pleistocene highstands were similar, in this area, to the modern nearshore.

Comparing the oxygen isotopic composition of Pleistocene *A. antiqua* shells collected from various beach ridges along the Patagonia Atlantic coast it is possible to observe that, unlike Holocene (when in older periods this signal is lost) the shells selected from beach sediments deposited during Mid-Late Pleistocene interglacials in the southern part of the study area (Caleta Olivia), in particular during MIS 7 and MIS 9, have higher values of $\delta^{18}O$ than specimens collected further north (Fig. 233), while the carbon isotopic composition does not show this trend (Fig. 234). This suggest that the Malvinas/Falkland Current may have been active along the Patagonia Atlantic coast at least since Mid-Late Pleistocene, as also indicated by Patagonian fossil assemblages (Aguirre *et al.,* 2008) and that probably during the Middle Pleistocene interglacials the Malvinas/Falkland current was stronger than during the middle Holocene (and probably during the last interglacial period).

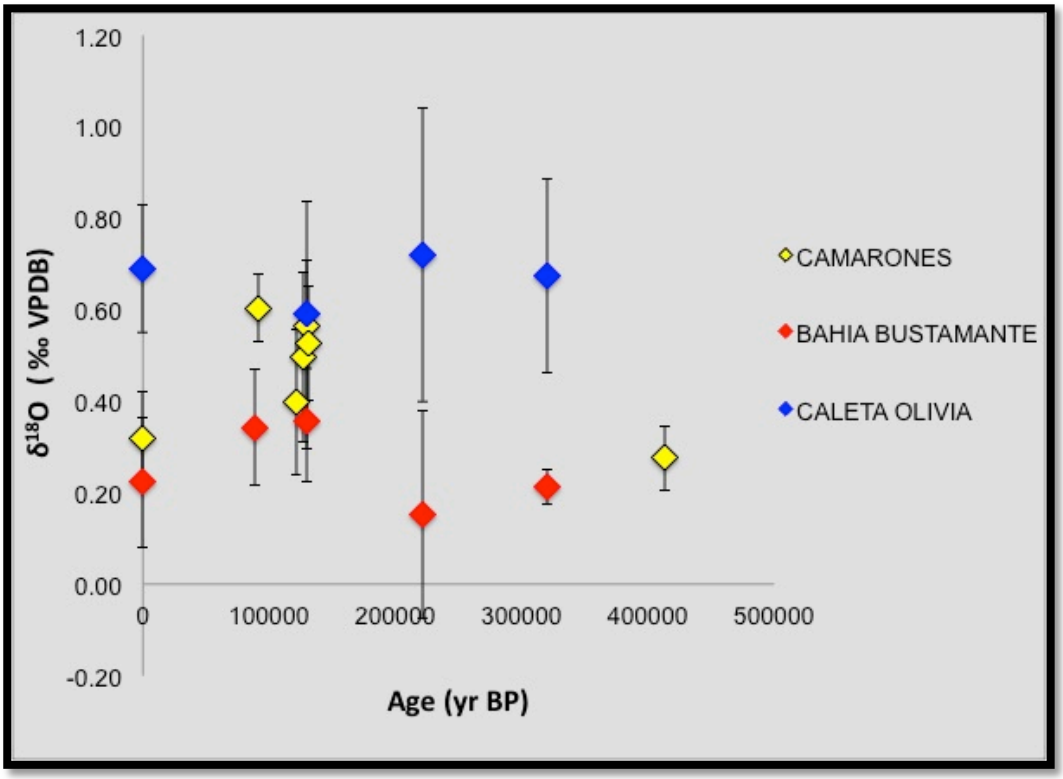

Figure 233 – Oxygen isotope composition of Pleistocene *Ameghinomya antiqua* shells collected from Atlantic Patagonia beach deposits.

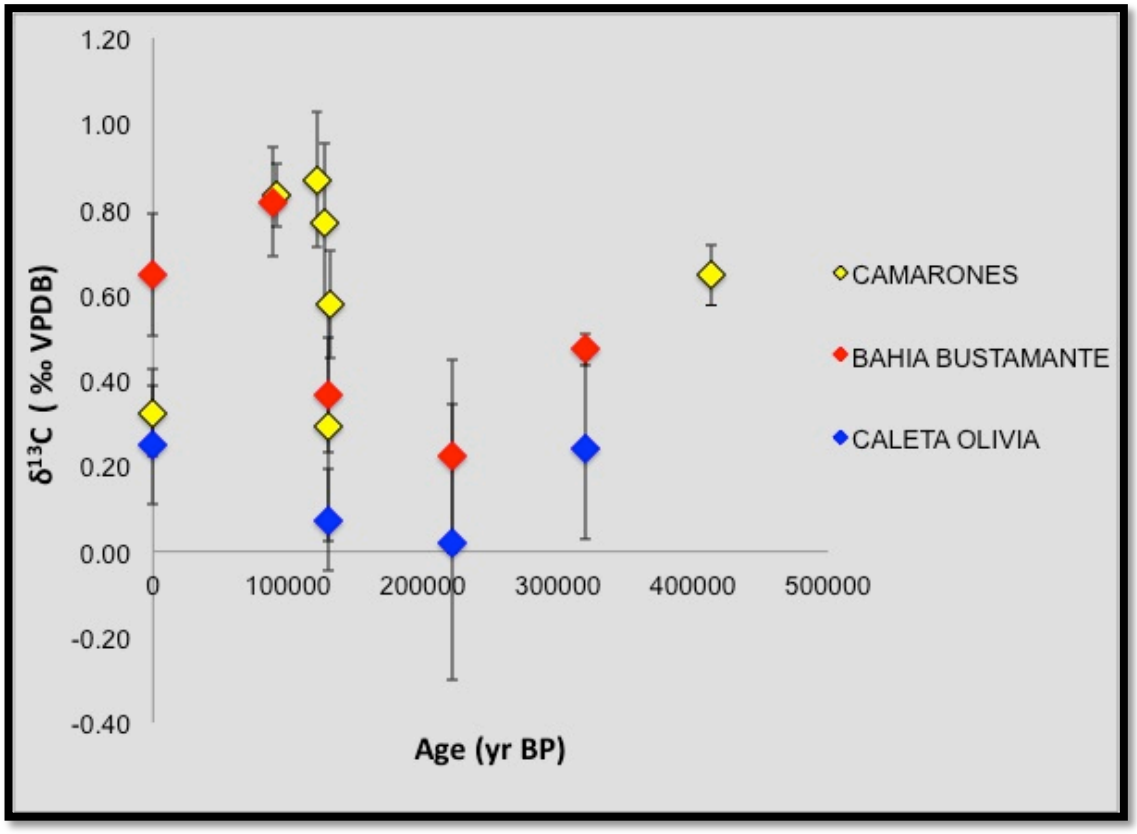

Figure 234 – Carbon isotope composition of Pleistocene *Ameghinomya antiqua* shells collected from Atlantic Patagonia beach deposits.

Trace element results obtained from fossil *A. antiqua* shells from Camarones area indicate that fossil specimens show lower contents of Fe, Mn and Mg (present in large concentrations in continental waters and paleosols from the study area) and higher values of Sr than the modern individuals (Fig. 235). These data could suggest a subtle mixing between seawater and freshwater for modern *Ameghinomya antiqua* shells, while fossil shells have characteristics more strictly marine.

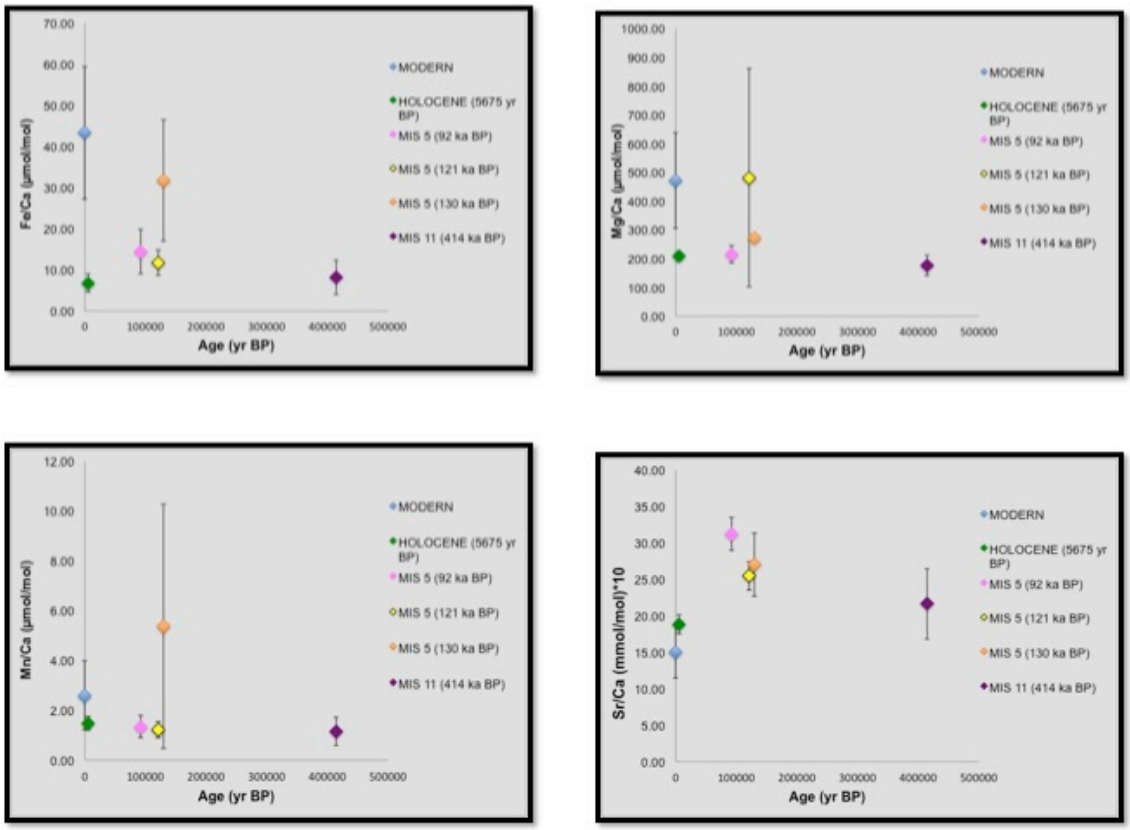

Figure 235 – Trace element concentrations (Fe/Ca, Mg/Ca, Mn/Ca, Sr/Ca) in modern and fossil *A. antiqua* shells from Camarones area.

Finally, fossil shells collected from the older Pleistocene deposits from Bahia Bustamante show slightly lower values of Mg/Ca ratio (Fig. 236) and of $\delta^{18}O$ (Fig. 233) and $\delta^{13}C$ (Fig. 234), suggesting a stronger influence of Malvinas/Falkland current during the Marine Isotope Stage 7 and 9 in comparison to more recent interglacial periods.

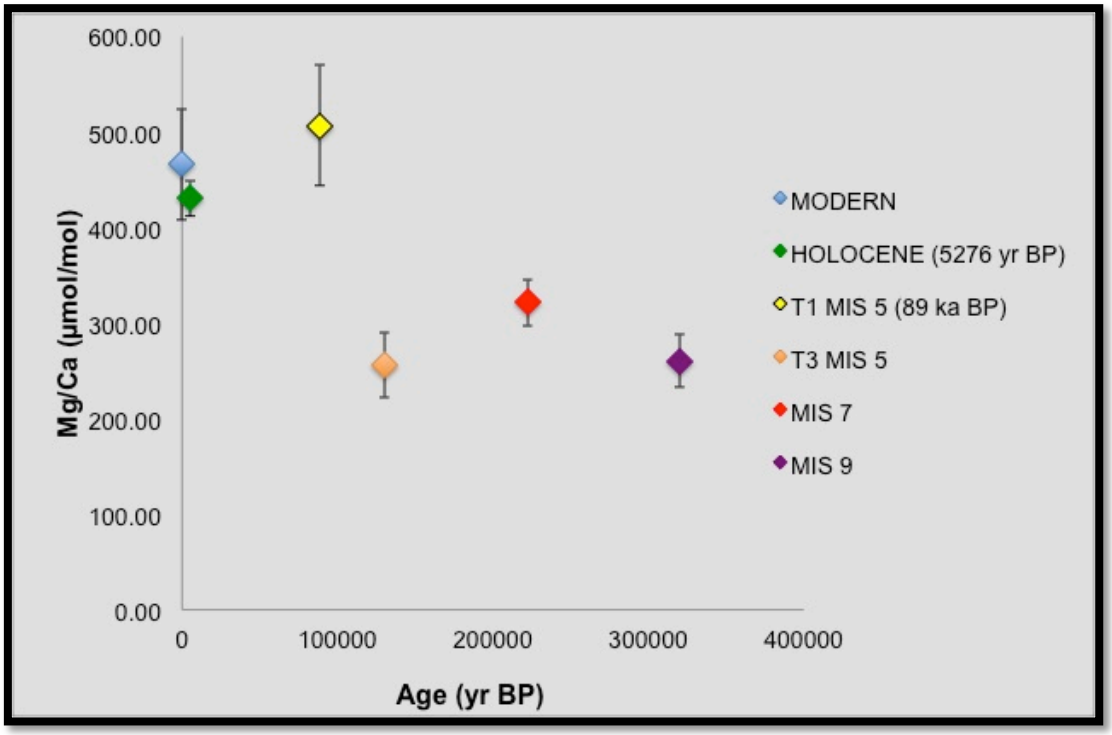

Figure 236 – Mg/Ca ratio in modern and fossil *A. antiqua* shells from Bahia Bustamante area.

8. CONCLUSIONS

In this study paleoenvironmental and paleoclimatic reconstructions based on geochemical analyses (stable isotopes and trace elements) of marine shells from Atlantic coast of Argentine Patagonia have been proposed in order to understand the effects of climate changes on this coastal environment. The general hypothesis which motivated this was linked to paleontological evidence that the position of the Falkland/Malvinas and Brazilian current boundaries were changed during time and can have been recognized in the spectacular raised beach deposit of Atlantic Patagonian coast. If this occurred we can except some differences between the different interglacials and within the same interglacials. For doing this, a good geological and chronological control of the studied section was necessary and this was achieved with very detailed fieldwork within the projects funded by the University of Pisa (Progetto Ateneo 2007) and the Ministry of Education, University and Research (PRIN 2009). In addition, in this thesis we have try to test the potential applicability of U/Th on marine shells, having in mind that this is not a simple task. The results were encouraging but still a lot of work has to do.

To have robust starting point for comparison of the data with the fossils, a significant number of modern shells along a latitudinal transect was analyzed for understanding the latitudinal patterns.

The values of the isotopic composition and trace elements of modern and fossil marine shells, despite complex, confirm that the “work hypothesis” was correct, and the data available have yielded important paleoclimatic and paleoenvironmental information in regard to areas and chronological intervals considered.

The achieved results are particularly important because the study was carried out on deposits practically unexplored as climatic archives.

Specifically conclusions derived from this study are:

1. The geochemical data of marine faunas analyzed demonstrate the suitability of *Ameghinomya antiqua* and Mytilidae family specimens as potential proxies for paleoclimatic studies (and for radiocarbon dating) even if the effects of diagenesis are present and can influence largely the U/Th dating, fact already

known but which is confirmed in this study. Because the samples (marine molluscs) are representative must not have undergone any mineralogical change. Thanks to the good state of preservation of the samples tested by appropriate analysis, it was possible to carry out the stable isotope and trace element analysis.

2. Modern *M. edulis* shells show an increase both in oxygen and in carbon isotope composition moving southward along the Patagonia Atlantic coast. The observed latitudinal gradient can be related to changes in seawater temperature. The modern data show that this gradient is in part difficult to understand for *A. antiqua* and this can be explained with phenomena of subtle local mixing with freshwater. This also opens the possibility (which is then used in the interpretation) that some elements such as Fe and Mn can be used as indicators of local mixing with freshwater, or at least on a certain range of concentrations; for too high values, in fact, we are in the presence of diagenetic phenomena.

3. Albeit in a complex way, Holocene data suggest that geochemical data can be used both as indicators of a progressive variation of coastal morphology and of the presence of more or less closed environments that progressively go to conditions of full opening to the sea as Holocene transgressive regressive cycle progress (and in this area in concomitance with strong glacioisostatic adjustments), but can be used also in relation to a greater influence of the Brazilian current, which took place about 6000 yr ago, than it does nowadays. Variations in the relative position between the two oceanic currents may have occurred during the Middle Holocene, as derived from two different species of marine bivalves (*A. antiqua* and *M. edulis*).

4. The data of Mid-Late Pleistocene interglacials suggest that the Marine Isotope Stage 5 was different from an isotopic point of view, having higher oxygen isotopic compositions and suggesting a greater influence of the Brazilian current down to Bahia Bustamante.

5. In the end, the obtained data, if placed in a well-defined chronological framework, allow us to affirm that these archives have a substantial potential to

unravel the paleoceanographic evolution of unexplored coastal areas. Such data can elucidate regional and continental-scale climate patterns. The importance of marine recorders from southern South America becomes apparent when considering the well-known role of the Southern Ocean in regulating the global climate.

Ringraziamenti

Ringrazio il mio Tutor, il Dott. Gianni Zanchetta, per avermi permesso di seguire un mio sogno.
Ringrazio i miei “compagni di viaggio e di progetto” (la Dott.ssa Monica Bini, la Dott.ssa Ilaria Isola, la Prof.ssa Marta Pappalardo, il Dott. Adriano Ribolini e il Dott. Luca Ragaini). Da ognuno di loro ho imparato qualcosa.
Grazie ai colleghi argentini (Marina Aguirre, Enrique Fucks, Gabriella Boretto e Melisa Charò) e in particolare a Juan Carlos e al suo mitico coche che ci ha permesso di arrivare più o meno ovunque.
Ringrazio il Dott. Guidi e il Dott. Dallai per avermi permesso di utilizzare i laboratori dell’Istituto di Geoscienze e Georisorse del C.N.R. di Pisa, in cui mi sono persa spesso all’inizio e che poi sono diventati una seconda casa.
Grazie di cuore alla Dott.ssa Ilaria Baneschi per i lunghi periodi trascorsi insieme in laboratorio.
E, infine, grazie alla mia famiglia, che mi ha permesso di lavorare con serenità a questo dottorato. Qualsiasi cosa succedesse, bastava tornare a casa per ritrovare il sorriso.

REFERENCES

A

Aguirre, M. L. (2001). *Molluscs as indicators of climatic changes in the marine Holocene of Argentina (South America). I*n Expanded Abstracts, V Iberian Quaternary Meeting and I Quaternary Congress of Countries of Iberian Languages (pp. 382-385).

Aguirre, M. L. (2002). *Optimo climático en el Holoceno marino de la Argentina: evidencias malacológicas.* In Actas XV Congreso Geológico Argentino (Vol. 1, pp. 548-553).

Aguirre, M.L. (2003) – *Late Pleistocene and Holocene palaeoenvironments in Golfo San Jorge, Patagonia: molluscan evidence.* Marine Geology, **194**, 3-30.

Aguirre, M. L., & Farinati, E. A. (2000) – *Aspectos sistemáticos, de distribución y paleoambientales de Littoridina australis (D'Orbigny, 1835)(Mesogastropoda) en el Cuaternario marino de Argentina (Sudamerica).* Geobios, **33**(5), 569-597.

Aguirre, M. L., Leng, M. J., & Spiro, B. (1998) – *Variation in isotopic composition (C, O and Sr) of Holocene Mactra isabelleana (Bivalvia) from the coast of Buenos Aires Province, Argentina*. The Holocene**, 8**(5), 613-621.

Aguirre, M. L., Zanchetta, G., & Fallick, A. E. (2002) – *Stable isotope composition of Littoridina australis from the coast of Buenos Aires province, Argentina, during Holocene climatic fluctuations.* Geobios, **35**(1), 79-88.

Aguirre, M. L., Sirch, Y. N., & Richiano, S. (2005) – *Late Quaternary molluscan assemblages from the coastal area of Bahia Bustamante (Patagonia, Argentina): paleoecology and paleoenvironments*. Journal of South American Earth Sciences, **20**(1), 13-32.

Aguirre, M. L., Richiano, S., & Negro Sirch, Y. (2006) – *Palaeoenvironments and palaeoclimates of the Quaternary molluscan faunas from the coastal area of Bahía Vera-Camarones (Chubut, Patagonia).* Palaeogeography, Palaeoclimatology, Palaeoecology, **229**(4), 251-286.

Aguirre, M. L., Hlebszevitsch Savalscky, J. C., & Dellatorre, F. (2008) – *Late Cenozoic invertebrate paleontology of Patagonia and Tierra del Fuego, with emphasis on molluscs.* Developments in Quaternary Sciences, **11**, 285-325.

Aguirre, M. L., Richiano, S., Álvarez, M. F., & Eastoe, C. (2009) – *Malacofauna Cuaternaria del litoral norte de Santa Cruz (Patagonia, Argentina)*. Geobios, **42(**4), 411-434.

Aguirre, M. L., Richiano, S., Farinati, E., & Fucks, E. (2011) – *Taphonomic comparison between two bivalves Mactra and Brachidontes from Late Quaternary deposits in northern Argentina: Which intrinsic and extrinsic factors prevail under different palaeoenvironmental conditions?*. Quaternary International, **233**(2), 113-129.

Almada-Villela, P. C., Davenport, J., & Gruffydd, L. D. (1982) - *The effects of temperature on the shell growth of young mytilus edulis L.* Journal of Experimental Marine Biology and Ecology, **59**(2), 275-288.

Almeida, F.F.M.de, Hasui, Y., Brito Neves, B.B. (1976) – *The Upper Precambrian of South America.* Universidade de Sao Paulo, Instituto de Geociencias, Boletim, **7**, 45-80.

Anagnostou, E., Sherrell, R. M., Gagnon, A., LaVigne, M., Field, M. P., & McDonough, W. F. (2011) – *Seawater nutrient and carbonate ion concentrations recorded as P/Ca, Ba/Ca, and U/Ca in the deep-sea coral Desmophyllum dianthus.* Geochimica et Cosmochimica Acta, **75**(9), 2529-2543.

Ariztegui, D., Anselmetti, F. S., Gilli, A., & Waldmann, N. (2008) – *Late pleistocene environmental change in Eastern Patagonia and Tierra del Fuego–A limnogeological approach*. Developments in Quaternary Sciences, **11**, 241-253.

Assireu, A. T., Stevenson, M. R., & Stech, J. L. (2003) – *Surface circulation and kinetic energy in the SW Atlantic obtained by drifters.* Continental Shelf Research, **23**(2), 145-157.

B

Baldi, J. E., & Nevistic, V. A. (1996) – *Cuenca costa afuera del Golfo San Jorge.* Geologia y Recursos naturales de la plataforma continental Argentina. Association Geológica Argentina/Institute Argentine del Petróleo, Buenos Aires, Argentina, 171-192.

Barros, V., Castañeda, M., & Doyle, M. (1996). *Recent precipitation trends in Southern South America to the East of the Andes, an indication of a mode of climatic variability Green House Emission Under Developing Country Point of View.* In Proceeding of the Latin America Workshop on Green House Emission of Energy Sector and their Impacts. Rio de Janeiro.

Bathurst, R. G. (1975). *Carbonate sediments and their diagenesis* (Vol. 12). Elsevier Science.

Beck, J. W., Edwards, R. L., Ito, E., Taylor, F. W., Recy, J., Rougerie, F., ... & Henin, C. (1992) – *Sea-surface temperature from coral skeletal strontium/calcium ratios.* Science, **257**(5070), 644-647.

Bernard, F.R. (1983) – *Catalogue of the living Bivalvia of the Eastern Pacific Ocean: Bering Strait to Cape Horn.* Canadian Special Publication of Fisheries and Aquatic Sciences **61**. Government of Canada, Fisheries and Oceans, Scientific Information and Publications Branch, Ottawa, 103 p.

Bertiller, M. B., Elissalde, N. O., Rostagno, C. M., & Defossé, G. E. (1995) – *Environmental patterns and plant distribution along aprecipitation gradient in western Patagonia*. Journal of Arid Environments, **29**(1), 85-97.

Beu, A.G. (2004) – *Marine Mollusca of oxygen isotope stages of the last 2 million years in New Zealand. Part 1: Revised generic positions and recognition of warm-water and cool-water migrants.* Journal of the Royal Society of New Zealand, **44** (2), 111-265.

Beu, A. G., Griffin, M., & Maxwell, P. A. (1997) – *Opening of Drake Passage gateway and Late Miocene to Pleistocene cooling reflected in Southern Ocean molluscan dispersal: evidence from New Zealand and Argentina*. Tectonophysics, **281**(1), 83-97.

Blanchard, R. L., Cheng, M. H., & Potratz, H. A. (1967) – *Uranium and thorium series disequilibria in recent and fossil marine molluscan shells*. Journal of geophysical research, **72**(18), 4745-4757.

Boebel, O., Davis, R. E., Ollitrault, M., Peterson, R. G., Richardson, P. L., Schmid, C., & Zenk, W. (1999) – *The intermediate depth circulation of the western South Atlantic.* Geophysical Research Letters, **26**(21), 3329-3332.

Bonadonna, F. P., Leone, G., & Zanchetta, G. (1995) – *Composición isotópica de los fósiles de gasterópodos continentales de la provincia de Buenos Aires. Indicaciones paleoclimáticas.* Evolución biológica y climática de la región pampeana durante los últimos cinco millones de años. Alberdi MT, Leone G, Tonni EP, Eds. *CSIC, Madrid*, 77-104.

Bonadonna, F. P., Leone, G., & Zanchetta, G. (1995) – *Algunos datos de la composicion isotopica de la crostas carbonatadas de los acantilados marino entre Mar Del Plata y Miramar.* Evolución Biológica y Climática de la Región Pampeana Durante Los últimos Cinco Millones de Años: Un Ensayo de Correlación con el Mediterráneo Occidental, 12, 121.

Bonadonna, F. P., Leone, G., & Zanchetta, G. (1999) – *Stable isotope analyses on the last 30 ka molluscan fauna from Pampa grassland, Bonaerense region, Argentina.* Palaeogeography, Palaeoclimatology, Palaeoecology, **153**(1), 289-308.

Bourgoin, B. P. (1990) – *Mytilus edulis shell as a bioindicator of lead pollution: Considerations on bioavailability and variability*. Mar. Ecol. Prog. *Ser.* **61,** 253–262.

Bowen, R. (1988) - *Isotopes in the earth sciences*. Elsevier, New York.

Branch, G.M. et al. (2002). *Two Oceans*. 5th impression. David Philip, Cate Town & Johannesburg.

Brand, U. (1989) – *Global climatic changes during the Devonian-Mississippian: Stable isotope biogeochemistry of brachiopods.* Global and Planetary Change, **1**(4), 311-329.
Brand, U., & Morrison, J. O. (1987) – *Paleoscene# 6. Biogeochemistry of fossil marine invertebrates*. Geoscience Canada, **14**(2).
Brand, U., & Veizer, J. (1980). *Chemical diagenesis of a multicomponent carbonate system; 1, Trace elements*. Journal of Sedimentary Research, **50**(4), 1219-1236.
Brandini, F. P., Boltovskoy, D., Piola, A., Kocmur, S., Röttgers, R., Cesar Abreu, P., & Mendes Lopes, R. (2000) – *Multiannual trends in fronts and distribution of nutrients and chlorophyll in the southwestern Atlantic (30–62 S).* Deep Sea Research Part I: Oceanographic Research Papers, **47**(6), 1015-1033.
Broecker, W. S. (1963) – *A preliminary evaluation of uranium series inequilibrium as a tool for absolute age measurement on marine carbonates.* Journal of Geophysical Research, **68**(9), 2817-2834.
Broecker, W.S., Olson, E.A. (1961) – *Lamont radiocarbon measurements VIII.* Radiocarbon, **3**, 176–204.
Brunet, F., Gaiero, D., Probst, J. L., Depetris, P. J., Gauthier Lafaye, F., & Stille, P. (2005) – *$\delta^{13}C$ tracing of dissolved inorganic carbon sources in Patagonian rivers (Argentina)*. Hydrological processes, **19**(17), 3321-3344.
Butzin, M., Prange, M., & Lohmann, G. (2005) – *Radiocarbon simulations for the glacial ocean: the effects of wind stress, Southern Ocean sea ice and Heinrich events.* Earth and Planetary Science Letters, **235**(1), 45-61.

C

Capo, R. C., & DePaolo, D. J. (1990) – *Seawater strontium isotopic variations from 2.5 million years ago to the present.* Science, **249**(4964), 51-55.
Carcelles, A. (1944) – *Catálogo de los moluscos marinos de Puerto Quequén*. Revista del Museo Argentino de Ciencias Naturales, Sección Zoología **3**, 233-309.
Carcelles, R. A. (1950) – *Catálogo de los moluscos mari- nos de la Patagonia*. Anales del Museo del Nahuel Huapi **2**, 41-99
Carter, J. G. (1990) – *Shell microstructural data for the Bivalvia. In* Carter, J. G., editor. ed. Skeletal Biomineralization: Patterns, Processes and Evolutionary Trends vol. 1:p. 297–411.Van Nostrand Reinhold. New York.
Castellanos, Z.J.A. (1967) – *Catálogo de los moluscos marinos bonaerenses.* Anales de la Comisión de Investigación Científica de la Provincia de Buenos Aires (CIC) **8,** 1–365.
Chave, K. E. (1954) – *Aspects of the biogeochemistry of magnesium 2. Calcareous sediments and rocks.* The Journal of Geology, 587-599.
Chen, J. H., Wasserburg, G. J., Von Damm, K. L., & Edmond, J. M. (1986) – *The U-Th-Pb systematics in hot springs on the East Pacific Rise at 21 N and Guaymas Basin*. Geochimica et Cosmochimica Acta, **50**(11), 2467-2479.
Chiessi, C. M., Ulrich, S., Mulitza, S., Pätzold, J., & Wefer, G. (2007) – *Signature of the Brazil-Malvinas Confluence (Argentine Basin) in the isotopic composition of planktonic foraminifera from surface sediments.* Marine Micropaleontology, **64**(1), 52-66.
Chung, G. S., & Swart, P. K. (1990) – *The concentration of uranium in freshwater vadose and phreatic cements in a Holocene ooid cay; a method of identifying ancient water tables*. Journal of Sedimentary Research, **60**(5), 735-746.
Cionchi, J.L. (1985) – *Geomorfologıa y estratigrafıa del Cuaternario de Bahıa Bustamante y zonas adyacentes, provincia de Chubut.* Doctoral thesis (Geol.), FCNYM, Universidad Nacional de La Plata.
Cionchi, J.L. (1987) – *Depositos marinos Cuaternarios de Bahia Bustamante, Provincia del Chubut*. Rev. Asoc. Geol. Argent., **42**, 61-72.
Cionchi, J. L. (1988). *Geomorfología de Bahía Bustamante y zonas adyacentes, Chubut.* Revista de la Asociación Geológica Argentina, **43**, 51-62.
Clapperton, C. (1993) – *Nature of environmental changes in South America at the Last Glacial Maximum*. Palaeogeography Palaeoclimatology Palaeoecology, **101**, 189-208.

Clark, S. P. (1957) – *A note on calcite-aragonite equilibrium.* Am. Mineralogist, **42**(7), 8.
Clasing, E., Brey, T, Otead, R., Navarro, J., Asencio, G. (1994) - *Population dynamics of Venus Antigua (Bivalvia: Veneracea) in the Bahía de Yaldad, Isla de Chiloé, Southern Chile.* Journal of Experimental Marine Biology and Ecology, **177**, 171-186.
Codignotto, J.O. (1983) – *Depositos elevados y/o de Acrecion Pleistoceno-Holoceno en la costa Fueguino-Patagonica.* Simposio Oscilaciones del Nivel del Mar Durante el Ultimo Hemiciclo Deglacial en la Argentina. (IGCP200), Univ. Nac. Mar del Plata, Actas, pp. 12-26.
Codignotto, J. O. (1987). *Cuaternario marino entre Tierra del fuego y Buenos Aires.* Revista de la Asociación Geológica Argentina, **42**(1-2), 208-212.
Codignotto, J. O., Marcomini, S. C., & Santillana, S. (1988) – *Terrazas marinas entre Puerto Deseado y Bahía Bustamante, Santa Cruz-Chubut.* Revista de la Asociación Geológica Argentina, **43**(1), 43-50.
Codignotto, J. O., Césari, O., & Beros, C. A. (1990). *Morfocronología secuencial evolutiva holocena en Bahía Solano, Chubut*. Revista de la Asociación Geológica Argentina, **45(**3-4), 205-212.
Codignotto, J., Kokot, R., Marcomini, S. (1992) – *Neotectonism and sea-level changes in the zone of Argentina.* Journal of Coastal Research, **8**, 125-133.
Colonese, A. C., Camarós, E., Verdún, E., Estévez, J., Giralt, S., & Rejas, M. (2011) – *Integrated Archaeozoological Research of Shell Middens: New Insights Into Hunter-Gatherer-Fisher Coastal Exploitation in Tierra Del Fuego*. The Journal of Island and Coastal Archaeology, **6**(2), 235-254.
Colonese, A. C., Verdún-Castelló, E., Álvarez, M., Briz i Godino, I., Zurro, D., & Salvatelli, L. (2012) - *Oxygen isotopic composition of limpet shells from the Beagle Channel: implications for seasonal studies in shell middens of Tierra del Fuego.* Journal of Archaeological Science, **39**(6), 1738-1748.
Conti, M. E., Stripeikis, J., Finoia, M. G., & Tudino, M. B. (2011*) – Baseline trace metals in bivalve molluscs from the Beagle Channel, Patagonia (Argentina).* Ecotoxicology, **20**(6), 1341-1353.
Conti, M. E., Stripeikis, J., Finoia, M. G., & Tudino, M. B. (2012) – *Baseline trace metals in gastropod mollusks from the Beagle Channel, Tierra del Fuego (Patagonia, Argentina).* Ecotoxicology, **21**(4), 1112-1125.
Coplen, T. B. (1994) – *Reporting of stable hydrogen, carbon, and oxygen isotopic abundances.* Pure and Applied Chemistry, **66**, 273-273.
Coplen, T. B. (1997) – *Atomic weights of the elements 1995.* Journal of Physical and Chemical Reference Data, **26**, 1239.
Coplen, T.B., Kendall, C., Hopple, J. (1983) – *Comparison of stable isotope reference samples*. Nature, **302**, 236–238.
Cordero, R.R., Panarello, H., Lanzelotti, S., Dubois, C.M.F. (2003) – *Radiocarbon age offsets between living organisms from the marine and continental reservoir in coastal localities of Patagonia (Argentina).* Radiocarbon, **45**, 9–15.
Coronato, A. M., Coronato, F., Mazzoni, E., & Vázquez, M. (2008) – *The physical geography of Patagonia and Tierra del Fuego.* Developments in Quaternary Sciences, **11**, 13-55.
Corrège, T. (1993) – *The relationship between water masses and benthic ostracod assemblages in the western Coral Sea, Southwest Pacific.* Palaeogeography, palaeoclimatology, palaeoecology, **105**(3), 245-266.
Cortiñas, J.S. (1996) – *La cuenca de Somuncurá – Cañadón Asfalto: sus límites, ciclos evolutivos del relleno sedimentario y posibilidades exploratorias.* 13° Congreso Geológico Argentino y 3° Congreso de Exploración de Hidrocarburos, Buenos Aires, Actas I, 147–163.
Craig, H. (1957) – *Isotopic standards for carbon and oxygen and correction factors for mass-spectrometric analysis of carbon dioxide*. Geochimica et cosmochimica acta, **12**(1), 133-149.

Craig, H. (1961) – *Standard for reporting concentrations of deuterium and oxygen-18 in natural waters.* Science, **133** (3467), 1833-1834.
Craig, H. (1965) – *The measurement of oxygen isotope paleotemperatures*. in Stable Isotopes in Oceanographic Studies and Paleotemperatures, edited by E. Tongiorgi, Consiglio nazionale delle ricerche, Laboratorio de geologia nucleare, 23, Spoleto, Italy.
Craig, H., & Gordon, L. I. (1965) – *Deuterium and oxygen 18 variations in the ocean and the marine atmosphere*. in Stable Isotopes in Oceanographic Studies and Paleotemperatures, edited by E. Tongiorgi, Consiglio nazionale delle ricerche, Laboratorio de geologia nucleare, pp. 9–130, Spoleto, Italy.
Cross, T. S., & Cross, B. W. (1983) – *U, Sr, and Mg in Holocene and Pleistocene corals A. palmata and M. annularis.* Journal of Sedimentary Research, **53**(2), 587-594.

D

D'Orbigny, A. (1834–1847) – *Voyage dans l'Amérique Méridionale. Mollusques. Tome* V(3), xliii + 758 pps., atlas (Tome 9), 85 pls. Paris.
D'Orbigny, A. (1834–1847) – *Voyage dans l'Amérique Méridionale. Paléontologie*. Tome III(4): 1-152, pls. 1-22. Paris & Strassbourg.
Dansgaard, W., & Tauber, H. (1969) – *Glacier oxygen-18 content and Pleistocene ocean temperatures.* Science, **166**(3904), 499-502.
Darwin, C. (1846) – *Geological observations on South America.* Smith, Elder and Co., 65 Cornhill, London, pp. 279.
Depaolo, D. J., & Ingram, B. L. (1985) – *High-resolution stratigraphy with strontium isotopes*. Science, 227(4689), 938-941.
de Villiers, S. (1999) – *Seawater strontium and Sr/Ca variability in the Atlantic and Pacific oceans*. Earth and Planetary Science Letters, **171**(4), 623-634.
De Wit, M. (1977) – *The evolution of the Scotia Arc as a Key to the reconstruction of southwestern Gondwanaland.* Tectonophysics, **37** (1–3), 53–81.
Dodd, J.R. (1965) – *Environmental control of strontium and magnesium in Mytilus.* Geochimica et Cosmochimica Acta, **29**, 385-398.
Dodd, J. R. (1967) – *Magnesium and strontium in calcareous skeletons: a review.* Journal of Paleontology, 1313-1329.
Dodd, J. R., & Stanton, R. J. (1975*)* – *Paleosalinities within a Pliocene bay, Kettleman Hills, California: a study of the resolving power of isotopic and faunal techniques*. Geological Society of America Bulletin, **86**(1), 51-64.
Drever, J. I. (1997) - *The geochemistry of natural waters: surface and groundwater environments*.
Duarte, C. A., Giarratano, E., & Gil, M. N. (2012) – *Trace metal content in sediments and autochthonous intertidal organisms from two adjacent bays near Ushuaia, Beagle Channel (Argentina).* Marine environmental research, **79**, 55-62.

E

Eisma, D., Mook, W. G., & Das, H. A. (1976) – *Shell characteristics, isotopic composition and trace-element contents of some euryhaline molluscs as indicators of salinity*. Palaeogeography, Palaeoclimatology, Palaeoecology, **19**(1), 39-62.
Elliot, M., Welsh, K., Chilcott, C., McCulloch, M., Chappell, J., & Ayling, B. (2009) – *Profiles of trace elements and stable isotopes derived from giant long-lived Tridacna gigas bivalves: Potential applications in paleoclimate studies.* Palaeogeography, Palaeoclimatology, Palaeoecology, **280**(1), 132-142.
Emiliani, C. (1955) – *Pleistocene temperatures*. The Journal of Geology, 538-578.
Epstein, S., & Mayeda, T. (1953) – *Variation of ^{18}O content of waters from natural sources.* Geochimica et cosmochimica acta, **4**(5), 213-224.

Epstein, S., Buchsbaum, R., Lowenstam, H. A., & Urey, H. C. (1953) – *Revised carbonate-water isotopic temperature scale*. Geological Society of America Bulletin, **64(**11), 1315-1326.

Erez, J., & Luz, B. (1983) – *Experimental paleotemperature equation for planktonic foraminifera.* Geochimica et Cosmochimica Acta, **47**(6), 1025-1031.

España, M. A., Rodríguez, E. R., & Romero, C. D. (2005) – *Sodium, K, Ca, Mg, Fe, Cu, and Zn concentrations in molluscs from the Magellan Strait (Chile): Their contribution to dietary intake.* International journal of food sciences and nutrition, **56**(5), 337-347.

España, A., Rodríguez Rodríguez, E. M., & Díaz Romero, C. (2007) – *Comparison of mineral and trace element concentrations in two molluscs from the Strait of Magellan (Chile).* Journal of Food Composition and Analysis, **20**(3), 273-279.

Esteves, L.S. Pivel, M.A.G., Silva, A.R.P., Barletta, R.C., Vranjac, M.P., Oliveira, U.R., and Vanz, A. (2000) – *Beachfront owners perception of erosion along an armored shoreline in southern Brazil*. Pesquisas, **27**(2), 97-109.

F

Fairbanks, R. G., C. D. Charles, and J. D. Wright (1992) – *Origin of global meltwater pulses*, in Radiocarbon After Four Decades: An Interdisciplinary Perspective, edited by R. E. Taylor, A. Long, and R. S. Kra, pp. 473–500, Springer, New York.

Falabella, V*.,* **Campagna, C., Croxall, J.** (2009) – *Atlas del Mar Patagónico: especies y espacios*. Wildlife Conservation Society y Birdlife International.

Feruglio, E. (1933) – *I terrazzi marini della Patagonia.* Giornali di Geologia. Annali del Reale Museo geologico di Bologna, **8**, 1–288.

Feruglio, E., (1947) – *Nueva contribución al estudio de las terrazas marinas de la Patagonia.* Revista de la Sociedad Geologica Argentina II, 223–238 (Buenos Aires).

Feruglio, E. (1949) – *Descripcion Geologica de la Patagonia.* Direccion General de Y.P.F., Tomo 2, 1–349. Buenos Aires.

Feruglio, E. (1950) – *Descripcion Geologica de la Patagonia.* Direccion General de Y.P.F., Buenos Aires, **3**, 431 pp.

Figari, E. G. (2005) – *Evolución tectónica de la Cuenca de Cañadón Asfalto (Zona del valle medio del Río Chubut)* (Doctoral dissertation, Universidad de Buenos Aires).

Figueiras, A., Sicardi O.E. (1969) – *Catálogo de los moluscos marinos del Uruguay.* Comunicaciones de la Sociedad Malacologica del Uruguay, **2**, 355-378.

Figueiras, A., Sicardi O.E. (1980) – *Catálogo de los moluscos marinos del Uruguay. Parte X. Revisión actualizada de los moluscos marinos del Uruguay con descripción de las especies agregadas. Sección II, Gastropoda y Cephalopoda.* Com. Soc. Malac. Uruguay, **5**, 179–272

Fisher-Piette, E. (1975) - *Revision des Venerinae s.s. (Mollusques Lamellibranches).* Mem. Mus. Nat. Hist. Nat. Par^s, Nouvelle Serie, Seri A, Zoologie**, 93**, 1-64.

Fisher-Piette, E. & Vukadinovic, D. (1977) – Suite de *revisions des Veneridae s.s. (Mollusques Lamellibranche) Chioninae, Samaranginae et complement aux Venus.* Mem. Mus. Nat. Hist. Nat. Par^s, Nouvelle Serie, Seri A, Zoologie, **106**, 1-186.

Fitzgerald, M. G., Mitchum Jr, R. M., Uliana, M. A., & Biddle, K. T. (1990) – *Evolution of the San Jorge Basin, Argentina (1). AAPG bulletin*, ***74*(6)**, 879-920.

Foster, L. C., Finch, A. A., Allison, N., Andersson, C., & Clarke, L. J. (2008) – *Mg in aragonitic bivalve shells: Seasonal variations and mode of incorporation in Arctica islandica*. Chemical Geology, **254**(1), 113-119.

Freitas, P.S., Clarke, L.J., Kennedy, H., Richardson, C., Abrantes, F. (2006) – *Environmental and biological controls on elemental (Mg/Ca, Sr/Ca and Mn/Ca) ratios in shells of the king scallop* Pecten maximus. Geochimica et Cosmochimica Acta, **70**, 5119-5133.

Freitas, P. S., Clarke, L. J., Kennedy, H. A., & Richardson, C. A. (2008) – *Inter-and intra-specimen variability masks reliable temperature control on shell Mg/Ca ratios in*

laboratory and field cultured Mytilus edulis and Pecten maximus (bivalvia). Biogeosciences Discussions, 5(1), 531-572.
Frizzell, D. L. (1936) – *Preliminary reclassification of veneracean pelecypods (1).* Bulletin du Musée royal d'Histoire naturelle de Belgique= Mededeelingen van het Koninklijk Natuurhistorisch Museum van België, ***7***(34).

G

Garcia, N. O., Ferreira, R. N., & Latrubesse, E. M. (2009) – *Climate and Geomorphologic-related disasters in Latin America*. Developments in Earth Surface Processes, 13, 1-27.
Garfield, N. (1990). *The Brazil Current at subtropical latitudes*.
Garlick, G.D. (1974) – *The stable isotopes of oxygen, carbon, hydrogen in the marine environment.* In: Goldberg, E.D. (Ed.), The Sea, Vol. 5. John Wiley & Sons, New York, pp. 393-425.
Garreaud, R. D., Vuille, M., Compagnucci, R., & Marengo, J. (2009). *Present-day south american climate.* Palaeogeography, Palaeoclimatology, Palaeoecology, **281**(3), 180-195.
Garzoli, S. L. (1993) – *Geostrophic velocity and transport variability in the Brazil-Malvinas Confluence*. Deep Sea Research Part I: Oceanographic Research Papers, **40**(7), 1379-1403.
Garzoli, S. L., & Bianchi, A. (1987) – *Time–space variability of the local dynamics of the Malvinas–Brazil confluence as revealed by inverted echo sounders.* Journal of Geophysical Research: Oceans (1978–2012), **92(**C2), 1914-1922.
Garzoli, S. L., & Garraffo, Z. (1989) – *Transports, frontal motions and eddies at the Brazil-Malvinas Currents Confluence.* Deep Sea Research Part A. Oceanographic Research Papers, **36**(5), 681-703.
Ghidella, M.E., Yañez, G., LaBrecque, H.L. (2002) – *Revised tectonic implications for the magnetic anomalies of the Western Weddell Sea.* Tectonophysics **347** (1-3), 65–86.
Gil, M. N., Torres, A., Harvey, M., & Esteves, J. L. (2006) – *Metales pesados en organismos marinos de la zona costera de la Patagonia argentina continental.* Revista de biología marina y oceanografía, **41**(2), 167-176.
Gillikin, D.P., Lorrain, A., Navez, J., Taylor, J.W., André, L., Keppens, E., Baeyens W., Dehairs, F. (2005) – *Strong biological controls on Sr/Ca ratios in aragonitic marine bivalve shells.* Geochemistry, Geophysics, Geosystems, **6**, 1-15.
Gillikin, D.P., Dehairs, F., Lorrain, A., Steenmans, D., Baeyens, W., André, L. (2006) – *Barium uptake into the shells of the common mussel (*Mytilus edulis) *and the potential for estuarine paleo-chemistry reconstruction.* Geochimica et Cosmochimica Acta, **70**, 395-407.
Goman, M., Malamud-Roam, F., & Ingram, B. L. (2008) – *Holocene environmental history and evolution of a tidal salt marsh in San Francisco Bay, California.* Journal of Coastal Research, 1126-1137.
Goman, M., Ingram, B. L., & Strom, A. (2008) – *Composition of stable isotopes in geoduck Panopea abrupta shells: A preliminary assessment of annual and seasonal paleoceanographic changes in the northeast Pacific*. Quaternary International, **188**(1), 117-125.
Gomez, D. M. E. A., Borel, C. M., Aguirre, M. L., & Martinez, D. E. (2008) – *Radiocarbon reservoir ages and hardwater effect for the northeastern coastal waters of Argentina.* Radiocarbon, **50**(1), 119-129.
Gonfiantini, R., Stichler, W., Rozanski, K. (1995) – *Standards and intercomparison materials distributed by the International Atomic Energy Agency for stable isotope measurements. Reference and intercomparison materials for stable isotope materials for stable isotopes of light elements.* International Atomic Energy Agency, Vienna, pp. 13–30.

Goni, G., Kamholz, S., Garzoli, S., & Olson, D. (1996) – *Dynamics of the Brazil-Malvinas Confluence based on inverted echo sounders and altimetry.* Journal of Geophysical Research, **101**(C7), 16273-16.

Goni, G. J., & Wainer, I. (2001) – *Investigation of the Brazil Current front variability from altimeter data.* Journal of Geophysical Research: Oceans (1978–2012), **106**(C12), 31117-31128.

Gonzáles-Wevar C.A., Nakano T., Cañete J.I., Poulin E. (2011) - *Concerted genetic, morphological and ecological diversification in Nacella limpets in the Magellanic Province.* Molecular Ecology, **20**, 1936–1951.

Goodkin, N. F., Hughen, K. A., & Cohen, A. L. (2007) – *A multicoral calibration method to approximate a universal equation relating Sr/Ca and growth rate to sea surface temperature.* Paleoceanography, **22**(1).

Gordillo, S., Rabassa, J., Coronato, A. (2008) – *Paleoecology and paleobiogeograohic patterns of mid-Holocene mollusks from the Beagle Channel (southern Tierra del Fuego, Argentina).* Revista Geologica de Chile, **35**, 321-333.

Gordillo, S., Cusminsky, G., Bernasconi, E., Ponce, J. F., Rabassa, J. O., & Pino, M. (2010) – *Pleistocene marine calcareous macro-and-microfossils of Navarino Island (Chile) as environmental proxies during the last interglacial in southern South America.* Quaternary International, **221**(1), 159-174.

Gordon, A. L. (1981) – *South Atlantic thermocline ventilation.* Deep Sea Research Part A. Oceanographic Research Papers, **28**(11), 1239-1264.

Gordon, A. L., & Greengrove, C. L. (1986). *Geostrophic circulation of the Brazil-Falkland confluence*. Deep Sea Research Part A. Oceanographic Research Papers, **33**(5), 573-585.

Grossman, E. L. (1984) – *Carbon isotopic fractionation in live benthic foraminifera—comparison with inorganic precipitate studies.* Geochimica et Cosmochimica Acta, **48**(7), 1505-1512.

Grossman, E. L., & Ku, T. L. (1986). *Oxygen and carbon isotope fractionation in biogenic aragonite: temperature effects.* Chemical Geology: Isotope Geoscience Section, **59**, 59-74.

Guevara, S. R., Bubach, D., Vigliano, P., Lippolt, G., & Arribére, M. (2004) – *Heavy metal and other trace elements in native mussel Diplodon chilensis from Nothern Patagonia Lakes, Argentina.* Biological trace element research, **102**(1-3), 245-263.

Guzmán, N., Saá, N., Ortlieb, L. (1998) – *Catálogo descriptivo de los moluscos litorales (Gastropoday Pelecypoda) de la zona de Antofagasta, 23°S, Chile.* Estudios Oceanológicos, **17**, 17-86.

H

Harrington, H. J. (1962) – *Paleogeographic development of South America*. AAPG Bulletin, **46**(10), 1773-1814.

Hayes, J. M. (1983) – *Practice and principles of isotopic measurements in organic geochemistry.* Organic geochemistry of contemporaneous and ancient sediments, *5*, e5.

Hellstrom, J. (2003) – *Rapid and accurate U/Th dating using parallel ion-counting multi-collector ICP-MS.* Journal of Analytical Atomic Spectrometry, **18**(11), 1346-1351.

Hellstrom, J. (2006) – *U–Th dating of speleothems with high ^{230}Th using stratigraphical constraint.* Quaternary Geochronology, **1**(4), 289-295.

Henderson, G. M. (2002) – *Seawater (^{234}U/^{238}U) during the last 800 thousand years*. Earth and Planetary Science Letters, **199**(1), 97-110.

Hendry, J. P., & Kalin, R. M. (1997) – *Are oxygen and carbon isotopes of mollusc shells reliable palaeosalinity indicators in marginal marine environments? A case study from the Middle Jurassic of England*. Journal of the Geological Society, **154**(2), 321-333.

Herm, D. (1969) – *Marines Pliozin und Pleistozln in Nord- und Mittel-Chile, unter besonderer Bertlck- sichtigung der Entwicklung der Mollusken-Faunen.* Zietteliana **2**, 1-159.

Hoefs, J. (2009). *Stable isotope geochemistry*. Springer.

Holmes, J. A., & Chivas, A. R. (2002) – *The Ostracoda: applications in Quaternary research* (Vol. 131, pp. 1-313). American Geophysical Union

http://earthobservatory.nasa.gov/IOTD/view.php?id=48244

http://data.giss.nasa.gov/o18data/grid.html

http://www.radiocarbon.ldeo.columbia.edu

Huber, M. (2010) - *Compendium of Bivalves*. ConchBooks, Hackenheim, 901 p.
Hudson, J. D., Clements, R. G., Riding, J. B., Wakefield, M. I., & Walton, W. (1995) – *Jurassic paleosalinities and brackish-water communities: A case study.* Palaios, 392-407.
Hughen, K.A., Baillie, M.G.L., et al. (2004) - *Marine 04 marine radiocarbon age calibration, 0–26 kyr BP.* Radiocarbon, **46**(3), 1059–1086.

I

Ihering, H. von (1907) – *Les Mollusques fossiles du Tertiaire et du Cretacé Supérieur de l' Argentine.* Anales del Museo Nacional de Buenos Aires, serie.3**, 14** (7), 1 - 611.
Ingram, B. L., Conrad, M. E., & Ingle, J. C. (1996) – Stable isotope and salinity systematics in estuarine waters and carbonates: San Francisco Bay. Geochimica et Cosmochimica Acta**, 60**(3), 455-467.
Isla, F. I., & Bujalesky, G. G. (1995) – *Tendencias evolutivas y disponibilidad de sedimento en la interpretación de formas costeras: Casos de estudio de la costa argentina.* Revista de la Asociación Argentina de Sedimentología, **2**(1-2), 75-89.
Isla, F.I., and Bujalesky, G.G. (2008) – *Coastal geology and morphology of Patagonia and the Fuegian Archipelago.* Developments in Quaternary Sciences, **11**, 227-239.
Isla, F.I., Spagnuolo, J.O. and Gelo´s, E.M. (2000*). Sedimentologia y mineralogia de playas de Tierra del Fuego y sector Antartico Argentino (Arco de Scotia e islas asociadas).* Asociacion Geologica Argentina, Revista **55**, 3, 216–228. Buenos Aires.
Isla, F. I., Bértola, G. R., & Schnack, E. J. (2001) – *Morfodinámica de playas meso y macromareales de Buenos Aires, Río Negro y Chubut.* Revista de la Asociación Argentina de Sedimentología, **8**(1), 51-60.
Isla, F. I., Bujalesky, G. G., Bértola, G. R., Iantanos, N., & Estrada, E. (2006) – *Typology of Argentine beaches: composition, tidal range and wave energy.* Journal of Coastal Research, 375-378.
Isola, I., Bini, M., Ribolini, A., Pappalardo, M., Consoloni, I., Fucks, E., ... & Zanchetta, G. (2011) – *Geomorphologic Map of Northeastern Sector of San Jorge Gulf (Chubut, Argentina).* Journal of Maps, **7**(1), 476-485.
Izumida, H., Yoshimura, T., Suzuki, A., Nakashima, R., Ishimura, T., Yasuhara, M., ... & Kawahata, H. (2011) – *Biological and water chemistry controls on Sr/Ca, Ba/Ca, Mg/Ca and $\delta^{18}O$ profiles in freshwater pearl mussel Hyriopsis sp*. Palaeogeography, Palaeoclimatology, Palaeoecology, **309**(3), 298-308.

J

Jobbágy, E. G., Paruelo, J. M., & León, R. J. (1996) – *Vegetation heterogeneity and diversity in flat and mountain landscapes of Patagonia (Argentina).* Journal of vegetation Science**, 7**(4), 599-608.

K

Kappner, I., & Bieler, R. (2006) – *Phylogeny of venus clams (Bivalvia: Venerinae) as inferred from nuclear and mitochondrial gene sequences.* Molecular Phylogenetics and Evolution, **40**(2), 317-331.

Kaufman, A., Broecker, W. S., Ku, T. L., & Thurber, D. L. (1971) – *The status of U-series methods of mollusk dating.* Geochimica et Cosmochimica Acta, **35**(11), 1155-1183.

Kaufman, A., Ghaleb, B., Wehmiller, J. F., & Hillaire-Marcel, C. (1996) – *Uranium concentration and isotope ratio profiles within Mercenaria shells:* Geochronological implications. Geochimica et Cosmochimica Acta, **60**(19), 3735-3746.

Kim, S. T., & O'Neil, J. R. (1997) – *Equilibrium and nonequilibrium oxygen isotope effects in synthetic carbonates.* Geochimica et Cosmochimica Acta, **61**(16), 3461-3475.

Kim, S. T., O'Neil, J. R., Hillaire-Marcel, C., & Mucci, A. (2007) – *Oxygen isotope fractionation between synthetic aragonite and water: Influence of temperature and Mg^{2+} concentration*. Geochimica et Cosmochimica Acta, **71**(19), 4704-4715.

Kitano, Y., & Oomori, T. (1971). *The coprecipitation of uranium with calcium carbonate*. Journal of the Oceanographical Society of Japan, **27**(1), 34-42.

Klein, R.T., Lohmann, K.C., Thayer, C.W. (1996) – *Sr/Ca and $^{13}C/^{12}C$ ratios in skeletal calcite of* Mytilus trossulus: *Covariation with metabolic rate, salinity, and carbon isotopic composition of seawater.* Geochimica et Cosmochimica Acta, **60**, 4207-4221.

Kroopnick, P. (1980) – *The distribution of ^{13}C in the Atlantic Ocean.* Earth and Planetary Science Letters, **49**(2), 469-484.

Ku, T. L., Knauss, K. G., & Mathieu, G. G. (1977) – *Uranium in open ocean: concentration and isotopic composition.* Deep Sea Research, **24**(11), 1005-1017.

L

Labonne, M., & Hillaire–Marcel, C. (2000). *Geochemical gradients within modern and fossil shells of Concholepas concholepas from northern Chile: an insight into U–Th systematics and diagenetic/authigenic isotopic imprints in mollusk shells.* Geochimica et Cosmochimica Acta, **64**(9), 1523-1534.

Land, L. S. (1967) – *Diagenesis of skeletal carbonates*. Journal of Sedimentary Research, **37**(3), 914-930.

Langmuir, D. (1978) – *Uranium solution-mineral equilibria at low temperatures with applications to sedimentary ore deposits*. Geochimica et Cosmochimica Acta, **42**(6), 547-569.

Lazareth, C. E., Putten, E. V., André, L., & Dehairs, F. (2003) – *High-resolution trace element profiles in shells of the mangrove bivalve Isognomon ephippium: a record of environmental spatio-temporal variations?.* Estuarine, Coastal and Shelf Science, **57**(5), 1103-1114.

Leanza, A.F. (1958) – *Geología Regional*. In La Argentina, Suma de Geografía, Editorial Peuser **1** (3), 217–349. Buenos Aires.

Legeckis, R., & Gordon, A. L. (1982) – *Satellite observations of the Brazil and Falkland currents—1975 1976 and 1978.* Deep Sea Research Part A. Oceanographic Research Papers, **29**(3), 375-401.

Lisiecki, L. E., & Raymo, M. E. (2005) – *A Pliocene-Pleistocene stack of 57 globally distributed benthic $\delta^{18}O$ records.* Paleoceanography, **20**(1).

LeGrande, A. N., & Schmidt, G. A. (2006) – *Global gridded data set of the oxygen isotopic composition in seawater.* Geophysical Research Letters, 33(12).

Lema, H., Busteros, A., Franchi, M. (2001). *Hoja Geológica 4466 II y IV Camarones, Provincia del Chubut.* Servicio Geológico Minero Argentino, Instituto de Geología y Recursos Minerales. Boletín N° 261: 60 p.

Lentini, C. A. D., Podestá, G. G., Campos, E. J. D., & Olson, D. B. (2001) – *Sea surface temperature anomalies on the Western South Atlantic from 1982 to 1994.* Continental Shelf Research**, 21**(1), 89-112.

Lentini, C. A., Olson, D. B., & Podestá, G. P. (2002) – *Statistics of Brazil Current rings observed from AVHRR: 1993 to 1998*. Geophysical Research Letters, **29(**16), 1811.
León, R. J., Bran, D., Collantes, M., Paruelo, J. M., & Soriano, A. (1998) – *Grandes unidades de vegetación de la Patagonia extra andina*. Ecología Austral, **8**(2), 125-144.
León, R. J. C., & Facelli, J. M. (1981) – *Descripción de una coenoclina en el sudeste del Chubut [ecología vegetal, lluvia, comunidad vegetal, gradiente, Argentina].;[Description of a coenocline in the South-western region of Chubut [plant ecology, rain, plan community, slope, Argentina]].* Revista de la Facultad de Agronomía-Universidad de Buenos Aires (Argentina). **2(**3), 163-171.
Lloyd, M. R. (1964) – *Variations in the oxygen and carbon isotope ratios of Florida Bay mollusks and their environmental significance.* Journal of Geology, **72**, 84-111.
Lorens, R. B., & Bender, M. L. (1980) – *The impact of solution chemistry on Mytilus edulis calcite and aragonite.* Geochimica et Cosmochimica Acta, **44**(9), 1265-1278.
Lorrain, A., Gillikin, D.P., Paulet, Y-M., Chauvaud, L., Le Mercier, A., Navez, J., André, L. (2005) – *Strong kinetic effects on Sr/Ca ratios in the calcitic bivalve* Pecten maximus. Geology, **33**, 965-968.
Lowenstam, H. A. (1961) – *Mineralogy, ratios, and strontium and magnesium contents of recent and fossil brachiopods and their bearing on the history of the oceans.* The Journal of Geology, 241-260.
Lozada, E., Bustos, H. (1984) – *Madurez sexual y fecundidad de Venus antigua (King and Broderip, 1835) en la Bahía Ancud (Molusco: Bivalvia: Veneridae).* Revista de Biología Marina, **20** (2), 91-112.
Lozan, J. L., R. Lampe, W. Matthaus, E. Rachor, H. Rumhor and H. V. Westernagen, EDS. (1996) - *Warnsignale aus der Ostsee: wissenschaftliche Fakten.* Berlin: Parey. 385 S.

M

Maamaatuaiahutapu, K., Garçon, V. C., Provost, C., Boulahdid, M., & Osiroff, A. P. (1992) – *Brazil-Malvinas Confluence: Water mass composition.* Journal of Geophysical Research: Oceans (1978–2012), **97**(C6), 9493-9505.
Maamaatuaiahutapu, K., Garcon, V., Provost, C., & Mercier, H. (1998) – *Transports of the Brazil and Malvinas Currents at their confluence.* Journal of marine research, **56**(2), 417-438.
Maamaatuaiahutapu, K., Provost, C., Andrié, C., & Vigan, X. (1999) – *Origin and ages of mode waters in the Brazil-Malvinas Confluence region during austral winter 1994.* Journal of Geophysical Research: Oceans (1978–2012), **104**(C9), 21051-21061.
Malanga, M.S. Estévez, J. Calvo, D. Abele, S. Puntarulo (2005) **–***Oxidative stress in gills of limpets from the Beagle Channel: comparisons with limpets from the Antarctic.* Scientia Marina, **69** (2), 297–304
Markgraf, V., Bradbury, J. P., Schwalb, A., Burns, S. J., Stern, C., Ariztegui, D., ... & Maidana, N. (2003) – *Holocene palaeoclimates of southern Patagonia: limnological and environmental history of Lago Cardiel, Argentina.* The Holocene, **13**(4), 581-591.
Martin J. M., Meyback M. (1979) – *Elemental mass-balance of material carried by major world rivers.* Mar. Chem. **7,** 173–206.
Maslin, M. A., & Swann, G. E. (2006). *Isotopes in marine sediments* (pp. 227-290). Springer Netherlands.
Mazzonia, E., & Vazquez, M. (2009) – *Desertification in Patagonia.* Developments in Earth Surface Processes**, 13**, 351-377.
McArthur, J. M., Doyle, P., Leng, M. J., Reeves, K., Williams, C. T., Garcia-Sanchez, R., & Howarth, R. J. (2007) – *Testing palaeo-environmental proxies in Jurassic belemnites: Mg/Ca, Sr/Ca, Na/Ca, $\delta^{18}O$ and $\delta^{13}C$.* Palaeogeography, Palaeoclimatology, Palaeoecology, **252**(3), 464-480.

Mac-clintock, C. (1967) – *Shell structure of patelloid and bellerophontoid gastropods*

(Mollusca). Bulletin of the Peabody Museum of Natural History, **22**,1-140
McCrea, J. M. (1950) – *On the isotopic chemistry of carbonates and a paleotemperature scale.* The Journal of Chemical Physics, **18**, 849.
McIntire, W. L. (1963) – *Trace element partition coefficients—a review of theory and applications to geology.* Geochimica et Cosmochimica Acta, **27**(12), 1209-1264.
McLaren, S. J., & Rowe, P. J. (1996). *The reliability of uranium-series mollusc dates from the western Mediterranean basin*. Quaternary Science Reviews, **15**(7), 709-717.
Mémery, L., Arhan, M., Alvarez-Salgado, X. A., Messias, M. J., Mercier, H., Castro, C. G., & Rios, A. F. (2000) – *The water masses along the western boundary of the south and equatorial Atlantic*. Progress in Oceanography, **47**(1), 69-98.
Milani, E. J., & Thomaz Filho, A. (2000) – *Sedimentary basins of South America.* Tectonic Evolution of South America. In-Fólio Produção Editorial, 389-449.
Milliman, J.D. (1974) – *Marine carbonates*. Springer, Berlin Heidelberg New York, 375 p.
Min, G.R., Edwards, R.L, Taylor, F.W, Recy, J., Gallup, C.D., Beck, J.W. (1995) – *Ann. cycles of U/Ca in coral skeletons and U/Ca thermometry* Geochim. Cosmochim. Acta, **59**, 2025–2042
Mitsuguchi, T., Matsumoto, E., Abe, O., Uchida, T., & Isdale, P. J. (1996) – *Mg/Ca thermometry in coral skeletons*. Science, ***274***(5289), 961-963.
Möller, P., & Kubanek, F. (1976) – *Role of magnesium in nucleation processes of calcite, aragonite and dolomite.* Neues Jarb Abh, **126**, 199-220.
Mook, W.G. (1971) – *Paleotemperatures and chlorinities from stable carbon and oxygen isotopes in shell carbonate.* Palaeogeography, Palaeoclimatology, Palaeoecology, **9**, 245-263.
Mook, W. G., & Vogel, J. C. (1968) – *Isotopic equilibrium between shells and their environment*. Science, **159**(3817), 874-875.
Mook WG, Tan FC. (1991) – *Stable carbon isotopes in rivers and estuaries.* In: iogeochemistry of Major World Rivers, Degens ET, Kempe S, Richey E (eds). John Wiley: New York; 245–264.
Morriconi, E. (1999) – *Reproductive biology of the limpet Nacella (P.) deaurata (Gmelin, 1791) in bahía Lapataia (Beagle Channel*). Scientia Marina, **63**(S1), 417-426.
Morrison, J. O., & Brand, U. (1986) – *Paleoscene# 5. Geochemistry of recent marine invertebrates.* Geoscience Canada, **13**(4).
Morrison, J. O., & Brand, U. (1988) – *An evaluation of diagenesis and chemostratigraphy of Upper Cretaceous molluscs from the Canadian Interior Seaway.* Chemical Geology: Isotope Geoscience section, **72**(3), 235-248.

N

Nagaya, Y., Nakamura, K., & Saiki, M. (1971) – *Strontium concentrations and strontium-chlorinity ratios in sea water of the North Pacific and the adjacent seas of Japan*. Journal of the Oceanographical Society of Japan, **27**(1), 20-26.
Noy-Meir, I. (1973). *Desert ecosystems: environment and producers.* Annual review of ecology and systematics, **4**, 25-51.
Nürnberg, D., Bijma, J., & Hemleben, C. (1996) – *Assessing the reliability of magnesium in foraminiferal calcite as a proxy for water mass temperatures.* Geochimica et Cosmochimica Acta, **60**(5), 803-814.

O

Obelic, B., Alvarez, A., Argullos, J., Piana, E.L. (1998) – *Determination of water palaeotemperature in the Beagle Channel (Argentina) during the last 6000 yr through stable isotope composition of Mytilus edulis shells.* Quaternary of South America & Antarctica Peninsula, **11**, 47-71.

Olson, D. B., Podestá, G. P., Evans, R. H., & Brown, O. B. (1988) – *Temporal variations in the separation of Brazil and Malvinas Currents.* Deep Sea Research Part A. Oceanographic Research Papers, **35**(12), 1971-1990. Balicema Publishers. Rotterdam.

Olsson, I. U. (1970) – *The use of Oxalic acid as a Standard*, in Olsson, I U, ed, Radiocarbon Variations and Absolute Chronology, Nobel symposium, 12th Proc: New York, John Wiley & Sons, p 17.

O'Neil, J. R., Clayton, R. N., & Mayeda, T. K. (1969) – *Oxygen isotope fractionation in divalent metal carbonates.* The Journal of Chemical Physics**, 51**, 5547.

Orquera, L.A., Piana, E.L. (2001) – *Composición de conchales de la costa del Canal Beagle.* Primera parte: Relaciones de la Sociedad Argentina de Antropología, XXV, 249–274.

Orquera, L.A., Piana, E.L. (2002) – *Composición de conchales de la costa del Canal Beagle.* Segunda parte: Relaciones de la Sociedad Argentina de Antropología, XXVI, 345-368.

Ortlieb, L., Guzmán, N, Marquardt, C. (2003) – *A Longer-Lasting and Warmer Interglacial Episode During Isotopic Stage 11: Marine Terrace Evidence in Tropical Western Americas*. American Geophysical Union. Geophysical Mongraph, **137**, 157-180.

Osorio, C. & Bahamonde, N. (1970) – *Lista preliminar de lamelibranquios de Chile*. Boletín del Museo Nacional de Historia Natural, Chile, **31**, 185-256.

Osorio, C., Atria, J., Mann, S. (1979) – *Moluscos marinos de importancia económica en Chile*. Biología Pesquera **11**, 3-47.

Osorio, C, Frassinetti, D., Bustos, E. (1983) – *Taxonomía y Morfometría de Venus antigua (King y Broderip, 1835) (Mollusca, Bivalvia, Veneridae).* Tethys **11,** 49-56.

P

Palacios, R., Orensanz, J. M., & Armstrong, D. A. (1994) – *Seasonal and Life-long Variation of Sr/Ca Ratio in Shells of Mya arenaria from Grays Harbor (Washington)—an Ancillary Criterion in Demographic Studies.* Estuarine, Coastal and Shelf Science, **39**(4), 313-327.

Panarello, H. O. (1987) – *Oxygen-18 temperatures on present and fossil invertebrated shells from Túnel Site, Beagle Channel, Argentina*. In INQUA international congress. **12** (pp. 83-91).

Pappalardo, M., Aguirre, M., Bini, M., Consoloni, I., Fucks, E., Hellstrom, J., Isola, I., Ribolini, A., Zanchetta, G. (2013) - *Coastal landscape evolution and sea-level change: a case study from Central Patagonia (Argentina).* Zeitschrift für Geomorphologie. Accepted Manuscript.

Park, R., & Epstein, S. (1960) – *Carbon isotope fractionation during photosynthesis*. Geochimica et Cosmochimica Acta, **21**(1), 110-126.

Paruelo, J. M., & Lauenroth, W. K. (1996) – *Relative abundance of plant functional types in grasslands and shrublands of North America*. Ecological Applications, 1212-1224.

Paruelo, J. M., Beltran, A., Jobbagy, E., Sala, O. E., & Golluscio, R. A. (1998) – *The climate of Patagonia: general patterns and controls on biotic.* Ecología Austral, **8**, 85-101

Passariello, I., Marzaioli, F., Lubritto, C., Rubino, M., D'Onofrio, A., De Cesare, N., ... & Terrasi, F. (2007) – *Radiocarbon sample preparation at the CIRCE AMS laboratory in Caserta, Italy.* Radiocarbon, **49**(2), 225-232.

Pérez, D.E., Del Rio, C.J., Nielsen, S.N. (2013) – *Sistematica y filogenia del género Ameghinomya Ihering, 1907 (Bivalvia: Chioninae) del Cenozoico de Argentina y Chile.* Ameghiniana, Tomo 50.

Peroni, G.O., Hegedus, A.G., Cerdan, J., Legarreta, L., Uliana, M.A., Laffitte, G., (1995) – *Hydrocarbon accumulation in an inverted segment of the Andean foreland: San Bernardo Belt, central Patagonia.* In: Tankard, A.J., Suárez Soruco, R., Welsink, H.J. (Eds.), Petroleum Basins of South America. Mem., vol. **62**. AAPG, 403–419.

Peterson, R. G. (1992) – *The boundary currents in the western Argentine Basin.* Deep Sea Research Part A. Oceanographic Research Papers, **39**(3), 623-644.
Peterson, R. G., & Stramma, L. (1991) - *Upper-level circulation in the South Atlantic Ocean.* Progress in Oceanography, **26**(1), 1-73.
Pia Mena, C.I., Gonzalez, C.A.W., Clasing, E.O., Gallardo, M.H.N. (2001) – *Variabilidad genética en Aulacomya atra (Molina, 1782) en el sur de Chile*. Cienc. Tecnol. Mar., **24**, 71-79.
Pidwirny, M. (2006). *Fundamentals of physical geography.* Date Viewed, **19**, 2009.
Pilkey, O. H., & Hower, J. (1960*). The effect of environment on the concentration of skeletal magnesium and strontium in Dendraster*. The Journal of Geology, 203-214.
Piola, A. R., & Matano, R. P. (2001) – *Brazil and Falklands (Malvinas) currents.* Ocean Currents: A Derivative of the Encyclopedia of Ocean Sciences, 35-43.
Piola, A. R., Campos, E. J., Möller, O. O., Charo, M., & Martinez, C. (2000) – *Subtropical shelf front off eastern South America.* Journal of Geophysical Research: Oceans (1978–2012), **105(C3)**, 6565-6578.
Pitts, L. C., & Wallace, G. T. (1994) – *Lead Deposition in the Shell of the Bivalve, Mya arenaria: an Indicator of Dissolved Lead in Seawater*. Estuarine, Coastal and Shelf Science, **39**(1), 93-104.
Podesta, G., Brown, O., & Evans, R. (1991) - *The annual cycle of satellite-derived sea surface temperature in the southwestern Atlantic Ocean*. Journal of climate, **4**(4), 457-467.
Powell, M. G., Schöne, B. R., & Jacob, D. E. (2009) – *Tropical marine climate during the late Paleozoic ice age using trace element analyses of brachiopods.* Palaeogeography, Palaeoclimatology, Palaeoecology, **280**(1), 143-149.
Prohaska, F. (1976) – *The climate of Argentina, Paraguay and Uruguay.* Climates of Central and South America, **22,** 13-112.
Purton, L., & Brasier, M. (1997) – *Gastropod carbonate δ18O and δ13C values record strong seasonal productivity and stratification shifts during the late Eocene in England*. Geology, **25**(10), 871-874.

R

Rabassa, J., & Coronato, A. (2009) – *Glaciations in Patagonia and Tierra del Fuego during the Ensenadan Stage/Age (Early Pleistocene–earliest Middle Pleistocene).* Quaternary International, ***210*****(1)**, 18-36.
Radtke, U. (1989). *Marine Terrassen und Korallenriffe: das Problem der quartären Meeresspiegelschwankungen erläutert an Fallstudien aus Chile, Argentinien und Barbados* (Vol. 27). Im Selbstverlag des Geographischen Institutes der Heinrich-Heine-Universität Düsseldorf.
Railsback (2012) – *X-ray diffraction (XRD) of aragonite and calcite http://www.gly.uga.edu/railsback/Fundamentals/A&CmixturesXRD01.pdf.*
Railsback, L. B., Anderson, T. F., Ackerly, S. C., & Cisne, J. L. (1989) – *Paleoceanographic modeling of temperature-salinity profiles from stable isotopic data*. Paleoceanography, **4**(5), 585-591.
Ramorino, L. (1968) - *Pelecypoda del fondo de la Bahía Valparaíso.* Revista de Biología Marina, **13** (3), 175-285.
Ramos, V.A. (1984) – *Patagonia: ¿Un continente paleozoico a la deriva?*.9° Cong. Geol. Argentino, Actas, 2, 311-325.
Ramos, V. A. (1996) – *Evolucion tectonica de la Plataforma Continental.* In: Ramos, V. and Turic, M. (eds), Geologıa y recursos naturales de la Plataforma Continental Argentina. Asociacion Geologica Argentina and Instituto Argentino del Petroleo, Relatorio, **21**, 385–404. Buenos Aires.
Ramos, V. (1999) – *Las provincias geolo´gicas del territorio argentino*. In: SEGEMAR (ed.), Geologı´a Argentina, Anales, **29**, 341–96. Instituto de Geologı´a y Recursos Minerales. Buenos Aires.

Ramos, V.A. (2004a) – *Tectonics of the southernmost Andes: a comparison between the Patagonian and the Fuegian Cordilleras.* Bolletino di Geofisica Teorica ed Applicata, **45,** 1–10 (2, supplement, Trieste).
Ramos, V.A. (2004b) – *La Plataforma Patagónica y sus relaciones con la Plataforma Brasilera*. In: Mantesso-Neto, V., Bartorelli, A., Ré Carneiro, C.D., Brito Neves, B.B. (Eds.) Geologia do Continente Sul-Americano, Sao Paulo, **22**, 371–381.
Ramos, V.A. (2008) – *Patagonia: A paleozoic continent adrift?.* Journal of South American Earth Sciences, **26**, 235-251.
Ramos, V. A., & Ghiglione, M. C. (2008) – *Tectonic evolution of the Patagonian Andes.* Developments in Quaternary Sciences, **11**, 57-71.
Reíd, D.; Osorio, C. (2000) – *The shallow-water marine mollusca of the Estero Elefantes and Laguna San Rafael, southern Chile.* Bulletin of the Natural History Museum of London, Zoology **66,**109-146.
Reimer, P. J., Bard, E., Bayliss, A., Beck, J. W., Blackwell, P. G., Ramsey, C. B., ... & van der Plicht, J. (2013) – *IntCal13 and Marine13 radiocarbon age calibration curves 0–50,000 years cal BP.* Radiocarbon, **55**(4), 1869-1887.
Ribolini, A., Aguirre, M., Baneschi, I., Consoloni, I., Fucks, E., Isola, I., ... & Bini, M. (2011). *Holocene beach ridges and coastal evolution in the Cabo Raso Bay (Atlantic Patagonian Coast, Argentina).* Journal of Coastal Research, **27**(5), 973-983.
Ribolini, A., Bini, M., Consoloni, I., Isola, I., Pappalardo, M., Zanchetta, G., Fucks, E., Panzeri, L., Martini, M., Terrasi, F. (2013) – *Late-Pleistocene wedge structures along the Patagonian coast (Argentina): chronological constraints and paleo-environmental implications.* Geografiska Annaler: Series A, Physical Geography. Accepted manuscript.
Ríos, E. (1975) – *Brazilian marine mollusks iconography.* Rio Grande, Fundacao Cidade do Rio Grande, Fundacao Universidade do Rio Grande,, 331 p.
Ríos, E. (1994) – **Seashells of the Brazil**. Editora da Fun-dacao Universidade do Rio Grande: 368 p. Brazil.
Roden, G. I. (1986) – *Thermohaline fronts and baroclinic flow in the Argentine Basin during the austral spring of 1984.* Journal of Geophysical Research: Oceans (1978–2012), **91**(C4), 5075-5093.
Rohling, E. J. (2007) – *Progress in paleosalinity: Overview and presentation of a new approach.* Paleoceanography, **22**(3).
Rohling, E.J. and Cooke, S. (1999) **–** *Stable oxygen and carbon isotope ratios in foraminiferal carbonate*, chapter 14 in B.K. Sen Gupta (ed.) *Modern Foraminifera*, Kluwer Academic, Dordrecht, The Netherlands, pp.239-258.
Rosenbluth, B., Casassa, G., Fuenzalida, H. (1995) – *Recent climatic changes in Western Patagonia*. Bull. Glacier Res. **13**, 127–132.
Rosenheim, B. E., Swart, P. K., Thorrold, S. R., Willenz, P., Berry, L., & Latkoczy, C. (2004) – *High-resolution Sr/Ca records in sclerosponges calibrated to temperature in situ*. Geology, **32**(2), 145-148.
Rosman, K. J. R., & Taylor, P. D. P. (1998) – *Isotopic compositions of the elements 1997.* Journal of Physical and Chemical Reference Data, ***27***, 1275
Rostami, K., Peltier, W.R., Mangini, A. (2000) – *Quaternary marine terraces, sea-level changes and uplift history of Patagonia, Argentina: comparisons withpredictio ns of the ICE-4G (VM2) model of the global process of glacial isostatic adjustment.* Quaternary Science Reviews, **19**, 1495-1525.
Ruddiman, W. (2008) – *Earth's Climate: Past and Future*.
Russell, A. D., Hönisch, B., Spero, H. J., & Lea, D. W. (2004) – *Effects of seawater carbonate ion concentration and temperature on shell U, Mg, and Sr in cultured planktonic foraminifera*. Geochimica et Cosmochimica Acta, **68**(21), 4347-4361.
Rutter, N., Schnack, E. J., Rio, J. D., Fasano, J. L., Isla, F. I., & Radtke, U. (1989) – *Correlation and dating of Quaternary littoral zones along the Patagonian coast, Argentina.* Quaternary Science Reviews, **8**(3), 213-234.
Rutter, N., Radtke, U. and Schnack, E. (1990) – *Comparison of ESR and amino acid data in correlating and dating Quaternary shorelines along the Patagonian coast, Argentina.*

Journal of Coastal Research, **6**, 391–411.

S

Saporiti, F., Bala, L. O., Crespo, E. A., Gómez Otero, J., Zangrando, A. F. J., Aguilar, A., & Cardona, L. (2013) – *Changing patterns of marine resource exploitation by hunter-gatherers throughout the late Holocene of Argentina are uncorrelated to sea surface temperature.* Quaternary International, **299**, 108-115

Saraceno, M., Provost, C., Piola, A. R., Bava, J., & Gagliardini, A. (2004) – *Brazil Malvinas Frontal System as seen from 9 years of advanced very high resolution radiometer data.* Journal of Geophysical Research: Oceans (1978–2012), **109(**C5).

Saunders, P. M., & King, B. A. (1995) – *Bottom currents derived from a shipborne ADCP on WOCE cruise A11 in the South Atlantic*. Journal of physical oceanography, **25**(3), 329-347.

Schellmann, G. (1998) – *Jungkänozoische Landschaftsgeschichte Patagoniens (Argentinien). Andine Vorlandvergletscherungen, Talentwicklung und marine Terrassen.* Essener Geographische Arbeiten 29; Essen.

Schellmann, G. (2007) – *Holozane Meeresspiegelschwankungen – ESR Datierungen aragonitischer Muschelschalen - Palaotsunamis*. Bamberger Geographische Schriften **22**, 1–152 (Bamberg).

Schellmann, G., & Radtke, U. (1997) – *Electron spin resonance (ESR) techniques applied to mollusc shells from South America (Chile, Argentina) and implications for palaeo sea-level curve.* Quaternary Science Reviews, **16**(3), 465-475.

Schellmann, G., Radtke, U. (2000) – *ESR dating stratigraphically well-constrained marine terraces along the Patagonian Atlantic coast (Argentina).* Quaternary International, **68-71**, 261-273.

Schellmann, G., & Radtke, U. (2003) – *Coastal terraces and Holocene sea-level changes along the Patagonian Atlantic coast.* Journal of Coastal Research, 983-996.

Schellmann, G., Radtke, U. (2007) – *Neue Befunde zur Verbreitung und chronostratigraphischen Gliederung holozäner Küstenterrassen an der mittel- und südpatagonischen Atlantikküste (Argentinien)— Zeugnisse holozäner Meeresspiegelveränderungen*. Bamberger Geographische Schriften, **22**, 1–91 (Bamberg).

Schellmann, G., & Radtke, U. (2010) – *Timing and magnitude of Holocene sea-level changes along the middle and south Patagonian Atlantic coast derived from beach ridge systems, littoral terraces and valley-mouth terraces.* Earth-Science Reviews, **103**(1), 1-30.

Schellmann, G., Radtke, U., Potter, E. K., Esat, T. M., & McCulloch, M. T. (2004) – *Comparison of ESR and TIMS U/Th dating of marine isotope stage (MIS) 5e, 5c, and 5a coral from Barbados—implications for palaeo sea-level changes in the Caribbean.* Quaternary International, **120**(1), 41-50.

Schellmann, G., Beerten, K., & Radtke, U. (2008) – *Electron spin resonance (ESR) dating of Quaternary materials.* Eiszeitalter und Gegenwart, **57**, 150-178.

Schöne, B. R., Zhang, Z., Jacob, D., Gillikin, D. P., Tütken, T., Garbe-Schönberg, D., ... & Soldati, A. (2010) – *Effect of organic matrices on the determination of the trace element chemistry (Mg, Sr, Mg/Ca, Sr/Ca) of aragonitic bivalve shells (Arctica islandica)— Comparison of ICP-OES and LA-ICP-MS data.* Geochemical Journal, **44**(1), 23.

Schöne, B.R., Zhang, Z., Radermarcher, P., Thébault, J., Jacob, D.E., Nunn, E.V., Maurer, A.-F. (2011) – *Sr/Ca and Mg/Ca ratios of ontogenetically old, long-lived bivalve shells (*Arctica islandica) *and their function as paleotemperature proxies.* Palaeogeography, Palaeoclimatology, Palaeoecology, **302**, 52-64.

Schroeder, J. H. (1969). *Experimental dissolution of calcium, magnesium, and strontium from Recent biogenic carbonates; a model of diagenesis.* Journal of Sedimentary Research, **39(**3), 1057-1073.

Seed, R., and T. H. Suchanek (1992) – *Population and community ecology of Mytilus*, in The Mussel Mytilus: Ecology, Physiology, Genetics and Culture, Dev. Aquacult. Fish. Sci., vol. **25**, edited by E. M. Gossling, chap. 4, pp. 87–170, Elsevier, New York.

Shackleton, N. J. (1974). *Attainment of isotopic equilibrium between ocean water and the benthonic foraminifera genus Uvigerina: Isotopic changes in the ocean during the last glacial.* Colloques Internationaux du C.N.R.S, 219, es methodes quantitatives d'étude des variations du clima tau cours du Pléistocène.

Shackleton, N. J., & Kennett, J. P. (1975) – *Paleotemperature history of the Cenozoic and the initiation of Antarctic glaciation: oxygen and carbon isotope analyses in DSDP Sites 277, 279, and 281*. Initial reports of the deep sea drilling project, **29**, 743-755.

Shackleton, N. J., & Opdyke, N. D. (1973) – *Oxygen isotope and palaeomagnetic stratigraphy of Equatorial Pacific core V28-238: Oxygen isotope temperatures and ice volumes on a 10^5 year and 10^6 year scale.* Quaternary research, **3**(1), 39-55.

Shen, G. T., & Dunbar, R. B. (1995) – *Environmental controls on uranium in reef corals.* Geochimica et Cosmochimica Acta, **59**(10), 2009-2024

Soldati, A. L., Jacob, D. E., Schöne, B. R., Bianchi, M. M., & Hajduk, A. (2009). *Seasonal periodicity of growth and composition in valves of Diplodon chilensis patagonicus (d'Orbigny, 1835).* Journal of Molluscan Studies, **75**(1), 75-85.

Soot-Ryen, T. (1959) – *Reports of fue Lund University Chile Expedition 1948-49. 35. Pelecypoda*. Lunds Universitets Arsskrift N.F. Avd. 2, Bd.55, N° 6, 66p.

Sosdian, S., Gentry, D. K., Lear, C. H., Grossman, E. L., Hicks, D., & Rosenthal, Y. (2006). *Strontium to calcium ratios in the marine gastropod Conus ermineus: Growth rate effects and temperature calibration.* Geochemistry Geophysics Geosystems, **7**(11), Q11023.

Stead, R. A., Clasing, E. L. E. N. A., Navarro, J. M., & Asencio, G. (1997) – *Reproductive cycle and cohort formation of Venus antiqua (Bivalvia: Veneridae) in the intertidal zone of southern Chile.* Rev. Chil. Hist. Nat, **70**, 181-190.

Stecher III, H. A., Krantz, D. E., Lord III, C. J., Luther III, G. W., & Bock, K. W. (1996). *Profiles of strontium and barium in Mercenaria mercenaria and Spisula solidissima shells.* Geochimica et Cosmochimica Acta, **60**(18), 3445-3456.

Stramma, L., & Peterson, R. G. (1990) – *The South Atlantic Current*. Journal of Physical Oceanography, **20**(6), 846-859.

Stramma, L., Ikeda, Y., & Peterson, R. G. (1990) – *Geostrophic transport in the Brazil Current region north of 20 S*. Deep Sea Research Part A. Oceanographic Research Papers, **37**(12), 1875-1886.

Sunye, P. S., & Servain, J. (1998) – *Effects of seasonal variations in meteorology and oceanography on the Brazilian sardine fishery.* Fisheries Oceanography, **7**(2), 89-100.

Surge, D., & Walker, K. J. (2006). *Geochemical variation in microstructural shell layers of the southern quahog (Mercenaria campechiensis): Implications for reconstructing seasonality.* Palaeogeography, Palaeoclimatology, Palaeoecology, **237**(2), 182-190.

Swan, E. F. (1956). *The meaning of strontium-calcium ratios.* Deep Sea Research (1953), **4**, 71.

Sylwan, C.A. (2001) – *Geology of the Golfo San Jorge Basin, Argentina.* Journal of Iberian Geology, **27**, 123–157.

T

Takesue, R.K. and van Geen A. (2004) – *Mg/Ca, Sr/Ca, and stable isotopes in modern and Holocene* Protothaca staminea *shells from a northern California coastal upwelling region.* Geochimica et Cosmochimica Acta, **68**, 3845-3861.

Tanner, W. F. (1995) – *Origin of beach ridges and swales.* Marine Geology, **129**(1), 149-161.

Taylor, J. H. (1964) – *Some aspects of diagenesis*. Adv. Sci, **20**, 417-436.

Taylor, J. D, Kennedy, W. J., Hall, A. (1973) – *The shell structure and mineralogy of the Bivalvia II.* Bulletin of British Museum (Natural History). Zoology, **22**, 255-294.

Terrasi, F., De Cesare, N., D'Onofrio, A., Lubritto, C., Marzaioli, F., Passariello, I., ... & Palmieri, A. (2008) – *High precision ^{14}C AMS at CIRCE.* Nuclear Instruments and Methods in Physics Research Section B: Beam Interactions with Materials and Atoms, **266**(10), 2221-2224.

Torres, M. E., Barry, J. P., Hubbard, D. A., & Suess, E. (2001) – *Reconstructing the history of fluid flow at cold seep sites from Ba/Ca ratios in vesicomyid clam shells.* Limnology and oceanography, **46**(7), 1701-1708.

Thrush, P.W. & Staff, U.S. Bureau of Mines (1968), *A Dictionary of Mining, Mineral, and Related Terms,* U.S.Dept. of Interior.

Turekian, K. K. (1972) – *Fate of metals in estuaries* (No. COO--3573-6; CONF-721106--7). Yale Univ., New Haven, Conn.(USA). Dept. of Geology and Geophysics.

U

Urban, H.J. (1994a) – *Adaptations of six infaunal bivalve species of Chile: coexistence resulting from differences in morphology, burrowing depth and substrate preferences.* Archive of Fishery and Marine Research, **42**, 183-195.

Urban, H.J. (1994b) – *Upper temperatura tolerante of ten bivalve species of Peru and Chile related to El Niño.* Marine Ecology Progress Series, **107**, 139-145.

Urban, H.J. (1996) – *Population dynamics of the bivalves Venus antiqua, Tagelus dombeii and Ensis macha from Chile at 36°S.* Journal of Shellfish Research, **15** (3), 719-727.

Urban, H.J., Tesch, C. (1996) – *Aspects of the population dynamics of six bivalve species from southern Chile.* Archive of Fishery and Marine Research, **44**, 243-256.

Urey, H. C. (1947). *The thermodynamic properties of isotopic substances*. Journal of the Chemical Society (Resumed), 562-581.

Urey, H. C., Lowenstam, H. A., Epstein, S., & McKinney, C. R. (1951) – *Measurement of paleotemperatures and temperatures of the Upper Cretaceous of England, Denmark, and the southeastern United States.* Geological Society of America Bulletin, **62**(4), 399-416.

Urien, C. M., & Zambrano, J. J. (1973) – *The geology of the basins of the Argentine continental margin and Malvinas Plateau.* The ocean basins and margins, **1**, 135-169.

V

Van der Putten, E., Dehairs, F., Keppens, E., & Baeyens, W. (2000) – *High resolution distribution of trace elements in the calcite shell layer of modern mytilus edulis: environmental and biological controls.* Geochimica et Cosmochimica Acta, **64**(6), 997-1011.

Veizer, J. (1983*) – Trace elements and isotopes in sedimentary carbonates*. Reviews in Mineralogy and Geochemistry, **11**(1), 265-299.

Verdinellij, M.A., Schuldt, M. (1976) - *Consideraciones preliminares sobre aspectos de la dinámica poblacional y reproducción de la almeja rayada Ameghinomya antiqua (King, 1831) (Chionidae) en Punta Loma, Golfo Nuevo-Chubut.* Revista del Museo de La Plata**, 12**, 183-202.

Verdún, E. (2010) - *Molluscs as sedimentary components: another perspective of analys*is. Munibe, Suplemento 31, 294–301.

Verdun, E., Briz, I., Camarós, E., Colonese, A.C., Estévez, J.,. Zurro, D. (2010) - *Metodología de excavación y análisis de concheros: experiencias acumuladas después de 20 años de estudios etnoarqueológicos en la costa norte del Canal Beagle (Tierra del Fuego, Argentina).* Fervedes, **6**, 25–32.

Vigan, X., Provost, C., Bleck, R., & Courtier, P. (2000) – *Sea surface velocities from sea surface temperature image sequences: 1. Method and validation using primitive equation model output.* Journal of Geophysical Research: Oceans (1978–2012), **105**(C8), 19499-19514.

Vivier, F., & Provost, C. (1999a) – *Direct velocity measurements in the Malvinas Current.* Journal of Geophysical Research: Oceans (1978–2012), **104**(C9), 21083-21103.
Vivier, F., & Provost, C. (1999b) – *Volume transport of the Malvinas Current: Can the flow be monitored by TOPEX/POSEIDON?.* Journal of Geophysical Research: Oceans (1978–2012), **104**(C9), 21105-21122.

W

Wefer, G. and Berger, W. (1991) – *Isotope paleontology: growth and composition of extant calacreous species.* Marine Geology, **100**, 207-248.
Wilbur, K. M. (1972) – *Shell formation in molluscs*, in Chemical Zoology, vol. **7**, edited by M. Florkin, and B. T. Scheer, chap. 3, pp. 103–145, Elsevier, New York.
Willson, H. R., & Rees, N. W. (2000) – *Classification of mesoscale features in the Brazil-Falkland Current confluence zone.* Progress in Oceanography, **45**(3), 415-426.
Winland, H. D. (1969) – *Stability of calcium carbonate polymorphs in warm, shallow seawater.* Journal of Sedimentary Research, **39**(4), 1579-1587.

www.disc.sci.gsfc.nasa.gov

Z

Zaixso, H. E. (1999) – *Distribución submareal del mitílido Aulacomya atra atra (Molina) en el Golfo San José (Argentina) en relación a la profundidad, características del fondo y condiciones hidrográficas.* Physis, **57**, 1-10.
Zanchetta, G., Consoloni, I., Isola, I., Pappalardo, M., Rinolini, A., Aguirre M., Fucks, E., Baneschi, I., Bini, M., Ragaini, L., Terrasi, F., Boretto, G. (2012) – *New insights of the Holocene marine transgression in the Bahìa Camarones (Chubut, Argentina).* Italian Journal of Geosciences, **131**, 19-31.
Zavialov, P. O., Wainer, I., & Absy, J. M. (1999) – *Sea surface temperature variability off southern Brazil and Uruguay as revealed from historical data since 1854*. Journal of Geophysical Research: Oceans (1978–2012), 104(C9), 21021-21032.
Zemann, J. (1969) – *Crystal chemistry*. In: Wedepohl KH (ed) Handbook of geochemistry, vol I. Springer, Berlin Heidelberg New York, pp 12–36.

Appendix A

A.1 Powder X-ray diffraction analysis

Ameghynomya antiqua

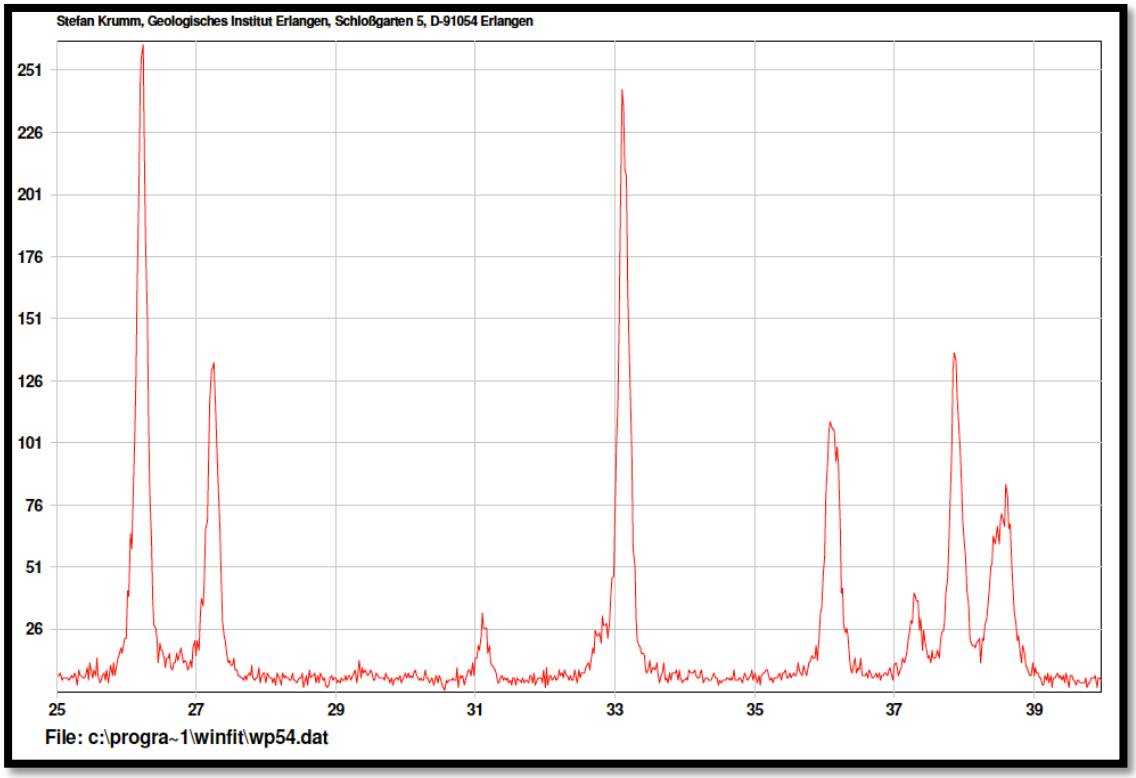

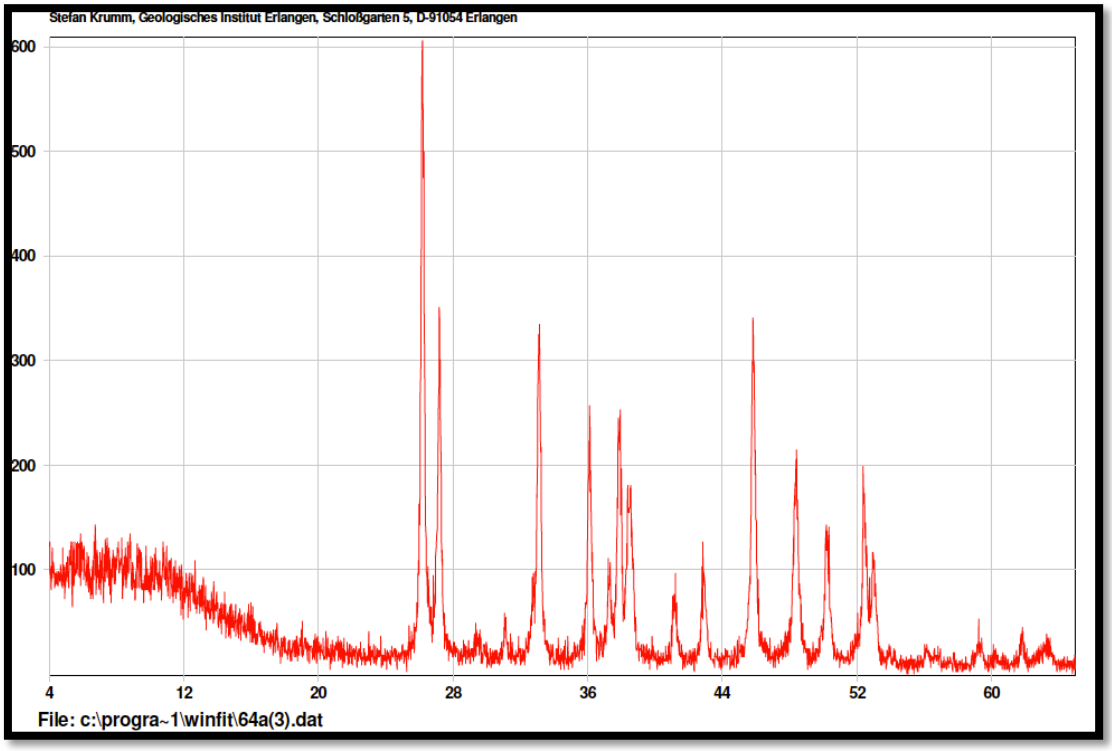
Stefan Krumm, Geologisches Institut Erlangen, Schloßgarten 5, D-91054 Erlangen
600
500
400
300
200
100
4
12
20
28
36
44
52
60
File: c:\progra~1\winfit\64a(3).dat

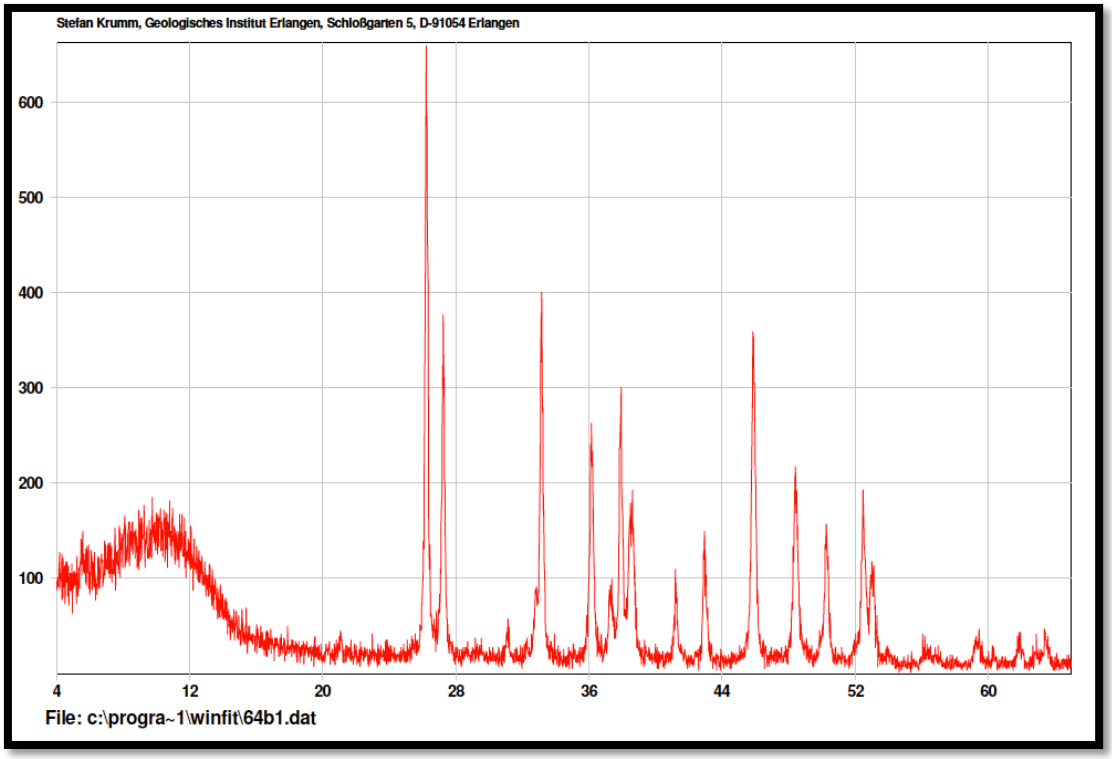
Stefan Krumm, Geologisches Institut Erlangen, Schloßgarten 5, D-91054 Erlangen
600
500
400
300
200
100
4
12
20
28
36
44
52
60
File: c:\progra~1\winfit\64b1.dat

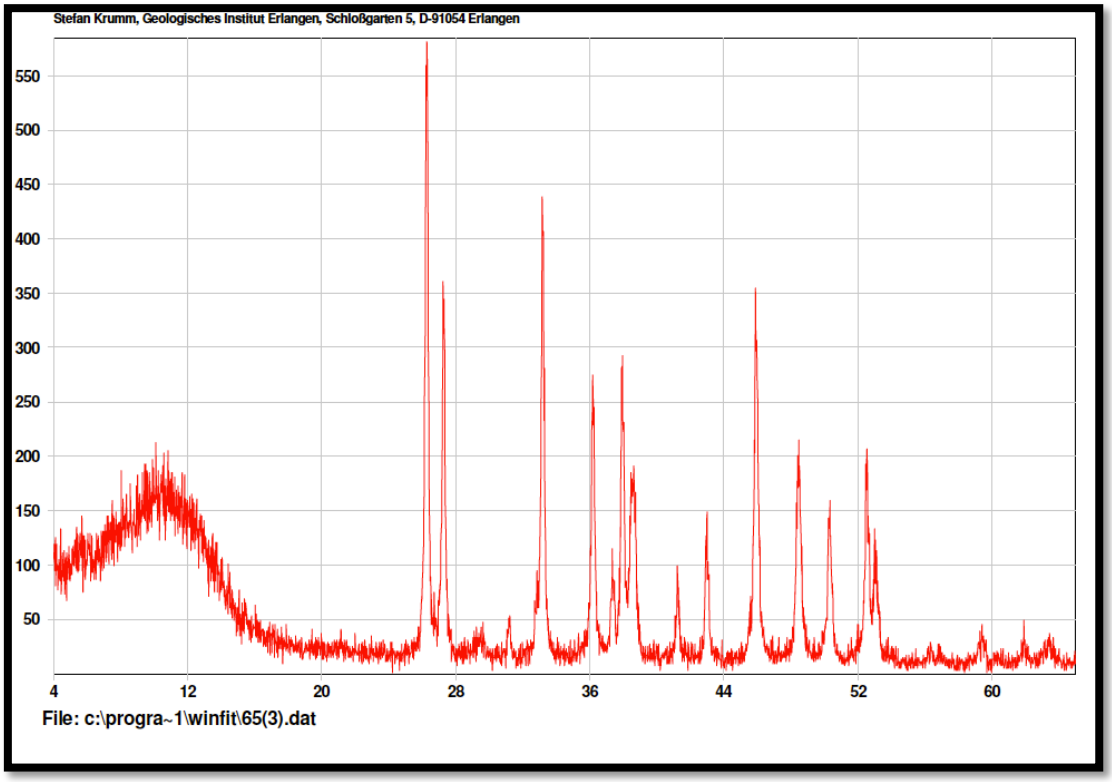
Stefan Krumm, Geologisches Institut Erlangen, Schloßgarten 5, D-91054 Erlangen
550
500
450
400
350
300
250
200
150
100
50
4
12
20
28
36
44
52
60
File: c:\progra~1\winfit\65(3).dat

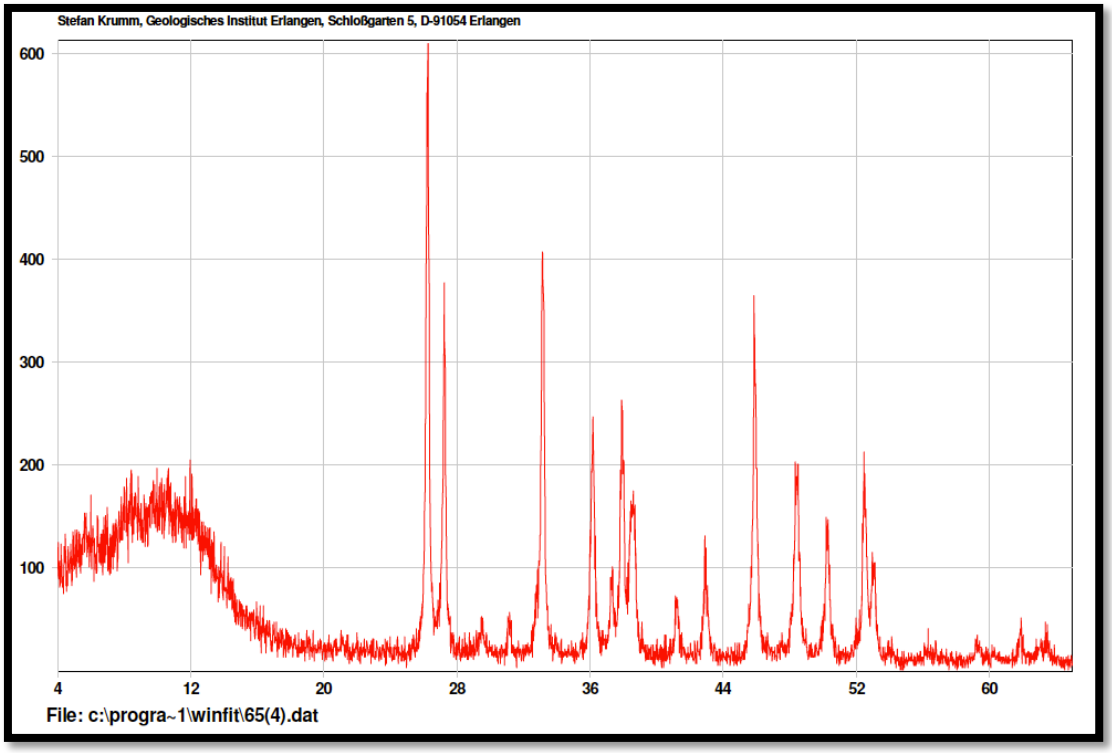
Stefan Krumm, Geologisches Institut Erlangen, Schloßgarten 5, D-91054 Erlangen
600
500
400
300
200
100
4
12
20
28
36
44
52
60
File: c:\progra~1\winfit\65(4).dat

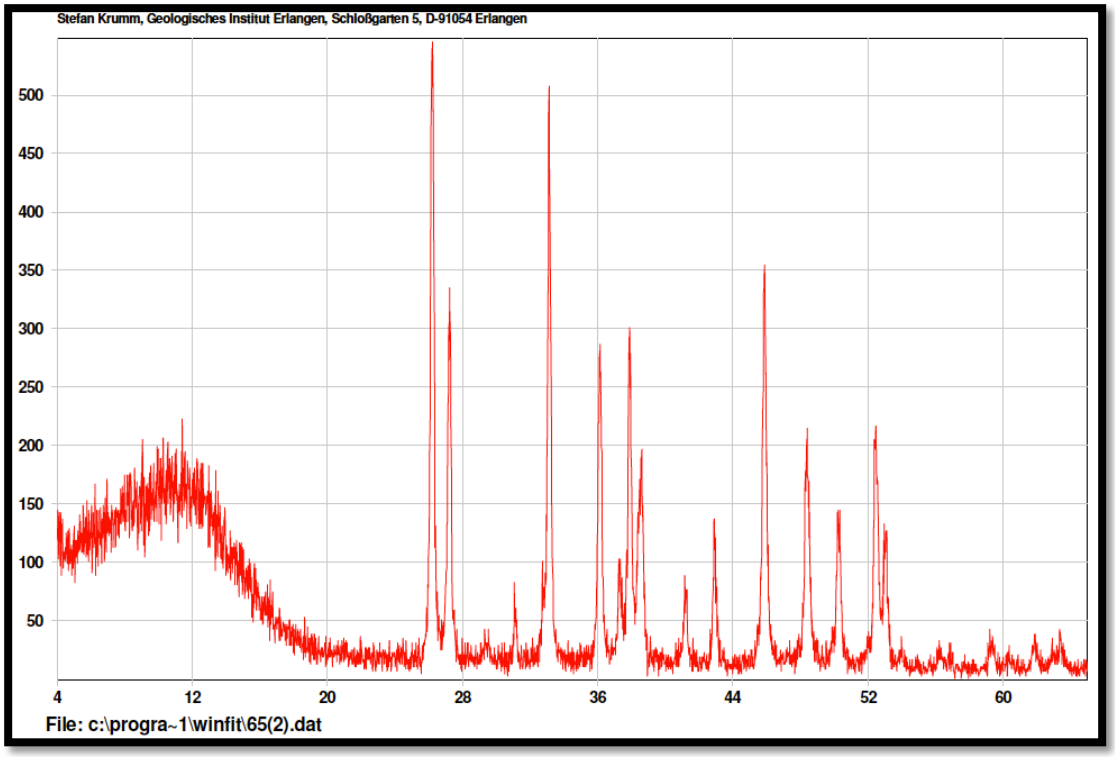
Stefan Krumm, Geologisches Institut Erlangen, Schloßgarten 5, D-91054 Erlangen
500
450
400
350
300
250
200
150
100
50
4
12
20
28
36
44
52
60
File: c:\progra~1\winfit\65(2).dat

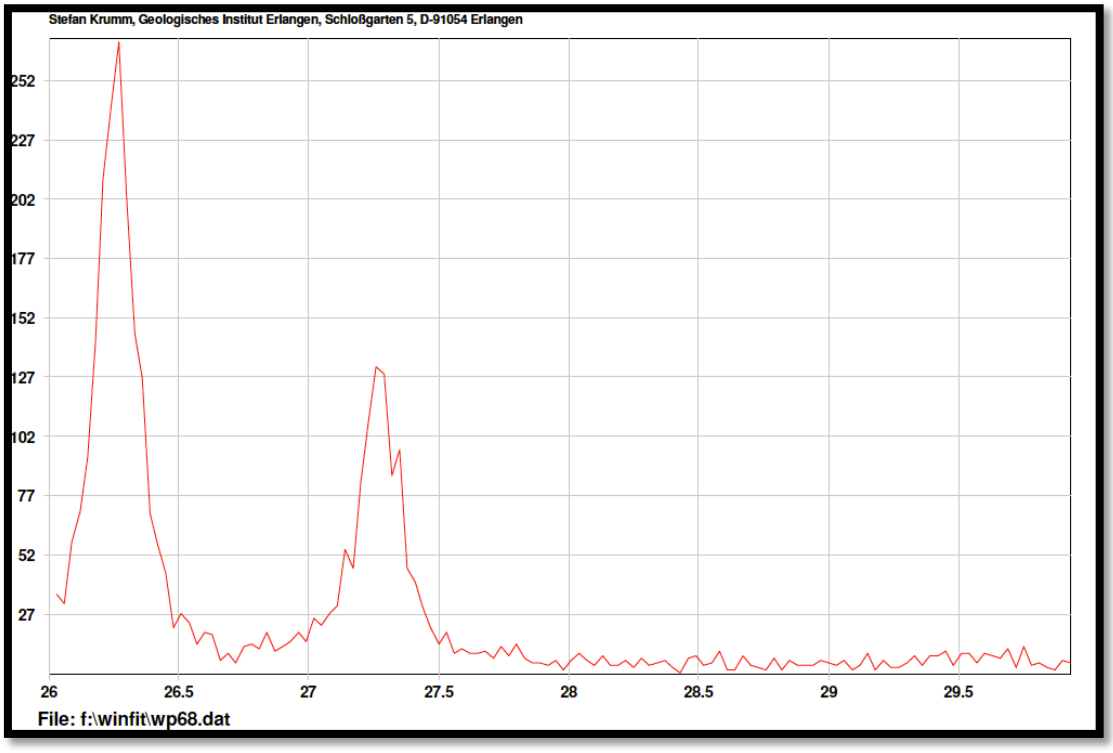
Stefan Krumm, Geologisches Institut Erlangen, Schloßgarten 5, D-91054 Erlangen
252
227
202
177
152
127
102
77
52
27
26
26.5
27
27.5
28
28.5
29
29.5
File: f:\winfit\wp68.dat

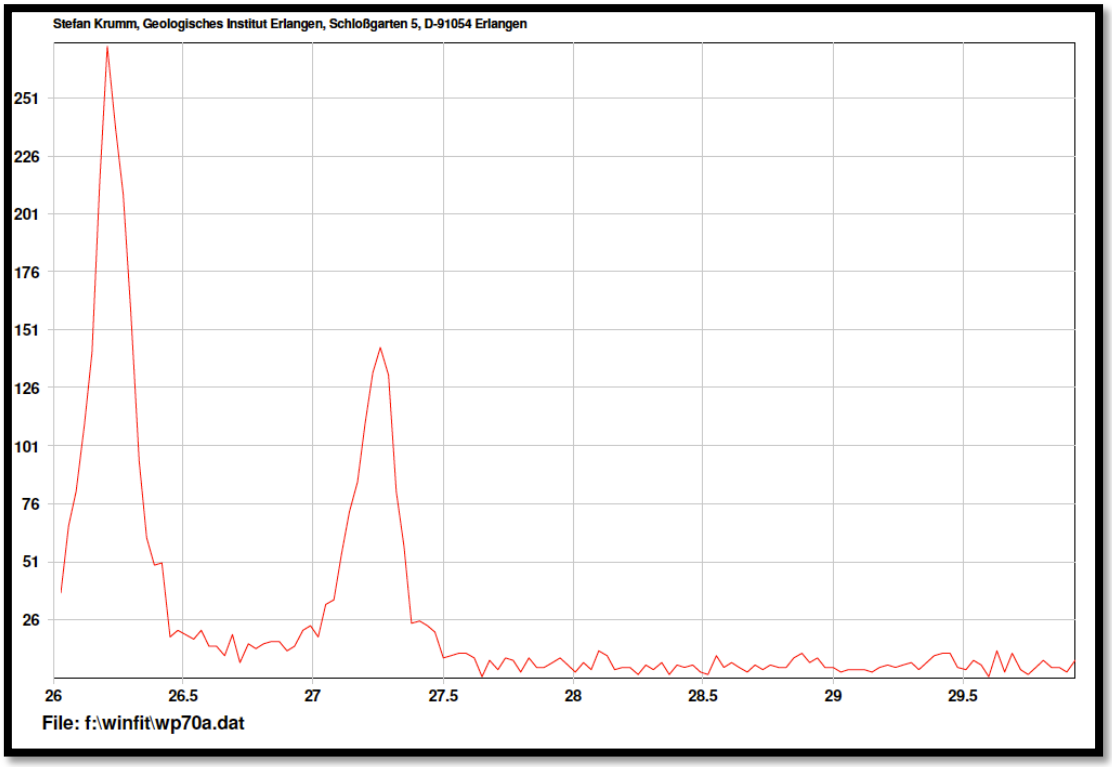
Stefan Krumm, Geologisches Institut Erlangen, Schloßgarten 5, D-91054 Erlangen
251
226
201
176
151
126
101
76
51
26
26
26.5
27
27.5
28
28.5
29
29.5
File: f:\winfit\wp70a.dat

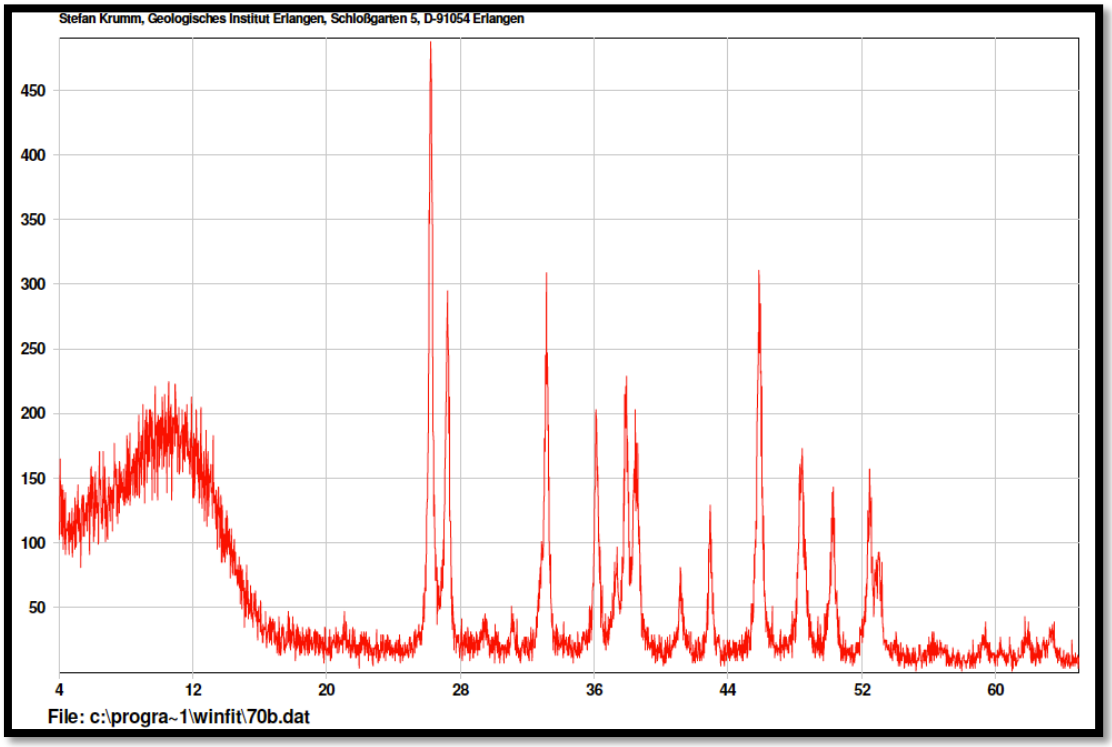
Stefan Krumm, Geologisches Institut Erlangen, Schloßgarten 5, D-91054 Erlangen
450
400
350
300
250
200
150
100
50
4
12
20
28
36
44
52
60
File: c:\progra~1\winfit\70b.dat

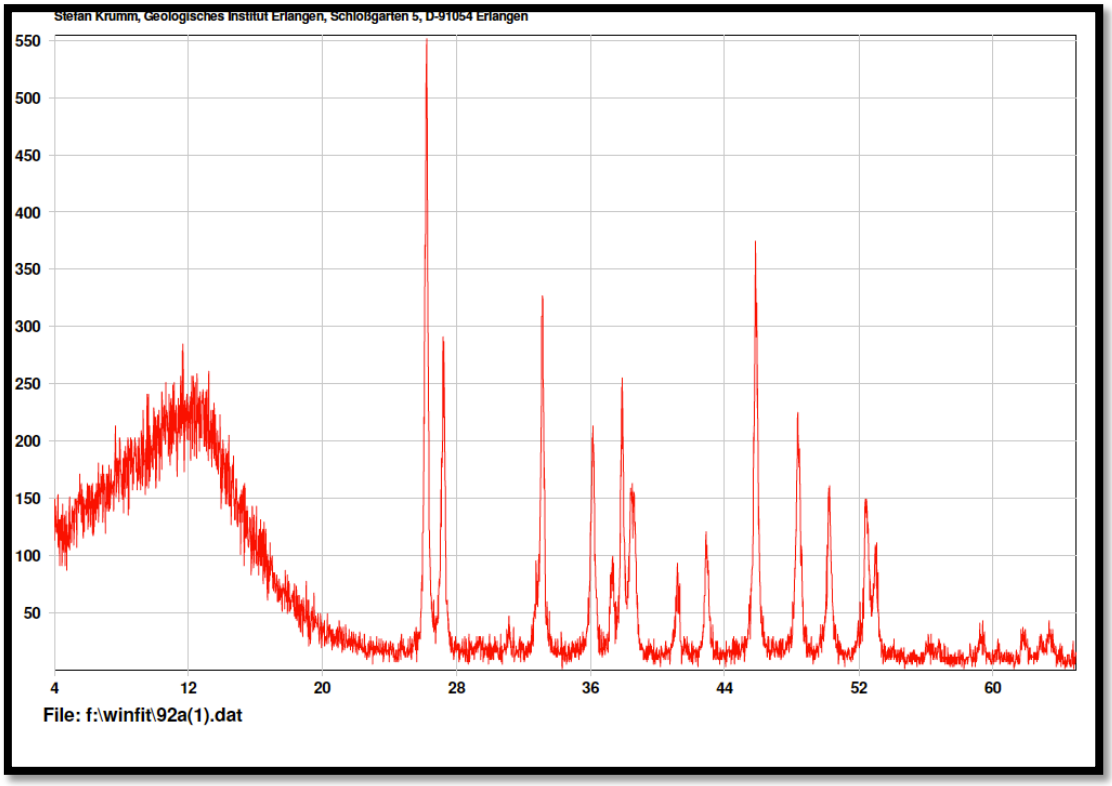
Stefan Krumm, Geologisches Institut Erlangen, Schloßgarten 5, D-91054 Erlangen
550
500
450
400
350
300
250
200
150
100
50
4
12
20
28
36
44
52
60
File: f:\winfit\92a(1).dat

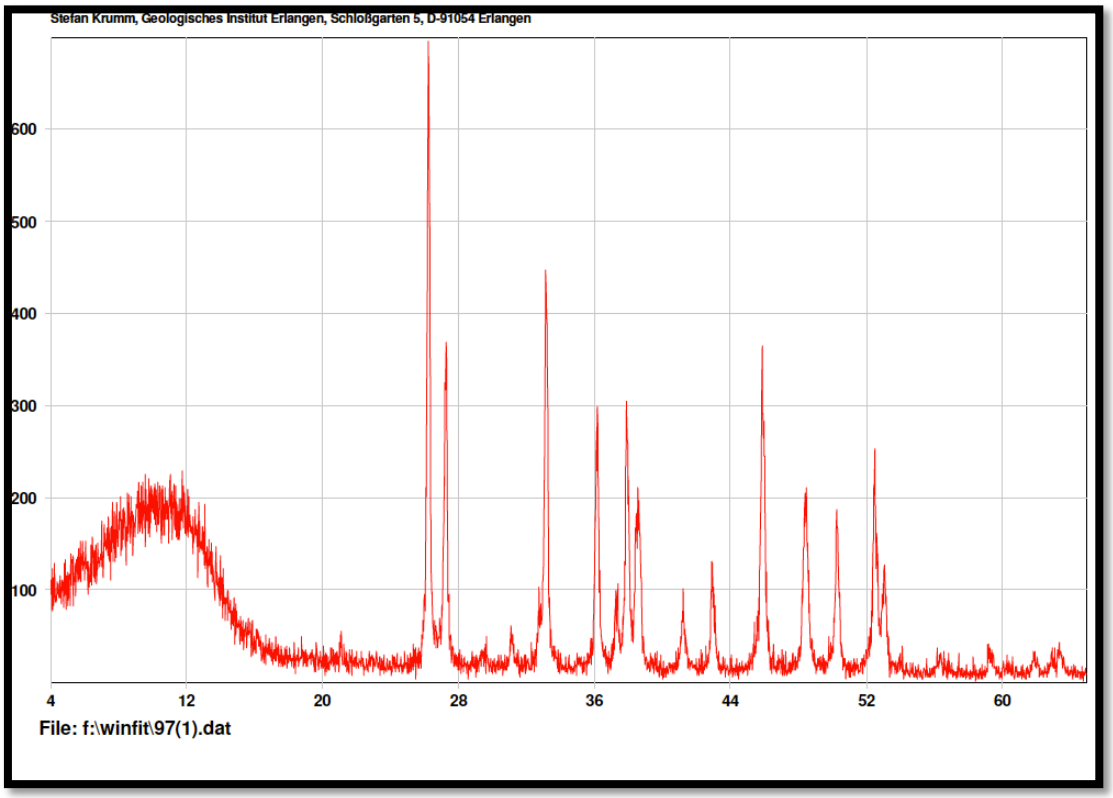
Stefan Krumm, Geologisches Institut Erlangen, Schloßgarten 5, D-91054 Erlangen
600
500
400
300
200
100
4
12
20
28
36
44
52
60
File: f:\winfit\97(1).dat

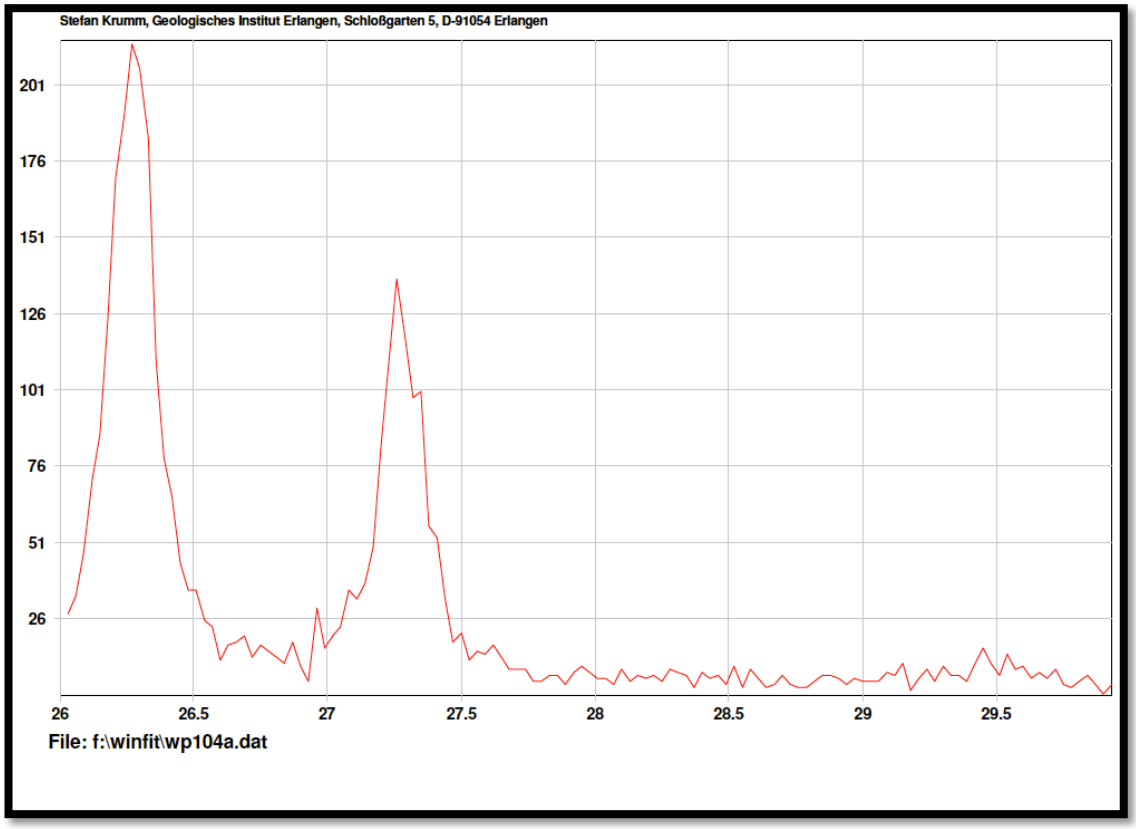
Stefan Krumm, Geologisches Institut Erlangen, Schloßgarten 5, D-91054 Erlangen
201
176
151
126
101
76
51
26
26
26.5
27
27.5
28
28.5
29
29.5
File: f:\winfit\wp104a.dat

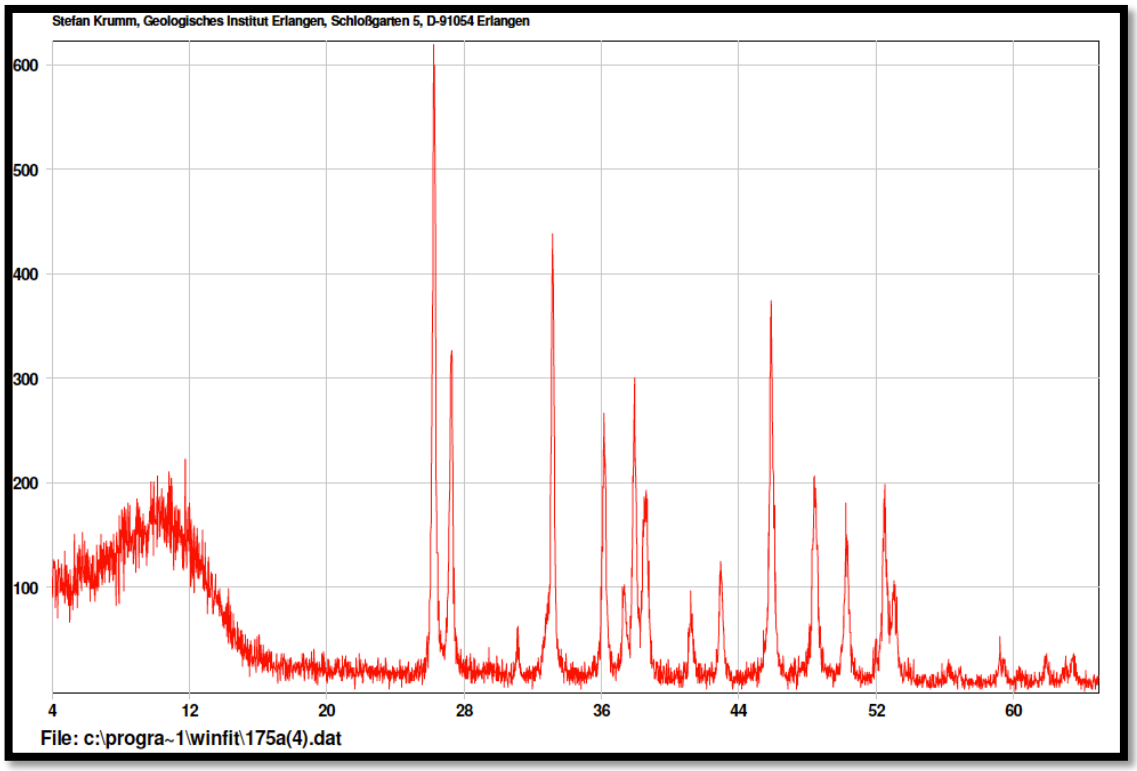
Stefan Krumm, Geologisches Institut Erlangen, Schloßgarten 5, D-91054 Erlangen
600
500
400
300
200
100
4
12
20
28
36
44
52
60
File: c:\progra~1\winfit\175a(4).dat

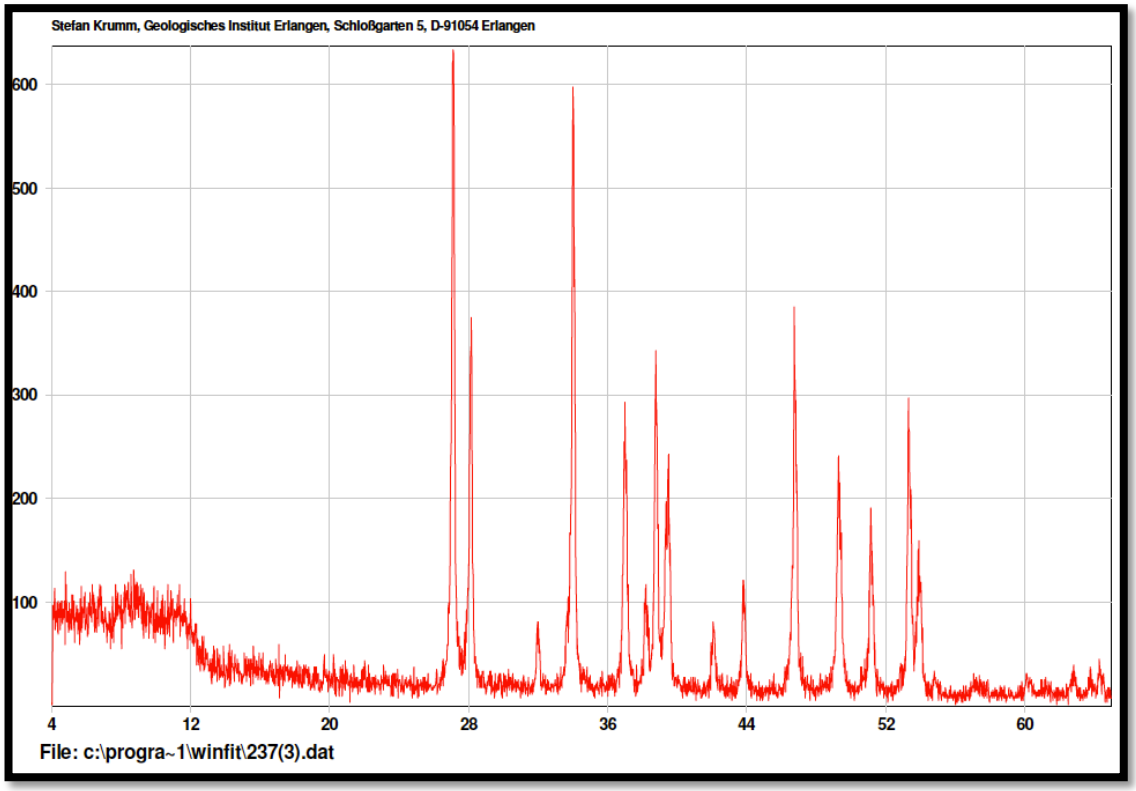
Stefan Krumm, Geologisches Institut Erlangen, Schloßgarten 5, D-91054 Erlangen
600
500
400
300
200
100
4
12
20
28
36
44
52
60
File: c:\progra~1\winfit\237(3).dat

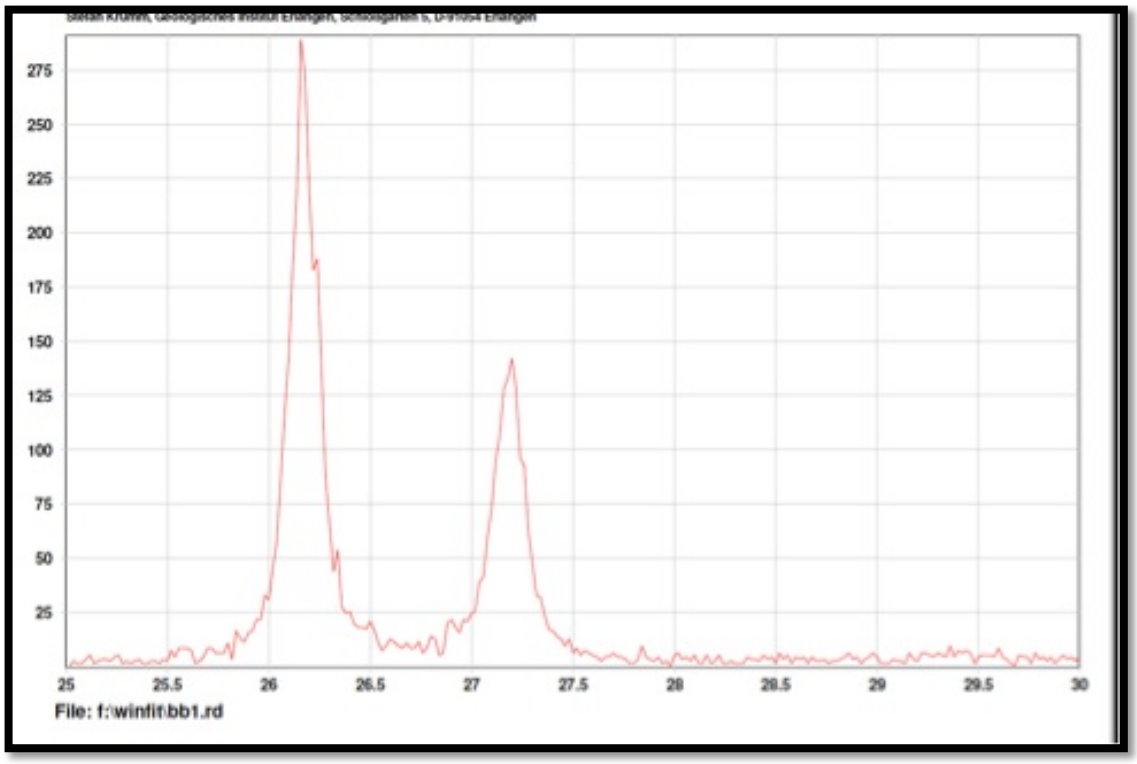
275
250
225
200
175
150
125
100
75
50
25
25
25.5
26
26.5
27
27.5
28
28.5
29
29.5
30
File: f:\winfit\bb1.rd

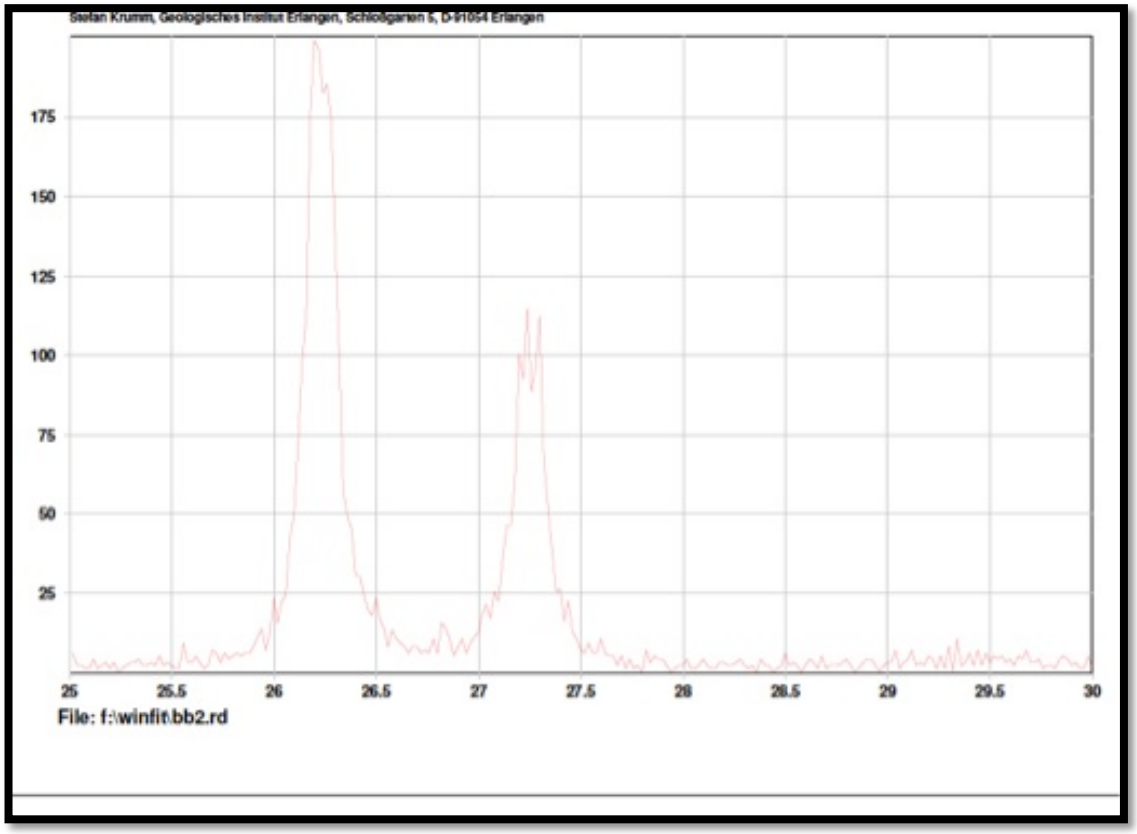
Stefan Krumm, Geologisches Institut Erlangen, Schloßgarten 5, D-91054 Erlangen
175
150
125
100
75
50
25
25
25.5
26
26.5
27
27.5
28
28.5
29
29.5
30
File: f:\winfit\bb2.rd

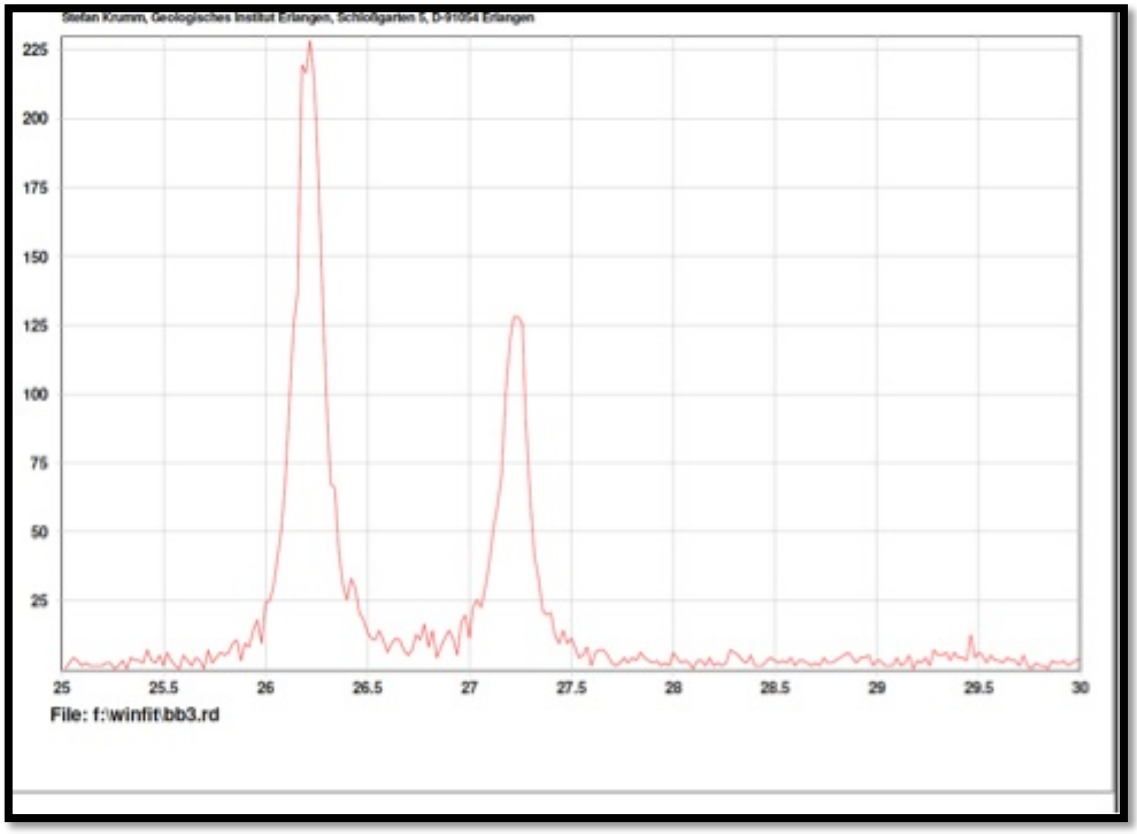
Stefan Krumm, Geologisches Institut Erlangen, Schloßgarten 5, D-91054 Erlangen
225
200
175
150
125
100
75
50
25
25
25.5
26
26.5
27
27.5
28
28.5
29
29.5
30
File: f:\winfit\bb3.rd

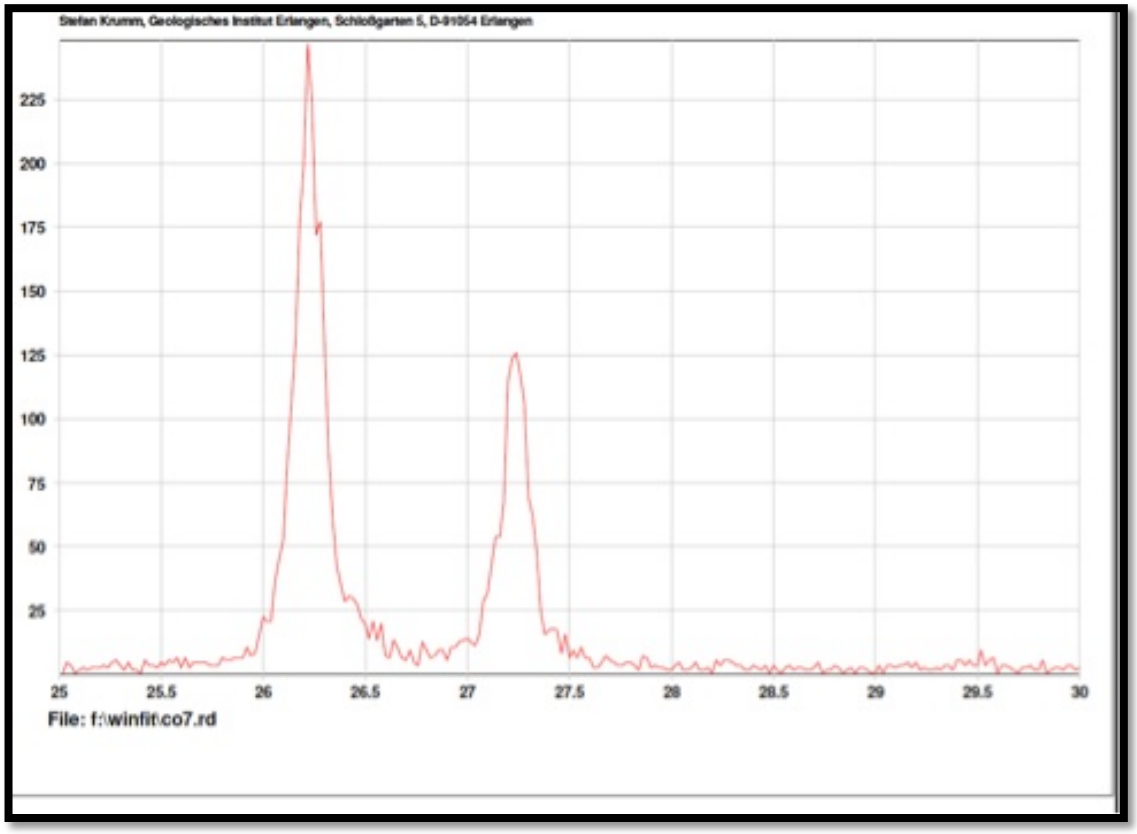
Stefan Krumm, Geologisches Institut Erlangen, Schloßgarten 5, D-91054 Erlangen
225
200
175
150
125
100
75
50
25
25
25.5
26
26.5
27
27.5
28
28.5
29
29.5
30
File: f:\winfit\co7.rd

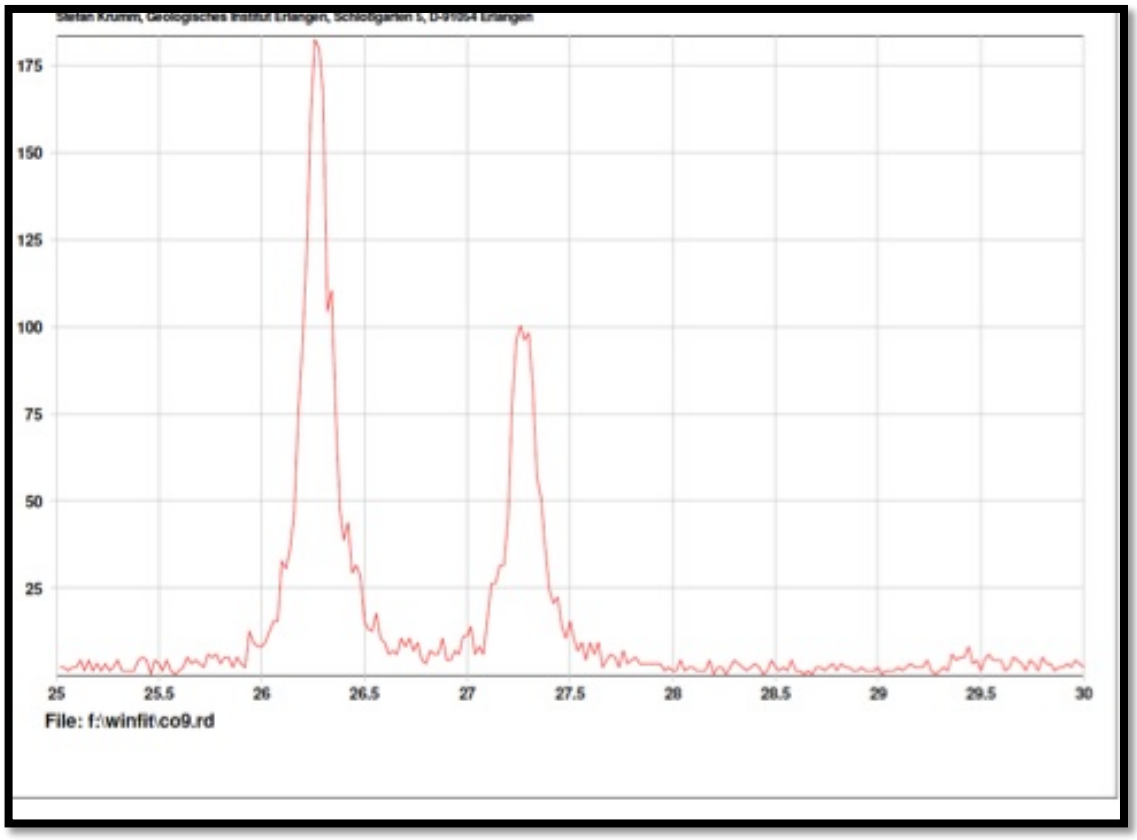
175
150
125
100
75
50
25
25
25.5
26
26.5
27
27.5
28
28.5
29
29.5
30
File: f:\winfit\co9.rd

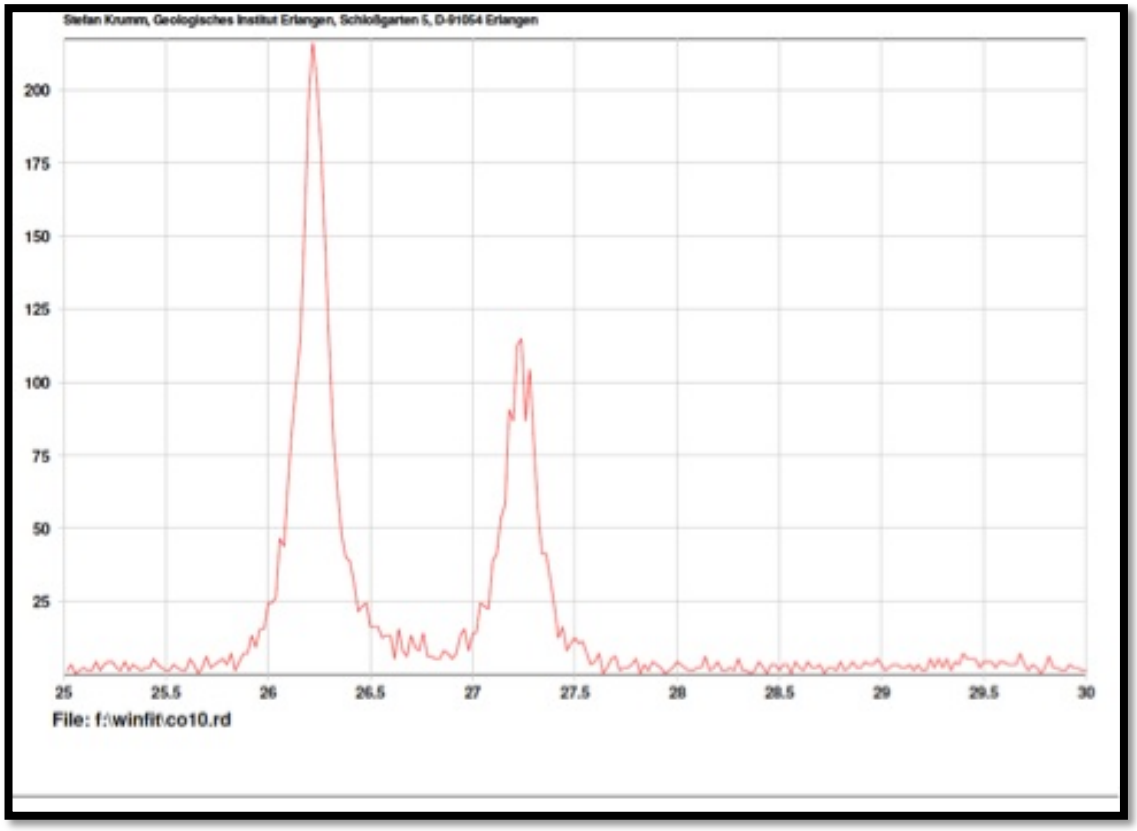

Aulacomya atra

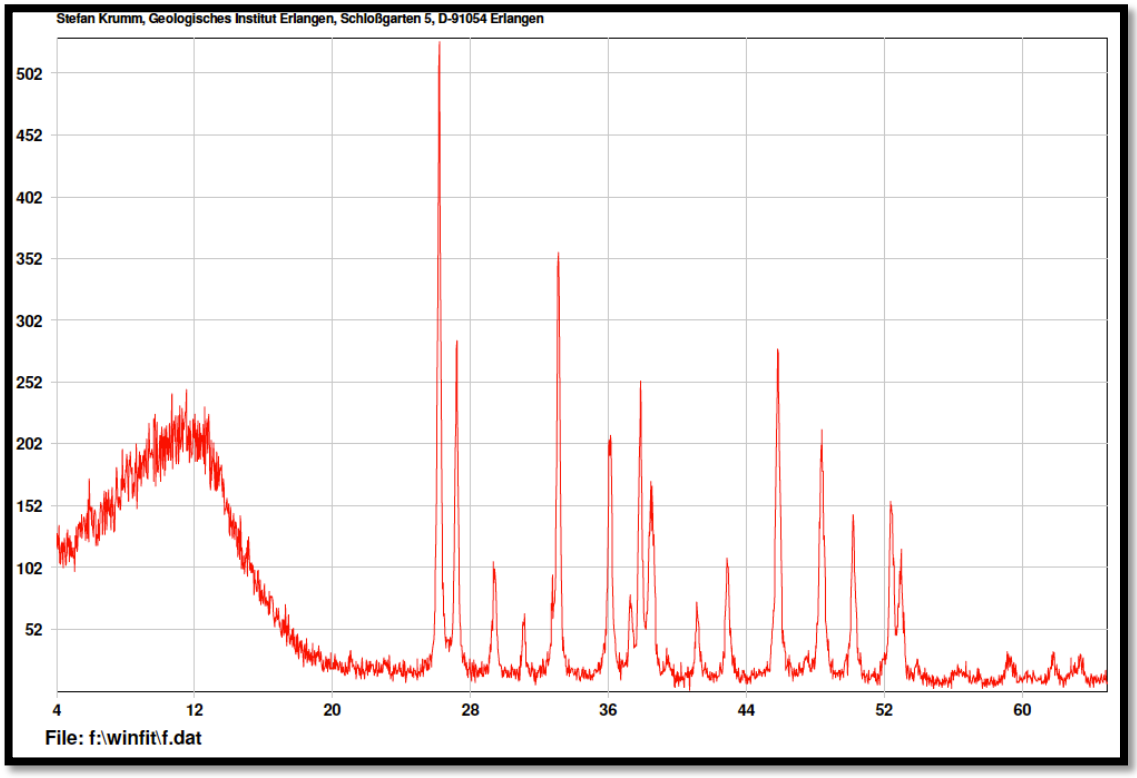

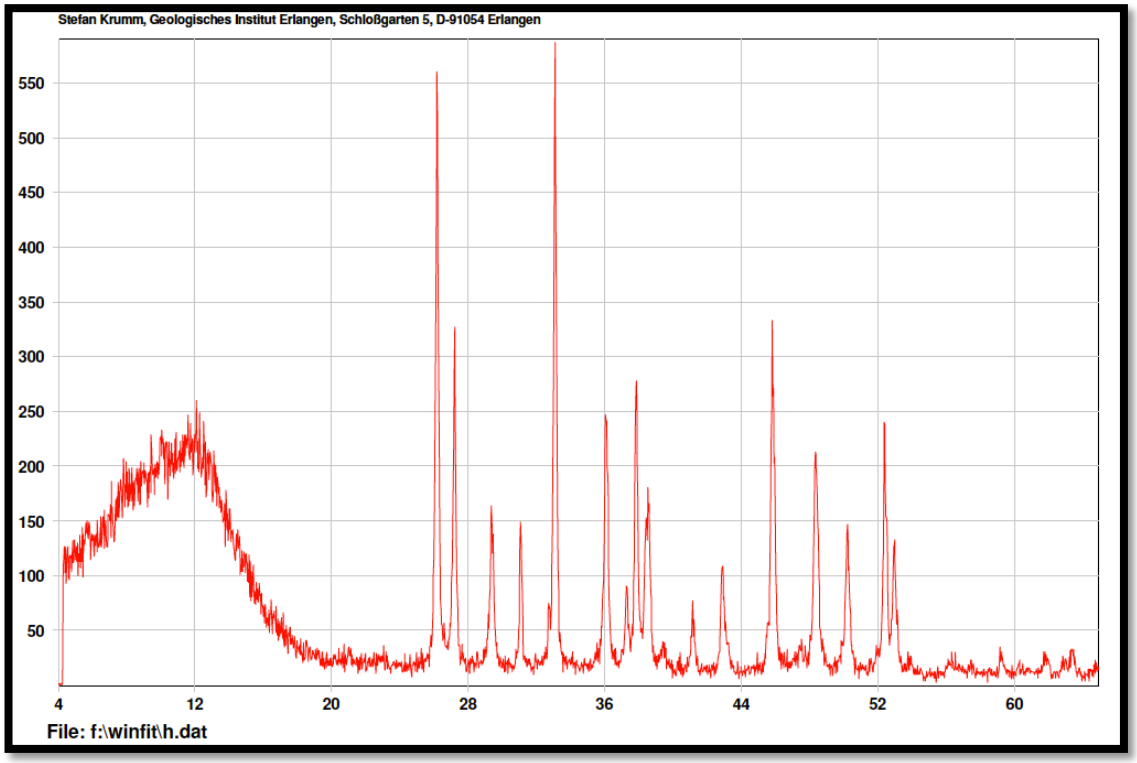
Stefan Krumm, Geologisches Institut Erlangen, Schloßgarten 5, D-91054 Erlangen
550
500
450
400
350
300
250
200
150
100
50
4
12
20
28
36
44
52
60
File: f:\winfit\h.dat

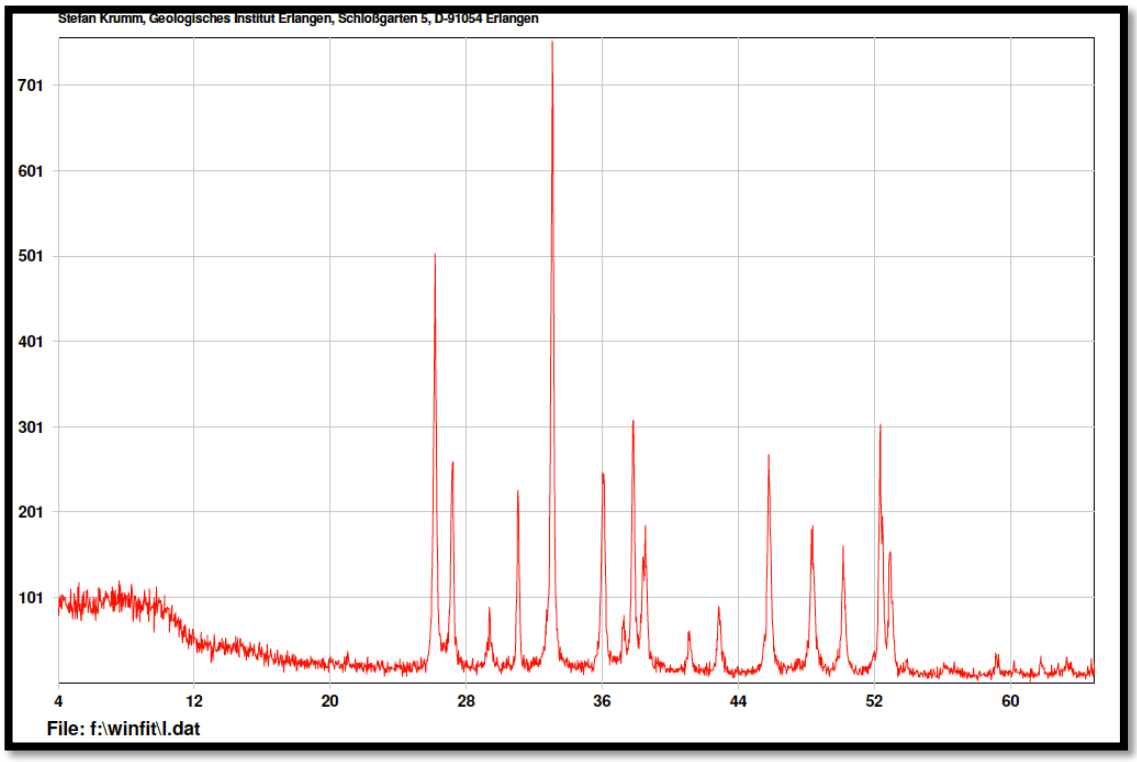
Stefan Krumm, Geologisches Institut Erlangen, Schloßgarten 5, D-91054 Erlangen
701
601
501
401
301
201
101
4
12
20
28
36
44
52
60
File: f:\winfit\l.dat

Mytilus edulis

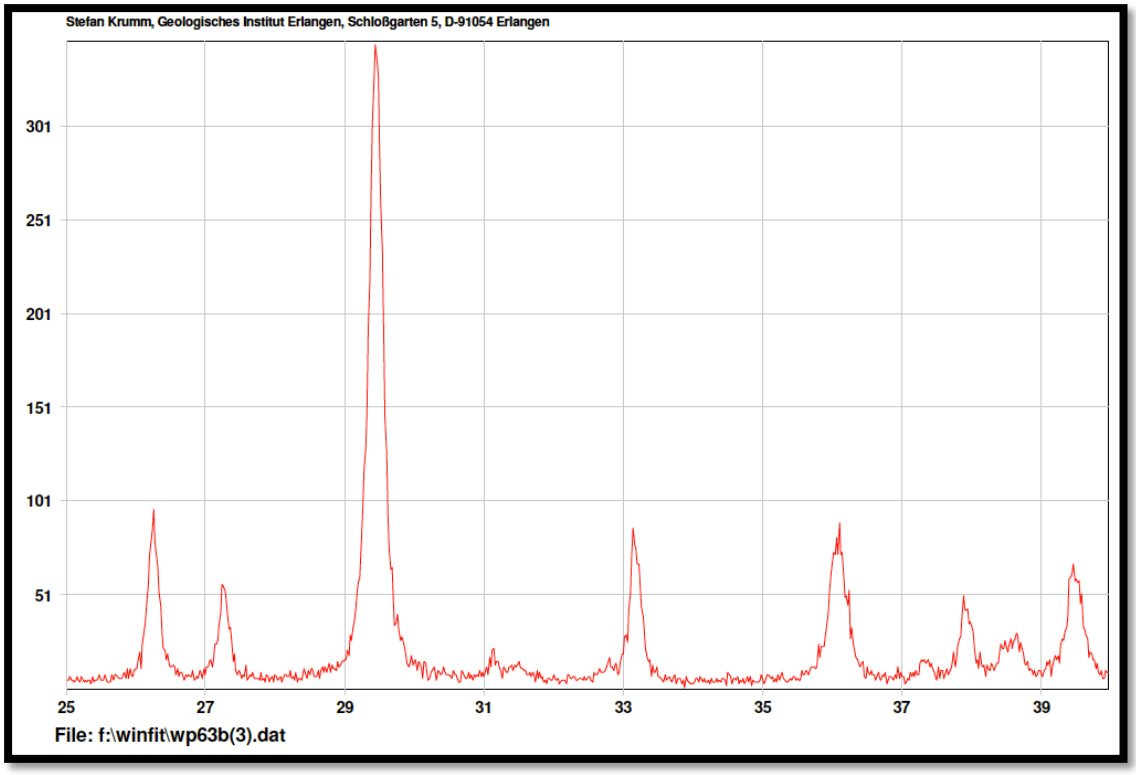

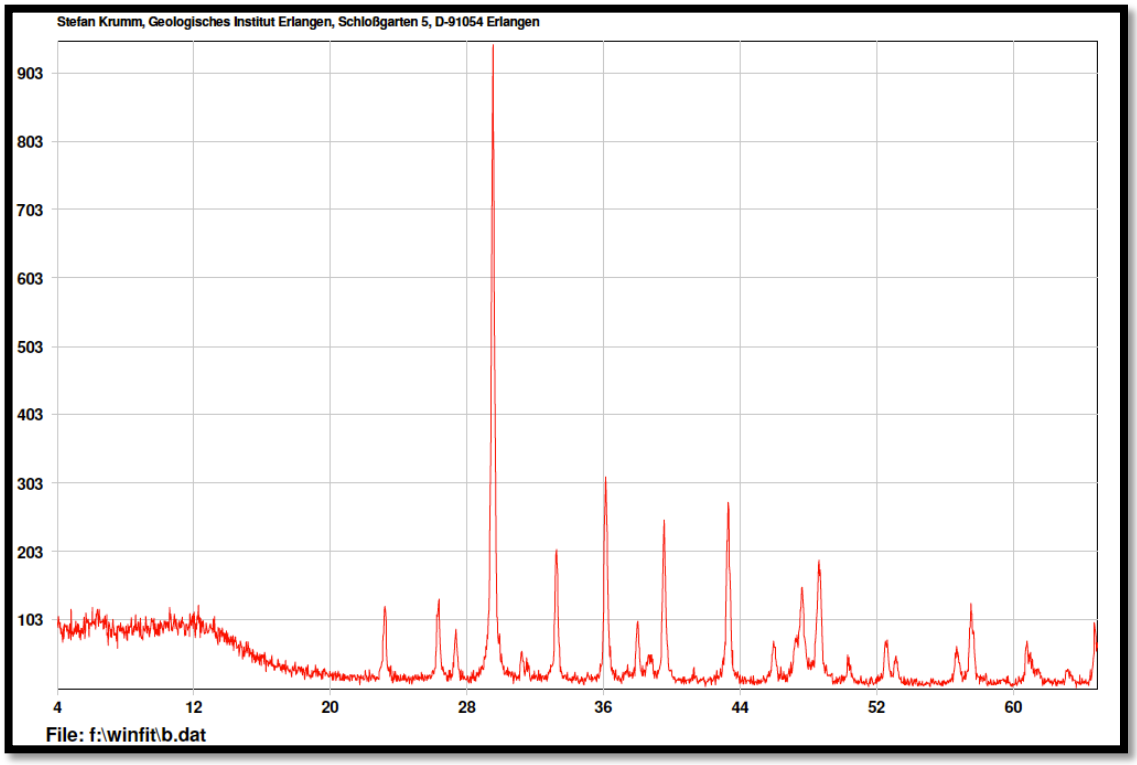

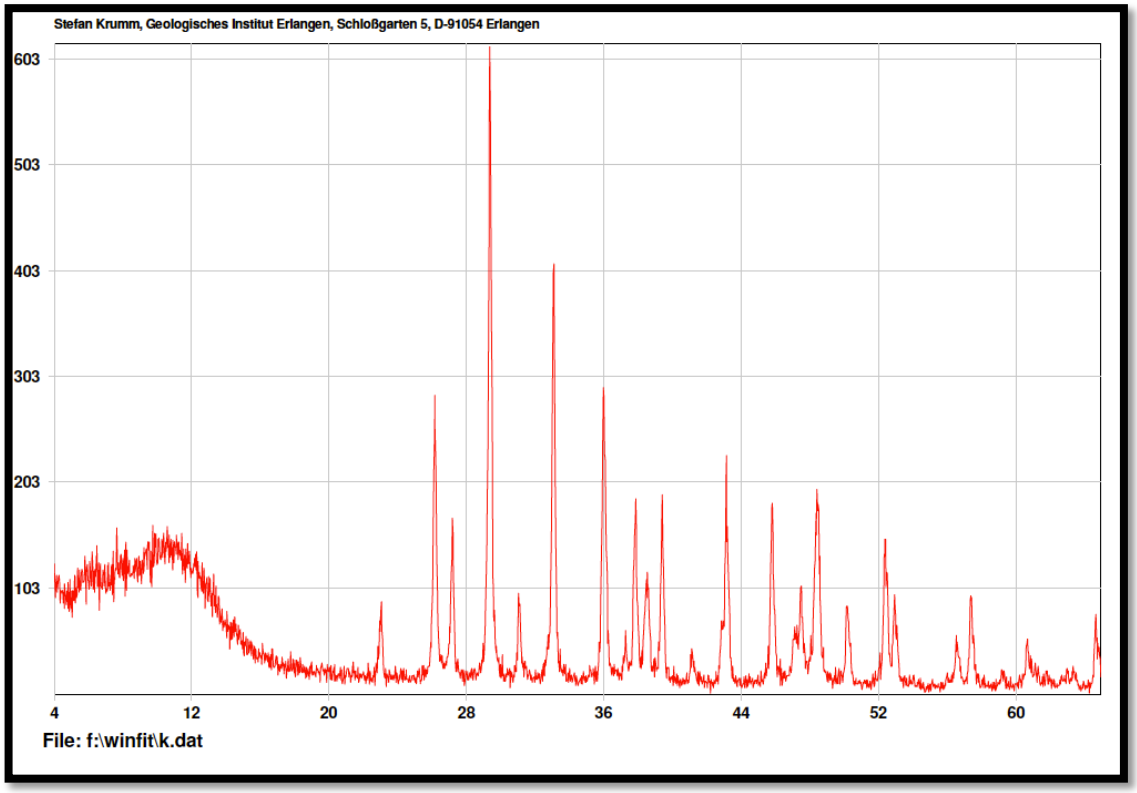
Stefan Krumm, Geologisches Institut Erlangen, Schloßgarten 5, D-91054 Erlangen
603
503
403
303
203
103
4
12
20
28
36
44
52
60
File: f:\winfit\k.dat

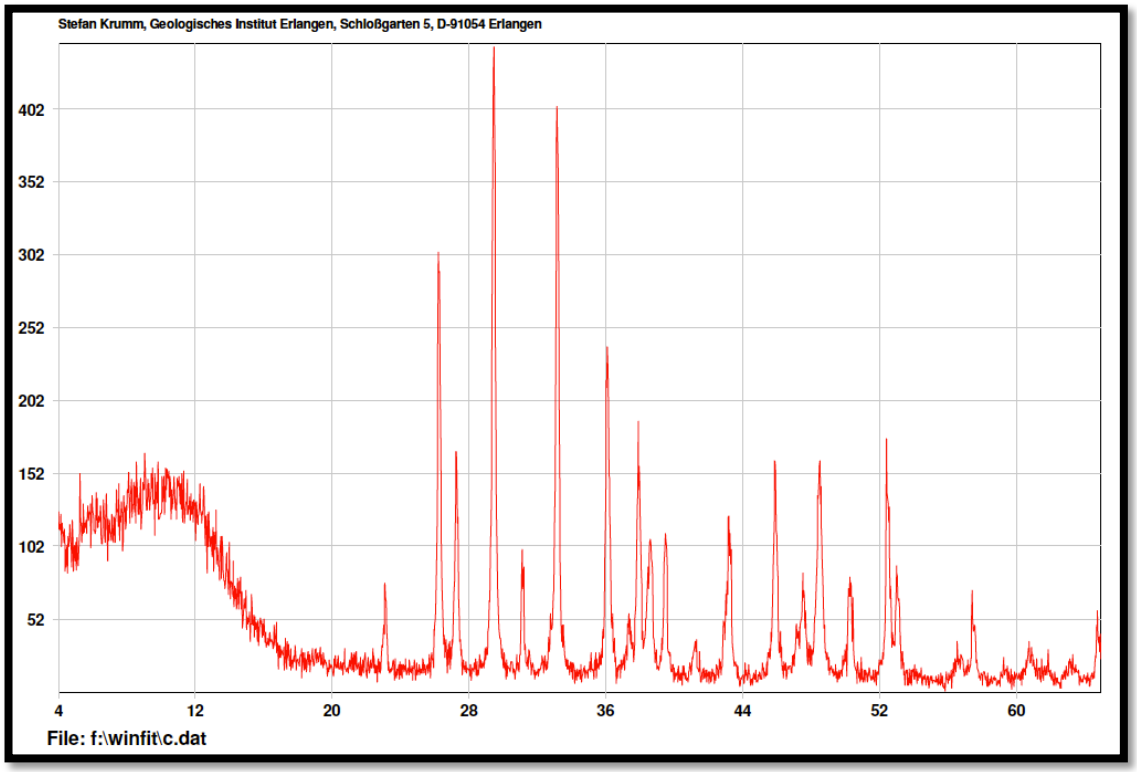
Stefan Krumm, Geologisches Institut Erlangen, Schloßgarten 5, D-91054 Erlangen
402
352
302
252
202
152
102
52
4
12
20
28
36
44
52
60
File: f:\winfit\c.dat

A.2 Radiocarbon dating

Sample name	species	Method	age yr BP	±	Area
WP39(1)	*Aulacomya atra*	^{14}C	**6055**	**20**	Cabo Raso
WP41(2)	*Brachidontes purpuratus*	^{14}C	**4500**	**20**	Cabo Raso
WP60A(2)	*Aulacomya atra*	^{14}C	**915**	**20**	Camarones North
WP60B(2)	*Aulacomya atra*	^{14}C	**-390**	**20**	Camarones North
WP63A(1)	*Ameghinomya antiqua*	^{14}C	**26110**	**100**	Camarones North
WP63A(2)	*Ameghinomya antiqua*	^{14}C	**38906**	**877**	Camarones North
WP63B(3)	*Mytilus edulis*	^{14}C	**6365**	**20**	Camarones North
G001	*Nacella (Patinigera) deaurata*	^{14}C	**4074**	**50**	Camarones North
WP 104A	*Ameghinomya antiqua*	^{14}C	**5675**	**45**	Camarones Sud
WP 139	*Ameghinomya antiqua*	^{14}C	**5276**	**47**	Bahia Bustamante
WP 144	*Ameghinomya antiqua*	^{14}C	**4693**	**59**	Bahia Bustamante
WP 145B	*Brachidontes purpuratus*	^{14}C	**1874**	**39**	Bahia Bustamante
WP 256B	*Ameghinomya antiqua*	^{14}C	**4138**	**41**	Bahia Bustamante
WP 272 A	*Ameghinomya antiqua*	^{14}C	**1930**	**24**	Bahia Solano
WP 275A	*Ameghinomya antiqua*	^{14}C	**2133**	**62**	Bahia Solano
WP344	*Nacella (Patinigera) deaurata*	^{14}C	**881**	**32**	Puerto Deseado
WP 307(1)	*Adelomelon ferussacii*	^{14}C	**3605**	**25**	Puerto Deseado
WP 307(2)	*Adelomelon ferussacii*	^{14}C	**3310**	**25**	Puerto Deseado
WP 383	*Nacella (Patinigera) deaurata*	^{14}C	**3519**	**24**	Puerto Deseado
WP 383	*Aulacomya atra*	^{14}C	**3527**	**42**	Puerto Deseado
WP 323	*Aulacomya atra*	^{14}C	**709**	**32**	Puerto Deseado
WP 301 D	*crosta*	^{14}C	**25780**	**160**	Puerto Deseado
WP 385	*Brachidontes purpuratus*	^{14}C	**41600**	**1200**	Puerto Deseado
WP 385	*Brachidontes purpuratus*	^{14}C	**45884**	**2061**	Puerto Deseado
WP 381	*Nacella (Patinigera) deaurata*	^{14}C	**2081**	**25**	Puerto Deseado
WP 312	*Adelomelon ferussacii*	^{14}C	**2382**	**60**	Puerto Deseado
WP 313	*Adelomelon ferussacii*	^{14}C	**1445**	**43**	Puerto Deseado
WP 315	*Nacella (Patinigera) deaurata*	^{14}C	**2343**	**48**	Puerto Deseado
WP 468A	*Ameghinomya antiqua*	^{14}C	**539**	**38**	Caleta Olivia
WP 462B	*suolo pedogenetico*	^{14}C	**27900**	**320**	Caleta Olivia
WPI 38	*Aulacomya atra*	^{14}C	**2226**	**60**	Puerto Deseado
WPI 39	*Aulacomya atra*	^{14}C	**476**	**59**	Puerto Deseado
AO 91	*Mytilus edulis*	^{14}C	**2798**	**65**	Bahia Bustamante
AO 92	*Mytilus edulis*	^{14}C	**2853**	**40**	Bahia Bustamante
AO 93a	*Ameghinomya antiqua*	^{14}C	**5154**	**60**	Bahia Bustamante
AO 95	*Aulacomya atra*	^{14}C	**626**	**36**	Bahia Bustamante
AO 154B	*balanide*	^{14}C	**5132**	**67**	Camarones Sud
AO 154D	*Mytilus edulis*	^{14}C	**5567**	**44**	Camarones Sud
AO 164	*Mytilus edulis*	^{14}C	**5370**	**60**	Camarones
AO 190	*Mytilus edulis*	^{14}C	**6486**	**46**	Camarones North
AO 194	*incrostazione*	^{14}C	**5432**	**60**	Camarones North
WPI 424	*balanide*	^{14}C	**5641**	**46**	Camarones Sud
WPI 436	*Mytilus edulis*	^{14}C	**5562**	**43**	Camarones Sud
WPI 436A	*balanide*	^{14}C	**5515**	**50**	Camarones Sud
WPI 436B	*incrostazione*	^{14}C	**4995**	**89**	Camarones Sud
PDP 1 (AO 79)	*Mytilus edulis*	^{14}C	**5851**	**39**	Puerto Deseado
PDP 2 (AO 78)	*Mytilus edulis*	^{14}C	**4259**	**92**	Puerto Deseado
PDN 1 (WPI 138)	*Nacella (Patinigera) deaurata*	^{14}C	**619**	**37**	Puerto Deseado

A.3 Stable isotope analysis

SAMPLE	LOCALITY	SPECIES	AGE	XRD	THIN SECTION	δ13C mean value (‰ VPDB)	st. dev.	δ18O mean value (‰ VPDB)	st. dev.	$^{87}Sr/^{86}Sr$
WP667(1)	PUERTO LOBOS	A. antiqua	MODERN			**1,01**	0,15	**0,45**	0,03	
WP667(2)	PUERTO LOBOS	A. antiqua	MODERN			**0,61**	0,07	**0,14**	0,04	
WP667(3)	PUERTO LOBOS	A. antiqua	MODERN			**0,25**		**0,01**		
WP667(4)	PUERTO LOBOS	A. antiqua	MODERN			**0,82**		**0,39**		
WP667(5)	PUERTO LOBOS	A. antiqua	MODERN			**0,44**	0,11	**0,15**	0,07	
WP04(1)	CABO RASO/BAHIA VERA	A. antiqua	MODERN			**1,13**		**0,71**		
WP04(2)	CABO RASO/BAHIA VERA	A. antiqua	MODERN			**1,40**	0,05	**0,70**	0,07	
WP04(3)	CABO RASO/BAHIA VERA	A. antiqua	MODERN			**0,68**		**0,51**		
WP04(4)	CABO RASO/BAHIA VERA	A. antiqua	MODERN			**0,55**		**0,62**		
WP04(5)	CABO RASO/BAHIA VERA	A. antiqua	MODERN			**0,57**		**0,84**		
WP54(1)	BAHIA SAN SEBASTIAN	A. antiqua	MODERN	X		**-0,33**	0,05	**0,08**	0,05	
WP54(2)	BAHIA SAN SEBASTIAN	A. antiqua	MODERN			**0,18**	0,02	**0,25**	0,07	
WP54(3)	BAHIA SAN SEBASTIAN	A. antiqua	MODERN			**0,12**		**0,43**		
WP54(4)	BAHIA SAN SEBASTIAN	A. antiqua	MODERN			**0,40**		**0,20**		
WP54(5)	BAHIA SAN SEBASTIAN	A. antiqua	MODERN			**0,24**	0,01	**0,28**	0,10	
WP54(6)	BAHIA SAN SEBASTIAN	A. antiqua	MODERN			**-0,08**	0,02	**0,28**	0,09	
WP60BBIS(1)	CAMARONES NORTH	A. antiqua	MODERN			**0,11**		**0,07**		
WP60BBIS(2)	CAMARONES NORTH	A. antiqua	MODERN			**0,49**		**0,40**		
WP623BIS(1)	CAMARONES NORTH	A. antiqua	MODERN			**0,07**		**0,42**		
WP623BIS(3)	CAMARONES NORTH	A. antiqua	MODERN		X	**0,36**		**0,33**		0,70917
WP623BIS(4)	CAMARONES NORTH	A. antiqua	MODERN			**0,30**		**0,23**		
WP623BIS(5)	CAMARONES NORTH	A. antiqua	MODERN			**-0,09**	0,03	**0,39**	0,04	
WP623BIS(6)	CAMARONES NORTH	A. antiqua	MODERN			**-0,43**		**0,37**		
WP95(2)	CAMARONES SOUTH	A. antiqua	MODERN			**0,59**		**0,38**		
WP95(3)	CAMARONES SOUTH	A. antiqua	MODERN			**0,62**		**0,30**		
WP95(4)	CAMARONES SOUTH	A. antiqua	MODERN			**0,89**		**0,35**		
WP110	CAMARONES SOUTH	A. antiqua	MODERN			**1,28**		**0,53**		
WP110(2)	CAMARONES SOUTH	A. antiqua	MODERN			**0,65**	0,03	**0,25**	0,10	
WP237(1)	BAHIA BUSTAMANTE	A. antiqua	MODERN	X		**-0,24**		**0,02**		
WP237(2)	BAHIA BUSTAMANTE	A. antiqua	MODERN			**-0,06**		**0,16**		
WP237(3)	BAHIA BUSTAMANTE	A. antiqua	MODERN	X		**0,41**		**0,27**		
WP237(4)	BAHIA BUSTAMANTE	A. antiqua	MODERN			**-0,36**		**0,23**		
WP237(5)	BAHIA BUSTAMANTE	A. antiqua	MODERN			**-0,21**	-0,03	**-0,03**	0,05	
WP613(1)	BAHIA BUSTAMANTE SOU	A. antiqua	MODERN			**-0,15**		**0,28**		
WP613(2)	BAHIA BUSTAMANTE SOU	A. antiqua	MODERN			**0,35**	0,01	**0,27**	0,04	
WP613(3)	BAHIA BUSTAMANTE SOU	A. antiqua	MODERN			**-0,22**		**0,23**		
WP 613(4)	BAHIA BUSTAMANTE SOU	A. antiqua	MODERN			**0,24**		**0,44**		
WP 613 (5)	BAHIA BUSTAMANTE SOU	A. antiqua	MODERN			**0,23**		**0,36**		
WP271(1)	BAHIA SOLANO	A. antiqua	MODERN			**-0,14**	0,08	**0,17**	0,06	
WP271(2)	BAHIA SOLANO	A. antiqua	MODERN		X	**-0,39**	0,00	**0,26**	0,01	0,70826
WP271(3)	BAHIA SOLANO	A. antiqua	MODERN			**-0,38**		**0,32**		
WP271(4)	BAHIA SOLANO	A. antiqua	MODERN			**-0,45**	0,03	**0,27**	0,08	
WP271(5)	BAHIA SOLANO	A. antiqua	MODERN			**0,01**	0,03	**0,33**	0,10	
MPA3(1)	BAHIA LANGARA	A. antiqua	MODERN			**0,43**		**0,62**		
MPA3(3)	BAHIA LANGARA	A. antiqua	MODERN			**1,13**		**0,97**		
MPA3(4)	BAHIA LANGARA	A. antiqua	MODERN			**1,04**		**0,55**		
WP473B(1)	CALETA OLIVIA	A. antiqua	MODERN			**0,06**		**0,71**		
WP473B(2)	CALETA OLIVIA	A. antiqua	MODERN			**0,45**		**0,81**		
WP473B(4)	CALETA OLIVIA	A. antiqua	MODERN			**0,37**		**0,75**		
WP 473B(6)	CALETA OLIVIA	A. antiqua	MODERN			**0,12**		**0,49**		
WP94B(1)	CAMARONES SOUTH	A. antiqua	HOLOCENE (LIT.5800±51 BP)			**1,10**		**0,82**		
WP94B(2)	CAMARONES SOUTH	A. antiqua	HOLOCENE (LIT.5800±51 BP)			**0,93**		**0,75**		
WP104A(1)	CAMARONES SOUTH	A. antiqua	5675±45	X		**0,59**		**0,64**		
WP104A(2)	CAMARONES SOUTH	A. antiqua	5675±45		X	**0,74**	0,13	**0,33**	0,13	
WP104A(3)	CAMARONES SOUTH	A. antiqua	5675±45			**0,38**	0,08	**0,58**	0,09	
WP104A(4)	CAMARONES SOUTH	A. antiqua	5675±45			**1,08**	0,02	**0,54**	0,02	
WP104A(5)	CAMARONES SOUTH	A. antiqua	5675±45			**0,50**	0,02	**0,39**	0,10	
WP 108A(1)	CAMARONES SOUTH	A. antiqua	HOLOCENE (LIT. 5754±62 BP)			**1,29**	0,09	**0,49**	0,02	
WP108A(2)	CAMARONES SOUTH	A. antiqua	HOLOCENE (LIT. 5754±62 BP)			**1,01**		**0,54**		
WP108A(3)	CAMARONES SOUTH	A. antiqua	HOLOCENE (LIT. 5754±62 BP)			**1,35**		**0,38**		
WP108A(4)	CAMARONES SOUTH	A. antiqua	HOLOCENE (LIT. 5754±62 BP)			**0,92**		**0,58**		
WP 114(1)	CAMARONES SOUTH	A. antiqua	HOLOCENE (LIT. 6620±65 BP)			**1,56**		**0,77**		
WP114(2)	CAMARONES SOUTH	A. antiqua	HOLOCENE (LIT. 6620±65 BP)			**1,75**		**0,83**		
WP114(3)	CAMARONES SOUTH	A. antiqua	HOLOCENE (LIT. 6620±65 BP)			**1,83**		**0,79**		
WP64A(2)	CAMARONES NORTH	A. antiqua	121000±900 BP			**0,87**		**0,22**		
WP64A(3)	CAMARONES NORTH	A. antiqua	121000±900 BP	X		**0,96**		**0,21**		
WP64A(4)	CAMARONES NORTH	A. antiqua	121000±900 BP			**0,75**		**0,44**		
WP64A(7)	CAMARONES NORTH	A. antiqua	121000±900 BP			**1,01**		**0,54**		
WP64B(2)	CAMARONES NORTH	A. antiqua	121000±900 BP			**0,82**		**0,37**		
WP64B(3)	CAMARONES NORTH	A. antiqua	121000±900 BP			**0,69**	0,02	**0,37**	0,04	
WP64B(4)	CAMARONES NORTH	A. antiqua	121000±900 BP			**0,95**		**0,21**		
WP65(1)	CAMARONES NORTH	A. antiqua	130000±2500 BP			**0,06**	0,00	**0,40**	0,40	
WP65(2)	CAMARONES NORTH	A. antiqua	130000±2500 BP	X		**-0,05**	0,03	**0,26**	0,08	
WP65(3)	CAMARONES NORTH	A. antiqua	130000±2500 BP	X		**0,83**	0,00	**0,47**	0,04	
WP65(4)	CAMARONES NORTH	A. antiqua	130000±2500 BP	X	X	**0,63**	0,01	**1,31**	0,10	
WP65(6)	CAMARONES NORTH	A. antiqua	130000±2500 BP			**0,28**		**0,91**		
WP65(7)	CAMARONES NORTH	A. antiqua	130000±2500 BP			**0,30**		**0,88**		
WP65(8)	CAMARONES NORTH	A. antiqua	130000±2500 BP			**0,34**		**0,46**		
WP 68(1)	CAMARONES NORTH	A. antiqua	131000±1100 BP	X		**0,23**		**0,70**		
WP 68(2)	CAMARONES NORTH	A. antiqua	131000±1100 BP			**0,85**	0,02	**0,63**	0,10	

APPENDIX A

WP68(3)	CAMARONES NORTH	A. antiqua	131000±1100 BP			**0,19**	0,02	**0,52**	0,02	
WP68(4)	CAMARONES NORTH	A. antiqua	131000±1100 BP			**0,33**	0,04	**0,37**	0,13	
WP 68(5)	CAMARONES NORTH	A. antiqua	131000±1100 BP			**0,93**		**0,51**		
WP 68(6)	CAMARONES NORTH	A. antiqua	131000±1100 BP			**0,92**		**0,43**		
WP70A(1)	CAMARONES NORTH	A. antiqua	127000±1200 BP	X		**0,20**	0,03	**0,28**	0,03	
WP70A(2)	CAMARONES NORTH	A. antiqua	127000±1200 BP			**1,12**	0,01	**0,34**	0,12	
WP70A(3)	CAMARONES NORTH	A. antiqua	127000±1200 BP			**0,25**	0,05	**0,44**	0,04	
WP70A(4)	CAMARONES NORTH	A. antiqua	127000±1200 BP			**0,64**	0,01	**0,43**	0,07	
WP70A(5)	CAMARONES NORTH	A. antiqua	127000±1200 BP			**0,54**		**0,59**		
WP70A(6)	CAMARONES NORTH	A. antiqua	127000±1200 BP			**1,02**		**0,74**		
WP70B	CAMARONES NORTH	A. antiqua	127000±1200 BP	X		**1,61**		**0,67**		
WP92A(1)	CAMARONES SOUTH	A. antiqua	92000±600 (LIT 198000±23000)			**1,10**	0,02	**0,61**	0,03	
WP92A(2)	CAMARONES SOUTH	A. antiqua	92000±600 (LIT 198000±23000)	X	X	**0,55**	0,03	**0,51**	0,03	
WP92A(3)	CAMARONES SOUTH	A. antiqua	92000±600 (LIT 198000±23000)			**0,82**	0,02	**0,52**	0,15	
WP92A(4)	CAMARONES SOUTH	A. antiqua	92000±600 (LIT 198000±23000)			**0,53**	0,01	**0,57**	0,12	
WP92A(5)	CAMARONES SOUTH	A. antiqua	92000±600 (LIT 198000±23000)			**1,10**		**0,71**		
WP97(1)	CAMARONES SOUTH	A. antiqua	414000±16000 BP	X		**0,43**		**0,23**		
WP97(2)	CAMARONES SOUTH	A. antiqua	414000±16000 BP		X	**0,57**	0,01	**0,18**	0,04	
WP97(3)	CAMARONES SOUTH	A. antiqua	414000±16000 BP			**1,14**	0,14	**0,29**	0,07	0,70889
WP97(4)	CAMARONES SOUTH	A. antiqua	414000±16000 BP			**0,65**		**0,25**		
WP97(5)	CAMARONES SOUTH	A. antiqua	414000±16000 BP			**0,32**		**0,30**		
WP138(1)	BAHIA BUSTAMANTE	A. antiqua	HOLOCENE	X		**0,95**		**0,59**		
WP138(2)	BAHIA BUSTAMANTE	A. antiqua	HOLOCENE			**0,75**		**0,27**		
WP138(3)	BAHIA BUSTAMANTE	A. antiqua	HOLOCENE			**0,96**	0,02	**0,31**	0,07	
WP138(4)	BAHIA BUSTAMANTE	A. antiqua	HOLOCENE			**0,74**	0,01	**0,34**	0,14	
WP139(1)	BAHIA BUSTAMANTE	A. antiqua	5276 ± 47			**0,36**	0,005	**0,26**	0,06	
WP139(2)	BAHIA BUSTAMANTE	A. antiqua	5276 ± 47			**0,41**	0,02	**0,25**	0,00	
WP139(3)	BAHIA BUSTAMANTE	A. antiqua	5276 ± 47			**0,58**		**0,38**		0,70917
WP139(4)	BAHIA BUSTAMANTE	A. antiqua	5276 ± 47			**0,54**		**0,45**		
WP139BIS(2)	BAHIA BUSTAMANTE	A. antiqua	5276 ± 47			**1,01**	0,00	**0,45**	0,04	
WP144(1)	BAHIA BUSTAMANTE	A. antiqua	4693 ± 59			**0,95**		**0,65**		
WP144(3)	BAHIA BUSTAMANTE	A. antiqua	4693 ± 59			**1,38**	0,01	**0,39**	0,07	
WP144(4)	BAHIA BUSTAMANTE	A. antiqua	4693 ± 59			**0,69**	0,01	**0,63**	0,06	
WP256A(1)	BAHIA BUSTAMANTE	A. antiqua	4138 ± 41			**1,58**	0,01	**0,72**	0,00	
WP256A(2)	BAHIA BUSTAMANTE	A. antiqua	4138 ± 41			**1,57**		**0,88**		
WP256A(3)	BAHIA BUSTAMANTE	A. antiqua	4138 ± 41			**1,17**	0,01	**0,42**	0,01	
WP256A(4)	BAHIA BUSTAMANTE	A. antiqua	4138 ± 41			**0,88**		**0,43**		
WP256B	BAHIA BUSTAMANTE	A. antiqua	4138 ± 41			**1,59**	0,004	**0,51**	0,04	
WP148(1)	BAHIA BUSTAMANTE	A. antiqua	MIS5			**0,50**	0,02	**0,31**	0,07	
WP148(2)	BAHIA BUSTAMANTE	A. antiqua	MIS5			**1,22**		**0,08**		
WP148(3)	BAHIA BUSTAMANTE	A. antiqua	MIS5	X		**1,08**		**0,56**		
WP148(4)	BAHIA BUSTAMANTE	A. antiqua	MIS5			**0,51**	0,01	**0,29**	0,01	
WP149(1)	BAHIA BUSTAMANTE	A. antiqua	89000 ± 800			**0,84**	0,001	**0,29**	0,042	0,70902
WP149(2)	BAHIA BUSTAMANTE	A. antiqua	89000 ± 800			**0,01**	0,01	**0,27**	0,16	
WP149(3)	BAHIA BUSTAMANTE	A. antiqua	89000 ± 800			**1,17**	0,002	**0,37**	0,14	
WP149(5)	BAHIA BUSTAMANTE	A. antiqua	89000 ± 800			**1,13**		**0,36**		
WP149(6)	BAHIA BUSTAMANTE	A. antiqua	89000 ± 800			**0,98**	0,01	**0,27**	0,06	
WP149(7)	BAHIA BUSTAMANTE	A. antiqua	89000 ± 800			**1,52**	0,03	**0,35**	0,07	
WP151(1)	BAHIA BUSTAMANTE	A. antiqua	MIS5			**1,22**		**0,37**		
WP151(2)	BAHIA BUSTAMANTE	A. antiqua	MIS5			**0,65**	0,02	**0,33**	0,03	
WP151(3)	BAHIA BUSTAMANTE	A. antiqua	MIS5			**0,62**		**0,48**		
WP151(4)	BAHIA BUSTAMANTE	A. antiqua	MIS5			**0,87**	0,00	**0,22**	0,01	
WP151(5)	BAHIA BUSTAMANTE	A. antiqua	MIS5			**-0,08**	0,00	**0,58**	0,00	
WP154A(1)	BAHIA BUSTAMANTE	A. antiqua	MIS5			**0,06**	0,04	**0,33**	0,20	
WP154A(2)	BAHIA BUSTAMANTE	A. antiqua	MIS5	X	X	**0,91**	0,09	**0,47**	0,13	
WP154B(1)	BAHIA BUSTAMANTE	A. antiqua	MIS5			**-0,29**	0,01	**0,34**	0,06	
WP154B(2)	BAHIA BUSTAMANTE	A. antiqua	MIS5			**0,05**		**0,26**		
WP154B(3)	BAHIA BUSTAMANTE	A. antiqua	MIS5			**-0,28**	0,03	**0,33**	0,03	
WP154B(4)	BAHIA BUSTAMANTE	A. antiqua	MIS5			**-0,99**	0,01	**-0,14**	0,01	
WP168(1)	BAHIA BUSTAMANTE	A. antiqua	MIS5	X		**0,40**		**0,31**		
WP168(2)	BAHIA BUSTAMANTE	A. antiqua	MIS5			**-0,09**	0,00	**0,25**	0,08	
WP168(3)	BAHIA BUSTAMANTE	A. antiqua	MIS5			**0,74**	0,002	**0,19**	0,014	
WP168(4)	BAHIA BUSTAMANTE	A. antiqua	MIS5			**1,02**		**0,36**		
WP171A	BAHIA BUSTAMANTE	A. antiqua	MIS5			**0,61**		**0,63**		
WP172(1)	BAHIA BUSTAMANTE	A. antiqua	MIS5			**0,56**	0,02	**0,53**	0,07	
WP172(2)	BAHIA BUSTAMANTE	A. antiqua	MIS5			**0,44**	0,00	**0,38**	0,02	
WP172(3)	BAHIA BUSTAMANTE	A. antiqua	MIS5			**0,97**		**0,33**		
WP172(4)	BAHIA BUSTAMANTE	A. antiqua	MIS5			**0,51**		**0,29**		
WP172(5)	BAHIA BUSTAMANTE	A. antiqua	MIS5			**0,55**		**0,42**		
WP173A(1)	BAHIA BUSTAMANTE	A. antiqua	MIS5			**0,05**		**0,26**		
WP173A(2)	BAHIA BUSTAMANTE	A. antiqua	MIS5			**0,89**		**0,40**		
WP175A(1)	BAHIA BUSTAMANTE	A. antiqua	MIS 7			**0,34**		**0,15**		
WP175A(2)	BAHIA BUSTAMANTE	A. antiqua	MIS 7			**0,52**		**0,34**		
WP175A(3)	BAHIA BUSTAMANTE	A. antiqua	MIS 7			**0,55**		**0,29**		
WP175A(4)	BAHIA BUSTAMANTE	A. antiqua	MIS 7	X		**1,18**		**0,41**		
WP175A(5)	BAHIA BUSTAMANTE	A. antiqua	MIS 7			**1,00**	0,01	**0,27**	0,15	
WP176BIS(1)	BAHIA BUSTAMANTE	A. antiqua	82500±500 BP (LIT.215000±24500)			**0,59**		**0,42**		0,70899
WP176BIS(2)	BAHIA BUSTAMANTE	A. antiqua	82500±500 BP (LIT.215000±24500)			**-0,17**	0,02	**-0,01**	0,02	
WP176BIS(3)	BAHIA BUSTAMANTE	A. antiqua	82500±500 BP (LIT.215000±24500)			**-0,55**	0,12	**-0,19**	0,14	
WP176BIS(4)	BAHIA BUSTAMANTE	A. antiqua	82500±500 BP (LIT.215000±24500)			**0,37**	0,01	**0,41**	0,19	
WP176BIS(5)	BAHIA BUSTAMANTE	A. antiqua	82500±500 BP (LIT.215000±24500)			**-0,02**		**-0,02**		
WP176BIS(6)	BAHIA BUSTAMANTE	A. antiqua	82500±500 BP (LIT.215000±24500)			**-0,39**	0,02	**-0,13**	0,05	

APPENDIX A

WP197(1)	BAHIA BUSTAMANTE	A. antiqua	PLEISTOCENE			**0,22**		**0,18**		
WP197(2)	BAHIA BUSTAMANTE	A. antiqua	PLEISTOCENE	X		**0,72**	0,07	**0,24**	0,04	
WP272A	BAHIA SOLANO	A. antiqua	1930±24		X	**0,55**		**0,28**		0,70905
WP272B(1)	BAHIA SOLANO	A. antiqua	1930±24			**0,50**	0,03	**0,54**	0,09	
WP272B(2)	BAHIA SOLANO	A. antiqua	1930±24			**0,16**	0,03	**0,52**	0,02	
WP272B(3)	BAHIA SOLANO	A. antiqua	1930±24			**0,80**		**0,29**	0,05	
WP272B(4)	BAHIA SOLANO	A. antiqua	1930±24			**0,86**		**0,55**		
WP272B(5)	BAHIA SOLANO	A. antiqua	1930±24			**0,28**		**0,40**		
WP274A(1)	BAHIA SOLANO	A. antiqua	<2133±62 upper layer			**1,62**		**0,08**		
WP274A(2)	BAHIA SOLANO	A. antiqua	<2133±62 upper layer			**0,37**		**0,61**		
WP274A(3)	BAHIA SOLANO	A. antiqua	<2133±62 upper layer			**0,10**		**0,54**		
WP274A(4)	BAHIA SOLANO	A. antiqua	<2133±62 upper layer			**0,78**		**0,77**		
WP274A(5)	BAHIA SOLANO	A. antiqua	<2133±62 upper layer			**0,82**		**0,10**		
WP274A(6)	BAHIA SOLANO	A. antiqua	<2133±62 upper layer			**0,62**		**0,30**		
WP274C(1)	BAHIA SOLANO	A. antiqua	<2133±62 upper layer			**0,45**		**0,13**		
WP274C(2)	BAHIA SOLANO	A. antiqua	<2133±62 upper layer			**0,30**		**0,27**		
WP274C(3)	BAHIA SOLANO	A. antiqua	<2133±62 upper layer			**0,48**		**0,51**		
WP274C(4)	BAHIA SOLANO	A. antiqua	<2133±62 upper layer			**0,86**		**0,40**		
WP274C(5)	BAHIA SOLANO	A. antiqua	<2133±62 upper layer			**0,29**		**0,39**		
WP274C(6)	BAHIA SOLANO	A. antiqua	<2133±62 upper layer			**0,82**		**0,35**		
WP278(1)	BAHIA SOLANO	A. antiqua	HOLOCENE			**0,95**		**0,75**		
WP278(2)	BAHIA SOLANO	A. antiqua	HOLOCENE			**0,64**		**0,37**		
WP278(3)	BAHIA SOLANO	A. antiqua	HOLOCENE			**1,00**		**0,40**		
WP278(4)	BAHIA SOLANO	A. antiqua	HOLOCENE			**1,26**		**0,49**		
WP468A(1)	CALETA OLIVIA	A. antiqua	539±38			**0,56**		**1,08**		
WP468A(2)	CALETA OLIVIA	A. antiqua	539±38			**0,86**		**0,92**		
WP468A(3)	CALETA OLIVIA	A. antiqua	539±38			**0,80**		**0,99**		
WP468A(4)	CALETA OLIVIA	A. antiqua	539±38			**1,23**		**0,99**		
WP475B(1)	CALETA OLIVIA	A. antiqua	LIT 4074±34			**0,47**		**1,34**		
WP475B(2)	CALETA OLIVIA	A. antiqua	LIT 4074±34			**0,28**		**0,78**		
WP475B(4)	CALETA OLIVIA	A. antiqua	LIT 4074±34			**0,23**		**0,66**		
WP523(1)	CALETA OLIVIA	A. antiqua	LIT 5450±100			**0,52**		**0,85**		
WP523(2)	CALETA OLIVIA	A. antiqua	LIT 5450±100			**0,15**		**0,48**		
WP523(3)	CALETA OLIVIA	A. antiqua	LIT 5450±100			**-0,35**		**0,43**		
WP446(1)	CALETA OLIVIA	A. antiqua	MIS 5			**0,30**		**0,58**		
WP446(2)	CALETA OLIVIA	A. antiqua	MIS 5			**-0,19**		**0,57**		
WP447B(1)	CALETA OLIVIA	A. antiqua	MIS 5			**-0,13**		**0,61**		
WP447B(2)	CALETA OLIVIA	A. antiqua	MIS 5			**-0,57**		**0,70**		
WP447B(3)	CALETA OLIVIA	A. antiqua	MIS 5			**-0,08**		**0,54**		
WP447B(4)	CALETA OLIVIA	A. antiqua	MIS 5			**-0,22**		**0,53**		
WP455(1)	CALETA OLIVIA	A. antiqua	MIS 5			**0,84**		**0,32**		
WP455(2)	CALETA OLIVIA	A. antiqua	MIS 5			**0,19**		**0,77**		
WP455(3)	CALETA OLIVIA	A. antiqua	MIS 5			**0,85**		**0,07**		
WP455(4)	CALETA OLIVIA	A. antiqua	MIS 5			**0,60**		**0,75**		
WP455(5)	CALETA OLIVIA	A. antiqua	MIS 5			**0,23**		**0,63**		
WP455(6)	CALETA OLIVIA	A. antiqua	MIS 5			**-0,18**		**0,55**		
WP455(7)	CALETA OLIVIA	A. antiqua	MIS 5	X		**0,10**		**0,54**		
WP447C(1)	CALETA OLIVIA	A. antiqua	MIS 7			**0,00**		**0,47**		
WP447C(2)	CALETA OLIVIA	A. antiqua	MIS 7			**-0,69**		**0,25**		
WP447C(3)	CALETA OLIVIA	A. antiqua	MIS 7			**-0,06**		**-0,16**		
WP447C(4)	CALETA OLIVIA	A. antiqua	MIS 7			**-0,02**		**0,64**		
WP454A(1)	CALETA OLIVIA	A. antiqua	MIS 7			**0,20**		**0,93**		
WP454A(2)	CALETA OLIVIA	A. antiqua	MIS 7			**0,23**		**1,01**		
WP454A(3)	CALETA OLIVIA	A. antiqua	MIS 7			**0,40**		**1,03**		
WP471(1)	CALETA OLIVIA	A. antiqua	MIS 9			**-0,88**		**0,52**		
WP471(2)	CALETA OLIVIA	A. antiqua	MIS 9			**1,01**		**0,63**		
WP471(3)	CALETA OLIVIA	A. antiqua	MIS 9			**0,93**		**1,11**		
WP479A(1)	CALETA OLIVIA	A. antiqua	MIS 9			**0,87**		**1,08**		
WP479A(2)	CALETA OLIVIA	A. antiqua	MIS 9			**0,80**		**0,71**		
WP479A(3)	CALETA OLIVIA	A. antiqua	MIS 9			**0,00**		**0,51**		
WP479B(1)	CALETA OLIVIA	A. antiqua	MIS 9			**0,02**		**0,34**		
WP479B(2)	CALETA OLIVIA	A. antiqua	MIS 9	X		**0,18**		**0,69**		
WP479B(3)	CALETA OLIVIA	A. antiqua	MIS 9			**0,75**		**0,80**		
WP479B(4)	CALETA OLIVIA	A. antiqua	MIS 9			**0,41**		**0,57**		
WP481(1)	CALETA OLIVIA	A. antiqua	MIS 9			**0,37**		**0,80**		
WP481(2)	CALETA OLIVIA	A. antiqua	MIS 9			**0,12**		**0,87**		
WP481(3)	CALETA OLIVIA	A. antiqua	MIS 9			**-0,19**		**0,90**		
WP481(4)	CALETA OLIVIA	A. antiqua	MIS 9			**0,06**		**0,52**		
WP481(5)	CALETA OLIVIA	A. antiqua	MIS 9			**0,11**		**0,64**		
WP481(6)	CALETA OLIVIA	A. antiqua	MIS 9			**-0,04**		**0,38**		
WP506(1)	CALETA OLIVIA	A. antiqua	MIS 9			**0,24**		**0,64**		
WP506(2)	CALETA OLIVIA	A. antiqua	MIS 9	X		**-0,43**		**0,44**		
WP506(3)	CALETA OLIVIA	A. antiqua	MIS 9			**0,27**		**0,68**		
WP667(7)	PUERTO LOBOS	M.edulis	MODERN			**0,96**		**0,52**		
WP95(6)	CAMARONES SOUTH	M.edulis	MODERN			**1,37**		**0,88**		
WP95(7)	CAMARONES SOUTH	M.edulis	MODERN			**1,37**		**1,18**		
WP191(5)	BAHIA BUSTAMANTE	M.edulis	MODERN			**1,71**		**0,91**		
WP191(6)	BAHIA BUSTAMANTE	M.edulis	MODERN			**1,66**	0,01	**0,98**	0,07	
WP191(7)	BAHIA BUSTAMANTE	M.edulis	MODERN			**1,63**		**0,96**		
WP191(8)	BAHIA BUSTAMANTE	M.edulis	MODERN			**1,48**		**0,81**		
WP271M(4)	BAHIA SOLANO	M.edulis	MODERN			**1,43**	0,015	**0,96**	0,08	
WP271M(5)	BAHIA SOLANO	M.edulis	MODERN			**1,69**		**1,03**		

APPENDIX A

MPA2(11)	RADA TILLY	M.edulis	MODERN			**1,75**		**1,15**		
MPA2(12)	RADA TILLY	M.edulis	MODERN			**1,30**		**1,01**		
MPA2(13)	RADA TILLY	M.edulis	MODERN			**1,31**		**1,23**		
WP330(1)	PUERTO DESEADO	M.edulis	MODERN			**1,06**		**1,43**		
WP330(2)	PUERTO DESEADO	M.edulis	MODERN			**1,98**		**1,89**		
WP330(3)	PUERTO DESEADO	M.edulis	MODERN			**1,61**		**1,30**		
WP330(4)	PUERTO DESEADO	M.edulis	MODERN			**1,45**		**1,31**		
WP330(5)	PUERTO DESEADO	M.edulis	MODERN			**0,89**		**1,35**		
AO 154D	CAMARONES SOUTH	M.edulis	5132±67			**1,72**		**1,29**		
AO 154D	CAMARONES SOUTH	M.edulis	5132±67			**1,71**		**1,26**		
WPi 436	CAMARONES SOUTH	M.edulis	5562±43			**1,86**		**1,19**		
WPi 436	CAMARONES SOUTH	M.edulis	5562±43			**1,87**		**1,22**		
WP104B(1)	CAMARONES SOUTH	M.edulis	5675±45 BP			**2,58**	0,02	**1,32**	0,08	
WP104B(2)	CAMARONES SOUTH	M.edulis	5675±45 BP			**2,75**		**1,46**		
WP104B(3)	CAMARONES SOUTH	M.edulis	5675±45 BP			**2,38**	0,05	**1,07**	0,03	
WP104B(4)	CAMARONES SOUTH	M.edulis	5675±45 BP			**2,82**	0,01	**1,24**	0,01	
WP108B(1)	CAMARONES SOUTH	M.edulis	LIT 5754±62 BP			**2,35**	0,01	**1,13**	**0,03**	
WP108B(2)	CAMARONES SOUTH	M.edulis	LIT 5754±62 BP			**2,29**		**1,17**		
WP108B(3)	CAMARONES SOUTH	M.edulis	LIT 5754±62 BP			**2,61**		**1,19**		
WP108B(4)	CAMARONES SOUTH	M.edulis	LIT 5754±62 BP			**1,99**		**1,11**		
WP108B(5)	CAMARONES SOUTH	M.edulis	LIT 5754±62 BP			**1,90**		**1,24**		
WP63B(1)	CAMARONES NORTH	M.edulis	6365±20	X		**2,08**	0,03	**2,50**	0,16	0,709127
WP63B(2)	CAMARONES NORTH	M.edulis	6365±20			**2,07**	0,02	**2,35**	0,01	
WP63B(3)	CAMARONES NORTH	M.edulis	6365±20	X		**2,65**	0,03	**2,51**	0,17	
WP63B(4)	CAMARONES NORTH	M.edulis	6365±20			**2,23**	0,05	**2,19**	0,19	
WP63B(5)	CAMARONES NORTH	M.edulis	6365±20			**1,75**		**2,23**		
WP63B(6)	CAMARONES NORTH	M.edulis	6365±20			**2,24**		**2,50**		0,709066
WP63B(7)	CAMARONES NORTH	M.edulis	6365±20			**1,99**		**2,16**		
WP63B(8)	CAMARONES NORTH	M.edulis	6365±20			**2,53**		**2,69**		
WP667	PUERTO LOBOS	*A.atra*	MODERN			**1,26**		**1,27**		
WP60B(2)	CAMARONES NORTH	*A.atra*	MODERN			**1,80**	0,037	**1,39**	0,041	
WP60B(3)	CAMARONES NORTH	*A.atra*	MODERN	X		**1,88**	0,141	**1,01**	0,142	0,7092
WP60B(4)	CAMARONES NORTH	*A.atra*	MODERN			**2,04**	0,005	**1,29**	0,028	
WP60B(5)	CAMARONES NORTH	*A.atra*	MODERN			**1,37**		**1,30**		
WP60B(6)	CAMARONES NORTH	*A.atra*	MODERN			**2,00**		**1,24**		
WP60B(10)	CAMARONES NORTH	*A.atra*	MODERN			**1,28**		**1,42**		
WP95(3)	CAMARONES SOUTH	*A.atra*	MODERN			**1,13**		**1,41**		
WP95(4)	CAMARONES SOUTH	*A.atra*	MODERN			**1,43**		**1,49**		
WP95(8)	CAMARONES SOUTH	*A.atra*	MODERN			**1,57**		**1,34**		
WP95(10)	CAMARONES SOUTH	*A.atra*	MODERN			**1,87**		**1,48**		
WP191(1)	BAHIA BUSTAMANTE	*A.atra*	MODERN			**1,32**	0,01	**1,28**	0,08	
WP191(2)	BAHIA BUSTAMANTE	*A.atra*	MODERN			**1,82**	0,03	**1,22**	0,06	
WP191(3)	BAHIA BUSTAMANTE	*A.atra*	MODERN			**1,75**	0,02	**1,42**	0,19	
WP191(4)	BAHIA BUSTAMANTE	*A.atra*	MODERN			**1,79**		**1,24**		
WP613(6)	BAHIA BUSTAMANTE	*A.atra*	MODERN	X		**1,78**		**1,33**		
WP613(7)	BAHIA BUSTAMANTE	*A.atra*	MODERN			**1,78**		**1,63**		
WP613(8)	BAHIA BUSTAMANTE	*A.atra*	MODERN			**1,44**		**1,39**		
WP613(9)	BAHIA BUSTAMANTE	*A.atra*	MODERN			**1,61**		**1,64**		
WP613(10)	BAHIA BUSTAMANTE	*A.atra*	MODERN			**1,68**		**1,60**		
WP271M(1)	BAHIA SOLANO	*A.atra*	MODERN	X		**1,72**		**1,52**		
WP271M(2)	BAHIA SOLANO	*A.atra*	MODERN			**1,65**		**1,06**		
MPA2(7)	RADA TILLY	*A.atra*	MODERN			**2,21**		**1,39**		
MPA2(8)	RADA TILLY	*A.atra*	MODERN			**2,21**	0,10	**1,22**	0,15	
MPA2(9)	RADA TILLY	*A.atra*	MODERN			**1,68**	0,05	**1,47**	0,15	
MPA2(10)	RADA TILLY	*A.atra*	MODERN			**2,30**	0,00	**1,50**	0,03	
WP473B(7)	CALETA OLIVIA	*A.atra*	MODERN			**1,50**		**1,46**		
WP473B(8)	CALETA OLIVIA	*A.atra*	MODERN			**1,66**		**1,51**		
WP473B(9)	CALETA OLIVIA	*A.atra*	MODERN			**1,85**		**1,73**		
WP473B(10)	CALETA OLIVIA	*A.atra*	MODERN			**1,87**		**1,68**		
WP473B(11)	CALETA OLIVIA	*A.atra*	MODERN			**1,48**		**1,53**		
WP473B(12)	CALETA OLIVIA	*A.atra*	MODERN			**1,56**		**1,39**		
WP60A(1)	CAMARONES NORTH	*A.atra*	915±20			**2,16**	0,01	**1,41**	0,09	
WP60A(2)	CAMARONES NORTH	*A.atra*	915±20			**2,71**	0,01	**1,55**	0,05	
WP60A(3)	CAMARONES NORTH	*A.atra*	915±20			**2,25**	0,01	**1,20**	0,09	
WP60A(4)	CAMARONES NORTH	*A.atra*	915±20			**2,27**	0,03	**1,34**	0,05	
WP60A(5)	CAMARONES NORTH	*A.atra*	915±20			**2,10**		**0,99**		
WP60A(7)	CAMARONES NORTH	*A.atra*	915±20	X		**1,65**	0,00	**1,36**	0,11	0,709051
WP60A(8)	CAMARONES NORTH	*A.atra*	915±20			**2,33**		**1,39**		
WP60A(9)	CAMARONES NORTH	*A.atra*	915±20			**1,51**		**1,42**		0,709188
WP60A(10)	CAMARONES NORTH	*A.atra*	915±20			**2,02**		**1,57**		
G001(1)	CAMARONES NORTH	*A.atra*	4074±50			**1,84**		**1,13**		0,709141
G001(4)	CAMARONES NORTH	*A.atra*	4074±50			**1,65**		**1,18**		
G001(5)	CAMARONES NORTH	*A.atra*	4074±50			**1,15**		**1,14**		
G001(6)	CAMARONES NORTH	*A.atra*	4074±50			**1,64**	0	**1,17**	0,02	
G001(7)	CAMARONES NORTH	*A.atra*	4074±50			**1,64**		**1,14**		0,70916
G001(2)	CAMARONES NORTH	*N. deaurata*	4074±50			**1,14**		**1,37**		
G001(3)	CAMARONES NORTH	*N. deaurata*	4074±50			**1,18**		**1,17**		

A.4 Trace element analysis

SAMPLE	Species	Ba µg/g	Ca µg/g	Fe µg/g	Mg ug/g	Mn µg/g	Sr µg/g	U µg/g
WP667(1)	A.antiqua	6,55	393019,65		131,01	0,07	1600,08	0,18
WP667(2)	A.antiqua	5,55	378867,40	21,34	153,95		1299,55	0,08
WP04(1)	A.antiqua	3,55	378867,40	12,94	139,95	1,00	1299,55	0,16
WP04(2)	A.antiqua	28,77	376212,12	16,17	104,87	1,73	1619,61	0,24
WP04(3)	A.antiqua	0,38	314526,54	5,15	101,46	2,93	1229,45	0,01
WP54(2)	A.antiqua	0,06	391452,24	31,71	109,09	1,57	1439,64	0,01
WP54(3)	A.antiqua	4,55	394039,40	43,35	135,01		1300,13	0,11
WP54(4)	A.antiqua	2,55	374018,70	31,35	129,01		1100,06	0,12
WP60BBIS(1)	A.antiqua	4,55	314259,36	12,74	106,20	0,32	1199,94	0,12
WP60BBIS(2)	A.antiqua	2,56	371318,30	35,42	123,31	2,51	741,85	0,15
WP60BBIS(3)	A.antiqua	26,66	294735,16	23,06	96,15	1,35	1099,56	
WP623BIS(1)	A.antiqua	23,40	360428,68	26,36	93,78	1,43	1399,65	0,33
WP623BIS(2)	A.antiqua	28,85	366882,60	9,74	84,63	1,05	1410,28	0,40
WP95(1)	A.antiqua		427489,81		125,80	0,16		
WP95(2)	A.antiqua	5,55	378399,20	14,35	176,09	1,30	880,44	0,22
WP95(3)	A.antiqua	23,19	338921,17	22,17	110,26	1,89	1359,80	0,07
WP110(1)	A.antiqua	13,53	391491,06	29,31	66,91	0,87	998,70	1,30
WP110(2)	A.antiqua	5,35	396012,91	20,54	50,72	0,58	1340,07	0,16
WP237(1)	A.antiqua	3,55	379000,00	8,15	122,00		1300,00	0,08
WP237(2)	A.antiqua	4,55	347721,82	10,64	87,93	0,12	1099,12	0,09
WP237(4)	A.antiqua	30,25	321526,70	7,31	88,08	0,66	1814,93	0,12
WP271(1)	A.antiqua	50,99	401071,8	10,00	100,91	0,837	1419,86	0,12
WP271(3)	A.antiqua	12,08	385245,34	30,17	104,08	1,89	2555,94	0,45
WP104A(2)	A.antiqua	16,07	377281,96	3,11	46,61	0,76	1656,59	1,60
WP104A(3)	A.antiqua	8,01	393773,19	2,80	53,92	0,66	1640,00	1,14
WP104A(4)	A.antiqua	12,58	394243,02	5,07	46,08	0,95	1499,93	1,24
WP92A(1)	A.antiqua	9,63	386851,51	8,09	51,71	0,87	2549,62	0,79
WP92A(2)	A.antiqua	7,10	370666,23	4,46	40,99	0,42	2738,90	0,79
WP92A(3)	A.antiqua	31,29	359386,34	9,71	52,20	0,75	2334,45	0,76
WP64B(1)	A.antiqua	48,39	383748,36	7,46	79,40	0,82	2299,48	0,62
WP64B(2)	A.antiqua	42,61	394496,31	7,18	218,15	0,61	2189,78	0,33
WP64B(3)	A.antiqua	40,38	386117,28	4,40	44,69	0,49	1989,10	0,28
WP65(2)	A.antiqua	14,65	370462,77	8,08	62,53	0,78	1952,84	2,35
WP65(3)	A.antiqua	37,54	377180,00	18,33	61,79	5,62	2639,33	2,29
WP65(4)	A.antiqua	54,43	371285,31	23,19	60,45	1,86	2026,26	1,79
WP97(1)	A.antiqua	4,43	340740,79	6,11	44,64	0,85	2029,59	1,54
WP97(2)	A.antiqua	1,09	395031,40	3,29	35,87	0,45	1659,75	2,04
WP97(3)	A.antiqua	29,02	380689,95	2,83	37,42	0,44	1539,85	1,94
WP139(2)	A.antiqua	22,29	409061,36	15,35	110,02		1000,15	0,20
WP139(4)	A.antiqua	18,52	389869,38	9,13	98,71	0,20	997,11	0,18
WP149(1)	A.antiqua	11,55	386864,60	7,25	130,95		1299,55	0,20
WP149(2)	A.antiqua	10,55	384961,50	17,35	101,99		1399,86	0,22
WP149(3)	A.antiqua	1,19	385942,11	8,75	122,98		1799,73	0,19
WP154A(1)	A.antiqua	2,10	381933,67	14,34	64,99		1499,74	0,87
WP154A(2)	A.antiqua	4,86	381000,00	17,35	53,60	0,15	1200,00	1,30
WP176BIS(1)	A.antiqua	5,77	385903,52	12,04	69,68	0,18	1499,63	1,60
WP176BIS(2)	A.antiqua	2,10	378363,25	17,34	73,29		1199,82	1,40
WP176BIS(3)	A.antiqua	5,77	398940,16	14,34	83,99		1899,72	1,10
WP197(1)	A.antiqua	12,55	388980,55	29,35	66,00	0,06	1099,95	0,00
WP197(2)	A.antiqua	1,19	376837,68	10,65	55,11		1300,13	1,70
WP 60B(1)	*A.atra*	98,02	309111,13	8,20	119,38	8,81	391,00	
WP 60B(4)	*A.atra*	59,22	274236,61	7,63	144,99	7,83	359,10	
WP 60B(10)	*A.atra*	41,19	334073,51	10,80	142,97	15,11	570,19	
WP 60A(4)	*A.atra*	71,43	340676,51	8,71	177,32	11,97	401,31	
WP 60A(7)	*A.atra*	66,94	337284,40	27,62	178,38	6,65	750,24	
WP 60A(9)	*A.atra*	58,42	341828,63	8,86	199,33	7,62	637,44	
G001(1)	*A.atra*	49,80	292609,40	24,65	295,48	9,18	625,66	
G001(6)	*A.atra*	43,11	332824,90	38,55	131,34	6,60	477,21	
G001(7)	*A.atra*	49,80	292609,40	24,65	295,48	9,18	625,66	
WP 63B(2)	*M.edulis*	92,41	344453,83	38,74	823,35	47,56	799,12	
WP 63B(5)	*M.edulis*	57,01	334673,27	45,15	983,08	40,75	149,67	
WP 63B(7)	*M.edulis*	53,19	325819,77	30,18	882,59	62,53	316,85	

APPENDIX A

WP70C	Paleosol	6,63	141381,42	4987,00	6402	31,83	219,00	2,00
WP70D	Paleosol	6,42	135243,76	5387,00	5890,50	32,84	194,55	2,20
WP70E	Paleosol	4,00	114763,06	3788,00	4356	23,84	219,50	1,48
WP18B	Paleosol	85,62	189484,38	8169,50	13010,50	115,70	271,10	0,76
WP18C	Paleosol	113,19	235989,42	7570,50	14897,00	97,70	343,10	1,00
WP18C	Paleosol	136,99	227772,85	10767,00	9845	135,60	339,00	0,84
WP18D	Paleosol	52,78	101401,06	27978,00	14343	719,60	151,50	1,00
WP38	Paleosol	166,34	177516,48	16364,50	12165,00	125,65	137,05	0,58
WP46A	Paleosol	12,83	92151,62	4387,00		55,83	77,50	0,68
WP46B	Paleosol	70,95	178439,08	5,00	11746,50	93,65	189,00	0,28
WP64C	Paleosol	74,61	179258,93	5,00	11961	99,60	195,00	1,48
WP 474	Paleosol	153,65	149973,67	6449,43	5273,15	103,47	245,32	
WP 462C	Paleosol	28,50	30487,43	17430,64	6100,71	652,49	49,94	
WP 462B	Paleosol	42,73	22249,81	20947,67	8878,68	244,41	54,93	
WP 175C	Paleosol	55,53	154162,03	1532,69	300,23	29,02	423,92	
WP 301E	Paleosol	111,14	125539,51	9915,59	2936,07	135,83	110,00	
WP 173B	Paleosol	114,98	94265,59	16793,96	7058,59	119,09	103,19	
WP 386	Paleosol	407,72	255441,07	6220,26	5941,30	166,71	242,85	

SAMPLE	Species	Ba/Ca (µmol/mol)	Fe/Ca (µmol/mol)	Mg/Ca (µmol/mol)	Mn/Ca (µmol/mol)	Sr/Ca (mmol/mol)*10	U/Ca (µmol*10/mol)
WP667(1)	A.antiqua	4,86		549,65	0,14	18,62	0,7712
WP667(2)	A.antiqua	4,27	40,4242	670,03	0,00	15,69	0,3643
WP04(1)	A.antiqua	2,73	24,5182	609,11	1,92	15,69	0,7108
WP04(2)	A.antiqua	22,32	30,8476	459,67	3,35	19,69	1,0738
WP04(3)	A.antiqua	0,35	11,7475	531,93	6,79	17,88	0,0535
WP54(2)	A.antiqua	0,04	58,1359	459,55	2,92	16,82	0,0430
WP54(3)	A.antiqua	3,37	78,9538	565,00	0,00	15,09	0,4701
WP54(4)	A.antiqua	1,99	60,1497	568,76	0,00	13,45	0,5402
WP60BBIS(1)	A.antiqua	4,23	29,1019	557,23	0,74	17,47	0,6694
WP60BBIS(2)	A.antiqua	2,01	68,4626	547,59	4,92	9,14	0,6819
WP60BBIS(3)	A.antiqua	26,40	56,1538	537,92	3,33	17,06	0,0000
WP623BIS(1)	A.antiqua	18,94	52,4850	429,04	2,90	17,76	1,5412
WP623BIS(2)	A.antiqua	22,95	19,0580	380,36	2,08	17,58	1,8361
WP95(1)	A.antiqua			485,25	0,28		
WP95(2)	A.antiqua	4,28	27,2179	767,34	2,51	10,64	0,9794
WP95(3)	A.antiqua	19,97	46,9502	536,43	4,06	18,35	0,3477
WP110(1)	A.antiqua	10,09	53,7385	281,84	1,62	11,67	5,5838
WP110(2)	A.antiqua	3,94	37,2310	211,19	1,07	15,48	0,6803
WP237(1)	A.antiqua	2,73	15,4257	530,80	0,00	15,69	0,3510
WP237(2)	A.antiqua	3,82	21,9637	416,98	0,25	14,46	0,4209
WP237(4)	A.antiqua	27,46	16,3127	451,72	1,50	25,82	0,6284
WP271(1)	A.antiqua	37,11	17,8919	414,89	1,52	16,19	0,5037
WP271(3)	A.antiqua	9,15	56,2114	445,50	3,57	30,35	1,9522
WP104A(2)	A.antiqua	12,43	5,9108	203,70	1,46	20,08	7,1556
WP104A(3)	A.antiqua	5,94	5,0955	225,80	1,23	19,05	4,8746
WP104A(4)	A.antiqua	9,31	9,2257	192,73	1,75	17,40	5,2956
WP92A(1)	A.antiqua	7,26	15,0028	220,43	1,65	30,15	3,4379
WP92A(2)	A.antiqua	5,59	8,6382	182,33	0,82	33,80	3,5871
WP92A(3)	A.antiqua	25,41	19,3970	239,53	1,53	29,71	3,5597
WP64B(1)	A.antiqua	36,80	13,9544	341,18	1,56	27,41	2,7417
WP64B(2)	A.antiqua	31,52	13,0529	911,85	1,13	25,39	1,4083
WP64B(3)	A.antiqua	30,52	8,1853	190,86	0,93	23,56	1,2204
WP65(2)	A.antiqua	11,54	15,6585	278,35	1,54	24,11	10,6902
WP65(3)	A.antiqua	29,05	34,8791	270,13	10,88	32,01	10,2200
WP65(4)	A.antiqua	42,79	44,8241	268,47	3,65	24,96	8,1008
WP97(1)	A.antiqua	3,80	12,8627	216,04	1,82	27,25	7,6083
WP97(2)	A.antiqua	0,81	5,9777	149,71	0,83	19,22	8,6938
WP97(3)	A.antiqua	22,25	5,3361	162,10	0,84	18,50	8,5795
WP139(2)	A.antiqua	15,90	26,9266	443,49		11,18	0,8233

APPENDIX A

WP139(4)	A.antiqua	13,87	16,8143	417,51	0,37	11,70	0,7751
WP149(1)	A.antiqua	8,71	13,4411	558,18		15,37	0,8702
WP149(2)	A.antiqua	8,00	32,3356	436,87		16,63	0,9621
WP149(3)	A.antiqua	0,90	16,2629	525,45		21,33	0,8288
WP154A(1)	A.antiqua	1,61	26,9541	280,58		17,96	3,8347
WP154A(2)	A.antiqua	3,72	32,6742	231,98	0,29	14,41	5,7451
WP176BIS(1)	A.antiqua	4,36	22,3993	297,75	0,34	17,77	6,9793
WP176BIS(2)	A.antiqua	1,62	32,8984	319,40		14,50	6,2292
WP176BIS(3)	A.antiqua	4,22	25,8055	347,15		21,78	4,6419
WP197(1)	A.antiqua	9,42	54,1414	279,77	0,12	12,93	0,0061
WP197(2)	A.antiqua	0,92	20,2764	241,13		15,78	7,5965
WP 60B(1)	*A.atra*	*92,55*	19,0311	636,83	20,80	5,79	
WP 60B(4)	*A.atra*	*63,03*	19,9789	871,83	20,82	5,99	
WP 60B(10)	*A.atra*	*35,98*	23,1908	705,70	33,01	7,81	
WP 60A(4)	*A.atra*	*61,19*	18,3452	858,28	25,63	5,39	
WP 60A(7)	*A.atra*	*57,92*	58,7726	872,07	14,38	10,17	
WP 60A(9)	*A.atra*	*49,88*	18,6101	961,56	16,26	8,53	
G001(1)	*A.atra*	*49,67*	60,4636	1665,14	22,88	9,78	
G001(6)	*A.atra*	*37,80*	83,1143	650,72	14,48	6,56	
G001(7)	*A.atra*	*43,99*	102,5923	968,61	17,83	10,76	
WP 63B(2)	*M.edulis*	*78,29*	80,7092	3941,54	100,72	10,61	
WP 63B(5)	*M.edulis*	*49,71*	96,8275	4843,72	88,82	2,05	
WP 63B(7)	*M.edulis*	*47,65*	66,4768	4466,77	140,01	4,45	
WP70C	Paleosol	13,69	25314,4481	74667,87	164,24	7,09	23,8185
WP70D	Paleosol	13,84	28585,8546	71819,99	177,11	6,58	27,3894
WP70E	Paleosol	10,17	23688,0425	62588,73	151,54	8,75	21,7138
WP18B	Paleosol	131,87	30941,6601	113222,04	445,44	6,54	6,7533
WP18C	Paleosol	139,97	23022,5571	104091,84	302,02	6,65	7,1348
WP18C	Paleosol	175,52	33924,5705	71272,86	434,30	6,81	6,2095
WP18D	Paleosol	151,92	198013,9788	233242,62	5177,04	6,83	16,6048
WP38	Paleosol	273,47	66158,5103	113001,41	516,37	3,53	5,5013
WP46A	Paleosol	40,63	34165,3637	0,00	441,98	3,85	12,4246
WP46B	Paleosol	116,03	20,0948	108549,78	382,87	4,84	2,6421
WP64C	Paleosol	121,48	20,0029	110026,45	405,33	4,98	13,9014
WP 474	Paleosol	299,00	30862,3078	57978,28	503,31	7,48	
WP 462C	Paleosol	272,85	410312,1286	329966,69	15612,92	7,49	
WP 462B	Paleosol	560,51	675664,5333	658010,14	8013,71	11,29	
WP 175C	Paleosol	105,13	7135,0779	3211,34	137,33	12,58	
WP 301E	Paleosol	258,38	56683,9364	38565,24	789,31	4,01	
WP 173B	Paleosol	355,96	127856,1828	123473,83	921,66	5,01	
WP 386	Paleosol	465,82	17475,8892	38353,19	476,10	4,35	